Production and Characterisation of Acellular Porcine Pulmonary Heart Valve Conduits

Ji Luo
BSc, MSc

Submitted in accordance with the requirements for the degree of
Doctor of Philosophy

School of Mechanical Engineering

The University of Leeds

October 2011

The candidate confirms that the work submitted is her own and that appropriate credit has been given where reference has been made to the work of others.

Acknowledgements

I would like to express my deepest thanks to my supervisor Professor Eileen Ingham, who is a very talented, wise and hard working scientist with great enthusiasm for science, for giving me the opportunity to carry out this research, and for her constant and endless guidance, advice, support and care throughout my study. I would also like to thank my co-supervisor, Dr Sotirios Korossis for his expert guidance in biomechanics. He has been so encouraging, helpful and patient. I think of him as a friend too. I cannot believe how lucky I am to have had both of you as my supervisors.

My heartfelt thanks go to Dr Daniel Thomas, my lab coach, for his kind support and guidance during my study. I will never forget the days working with the bioreactor with you. Every moment was challenging. You have been such a responsible and dependable lab partner.

I would like to thank Dr Stacy-Paul Wilshaw, Dr Thomas Stapleton, Dr Louise Jennings, Dr Helen Berry, Dr Catherine Bladen and Professor John Fisher for the instructions and help that they have given me throughout my studies. I was able to learn various techniques from you, without which this project could not have been accomplished.

I would like to express my appreciation to the technical staff in the IMBE, namely Mr Philip Wood, Mr Irvin Homan, Mr Lee Wetherill, Mr Keith Dyer, Mrs Amisha Desai and Mrs Jane Cardie, for their technical support during my study, especially the mechanical design, manufacture and maintenance of the equipment I needed.

I would like to thank Dr Rodolfo Paniagua for providing information on the surgical need for replacement heart valves, Miss Halina Norbertczak for her assistance in Alcian blue staining, and Mr Andrew Aldridge for providing me with the collagen gel to perform the contact cytotoxicity assays.

I would also like to thank everybody from Professor Ingham's lab especially from Office 6.56a, for their instructions on the experiments and assistance with questions and difficulties I encountered during this project.

My special thanks go to Mrs Sha Zhang, Professor Zhongmin Jin and Mrs Aiqin Liu. Mrs Zhang and Professor Jin, thank you so much for taking so much care of me all

through these years. You were always so nice even taking me out shopping. You provided me with so much information and suggestions which, to me, have been invaluable to understanding culture and life in the UK. Aiqin, you are a true friend who has always comforted and helped me in times of need. Thank you for being so supportive!

I would like to take this opportunity to thank my parents. You have been supportive and encouraging all through my life. You made me the person I am now. I cannot express in words just how grateful I am. You are the greatest parents in the world and I love you so much!

I would also like to thank my boyfriend, Yangwen. There has been joy and there have been tears, and you were there to share the good and bad times no matter what. Thank you for your encouragement and care, and above all, for always being around. You cannot imagine how important you have been to me in this foreign country.

My appreciation also goes to all of my friends that have been around to spend all the wonderful times with me during these years!

Finally I acknowledge the help received from numerous people, too many to mention in person who have directly or indirectly helped me in any way during my studies.

Abstract

Cardiac valve replacement is the second most common heart operation. Currently available replacement heart valves all have limitations. This study aimed to produce and characterise a decellularised, biocompatible porcine pulmonary root conduit for use in the Ross procedure. A process for the decellularisation of porcine pulmonary roots was developed incorporating trypsin (2.25×10^4 $Unit.ml^{-1}$) digestion of the adventitial surface of the scraped pulmonary artery and sequential treatment with: hypotonic Tris buffer (HTB; 10mM Tris pH 8.0, 0.1% (w/v) EDTA, 10KIU aprotinin), 0.1% (w/v) SDS in HTB, two cycles of DNase and RNase, and sterilisation with 0.1% (v/v) peracetic acid.

Histology confirmed an absence of cells and retention of the gross histoarchitecture. DNA levels were reduced by >90 % throughout the decellularised tissue and functional genes were not detected using PCR. Immunohistochemistry showed a lack of α-gal epitopes and confirmed cell removal but a loss of collagen IV. *In vitro* biocompatibility studies indicated the decellularised leaflets were not cytotoxic while the pulmonary wall was shown to reduce 3T3 cells viability in 3 out of 6 samples.

Uniaxial tensile testing to failure demonstrated no significant difference in the tensile properties between the fresh and decellularised leaflets and pulmonary walls in the circumferential and radial directions with the exception of the elastin phase slope of the pulmonary artery in both directions which showed a significant decrease in the decellularised tissue. Pulsatile flow testing indicated the decellularised pulmonary roots had excellent hydrodynamic function and leaflet kinematics in comparison to the fresh tissue. Initial attempts to culture fresh pulmonary roots in a heart valve bioreactor were unsuccessful, indicating a need to develop the physiological culture system further.

Overall the decellularised porcine pulmonary roots have excellent potential for development of a tissue engineered solution for right ventricular out flow tract reconstruction during the Ross procedure.

Contents

List of tables

List of Figures

Abbreviations

α-gal	Galα1,3-Galβ1-4GlcNAc-R
α-SMA	α-smooth muscle actin
Δp	Mean pressure difference
a.a.	Amino acid
ANOVA	Analysis of variance
AV	Atrioventricular
bp	Base pair
BSA	Bovine serum albumin
$CaCl_2$	Calcium chloride
CD	Cluster of differentiation
CHAPS	3-[(3-cholamidopropyl) dimethylammonio]-1-propanesulfonate
C.I.	Confidence intervals
cpm	Counts per minute
CSA	Cross-sectional area
Da	Dalton
DAB	3,3'-diaminobenzidine
DABCO	1,4-diazabicyclo[2.2.2]octane
DAPI	4',6-diamidino-2-phenylindole
Dil-Ac-LDL	Dil-labeled low density lipoprotein
DMEM	Dulbecco's modified Eagles Medium
DMSO	Dimethylsulphoxide
DNA	Deoxyribonucleic acid
DNAse	Deoxyribonuclease
ECM	Extracellular matrix
EDTA	Ethylenediaminetetraacetic acid
EOA	Effective orifice area
EPC	Endothelial progenitor cell
FBS	Foetal bovine serum
FC	Fully closed
FO	Fully open
GAG	Glycosaminoglycan
GAPDH	Glyceraldehyde 3-phosphate dehydrogenase
h	Hour
H&E	Haemotoxylin & Eosin
H_2O_2	Hydrogen peroxide
HBA	Heated blood agar
HCl	Hydrochloric acid
hEGF	Human epidermal growth factor
HMG-CoA	3-hydroxy-3-methyl-glutaryl-Coenzyme-A
HSC	Hematopoietic stem cells
$MgCl_2$	Magnesium chloride
MHC	Major histocompatibility complex

min	Minute
MO	Modified Orifice
MSC	Mesenchymal stem cell
MSD	Minimum significant difference
MTT	3-(4,5-Dimethylthiazol-2-yl)-2,5-diphenyltetrazolium bromide
N	Newton
NA	Nutrient agar
NaOH	Sodium hydroxide
NBF	Neutral buffered formalin
NCBI	National Center for Biotechnology Information
P4HB	Poly-4-hydroxybutyrate
PAA	Peracetic acid
PBS	Phosphate buffered saline
PCR	Polymerase chain reaction
PECAM-1	Platelet/endothelial cell adhesion molecule
PERV	Porcine endogenus retrovirus
PGA	Polyglycolic acid
PHA	Polyhydroxyalkanoate
PLA	Polylactide
PLC	Polycaprolactone
PLGA	Poly(lactic-co-glycolic acid)
PLLA	Poly-L-lactic acid
POE	Polyorthoesters
PPF	Polypropylene fumarates
RGD	Arginine-glycine-aspartic acid
RNA	Ribonucleic Acid
RNAse	Ribonuclease
rpm	Revolutions per minute
SAB	Saboraud dextrose agar
SC	Start closing
SDS	Sodium dodecyl sulfate
SE	Standard error
s	Second (SI unit)
SLA	Swine leukocyte antigen
SO	Start opening
StDev	Standard deviation
TBS	Tris buffered saline
TE	Tris-EDTA
TGA	Triglycidyl amine
Tm	Melting temperature
UEA-1	Ulex Europaeus agglutinin-1
v	Volume
V	Voltage
VEC	Valvular endothelial cell
VEGF	Vascular endothelial growth factor
VIC	Valvular interstitial cell

vWF	von Willebrand factor
w	Weight

Chapter 1

Introduction

From 1998 to 2005, an estimated 288,000 aortic or mitral valve replacement procedures were performed in the United States with an in-hospital death rate of 4.98 % (Barnett & Ad, 2009). Although heart valve repair is the gold standard for minor valve disease, heart valve replacement is the most common and effective treatment for severe valvular dysfunction. Thus, there is an increasing need for replacement heart valves. Currently, traditional replacement valves are either mechanical or biological, and each has its advantages and disadvantages. Mechanical valve replacement carries a risk of thromboembolism, and thus life-long anticoagulation therapy is required. Anticoagulation however may cause hemorrhage. Biological valves, including bioprosthetic and homograft valves, carry a lower risk of thromboembolism, but tend to fail sooner and more frequently. Homograft valves are associated with limited availability especially for children. An approach to design an “ideal replacement valve” would be through tissue engineering. A successful tissue engineered heart valve could overcome almost all of the drawbacks associated with the currently available valve replacements. Tissue engineered heart valves would have the potential to remodel and grow, which are important features especially for children undergoing heart valve replacement.

1.1 The human heart

The function of the heart is to pump blood to all tissues and organs in the body. It is thus essential to life. Oxygen, nutrients, waste products and heat are transported with the aid of the heart around the body at a very high speed (Levick, 2003). It is located slightly left of the middle of the chest (directly posterior to the sternum). The heart is protected and supported by the pericardium, which is a double layered membrane. Normally, the heart weighs 300 to 400 grams in human adults, and measures approximately 12.5 cm from the base to the apex, which reaches the fifth intercostal space (Martini, 2006). The heart acts as a strong pump, which is composed of myocardium, and beats an average of 100，000 times each day, pumping more than

7,000 litres of blood. A person's heart may have beaten more than 3 billion times by the end of his/her life (Martini, 1995).

The heart consists of four chambers, which are the left and right ventricles and the left and right atria. The four chambers are built around the *annulus fibrosus*, which is a ring of fibrous tissue. The heart is supplied by several large blood vessels, by which, blood can be carried into or away from the heart. The right atrium receives blood through the superior vena cava and the inferior vena cava. The left and right pulmonary arteries are connected to the right ventricle and carry blood from the right ventricle to the lungs. The left atrium receives oxygenated blood from the lungs via the two left and two right pulmonary veins, which are connected to the posterior wall of the left atrium. The aorta, which is responsible for carrying oxygenated blood away from the heart and into the systemic circuit, is connected to the left ventricle. The aorta is the largest vessel connected to the heart, and has a diameter of about 20 mm in human adults (Martini, 2006; Figure 1.1).

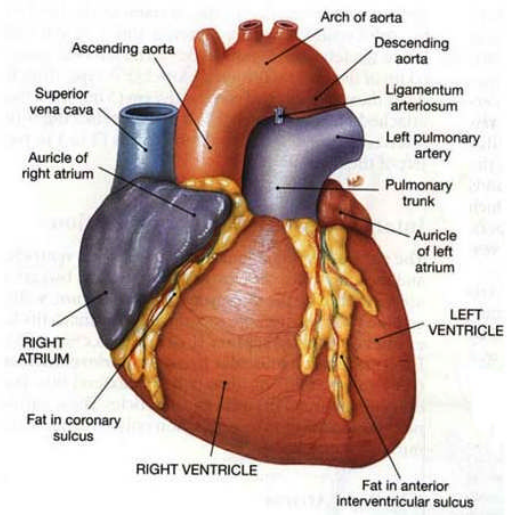

Figure 1.1 Schematic diagram of the structure of the heart. The heart consists of four chambers: left and right ventricles, and the left and right atria. Several large vessels are connected to the heart. The superior vena cava and the inferior vena cava are connected to the right atrium; the left and right pulmonary arteries are connected to the right ventricle; the left and right pulmonary veins are connected to the left atrium; the aorta is connected to the left ventricle. (Derived from BiologyDaily, 2005)

The ventricles receive blood from the atria, and are responsible for pumping the blood out of the heart to different parts of the body. The shape of the left ventricle is ellipsoidal while the shape of the right ventricle is more irregular. The left ventricle

appears to wrap around the right ventricle. The ventricle walls consist of cardiac muscle. Cardiac muscle is strong in order to carry out the pumping work of the ventricles. The left ventricle, which is responsible for systemic circulation, has to exert four to six times as much pressure, to push blood around the systemic circuit, as the right ventricle to push blood around the pulmonary circuit. Thus, the left ventricle has a much thicker wall than the right ventricle (almost twice as thick) because it requires more muscle and energy to do its work. The left ventricle also bulges into the right ventricular cavity as it contracts, improving the efficiency of the right ventricle (Martini, 2006; Levy & Pappano, 2007).

The atria reside above the ventricles. They are storage chambers for blood returning to the heart, rather than important pumps for the forward propulsion of blood. They are formed by a continuum of muscle fibres that originate from the fibrous skeleton at the base of the heart (Levy & Pappano, 2007). They perform a temporary storage function and then pump the blood into the corresponding ventricles. The contraction of the atria contributes to approximately one quarters of the blood that enters the ventricles. The other three quarters of blood enter the ventricles due to the vacuum force after the contraction of the ventricles. Since the atria only supply blood to the ventricles, the contraction force in the atria is much weaker than that in the ventricles. Thus, the walls of the atria are much thinner compared to that of the ventricles. However, the wall of the right atrium is slightly thicker than that of the left atrium due to the fact that the right atrium receives blood from the systemic circulation and experiences higher pressures (Korossis, 2002; Levick, 2003; Levy & Pappano, 2007).

The blood circulation in the heart is regulated by the cardiac cycle. According to the contraction of the atria and the ventricles, and the position of the inlet and outlet heart valves, the ventricular cycle can be divided into four phases: ventricular filling, isovolumetric contraction, ejection and isovolumetric relaxation (Levy & Pappano, 2007). The blood enters the heart via the left atrium through the pulmonary veins, and is then pumped into the left ventricle. After the contraction of the left ventricle (ventricular systole), blood is pumped into the aorta, and the systemic circulation starts. For the right heart, the right atrium receives blood after systemic circulation through the superior vena cava and the inferior vena cava. Then, blood enters the right ventricle and is pumped out of the heart through the pulmonary artery during right ventricular systole. The pulmonary circulation then starts, and the oxygenated blood returns to the heart

through the pulmonary veins (pulmonary veins – left atrium – left ventricle – aorta - systemic circulation – superior vena cava & inferior vena cava – right atrium – right ventricle – pulmonary artery – lungs – pulmonary veins; Figure 1.2).

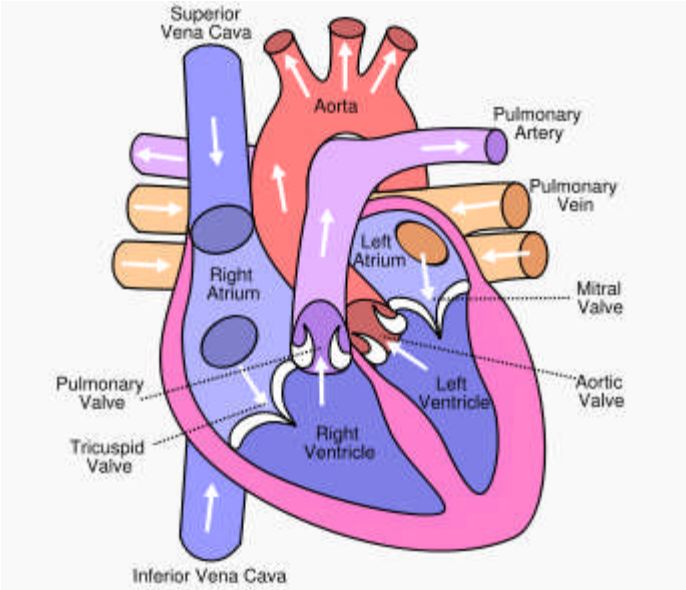

Figure 1.2 An illustration of the blood circulation in the human heart.
(http://en.wikipedia.org/wiki/File:Diagram_of_the_human_heart_(cropped).svg**)**

1.2 Heart valves

The cardiac valves are flexible, tough, endothelium-covered fibrous leaflets (also called cusps or flaps) present at the exits of the ventricles and atria. The movements of heart valves are passive, depending on the different transvalvular pressures. The main function of heart valves is to prevent or minimise backward blood flow, acting as one way inlets and outlets and allowing the unidirectional flow of blood through the heart during the cardiac cycle (Rector & Visitors, 2007). There are four valves in the heart including the tricuspid, mitral, aortic and pulmonary valves (Table 1.1 and Figure 1.3). The mitral valve has two leaflets whereas the other three have three leaflets. Since the tricuspid and mitral valves are located between the atria and the ventricles, they are known as atrioventricular (AV) valves. The aortic and pulmonary valves are classified as semilunar valves due to the shape of the leaflets, and are located between the ventricles and the great arteries (the aorta and the pulmonary artery, respectively).

Table 1.1 Heart valves and their locations.

Type	Name	Location
Atrioventricular valves	Tricuspid valve	Between the right atrium and the right ventricle
	Mitral valve	Between the left atrium and the left ventricle
Semilunar valves	Pulmonary valve	Between the right ventricle and the pulmonary artery
	Aortic valve	Between the left ventricle and the aorta

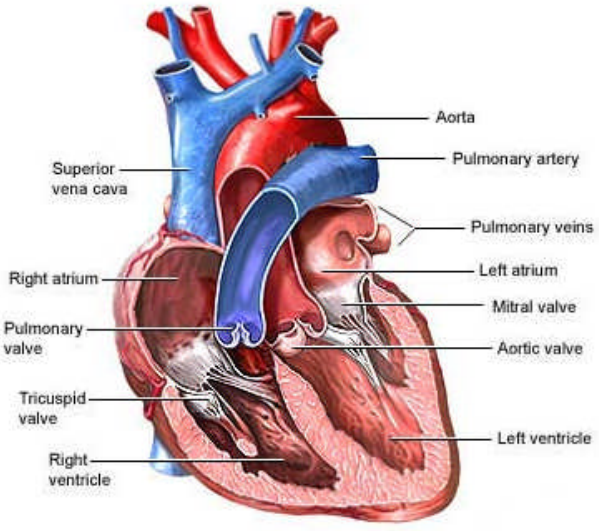

Figure 1.3 The locations of heart valves. (Lee, 2006)

During ventricular relaxation, the aortic and pulmonary valves close and the mitral and tricuspid valves open to allow blood from the left and right atria into the left and right ventricles, respectively. More blood flows into the ventricles as the atria contract. During ventricular contraction the mitral and tricuspid valves close and the aortic and pulmonary valves open, allowing blood flow into the aorta and the pulmonary artery, respectively (Rector & Visitors, 2007).

1.2.1 The atrioventricular valves

The main function of the AV valves is to prevent the back-flow of blood from the ventricles into the atria. The AV valves are composed of four primary elements: (1) the valve annulus; (2) the valve leaflets; (3) the papillary muscles; and (4) the chordae tendineae (Bronzino, 2000). The leaflets of the AV valves are thin and translucent

fibrous membranes, strong enough to prevent the back-flow of blood (Schoen, 1998). Similarly to all other tissues in direct contact with the blood, the leaflets of the atrioventricular valves are covered by endothelial cells. Smooth muscle cells are the main cell population of the mitral valve interstitium. In addition, non-myelinated nerve fibres, and blood vessels are also present (Bronzino, 2000). The total leaflet area of the AV valves is approximately twice that of their respective orifices and, therefore, there is a considerable coaptation region in the leaflets of the closed AV valves. The AV valve annulus resides at the base of the leaflets, and is attached to the atrial and ventricular walls. The chordae tendineae (also known as "heart strings") are fine, strong ligamentous tissues attached at the free edge of the leaflets. They insert the leaflets at multiple locations (about 5 to 60) and extend to the tips of the papillary muscles. The chordae tendineae play an important role in valve function by preventing eversion of the leaflets during ventricular systole (Levy & Pappano, 2007). The papillary muscles arise from the wall of the ventricle and are responsible for generating the tension which is transferred to the leaflets by the chordae during ventricular contraction. The structures and arrangement of these valve components are important in providing continuity between the valve and ventricular wall (Bronzino, 2000).

The mitral valve is the only valve in the heart to have two leaflets; the posterior and anterior leaflets. These two leaflets are actually one continuous piece of tissue with the anterior portion being shorter and wider than the posterior. The mitral valve owes its name to its shape which resembles a mitre (Latin; from the Greek mítra), or bishop's cap. Since the pressure in the left side of the heart is higher than that in the right side, the mitral valve, together with aortic valve, are the most stressed valves in the heart and are associated with a high incidence of valvular disease. The tricuspid valve is so named because it has three leaflets: anterior, inferior and septal (Martini, 1995; Martini, 2006).

1.2.2 The semilunar valves

The semilunar valves (pulmonary and aortic valves) prevent blood from returning back to the ventricles from the arteries. They consist of three half-moon-shaped cusps, and thus have been named semilunar. The leaflets of these valves are attached to the artery wall and are composed of passive, thin fibrous tissue, which is translucent (Schoen, 1999a). At the end of the reduced ejection phase of ventricular systole, the cusps snap

together due to a brief reversal of the blood flow towards the ventricles, therefore, preventing blood regurgitation. During ventricular systole, instead of lying back against the walls of the pulmonary artery and aorta, the leaflets float in the bloodstream approximately midway between the vessel walls and their closed position (Levy & Pappano, 2007). Since the arterial walls do not contract, muscular braces are not required for the semilunar valves. Thus, unlike the atrioventricular valves, semilunar valves do not have papillary muscles or chordae tendineae.

The pulmonary valve, which is located between the right ventricle and the pulmonary artery, prevents deoxygenated blood returning to the right ventricle during ventricular relaxation. It opens during the contraction of the right ventricle, and allows deoxygenated blood to flow through to the lungs. The aortic valve is the other semilunar valve. When it opens during the contraction of the left ventricle, the oxygenated blood flows through the aortic valve to the aorta. It is closed as the ventricle relaxes, and this prevents blood from returning to the left ventricle.

The aortic valve is the most well-studied heart valve and is prone to valve dysfunction requiring surgical intervention. It has three leaflets, the left-coronary, right coronary, and the non-coronary (also named the posterior) leaflets. The left and right coronary leaflets have coronary arteries, which supply the heart with blood, arising from the corresponding sinuses. The non-coronary leaflet does not have such an artery. The right coronary leaflet of the porcine aortic valve has a piece of muscle at its base, which makes it distinguishable from the left coronary leaflet (Sutton *et al*., 1995). A cut-open porcine aortic valve is illustrated in Figure 1.4 A. The orifices of the coronary arteries can be seen above the left and right coronary leaflets. The position of each leaflet and the position of the mitral and aortic valves relative to each other are illustrated in Figure 1.4 B. The difference between the human and porcine aortic heart valve is that in pigs the myocardium is in contact with the right coronary leaflet, forming a muscular shelf. In humans, however, there is no such shelf. For a single aortic valve leaflet, as illustrated in Figure 1.4 D, the free edge is along the top of the leaflet. Just in from the free edge along the superior portion of the leaflet is the coaptation region which is the portion that contacts the neighbouring cusps. The leaflet is connected to the aortic wall by the curved inferior portion. The commissure is the region where the free edge meets the aorta, and the *corpus arantii* is a large collagenous mass in the coaptation region which supposedly aids in valve closure and reduces regurgitation (Robarts *et al*., 1997).

A histological section of a single aortic leaflet illustrating the different layers stained with Masson's trichrome is shown in Figure 1.4 E.

The pulmonary valve has been reported to share similar structural characteristics with the aortic valve, although some differences have been found (Martini, 2006; Levy & Pappano, 2007). It also consists of three leaflets, which are attached by convex edges partly to the infundibular wall of the right ventricle and partly to the origin of the pulmonary trunk. An image of a cut-open porcine pulmonary valve is presented in Figure 1.4 F. The pulmonary leaflets are attached to the pulmonary sinuses through three crescents of infundibular musculature, and there is an incomplete annulus supporting the leaflets. The three pulmonary leaflets are named the right leaflet (comparable to the right aortic leaflet), left leaflet (comparable to the left coronary aortic leaflet), and anterior leaflet (Standring, 2008; Figure 1.4 G). The term "pulmonary root" refers to the pulmonary valve together with the pulmonary artery (approximately 5 cm in length) and myocardium (approximately 5 mm in length) that connects to the valve annulus. The pulmonary root is hardly supported since the pulmonary annulus inserts into the relatively thin right ventricular myocardium, whereas the aortic root annulus inserts into the thick left ventricular myocardium. However, the pulmonary root has myocardium up to the leaflet connections around the whole circumference. Although thicker, only approximately two thirds of the aortic root circumference has myocardium (the remaining third is the mitral valve anterior leaflet). The pulmonary artery wall is thinner than the aorta, and the pulmonary leaflets are generally thinner than the aortic leaflets. Also, there are no blood vessel associated with the pulmonary valve leaflets (Fisher & Watterson, 1997). David and colleagues (1994a) conducted a comparative study in which the thickness of 72 porcine pulmonary leaflets and 72 porcine aortic leaflets was measured. The mean thickness of pulmonary leaflets was 0.49 mm whereas the mean thickness of aortic leaflets was 0.67 mm. Porcine pulmonary valve leaflets exhibited similar tensile properties to aortic valve leaflets in the circumferential direction, but slight differences existed between the radial directions (David *et al*., 1994a; Gerosa *et al*., 1994). The calcium level in pulmonary walls was on average less than half of that in the aortic walls, which suggests that pulmonary roots may exhibit less calcification after implantation. The pulmonary root also has less elastic tissue than the aortic root (Livi *et al*., 1987; Hokken *et al*., 1997).

1.2.2.1 Structure of the semilunar valve leaflets

The leaflets of the semilunar valves have a total thickness of approximately 300-700μm (Martini, 2006). Both collagen and elastin are connective tissue proteins and are the most abundant extracellular matrix (ECM) proteins in heart valves. Collagen is strong and stiff while elastin is more flexible. The cross-section of a leaflet shows three distinct layers; the *fibrosa*, *spongiosa* and *ventricularis* (ordered from the direction of the artery to the ventricle, Figure 1.4 E). The *fibrosa* is mainly composed of collagen and elastin, and has a thickness of about 150-350μm. The collagen in the *fibrosa* is organised into large bundles which are oriented predominantly in the circumferential direction of the leaflets. This directional arrangement of the collagen makes the leaflets highly compliant in the radial direction and relatively stiff and inextensible in the circumferential direction. These features are important in accommodating the cyclical pressure fluctuations during the cardiac cycle since the circumferentially orientated, stiff collagen bundles are responsible for bearing the diastolic stress. During systole, the collagen fibres start crimping, and corrugations of the *fibrosa* produce a visible surface rippling which disappear during diastole (Figure 1.4 H). When the valve is closed, the crimping expands in the radial direction, permitting an initial increase in leaflet size (Figure 1.4 I). The stiffening induced by fully extended collagen crimps during valve closing contributes to the prevention of leaflet prolapse (Schoen, 1999b). Surrounding the collagen bundles, there is an elastin matrix which maintains the valve's microstructure by restoring the contracted configuration of the leaflets during systole. The *ventricularis* is the leaflet layer facing the inflow surface of the valve. It also consists of collagen and elastin. However, unlike the *fibrosa*, the collagen is not organised in any specific direction. Thus, the *ventricularis* is less stiff than the *fibrosa* (Robarts *et al*., 1997; Schoen, 1999a; Mendelson & Schoen, 2006). The *spongiosa* is more of a gap between the *fibrosa* and *ventricularis* than a definable structure on its own. It is primarily composed of water, glycosaminoglycans (GAG`s) and a small amount of loosely arranged collagen and elastin. GAG`s in this layer are important in resisting compression, and the loose arrangement of this layer allows it to absorb shock during the cardiac cycle.

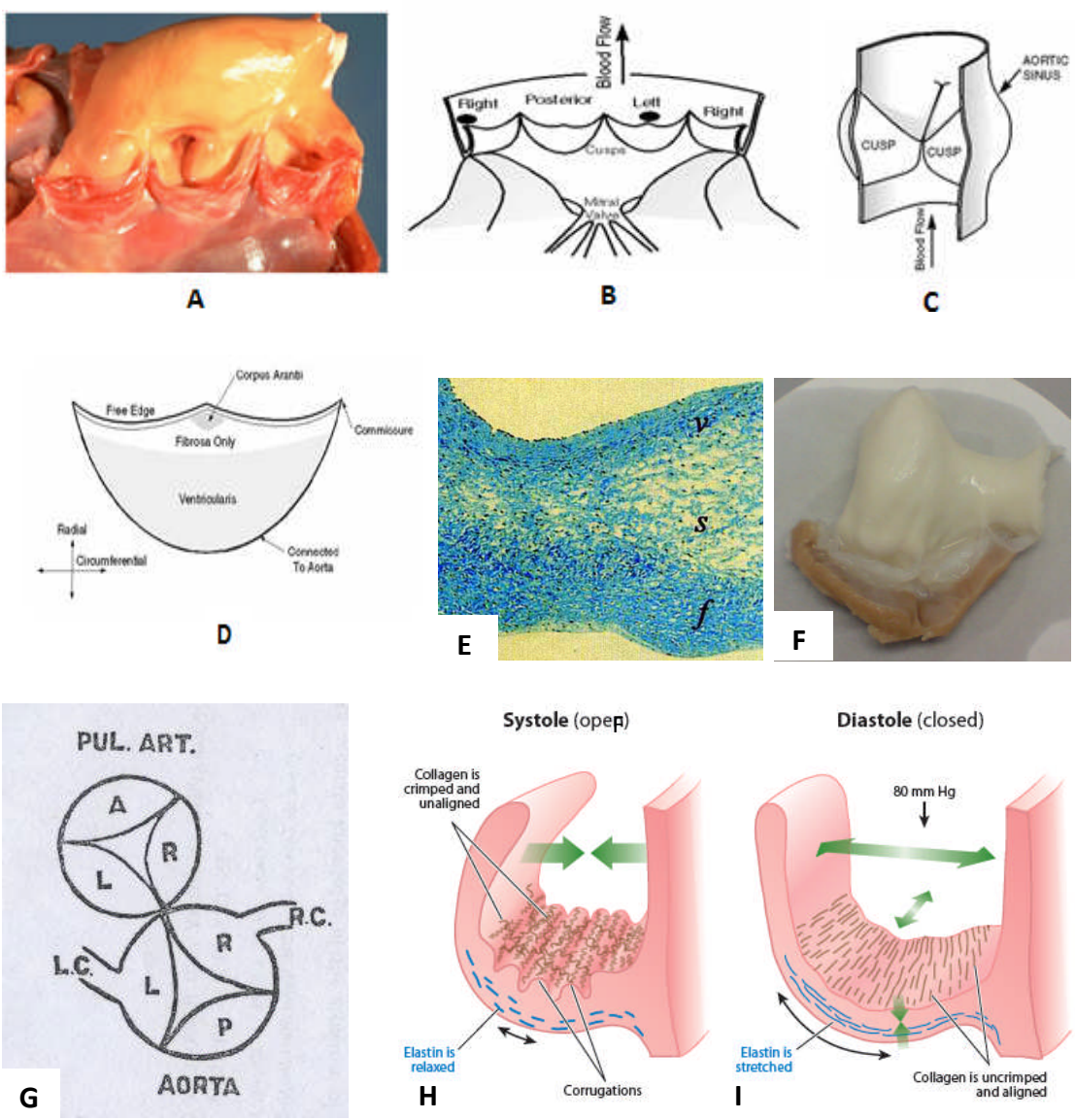

Figure 1.4 The semilunar valves. (A) A cut-open porcine aortic valve. From left: non-coronary, left-coronary, right coronary leaflets; **(B)** Schematic of cut-open porcine aortic valve; **(C)** Schematic of the aortic root; **(D)** Schematic of the semilunar leaflet; **(E)** Masson's trichrome stained section of a porcine aortic valve leaflet, collagen stained blue; (v: *ventricularis*; s: *spongiosa*; f: *fibrosa*) (Source: The University of Utah Cardiovascular Pathology Index, 2007b; The Robarts *et al*., 1997; Booth *et al*., 2002). **(F)** A cut-open porcine pulmonary valve; **(G)** Terminology of pulmonary and aortic valve leaflets (Gross & Kugel, 1931); **(H)** A 3D illustration of the three layered structure of the aortic valve during systole (Schoen, 2011a); **(I)** A 3D illustration of the three layered structure of the aortic valve during diastole (Schoen, 2011a). L: left leaflet; R: right leaflet; P: posterior leaflet; A: anterior leaflet; L.C.: left coronary artery; R.C.: right coronary artery.

1.2.2.2 Cells of the semilunar valve leaflets

Heart valve leaflets contain two types of cells: valvular endothelial cells (VEC`s) and valvular interstitial cells (VIC`s). VEC`s form a single layer on the surface of the leaflet, and are considered to be morphologically different from aortic endothelial cells (Butcher *et al*., 2004; Butcher & Nerem 2004; Sacks & Yoganathan, 2007). For example, in response to mechanical stress, porcine aortic valve endothelial cells align perpendicular to flow whereas endothelial cells from the aorta align parallel to flow (Mendelson & Schoen, 2006). By studying the porcine valvular and vascular endothelial cells *in vitro* with 20 dynes.cm^{-2} steady laminar shear stress for up to 48 hours, Butcher *et al*. (2004) reported the vascular endothelial alignment is calpain-, Rho-kinase–, and PI3K-dependent, whereas valvular endothelial cell alignment is calpain- and Rho-kinase–dependent, but PI3K-independent. VEC`s are important in regulating vascular tone, thrombosis, inflammation and remodelling and VEC dysfunction may lead to multiple disorders including atherosclerosis (Leask *et al*., 2003). Endothelial cell dysfunction can be caused by mechanical forces, bacterial infection, autoantibodies and circulating modulators of endothelial cell function. Common valvular diseases such as senile degenerative valve disease, myxomatous (or floppy) valves, rheumatic valves, and infected (endocarditis) valves show changes in the synthetic, morphologic and metabolic functions of the VEC`s (Leask *et al*., 2003).

The VIC`s reside within the three layers of the heart valve leaflets, and primarily serve to maintain the structural integrity of the leaflet tissue by remodelling via protein synthesis and enzymatic degradation (Bairati & DeBiasi, 1981; Taylor *et al*., 2003; Merryman *et al*., 2006). The VIC`s have characteristics of both fibroblasts and smooth muscle cells (which range from fibroblast-like to myo-like). The phenotype of VIC`s is believed to be reversible (Sacks & Yoganathan, 2007). When the phenotype of the resident VIC population is myo-like, the cells are actively remodelling the ECM, which indicates that the VIC phenotypic state at any given time is likely related to the current remodelling demands of the tissue (Rabkin *et al*., 2002). It is believed that there is a feedback mechanism between the VEC`s and VIC`s although no direct junctions have been observed between the two types of cells (Filip *et al*., 1986; Marron *et al*, 1996; Sacks & Yoganathan, 2007; Sacks *et al*., 2009). In an *in vitro* study carried out by Butcher & Nerem (2006), VIC alone or VIC and VEC mixtures were cultured in Type I collagen hydrogels and exposed to 20 dynes.cm^{-2} steady shear for up to 96 hours. VIC`s

proliferated when not in communication with VEC`s. VIC`s secreted matrix in a valvular endothelial– and flow-dependent manner and VEC`s decreased α-SMA expression in VIC`s. Although the exact mechanism was unclear, it was apparent from the results that the VEC was the key regulator of VIC phenotype and shear flow enhanced this regulation.

1.2.2.3 Mechanical properties of the semilunar heart valves

The mechanical behaviour of a material refers to its deformation under load. Most frequently, the mechanical behaviour is expressed as the stress generated in a material subjected to a particular strain (stress-strain behaviour). The biomechanical testing of soft tissues such as heart valves is problematic. Soft tissues are non-homogeneic and their complex nature makes it difficult to obtain fundamental physical parameters. Generally, in order to characterise the mechanical properties of valvular tissue, uniaxial tensile tests on strips of tissue (Sauren *et al*., 1983; Mayne *et al*., 1989; Korossis *et al*., 2002; Stradins *et al*., 2004; Korossis *et al*., 2005; Seebacher *et al*., 2007; Tudorache *et al*., 2007) or biaxial mechanical tests on intact valves (Mayne *et al*., 1989; Billiar & Sacks, 2000; Vesely *et al*., 2000) have been frequently used.

Uniaxial tensile testing is more popular since in comparison to biaxial testing it is easier to perform. However, although important information can be generated, uniaxial tensile testing is not ideal for determination of the mechanical properties of soft tissue, since the stress/strain relationship in different directions cannot be obtained at the same time and on the same point of a tissue specimen. Moreover, the mechanical coupling between the material axes and the physiological fibre kinematics is not taken into account during uniaxial tensile testing (Billiar & Sacks, 2000). Uniaxial tensile testing is more representative of the physiological state of the heart valve tissue although it is a complex methodology to establish and perform especially on heart valve leaflet tissue, which has a heterogeneous structure and is small in size (Billiar & Sacks, 2000; Sacks & Yoganathan, 2007). Both uniaxial and biaxial tensile testing requires flattening of the tissue, and the force is only applied in 2D. Thus, the true 3D stress-strain behaviour of the tissue is not achievable using these tests. On the other hand, tensile testing, either uniaxial or biaxial, can provide quantitative stress-strain information of heart valve tissue *in vitro*, which is useful for understanding the mechanical behaviour, as well as

for comparison of the heart valve replacements to natural tissue. Preconditioning has been used by many researchers prior to uniaxial tensile testing when determining the mechanical properties of heart valve tissue in order to generate repeatable results (Korossis *et al*., 2002; Fitzpatrick *et al*., 2010). However, it has been reported that tissue preconditioning does not contribute to the generation of repeatable stress-strain curves for heart valve tissue (Carew *et al*., 2004). Whether there is a need for preconditioning in the determination of heart valve tissue mechanical properties will be dependent upon the purpose of the study. For example, for comparative studies, preconditioning can be omitted as long as the test conditions for each test groups stay the same.

Both uniaxial and biaxial tensile tests (Sauren *et al*., 1983; Courtman *et al*., 1994; Billiar & Sacks, 2000; Korossis *et al*., 2002; Stradins *et al*., 2004; Tudorache *et al*., 2007) have shown that the stress-strain behaviour of heart valve leaflet tissue has three distinct phases. The initial phase is linear with a low elastic modulus, during which the resistance to stretch and force transmission is provided solely by the elastin fibres (Sauren *et al*., 1983). The next phase is a transition phase in which the collagenous crimps of the leaflets is gradually removed (Clarke, 1973; Broom, 1978) and their contribution to force transmission is increased. The second linear portion represents the collagen phase and it is characterised by a high modulus. During this phase, the tissue has a reduced compliance and a small extension of the tissue would produce a high tension. This reflects the material properties of the strong network of collagen fibres (Sauren *et al*., 1983). Of all the tensile parameters that can be acquired from the tensile testing results, the elastin phase slope, collagen phase slope, and failure stress and strain give the most information regarding the properties of the tissue such as the extensibility and the strength. Korossis (2002) reported on the uniaxial tensile properties of the porcine aortic leaflet. The elastin phase slope, collagen phase slope, failure stress and failure strain in the circumferential direction were: $(7.24 \pm 1.95) \times 10^{-5}$ GPa, $(3.79 \pm 0.61) \times 10^{-2}$ GPa, 6.26 ±0.83 MPa and 47.21 ± 5.68 %, and the above parameters in the radial direction were: $(4.01 \pm 0.87) \times 10^{-5}$ GPa, $(2.10 \pm 0.30) \times 10^{-3}$ MPa, 0.93 ± 0.21 MPa and 101.70 ± 9.18 %. Tudorache *et al*. (2007) reported the failure stress and strain for porcine pulmonary valve leaflet to be 0.8 ± 0.12 MPa and 80 ± 33 % in the circumferential and 0.52 ± 0.23 MPa and 70 ± 20 % in the radial direction. The reported tensile testing results showed a wide range of variability. This was probably due to the different tensile testing methods that were applied by each research group. Differences

in the experimental methods including tissue sampling, processing, testing equipment and experimental settings will all affect the tensile test results. Thus, it is essential in comparative studies of the tensile properties of tissues that the same methods are applied. A study carried out by Strandis *et al.* (2004) reported the failure stress and strain for human pulmonary valve leaflet to be 2.78 ± 1.05 MPa and 19.40 ± 3.91 % in the circumferential and 0.29 ± 0.06 MPa and 29.67 ± 4.41 % in the radial direction. The human pulmonary valve leaflets seemed to be weaker than the porcine tissue. The results of these studies showed the leaflets to be much more extensible in the radial direction compared to the circumferential direction, which corresponds to the anisotropy of the leaflets.

Uniaxial tensile testing has been applied to study the mechanical properties of the aortic or pulmonary root wall by a number of groups (Sauren *et al*., 1983; Lokie *et al*., 1993; Zhou *et al*., 1997; Jennings, 2001; Korossis, 2002). The stress-strain behaviour of the semilunar root wall has a similar three-phased behaviour to the leaflet tissue, with a higher elastic and collagen modulus. The aortic root wall has been reported to have no directional differences (Sauren *et al*., 1983) or a reduced anisotropy (Ferraresi *et al*., 1999; Jennings, 2001; Korossis, 2002) compared to the leaflet tissue. Korossis (2002) reported the uniaxial tensile properties of the fresh porcine aortic wall in his study The elastin phase slope, collagen phase slope, failure stress and failure strain in the circumferential direction were: $(1.22 \pm 0.15) \times 10^{-4}$ GPa, $(3.60 \pm 0.77) \times 10^{-3}$ GPa, 1.91 ±0.30 MPa and 149.63 ± 6.15 %. The above parameters in the axial direction were: $(8.67 \pm 2.13) \times 10^{-5}$ GPa, $(6.58 \pm 1.34) \times 10^{-4}$ MPa, 0.44 ± 0.04 MPa and 141.97 ± 19.99 %. The same trend might be expected for the pulmonary root wall, which does not differ significantly in structure from that of the aortic root wall (Hokken *et al*., 1997).

1.2.2.4 The hydrodynamic function of the semilunar heart valves

The function of the heart valve tissue is essentially related to the surrounding haemodynamic environment. Understanding the interactions between the heart valve and the local haemodynamic environment is critical to understand normal valve function and disease progression, as well as to provide a standard to test the function of a replacement heart valve. Although some anatomical differences do exist, the essential

function of the semilunar heart valves, which is to facilitate the unidirectional flow of blood while maximizing flow rate and minimizing flow resistance stays the same.

The aortic valve opens during systole when the ventricle is contracting and then closes during diastole as the ventricle relaxes. The valve closes near the end of the deceleration phase of systole with very little reverse flow through the valve. The axial pressure differences cause the low inertial flow along the aortic wall to decelerate and then to reverse direction, resulting in vortices in the sinuses behind the aortic valve leaflets (Reul & Talukder, 1989). This action is thought to facilitate movement of the aortic valve leaflets away from the aorta and towards the closed position, thus to assist the effective and fast closure of the leaflets. Although *in vitro* studies have suggested that the axial pressure difference alone is sufficient for valve closure (Reul & Talukder, 1989), the closure is not as efficient as when the vortices are present. In fact, the aortic valve should functionally be considered as part of the entire left ventricular outflow tract. For instance, during the cardiac cycle, the aortic annulus expands and contracts, which clearly assists the opening and closure of the leaflets (Sacks *et al*., 2009).

The pulmonary flow profile has been reported to be similar to that of the aortic valve with lower velocity magnitude (Sacks & Yoganathan, 2007). During acceleration of the blood flow, the peak velocity is observed after the peak flow. The mean temporal velocity profile is relatively flat and reverse flow occurs in late systole with an instantaneous skewness that rotates counter clockwise, which may be representative of flow separation (Sloth *et al*., 1994). Secondary flow patterns have also been observed in the pulmonary artery and its bifurcation. *In vitro* laser Doppler anemometry experiments have shown that these flow patterns are dependent on the valve geometry and thus can be used to evaluate function and fitness of the heart valve (Sung & Yoganathan, 1990; Sung *et al*., 1990).

Understanding valve hydrodynamics requires a knowledge of the dynamic deformations that occur during valve function. However, due to the complexity of valve anatomy, it is difficult to theoretically determine the functional role of each individual component (Arts *et al*., 1983). Studies of heart valve root dynamics are limited due to difficulties in performing *in vivo* studies (Thubrikar *et al*., 1993). A study carried out by Dagum *et al*. (1999) showed that the ovine aortic root undergoes complex, asymmetric deformations during the various phases of the cardiac cycle including elongation, compression, shear,

and torsional deformation. Sacks *et al*. (2009) summarised the common behaviour of all valvular tissues which are required for valve function as: (i) leaflets cycle between the fully unloaded to fully loaded state every cardiac cycle, which is different to other connective tissues that remain preloaded (e.g. blood vessels); (ii) leaflets experience large, anisotropic stretches during closure in response to small transvascular gradients; (iii) corresponding tension levels have been estimated to be in the range of 50 – 100 $N.m^{-1}$ during peak loading; (iv) peak strain rates are very high, reaching values of 1000 $\%.s^{-1}$; (v) once the valve is closed, further leaflet deformation ceases; (vi) valve tissue deformations are highly sensitive to the deformations of the surrounding tissues.

In vitro hydrodynamic testing using a pulsatile flow simulator has been employed to evaluate the hydrodynamic function of heart valves (Fisher *et al*., 1986; Weerasena *et al*., 1992; Zsolt *et al*., 2000; Jennings, 2001; Korossis *et al*., 2005). During the opening phase, the semilunar valves experience the stellate, triangular and circular configurations as described by Thubrikar *et al*. (1979). The bending deformations of the valve leaflets can be analysed by high-speed image analysis throughout the cardiac cycle during pulsatile flow testing by the determination of the curvatures of the free leaflet edge (Corden *et al*., 1995; Korossis, 2002). The mean pressure difference across the valve as a function of the root mean squared flow (which can be expressed as the effective orifice area (EOA), with the larger the EOA the less obstruction to flow), together with the reverse flow and the total energy loss, can be used to characterise overall valve function (Fisher & Wheatley, 1988). The EOA also has an impact on the specific flow behaviour of the heart valve (Sacks & Yoganathan, 2007).

Porcine and human aortic and pulmonary valve roots have been reported to have a low pressure difference across their leaflets since the resistance to flow is very low (Lockie *et al*., 1994; Nagy *et al*., 2000; Jennings, 2001). Normally, a peak pressure gradient of 40 mm Hg would be considered as conduit dysfunction following heart valve replacement surgery (Brown, *et al*., 2011). Porcine and homograft pulmonary roots have shown similar pressure/flow characteristics and EOA`s to aortic roots when tested at systemic pressure. The pulmonary roots demonstrated better performance than their aortic counterparts due to the larger dilation of the pulmonary root at systemic pressure (Weerasena *et al*., 1992; Nagy *et al*., 2000; Jennings, 2001).

1.3 Heart valve disease

Heart valve associated disease is one of the main causes of heart failure. Valvular dysfunction usually involves regurgitation and/or stenosis. Regurgitation occurs when the valve is not able to close completely, causing part of the blood to flow back to the atrium or ventricle. In this case, the heart is required to increase its effort in pumping blood, resulting in cardiac hypertrophy. In valvular stenosis the effective orifice of the valve narrows or does not form properly, restricting the flow of blood out of the atria or the ventricle. Thus, the heart is required to pump harder in order to pump enough blood through the stenotic valve. Heart valves can have either one or both of the conditions at the same time hampering the heart's ability to pump blood adequately through the body and, consequently, causing serious cardiac implications (Rector & Visitors, 2007). As discussed previously, the left side of the heart is responsible for pumping blood through the high-pressure systemic circulation whereas the right side of heart pumps blood to the low-pressure pulmonary circulation. Therefore, the valves associated with the left side of the heart (mitral and aortic) are more prone to disease than the valves of the right heart. Statistics have shown that acquired valvular disease involves the mitral valve in ~80% of the cases, the aortic valve in ~50% of the cases, and the tricuspid valve in only ~10% of the cases. The pulmonary valve is almost never affected (Marks & Marks, 1993). When a heart valve is diseased severely and cannot be repaired, replacement is normally the therapeutic choice. Although the mitral valve is most likely to be diseased among the four heart valves, valve repair rather than replacement is most commonly required. Heart valve replacement is mostly required for the aortic valve since severe valve failure happens most frequently in the aortic position.

Researchers in the area have identified a number of underlying reasons for valvular disease. According to Boudoulas *et al*. (1994), valvular disease can be classified as:

1. Heritable-congenital causes of valvular heart disease e.g., floppy mitral valve with mitral valve prolapse, bicuspid aortic valve, and Marfan syndrome;

2. Inflammatory-immunologic causes such as rheumatic fever, acquired immune deficiency syndrome, endocardial proliferative disorders, and antiphospholipid syndrome;

3. Myocardial dysfunction-ischemic cardiomyopathy, dilated or hypertrophic cardiomyopathy-resulting in valvular heart disease;

4. Diseases and disorders of other organs as causes of valvular heart disease, e.g., chronic renal failure and carcinoid heart disease;

5. Valvular heart disease related to aging: calcific aortic stenosis and mitral annular calcification;

6. Valvular disease following interventions such as valvuloplasty, valve reconstructive surgery and valve replacement;

7. Valvular disease related to drugs and physical agents, such as chronic ergotamine use, radiation therapy and trauma.

1.4 Heart valve replacement

Heart valve replacement is the second most common surgical operation in the heart in the Western world (Brody & Pandit, 2007). Cardiac valve replacement was first introduced in the 1950's, by Charles Hufnagel who implanted caged-ball heart valves in ten patients (six survived the operation). A similar valve was invented by Miles Edwards and Albert Starr in 1960 (Lefrak & Starr, 1979; Starr *et al.*, 2002; Winters & Obriot, 2007). During the past 50 years, a variety of replacement valves have become available, with the most commonly used being the mechanical and biological tissue valves. Since the aortic valve is most likely to fail and replaced among the four valves, it is important that a replacement valve can be used in the aortic position. Almost all of the available mechanical or biological valves can be used in aortic valve replacement if required. When selecting an appropriate valve replacement, the surgeon needs to take into account a number of issues including age, sex, associated medical conditions, risk factors, and even cultural beliefs (Treasure, 1990; Women's heart foundation, 2007).

Currently, there is no ideal valve replacement. As more advanced understanding of cardiac physiology, biomechanics and materials science, and clinical experience is accumulated, workers in the field have concluded that an ideal valve replacement should meet the following criteria (Schoen *et al.*, 1982; Marks & Marks, 1993; Sapirstein & Smith, 2001):

- Function like a native valve, permitting unimpeded forward flow when open while preventing regurgitant flow when closed, without leaking;
- Not generate turbulence so that haemolysis and stimulation of the clotting cascade is limited;
- Biocompatible, and its blood-contacting surfaces not thrombogenic;
- Easy and safe to implant with surgical results comparable among surgeons;
- An associated morbidity which is low enough to yield reproducible clinical outcomes;
- Durable and the need for re-operation minimal.
- Only affects the daily activities of the patient to a very limited level. This means that anticoagulation should be unnecessary after the surgery, the risk of endocarditis is low, and the sounds of the prosthetic valve are unnoticeable.

Although there is no replacement valve that can meet all these criteria, current replacement valve designs offer acceptable solutions in most cases. In general, clinically available heart valve replacements can be classified into two types: mechanical and biological. Biological valves include bioprosthetic valves and human tissue valves. Each has its own advantages and disadvantages.

1.4.1 Mechanical valves

Mechanical valves are entirely made from artificial components, according to understanding of cardiac physiology and biomaterials. They were the first type of replacement valve to be developed. To date, three types of mechanical valve have been developed including the caged-ball valve, the tilting-disc valve and the bileaflet valve.

The first mechanical valve to be developed was the Starr-Edwards caged-ball valve. This valve was designed as a mitral valve prosthesis using a silastic ball (Starr & Edwards, 1961a; Figure 1.5 A). The first clinical operation was performed in 1960, and in the following 4 to 5 years, further modifications were conducted with the first commercial model developed in 1965 (Starr & Edwards, 1961b; Starr *et al*., 1967). The

caged-ball mechanical valve retained its fundamental design for over 30 years of use. The main problem with the caged-ball valve was that turbulence was caused due to the ball's central location in the outflow blood. Although there was an attempt to reduce thromboembolic complications by covering the valve housing with cloth, this failed because the cloth wear and unpredictable overgrowth of tissue could stop the motion of the poppet (Khan, 1998; Sapirstein & Smith, 2001; Figure 1.5 B). The latest version of the caged-ball valve was brought to market in 1980s. It was improved and subject to reduced failure (Wernly & Crawford, 1998). An occluding poppet was used in the cage in order to direct the blood flow. However, this poppet could result in turbulence and the implantation of the valve required a relatively large dose of anticoagulants. Moreover, these valves generated high transvalvular pressure gradients especially with smaller diameter valves (Fisher & Wheatley, 1988). Another problem with the caged-ball mechanical valve is that it had a relatively high profile due to the cage. Thus, it could only be implanted in patients with relatively large left ventricular cavities or aortic roots. Nowadays, the caged-ball valve is rarely used clinically (Sapirstein & Smith, 2001).

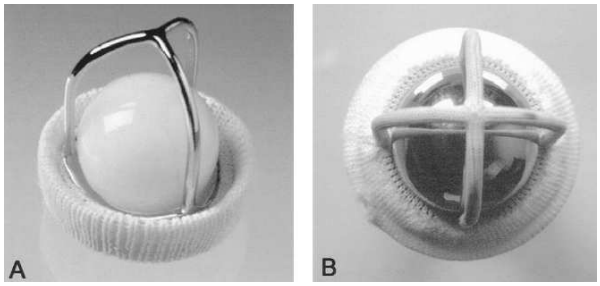

Figure 1.5 The caged-ball mechanical valve. (A) The aortic model 1260 Starr Edwards valve. **(B)** A four-strut mitral model 6400 Starr-Edward valve with a hollow metal ball and the struts covered by cloth. (Modified from Butany *et al*., 2003a).

The second generation of mechanical valves was based on a tilting-disc principle. This type of valve used a thin wafer to replace the ball in the caged-ball valve. Tilting-disc valves experienced a number of problems when first developed, including low-velocity eddy currents caused by turbulence, retrograde leaks (which occurred when the disc approached the vertical position when fully open; Collins, 1991). Towards the end of the 1960s, the Bjork-Shiley tilting disc valve (Figure 1.6 A), was developed (Bjork, 1969). This valve consisted of a spherically-shaped disc, which was made of pyrolytic

carbon and positioned within a metal ring and sewing cuff. Across the inflow and outflow of the valve orifice, two arching struts were designed, thus permitting the disk to pivot between opened and closed positions. In order to decrease turbulence, an occluder was designed within the valve ring. The free-floating disc occluder was also retained by the struts. The Bjork-Shiley valve was widely used for several decades since it had a much lower profile than the caged-ball valve, and thus had fewer limitations. Nevertheless, the Bjork-Shiley valve still had several drawbacks that could cause serious valve failure. During ventricular contraction, due to the repetitive stress of valve closure, some larger-diameter mitral valves fractured at their welds, or the strut completely separated from the ring. The Bjork-Shiley valve was withdrawn from the market in 1986 (van Gorp *et al*., 2004).

Following the Bjork-Shiley valve, three other improved tilting disk valves became clinically available. These include the Alliance Medical Technologies' Monostrut valve (uses a re-engineered strut contiguous with the metal of the valve ring; Figure 1.6 B), the Omniscience valve (it moves by "hinging" against 2 sides of the valve ring; Figure 1.6 C), and the Medtronic-Hall valve (Figure 1.6 D). All have been used for either mitral valve or aortic valve replacement. An improvement in the tilting disc valves is that the opening angle is about 70°-80°, generating fairly low transvalvular pressure gradients (Sapirstein & Smith, 2001).

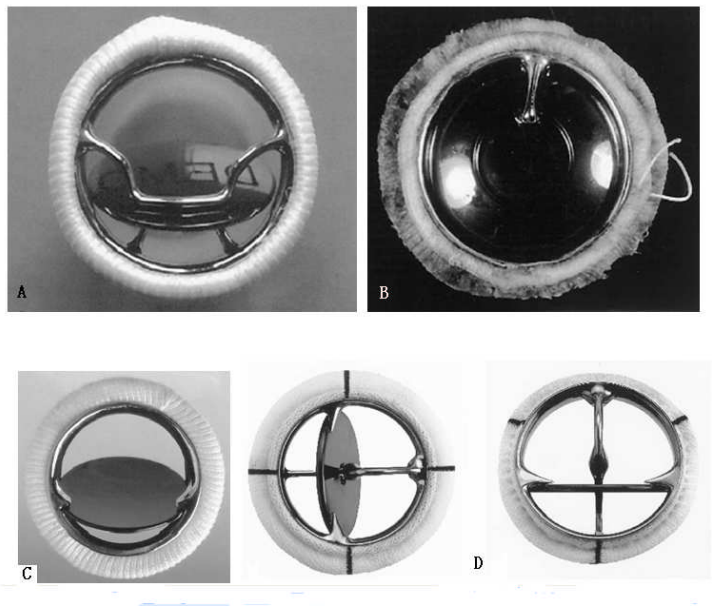

Figure 1.6 Tilting disc valves. (A) Bjork-Shiley; **(B)** Alliance Medical Technologies **(C)** Monostrut; Omniscience; **(D)** Medtronic-Hall. (Modified from Butany *et al*., 2003a)

The invention of pyrolytic carbon by Dr Jack Bokros in 1969 was a great contribution to the development of mechanical valves (DeBakey *et al*., 1971). Although this material was originally developed for the encapsulation of nuclear fuel rods, it was widely used in almost all new mechanical valves over the decade following its invention (Bokros, 1989; Gott *et al*., 2003). The discs in each of the tilting disk valves discussed above were composed of graphite, and coated with pyrolytic carbon, which was synthesized through repetitive heating. The use of this material gives the disc a very smooth and strong surface, and thus reduces the formation of thrombus.

The most recent generation of mechanical valves is the bileaflet prosthesis. The bileaflet mechanical valves are manufactured by St Jude Medical Inc. and Sulzer CarboMedics,. The St Jude bileaflet valve (Figure 1.7) also used pyrolytic carbon as the disc material. It contains 2 semicircular discs that open with independent hinge mechanisms with nearly 90° opening angles. The larger opening angles provide excellent valve haemodynamic function. Compared to the tilting-disc, the excursion of the occluder beyond the plane is considerable less due to the fact that each leaflet covers only half of the valve orifice. St Jude mechanical valves have been used for mitral, tricuspid, and aortic valve replacement (Sapirstein & Smith, 2001; Starr *et al*., 2002).

Figure 1.7 The St Jude Mechanical valve. (obtained from St Jude Medical, Inc., 2011)

It is generally believed that the second and third generation mechanical valves are much more superior to the caged-ball valves. They have a lower profile, longer durability, reduced turbulence, and require a smaller dose of anticoagulants following implantation. In addition, the second and third generation mechanical valves cause less frequent thromboembolic complications after surgery compared with the caged-ball valves.

The most important advantage of the mechanical valves is their long-term durability compared to bioprosthetic and human tissue valves. However, even though the second and third generation mechanical valves are significantly improved compared to older designs, they are still highly thrombogenic due to the blood turbulence at the interface with the device (Schoen, 1982; Grunkemeier & Rahimtoola, 1990; Butany *et al*., 2003a). The occurrence of thrombosis may have catastrophic consequences because it can occlude the valve and embolise to the brain or other vital organs. Among the available mechanical valves, the St Jude valve has been reported to cause the least thrombosis. In addition, blood clots are more likely to form after mechanical valve replacement due to the more severe red blood cell damage that mechanical valves cause compared to biological valves (Edmunds *et al*., 1987). Consequently, it is not surprising that life-long administration of oral anticoagulants such as warfarin is mandatory following valve replacement with a mechanical valve. Regular control of the coagulation state by the plasma thromboplastin time is also necessary (Marks & Marks, 1993). Haemorrhage is another complication associated with mechanical valve implantation due to the necessary use of anticoagulants (Hammermeister *et al*., 2000; Grunkemeier e*t al*., 2000; Oxenham *et al.*, 2003; Wheatley & Will, 2004). The structural deterioration of these valves has become an increasingly recognized complication from the early 1980s, particularly in younger patients (Wheatley & Will, 2004).

1.4.2 Biological valves

Biological valves are derived from animal or human tissue. Depending on their source, biological valves are divided into bioprosthetic valves (porcine or bovine tissue valves) and human tissue valves (further classified as homografts and autografts).

1.4.2.1 Bioprosthetic valves

Bioprosthetic valves are also referred to as xenografts or heterografts. They are chemically-treated animal tissue valves which were first developed in the late 1960s in an attempt to overcome the haemodynamic problems of the mechanical valves. Bioprosthetic valves are generally designed to imitate the flow and materials properties of the native counterpart. Thus, they are a much closer match than mechanical valves

(Butany *et al*., 2003b). Both valvular tissue (such as porcine aortic or pulmonary valve) and non-valvular tissue (typically bovine pericardium) have been used in the manufacture of bioprosthetic valves. In bioprosthetic valves, the animal tissue is treated with a cross-linking agent, usually glutaraldehyde, in order to strengthen the tissue, reduce its immunogenicity, and provide tissue stability against biological breakdown (Korossis *et al*., 2000; Mercuri *et al*., 2007). Subsequently, the cross-linked tissue is mounted on a fabric-covered frame (sewing ring) or stent made of metal or plastic. Nowadays, bioprosthetic valves are used in half or more of valve replacements (Rahimtoola, 2010).

The first generation bioprosthetic valves were the Carpentier-Edwards and Hancock Standard (Medtronic Inc) stented porcine aortic xenografts, which became available during the 1970s. These prostheses were cross-linked with glutaraldehyde at high pressure and mounted on stents. The Carpentier-Edwards valve utilised a stent which was flexible and eccentric to compensate for the restricting muscle shelf which resides under the right coronary cusp of the porcine aortic valve (Figure 1.8). The Hancock Standard valve (Figure 1.9 A) utilised a semi-flexible stent with a radiopaque sewing ring and demonstrated inferior hemodynamic performance in smaller sizes. In the Hancock Modified Orifice (MO) valve (Figure 1.9 B) the right leaflet was replaced by a non-coronary leaflet from another porcine aortic valve in order to eliminate the muscle shelf. The Carpentier-Edwards and Hancock (Medtronic Inc) Standard xenografts had an overall thromboembolic incident rate equivalent to those of fully anticoagulated mechanical prostheses. Although low doses of anticoagulation were used postoperatively for only several months, the increased risk of embolization after surgery in some cases required long term anticoagulation (Sapirstein & Smith, 2001). The postoperative results with the Carpentier-Edwards and Hancock Standard bioprostheses were clinically acceptable. The most significant drawback with these valves was that they faced predictable structural failure after several years (Bernal *et al*., 1995). A 10-year clinical study of the Carpentier-Edwards (98 patients) and Hancock Standard valves (65 patients) showed an average implant duration of 13.9 ± 3.9 years for the Carpentier-Edwards valves, and 10.0 ± 5.1 years for the Hancock Standard valves. Compared with Hancock Standard valves, Carpentier-Edwards valves also had a higher incidence of stent deformation (41.5% vs. 14.3%), calcification (75.4% vs. 54.1%), and pannus (100% vs. 91.8%) (Butany *et al*., 2007b). Butany *et al*. (2007a) reported on the

longest duration of implantation of a porcine bioprosthesis Carpentier-Edwards valved conduit excised after 25 years at the tricuspid valve position from a 50-year-old man. They found significant thrombus (on the sinus surface of a cusp), mild structural valve deterioration and pseudo-intimal formation within the conduit. The bioprosthesis' longevity was likely related to low-pressure circulation in the right heart and to host tissue (pannus) overgrowth that covered the cusps and thereby reduced tissue degeneration.

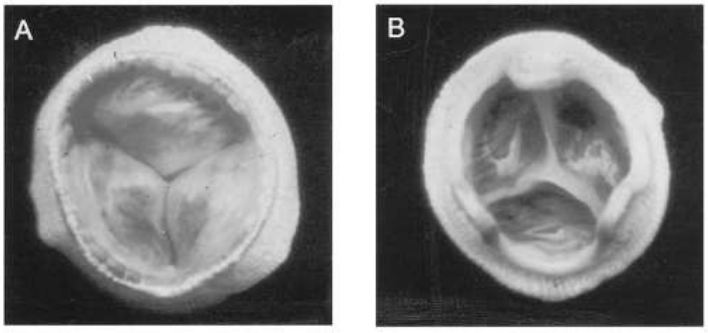

Figure 1.8 The Carpentier-Edwards valves. (A) The inflow; **(B)** The outflow. (Modified from Butany *et al*., 2003b)

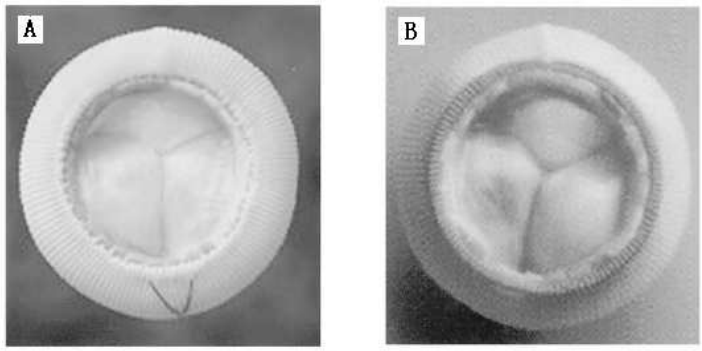

Figure 1.9 The Hancock bioprosthetic valves. (A) Hancock standard valve; **(B)** Hancock MO valve. (Modified from Butany *et al*., 2003b)

The second generation of porcine valves was developed with a view to improving the durability of their predecessors. Attempts were made to treat the tissue with anti-mineralization agents and the valve was fixed in glutaraldehyde at low pressure, to prevent distorting the ECM. The outcome of the second generation valves has been

good for older patients (lower than 10% failure after 10 years), yet not very satisfying in younger patients (David *et al*., 1995; Jamieson *et al*., 1995).

In an effort the overcome the problems of the elevated transvalvular pressure gradient associated with the stented porcine bioprostheses, stentless porcine bioprostheses were developed (Figure 1.10 A). These valves were considered to have very low to zero transvalvular pressure gradients, good to excellent haemodynamics and are associated with regression of left ventricular hypertrophy (O'Brien *et al*., 1987; Bernard *et al*., 1989; David *et al*., 1994b; Kon *et al*., 1999; Butany *et al*., 2003b). Recent clinical outcomes in Toronto have shown that the stentless valves have a much lower freedom from reoperation rate at 12 years than the Carpentier-Edwards valves. Cusp tear with consequent aortic regurgitation was the most common cause of structural valve deterioration. There is no general recommendation to use stentless bioprostheses in all patients in the aortic position (Kobayash, 2011).

Bovine pericardial bioprosthetic valves, such as the Ionescu-Shiley valve (Figure 1.10 B), were designed in the 1970s. They were made of glutaraldehyde-treated bovine pericardium and demonstrated better haemodynamics compared to the stented porcine valves. However, these valves have demonstrated limited durability, especially in patients younger than 60 (Sapirstein & Smith, 2001; Butany *et al*., 2003b).

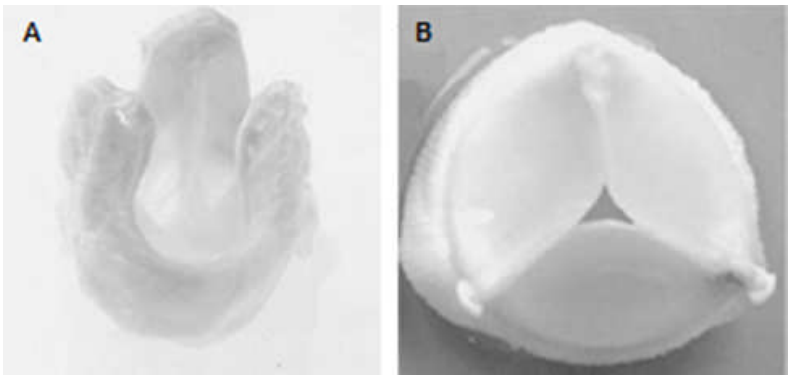

Figure 1.10 Stentless porcine bioprosthetic valves. (A) Stentless porcine bioprosthetic valve; **(B)** Ionescu-Shiley stentless bovine valve. (Modified from Butany *et al*., 2003b).

Bioprosthetic heart valves have acceptable haemodynamic function, and have become an important clinical choice in heart valve replacement (Schoen, 2011a). One of their

major advantages is that they are more thromboresistant than mechanical valves, and therefore, life-long anticoagulation treatment is not necessary (Butany *et al*., 2003b). On the other hand, functional deterioration and progressive structural failure are the major drawbacks of bioprosthetic valves, which fail sooner and more frequently than mechanical valves (Sapirstein & Smith, 2001). Clinical studies using bioprosthetic valves in the pulmonary position in 181 patients suggested valve function was stable in most patients until 5 years after operation. By 10 years, however, about 80% will require reoperation or manifest valve dysfunction. It has also been suggested that the stentless valve was less durable than stented valves (Lee *et al*., 2011).

Both biological responses and design criteria can contribute to bioprosthetic valve failure: leaflet calcification leads to tearing and loss of adequate coaptation (Jamieson *et al*., 1990; Schoen & Levy, 1986; Grabenwoger *et al*., 1996); high levels of cyclic bending stress within the valve leaflets also exacerbate the structural deterioration (Vesely *et al*., 1988; Butterfield *et al*., 1990); abrasion, thinning, as well as tearing can cause the local fatigue of bioprosthetic valves in the stressed regions, and thus lead to valve failure (Korossis, 2002). Furthermore, studies have indicated that bioprosthetic valves do not perform as well in younger patients as they do in older patients, making them unsuitable for this patient group and especially children (David *et al*., 1995; Jamieson *et al*., 1995; Schoen, 1999a; Sapirstein & Smith, 2001; Butany *et al*., 2003b). Relevant studies have demonstrated that bioprosthetic mitral valve structural degeneration typically affects 20-40% patients at 10 years and 60% at 15 years (Hammermeister *et al*., 2000; Grunkemeier e*t al*., 2000; Oxenham *et al*., 2003; Wheatley & Will, 2004).

During the preparation of bioprosthetic valves, chemical fixation with glutaraldehyde destroys the viability of the resident cells of the tissues, which are either VIC`s of the porcine valves, or fibroblasts of the bovine pericardial valves (Schoen, 2011a). This process decreases the immunogenicity of the bioprosthetic valves through the cross-linking and masking of the antigens (Okamura *et al*., 1980; Villa *et al*., 1980). However, the glutaraldehyde fixation has several key consequences that contribute to durability limitations of the bioprosthetic valves as summarised by Schoen (2011a): Firstly, because non-viable cells are incapable of tissue remodelling, ongoing repair of the bioprosthetic valve ECM by the cells of the transplanted tissue is impossible, and any damage to the ECM is cumulative. Secondly, VIC fragments which are not removed

from the matrix serve as nuclei for calcification. Thirdly, devitalized VEC`s of porcine valve bioprostheses are largely denuded by handling, thereby increasing the permeability of the tissue to fluid. Finally, fixation locks the collagenous network mechanically into a configuration that inhibits the smooth, internal cuspal structural rearrangements of the ECM that accompany normal valvular function, thereby inducing buckling of the cuspal tissue during functional opening and closing of a fixed bioprosthesis and causing cumulative internal structural damage (Vesely *et al*., 1988).

Of all the possible causes for bioprosthetic valve failure, calcification is the principal mechanism of tissue damage. The major factors involved in the calcification are believed to be associated with host related factors, mechanical stress and chemical treatment (Simionescu, 2004). Host factors such as age of the recipient and altered calcium metabolism have been reported to affect the durability of bioprosthetic valves (Diaz-Jauanen *et al*., 1975, Manji *et al*., 2006). This has been explained by some researchers as the high levels of blood calcium, phosphate, and enhanced parathyroid hormone and vitamin D metabolism in the young patient population (Berrebi *et al*., 2001; Simionescu, 2004). In addition, the areas in which mechanical stress is concentrated, such as the points of flexion in heart valves have been found to be more likely to calcify (Schoen *et al*., 2011).

However, whether calcification is also associated with immunological reactions remains unclear and under debate (Schoen, 2001; Manji *et al*., 2006). Some researchers believe that there is no obvious relationship between bioprosthetic valve calcification and the immune system (Gong *et al*., 1993; Trantina-Yates *et al*., 2001). Others have reported that immunological rejection mechanisms leading to secondary dystrophic calcification is potentially a reason for glutaraldehyde-fixed bioprosthetic heart valve failure, especially in young patients who are more immunocompetent than the elderly (Manji *et al*., 2006). A better understanding of the role of the immune system in calcification mechanisms in bioprosthetic valves would provide information that would benefit the design of future longer-lasting valves for the treatment of the younger patient population.

Attempts have been made to prevent calcification in bioprosthetic valves. Schoen and Levy (2005) summarised the calcification-preventing strategies for biomaterial implants and classified them into three generic categories: (1) systemic therapy with anti-

calcification agents; (2) local therapy with implantable drug delivery devices; (3) biomaterial modifications such as removal of a calcifiable component, addition of an exogenous agent, or chemical alteration. For instance, ethanol pre-incubation of glutaraldehyde cross-linked porcine valves has been suggested as an approach to prevent cuspal calcification. It is believed that pre-treatment with ethanol can extract almost all phospholipids and cholesterol from cusps, cause a permanent alteration in collagen conformation, affect cuspal interactions with water and lipids, and enhance cuspal resistance to collagenase (Vyavahare *et al*., 1997; Vyavahare *et al*., 1998; Connolly *et al*., 2004). Other efforts have also been made to develop new cross-linking systems. Rapopor *et al*. (2007) reported that porcine aortic xenografts treated with triglycidyl amine (TGA) and mercapto bisphosphonate demonstrated superior biocompatibility, mechanics, and calcification resistance (although not completely) compared to glutaraldehyde-treated groups. In an attempt to reduce calcification, high concentrations of the cross-linking agent have also been used. However, bioprosthetic valves fixed with a high concentration of glutaraldehyde (about 5 to 10 times than the conventional concentration, which is about 0.2-0.3%) were too stiff to be used clinically (Zilla *et al*., 1997, Zilla *et al*., 2000; Schoen & Levy, 2005).

1.4.2.2 Human tissue valves

Autografts are tissues that are re-implanted in the same individual that they come from. The first successful replacement of the aortic valve with a pulmonary valve autograft was conducted by Donald Ross in 1967 (Ross, 1967). This operation is now commonly referred to as the “Ross procedure”, which is usually used for patients (especially young patients) suffering from serious aortic valve disease. The diseased valve is removed, and replaced with the pulmonary valve of the same patient. The pulmonary valve is then replaced with a homograft valve. The replacement of the pulmonary valve with a homograft valve carries less risk since the stresses in the right side of the heart are much lower than in the left side of the heart. The pulmonary autograft is considered to be the perfect substitute for the diseased aortic valve, because it is a living tissue with very similar structure to the native aortic valve.

The Ross procedure is considered as the best choice to treat complex multilevel left ventricular outflow tract obstruction. The replacement valve functions well, and shows a central and laminar flow. Also, anticoagulation is usually unnecessary. In addition, the

grafted valve is from the same patient so it causes minimal host response after implantation. Last but not least, the replacement valve has the ability to grow with the patient, which makes this procedure very popular in children (Concha *et al*., 2004; Brown *et al*., 2006a). Nevertheless, the Ross procedure is technically difficult to perform since it actually involves two valve replacements. Moreover, endocarditis may occur in the pulmonary position due to the homograft valve (Ross, 1989).

Homograft (or allograft) valves are aortic or pulmonary valves obtained from human donors. They are cryopreserved in liquid nitrogen after harvesting until required (Butany *et al*., 2003b). The first homograft was implanted in 1962 by Ross (Ross, 1962). Although the surgical techniques for implanting homografts have gradually improved since 1962, the optimum techniques for homograft procurement, preservation and implantation have yet to be determined. The advantages of the homograft include: haemodynamic function similar to the native valve with very low transvalvular pressure gradients; reduced thromboembolic complications and infections compared to bioprosthetic or mechanical valves; no need for anticoagulation (Barratt-Boyes *et al*., 1977; Haydock *et al*., 1992). However, homograft valves lack long term durability and have limited availability.

Homograft valve failure is multifactorial, depending on patient age, surgical technique, homograft sizing and type, procurement and processing methods. Early investigations of the failure mechanism covered the relevance of cellular viability (Messier *et al*., 1999; Kitagawa *et al*., 2001), the biochemical aspects of ECM such as elastin and collagen (Kano *et al*., 2001; Yokose *et al*., 2002), the role of immune response (Oei *et al*., 2002), as well as the impact of damage caused by ice formation after preservation (Brockbank *et al*., 2000). It has become clear though that immunogenicity of homograft valves is the main reason for homograft valve failure. Blood group (ABO) or human leukocyte antigen (HLA class I and class II) mismatching may trigger both humoral and cellular immune responses in the host. In addition, the specific increase in the fraction of high-avidity cytotoxic T-lymphocyte precursors (CTLp) may indicate immune-mediated cellular destruction of homograft valves (Oei *et al*., 2000; Dignan *et al*., 2000). The allogeneic T-cell response is initiated by recognition of non-self HLA-DR (major histocompatibility complex (MHC) Class II) on graft dendritic and endothelial cells, followed by an amplification phase against HLA-A and HLA-B (MHC Class I) molecules in addition to HLA-DR on most parenchymal cells (Hogan & O'Brien, 2003).

The clinical experience confirms that, although homografts have normal hemodynamic function immediately after surgery, a mild to moderate increase in gradients is a frequent observation associated with elevated anti- MHC class I and MHC Class II antibodies in the circulation of patients receiving cryopreserved homografts (da Costa *et al*., 2009).

Despite the disadvantages of lacking long term durability and having limited availability, homografts have been widely used in heart valve replacement surgeries in the aortic, pulmonary and mitral valve positions (Kitamura, 2011). The most important indications for use of cryopreserved allograft valves are: important cardiac and valve malformation in children, female patients of child-bearing age with diseased cardiac valves, cases with contra-indications for anti-coagulation and patients with severe endocarditis with septal or annular abscesses. Since 1988, a total of 4516 allograft valves (1391 aortic, 2620 pulmonary and 48 mitral) supplied by the European Homograft Bank (EHB) were implanted in the left or right ventricular outflow tract for replacement of the diseased aortic or pulmonary valve and for mitral or tricuspid valve replacement or repair (Jashari *et al*., 2010).

The general outcome of homograft valve transplantation is acceptable. Kilian *et al*. (2010) reported the clinical outcome of homografts used as aortic valve replacements after 15 years. In total 360 homografts had been implanted in adult patients since 1992, and the survival rates after 5, 10, and 15 years were 88.3%, 84.6%, and 76.0%, respectively. By echocardiography, the transvalvular pressure gradient changed from 10.55 to 15.02, 19.9 and 37 mm Hg after 5, 10, and 15 years, respectively. The hemodynamic performance was generally good, and hemorrhagic or thrombo-embolic events were rare.

Pulmonary homografts have been widely used during the Ross procedure (Haydock *et al*., 1992; da Costa *et al*., 2005b; da Costa *et al*., 2007). The general outcome has been satisfactory with a high survival rate and low reoperation rate. A study of 259 patients implanted with cryopreserved pulmonary homograft valves during the Ross procedure showed a satisfactory result at mid-term follow-up. The mean follow up period was 3.8 years (range: 0.2-11.2 years). Homograft failure occurred in 9% patients, and homograft dysfunction was 12 %. It was reported that a younger donor age was somehow related to increased immunogenicity of the homograft and that this may be associated with

severe homograft stenosis which developed within the first postoperative year in some patients undergoing the Ross procedure (Niwaya *et al*., 1999).

Another intermediate-term follow-up (mean follow-up period: 3.2 years) reviewed the results after the Ross procedure (in which cryopreserved pulmonary homografts were used in the right ventricular outflow tract) in children and young adults (Ward *et al*., 1997). A total of 113 children or young adults who received pulmonary homografts at the Children's Hospital of Oklahoma were evaluated. The result of this study also indicated the occurrence of stenosis, as stated by Niwaya and Colleagues (1999). No investigation of the relationship between age of the donor and increased immunogenicity was undertaken. In this study, the following conclusions were drawn: pulmonary homografts undergo significant annular reduction in most patients, though this is usually not associated with the development of significant obstruction; in most cases, the gradient was increased across the homograft after the operation; severe homograft valve degeneration usually occurred within one year of implantation, which may reflect an immune-mediated response.

During 1995 and 2005, the Ross procedure was conducted in 202 patients with aortic valve diseases at the Cardiac Surgery Service of *Alianca Saude Santa Casa- PUCPR*. For the reconstruction of the right ventricular outflow tract, cryopreserved pulmonary homografts were used in 160 patients. None of the patients received anticoagulation drugs, and no case of thromboembolism was detected in the late follow-up. The late actuarial survival was considerably high (96.9%) (da Costa *et al*., 2005a).

In conclusion, nowadays, for patients suffering from serious heart valve disease, different options for replacement valves are available with relatively mature surgical techniques. Nevertheless, none of the currently available valve replacements meet all the requirements of an "ideal heart valve". Mechanical valve replacement carries a risk of thromboembolism, and thus life-long anticoagulation therapy is required, increasing the risk of haemorrhages. Biological valves, including bioprosthetic and homograft valves, have a lower risk of thromboembolism but tend to fail sooner and more frequently. Furthermore, the performance of most of the existing valve replacements is highly variable in children. Although homograft valves are considerably superior to other candidates, they are hard to implant, risky, and rarely available for the paediatric population since they can only be obtained from donors of a similar size. A promising

approach for reaching the holy grail of an "ideal valve replacement" is tissue engineering. Especially for the paediatric population, tissue-engineered heart valves are considered to be the best potential solution for valve replacement (Booth, *et al*., 2002; Sapirsten & Smith, 2001; Veseley, 2005).

1.5 Tissue engineering of heart valves

Tissue engineering offers an attractive alternative for tissue reconstructions, involving the development of biological or hybrid substitutes for implantation into the body with the purpose of fostering remodelling and regeneration of diseased tissue. Potential applications of tissue engineering range from structural tissues such as skin, cartilage, bone, and cardiovascular tissues (blood vessels, myocardium, and heart valves), to complex organs such as the liver, kidney, lungs and heart (Langer & Vacanti, 1993; Booth *et al*., 2002; Dimmeler *et al*, 2005; Mendelson & Schoen, 2006; Lanza *et al*., 2007).

A tissue-engineered heart valve has the potential to offer advantages, including low risk of thrombosis, reduced risk of degradation and calcification, resistance to infection, as well as ability to repair injury, remodel and grow. Effectively, a living tissue-engineered heart valve, would overcome the drawbacks inherent in the currently available valve replacements, by providing adequate strength, flexibility and durability and accommodating the repetitive changes in shape, dimensions, and stress during valve opening and closing (Mendelson & Schoen, 2006). The fact that tissue engineered heart valves have the potential to grow, repair, and remodel makes them particularly attractive for the paediatric population.

1.5.1 Scaffolds for heart valve tissue engineering

An ideal heart valve scaffold should be a template directing neo-tissue growth and organization, and regulating cellular adhesion, proliferation, migration, and differentiation. In addition, the scaffold should be able to degrade and be gradually replaced by functionally integrated extracellular matrix (ECM). According to Brody & Pandit (2006), an ideal scaffold for tissue engineering heart valves would:

- Possess adequate mechanical properties to withstand the dynamic conditions in the heart, in particular be sufficiently elastic to maintain a tight seal during the diastole phase of the cardiac cycle.

- Have a micro-architecture and constituent content mimicking that of the native heart valve, since collagen and elastin fibres, as well as the structural orientation of the fibres may all influence cellular orientation through contact guidance, and thus contribute to the mechanical properties of the heart valves.

- Incorporate nanotopography which is similar to that of the native valve basement membrane since cellular growth is significantly influenced by nanotopography and a confluent endothelium is critical in maintaining a non-thrombogenic surface.

- Support the adhesion, proliferation and phenotypic expression of VEC`s and VIC`s, or any cell type, which is chosen to replicate their behaviour.

- Have a degradation rate similar to that at which extracellular matrix is being produced, thus maintaining the ability of the construct to withstand the high pressure fluctuations and a tight seal during diastole.

Currently, scaffolds being investigated for heart valve tissue engineering can be divided into three broad categories, synthetic scaffolds, scaffolds made from natural materials and acellular biological scaffolds.

1.5.1.1 Synthetic scaffolds

Generally, synthetic scaffolds can be fabricated using one of the following processes: weaving, meshing, porogen leaching, emulsion freeze drying, expansion in high pressure gas, 3D-printing, phase separation, and stereolithography (Sodian *et al*., 2000; Shi *et al*., 2002; Brody & Pandit, 2007).

A range of biodegradable polymers have been investigated as scaffolds for heart valves (Tuzlakoglu & Reis, 2009; Schoen, 2011b). Polyesters such as polyglycolic acid (PGA), polylactide (PLA) and their copolymers are currently the most widely researched in tissue engineering. PGA is a highly crystalline, linear, aliphatic polyester, which has a high melting point and low solubility in organic solvents except for highly fluorinated

organic solvents such as hexafluoro-isopropanol. PGA can be fabricated into different forms using techniques such as extrusion, injection and compression moulding under careful control of processing conditions due to its high sensitivity to hydrolytic degradation (Mikos & Temenoff, 2000). An attractive feature of PGA is that its degradation product (glycolic acid) is a natural metabolite. The degradation of PGA occurs by the diffusion of water into the amorphous regions of the scaffold causing hydrolytic chain scission of the ester groups (Gunatillake & Adhikari, 2003). PLA is more hydrophobic, and more resistant to hydrolytic degradation compared to PGA. The combination of PGA and PLA in different proportions increases the range of material properties (Grayson *et al*., 2004; Mendelson & Schoen, 2006). Nonwoven PGA and composites of poly(lactic-co-glycolic acid) (PLGA) layered with nonwoven PGA were firstly investigated as valvular scaffolds by Shinoka *et al*. (1995; 1996; 1997) in the late 1990s. The results were generally favourable, although the leaflets were thicker and less flexible than the native ones. However, it is generally considered that PGA, PLA, and their copolymers are not suitable for cell growth *in vitro* (Kohn *et al.*, 2004).

Other polymers such as polycaprolactone (PLC), polypropylene fumarates (PPF), polyanhydrides, polyorthoesters (POE), poly-L-lactic acid (PLLA), poly-4-hydroxybutyrate (P4HB), polyhydroxyalkanoates (PHA) have also been investigated as scaffold materials. Both P4HB and PHA have been used to create heart valve scaffolds using stereolithography (Sodian *et al*., 2000, Sodian *et al*., 2002). In a study reported by Hoerstrup *et al*. (2000), P4HB was coated on PHA for use as a valvular scaffold. Valvular scaffolds made of highly porous PGA combined with P4HB produced promising results in a sheep model. Moreover, Schmidt *et al*. (2004, 2007) reported that P4HB/PHA scaffolds demonstrated excellent attachment of human umbilical cord blood-derived endothelial progenitor cells. Sutherland and colleagues (2005) developed a valve scaffold by melt-extruding PGA/PLLA fibres and processing them into flat, nonwoven sheets. The valve scaffolds were then assembled over moulds using needle punching to provide bonding between layers. Subsequently, the scaffold was seeded with ovine bone marrow mesenchymal derived stem cells (MSC`s) and implanted in an ovine model, demonstrating satisfactory function for periods of over 4 months.

Synthetic scaffolds are relatively easy to control and produce. They can be fabricated into various shapes with appropriate pore size, conducive to tissue growth. They can also be tailored to possess certain mechanical properties and degradation rates.

Chemically functional groups can also be introduced into the synthetic scaffolds to induce the tissue growth. Moreover, the raw materials of synthetic scaffolds are relatively easy to obtain and to preserve. However, synthetic scaffolds have the potential to induce a toxic response due to degradation products, and lack the natural histioarchitecture of the native tissue. In addition, inflammation may occur due to the introduction of foreign material and incomplete scaffold degradation (Gunatillake & Adhikari, 2003).

1.5.1.2 Scaffolds made from natural materials

Another approach that has been employed for generating valvular scaffolds is to synthesise them using natural biological materials. Such materials include collagen, chitosan, hyaluronic acid, fibrin and chondroitin sulphate (Schmidt & Baier, 2000; Brody & Pandit, 2007; Owen & Shoichet, 2010).

Collagen is the principal structural component of the heart valve leaflets and is weakly immunogenic compared to other structural proteins (Chevallay *et al*., 2000). Collagen type I scaffolds manufactured using collagen from bovine tendons have been developed using the rapid prototyping method. The 3D structure of the scaffold was created by using 3D inkjet printing. In order to induce pore generation, the bovine collagen solution was dispersed into the mould and then frozen at -30°C. The mould was then dissolved away by immersion in ethanol and the collagen scaffold was critical point dried with liquid carbon dioxide for 3 hours. Cross-linking was conducted with a non-toxic, dehydrothermal treatment under vacuum. This scaffold has been used for seeding human aortic VIC`s, as well as human bone marrow-derived MSC`s (Terrovitis *et al*., 2006; Dreger *et al*., 2006; Taylor *et al*., 2006a).

Chitosan is a derivative of chitin. Advantages to use chitosan may include minimal foreign body reaction, mild processing conditions, controllable degradation, structural similarity to GAG`s, and availability of hydroxyl and amino functional groups, which may be conjugated to molecules when used to produce bioactive scaffolds (Suh & Mathew, 2000). Chitosan has been shown to support the growth of VEC`s and showed better performance in terms of optimal VEC attachment, proliferation, and morphology when compared to some synthetic materials such as polyhydroxyalkanoate (PHA)

(Brody & Pandit, 2007). Chitosan may therefore be considered as a candidate for tissue engineered heart valve scaffold design (Cuy *et al*., 2003)

Fibrin promotes cellular migration, proliferation, and matrix synthesis through the release of platelet derived growth factor and transforming growth factor-β (Sierra *et al*., 1998). It can also serve as a reservoir for cell mediators, such as bioactive peptides, alternative growth factors, and proteins (Lewis *et al*., 1997). These characteristics have led to the investigations on the use of fibrin gel in heart valve tissue engineering (Jockenhoevel *et al*., 2001). Injection molding was used to create heart valve constructs from fibrin gel supplemented with aprotinin and chemically fixed with poly-L-lysine. Constructs were seeded with human aortic myofibroblasts and after 4 weeks in culture, a homogenous cell distribution and a well-developed ECM with organized collagen bundles was formed (Brody & Pandit, 2007). However, the two main disadvantages of fibrin gel, shrinking and low initial mechanical stiffness, may limit its potential use in tissue engineered heart valve scaffold.

Although much research has been conducted on the design and manufacture of scaffolds using synthetic or natural materials, this approach is still a long way from clinical translation.

1.5.1.3 Acellular biological scaffolds

An alternative approach to synthetic polymer scaffolds or scaffolds made from natural materials is the utilisation of decellularised natural allogeneic or xenogeneic heart valves. Allogeneic valves are the optimal choice, however this approach is limited by availability. Thus, recent research has focused on the development of decellularised xenogeneic heart valve scaffolds. A ready-available xenogeneic scaffold with optimal biological, histological and mechanical features similar to native valves holds great potential. For a successfully decellularised valvular scaffold, all of the cells and cellular debris should be removed from the tissue and damage to the surrounding ECM should be minimal. The growth of seeded cells should not be inhibited and immunogenic reactions and calcification should not be induced after implantation (Stock & Schenke-Layland, 2006). Complete decellularisation is crucial for xenogeneic scaffolds, since

residual animal cells or cell debris could lead to inflammatory reactions and immunological rejection.

In the development of acellular xenogeneic scaffolds, the removal the α-gal (Galα1,3-Galβ1-4GlcNAc-R) epitope is of particular concern. The α-gal epitope is the major xenoantigen causing hyperacute rejection of animal tissue in Man, and is an additional blood group antigen in pigs (homologous to the ABO blood group antigens in humans). It has a unique carbohydrate structure, which is conserved in all mammalian species except old world primates and Man. Humans and Old World monkeys do not express the α-gal epitope due to two frameshift mutations in the α 1,3-galactosyl-transferase gene (Galili & Swanson, 1991; Joziasse *et al*., 1991), and produce large amounts of anti-α-Gal antibodies including IgG, IgM and IgA as a result of the constant exposure to intestinal bacterial that carry cross-reacting epitopes (Badylak & Gilbert, 2008). It has been estimated that up to 1 % of circulating human antibodies are anti-α-Gal (Galili *et al*., 1984; Galili *et al*., 1985). The presence of the α-gal epitope on the surface of the vascular endothelium is the primary cause of rejection of xenogeneic organ transplants (Cooper *et al*., 1993; Oriol *et al*., 1993). The α-gal epitope is expressed in porcine valve endothelium (Fariva *et al*., 2003). When implanted, porcine tissue expressing the α-gal epitope elicits a specific hyperacute host immune response mediated by IgM antibodies directly against α-gal (Farivar *et al*, 2001; Farivar *et al*., 2003; Konakci *et al*., 2005). In order to eliminate the α-gal epitope in xenogeneic tissue transplants, there have been attempts to use transgenic pigs with the 1,3-galactosyl transferase gene knocked out (Lai *et al*., 2002; Phelps *et al*., 2003). The α-gal epitope was not detected in the α-gal deficient tissues after transplantation in rat models (Lila *et al*., 2010; McGregor *et al*., 2011). However, xenotransplants of 1,3-galactosyl transferase gene knockout hearts were rejected over periods of 6 months due to an immune response that included the formation of anti-non-α-Gal antibodies specific to porcine antigens (Kuwaki, *et al*., 2005). Although the level of anti-non-α-Gal antibodies to xenoantigens in humans is low compared to total anti-α-gal antibodies, they can result in acute rejection. It has been suggested by Burcin & Cooper (2008) that further genetic modification of 1,3-galactosyl transferase gene knockout pigs might overcome the remaining immunological barrier to xenotransplantation.

Hence the approach to utilising acellular biological scaffolds derived from xenogeneic heart valve tissues is based upon removal of all the cells and cellular antigens. Porcine

heart valves are considered to be the best candidate for use in the development of acellular xenogeneic heart valve scaffolds because they are of similar size to the human heart valves. In addition, the ECM proteins are highly conserved between pigs and humans. Thus, a completely decellularised porcine heart valve scaffold should exhibit very low immunogenicity in Man.

A successful decellularisation method should successfully remove all cellular components without impairing the architecture and integrity of the ECM. In early attempts, freeze-drying was used for heart valve decellularisation to produce a porous scaffold for cellular growth. This method preserved the general histoarchitecture of the scaffold, but ice crystals formed during freeze-drying caused the collapse of the scaffold ECM. Moreover, adequate porosity of the scaffold, which is important for cellular infiltration, was not achieved by this method (Curtil *et al*., 1997; Brody & Pandit, 2007).

Other attempts to produce decellularised porcine valves scaffolds have also been reported. Wilson *et al*. (1995) reported a four-step decellularisation process utilising 1% (w/v) Triton X-100, 1% (w/v) sodium dodecyl sulphate (SDS), deoxyribonuclease (DNAse) and ribonuclease (RNAse). This protocol was reported to completely decellularise the porcine valve while maintaining the integrity of the ECM. A triton X-100 detergent based decellularisation protocol was also reported by Bader *et al*. (1998), which also completely decellularised the porcine valve while maintaining the ECM. Further attempts to decellularise heart valves focused on the utilization of ionic and nonionic detergents, hypo- and hypertonic salt solutions and enzymes (generally including ehylenediaminetetraacetic acid (EDTA), trypsin, SDS, DNAse, RNAse), triton X-100 etc.; Booth *et al*, 2002). An enzyme based decellularisation protocol was reported by Schenke-Layland *et al*. (2003, 2004), which utilised 0.05% (w/v) trypsin and 0.02% (w/v) EDTA.

A successful decellularisation method for aortic valve leaflets was also developed by Booth *et al*. (2002) using the detergents SDS at 0.03% -0.01 % (w/v) or sodium deoxycholate at 0.5% w/v in hypotonic buffer. Following treatment, the major structural components of the valve ECM were successfully maintained and functional analysis showed the valve cusps to be fully competent under physiological pressures (120 mm Hg) along with physiological leaflet kinematics (Korossis *et al*., 2002). It was also reported that this method produced increased extensibility in the aortic leaflets but did

not impair their strength. Since SDS alone was not sufficient to decellularise the whole aortic root, and a modified protocol was developed by including a 1.25% (w/v) trypsin digestion step. In this protocol, SDS was used at a concentration of 0.1% (w/v) (Wilcox *et al*., 2005). Cytotoxicity studies showed that the decellularised scaffold was free of residual SDS and biocompatible with porcine smooth muscle cells. This decellularisation method was, subsequently, utilized by Vincentelli and colleagues (2007) to decellularise porcine pulmonary valve scaffolds. The decellularised scaffolds were seeded with ovine MSC`s and implanted to sheep. The valves demonstrated satisfactory haemodynamic and histological aspects after 4 months.

Over the past few years, two general strategies have been employed by researchers in the field of heart valve tissue engineering. These include: (1) implantation of heart valve scaffolds without prior *in vitro* cell seeding with a view to the valves being repopulated *in vivo* by endogenous cells; and (2) implantation of scaffolds which have been seeded with cells *in vitro* either passively or dynamically in bioreactors. To seed or not seed cells before implantation has become an important issue in the field of tissue engineered heart valve conduits (Versely, 2005). It has been reported that cryopreserved homograft valves fail to repopulate with recipients cells and become completely acellular within months of implantation (Schoen, 1995). This finding was of particular concern because the homograft was expected to be the ideal matrix for cell repopulation. Possibly due to these findings, a number of investigators have attempted to seed the decellularised scaffolds *in vitro* prior to implantation (Schenke-Layland *et al*., 2003). Some researchers choose to seed decellularised valvular scaffolds only with endothelial cells derived from patients, and the clinical outcome has demonstrated excellent hemodynamic performance during long-term follow up (Dohmen *et al*., 2011). With regards to *in vivo* tissue engineering, the scaffold may be implanted unseeded with a view to attracting endogenous cells by facilitating repair mechanisms. In a long-term animal model study in which decellularised seeded and non-seeded porcine valve leaflets were implanted into goats, Kim *et al*. (2004) demonstrated good valve function with no thrombosis and abundant cellular ingrowth was observed. Thus, the authors suggested it was feasible to use decellularised valve conduits.

1.5.2 Cells for heart valve tissue engineering

In the approach which utilises preseeding of heart valve scaffolds prior to implantation, cells are required. Cells should have similar properties to that of the native tissue and must be autologous from the patient. Basically, two types of cells exist in native heart valves, the VEC`s (which are important to prevent thrombus formation), and the VIC`s (which are responsible for synthesising and remodelling the ECM; Latif *et al*., 2007). Potential cell sources for scaffold seeding *in vitro* include differentiated endothelial and/or smooth muscle cells and stem cells.

Stem cells, with their unique properties such as multilineage differentiation and self-renewing ability, are very attractive for tissue engineering applications (Oswald *et al*., 2004; Mendelson & Schoen, 2006). There are two types of stem cells present in adult bone marrow: hematopoietic stem cells (HSC`s; blood forming cells) and mesenchymal stem cells (MSC`s; may develop into cells that form bone, muscle, cartilage, etc.) (Majumdar *et al.*, 1998). Bone marrow MSC`s are easily accessible, isolated and cultured which has made them an ideal cell source for tissue engineering.

Endothelial progenitor cells (EPC`s) are stem cells which have the ability to differentiate into the endothelial cells that line the blood vessels and cardiac valves. EPC`s can be derived from either bone marrow or blood. EPC`s from bone marrow can be mobilised either endogenously by tissue ischemia or exogenously by cytokine stimulation or 3-hydroxy-3-methyl-glutaryl-Coenzyme-A (HMG-CoA) reductase inhibitors (Llevadot *et al*., 2001; Dimmerler *et al*, 2001). Peripheral blood EPC`s can be isolated by magnetic bead selection on the basis of CD34, CD133 expression and vascular endothelial growth factor (VEGF) receptor 2 (Asahara *et al*, 1997; Oswald *et al*., 2004). Wu *et al.* (2004) have reported that when blood-derived EPC`s are expanded *in vitro* and consequently seeded on a biodegradable PGA-PLLA scaffold, they successfully formed micro-vessels on the scaffold. Fang and colleagues (2007) have successfully isolated and differentiated human umbilical cord blood-derived EPC`s into EC`s by culturing them in endothelial basal medium EGM-2MV medium, containing vascular endothelial growth factor (VEGF), human fibroblast growth factor (hFGF), human recombinant long-insulin-like growth factor-1 (R3-IGF), human epidermal growth factor (hEGF), gentamicin and amphotericin, hydrocortisone, heparin, ascorbic acid and 5% (v/v) fetal bovine serum (FBS). The EPC-derived endothelial cells were

histiocytic cobblestone in morphology and expressed specific markers of the endothelial cell lineage, including von Willebrand factor (vWF) and CD31. They could bind to human endothelial cell-specific lectin Ulex Europaeus agglutinin-1 (UEA-1) and took up Dil-labeled low density lipoprotein (Dil-Ac-LDL). These cells were then seeded onto a decellularised porcine heart valve scaffold, and showed excellent metabolic activity and proliferation. As reported by Sales *et al*. (2010), EPC`s isolated from blood appeared to have the potential to provide both interstitial and endothelial functions and could potentially serve as a single-cell source for construction of tissue engineered heart valves. These studies suggest that EPC`s may be a promising cell source for the endothelialisation of tissue-engineered heart valves.

MSC`s have received much interest due to their clinical potential for tissue engineering not only because they are multipotent and can easily be expanded in culture, but they can also secrete a variety of paracrine angiogenic and cytoprotective factors, which have the potential advantage to suppress many immune cell functions and to decrease immune-mediated reactions (Uccelli *et al*., 2006; Ohnishi & Nagaya, 2007; Vincentelli *et al*., 2007). Apart from bone marrow, MSC`s and MSC-like cells can also be found in various other tissues including adipose tissue, amniotic fluid, periosteum, and foetal tissues. MSC`s can be isolated from the mononuclear layer of the bone marrow after density gradient centrifugation. The mononuclear cells are cultured in medium with 10% (v/v) foetal calf serum, and the MSC`s adhere to plastic (Chamberlain *et al*., 2007).

Phenotypically, although not specific, MSCs express a number of markers. It is generally agreed that they do not express the hematopoietic markers CD45, CD34, CD14, or CD11, the adhesion molecules CD31 (platelet/endothelial cell adhesion molecule-1 (PECAM-1)), CD18 (leukocyte function-associated antigen-1) or CD56, and the co-stimulatory molecules CD80, CD86, or CD40. However, they can express CD105, CD73, CD44, CD90, CD71, and Stro-1, as well as the adhesion molecules CD106, CD166 and CD29 (Haynesworth *et al.*, 1992; Chamberlain *et al*., 2007; Kolf *et al*., 2007).

Numerous studies have been carried out demonstrating the migration and multi-organ engraftment potential of MSC`s in animal models as well as in humans (Lanza *et al*., 2007). Elaborating, MSC`s have the capability to migrate from the blood, across endothelial cells, and into tissues. This is an exciting feature for tissue engineered heart

valve scaffold seeding. Together with their capacity to differentiate into cardiac VIC`s, MSC`s are believed to be a good candidate for VIC seeding in heart valve tissue engineering (Jiang et al., 2005; Chamberlain *et al*., 2007).

Latif and colleagues (2007) compared the phenotypes of MSC`s and VIC`s with the aim to demonstrate the potential application of MSC`s in heart valve tissue engineering. A number of cell surface molecules, cytoskeletal proteins, cell junction and cell communication molecules and ECM components were expressed by both MSC`s and VIC`s. MSC`s and more than 80% of VIC`s expressed fibroblast surface antigen α-smooth muscle actin (α-SMA), vimentin and CD44. The expression of MHC class I and II, and calponin were also comparable between the two cell types. CD105 was weakly expressed by 10% of VIC`s while the expression level in MSC`s was more than 90%. Both cell types made similar levels and patterns of ECM components. Elastin expression was detected in neither of the cell types. Adhesion molecule expression was highly variable among the MSC isolates and between the two cell types, with the predominant integrins being α1, α3, α5, and β1 in both cell types. The WNT gene family is considered to secrete critical regulator proteins. The secreted proteins are involved in cell proliferation, motility, cell polarity generation, and specification of cell fate. Polymerase chain reaction (PCR) analysis of *WNT/FZD/SFRP/LRP* family members revealed a greater range of the *WNT* family of genes being expressed in MSC`s compared to VIC`s. The *in vitro* differentiation of MSCs into VIC`s could possibly be controlled by mechanical and biological conditioning which mimics the *in vivo* environment of the native valve (Ku *et al*., 2006). The composition of the scaffold would also be crucial in the differentiation of the MSCs. A valvular scaffold closely comparable to the native valve might contribute to the differentiation of MSC`s into VIC`s.

Currently, detailed understanding of the pathways and processes involved in the differentiation of MSC from different sources is insufficient. This information is desired for the clinical application of MSC towards the *in vitro* generation of functional tissue for implantation (Hilfiker *et al*., 2011).

1.5.3 Bioreactors for heart valve tissue engineering

A tissue engineering heart valve bioreactor is a device able to ensure the biological and physiological environment of the heart and the circulatory system (Gandaglia *et al*., 2011). In general, a tissue engineering heart valve bioreactor should enable the culture of bioartificial tissue under sterile, physiological (37 °C and 5 % v/v CO_2) conditions and should be easy to clean and maintain. In order to engineer functional valvular tissue, it is essential that bioreactor systems are able to simulate the dynamic physiological, biomechanical and biochemical conditions *in vitro* which mimics the human *in vivo* circulation (Mertsching & Hansmann, 2009). Heart valve tissue engineering bioreactors have been designed for two major purposes. The first is to study the mechanisms by which the biochemical or biomechanical environment influences the interaction between the valvular cell types or between cells and scaffold material, and the tissue remodelling process *in vitro*. The second is to prepare cell-seeded tissue engineered heart valve conduits for implantation (Berry *et al*., 2010).

The first attempt to assemble a bioreactor for the culture of heart valves dates back to the year 2000 by Sodian *et al*. (2000). The authors applied a simple pulsatile flow system which was designed to induce different levels and conditions of flow and pressure in the bioreactor. Cells from ovine carotid artery were statically seeded onto PHA scaffold prior to placing the conduit in the bioreactor. The results indicated an increase in cell proliferation when compared to static culture. The cells were found to have secreted ECM components collagen and GAG`s but not elastin following culture.

In the same year, Hoerstrup and colleagues (2000) developed a compact heart valve bioreactor which consisted of an air chamber, medium chamber, and perfusion chamber that held the heart valve. Ovine myofibroblasts and endothelial cells were seeded on a biopolymeric scaffold (a combination of PGA and P4HB) statically prior to placing the conduit in the bioreactor. The cultured tricuspid valve leaflets were subsequently implanted into lambs. However, these tissue engineered valvular conduits had a poor hemodynamic performance *in vivo*.

The use of a heart valve bioreactor for the culture of cell-seeded decellularised biological xenograft (porcine) valve conduits was carried out by Zeltinger *et al*. (2001). The bioreactor included a medium reservoir, pneumatic pressure chamber with an elastomeric bladder which was placed below the heart valve to produce a back flow on

the valve in order to generate negative pressure allowing the valve to the close. Human neonatal fibroblasts were seeded onto the decellularised scaffold dynamically. Unfortunately, the repopulated conduit resulted in a thickening of the leaflets which finally lead to valve stenosis after implantation in an animal model.

A very compact diastolic pulse duplicator which consisted of a valve holding device and a medium container was developed by Mol *et al*. (2005). Pulsatile flow was produced by the release of air into a cylinder which compressed or decompressed tubing resulting in a pressure differential. Cells harvested from the human saphenous vein were seeded on trileaflet heart valve scaffolds which were fabricated on a Fastacryl® stent, and cultured in the system for up to 4 weeks. Histological staining showed superior tissue formation in the leaflets. Collagen could be identified in the leaflets. However, the leaflets lost coaptation after releasing them from one another following culture, as they had partly grown together.

Lichtenberg *et al*. (2006) engineered a heart valve bioreactor which included a pulsatile pump, a heart valve reservoir, a medium reservoir, and a compliance chamber. This system allowed the direct control of the flow rate via a pulsatile pump. The culture conditions within the bioreactor were closely monitored by flow, pressure and temperature transducers. Autologous EPC`s were seeded onto human cadaveric pulmonary valves and preconditioned in the bioreactor for up to 21 days, and the seeded conduits were implanted in two pediatric patients as pulmonary valve replacements. The 3.5 years follow-up showed normal patient growth and normal valve growth (Cebotati *et al*., 2006).

Flanagan *et al*. (2007) developed a ventricular pulse duplicator lodged in an incubator. The pulsatile flow was provided by the displacement of a silicon membrane, forcing the medium to pass through the above ventricular chamber during the systolic phase, where the heart valve was located (Gandaglia *et al*., 2011). Moulded fibrin-based tissue-engineered heart valves seeded with ovine carotid artery-derived cells were subjected to 12 days of mechanical conditioning in the system. The authors demonstrated that the pulsatile flow conditions in the bioreactor not only enhanced seeded cell attachment and alignment within the fibrin-based heart valve scaffolds, but dramatically changed the manner in which the cells generated ECM proteins and remodelled the valve matrix in comparison to stirred controls in a beaker. This model was able to simulate the most

appropriate stimulus for cardiovascular tissue engineering as described by Stock & Vacanti (2001).

Lee *et al*. (2009) developed a computer-assisted pulsatile heart valve bioreactor for the endothelialisation of decellularised pulmonary valves. The bioreactor was comprised of a digital gear pump, and was suitable for shear stress modulation, but lacked the ability to evaluate the transvalvular gradients. EPC`s derived endothelial cells were seeded on decellularized porcine valve scaffolds and cultured in the bioreactor for 7 days. Successful endothelialization was achieved by preconditioning the cell-seeded valves with stepwise increases in volume flow rate up to 2 $L.min^{-1}$ following culture.

A heart valve bioreactor developed by Ruel and Lachance (2009) used a compliance chamber positioned between the valve holder and the variable resistance to reproduce the elastic characteristic. This device was reported to be able to generate flow and pressure waveforms comparable with that of healthy patients with a custom designed bileaflet mechanical valve. However, no cells or tissue was tested in this bioreactor. The success of this bioreactor still needs to be verified.

In addition to the clinical application of the pre-seeded allogeneic pulmonary valve conduits in a bioreactor which has been described previously in this section (Cebotati *et al*., 2006), Dohmen *et al*. (2002) reported the clinical use of tissue engineered pulmonary heart valve scaffolds preseeded with endothelial cells in a specially designed heart valve bioreactor. The long-term follow-up demonstrated the tissue engineered pulmonary valves had excellent hemodynamic performance with no calcification for up to 10 years (Dohmen *et al*., 2011).

A major step towards the understanding the design of efficient bioreactors for use in heart valve tissue engineering has been achieved, but many unsolved issues remain. The physiological hydrodynamics (e.g. cyclic stretch, flexure and shear stress) *in vivo* has proved difficult to reproduce in the heart valve bioreactors to date (Gandaglia *et al*., 2010). Currently, there is no agreement upon the conditioning protocol for heart valve bioreactors. However, bioreactors should gradually introduce physiologic flex, stretch and flow in order to properly condition the valves (Berry *et al*., 2010). Future studies are needed to identify those forces and conditions within the heart valve bioreactors to achieve appropriate physiological culture conditions.

1.5.4 Heart valve replacement using natural acellular scaffolds

Currently, cryopreserved homografts are generally accepted as the 'gold standard' for right ventricular outflow tract reconstruction. However, there are associated risk factors including younger recipient age, previous bioprosthetic valve, low weight at operation, small graft size and reoperation (Clarke, *et al*., 1993; Brown *et al*., 2001). Brockbank *et al*. (2000) also suggested a possible cause of tissue failure and calcification due to interstitial ice formation in cryopreserved homografts. The use of tissue engineered valves in the pulmonary position is of major interest since they are potentially the best substitute for use in the Ross procedure to reconstruct the right ventricular outflow tract.

Different decellularisation methods have been utilised to generate acellular pulmonary valve conduits including the use of 0.1 % (w/v) SDS (da Costa *et al*., 2009; Navarro *et al*., 2010) 0.1 % (w/v) deoxycholic acid (da Costa *et al*., 2004; da Costa *et al*., 2007). Currently, some of the acellular pulmonary valves have been tested biologically and biomechanically *in vitro* and have been studied in animal models or used clinically. Two types of acellular pulmonary valves have been marketed: the decellularised pulmonary homograft (SynerGraft™) which is marketed by Cyrolife Inc, USA, and the decellularised xenogeneic heart valve Matrix P™ and Matrix P™ Plus porcine pulmonary valve (AutoTissue, Germany).

The most widely reported attempt to develop an acellular heart valve scaffold was that of Synergraft™ (Cryolife, USA), which comprised decellularised porcine valve tissue. Preclinical reports on this valve indicated that the decellularisation process rendered a completely acellular scaffold with biomechanical features comparable to those of the native human aortic valve. Following the initial encouraging pre-clinical reports (O`Brien *et al*., 1999; Goldstein *et al*., 2000), Synergraft valves were implanted in four male children in 2001. Two of them were implanted in the aortic position and two in the pulmonary position. All of the four grafts were cryopreserved after decellularisation and prior to implantation. Unfortunately, a strong inflammatory response and structural degradation of the valves lead to the death of three of the patients within one year. Later, traces of α-gal epitope were found in the leaflets of the Synergraft™ valves, which could have been responsible for their failure (Simon *et al*., 2003; Kasimir *et al*., 2006; Brody & Pandit, 2007).

Although the decellularised SynerGraft™ xenogeneic porcine valve for the aortic position was a major failure probably due to the presence of residual xenogeneic cells, the setbacks were not reflected in the SynerGraft™ human homograft pulmonary valves (Knight *et al*., 2008). The SynerGraft™ pulmonary homograft was treated by a proprietary process designed to substantially reduce leaflet and conduit cellularity (Sievers *et al*., 2003). Biomechanical analysis showed no corresponding change in the *in vitro* biomechanics, including suture retention, tissue extensibility and strength (Knight *et al*., 2008). Compared to cryopreserved homografts, the SynerGraft™ pulmonary homograft has low pressure gradients at all flow conditions. Short term clinical studies showed comparable or better outcomes than the conventional cryopreserved human allografts, with regard to pressure gradients and subsequent recipient immune response (Sievers *et al*., 2003; Hawkins *et al*., 2003; Bechtel *et al*., 2003; Tavakkol *et al*., 2005). A mid-term follow up (mean: 52 months) conducted by Bechtel *et al*. (2008) using SynerGraft™ pulmonary homografts in 23 patients, compared to 49 patients implanted with cryopreserved homografts showed no reoperations were required, and the echocardiographic results were stable after the first postoperative year. Brown *et al*. (2011) reported the clinical outcome of 29 patients who received the SynerGraft™ pulmonary homograft and 34 patients who received standard cryopreserved homografts during the Ross procedure between the year 2000 and 2009. No early or late deaths occurred during the mean follow-up of 4.9 ± 2.7 years. No patient required reoperation. No deterioration in conduit valve function occurred in the SynerGraft™ homograft group, while mild conduit regurgitation developed in several patients in the cryopreserved homograft group. No patient from either group reached conduit dysfunction by the authors' definition (peak gradient: 40 mm Hg or > 2+ regurgitation). The SynerGraft™ pulmonary homografts appeared to be safe and have comparable hemodynamic performance, and have been proposed to be an alternative to the cryopreserved homografts according to current experience (Brown *et al*., 2010; Brown *et al*., 2011). Further long term follow up will however be needed to evaluate the SynerGraft™ pulmonary homografts.

The Matrix P™ porcine pulmonary valve (AutoTissue, Germany) is an acellular porcine pulmonary valve which is surrounded by three glutaraldehyde-fixed equine pericardial patches forming the conduit wall (Ruffer *et al*., 2010). It has been available since February 2004. Decellularisation is achieved using 1% (w/v) deoxycholic acid (Konertz

et al., 2005). Histology showed removal of the porcine cells from the pulmonary valve matrix while the mechanical properties were maintained. The valve closing times, closing volumes, and gradients were all superior compared to glutaraldehyde-fixed xenograft bioprostheses (Dohmen *et al*., 2002). When used clinically, no cell reseeding was conducted for Matrix P™. The general outcome was satisfying, with low transvalvular gradients that did not tend to increase over time. The hemodynamic characteristics of the Matrix P™ decellularised pulmonary xenograft were reported to be similar to a physiologically normal valve in healthy subjects following short term follow-up of 50 patients undergoing the Ross procedure (Konertz *et al*., 2005).

Konertz *et al*. (2011) reported on the clinical outcome of Matrix P™ (n=9) and Matrix P™ Plus (n=52) implantation in 61 patients between 2006 and 2008. The early mortality was 8.2 %, and no deaths occurred during the follow up period. In the authors' opinion, the intermediate-term performance of the grafts was favourable compared to that of other currently available implants, and only four patients underwent reoperation due to valve failure. However, Cicha *et al*. (2011) reported that the Matrix P™ Plus valve displayed early obstruction following implantation in paediatric patients. A foreign body-type reaction accompanied by severe fibrosis and massive neointima formation around the Matrix P™ valve wall was found. Examination of the explanted valves showed an inflammatory infiltrate, composed of T cells, B cells, plasma cells, dendritic cells, macrophages and mast cells, in the tissue surrounding the conduit (Mahler & Butcher). Inflammation and predominantly peripheral conduit narrowing were also observed by Ruffer *et al*. (2010) in the clinical application of Matrix P™ Plus conduits in 16 paediatric patients. The Matrix P™ and Matrix P™ Plus xenogeneic pulmonary valve conduits do not seem to be an ideal conduit for right ventricular outflow tract reconstruction according to the current outcomes. Due to the clinical outcomes, it is possible that there may be toxicological problems due to glutaraldehyde preservation of the equine pericardial patches present in the grafts. The quality control of decellularisation during the manufacture of the Matrix P™ and Matrix P™ Plus grafts should also be questioned in order to determine if complete decellularisation was achieved.

Da Costa *et al*. (2005b) showed that homografts decellularised using deoxycholic acid demonstrated a significantly reduced immune response and better hemodynamic performance when compared to cryopreserved homografts over an 18 month clinical

follow up when used in the Ross procedure. However, in a longer-term assessment with a greater number of patients, the deoxycholic acid decellularised homografts showed some rise in gradients due to residual cell persistence in some grafts (da Costa *et al*., 2007).

Xenografts (porcine) decellularised with 0.1 % (w/v) SDS using the technique developed in Leeds (Booth *et al*., 2002; Korossis *et al*., 2002) demonstrated more complete repopulation than deoxycholic acid decellularised valves in sheep studies, and a late rise in gradient was not observed in a short to medium term clinical study (da Costa *et al*., 2007). da Costa *et al*. (2009) compared the clinical outcomes using cryopreserved, deoxycholic acid decellularised, and SDS decellularised homografts for the reconstruction of the right ventricular out flow tract in a report of their thirteen years' experience with the Ross procedure. They demonstrated that the homografts decellularised using 0.1 % (w/v) SDS had significantly lower gradients with not a single case being observed with a gradient more than 40 mm Hg over a 24 months follow up. During a reoperation due to the pulmonary autograft dysfunction in the aortic position, it was shown that the SDS decellularised homograft was soft and pliable, while the adventitia showed neovascularisation with no adhesions. A biopsy of the homograft conduit wall showed good preservation of the ECM and partial repopulation with autologous cells at 17 months postoperatively. An absence of any immunological reaction without elevation of MHV Class I and II antibodies was further confirmed (da Costa *et al*., 2009). Aortic valve homografts decellularised using 0.1% (w/v) SDS also demonstrated stable structural integrity, low rate of calcification, and adequate hemodynamics as shown in early and midterm clinical results (da Costa *et al*., 2010).

Based on the outcomes of the clinical use of acellular homograft pulmonary valve conduits, it is apparent that acellular heart valve scaffolds implanted without a complex, costly cell pre-seeding procedure have important clinical potential. However, homografts, either cryopreserved or decellularised have limited availability. It would be advantageous if an acellular xenogeneic heart valve scaffold could be developed. This would have the potential of availability "off the shelf" in a range of different sizes. Therefore in this project, porcine pulmonary roots will be decellularised using SDS detergent based on the previous method developed by Booth *et al*. (2002), Wilcox *et al*. (2005) and Korossis *et al*. (2002; 2005), which is similar to the method used by da Costa *et al*. (2009).

1.6 Aims and objectives

Aims:

The aims of this study were to develop methods to produce a decellularised, biocompatible porcine pulmonary root conduit for the use in the Ross procedure to reconstruct the right ventricular outflow tract. The biological and biomechanical characteristics were determined by comparison to the fresh tissue. In addition, the conditions for the culture of fresh porcine pulmonary roots under sterile conditions in a novel dynamic heart valve bioreactor and a static culture system were investigated.

Objectives:

- To develop and optimise a process for the decellularisation of porcine pulmonary valve conduits.
- To assess the effects of decellularisation on the histoarchitecture, the total amount of DNA and the presence of functional DNA, the presence of specific matrix and cytoskeletal proteins, and the presence of the α-gal epitope by comparison with the fresh tissue.
- To determine the *in vitro* biocompatibility of the decellularised porcine pulmonary valve conduits.
- To assess the effects of decellularisation on the uniaxial tensile properties, the hydrodynamic behaviour, and the leaflet kinematics of the decellularised tissues by comparison to fresh porcine pulmonary root tissues.
- To determine the conditions for the culture of fresh porcine pulmonary roots in a dynamic heart valve bioreactor by assessing the cell distribution, tissue histoarchitecture, localisation of the specific matrix and cellular proteins, and cell viability of the tissue.

Chapter 2

General Materials and Methods

2.1 Materials

2.1.1 Equipment

The equipment used in this study and the UK suppliers are listed in Table 2.1.

Table 2.1 Equipment used throughout the study.

Equipment	Model	Supplier
Automatic pipettes	Gilson P2-P1000	Anachem Ltd
Automatic Pipettes	Finnipipette® P2-P1000	Thermo Fisher Scientific Inc
Balances (Accuracy: 0.01g/0.0001g)	GR200/GX2000	Jencons PLC
Bench top centrifuge	5415R	Eppendorf
Blood tissue spinner	SB3	Stuart
Cell medium aspirator	Vacusafe comfort	Integra Biosciences
Centrifuge	Harrier 15/80	SANYO Biomedical Europe BV
Class II safety cabinet	Heraeus 85	Kendro
Class II safety cabinet (for heart valve bioreactor)	Model 1.8	Holten
CO_2 Incubator	MCO-20AIC	SANYO Biomedical Europe BV
Confocal microscope	LSM510 META	Carl Zeiss Ltd
Cryo freezing pots (Nalgene®)	-	Thermo Fisher Scientific Inc
E-gel DNA gel electrophoresis	E Gel®	Invitrogen
Freezer (-20°C)	Electrolux 3000	Jencons Plc
Fridge	Electrolux ER8817C	Jencons Plc
Fume cupboard/fume hood	-	Whiteley
Gel imaging system	LOGIC1500	KODAK
Heating forceps	Speci-leps System II	BIOS EUROPE
Histology cassettes	CMB-160-030R	Thermol Fisher Scientific Ltd
Histology water bath	MH8515	Barnstead Electrothermal
Hot forcepts	Speci-leps	BIOS EUROPE

Hot plate	E18.1 hotplate	Raymond A Lamb
Hot wax dispenser	E66 wax dispenser	Raymond A Lamb
Magnetic stirrer	Stuart SB161	Scientific Laboratory Systems Ltd
Magnifying lamp	D20251	Fisher Scientific
Micro plate spectrophotometer	Multiskan spectrum	Thermo Scientific
Microscope (upright)	Olympus BX51	Microscopes, medical Diagnostic Systems and Olympus Patient systems Ltd
Microtome	RM2125 RTR	Leica Microsystems
Microwave	KM19W, 800w	PROLINE
Nanodrop Spectrophotometer	ND-1000	Labtech Int
Orbital shaker	IKA KS130 basic	Jencons Plc
Oven (hot air)	OMT225	SANYO Biomedical Europe BV
PCR machine	PCR SPRINTThermal Cycler	Thermo Electron Corporation
pH meter	Jenway 3010	VWR International
Plastic histology cassettes	CMB-160-030R	Thermo Fisher Scientific Ltd
Plate reader	Multiskan Spectrum 1500	Thermo
Plate shaker	IKA KS130 basic	Jencons Plc
Plate shaker 2	Cooke AM69 microshaker	Dynatech Laboratories Ltd
Pipette boy	Acu	Intergra Biosciences
RT-PCR machine	MX3000P	Stratagene
Slide holder	E102	Raymond A Lamb
Tensile testing machine	AGS-10KNG	Shimazu
Thickness gauge	-	Mitutoya
Tissue processor	TP11020	Leica Microsystems
Tube-strip centrifuge	Picofuge PMC-860	Stratagene
Vortexer	TopMix FB15024	Fisher Scientific
Vortexer 2	MS2 minishaker	IKA
Water bath	Grant	Jencons Plc
Water purifier	Option 7	ELGA
Wax oven	Windsor E18/31	Scientific Laboratory Supplies

2.1.2 Chemicals

The chemicals and reagents used in this study and the UK suppliers are listed in Table 2.2.

Table 2.2 Chemicals and reagents used throughout the study.

Chemical/Reagent	Supplier
Acetone	European Bios
A-Gal BSA	Dextra laboratories Ltd
A-SMA	Sigma
Acetic acid	Thermo Fisher Scientific Ltd
Acetone	European Bios
Agarose (Low melting point)	Invitrogen
Alcian blue	Raymond A Lamb
Aprotinin (10,000KIU.ml^{-1})	Mayfair house
Blue Juice^{TM} gel loading buffer (10×)	Invitrogen
Bovine serum albumin	Sigma-Aldrich
Calcium chloride	VWR International
Citric acid	VWR International
Collagen type IV	DAKO
DABCO	Sigma-Aldrich
Desmin	Vector
DMSO	Sigma-Aldrich
DNeasy blood & tissue kit	QIAgen
DNAse	Sigma-Aldrich
DPX mountant	Thermo Fisher Scientific Ltd
Dulbecco's modified Eagle's medium	Invitrogen Ltd
Dulbecco's PBS tablets	Oxoid
E-gel 0.8% agarose	Invitrogen
E-gel 4 % agarose	Invitrogen
E-gel low range quantitative DNA ladder	Invitrogen
Eosin	VWR International
Ethanol	Thermo Fisher Scientific Ltd
Ethylenediaminetetraacetic acid (EDTA)	VWR International
Fibronectin	DAKO
Foetal calf serum	Biosera
Gel Elute^{TM} PCR clean-up kit	Sigma-Aldrich
Gentamycin	Sigma-Aldrich
Giemsa solution	VWR International
Glycerol	Sigma-Aldrich
Haematoxylin	Thermo Fisher Scientific Ltd
Heated blood agar	University of Leeds
Hoechst 33258	Sigma-Aldrich
Horseradish peroxidise-conjugated secondary rabbit anti-mouse antibody	DAKO
Hydrochloric acid (6M)	VWR International
Hydrogen peroxide (30%, v/v)	Sigma-Aldrich
IgM purification kit	Pierce (Thermo Fisher scientific Ltd)
Isotype control	DAKO
L-glutamine	Invitrogen

Live/Dead assay kit	Invitrogen
Magnesium chloride	Thermo Fisher Scientific Ltd
Methanol	Vichers Laboratories
Miller's stain	Raymond A Lamb
Molecular grade water	Sigma-Aldrich
Monoclonal IgG1	DAKO
Monoclonal IgG2a	DAKO
Monoclonal IgM against α-Gal epitope	Alexis
MTT reagent	Sigma-Aldrich
Neutral buffered formalin (10%, w/v)	Genta Medical
Nuclease free water	Fermentas
Nutrient agar	University of Leeds
OPD*fast* tablets	Sigma-Aldrich
Oxalic acid	VWR International
Paraffin wax	Thermo Fisher Scientific Ltd
PBSa tablets	Oxoid
PCR master mix	Fermentas
Penicillin	Invitrogen Ltd
Peracetic acid	Sigma-Aldrich
pH standards (4,7,10)	Scientific Laboratory Supplies Ltd
Picric acid	Sigma-Aldrich
Potassium permanganate	Thermo Fisher Scientific Ltd
Quick-load PCR marker	Biolabs
Rabbit immunoglobulin Fraction	DAKO
RNAse	Sigma-Aldrich
SAB agar	University of Leeds
Sodium azide	Sigma-Aldrich
Sodium chloride	Thermo Fisher Scientific Ltd
Sodium dodecyl sulphate (SDS)	Sigma-Aldrich
Sodium hydrogen carbonate	VWR International
Sodium hydroxide	VWR International
Streptomycin	Invitrogen
Sulphuric acid	Sigma-Aldrich
TE buffer	Sigma-Aldrich
Trigene	Scientific Laboratory Supplies Ltd
Tripsin	Sigma-Aldrich
Tripsin inhibitor	Sigma-Aldrich
Trizma base	Sigma-Aldrich
Tween 20	Sigma-Aldrich
Ultravision Detection system	Thermo Scientific
Vimentin	Novacastra
Virkon	Scientific Laboratory Supplies Ltd
Von Willebrand factor	DAKO
Xylene	Genta medical
Zinc acetate	Thermo Fisher Scientific Ltd
Zinc Chloride	Thermo Fisher Scientific Ltd

2.1.3 Consumables

The consumables and plasticware used in this study are listed in Table 2.3 and Table 2.4 respectively.

2.1.3.1 General consumables

Table 2.3 General consumables used in this study.

Item	Model/Size	Supplier
Glass coverslips	MIC3228	Scientific Laboratory Supplies
Filter paper	Whatman® Grades 1-5	Whatman International Ltd
ImmEdge Hydrophobic Barrier Pen	H-000	Vector Laboratories
Microtome blades	SD3050835	Fisher Scientific
Parafilm M	-	Sigma-Aldrich Ltd
Scalpel blade	Size 22	Fisher Scientific
Superfrost Microscope Slide	MIC3040	Scientific Laboratory Supplies
Sutures	Ethicon 4-0 Prolene	Ethicon (Johnson & Johnson Ltd)
Superfrost Plus Microscope Slide	MIC3022	Scientific Laboratory Supplies
Syringe needles	-	Thermo Fisher Scientific Ltd

2.1.3.2 Plasticware

Table 2.4 Plasticware used in this study.

Item	Model/Size	Supplier
8 Strip PCR tubes	0.2 ml	Starlab
Bijous	5 ml	Scientific Laboratory Supplies Ltd
Cell culture flasks	75 cm^2	Thermo Fisher Scientific Ltd
Conical tubes	15 ml	Thermo Fisher Scientific Ltd
Disposable plastic syringes	1 ml, 2 ml, 5 ml, 10 ml, 20 ml, 50 ml	Scientific Laboratory Supplies
Micro tube 1.5ml, loop cap-simport	212-9573	VWR International
Nunc-Immuno™ 96 well plate, Maxisorb™	456537	Scientific Laboratory Supplies
Pipette tips (filtered and	10 µl, 20 µl, 200 µl, 1000	Star Labs

non filtered)	µl, 5000 µl	
Optiplate™	96-well	PerkinElmer™
Sterile containers	60 ml, 150 ml, 250 ml	Scientific Laboratory Supplies
Stripette™ (disposable pipettes)	1 ml, 2 ml, 5 ml, 10 ml, 25 ml	Sigma Aldrich Ltd
Universals	25 ml	Scientific Laboratory Supplies
Well plates, Nunc® (flat and round bottomed)	6-well, 12-well, 24-well, 48-well, 96-well plates	Thermo Fisher Scientific Ltd

2.1.4 Cells

Cells used in the biocompatibility assays are listed in Table 2.5.

Table 2.5 Cell lines used in this study.

Cells	Type	Species	Supplier
3T3 cells	Fibroblast	Murine	European Collection of Cell cultures
L929 cells	Fibroblast	Murine	European Collection of Cell cultures

2.1.5 General stock solutions

2.1.5.1 Phosphate buffered saline (PBS)

One PBS tablet was dissolved in 100ml of distilled water and the pH adjusted to pH 7.4-7.6. The solution was sterilised by autoclaving and stored at room temperature until needed.

2.1.5.2 Tris buffered saline (TBS)

Tris solution (pH 7.6), 2M 25 ml was mixed with 50 ml 3M NaCl solution. The volume was made up to 1 L using distilled water. The pH of the solution was adjusted to pH 7.6. The solution was sterilised by autoclaving and stored at room temperature until needed.

2.1.5.3 Cell culture medium

The standard cell culture medium used in this project was Dulbecco's modified Eagle's medium (DMEM) with 10% (v/v) foetal bovine serum (FBS), 100 $U.ml^{-1}$ penicillin, 100 $U.ml^{-1}$ streptomycin, and 100 µM L-glutamine. The culture medium was stored at 4 °C for up to 7 days.

2.2 Methods

2.2.1 pH measurement

The pH of solutions was measured using a Jenway 3010 pH meter. Before each measurement, the pH meter was calibrated using pH standard solutions at pH 4, 7 and 10. The solution for measurement was gently stirred using a magnetic stirrer while measuring with the pH probe, and the values were taken when the reading reached a steady state. To adjust the pH of the solutions, 1-6 M hydrochloric acid (HCl) or 1-6 M sodium hydroxide (NaOH) was used.

2.2.2 Light Microscopy

Light microscopy was carried out using an Olympus BX51 microscope. In order to perform polarized microscopy, the microscope was incorporated with a polarizer and an analyser into the normal bright field set-up. With the fluorescent vertical illuminator (BX51-RFA) and appropriate filters, fluorescent microscopy was also carried out using this microscope. Images were taken using an Olympus XC50 digital camera controlled through Cell B software (Olympus®, UK).

2.2.3 Sterilisation

2.2.3.1 Dry heat sterilisation

Items sterilised by dry heat sterilisation were placed in a hot air oven and sterilised at a temperature of 190 °C for 4 h.

2.2.3.2 Moist heat sterilisation

Items sterilised by autoclaving were sterilised at 121 °C for 20 min, at 103 kPa pressure.

2.2.3.3 Filter sterilisation

Filter sterilisation was used for solutions that were not suitable for moist heat sterilisation. The solutions were filtered through a filter with 0.2 µm pore size using a disposable syringe. This procedure was carried out in a Class II safety cabinet.

2.2.4 Dissection of porcine pulmonary heart valve tissue

Fresh porcine hearts were obtained from a local abattoir (Leeds) within 4 hours of slaughter (Figure 2.1 A). The pericardium was removed to expose the aorta and pulmonary artery. The aorta and the pulmonary artery were carefully separated using a scalpel blade, forceps and dissecting scissors. Then, using a scalpel blade, the pulmonary heart valve together with pulmonary artery and a myocardium skirt (from the right ventricle) were separated from the heart. Any excess fat and connective tissue were removed from the surface of the pulmonary artery and the myocardium skirt. Special care was taken to remove the fat and connective tissue from the connection part of the pulmonary artery, the myocardium, and the pulmonary leaflets. The pulmonary artery wall and the myocardium skirt were trimmed to the appropriate length required for the different experiments. The macroscopic integrity of the three pulmonary leaflets as well as the pulmonary artery wall and the myocardium skirt was checked, and only non-damaged pulmonary conduits were used in further experiments (Figure 2.1B). The pulmonary conduits were washed in PBS to remove the excess blood. The dissected porcine pulmonary roots were either used fresh, or wiped dry and wrapped in PBS-soaked filter paper in a sealed container and stored at -20 °C for later use.

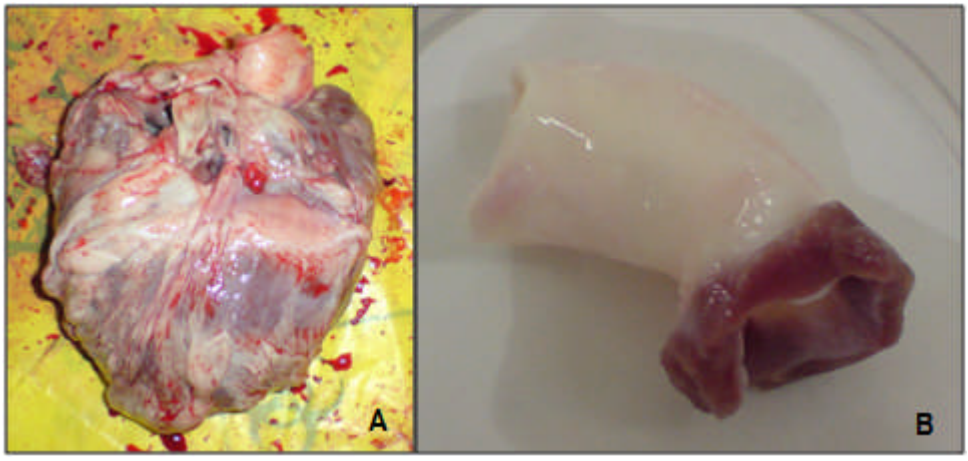

Figure 2.1 Dissection of porcine pulmonary valve roots. (A) Fresh porcine heart; **(B)** The dissected and cleaned porcine pulmonary valve conduits.

2.2.5 Sizing of porcine pulmonary roots

Following the isolation and trimming of the porcine pulmonary roots, their internal diameter was estimated using surgical obturators (Figure 2.2) and their external

diameter using vernier callipers. The internal diameter was recorded as the size of the obturator which fitted best the interior of the root (neither loose nor stretching the root). The external diameter was measured while the roots were gently lifted with forceps to allow the roots to open. The internal and external diameters of the roots were measured from the pulmonary artery side.

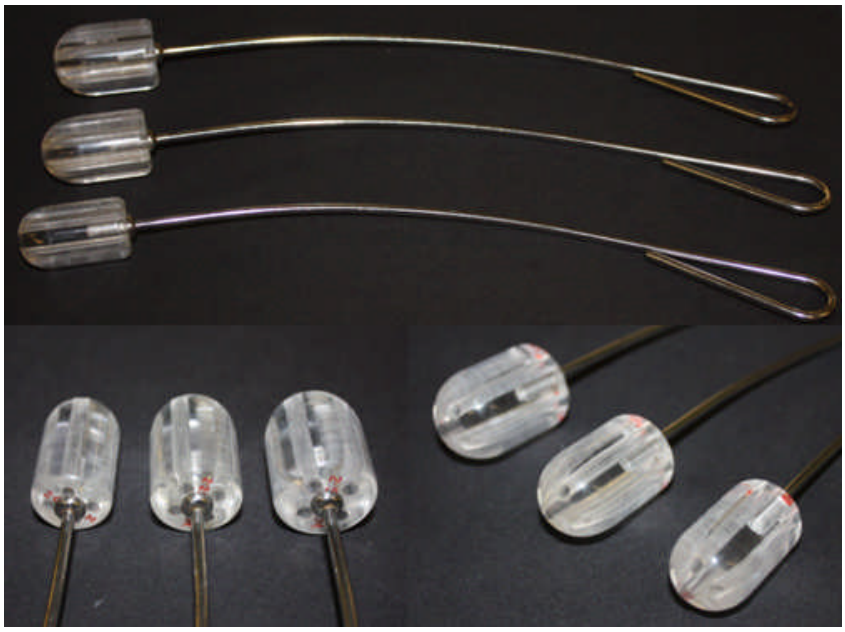

Figure 2.2 Obturators used for measuring the internal diameter of valve conduits.

2.2.6 Histological techniques

2.2.6.1 Paraffin embedding

Tissue samples were completely immersed in 10% (v/v) neutral buffered formalin (NBF) for 24 hrs at room temperature prior to further processing. Each root was cut into 6 pieces vertically (as illustrated in Figure 2.3). Thus, each piece incorporated a part of the pulmonary wall, a part of the myocardium and half of a leaflet. The samples were then placed in plastic cassettes (Histocasette®), and the cassettes placed into an automated tissue processor for dehydration. The tissue processor sequentially immersed the cassettes containing the tissue samples in: 10 % (v/v) NBF for 1 h, 70 % (v/v) ethanol for 1 h, and 90 % (v/v) ethanol for 1 h, followed by three consecutive 1-hour immersions in 100 % (v/v) ethanol, three consecutive 1-hour immersions in xylene, and three consecutive 1-hour immersions in paraffin wax. The cassettes were transferred

into a wax oven in hot wax at 60 °C for a maximum of 12 h. The tissue blocks were removed quickly from the cassettes and oriented into metal wax block moulds using hot forceps and fully covered in wax. The blocks were placed on ice to allow them to completely cool and fully solidify. The moulds were then removed and the excess wax was trimmed.

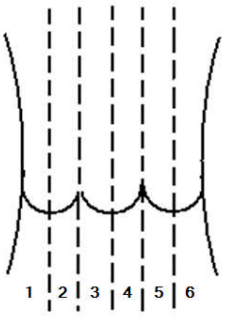

Figure 2.3 Schematic of the method used to cut the pulmonary roots for paraffin embedding.

2.2.6.2 Tissue sectioning, and slide preparation of paraffin embedded tissues

The embedded tissue was sectioned in 10 µm thickness sections using a microtome. The tissue sections were transferred to a water bath set at 42 °C and collected onto Superfrost Plus® slides. These slides were electrostatically charged to prevent the sections from floating off the slides during staining. The slides were placed onto a drying rack to briefly drain the excess water, and then transferred onto a hot plate at 60 °C for at least 20 min to completely dry and melt the wax. This step also provided firmer tissue fixation to the slides. The prepared slides were stored at room temperature until stained.

2.2.6.3 Dewaxing and rehydration of paraffin embedded tissue sections

The slides with the tissue sections were placed twice in xylene for 10 min each time to remove all the wax. They were then placed thrice into absolute alcohol for 3, 2, and 1 min respectively. Finally, the slides were placed into 70 % (v/v) ethanol for 1 min and then rinsed gently in running tap water for 3 min.

2.2.6.4 Dehydrating of tissue sections

Following staining of the sections, the slides were placed into 70 % (v/v) ethanol for 5 s before they were immersed into absolute alcohol thrice for 1, 2 and 3 min respectively. Subsequently, they were placed in xylene twice for 10 min each time.

2.2.7 Histological staining methods

2.2.7.1 Haematoxylin & eosin (H&E) staining

H&E staining was used to visualise tissue histoarchitecture and spatial distribution of cell nuclei. The tissue sections for staining were dewaxed and rehydrated, then immersed in Mayers Haematoxylin solution for 1 min before being placed in running tap water until the water ran clear. The slides were then stained with eosin for 4 min before dehydrating. Each section was mounted using DPX mountant and a coverslip. The slides were left to completely dry overnight in a fume cupboard before viewing under the microscope.

2.2.7.2 Hoechst staining

Hoechst 33258 dye binds to DNA, and was used to visualise cell nuclei and DNA remnants. The Hoechst dye buffer contained 1.211 $g.L^{-1}$ tris base, 0.372 $g.L^{-1}$ EDTA, and 0.006 $g.L^{-1}$ NaCl, whereas the pH of the solution was adjusted to pH 7.4. This solution was stored in a dark bottle away from light. The tissue sections for staining were dewaxed and rehydrated as stated in Section 2.2.6.3. Subsequently, a hydrophobic marker pen was used to mark out the tissue sections on the slides in order to keep the following applied dye in the circled area. The tissue sections were then incubated in 1 $\mu g.ml^{-1}$ Hoechst dye in Hoechst working solution for 30 min at room temperature in the dark. Each slide was washed three times, each for 10 min, using TBS (pH 7.4). The slides were mounted using glycerol: 1,4-diazabicyclo[2.2.2]octane (DABCO) (1:9). The slides were kept in the dark until ready to view under a 4',6-diamidino-2-phenylindole (DAPI) filter using fluorescence microscopy at a wavelength of 415 nm.

2.2.7.3 Alcian blue staining

Alcian blue staining was used to stain the GAG`s in the tissue. The sections were dewaxed and rehydrated before rinsed in 3% (v/v) acetic acid for 5-10 s. The sections were then immersed in 1% (v/v) alcian blue in 3 % (v/v) acetic acid for 5 min. After briefly blot drying with filter paper, the sections were immediately stained with 0.5 % (w/v) neutral red for 3 min and washed with distilled water. The slides were then mounted with warmed up glycerol and coverslip. Microscopic visualization was performed within hours after staining.

2.2.7.4 Miller's staining

Miller's staining was used to visualise elastin in the tissue. Following dewaxing and rehydration, the tissue sections were immersed in 0.25 % (w/v) potassium permanganate for 5 min. The tissue sections were washed thoroughly with running tap water and then with distilled water, and bleached with 0.1 % (w/v) oxalic acid for 3 min. Subsequently, the sections were washed again with running tap water and then distilled water, and transferred to 95 % (v/v) alcohol. The sections were then immersed in undiluted Miller's stain for 2 h before being washed with 96 % (v/v) ethanol and then with distilled water. Van Gieson's stain was used to counterstain the tissue sections for 5 min prior to dehydration. DPX mountant and a coverslip were used to mount each section.

2.2.8 Immunohistochemical labelling

2.2.8.1 Tissue fixation methods

Depending on the antibody, either 10 % (v/v) NBF fixation, or zinc fixation was used. Tissue fixed using 10 % (v/v) NBF was directly placed into an automated tissue processor as described in Section 2.2.6.1. The zinc fixation solution was 0.1 M Tris solution with 0.5 % (w/v) calcium acetate, 0.5% (w/v) zinc acetate, and 0.05% (w/v) zinc chloride. The pH was adjusted to pH 7.4, and the solution was stored at room temperature until needed. The tissue was placed into the zinc fixative for 16-24 h, before it was placed into the automated tissue processor (omitting the 10 % (v/v) NBF for 1 h step) for paraffin embedding (Section 2.2.6.1). The optimal fixation method was determined for each antibody. Fresh tissue samples were fixed with different methods

and went through immunohistochemistry. The optimal fixation method was considered as the one that gave strongest staining results for the fresh tissue samples.

2.2.8.2 Antigen retrieval methods

2.2.8.2.1 Citric acid microwave treatment

Reagents:

Citric acid solution (10mM citric acid) buffer was used as reagent. Prior to use, the pH of the solution was adjusted to pH 6.0 using NaOH.

Method:

Slides were placed in a Pyrex dish, with the tissue sections facing upwards, and were immersed in citric acid solution buffer (completely covering the tissue sections). The Pyrex dish was covered with pierced cling film and then microwaved on full power (800W) for 10 min. The slides were removed after the dish was cooled.

2.2.8.2.2 Trypsin retrieval method

2.2.8.2.2.1 Trypsin retrieval method 1 (0.1 % w/v trypsin)

Reagents:

Trypsin solution was prepared by dissolving 0.2 g trypsin and 0.2 g calcium chloride in 200 ml TBS (pH 7.6). The trypsin solution was warmed to 37 °C, and its pH was adjusted to 7.8 by adding 1M sodium hydroxide dropwise.

Method:

Slides were placed in distilled water, which was pre-warmed to 37 °C for a minimum of 5 min. The sections were then incubated in the trypsin solution at 37 °C for 30 min before being rinsed in running tap water.

2.2.8.2.2.2 Trypsin retrieval method 2 (0.5 % w/v trypsin)

This method was based on the trypsin retrieval method 1 (Section 2.2.8.2.2.1), but in this case, 1g of trypsin instead of 0.2 g was used to make up the trypsin solution. This gave a final trypsin concentration of 0.5 % (w/v).

2.2.8.2.3 Antibodies

The antibodies, secondary antibody, isotypes, fixation methods and the antigen retrieval methods used in this study are listed in Table 2.6. The concentration used for the isotype control was the same as the specific primary antibody.

Table 2.6 The antibodies, secondary antibody, isotypes, fixation methods and the antigen retrieval methods used in the study.

Antigen	Supplier	Clone	Isotype	Antigen Retrieval/ fixation method	Diluted concentration
A-SMA	Sigma A2547	1A4	Mouse IgG2a (Dako X0943)	Trypsin (method 1)/ 10 % (v/v) NBF	11.25 $mg.L^{-1}$
Vimentin	Novocastra NCL-VIM	VIM 3B4	Mouse IgG2a (Dako X0943)	Citrate/ 10 % (v/v) NBF	50 $mg.L^{-1}$
Desmin	Vector VP-D502	DE-R-11	Mouse IgG1(Dako X0931)	Citrate 10 % (v/v) NBF	54 $mg.L^{-1}$
Collagen-IV	DAKO M0785	CIV22	Mouse IgG1(Dako X0931)	Citrate/ Zinc fixative	1.6 $mg.L^{-1}$
Fibronectin	DAKO A0245	-	DAKO rabbit immunoglobilin Fraction, code X0936	Trypsin (Method 2)/ 10 % (v/v) NBF	10.2 $mg.L^{-1}$
Von Willebrand	DAKO A0082	-	DAKO rabbit immunoglobilin Fraction, code X0936	Citrate/ 10 % (v/v) NBF	15.5 $mg.L^{-1}$
Galα1-3Galβ1-4GlcNAc-R (α-gal)	ALEXIS Biochemicals 801-090	M86	-	-/ Zinc fixative	0.51 $mg.ml^{-1}$
Horseradish peroxidise-conjugated secondary rabbit anti-mouse antibody	DAKO P0260	-	-	-	1.3 $mg.L^{-1}$

2.2.8.3 Immunohistochemistry procedure

Reagents:

- TBS pH 7.6
- TBS containing 0.05 % (v/v) Tween 20, pH 7.6
- Antibody diluent: 100 ml TBS (pH 7.6) containing 0.01 % (w/v) sodium azide and 0.01 % (w/v) bovine serum albumin (BSA). The pH was adjusted to pH 7.6, and the solution was stored at 4 °C and used within 1 month.
- PBS pH 7.6
- 3 % (v/v) hydrogen peroxide (H_2O_2): 30 % (v/v) H_2O_2 was diluted 10 times using PBS pH 7.6.
- Ultravision Detection kit (for antibodies raised in either mouse or rabbit)

Method:

Tissue sections were dewaxed and rehydrated before the appropriate antigen retrieval was carried out. The sections were then placed into 3 % (v/v) H_2O_2 for 20 minutes at room temperature for blocking, and washed in running tap water for three minutes. Each section on the slides was ringed using a hydrophobic marker pen. The slides were then placed into four well plastic slide holders. The sections were washed with TBS pH 7.6, and incubated with V block from the Ultravision kit for 10 min. Slides were washed twice using TBS pH 7.6 for 10 min on a plate rocker. The primary antibody or the appropriate isotype control was then applied at a suitable dilution (diluted with antibody dilute), and the slides were placed in a sealed container (containing moist tissue paper) at room temperature for 1 h (90 min for α-gal). Subsequently, the sections were washed twice with TBS containing 0.05 % (v/v) Tween 20 pH 7.6, followed by two more washes with TBS pH 7.6, each for 10 minutes on a plate rocker. The Ultravision One HRP Polymer from the Ultravision kit was applied to the sections, and the sections were incubated for 30 min at room temperature in the dark. The slides were then washed twice with TBS containing 0.05 % (v/v) Tween 20 pH 7.6, followed by two more washes with TBS pH 7.6, each for 10 min on a plate rocker. 3,3'-diaminobenzidine (DAB) plus Chromogen from the Ultravision kit (made up by adding 20 µl of DAB plus chromagen to 1 ml of substrate buffer and mixing thoroughly) was applied to each section, and the sections were incubated for 10 min at room temperature. The sections

were washed gently under running tap water and counterstained with haematoxylin for 15 seconds. The slides were rinsed using tap water until the water ran clear, prior to dehydrating and mounting using DPX mountant and coverslips. The slides were air dried overnight in a fume cupboard and viewed using an upright microscope.

2.2.9 Cell culture techniques

All cells used in this study were cultured in standard DMEM cell culture medium (Section 2.1.5.3). All medium changes were performed aseptically in a Class II cabinet. All medium and reagents added to the cells were allowed to equilibrate to 37 °C before use. Cells were cultured at 37 °C in 5 % CO_2 (v/v) in air.

2.2.9.1 Resurrection and maintenance of cells

Cells were removed from liquid nitrogen storage, and thawed in a 37 °C water bath. A T75 cell culture flask with 13 ml cell culture medium was prepared. When the cells were defrosted, 2 ml of the defrosted cell stock was slowly added into the T75 flask. The flask was incubated at 37 °C in 5 % CO_2 (v/v) in air for at least overnight to allow the cells to attach to the flask. The medium was changed every two days until the cells became confluent and ready to be passaged.

2.2.9.2 Cell Passaging

The culture medium was aspirated from the cell culture flasks, and the cell layer was washed in PBS without calcium or magnesium for 2 min. Trypsin/EDTA (1.5 ml) was added to each T75 culture flask, and the flasks were then incubated in 5 % CO_2 (v/v) in air at 37 °C for 3 min. Following incubation, the cells were detached by gently tapping the flasks. The action of the trypsin/EDTA was terminated by adding 10 ml of culture medium to each flask. The cell suspension was transferred into a universal tube and centrifuged for 10 min at 150 g. Following centrifugation, the supernatant was carefully removed and the cell pellet was resuspended in 5 ml of cell culture medium. A viable cell count (Section 2.2.9.3) was performed to allow the cells to be seeded into fresh flasks at the appropriate density. The cell culture medium was changed every other day until the cells became confluent and ready to be passaged again.

2.2.9.3 Cell viability using Trypan blue

Trypan blue dye permeates into dead cells due to the loss of their membrane potential. Thus, live cells appeared transparent while dead cells were stained blue when examined under the microscope after staining with Trypan blue.

In order to perform the viability test, 20 µl of cell suspension was mixed with 20 µl of Trypan blue dye in a bijou tube. This mixture was added to an Improved Neubauer counting chamber. Viable cells were counted in *n* of the 9 grids (*n* = the number of grids which allowed the viable cell count to fall between 100 and 300). The total number of viable cells per ml in the cell suspension was calculated as follows:

$$\text{Number of cells.ml}^{-1} = \frac{\text{number of viable cells}}{n} \times 10^4 \times \textit{Dilution factor}$$

n was the number of grids used to count the cells

Dilution factor was the correction required due to the dilution of the cell suspension with Trypan blue dye (in this case, *Dilution factor* = 2)

2.2.9.4 Cell storage

Cells were isolated from the flasks (Section 2.2.9.2), and then diluted to 10^6.ml^{-1} with chilled cryopreservation medium (DMEM containing 20 % (v/v) FBS, 10 % (v/v) filter sterilised Dimethyl sulfoxide (DMSO)). The addition of DMSO prevented the formation of ice crystals during freezing, but it is toxic to the cells. In order to avoid the toxic effects, the cells were frozen immediately after the addition of DMSO. The cell suspension was aliquoted to 1 ml into cryovials, and placed into a cryo freezing pot which contained isopropanol. The pot was then placed in a -80 °C freezer for 12-36 hrs. The cell vials were subsequently transferred to liquid nitrogen for long-term storage.

2.2.10 Uniaxial tensile testing

The biomechanical properties of fresh and acellular porcine pulmonary valve conduits were compared using uniaxial tensile testing to failure in order to determine any significant effects of the decellularisation procedure on the mechanical properties of the tissue. The method used in this project was based to the protocol described by Korossis *et al*. (2002).

2.2.10.1 The uniaxial tensile test system

The uniaxial tensile testing was performed in a Shimadzu tensile testing system (Figure 2.4).

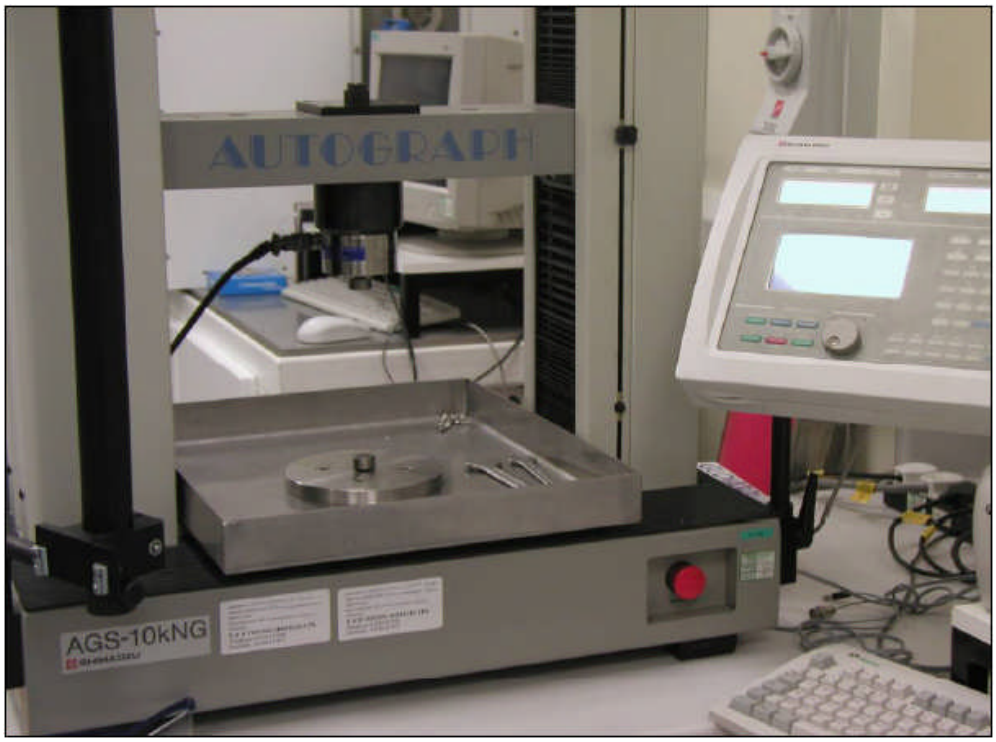

Figure 2.4 The Shimadzu tensile testing system.

A purpose built stainless steel tissue holder system (Figure 2.5) was used to hold the tissue samples for testing and to define their gauge length. The two holder parts (load cell and base), which were used to attach the tissue holder to the tensile tester, were aligned with a removable bracket. A central stainless steel block which was fixed onto the bracket was used to separate the two holder parts in order to define the gauge length of the tissue samples. A 10 mm wide separating block was used for the pulmonary artery wall samples to define a gauge length of 10 mm, and a 6 mm wide separating block was used for pulmonary leaflet samples to define a gauge length of 6 mm. The specimen was clamped in the holder with two grip blocks which were screwed onto each of the holder parts. Special care was taken during clamping to make sure that the tissue sample was in a completely un-stretched state. Once the tissue was secured onto the holder, the base part was fitted onto the base of the tensile tester, and the top part was screwed onto the load cell of the tensile tester. Subsequently, the bracket was removed, without disturbing the gauge length of the specimen.

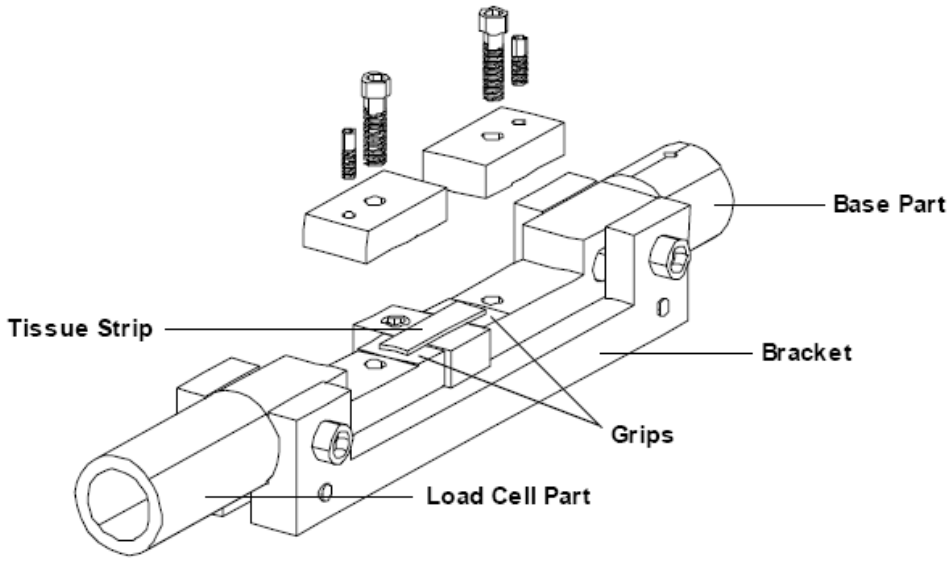

Figure 2.5 Tissue sample holder for tensile testing machine.

2.2.10.2 Tissue sample preparation

The specimens were dissected using parallel razor blades fitted onto a cutting block (Figure 2.6). The spacer between the two blades defined the width of the tissue strip. Using spacers of different thickness, the tissue was cut to its desired width. The length of the specimen was kept to approximately 20 mm for the pulmonary artery, and 15mm for the pulmonary valve leaflets, in order to allow mounting to the tissue holder. The thickness of the tissue was measured using a Mitutoya thickness gauge (Figure 2.7) with a resolution of 0.01 mm. Three measurements were taken for each specimen at different positions along its long axis, and the average thickness was recorded.

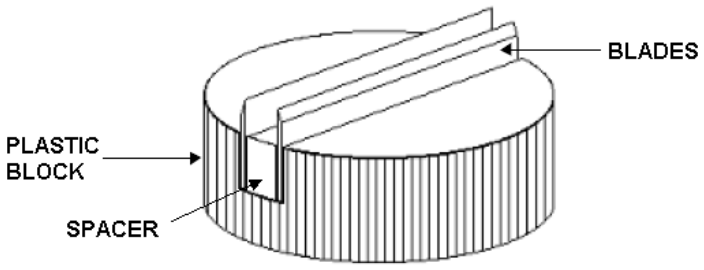

Figure 2.6 Cutting block used for the dissection of tissue strips.

Figure 2.7 Thickness gauge.

The specimen groups used in the study, as illustrated in Figure 2.8, were:

- Circumferential and radial leaflet strips: 6mm long by 3 mm wide;
- Circumferential and axial pulmonary wall strips: 10 mm long by 5 mm wide.

(The lengths stated here were the specimen gauge lengths used in the tests)

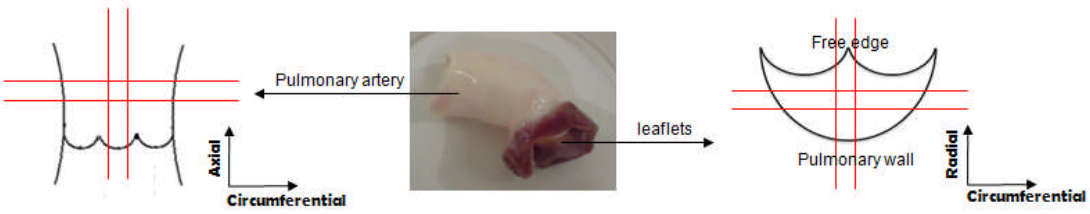

Figure 2.8 Specimen dissection for pulmonary wall and pulmonary valve leaflets.

2.2.10.3 Test procedure

All specimens were tested under uniaxial low-strain-rate loading to failure. The test sample was mounted onto the tissue holder with the bracket, and then fitted onto the tensile testing machine. Once the bracket was removed, the state of the tissue (at its relaxed state with no stress applied) was used to zero the load and the stroke channels. Specimen information, including thickness, gauge length, width, tissue type, treatment

type and serial numbers were inputted in the operating programme (MTTE.exe), which was installed on a personal computer.

To obtain an accurate measure of the tissue gauge length, the tensile machine was set to produce a sample preloading of 0.02 N before the operating program started to acquire any data. Therefore, zero extension was taken at the point where a 0.02 N was detected. The final gauge length, which was used for strain calculations, was automatically recorded by the programme as the manually inputted gauge length plus the extension that was needed to produce the 0.02 N preloading. A crosshead speed of 10 mm per minute was applied during testing, using a positive ramp function. Specimen failure was taken as the first decrease in the recorded load during extension. The real-time load was observed during the test run, to ensure the sample behaviour was normal (without slipping from the grips or being torn). During testing, load and extension data was recorded automatically at a rate of 20 Hz and stored in DAT files together with the specimen parameters. All tests were performed at 20 °C. Preconditioning was not performed in this study since it has been reported that preconditioning does not contribute to the generation of repeatable stress-strain curves for heart valve tissue (Carew *et al*., 2004). In addition, the major purpose of the testing was to compare the mechanical properties before and after treatment and not to determine the material properties of the tissue *persay.*

2.2.10.4 Data processing

The tensile testing machine operating programme, MTTE.exe, was used to analyze the data for each test run. Using the recorded force/extension data, the engineering stress was calculated for each data point according to:

$$\sigma_{Eng} = \frac{F}{A}$$

where σ_{Eng} represents the engineering stress in MPa, F the recorded force in Newtons (N) and A the cross-sectional area (CSA) of the specimen in mm^2. The CSA was calculated as A = specimen width × specimen thickness. The changes in thickness and width during preloading to 0.02 N were very small and considered negligible. The engineering strain for each corresponding data point was calculated according to:

$$\varepsilon_{Eng} = \frac{\Delta l}{l+lo}$$

where ε_{Eng} represents the unitless engineering strain, Δl the extension of the specimen in mm, l the original gauge length (10 mm for pulmonary wall strips, and 6 mm for pulmonary leaflet strips), and l_0 the length increased by the extension needed to produce the 0.02 N preloading. The stress-strain behaviour of each tested sample was characterised using six parameters; namely the elastic phase slope, the collagen phase slope, the transition stress, the transition strain, the ultimate tensile strength, and the failure strain. A typical stress-strain curve of heart valve leaflet tissue is illustrated in Figure 2.9, indicating how the six parameters were determined.

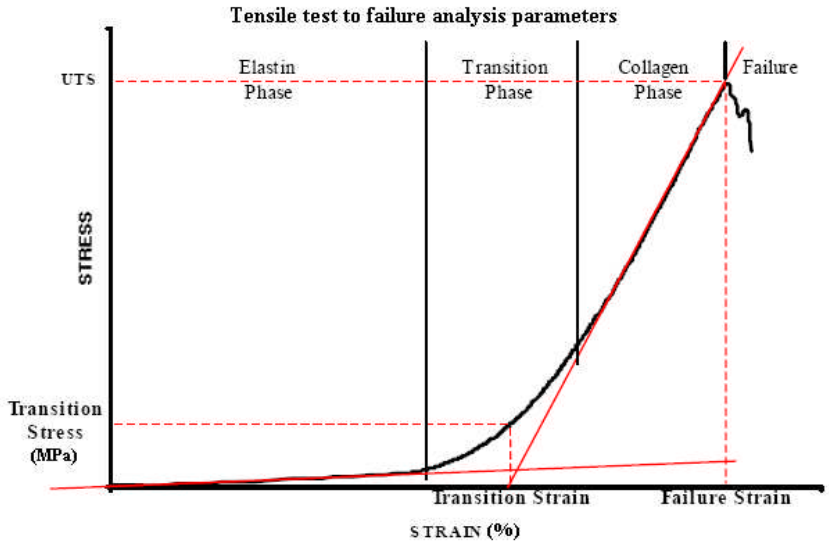

Figure 2.9 Typical stress-strain curve of heart valve leaflet tissue subjected to uniaxial tensile loading to failure.

The DAT files that were obtained during testing were exported from the operating program of the tensile testing machine and imported to Microsoft Excel (version 2003 and 2007, Microsoft Corporation) as spreadsheets for further processing. In Excel, the load and extension data was manually converted to stress and strain, respectively, as described above.

The analysis of the results was carried out per treatment group (at least 5 replicates from 6 different pig hearts per group). The engineering stress-strain curves for the specimens of each group, calculated in Excel, were averaged over the number of samples in each test group using the Origin software program (Version 8.5, Microbal). In addition, the

six parameters for each specimen obtained from MTTE.exe and described above, were averaged over the number of specimens in the group, and the results were presented as means ± 95 % confidence intervals (C.I.). The comparisons of the different groups were analysed by one-way analysis of variance (ANOVA) or the Student's t-test.

2.2.11 Statistical analysis

In this study, all numerical data was analysed using Microsoft Excel (Version 2003 or 2007, Microsoft), and all numerical values are presented as means ± 95 % C.I. The Student's t-test was used for comparison of groups of two means, and one-way ANOVA was applied for the comparison of data from more than two groups. Individual differences between group means were calculated using the minimum significant difference (MSD) (Sokal & Rohlf, 1981). The difference was considered as significant when the p value was smaller than 0.05.

x: individual value

n: sample number

$$\text{StDev} = \frac{\sum x}{n}$$

$$\text{SE Mean} = \frac{\text{StDev}}{\sqrt{n}}$$

$$95\ \%\ \text{C.I.} = \text{Mean} \pm t \times \text{SE Mean}$$

MSD = critical value × SE Mean

Critical value = Q α [k, v]

α = p = 0.05

k = number of groups

v = degrees of freedom (n-1)

Chapter 3

Development of methods for the decellularisation of porcine pulmonary valve conduits

3.1 Introduction

3.1.1 Decellularisation

Ideally, a successfully decellularised porcine heart valve should have close to 100 % of the cells and cell remnants removed, with its ECM well retained. The ECM has been shown to have an impact on cell mitogenesis and chemotaxis (Bornstein & Sage, 2002; Vorotnikova *et al*., 2010), cell differentiation (Stern *et al*., 2009; Allen *et al*., 2010; Barkan *et al*., 2010), and constructive host tissue remodelling responses (Valentin *et al*., 2010). Since there is evidence that residual cellular material can reduce the constructive tissue remodelling advantages of biologic scaffold materials *in vivo*, the tissue processing methods, especially decellularisation, can be critical for the success of acellular heart valves *in vivo* (Brown *et al*., 2009; Zhang *et al*., 2010; Burch *et al*., 2010; Crapo *et al*., 2011). The decellularisation process should ideally retain the macro and micro-scale biomechanical and biological properties of the ECM in order to facilitate appropriate cell response *in vivo*. A fully decellularised porcine heart valve scaffold with similar biological, histological and mechanical characteristics to the native heart valve has the potential to be used in heart valve replacement surgeries.

Although single treatment methods have been studied for their decellularisation potential, decellularisation methods have included a combination of physical, chemical and enzymatic treatments. Normally, physical treatments are applied at the beginning of a decellularisation method to lyse the cell membranes, followed by enzymatic treatments to separate the cellular components from the ECM and to remove nuclear material. Detergents are utilised to solubilise cell membranes by disrupting lipid/protein and protein/protein interactions. Mechanical agitation can be coupled with these steps to increase the effectiveness of the treatments. Washing steps are necessary to remove the products of cell lysis and detergent action and residual chemicals to avoid host tissue responses.

Physical methods such as freeze-thawing, direct pressure, sonication and agitation have been used to facilitate tissue decellularisation. The freeze-thawing of tissue causes the formation of intracellular ice crystals, which disrupts the cellular membranes, therefore lysing the cells. Freeze-thawing treatments have previously been applied for ligamentous tissue, tendons and nerve tissues (Jackson *et al*., 1988; Gulati, 1988; Jackson *et al*., 1991; Roberts *et al*., 1991). One cycle of freeze-thawing has been reported to reduce adverse immune responses such as leukocyte infiltration following vascular tissue decellularisation (Lehr *et al*., 2011). Multiple cycles of freeze-thawing have also been used in decellularisation (Stapleton *et al*., 2008) without significantly decreasing the amount of ECM proteins (Patel *et al*., 2008). Kim and colleagues (2002) have also studied the effects of freeze-thawing on porcine pulmonary heart valve leaflet decellularisation. However, the treatment failed to produce decellularisation since the tissue remained cellular as revealed by histology. Direct pressure provides mechanical force on the tissue with a view to bursting the cells (Freytes *et al*., 2004). However, the applied force can cause damage to the ECM. Mechanical agitation has been used together with chemicals to facilitate the removal of cellular materials (Schenke-Layland *et al*., 2003; Wilcox *et al*., 2005). In general, physical treatments have been shown to be effective for cell lysis, but additional processes are required to achieve complete cell removal.

Enzymes that have been used in tissue decellularisation methods include nuclease, trypsin, collagenase, thermolysin, lipase, dispase and α-galactosidase (Kasimir *et al*., 2003; Rieder *et al*., 2004; Chen *et al*., 2004; Wilcox *et al*., 2005; Xu *et al*., 2008; Yang *et al*., 2010; Funamoto *et al*., 2010; Broun *et al*., 2010). Nucleases, such as DNAses and RNAses have been reported to aid in the removal of nuclear material by cleaving DNA and RNA in tissues after cell lysis (Crapo *et al*., 2011). Trypsin is the most commonly used proteinase. It works by cleaving proteins at peptide bonds on the C-side of arginine and lysine. Schenke-Layland and colleagues (2003) reported efficient removal of cellular material from porcine pulmonary valves after treatment with 0.05 % (w/v) trypsin and 0.02 % (w/v) EDTA for 24 h with agitation. Wang and colleagues (2005) also reported complete decellularisation of porcine aortic valve leaflet tissue using 0.05 % (w/v) trypsin. However, there have been other studies, which have shown less efficient decellularisation using trypsin for 17 h (Grause *et al*., 2005). Schenke-Layland *et al*. (2003) reported that the effect of trypsin is time-dependent, and complete

decellularisation by trypsin alone may require long incubation, even for thinner tissues such as heart valve leaflets. The main concern regarding the use of trypsin in tissue decellularisation is its adverse effects on the ECM. Although trypsin has been reported to give better preservation of GAG content, it has also been reported to disrupt the elastin and collagen network of the ECM. Trypsin disruption of the ECM proteins can also result in detrimental changes to the mechanical properties of the tissue (Yang *et al*., 2009). Following trypsin treatment of heart valves, the remaining ECM has been shown to support endothelial cell growth despite the removal of ECM components (Schenke-Layland *et al*., 2003; Grause *et al*., 2005). Trypsin is effective at disrupting the ECM of the tissue and, subsequently, at improving the penetration of decellularisation agents. Therefore, the use of trypsin as the initial step in a tissue decellularisation protocol may be necessary, especially for denser tissues (Yang *et al*., 2010)

Hypotonic and hypertonic solutions have been widely used in tissue decellularisation. Hypotonic solutions cause cell lysis by the osmotic flow of water into the intracellular space, causing cell bursting, with minimal changes to the ECM proteins (Xu *et al*., 2007). Hypertonic saline has been shown to dissociate DNA from proteins (Cox & Emili, 2006). Additional treatments are required to facilitate the removal of cellular fragments. Hypo- and hypertonic solutions have also been reported to rinse cell residues from tissues following lysis (Cox & Emili, 2006; Xu *et al*., 2007).

Non-ionic, ionic, and zwitterionic detergents have been shown to be effective in removal of cellular material by solubilising cell membranes and dissociating DNA from proteins (Cox & Emili, 2006; Giusti *et al*., 2009). However, these detergents may also disrupt and dissociate proteins in the ECM. By increasing the tissue exposure time to detergents, more complete decellularisation can be achieved, but also more ECM proteins may be denatured.

Non-ionic detergents contain uncharged, hydrophilic head groups. They disrupt lipid-lipid and lipid-protein interactions, but leave protein-protein interactions intact so that proteins within a tissue following non-ionic detergent treatment are generally left in their functional conformation (Gilbert *et al*., 2006; Bhairi & Mohan, 2007). Triton X-100 is the most commonly used non-ionic detergent in tissue decellularisation. It has been reported to effectively remove cell residues from thicker tissues such as heart valve conduits in which enzymatic and osmotic methods are insufficient. Triton X-100

has also been associated with ECM protein loss accompanied by decreased adverse immune responses *in vivo* (Meyer *et al*., 2006). Mixed results have been reported of the decellularisation efficacy using Triton X-100. The removal of cells seems to be more effective for thin tissues. Some studies have reported that Triton X-100 caused disruption of the ECM ultrastructure and removal of GAG`s (Cho *et al*., 2005). Wang *et al.* (2005) applied 0.25 % (v/v) Triton X-100 in porcine aortic heart valve leaflet decellularisation for 48 h. Although complete decellularisation was achieved, strong structural alterations and changes to the tissue's tensile properties were reported. When Triton X-100 was used to decellularise whole aortic roots, although complete removal of nuclear material was observed in the valve leaflets, cellular material was found in the adjacent myocardium and aortic wall (Grause *et al*., 2005).

Ionic detergents, such as SDS and Triton X-200, contain a head group with a net charge, and are effective for solubilising both cytoplasmic and nuclear cellular membranes, but may denature proteins by disrupting protein-protein interactions when used in high concentrations (Seddon *et al*., 2004; Gilbert *et al*., 2006). SDS is the most widely used ionic detergent. It solubilises membrane proteins by mimicking the lipid bi-layer and solubilises proteins by inducing conformational changes. SDS has been shown to be very effective in removing cellular components of tissues at different concentrations, including pericardium, porcine heart valves, human amniotic membrane, tendon (Booth *et al*., 2002; Wilcox *et al*., 2005; Grauss *et al*., 2005; Wilshaw *et al*., 2006). SDS appears to be more effective in removing cell residues from tissues compared to other detergents, but it has also been associated with ECM disruption (such as loss of GAG`s and collagen integrity) and growth factor elimination (Courtman *et al*., 1994; Kasimir *et al*., 2003; Reing *et al*., 2010). Booth *et al*. (2002) tested a range of detergents including SDS, Triton X-100, sodium deoxycholate and Tween 20, and found that low concentration SDS (0.03-0.1 %) achieved complete porcine aortic heart valve leaflet decellularisation. Korossis *et al*. (2002) reported that porcine aortic leaflets treated with this method had equal strength compared to fresh samples. Complete decellularisation was also achieved using 0.1 % (w/v) SDS for porcine aortic whole roots (Wilcox *et al*., 2005). Korossis *et al*. (2005) reported that whole porcine roots treated with this method demonstrated complete valve leaflet competence and kinematics achieved under physiological conditions.

Zwitterionic detergents offer the combined properties of ionic and non-ionic detergents (Bhairi & Mohan, 2007). They have a greater tendency to denature proteins than non-ionic detergents but do not have the same effect of solubilising lipid membranes as ionic detergents (Gilbert *et al*., 2006). The 3-[(3-cholamidopropyl) dimethylammonio]-1-propanesulfonate (CHAPS) is an example of a zwitterionic detergent. It has been shown to be most effective for cell removal from thinner tissues (Peterson *et al*., 2010) and less effective for thicker tissues (Du *et al*., 2011). A study on peripheral nerve decellularisation showed better preservation of the ECM using non-ionic and zwitterionic detergents but better cell removal using ionic detergents (Hudson *et al*., 2004). However, due to the low concentration of cell bodies in peripheral nerves and the size of the tissue, the translation of these results to other tissues is limited. In the study conducted by Booth *et al*. (2002) for porcine heart valve decellularisation, it was found that although no significant damage to the ECM was observed, the use of CHAPS was not able to achieve complete decellularisation even when extending the incubation time to up to 72 h.

Following the production of the scaffold, it is necessary to be sterilised prior to implantation or *in vitro* cell seeding. Sterilisation methods have included incubation in acids or solvents, ethylene oxide exposure, gamma irradiation and electron beam irradiation (Hodde & Hiles, 2002; Corschewsky *et al*., 2005). However, the use of oxide exposure, gamma irradiation and electron beam irradiation has been shown to change the ECM histoarchitecture and biomechanical properties (Freytes *et al*., 2008; Sun & Leung, 2008; Gouk *et al*., 2008). Peracetic acid (PAA) is an oxidising agent and an effective chemical sterilant (Hodde & Hiles, 2002; Pruss *et al*., 1999), without any adverse effect on the mechanical behaviour of scaffolds (Freytes *et al*., 2004). It can also aid in the solubilisation of the cytoplasmic component of the cells and remove nucleic acids (Badylak *et al*., 1995).

This chapter describes the development of a method for the decellularisation of porcine pulmonary roots, based on a previously developed method for porcine aortic roots (Booth *et al*., 2002; Wilcox *et al*., 2005). In the studies conducted by Booth *et al*. (2002) and Wilcox *et al.* (2005), the porcine aortic roots were successfully decellularised while maintaining the integrity and biomechanical properties of the ECM. The decellularisation process developed in the present study included freeze-thawing, a

combination of trypsin, SDS, hypotonic and hypertonic buffers and nuclease treatments, as well as a final sterilisation step using PAA.

3.1.2 Mechanical behaviour of valvular tissue

The mechanical behaviour of a material refers to its deformation under load. Most frequently, the mechanical behaviour is expressed as the stress generated in a material subjected to a particular strain (stress-strain behaviour). Uniaxial tensile testing is a popular method used in the characterisation of the mechanical behaviour of soft tissues since it is a relatively straightforward procedure. It has been frequently used for the evaluation of the mechanical properties of both fresh and acellular heart valve tissue (Mayne *et al*., 1989; Korossis *et al*., 2002; Stradins *et al*., 2004; Korossis *et al*., 2005; Seebacher *et al*., 2007; Tudorache *et al*., 2007).

The typical stress-strain behaviour of valvular tissue has been illustrated in Section 2.2.10.4. This type of stress-strain behaviour has three distinct phases. The initial linear portion of the graph represents the elastin phase of the tissue and is characterised by a low elastic modulus (large increases in strain with small increases in stress). During this phase, the collagen layer in the tissue unfolds having a minimal contribution to load bearing. Force transmission in this phase is provided solely by the elastin fibres within the heart valve tissue. The next phase is the non-linear transition phase, during which the collagen fibres start to gradually uncrimp and align, increasing their contribution to force transmission. The second linear portion of the graph represents the collagen phase and it is characterised by a high modulus. During this phase, the tissue has a reduced compliance and a small extension of the tissue would produce a high tension. This reflects the material properties of the strong network of collagen fibres. The collagen phase of heart valve tissue usually continues beyond the physiological range, corresponding to its reserved strength. At the end of the collagen phase the slope of the graph starts decreasing and a further increase in the strain would result in tissue failure (Sauren *et al*., 1983).

Chemical treatment of biologically derived tissues has been shown to affect the mechanical properties of the ECM (Courtman *et al*., 1995, Palsson & Bhatia, 2004). Therefore, for tissues serving a mainly mechanical function in the body it is important

to study the effect of a particular tissue decellularisation protocol on the biomechanical properties of the tissue by comparing the behaviour of fresh decellularised tissue. Uniaxial tensile testing can be used to assess the effect of decellularisation on the mechanical integrity of a tissue scaffold and thus provide an insight on its potential function *in vivo*.

3.2 Aims and objectives

Aims:

The aim of the study presented in this chapter was to develop and optimise a process for the decellularisation of porcine pulmonary valve conduits.

Objectives:

- To characterise the fresh porcine pulmonary valve root histologically.
- To develop a decellularisation method for porcine pulmonary valve roots that is able to remove the cells and cellular remnants whilst preserving the histoarchitecture and the biomechanical integrity of the ECM.
- To characterise the decellularised porcine pulmonary valve roots histologically and biomechanically.

3.3 Methods

3.3.1 Decellularisation solutions

3.3.1.1 Antibiotic disinfection solution

This solution consisted of PBS containing 100 $U.ml^{-1}$ penicillin, 100 $\mu g.ml^{-1}$ streptomycin and 50 $\mu g.ml^{-1}$ gentamicin. This solution was prepared fresh before use.

3.3.1.2 Trypsin treatment paste

Trypsin solution: trypsin was dissolved in PBS at a concentration of 2.25×10^4 $U.ml^{-1}$.

Agarose solution (1 % w/v): 1 g low temperature melting point agarose was added to 100 ml distilled water. The agarose was dissolved and sterilised by autoclaving.

In order to make the trypsin treatment paste, the 1 % (w/v) agarose gel was heated in a water bath at 70 °C until fully melted. The water bath was adjusted to 40 °C, and the agarose solution was allowed to equilibrate. The 2.25×10^4 $Unit.ml^{-1}$ trypsin and the 1 % (w/v) agarose solution were mixed at a 1:1 ratio, and the mixture was allowed to cool at 4 °C until it became a paste. This trypsin treatment paste consisted of 1.125×10^4 $Unit.ml^{-1}$ trypsin and 0.5 % (w/v) agarose. This paste was prepared fresh prior to use.

3.3.1.3 Trypsin inhibitor solution

Buffer: 10 PBS tablets were dissolved in 1000 ml of distilled water containing 0.1 % (w/v) EDTA and 10 $KIU.ml^{-1}$ aprotinin. The PBS solution with EDTA was sterilised by autoclaving. Aprotinin was added to the PBS EDTA solution aseptically, using a needle and deposable syringe. The sterile buffer was stored at room temperature for up to one month. Trypsin inhibitor (45 mg; 1mg will inhibit 1.5 mg 10,000 $U.mg^{-1}$ trypsin) was added to 20 ml of the reaction buffer and filter sterilised prior to adding to the remaining 980 ml buffer just before use.

3.3.1.4 Hypotonic buffer (10mM Tris pH 8.0, 0.1 % w/v EDTA, 10 $KIU.ml^{-1}$ aprotinin)

Tris solution (2 M, pH 8.0): Tris (24.23 g) was dissolved in 75 ml distilled water. The pH was adjusted to 8.0 using 6 M HCl before the volume was made up to 100 ml with

distilled water to give 2 M Tris solution pH 8.0. The solution was sterilised by autoclaving and stored for up to one month at room temperature.

EDTA stock solution: EDTA (10 g) was dissolved in 80 ml distilled water and the pH was adjusted to 8.0 with NaOH pellets and 1 M NaOH solution. The solution was sterilised by autoclaving and stored for up to one month at room temperature.

The hypotonic buffer was prepared by adding 5 ml 2 M Tris solution pH 8.0, 10 ml of 10 % (w/v) EDTA to 900 ml of distilled water. The solution was made up to 1 L with distilled water and sterilised by autoclaving. The solution was stored at room temperature for up to one month. Aprotinin (1 ml, 10,000 $KIU.ml^{-1}$) was added aseptically to the solution just before use.

3.3.1.5 Hypotonic SDS buffer (0.1 % w/v SDS, 10mM Tris pH 8.0, 0.1 % w/v EDTA, 10 $KIU.ml^{-1}$ aprotinin)

SDS stock solution (10 % w/v): SDS (10 g) was added to 100 ml distilled water. The solution was sterilised by autoclaving and stored for up to one month at room temperature.

SDS (10 ml, 10 % w/v) was added to 990 ml sterile hypotonic buffer. The unused hypotonic SDS buffer was stored for up to one week at 4 °C if it was opened aseptically.

3.3.1.6 Nuclease treatment solution (RNase at 1 $U.ml^{-1}$ and DNase at 50 $U.ml^{-1}$ in treatment buffer)

Tris solution (2 M, pH 7.5): Tris (24.23 g) was dissolved in 75 ml distilled water. The pH was adjusted to 7.5 using 6 M HCl before the volume was made up to 100ml with distilled water to give 2 M Tris solution pH 7.5. The solution was sterilised by autoclaving and stored for up to one month at room temperature.

Magnesium chloride ($MgCl_2$) solution (1 M): $MgCl_2.6H_2O$ (20.3 g) was dissolved in 100 ml distilled water and autoclaved. The solution was stored at room temperature for up to one month.

BSA solution (5 $mg.ml^{-1}$): 250 mg BSA was dissolved in 50 ml distilled water. The solution was sterilised by filter sterilisation. Aliquots of 5 ml of the solution were made in sterile bijous, and stored frozen at -20 °C for up to six months.

DNAse reconstitution buffer (5 mM sodium acetate, 1 mM calcium chloride ($CaCl_2$), 50 % v/v glycerol): sodium acetate (0.68 g) and $CaCl_2$ (0.11g) were dissolved in 500 ml distilled water. Glycerol (500 ml) was added to this solution and mixed by inverting. The pH of the solution was adjusted to pH 5 by adding 6 M HCl or 6 M NaOH dropwise whist stirring using a magnetic stirrer. The buffer was stored at room temperature for up to three months.

DNAse stock solution (10,000 $U.ml^{-1}$): DNAse was rehydrated to a final concentration of 10,000 $U.ml^{-1}$ (according to the label of activity on the bottle) using DNAse reconstitution buffer. The solution was sterilised by filter sterilisation. Aliquots (5ml) were made in bijous and stored at -20 °C for up to three months.

RNAse stock solution (100 $U.ml^{-1}$): RNAse was rehydrated to a final concentration of 100 $U.ml^{-1}$ (according to the label of activity on the bottle) using distilled water. The solution was sterilised by filter sterilisation. Aliquots (5ml) were made in bijous and stored at -20 °C for up to three months.

Nuclease treatment buffer: 12.5 ml sterile Tris buffer (2 M, pH 7.5), 5 ml of 1 M sterile $MgCl_2$ solution, and 5 ml of 5 $mg.ml^{-1}$ filter sterilised BSA solution were mixed with 470 ml sterile distilled water. The buffer was made fresh prior to use.

Nuclease treatment solution: RNAse (5 ml, 100 $U.ml^{-1}$) and DNAse (2.5 ml, 10,000 $U.ml^{-1}$) were added to the nuclease treatment buffer just prior to use.

3.3.1.7 Hypertonic buffer (1.5 M NaCl, 50 mM Tris pH 7.5)

Tris buffer pH 7.5 (2 M, 12.5 ml) was added to 487.5 ml distilled water. NaCl (43.83g was dissolved in the buffer which was then sterilised by autoclaving. The hypertonic buffer was stored for up to one month at room temperature.

3.3.1.8 PAA solution

PAA (32 %, 1.56 ml) was added to 500 ml of PBS. The pH was adjusted to 6.0 by adding 6 M NaOH dropwise with agitation. The solution was made fresh just prior to use.

3.3.1.9 Wash buffer I (10 KIU.ml^{-1} aprotinin, 0.1 % w/v EDTA in PBS)

EDTA (10 % w/v, 10 ml) was added to 1 L of PBS. The buffer was sterilised by autoclaving. This solution was stored at room temperature for up to one month. Aprotinin (1 ml, 10,000 KIU.ml^{-1}) was added aseptically to the solution just before use.

3.3.1.10 Wash buffer II (10 KIU.ml^{-1} aprotinin in PBS)

Aprotinin (1 ml, 10,000 KIU.ml^{-1}) was added aseptically to autoclaved 1 L of PBS just before use.

3.3.2 Histological evaluation of fresh and decellularised porcine pulmonary heart valve roots

The histoarchitecture of fresh and decellularised porcine pulmonary valve roots was determined by histology. Tissue samples (n=6 for the fresh and each of the treatment groups) were fixed with 10 % (v/v) NBF for 24 to 48 hrs. Histological evaluation was performed as described in Section 2.2.7. Tissue sections of 10 µm were used for histological staining, and the slides were viewed under bright-field microscopy or fluorescent microscopy with a DAPI filter. Sections were collected when the leaflet, pulmonary artery and myocardium all appeared on the tissue section. At least 3 sections were examined by each histological method. For each decellularised tissue block, at least 10 tissue sections were collected every 20 sections, and these sections were all examined by histology to study the effects of decellularisation. H&E staining was used to study tissue architecture and cell distribution. Connective tissue was stained red/pink and cell nuclei were stained blue. Hoechst staining was performed to locate cell nuclei or DNA residues in the tissue. Cell nuclei were present as bright blue dots under fluorescent microscopy. This helped to evaluate the extent of decellularisation. Miller's staining was used to identify the distribution of elastin in the tissue. Elastin stained blue/black. Alcian blue staining was used to identify the GAG`s in the tissue. GAG`s were stained blue, and cell nuclei were stained red.

3.3.3 Decellularisation of porcine pulmonary roots (Method 1)

Six porcine hearts were procured from a local abattoir within 4 h of slaughter, and dissected immediately (Section 2.2.4). The pulmonary roots were trimmed of excess

tissue, rinsed in PBS and stored dry at -20 ºC. All decellularisation treatments were carried out in 150 ml containers (1 root per container).

Decellularisation commenced with defrosting the roots in a 37 ºC oven for 30 min or until the roots were completely defrosted. Using fine pointed forceps, the outside layer of the pulmonary wall was peeled off to thin it to approximately 1.5-2 mm thickness (Figure 3.1). The roots were then disinfected with antibiotic disinfection solution (100 ml per root) overnight (16-17 h) at 4 ºC. The following day, before trypsin treatment, the valve leaflets were masked using cotton wool soaked with 50 % (v/v) FBS in PBS (Figure 3.2). For each pulmonary root, three soaked cotton wool balls were placed between each of the three leaflets and the pulmonary artery (Figure 3.2 A, B, C), and a soaked cotton wool pad was placed at the ventricular side of the leaflets (Figure 3.2 D). The positions of the cotton wool balls and pad in a cut open pulmonary root are shown in Figure 3.2 D and Figure 3.2 E. Trypsin treatment was performed by brushing a layer of trypsin treatment paste on both the outside and the inside of the pulmonary artery wall, as well as the remaining myocardium bar using a hog haired wooden handle artists' paint brush (Figure 3.3 A). The roots were incubated for 2 h at 37 ºC in a humidified container (Figure 3.3 B). The trypsin treatment paste was removed and replaced, and the roots were incubated for a further 2 h under the same conditions. Following treatment, each pulmonary root was washed in 120 ml trypsin inhibitor solution at 45 ºC with shaking at 240 rpm (containers were placed horizontally) three times for 30 min. The pulmonary roots were then placed into hypotonic buffer (120 ml per root) for 24 h at 45 ºC with agitation at 240 rpm (containers were placed horizontally), followed by incubation in 120 ml of hypotonic SDS buffer for 24 h at 45 ºC with agitation at 240 rpm (containers were placed horizontally). Two 30-min washes and one overnight wash (16-17 h) were then performed using PBS containing 10 $KIU.ml^{-1}$ aprotinin (wash buffer II) at 45 ºC (120 ml per root each time, containers were placed horizontally, 240 rpm). The roots were then incubated in 120 ml nuclease solution for 4 hours at 37 ºC with agitation at 80 rpm (containers were placed horizontally). Subsequently, the roots were washed twice for 30 min in 120 ml wash buffer I at 45ºC, followed by a 66 h wash in the same solution (containers were placed horizontally; 240 rpm). The roots were incubated in hypertonic buffer for 24 h at 45ºC with agitation at 240 rpm (containers were placed horizontally), and then incubated in 120 ml 0.1 % (w/v) PAA solution for 3 h at room temperature with agitation at 240 rpm (containers were placed horizontally).

Three final washes were conducted using 120 ml wash buffer I at 45 ºC for 30 min each (containers were placed horizontally; 240 rpm). The process is summarised in Figure 3.4.

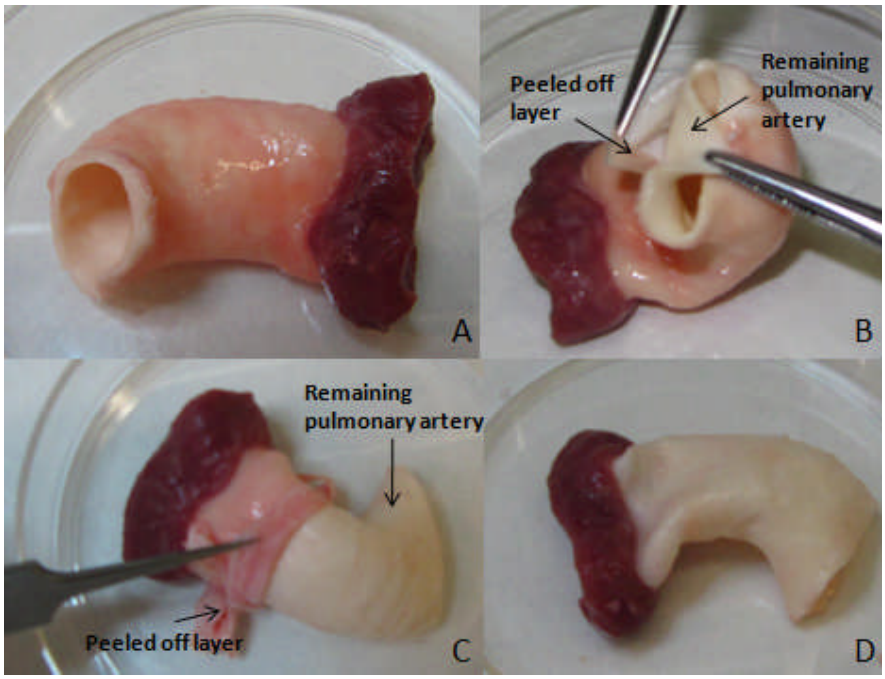

Figure 3.1 Peeling of porcine pulmonary roots. (A) fresh porcine pulmonary root for decellularisation; **(B)** A thin layer was peeled off with a pair of fine point forceps, starting from the pulmonary artery side; **(C)** The peeling continued all the way towards the ventricular side; **(D)** A thinned-wall porcine pulmonary root.

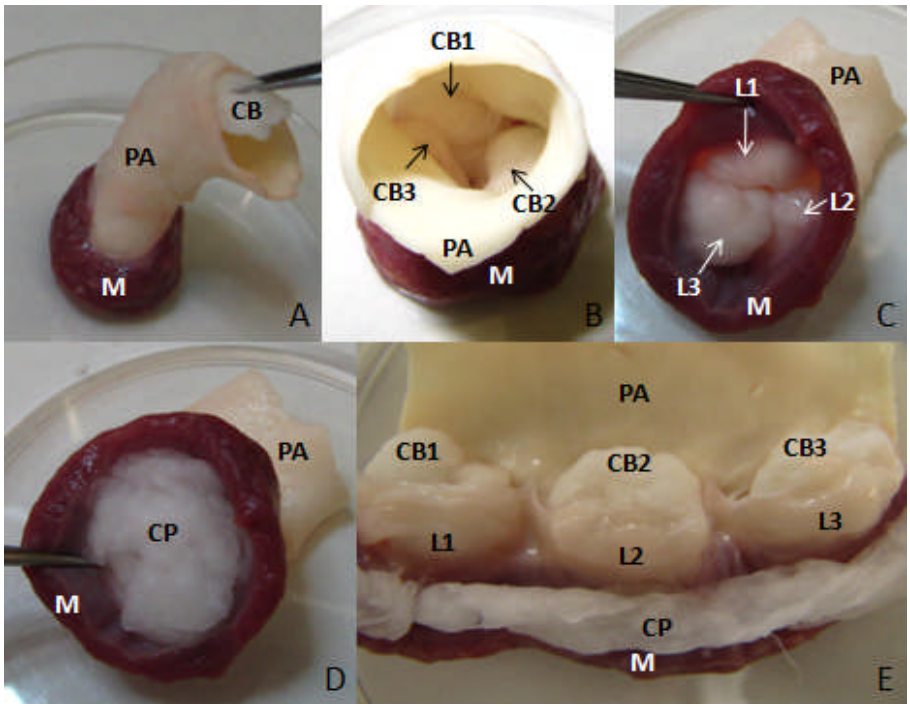

Figure 3.2 Protection of pulmonary leaflet during trypsin treatment. (A) Soaked cotton wool balls were placed between each of the three leaflets and the pulmonary artery; **(B)** Pulmonary artery view after the three soaked cotton wool balls were placed; **(C)** Ventricle view after the three soaked cotton wool balls were placed; **(D)** A soaked cotton wool pad was placed at the ventricular side to cover the leaflets; **(E)** The cut-open pulmonary root with the leaflets protected with soaked cotton wool balls and pad. PA: pulmonary artery; M: myocardium; L: pulmonary leaflet; CB: cotton wool ball; CP: cotton wool pad.

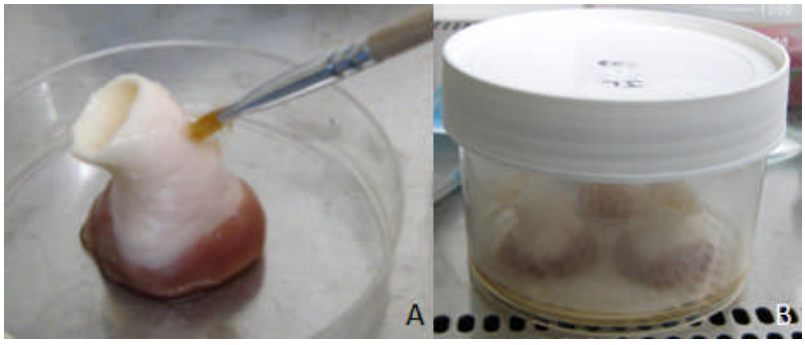

Figure 3.3 Trypsin treatment of porcine pulmonary roots. (A) Trypsin treatment paste was brushed onto the pulmonary artery and the myocardium bar; **(B)** The pulmonary roots with trypsin treatment paste were placed in a humidified container for incubation.

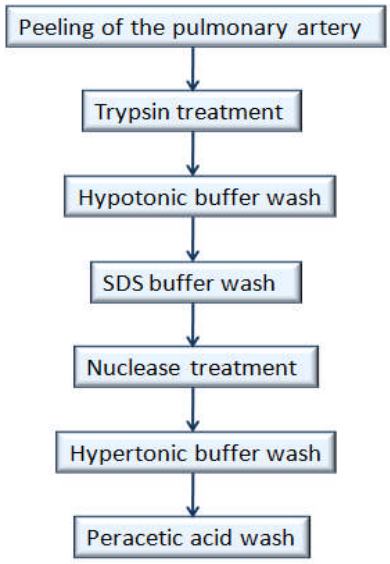

Figure 3.4 Process flow diagram of decellularisation Method 1.

3.3.4 Biomechanical evaluation of fresh and decellularised porcine pulmonary heart valve roots

The biomechanical properties of native and decellularised (Method 3, Section 3.4.4) porcine pulmonary roots were evaluated using uniaxial tensile testing. Circumferential and axial specimens were dissected from fresh intact porcine pulmonary arteries (n=7 and 6, respectively), fresh peeled porcine pulmonary arteries (n=6 and 6, respectively), and decellularised (according to Method 3, Section 3.4.4) porcine pulmonary arteries (n=6 and 9, respectively) and tested under uniaxial tensile loading to failure in order to characterised their stress-strain behaviour and failure characteristics. All pulmonary artery specimens tested were 5 mm in width and 10 mm in length (initial gauge length). The test samples and controls are listed in Table 3.1.

Table 3.1 The test samples and controls of uniaxial tensile testing for porcine pulmonary arteries. C: circumferential direction; A: axial direction.

	Fresh intact		Fresh peeled		Decellularised (Method 3)	
	C	A	C	A	C	A
Numbers of sample	7	6	6	6	6	9

Circumferential and radial fresh (n=6 and 6, respectively), and decellularised (Method 3, Section 3.4.4) (n=5 and 6, respectively) pulmonary leaflets were also tested under uniaxial tensile loading to failure. The pulmonary leaflet specimens were 3 mm in width and 6 mm in length (initial gauge length). Tissue specimens were taken from different animals within each test group, and randomly from the three pulmonary leaflets for both fresh and decellularised groups. The methodology followed during uniaxial tensile testing was described in Section 2.2.10. The test samples and controls are listed in Table 3.2.

Table 3.2 The test samples and controls of uniaxial tensile testing for porcine pulmonary leaflets. C: circumferential direction; R: radial direction.

	Fresh		Decellularised (Method 3)	
	C	R	C	R
Numbers of sample	6	6	5	6

The mean stress-strain curves for each group were generated using the Origin 8.0 software package. A cubic spline was fitted to each data set and equally spaced data points were interpolated from the cubic spline at 100 fixed intervals along the spline. The 100 fixed intervals were determined by dividing the mean engineering strain into 100 equal portions. The interpolated data set was then used to fit an exponential decay, thus the mean stress-strain behaviour was generated for each test group.

3.4 Results and further development of the decellularisation process

3.4.1 Histological evaluation of fresh porcine pulmonary valve conduits

In order to characterise the fresh pulmonary root tissue, tissue sections were stained with H&E, Hoechst, Miller's and Alcian blue. Images of the pulmonary root tissue stained with H&E are shown in Figure 3.5. Cells were stained blue after H&E staining, and could be seen throughout the fresh porcine pulmonary root. The VEC`s and the VIC`s were visible in the images of the leaflets (Figure 3.5 A). Connective tissue (collagen and elastin) were stained red with H&E, and seen in the pulmonary leaflet, pulmonary artery and myocardium. The red colour was deeper in the *ventricularis* and *fibrosa*, but lighter in the *spongiosa*, indicating more collagen and elastin distributed in the *ventricularis* and *fibrosa* layers than the *spongiosa* layer. The structure of the *spongiosa* seemed to be more loosely arranged and less organised than the other two layers. The myocardium bundles were recognised when stained with H&E (Figure 3.5 B). Depending on the orientation when preparing the tissue section, the myocardium bundles appeared in longitudinal or cross section. In Figure 3.5 B, both longitudinal and cross sectioned myocardium bundles could be recognised. The pulmonary artery was sectioned along its long axis. Both endothelial cells and valvular smooth muscle cells were present (Figure 3.5 C). The smooth muscle cells were aligned parallel to the long axis of the pulmonary artery. The leaflet connection is the region where the root of the pulmonary leaflet attaches to the myocardium and the pulmonary artery. The pulmonary leaflet appeared to be thickest in this region. Both leaflet tissue and myocardium tissue were recognisable in the image of the leaflet connection area (Figure 3.5D).

Images of the pulmonary root tissue stained with Hoechst are shown in Figure 3.6. The bright blue dots in the Hoechst stained tissue indicated cell nuclei. Hoechst staining further demonstrated that cells were distributed throughout the whole fresh pulmonary root tissue. The VEC`s were distributed closer to each other than the VIC`s (Figure 3.6 A). The cells in the pulmonary artery were clearly aligned parallel to the long axis of the artery (Figure 3.6 C). Images of the pulmonary root tissue stained with Miller's and Alcian blue are shown in Figure 3.7 and 3.8 respectively. Referring to the tissue sections stained with Millers stain, elastin fibres (stained black) were distributed mainly in the pulmonary wall, whereas they were hardly distinguishable in the myocardium (Figure 3.7 B, C). Elastin fibres could also be seen in the leaflets, with the *ventricularis*

layer demonstrating higher elastin content compared to the *fibrosa* and *spongiosa* layers (Figure 3.7 A). Elastin fibres were observed on the ventricular side of the myocardium (Figure 3.7 B). Following Alcian blue staining, blue coloured GAG`s were observed in the leaflets, pulmonary wall, and leaflet connection, but hardly in the myocardium (Figure 3.8). The centrally located *spongiosa* appeared to contain abundant GAG`s, which were less apparent in the *fibrosa* and *ventricularis* (Figure 3.8 A).

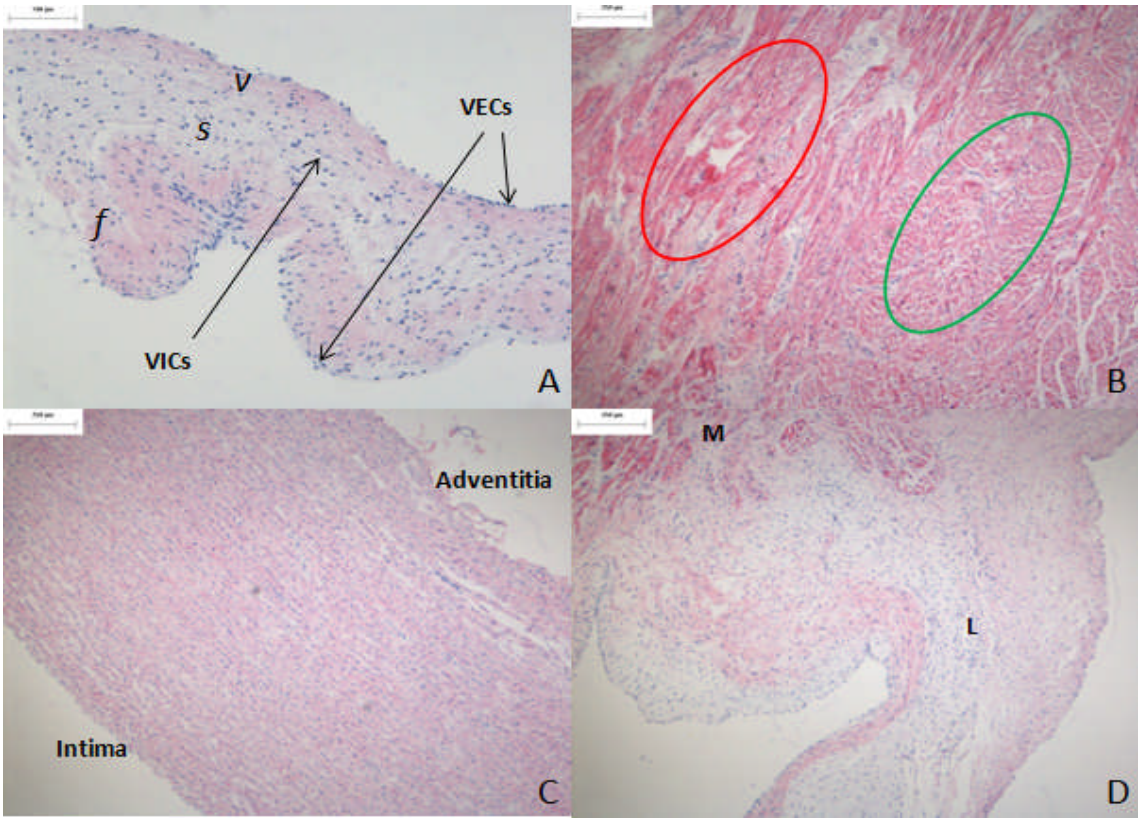

Figure 3.5 Sections of fresh porcine pulmonary root tissue stained with H&E. (A) Pulmonary valve leaflet, 100 × (*v*: *ventricularis*; *s*: *spongiosa*; *f*: *fibrosa*); The VEC`s and VIC`s are indicated by arrows; **(B)** Myocardium, 40 ×; The red circle indicates longitudinal section of myocardium bundles and the green circle indicated cross sectioned myocardium bundles **(C)** Pulmonary wall, 40 ×; **(D)** Leaflet connection, 40 ×. M: myocardium; L: leaflet. Scale bars are: (A) 100 µm; (B), (C), (D) 250 µm.

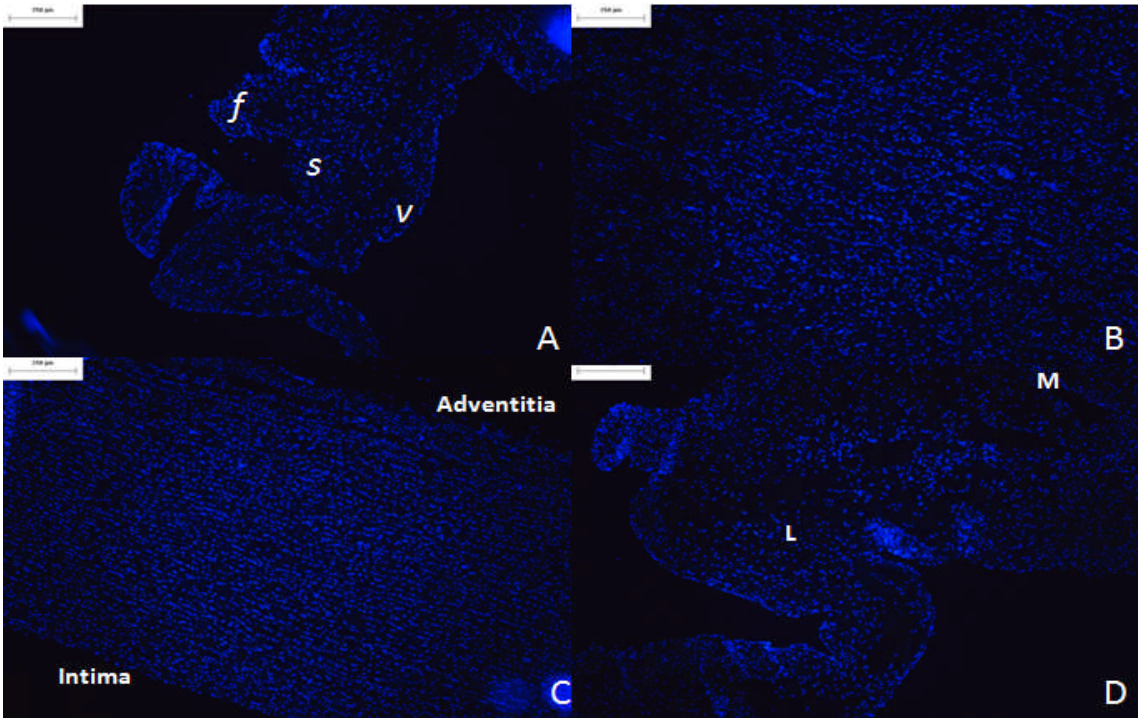

Figure 3.6 Sections of fresh porcine pulmonary root tissue stained with Hoechst. (A) Pulmonary valve leaflet, 40 × (*v*: *ventricularis*; *s*: *spongiosa*; *f*: *fibrosa*); **(B)** Myocardium, 40 ×; **(C)** Pulmonary wall, 40 ×; **(D)** Leaflet connection, 40 ×. M: myocardium; L: leaflet. Scale bars are: all 250 µm.

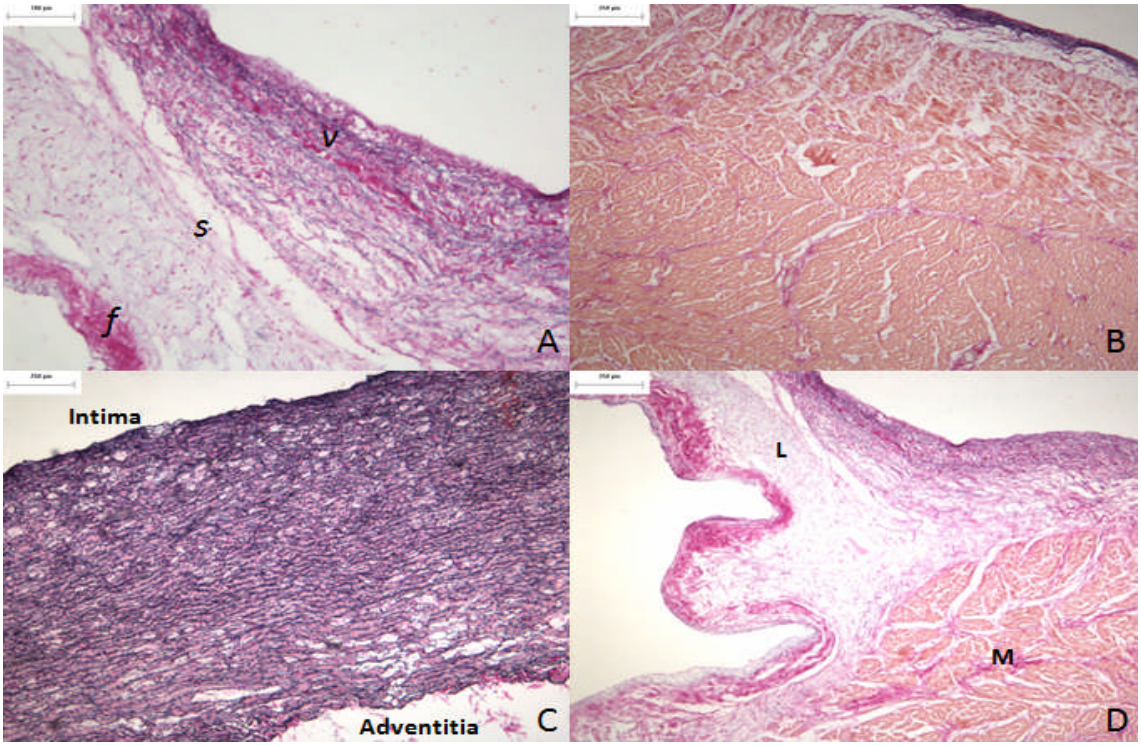

Figure 3.7 Sections of fresh porcine pulmonary root tissue stained with Miller's. (A) Pulmonary valve leaflet, 100 × (*v*: *ventricularis*; *s*: *spongiosa*; *f*: *fibrosa*); **(B)** Myocardium, 40 ×; **(C)** Pulmonary wall, 40 ×; **(D)** Leaflet connection, 40 ×. M: myocardium; L: leaflet. Scale bars are: (A) 100 µm; (B), (C), (D) 250 µm.

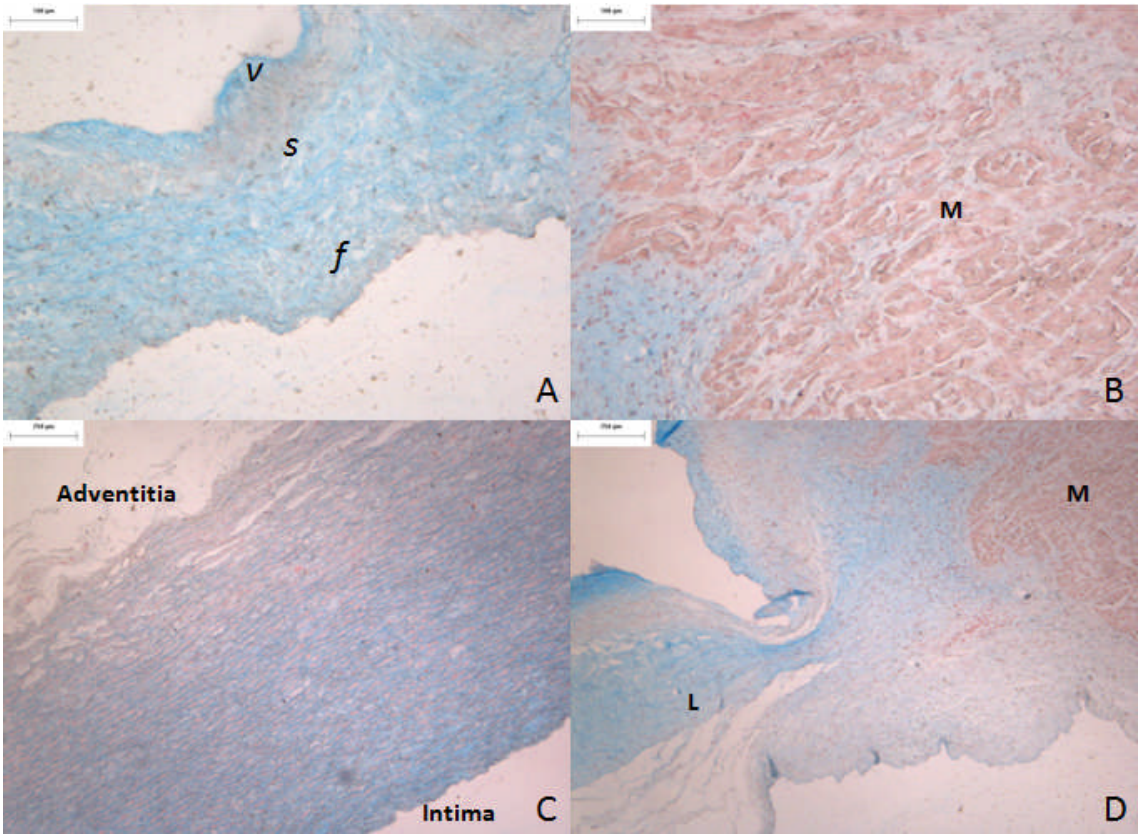

Figure 3.8 Sections of fresh porcine pulmonary root tissue stained with Alcian blue. **(A)** Pulmonary valve leaflet, 100 × (*v*: *ventricularis*; *s*: *spongiosa*; *f*: *fibrosa*); **(B)** Myocardium, 100 ×; **(C)** Pulmonary wall, 40 ×; **(D)** Leaflet connection, 40 ×. M: myocardium; L: leaflet. Scale bars are: (A), (B) 100 µm; (C), (D) 250 µm.

3.4.2 Histological evaluation of decellularised porcine pulmonary valve conduits (Method 1)

Following decellularisation of the porcine pulmonary roots using Method 1, decellularised tissue sections were stained with H&E (Figure 3.9) and Hoechst (Figure 3.10) to determine the extent of decellularisation. No cell nuclei could be observed in the leaflets, pulmonary wall or myocardium. However, cells or cell residues were observed in the connection area of the leaflet to the myocardium (Figure 3.9 B). Under 400 × magnification, cell nuclei in the pulmonary root-myocardium connection area were about the same size as those in fresh pulmonary roots from the same area (Figure 3.9 E, F). Blue fluorescent nuclei were identified in the connection area of the myocardium and leaflet connection in Hoechst stained images (Figure 3.10 C, D), but no nuclei were identified in the pulmonary leaflets or wall (Figure 3.10 A, B). The

results indicated the presence of cells or cell residues in the connection area of the leaflet and the myocardium after decellularisation using Method 1.

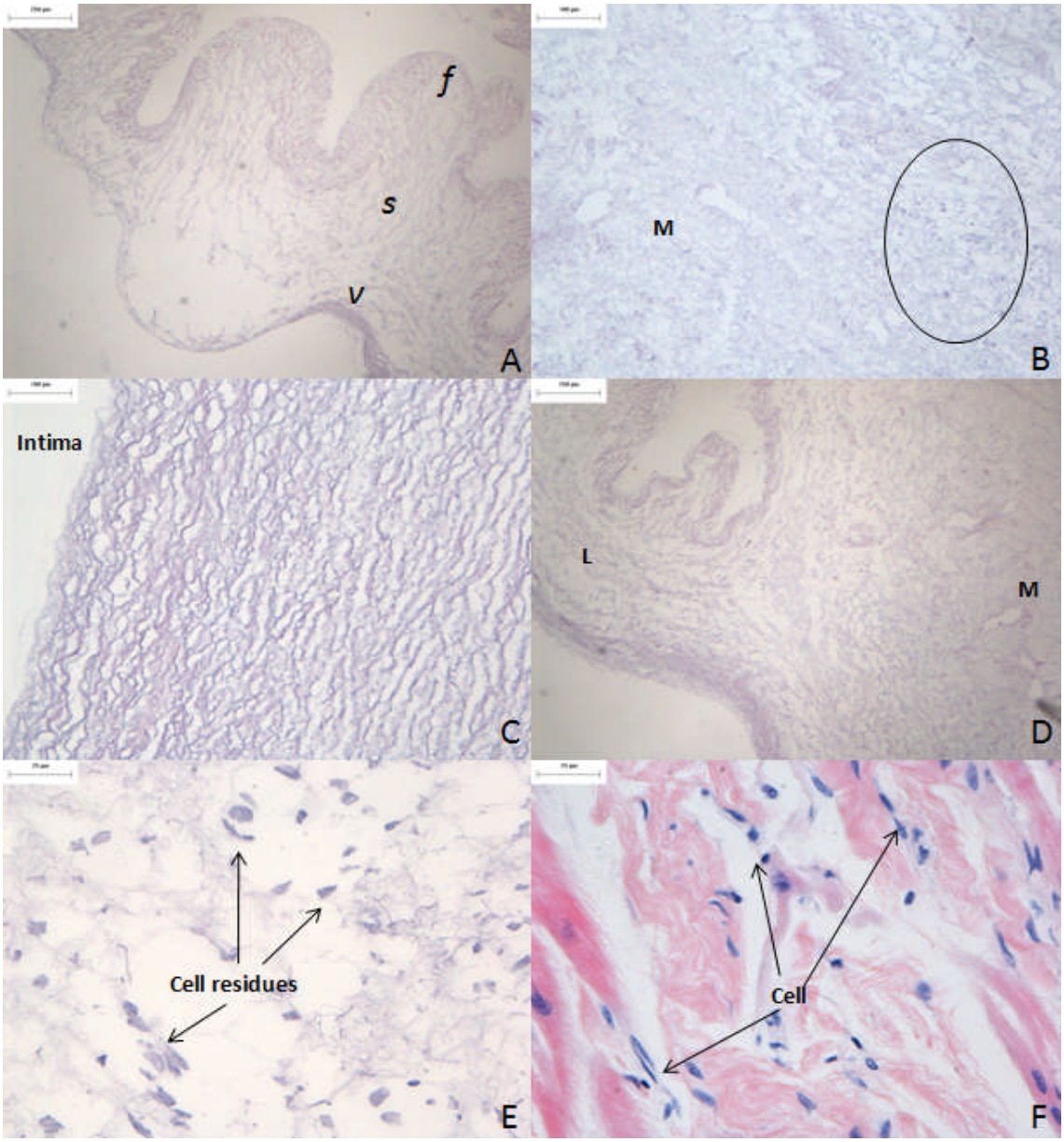

Figure 3.9 Sections of decellularised porcine pulmonary root tissue stained with H&E (Method 1). (A) Pulmonary valve leaflet, 40 × (*v*: *ventricularis*; *s*: *spongiosa*; *f*: *fibrosa*); **(B)** Myocardium, 100 ×, the circle indicates the remaining cells after decellularisation (Method 1); **(C)** Pulmonary wall, 100 ×; **(D)** Leaflet connection, 40 ×; **(E)** Cell residues at the connection area, 400 ×, arrows indicate cell residues; **(F)** Cells in the same area as (E) In fresh pulmonary root, 400 ×, arrows indicated cells. M: myocardium; L: leaflet. Scale bars are: (A), (D), (E), (F) 250 µm; (B), (C) 100 µm.

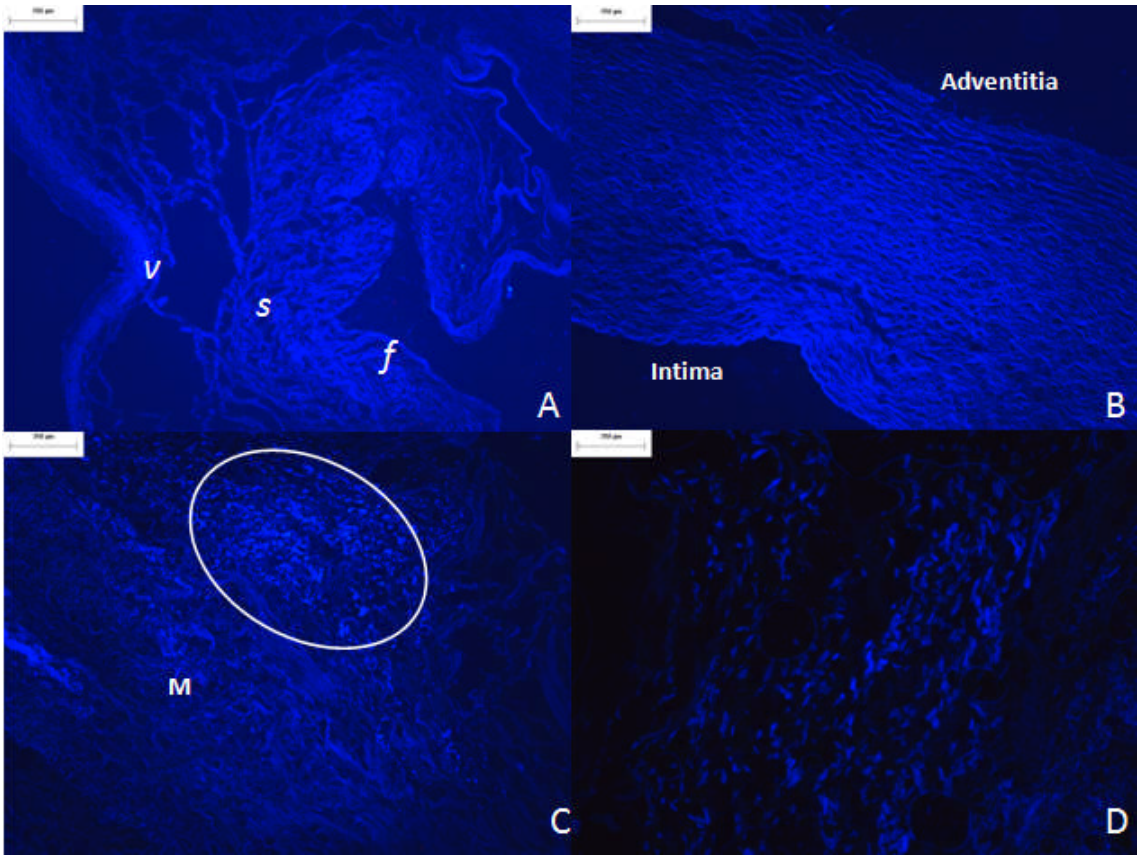

Figure 3.10 Sections of decellularised porcine pulmonary root tissue stained with Hoechst (Method 1). (A) Pulmonary valve leaflet, 40 ×, (*v*: *ventricularis*; *s*: *spongiosa*; *f*: *fibrosa*); **(B)** Pulmonary wall, 40 ×; **(C)**, Leaflet connection and myocardium, the circle indicates the remaining cells after decellularisation (Method 1), 40 ×; **(D)** Cell residues, 40 ×. M: myocardium; L: leaflet. Scale bars are: all 250 µm.

3.4.3 Further development of the decellularisation method for porcine pulmonary valve roots (Method 2)

3.4.3.1 Method

The results from the porcine pulmonary roots decellularised according to Method 1 showed cell residues present in the leaflet connection area. In order to improve the cell removal in the connection area, 2 cycles of the hypotonic SDS buffer wash were introduced in Method 2. Since the pulmonary roots were relatively small compared to the aortic roots, and the porcine pulmonary walls were thinner, it was considered that trypsin treatment might not be necessary to decellularise the pulmonary root. In addition, since the pulmonary wall was thinner than the aortic wall, it was hypothesised that it

might not be necessary to thin the wall prior to decellularisation. Thus, Method 2 was modified to Method 1 with the following changes:

a) the pulmonary wall was not peeled;
b) Trypsin treatment was not performed;
c) Two cycles of incubation in hypotonic buffer and hypotonic SDS buffer were performed instead of one.

Two porcine pulmonary roots were decellularised using Method 2.

3.4.3.2 Results

Sections of porcine pulmonary valve tissue were stained with H&E (Figure 3.11), Hoechst (Figure 3.12) and Miller's (Figure 3.13) to study the effect of decellularisation using Method 2. From the images of H&E stained sections, no cell nuclei were observed in the pulmonary leaflets, inside the pulmonary wall, or the myocardium (Figure 3.11 A, B, C). The connection of the leaflet and myocardium was also clear of cell nuclei (Figure 3.11 D). However, some residual nuclei were observed on the outside surface of the pulmonary wall (Figure 3.11 C). This was further confirmed by Hoechst stain (Figure 3.12 C, D), since some fluorescence was observed on the adventitia of the pulmonary wall. The fluorescence was not as defined as that observed in the Hoechst stained sections of the fresh pulmonary root, and was more diffuse. No blue fluorescence was present in the pulmonary leaflets, myocardium, or the inside of the pulmonary wall (Figure 3.12 A, B, C). Following Millers staining, elastin was observed in the pulmonary leaflets (mostly on the *ventricularis* layer), pulmonary wall, and the leaflet connection area, but not in the myocardium (Figure 3.13). The outside surface of the pulmonary wall demonstrated "fluffy" connective tissue, and not was not as smooth as the inside surface (Figure 3.11 C, Figure 3.13 C). The residual DNA observed in H&E and Hoechst stained sections was inside this "fluffy" area (Figure 3. 11 C, Figure 3.12 C).

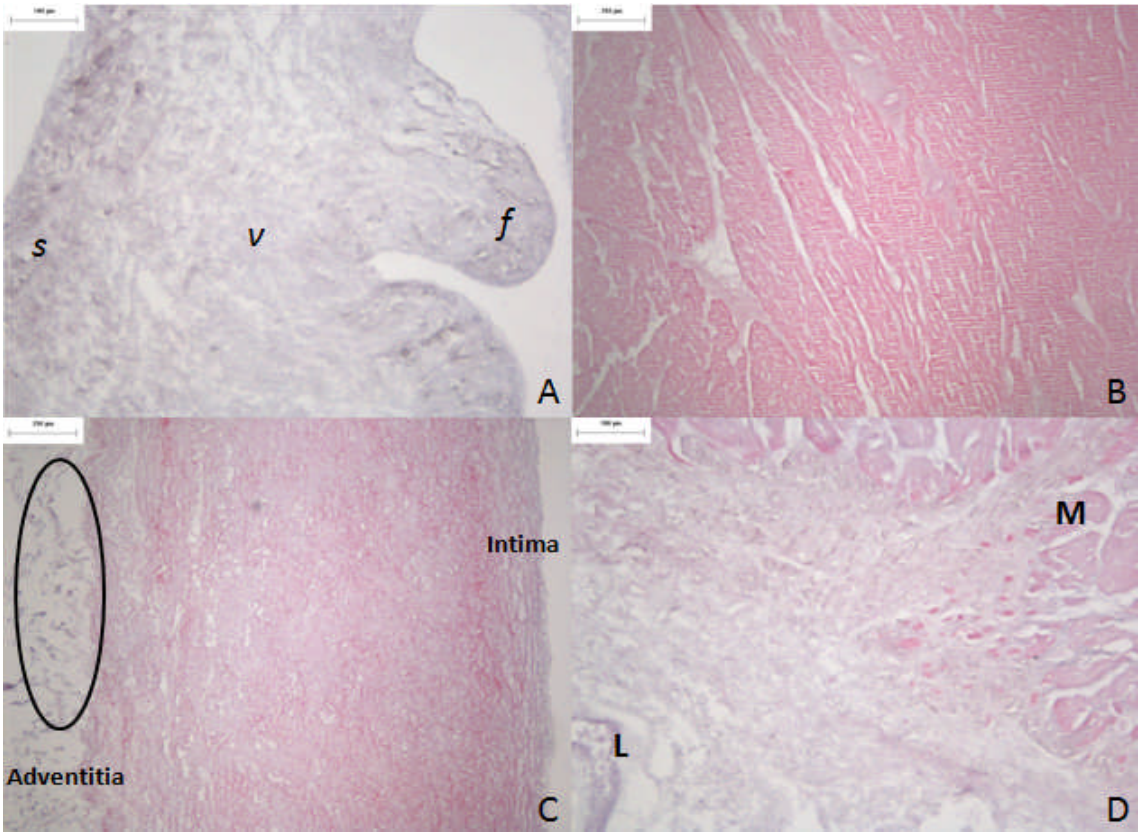

Figure 3.11 Sections of decellularised porcine pulmonary root tissue stained with H&E (Method 2). (A) Pulmonary leaflet, 100 × (*v*: *ventricularis*; *s*: *spongiosa*; *f*: *fibrosa*); **(B)** Myocardium, 40 ×; **(C)** Pulmonary wall, 40 ×, the circle indicated the remaining cells on the adventitial surface after decellularisation (Method 2); **(D)** Leaflet connection, 100 ×. M: myocardium; L: leaflet. Scale bars are: (A), (D) 100 µm; (B), (C) 250 µm.

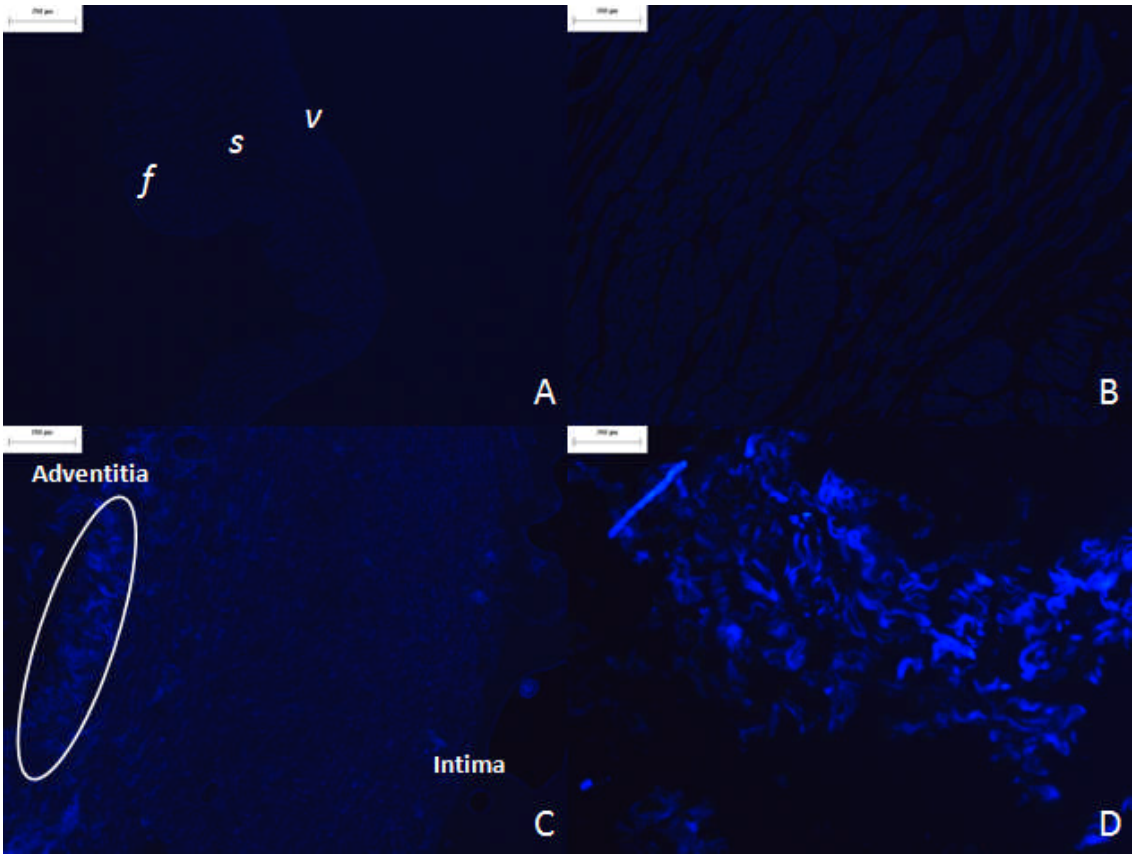

Figure 3.12 Sections of decellularised porcine pulmonary root tissue stained with Hoechst (Method 2). (A) Pulmonary leaflet, 40 × (*v*: *ventricularis*; *s*: *spongiosa*; *f*: *fibrosa*); **(B)** Myocardium, 40 ×; **(C)** Pulmonary wall, 40 ×, the circle indicates the remaining cells on the adventitia of the wall after decellularisation (Method 2); **(D)** Cell residues on the adventitia of the wall, 100 ×. Scale bars are: (A), (B), (C) 250 µm; (D) 100 µm.

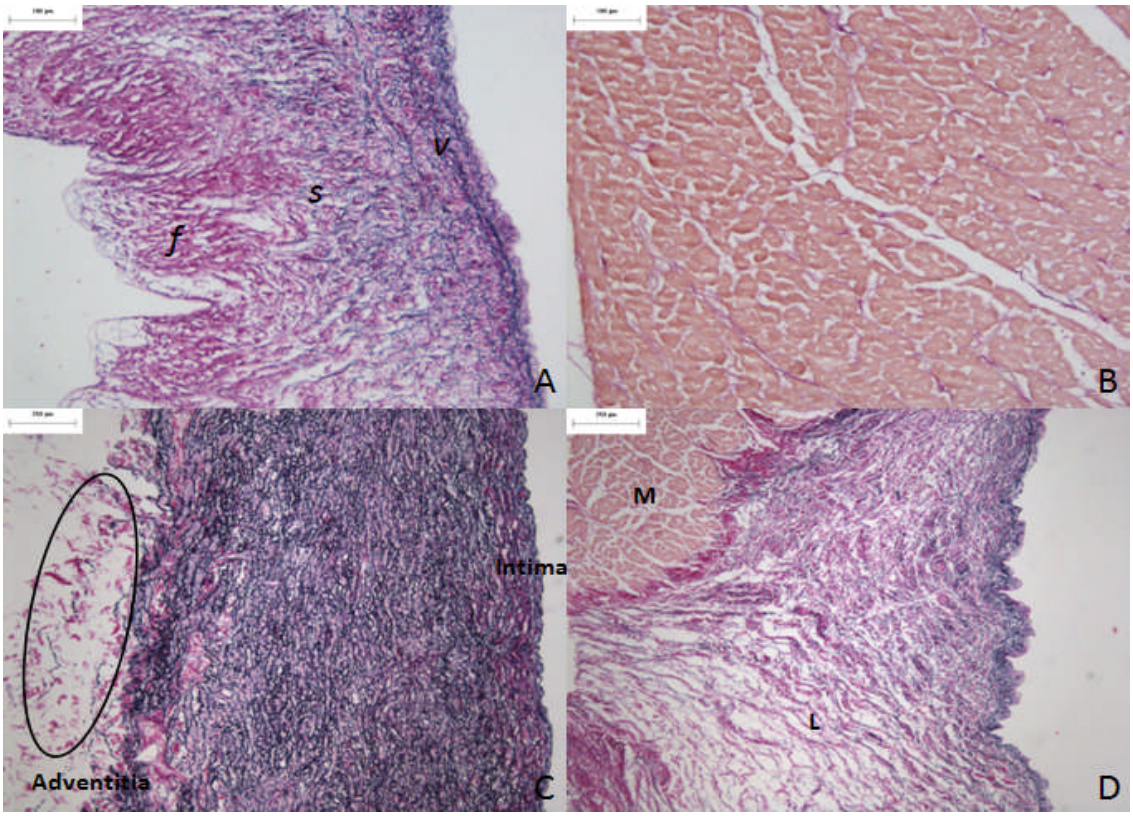

Figure 3.13 Sections of decellularised porcine pulmonary root tissue stained with Miller's (Method 2). (A) Pulmonary valve leaflet, 100 × (*v*: *ventricularis*; *s*: *spongiosa*; *f*: *fibrosa*); **(B)** Myocardium, 100 ×; **(C)** Pulmonary wall, 40 ×, the circle indicated the connective tissue on the adventitial surface of the pulmonary wall; **(D)** Leaflet connection, 40 ×. M: myocardium; L: leaflet. Scale bars are: (A), (B) 100 µm; (C), (D) 250 µm.

3.4.4 Further development of the decellularisation methods for porcine pulmonary roots (Method 3)

3.4.4.1 Method

The histological results of the tissue treated with Method 2 indicated that the only region that still retained cell residues was the outer layer of the adventitia of the pulmonary wall. Thus, it was realised that peeling of an external layer of the pulmonary artery was necessary to achieve complete decellularisation of the pulmonary roots. Method 3 was modified from method 2 with only one change: the external layer of the pulmonary artery wall was peeled prior to decellularisation. Six porcine pulmonary roots were decellularised using Method 3.

3.4.4.2 Results

Sections from the porcine pulmonary roots were stained with H&E (Figure 3.14), Hoechst (Figure 3.15) and Miller's (Figure 3.16) to study the effect of decellularisation using Method 3. No residual cell nuclei were observed in the H&E stained sections of decellularised pulmonary roots (Method 3) (Figure 3.14). In addition, no blue fluorescence was observed in the sections stained with Hoechst (Figure 3.15). The sections stained with Miller's stain indicated that elastin was mainly distributed in the pulmonary wall, the surface surrounding the myocardium, and the ventricle side of the pulmonary leaflets (Figure 3.16). Unlike the tissues treated with Method 2, the outer surface of the pulmonary wall treated with Method 3 was clear of cells (Figure 3.14 C, Figure 3.15 C). The adventitia layer of the pulmonary artery was peeled off from the roots treated with this decellularisation method (Figure 3.14 C, figure 3.16 C). Complete decellularisation of porcine pulmonary roots was achieved by using decellularisation Method 3.

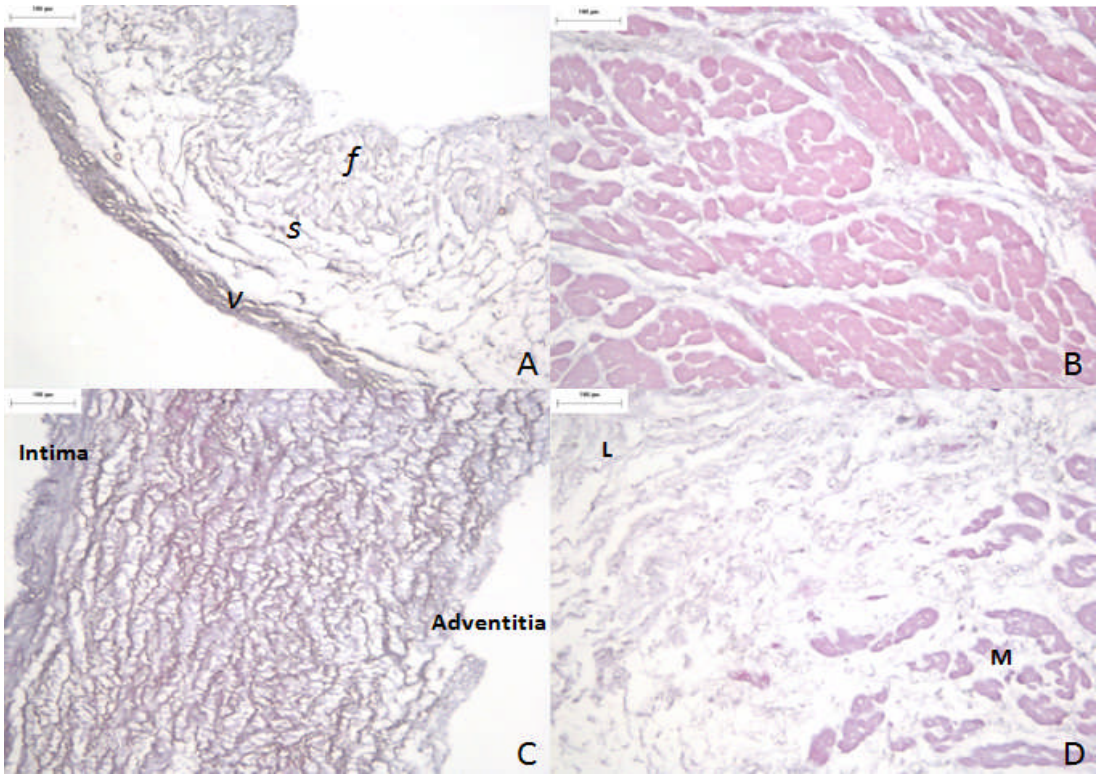

Figure 3.14 Sections of decellularised porcine pulmonary root tissue stained with H&E stain (Method 3). (A) Pulmonary valve leaflet, 100 × (*v*: *ventricularis*; *s*: *spongiosa*; *f*: *fibrosa*); **(B)** Myocardium, 100 ×; **(C)** Pulmonary wall, 100 ×; **(D)** Leaflet connection, 100 ×. M: myocardium; L: leaflet. Scale bars are: all 100 µm.

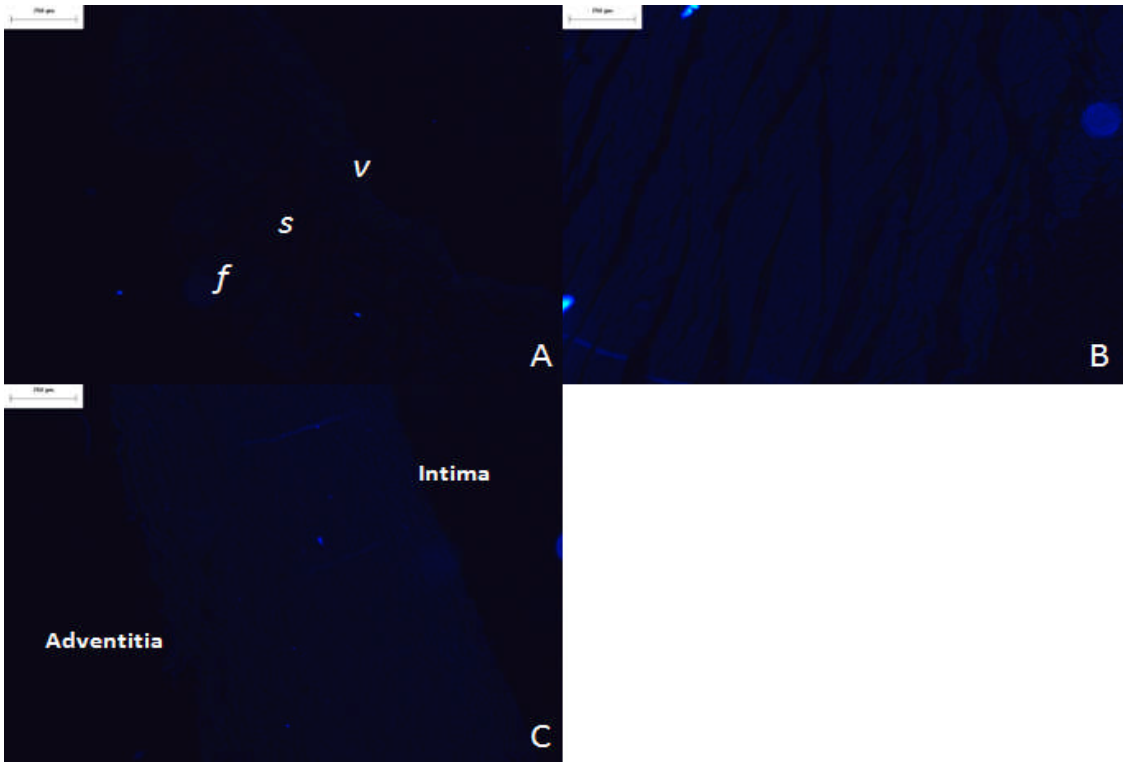

Figure 3.15 Decellularised porcine pulmonary root tissue stained with Hoechst (Method 3). (A) Pulmonary leaflet, 40 ×; **(B)** Myocardium, 40 ×; **(C)** Pulmonary wall, 40 ×. M: myocardium; L: leaflet. Scale bars: (A) 100 µm; (B), (C), (D) 250 µm.

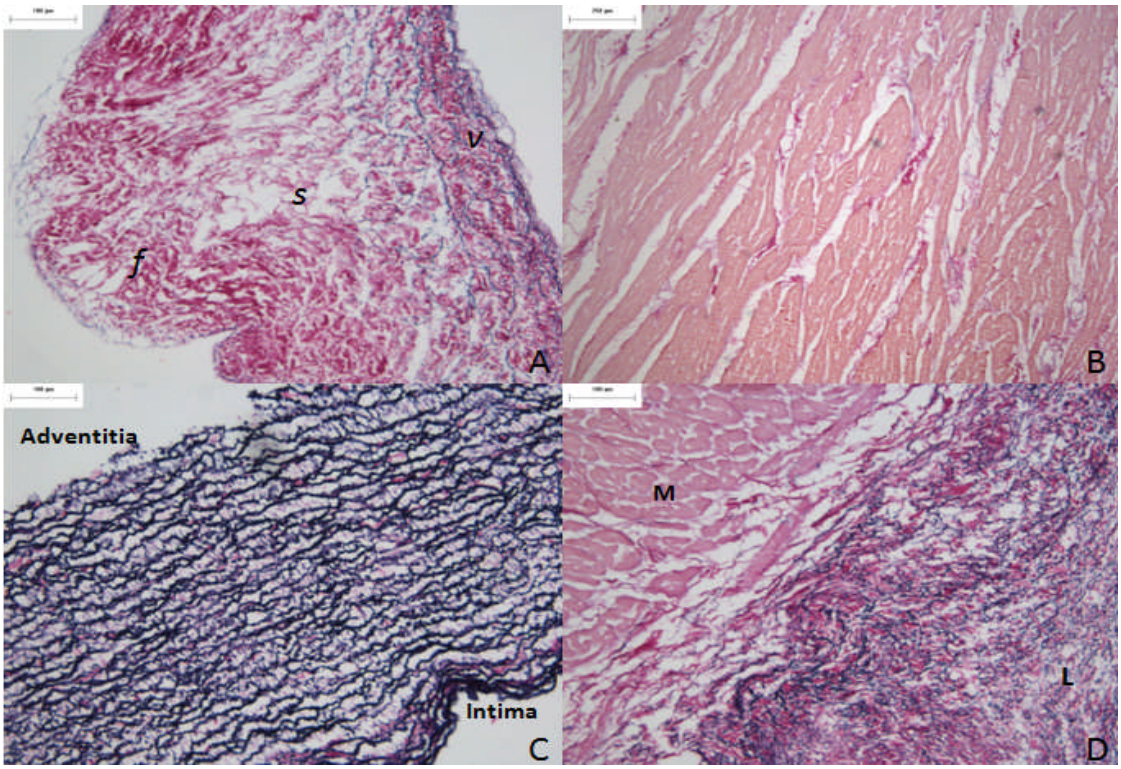

Figure 3.16 Sections of decellularised porcine pulmonary root tissue stained with Miller's (Method 3). (A) Pulmonary valve leaflet, 100 × (*v*: *ventricularis*; *s*: *spongiosa*; *f*: *fibrosa*); **(B)** Myocardium, 40 ×; **(C)** Pulmonary wall, 100 ×; **(D)** Leaflet connection, 100 ×.M: myocardium; L: leaflet. Scale bars are: (A), (C), (D) 100 µm; (B) 250 µm.

3.4.5 Biomechanics of fresh and decellularised (Method 3) porcine pulmonary valve roots

3.4.5.1 Biomechanical evaluation of pulmonary leaflets

Since decellularisation of the porcine pulmonary roots using Method 3 demonstrated complete removal of cells and cell nuclei as determined by H&E and Hoechst staining with no gross changes to the tissue histoarchitecture, it was decided to determine whether Method 3 had any effects on the biomechanical properties of the tissue. Therefore, circumferential and radial leaflet specimens were dissected from fresh pulmonary roots and pulmonary roots treated with Method 3 and subjected to uniaxial tensile loading to failure. The methodology followed for these tests has been described in Sections 2.2.10 and Section 3.3.4.

The mean stress-strain behaviour of the fresh and decellularised (Method 3) leaflet groups is illustrated in Figure 3.17 (circumferential) and Figure 3.18 (radial). The curves demonstrated the typical quasi-linear characteristics with a low modulus region during the elastin phase and a high modulus region during the collagen phase until the tissue failed. The analysis of the results showed no significant difference between the fresh and acellular groups for the following parameters: the elastin phase slope in circumferential and radial directions (Figure 3.19), the collagen phase slope in the circumferential and radial directions (Figure 3.20), the transition stress in the circumferential and radial directions (Figure 3.21), the transition strain in the circumferential and radial directions (Figure 3.22), the failure stress in the circumferential direction (Figure 3.23), the failure strain in the circumferential and radial directions (Figure 3.24), and the thickness of pulmonary leaflets in the circumferential and radial directions (Figure 3.25). The results indicated a significant decrease ($p<0.05$) in the failure stress of the decellularised radial leaflet (Figure 3.23).

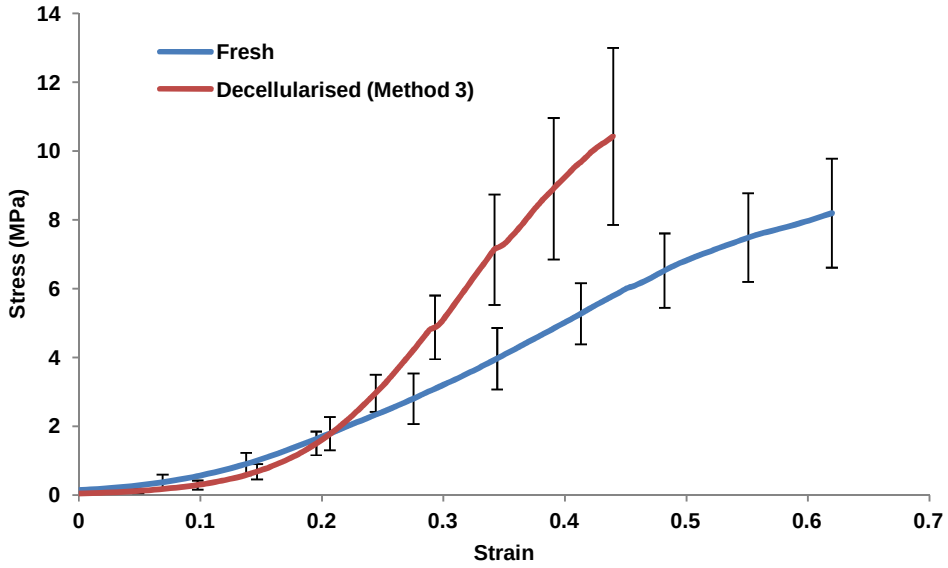

Figure 3.17 Mean stress-strain behaviour of the fresh (n=6) and decellularised (n=5; Method 3) circumferential leaflet groups. The error bars indicate the 95% C.I.s.

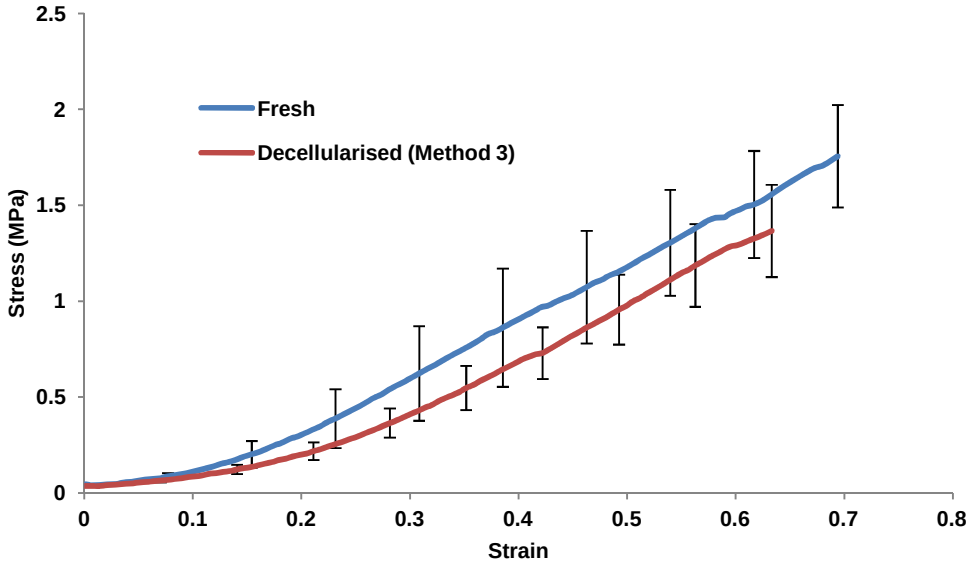

Figure 3.18 Mean stress-strain behaviour of the fresh (n=6) and decellularised (n=5; Method 3) radial leaflet groups. The error bars indicate the 95% C.I.s.

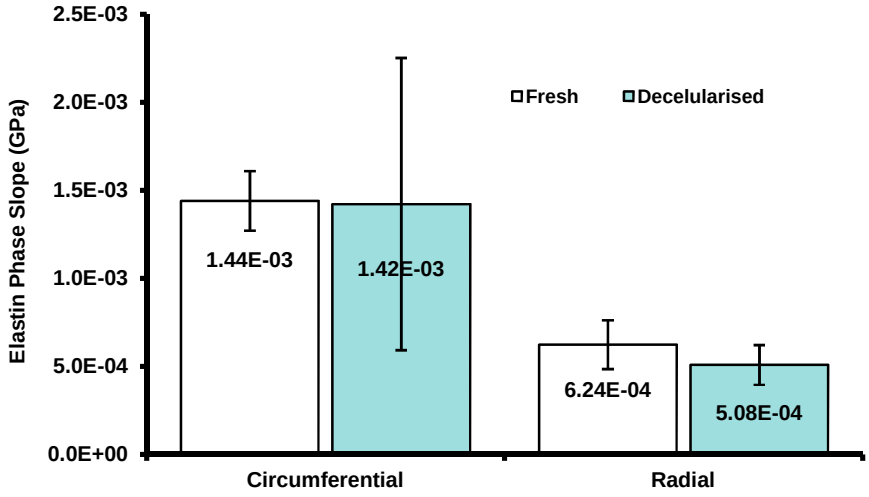

Figure 3.19 Elastin phase slope for the fresh and decellularised (Method 3) leaflets tested in the circumferential and radial directions. The error bars indicate the 95% C.I.s. Fresh circumferential and radial groups and decellularised radial group: n=6; decellularised circumferential group: n=5. The data was analysed using the student t-test, which showed no significant difference between fresh and decellularised tissue.

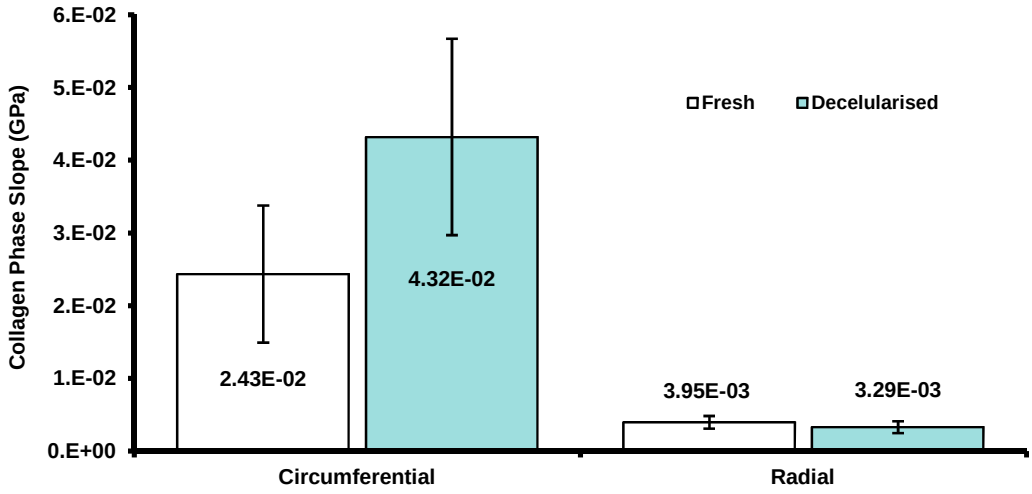

Figure 3.20 Collagen phase slope for the fresh and decellularised (Method 3) leaflets tested in the circumferential and radial directions. The error bars indicate the 95% C.I.s. Fresh circumferential and radial groups and decellularised radial group: n=6; decellularised circumferential group: n=5. The data was analysed using the student t-test, which showed no significant difference between fresh and decellularised tissue.

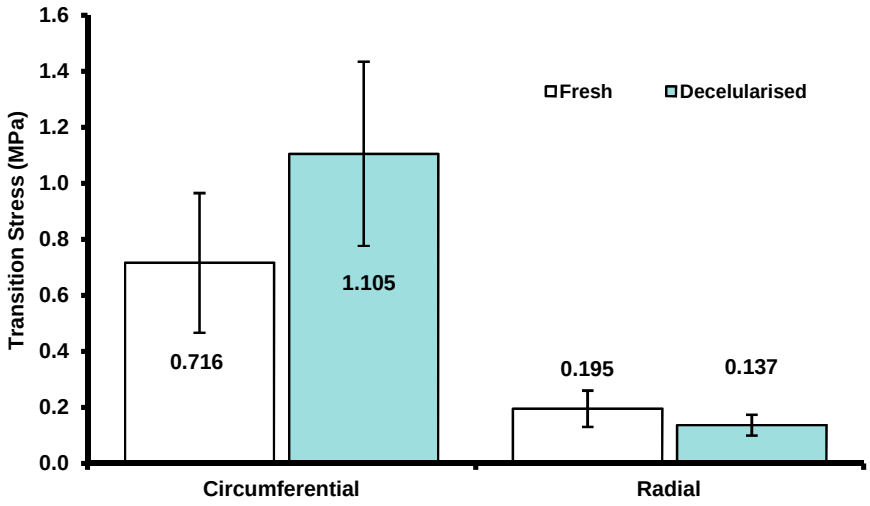

Figure 3.21 Average transition stress for the fresh and decellularised (Method 3) leaflets tested in the circumferential and radial directions. The error bars indicate the 95% C.I.s. Fresh circumferential and radial groups and decellularised radial group: n=6; decellularised circumferential group: n=5. The data was analysed using the student t-test, which showed no significant difference between fresh and decellularised tissue.

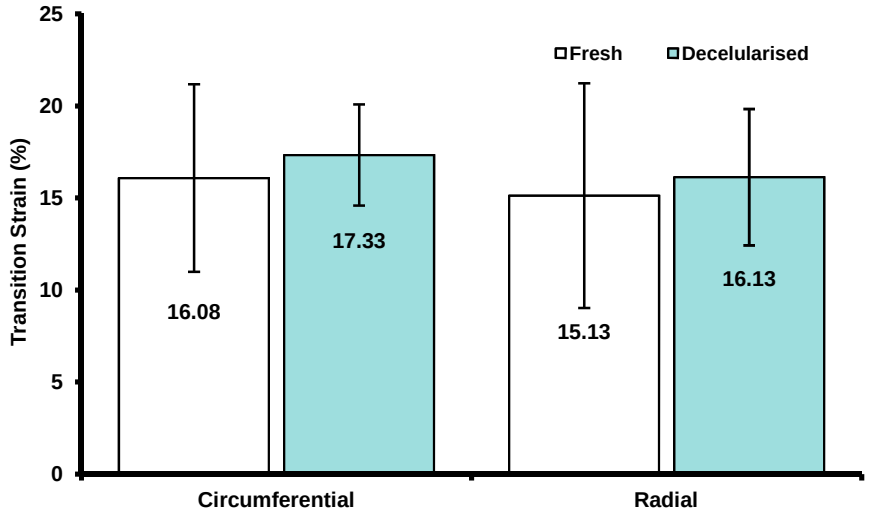

Figure 3.22 Average transition strain for the fresh and decellularised (Method 3) leaflets tested in the circumferential and radial directions. The error bars indicate the 95% C.I.s. Fresh circumferential and radial groups and decellularised radial group: n=6; decellularised circumferential group: n=5. The data was analysed using the student t-test, which showed no significant difference between fresh and decellularised tissue.

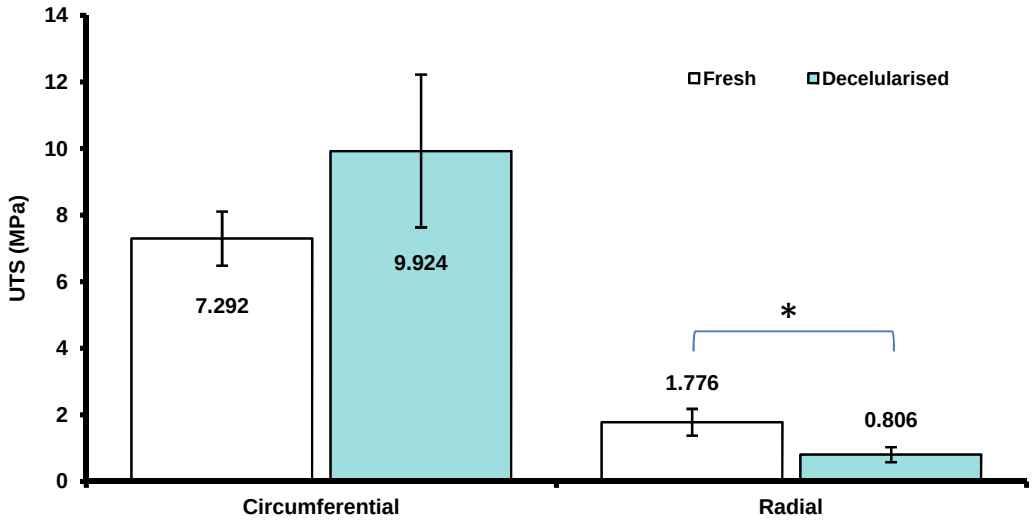

Figure 3.23 Average ultimate tensile stress for the fresh and decellularised (Method 3) leaflets tested in the circumferential and radial directions. The error bars indicate the 95% C.I.s. Fresh circumferential and radial groups and decellularised radial group: n=6; decellularised circumferential group: n=5. The data was analysed using the student t-test, which showed no significant difference in the circumferential direction fresh and decellularised groups, and a significant different in the radial direction (p=0.037).

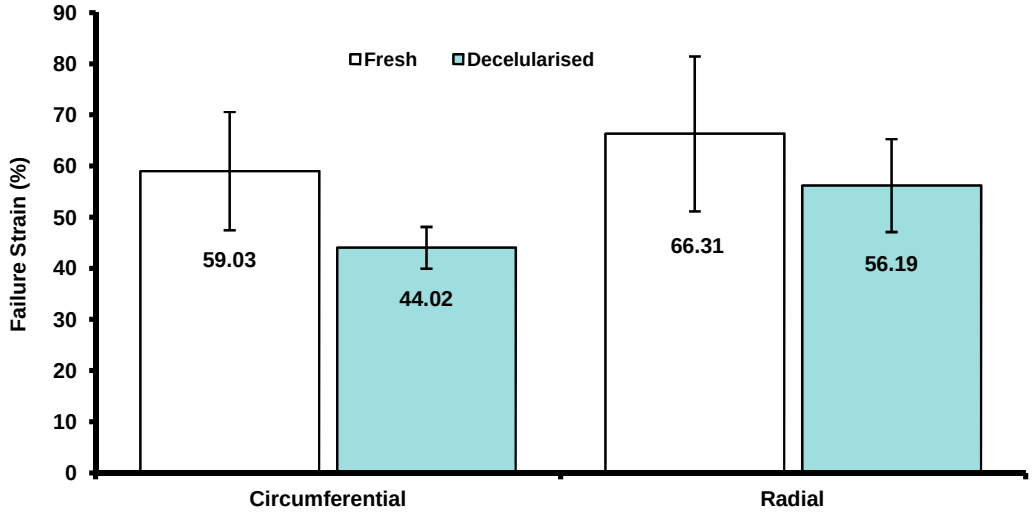

Figure 3.24 Average failure tensile strain for the fresh and decellularised (Method 3) leaflets tested in the circumferential and radial directions. The error bars indicate the 95% C.I.s. Fresh circumferential and radial groups and decellularised radial group: n=6; decellularised circumferential group: n=5. The data was analysed using the student t-test, which showed no significant difference between fresh and decellularised tissue.

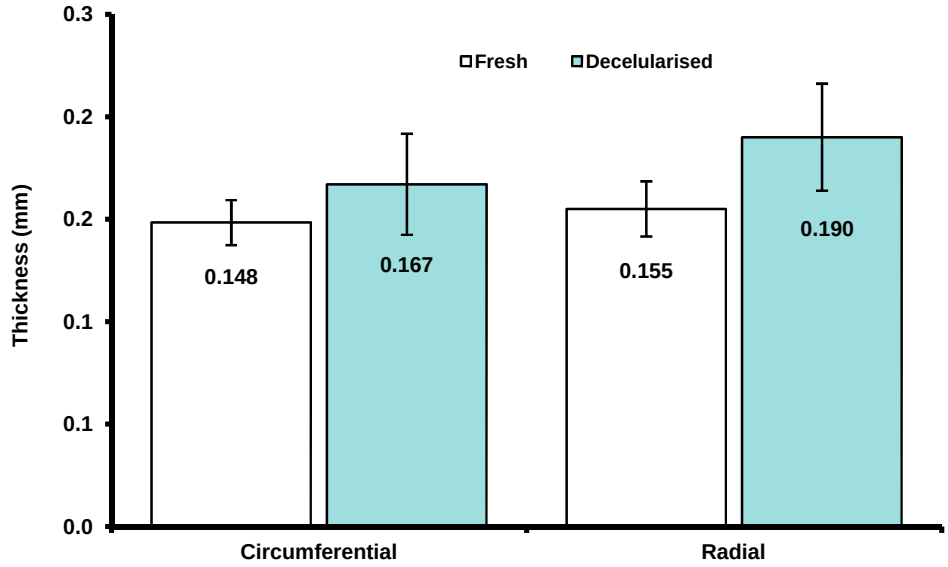

Figure 3.25 Average thickness for the fresh and decellularised (Method 3) leaflets tested in the circumferential and radial directions. The error bars indicate the 95% C.I.s. Fresh circumferential and radial groups and decellularised radial group: n=6; decellularised circumferential group: n=5. The data was analysed using the student t-test, which showed no significant difference between fresh and decellularised tissue.

3.4.5.2 Biomechanical evaluation of pulmonary artery

Uniaxial tensile loading to failure was also used to evaluate the changes in the mechanical behaviour of the porcine pulmonary artery tissue after decellularisation according to Method 3. According to this decellularisation method, the pulmonary artery was peeled of an external layer before SDS treatment. The pulmonary artery therefore had no adventitial layer during the decellularisation, which was a physical change that could directly affect the mechanical properties of the tissue. Thus, three groups were investigated to fully understand the mechanical changes to the pulmonary artery tissue after decellularisation: a fresh group (circumferential group: n=7; axial group: n=6), a peeled fresh group (circumferential and axial group: n=6) and a decellularised group (circumferential group: n=6; axial group: n=9).

The porcine pulmonary arteries mean stress-strain behaviours are illustrated in Figure 3.26 and Figure 3.27. The curves showed similar characteristics to the valve leaflet samples, with a low modulus region during the elastin phase and a high modulus region during the collagen phase. The results for the elastin phase slope, collagen phase slope,

transition stress and strain, failure stress and strain, and the average thickness for control and test groups are illustrated in Figure 3.28 through to Figure 3.34.

There was no significant difference among the three groups for the following parameters: the transition stress in the circumferential and axial directions (Figure 3.30), the transition strain in the circumferential direction (Figure 3.31), the failure stress in the axial direction (Figure 3.32), the failure strain in the circumferential direction (Figure 3.33) and the thickness in the circumferential direction (Figure 3.34). Significant differences were found in: the elastin phase slope between the fresh group and the decellularised group in the circumferential and the axial directions (Figure 3.28), the collagen phase slope between the fresh and peeled group in the circumferential direction and axial directions (Figure 3.29), the transition strain between the fresh group and the decellularised group in the axial direction (Figure 3.31), the failure stress between the fresh and peeled group in the circumferential direction (Figure 3.32), the failure stress between the peeled group and the decellularised group in the circumferential direction (Figure 3.32), the failure strain between the fresh group and the peeled group in the axial direction (Figure 3.33), the failure strain between the fresh group and the decellularised group in the axial direction (Figure 3.33), the porcine pulmonary wall thickness between the fresh and the peeled group (Figure 3.34), and the wall thickness between the fresh and decellularised group (Figure 3.34). The only significant difference found between the peeled fresh and the decellularised groups was for the failure stress along the circumferential direction (Figure 3.32).

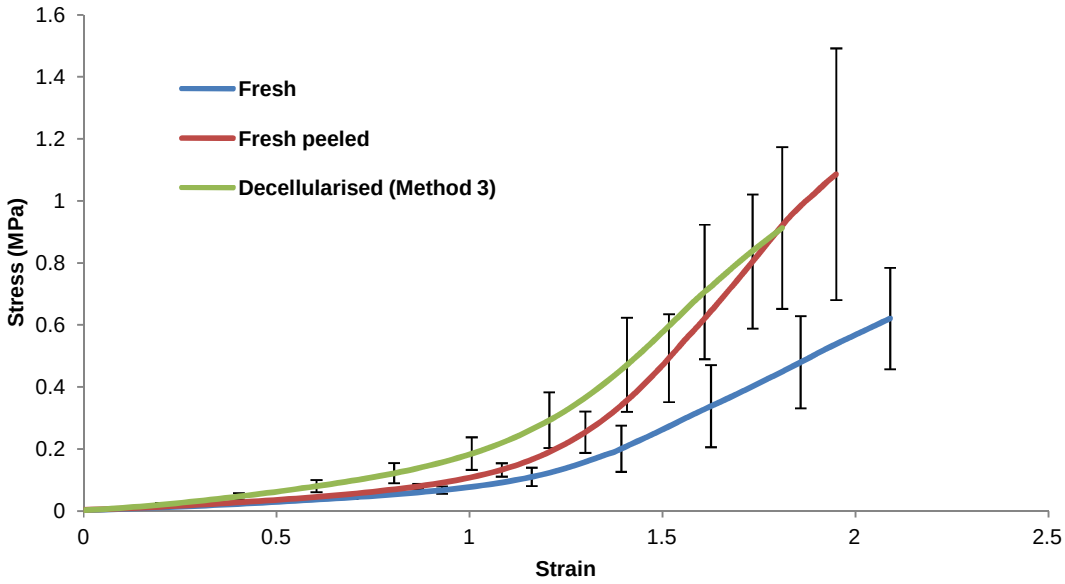

Figure 3.26 Mean stress-strain behaviour for the fresh (n=7), peeled fresh (n=6) and decellularised (n=6; Method 3) circumferential pulmonary artery groups. The error bars indicate the 95% C.I.s.

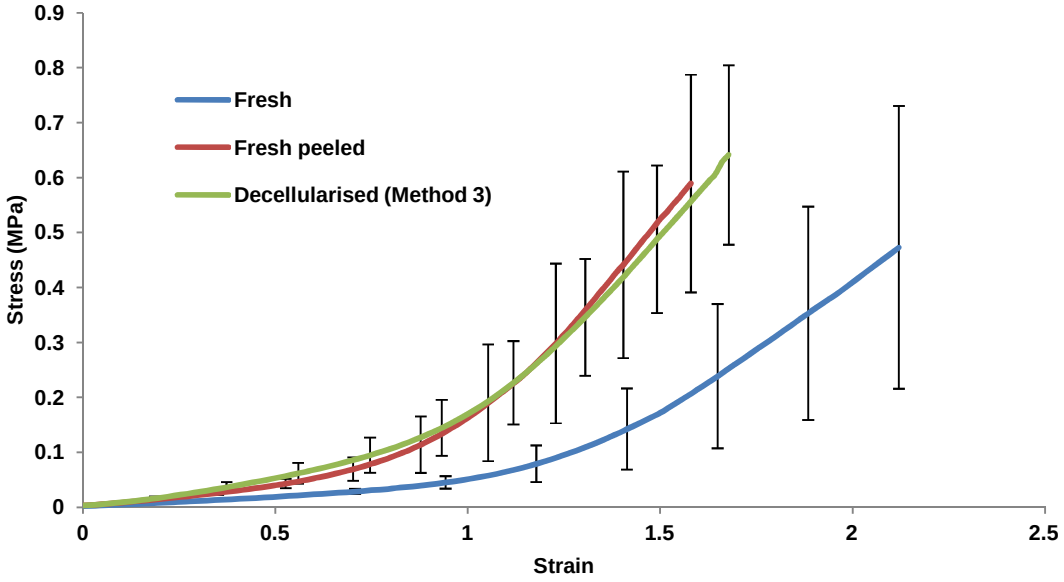

Figure 3.27 Mean stress-strain behaviour for the fresh (n=6), peeled fresh (n=6) and decellularised (n=9; Method 3) axial pulmonary artery groups. The error bars indicate the 95% C.I.s.

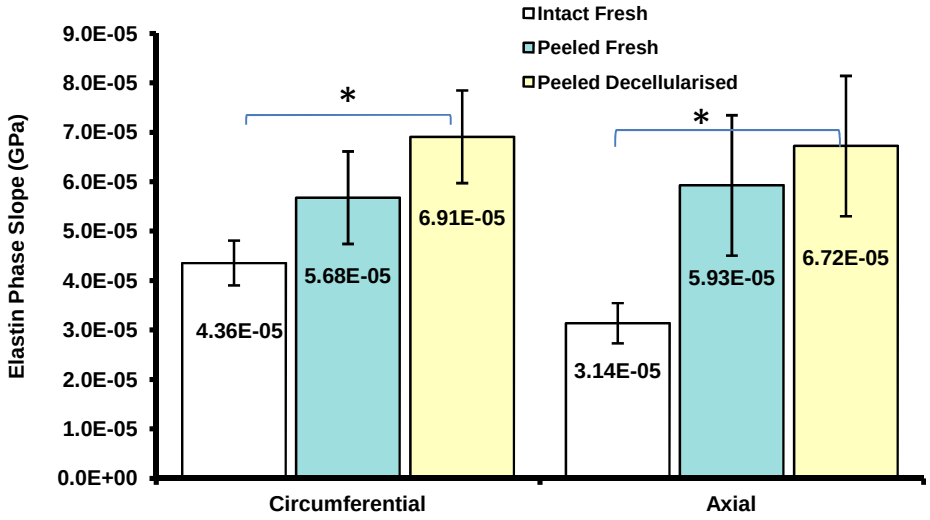

Figure 3.28 Average elastin phase slope for fresh, peeled fresh and decellularised (Method 3) pulmonary artery tested in the circumferential and axial directions. The error bars indicate the 95% C.I.s. Fresh circumferential: n=7; peeled fresh circumferential, decellularised circumferential, fresh axial and peeled fresh axial: n=6; decellularised axial: n=9. Data was analysed using the one way ANOVA that showed no significant difference between the circumferential and axial groups except for the fresh and decellularised groups in both directions. The asterisk indicates significant difference between the marked groups.

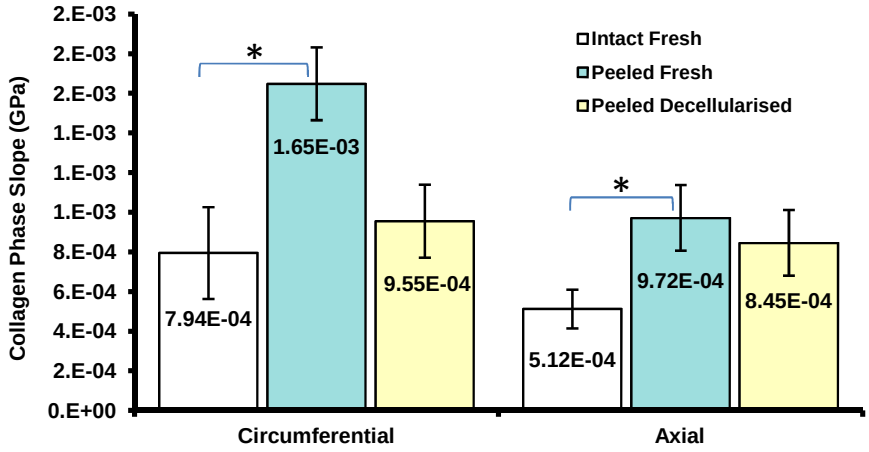

Figure 3.29 Average collagen phase slope for fresh, peeled fresh and decellularised (Method 3) pulmonary artery tested in the circumferential and axial directions. The error bars indicate the 95% C.I.s. Fresh circumferential: n=7; peeled fresh circumferential, decellularised circumferential, fresh axial and peeled fresh axial: n=6; decellularised axial: n=9. Data was analysed using the one way ANOVA test, which showed no significant difference within the circumferential and axial groups except for the fresh and peeled fresh groups in both directions. The asterisk indicates significant difference between the marked groups.

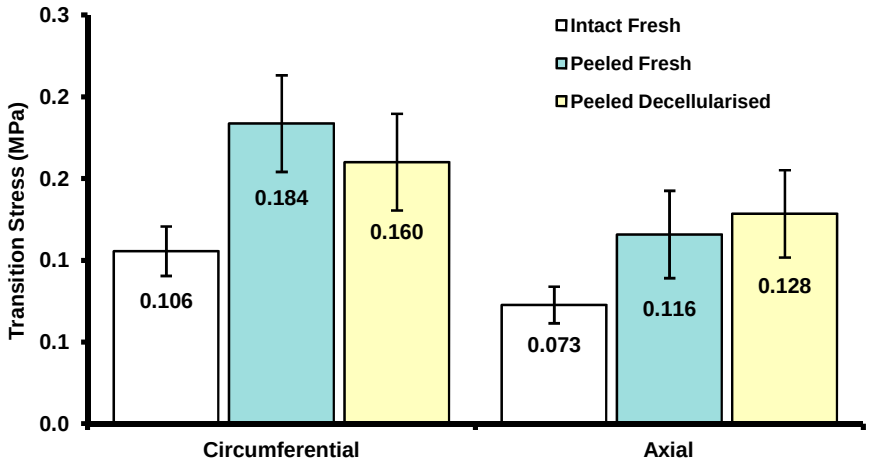

Figure 3.30 Average transition stress for fresh, peeled fresh and decellularised (Method 3) pulmonary artery groups tested in the circumferential and axial directions. The error bars indicate the 95% C.I.s. Fresh circumferential: n=7; peeled fresh circumferential, decellularised circumferential, fresh axial and peeled fresh axial: n=6; decellularised axial: n=9. Data was analysed using one way ANOVA, which showed no significant difference within the circumferential and axial groups.

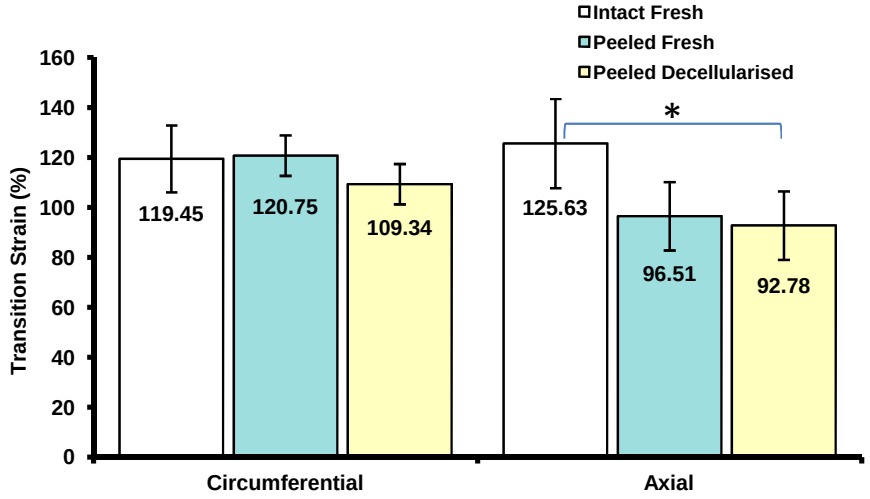

Figure 3.31 Average transition strain for fresh, peeled fresh and decellularised (Method 3) pulmonary artery tested in the circumferential and axial directions. The error bars indicate the 95% C.I.s. Fresh circumferential: n=7; peeled fresh circumferential, decellularised circumferential, fresh axial and peeled fresh axial: n=6; decellularised axial: n=9. Data was analysed using one way ANOVA, which showed no significant difference between the circumferential and axial groups except for the fresh and decellularised groups in the axial direction. The asterisk indicates significant difference between the marked groups.

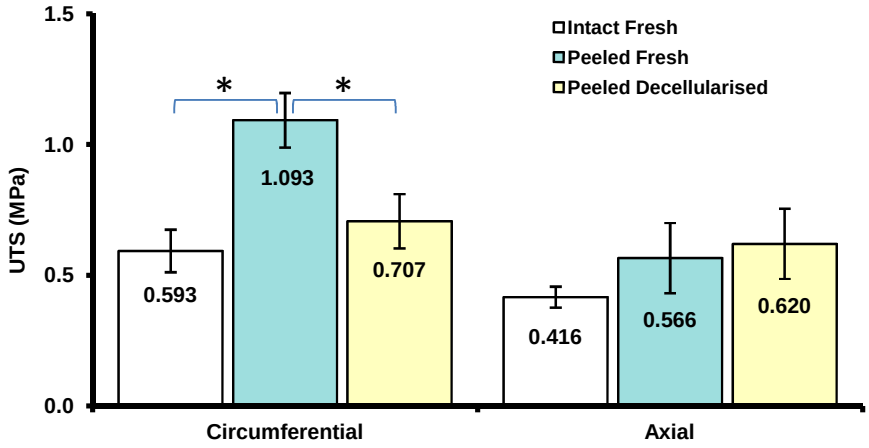

Figure 3.32 Average ultimate tensile stress for fresh, peeled fresh and decellularised (Method 3) pulmonary artery tested in the circumferential and axial directions. The error bars indicate the 95% C.I.s. Fresh circumferential: n=7; peeled fresh circumferential, decellularised circumferential, fresh axial and peeled fresh axial: n=6; decellularised axial: n=9. Data was analysed using one way ANOVA, which showed no significant difference within the circumferential and axial groups except for the fresh and peeled fresh groups, as well as the peeled fresh and the decellularised groups in the circumferential direction. The asterisk indicates significant difference between the marked groups.

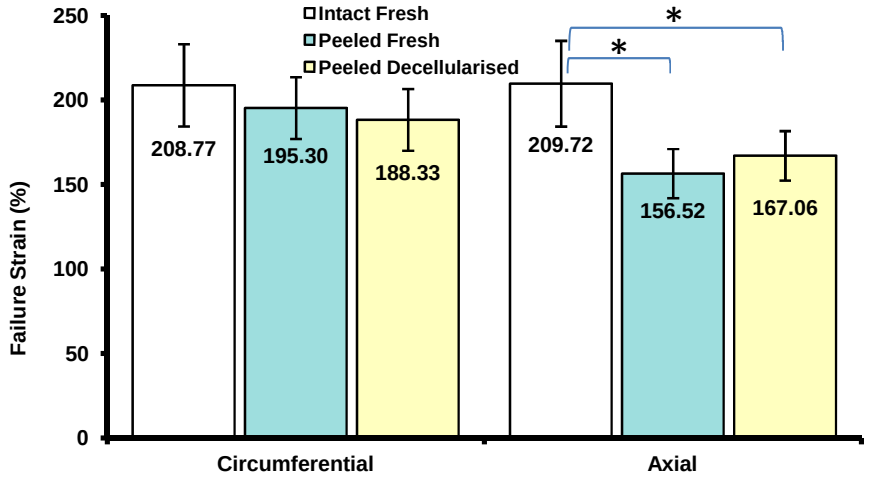

Figure 3.33 Average failure tensile strain for fresh, peeled fresh and decellularised (Method 3) pulmonary artery tested in the circumferential and axial directions. The error bars indicate the 95% C.I.s. Fresh circumferential: n=7; peeled fresh circumferential, decellularised circumferential, fresh axial and peeled fresh axial: n=6; decellularised axial: n=9. Data was analysed using one way ANOVA, which showed no significant difference within the circumferential and axial groups except for the fresh and peeled fresh groups, as well as the fresh and decellularised groups in the axial direction. The asterisk indicates significant difference between the marked groups.

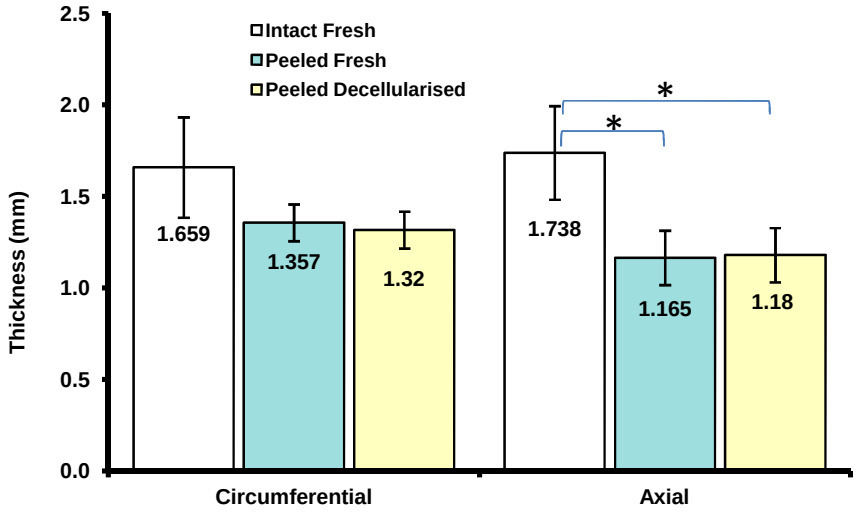

Figure 3.34 Average thickness for fresh, peeled fresh and decellularised (Method 3) pulmonary artery tested in the circumferential and axial directions. The error bars indicate the 95% C.I.s. Fresh circumferential: n=7; peeled fresh circumferential, decellularised circumferential, fresh axial and peeled fresh axial: n=6; decellularised axial: n=9. Data was analysed using one way ANOVA, which showed no significant difference within the circumferential and axial groups except for the fresh and peeled fresh groups, as well as the fresh and decellularised groups in the axial direction. The asterisk indicates significant difference between the marked groups.

3.4.6 Further development of the decellularisation method for porcine pulmonary roots (Method 4)

3.4.6.1Method

The uniaxial tensile results for the porcine pulmonary roots treated with Method 3 demonstrated a significant difference in the failure stress of the circumferential pulmonary artery group compared to the fresh control. Changes were made in the decellularisation method in order to retain the native structure of the pulmonary artery as much as possible. Since peeling of the pulmonary artery introduced physical changes to the pulmonary wall, an alternative solution of carefully scraping the outer surface of the adventitia of the pulmonary artery was introduced in Method 4 to replace the peeling procedure used in Method 3. The connective tissue and fat on the surface of the artery were easy to identify and removed by scraping. No other changes were made for

Method 4 compared to Method 3. Two porcine pulmonary roots were decellularised using method 4.

3.4.6.2 Results

Sections of porcine pulmonary roots were stained with H&E (Figure 3.35) and Hoechst (Figure 3.36) to study the effect of decellularisation using Method 4. No cells or cell residues were observed in the porcine pulmonary valve leaflets, the pulmonary artery or the myocardium (Figure 3.35 & Figure 3.36). The outer surface of the adventitia of the pulmonary artery was clear from cells or cell residues using scraping in Method 4 (Figure 3.35F & Figure 3.36E).

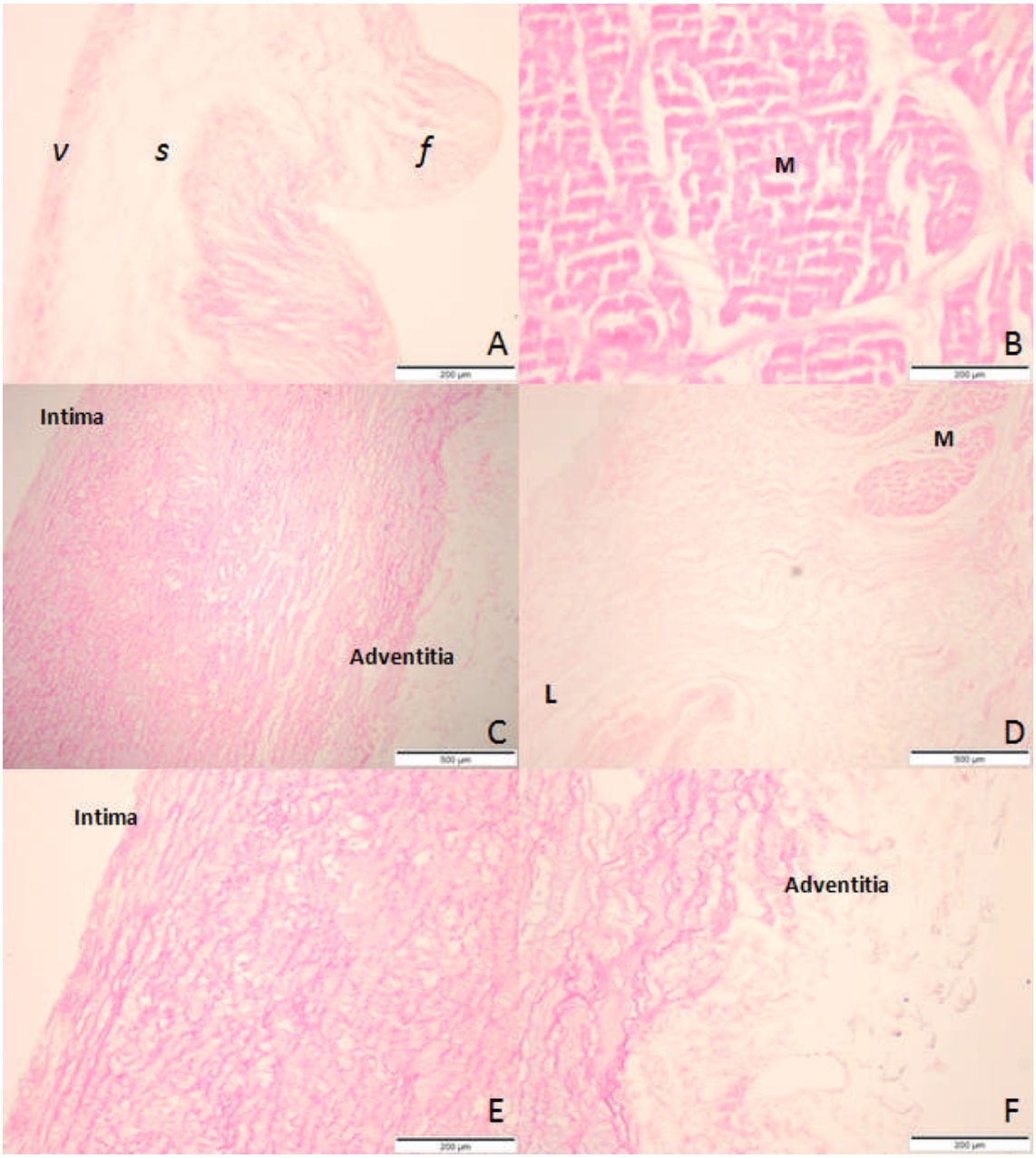

Figure 3.35 Sections of decellularised porcine pulmonary root tissue stained with H&E (Method 4). (A) Pulmonary valve leaflet, 100 × (*v*: *ventricularis*; *s*: *spongiosa*; *f*: *fibrosa*); **(B)** Myocardium, 100 ×; **(C)** Pulmonary wall, 40 ×; **(D)** Leaflet connection, 40 ×; **(E)** The lumen surface of the pulmonary wall, 100 ×; **(F)** The adventitial surface of the pulmonary wall 100 ×. M: myocardium; L: leaflet. Scale bars are: (A), (B), (E), (F) 200 µm; (C), (D) 500 µm.

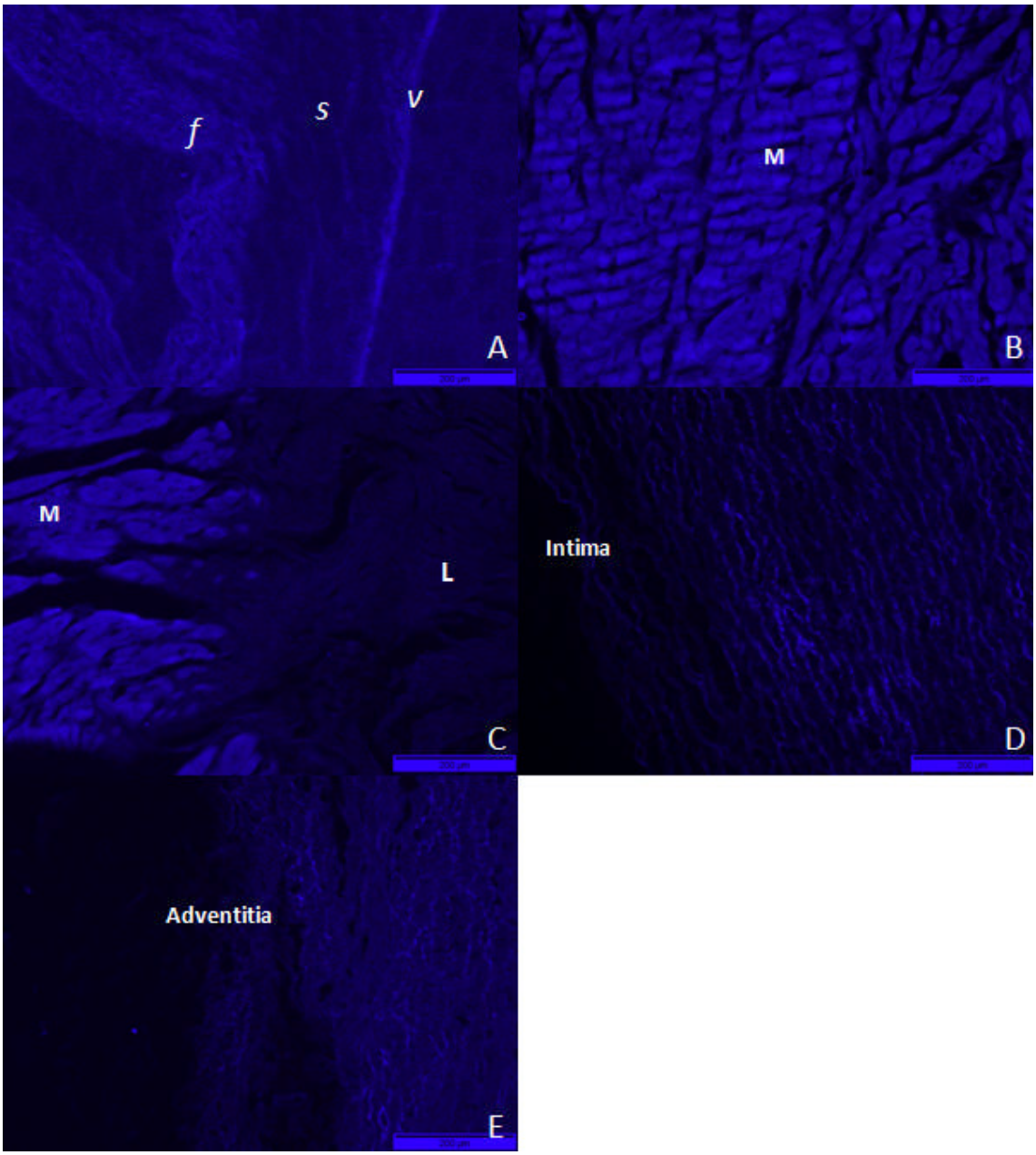

Figure 3.36 Sections of decellularised porcine pulmonary root tissue stained with Hoechst (Method 4). (A) Pulmonary valve leaflet, 100 × (*v*: *ventricularis*; *s*: *spongiosa*; *f*: *fibrosa*); **(B)** Myocardium, 100 ×; **(C)** Leaflet connection, 100 ×; **(D)** The lumen surface of the pulmonary wall, 100 ×; **(E)** The adventitial surface of the pulmonary wall 100 ×. M: myocardium; L: leaflet. Scale bars are: all 250 µm.

3.4.7 Further development of decellularisation method for porcine pulmonary roots (Method 5)

3.4.7.1 Method

Although no cells or cell residues were present in the roots decellularised according to Method 3, significant changes to the biomechanical properties were observed when compared to the fresh roots. Comparing decellularisation Method 3 of the present study and the decellularisation method for aortic roots used in the study by Korossis *et al.* (2002) in which no significant changes were observed for the failure stress after decellularisation, it was apparent that the difference was that Method 3 included another cycle of hypotonic buffer and 0.1 % (w/v) SDS. It was considered that the additional SDS buffer wash might have had an impact on the leaflets' failure stress properties. Changes were made to Method 1 as follows:

a) Instead of peeling an outer layer, the adventitia of the pulmonary artery was carefully scraped with a scalpel blade (since the results from Method 4 showed successful decellularisation of the pulmonary wall with the scraping);
b) Trypsin treatment was only applied on the outer surface of the adventitia of the pulmonary artery and the myocardium bar (considering that application of trypsin paste only on the adventitial surface could be sufficient to achieve complete decellularisation for the relatively thin pulmonary artery wall).

Six porcine pulmonary roots were decellularised using Method 5.

3.4.7.2 Results

Sections of the porcine pulmonary roots were stained with H&E (Figure 3.37) and Hoechst (Figure 3.38) to study the effect of decellularisation using Method 5. All roots were clear of cells in their leaflets, pulmonary arteries and myocardium (Figure 3.37 A, B, C and D, Figure 3.38 A, B, C and D). Regarding to the leaflet connection region, no cells were observed in the H&E stained sections for four out of the six roots that were subject to decellularisation (Figure 3.37E). For the other two roots, H&E staining showed some cell residues in the leaflet connection region (Figure 3.37F). Hoechst staining confirmed this observation. Blue nuclei were identified in the leaflet connection region for 2 out of 6 decellularised roots (Figure 3.35F).

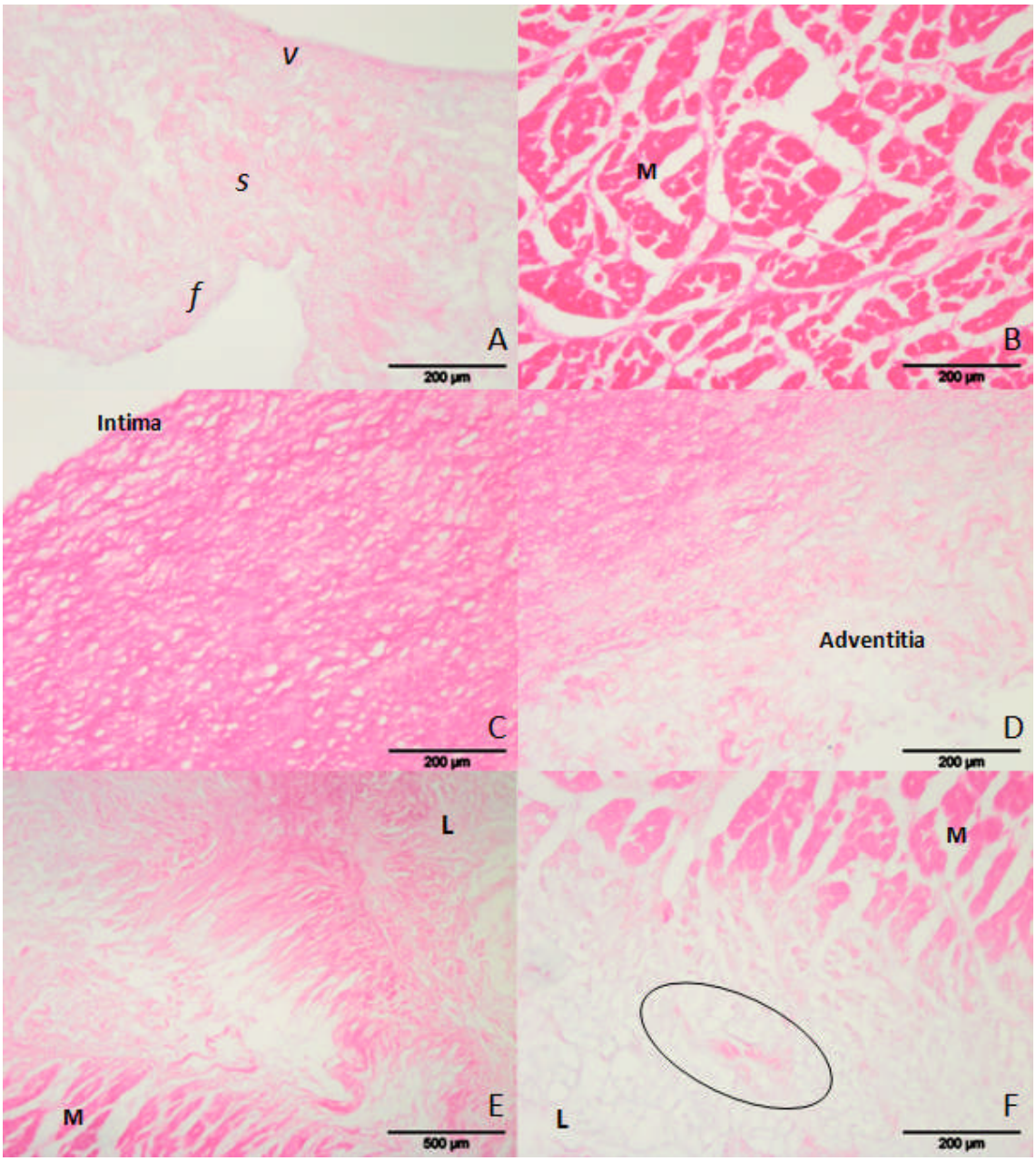

Figure 3.37 Sections of decellularised porcine pulmonary root tissue stained with H&E (Method 5). (A) Pulmonary valve leaflet, 100 × (*v*: *ventricularis*; *s*: *spongiosa*; *f*: *fibrosa*); **(B)** Myocardium, 100 ×; **(C)** The lumen surface of pulmonary wall, 100 ×; **(D)** The adventitial surface of pulmonary wall, 100 ×; **(E)** Leaflet connection, 40 ×; **(F)** Leaflet connection, 100 ×, the circle indicated the area with cell residues presented. M: myocardium; L: leaflet. Scale bars are: all 200 µm, except for (E) 500 µm.

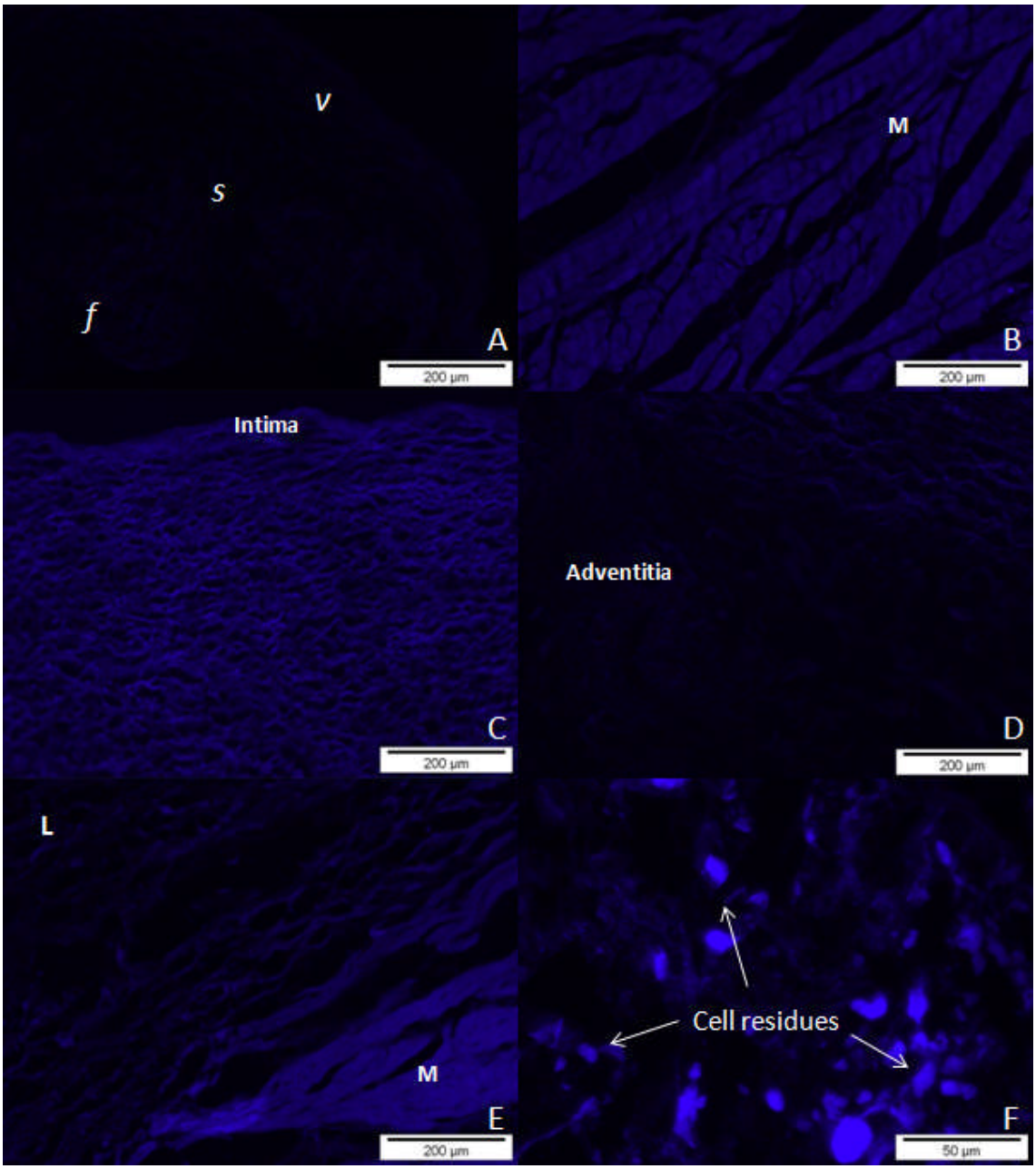

Figure 3.38 Sections of decellularised porcine pulmonary root tissue stained with Hoechst (Method 5). (A) Pulmonary valve leaflet, 100 × (*v*: *ventricularis*; *s*: *spongiosa*; *f*: *fibrosa*); **(B)** Myocardium, 100 ×; **(C)** The lumen surface of the pulmonary wall, 100 ×; **(D)** The adventitial surface of the pulmonary wall 100 ×; **(E)** Leaflet connection, 100 × ; **(F)** Leaflet connection, 400 ×, the arrows indicated cell residues. M: myocardium; L: leaflet. Scale bars are: all 200 µm, except for (F) 50 µm.

3.4.8 Further development of the decellularisation method for porcine pulmonary roots (Method 6)

3.4.8.1 Method

Since no intact cells were identified after decellularisation according to Method 5, but only nucleic residues were recognised in two out of six pulmonary roots, an additional nuclease wash was included in decellularisation Method 6 to completely remove the cell nuclei. Method 6 evolved from Method 5 with the following change: Two continuous 3 h treatments with nuclease buffer were carried out to replace the one 4 h nuclease wash in Method 5. The process is summarised in Figure 3.39. Six porcine pulmonary roots were decellularised according to Method 6.

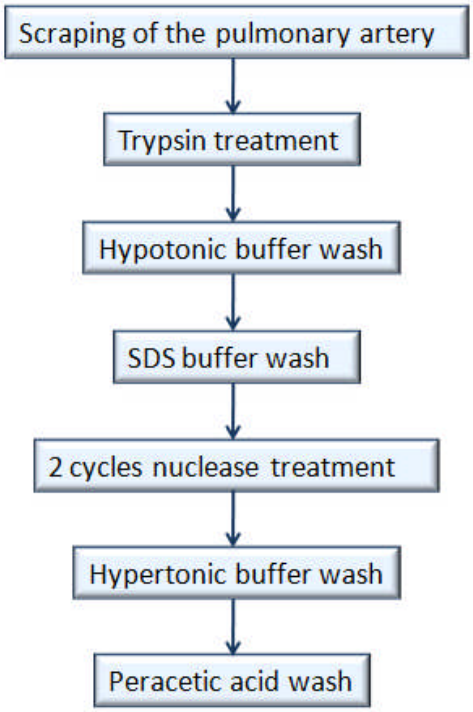

Figure 3.39 Flow diagram of decellularisation Method 6.

3.4.8.2 Results

Sections of the pulmonary roots were stained with H&E (Figure 3.40) and Hoechst (Figure 3.41) to study the effect of decellularisation using Method 6. No cells or cell residues were observed in any of the sections from the 6 porcine pulmonary roots that were subjected to decellularisation (Figure 3.40, Figure 3.41). Complete

decellularisation was achieved using decellularisation Method 6 as indicated by histology.

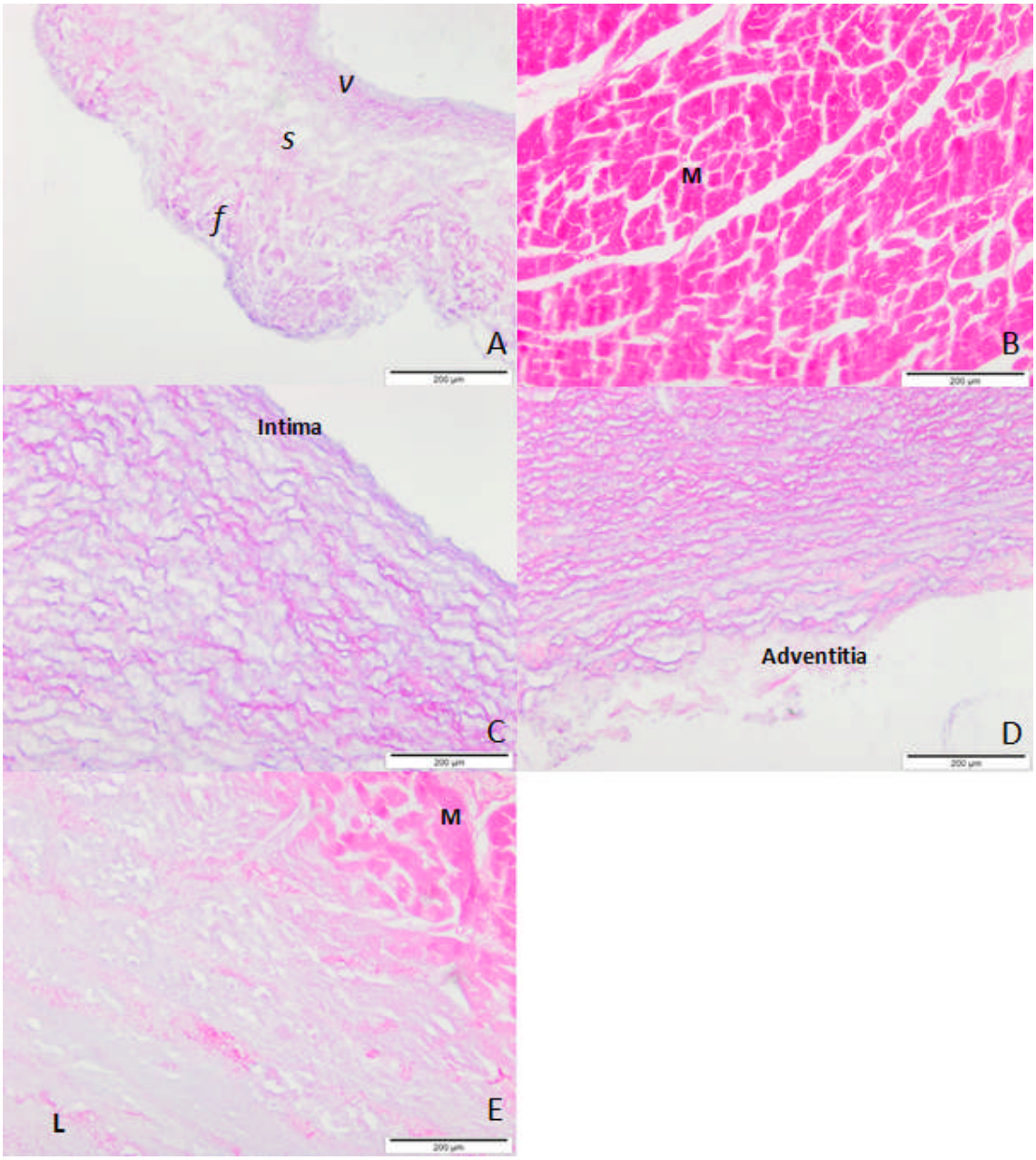

Figure 3.40 Sections of decellularised porcine pulmonary root tissue stained with H&E (Method 6). (A) Pulmonary valve leaflet, 100 × (*v*: *ventricularis*; *s*: *spongiosa*; *f*: *fibrosa*); **(B)** Myocardium, 100 ×; **(C)** The lumen surface of the pulmonary wall, 100 ×; **(D)** The adventitial surface of the pulmonary wall, 100 ×; **(E)** Leaflet connection, 100 ×. M: myocardium; L: leaflet. Scale bars are: all 200 µm.

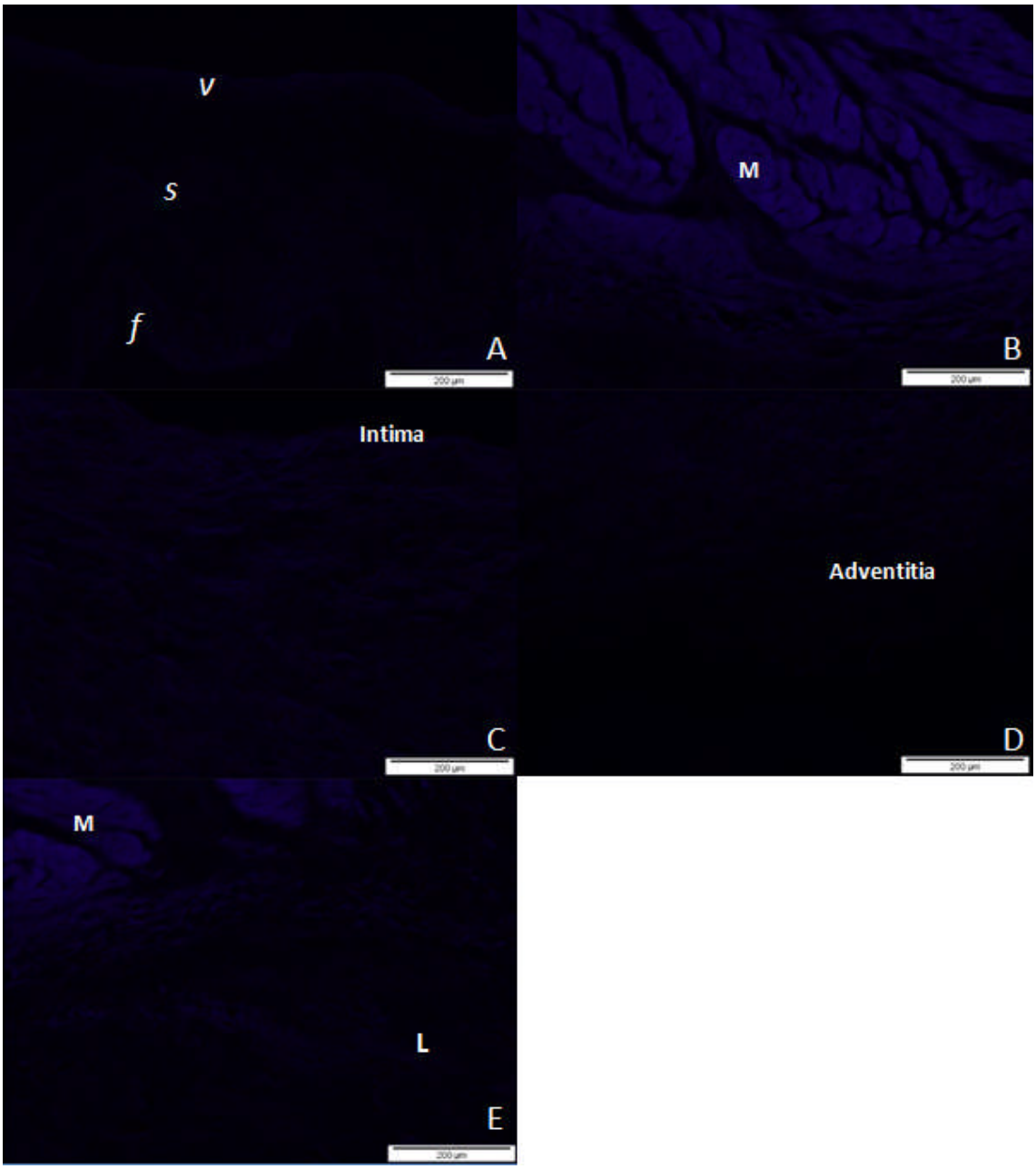

Figure 3.41 Sections of decellularised porcine pulmonary root tissue stained with Hoechst (Method 6). (A) Pulmonary valve leaflet, 100 × (*v*: *ventricularis*; *s*: *spongiosa*; *f*: *fibrosa*); **(B)** Myocardium, 100 ×; **(C)** The lumen surface of the pulmonary wall, 100 ×; **(D)** The adventitial surface of the pulmonary wall, 100 ×; **(E)** Leaflet connection, 100 ×. M: myocardium; L: leaflet. Scale bars are: all 200 µm.

3.4.9 Summary of the decellularisation method development for porcine pulmonary roots

In this study, in total 6 methods were assessed of their decellularisation effects. The differences of these methods concentrated on the following steps: the use of trypsin, the peeling or scraping method applied on the outer layer of the adventitia of the pulmonary arteries, the cycles of hypotonic SDS buffer washes, and the cycles and lengths of nuclease treatments. The other steps in the decellularisation procedure (hypotonic buffer wash, hypertonic buffer wash, and peracetic acid wash) stayed the same for all of the 6 methods used. A summary of the steps that were used differently in the decellularisation methods and the key results are demonstrated in Table 3.3.

Table 3.3 A summary of the steps that were used differently in the decellularisation methods and the accordingly key results.

Method	Pulmonary artery	Trypsin treatment	SDS wash	Nuclease treatment	Results
1	Peeled	Yes	1 ×	1 × 4 h	Cell residues in the leaflet connection area
2	Native	No	2 ×	1 × 4 h	Tissue DNA on the adventitial surface of the pulmonary arteries
3	Peeled	No	2 ×	1 × 4 h	Complete decellularisation, but biomechanical properties changed (significant decreases for failure stresses in the pulmonary leaflets (radial direction) and the pulmonary arteries (circumferential direction))
4	Scraped	No	2 ×	1 × 4 h	Scraping of the pulmonary arteries achieved similar decellularisation result to peeling
5	Scraped	Yes	1 ×	1 × 4 h	2 out of 6 roots had remaining DNA in leaflet connection area
6	Scraped	Yes	1 ×	2 × 3 h	Complete decellularisation

3.5 Discussion

The aim of the work presented in this chapter was to develop a method for the decellularisation of porcine pulmonary roots which retained the histoarchitecture and mechanical integrity of the fresh tissue. Initially, the histology of fresh pulmonary roots was evaluated. Cells were distributed throughout the fresh pulmonary roots. This was revealed by H&E staining, Millers elastin staining and Hoechst staining of pulmonary root sections. In the porcine pulmonary leaflets, the density of connective tissue (red/pink in H&E stain) was much higher in the *fibrosa* and *ventricularis* than that in *spongiosa* of the leaflets. The elastin content was higher in the *ventricularis* compared to the *fibrosa*, probably due to the *ventricularis* directly facing blood flow from the ventricle side, and the high elastin content could absorb the shock from the blood. Elastin fibres were also identified in the pulmonary artery, but they were quite sparse in the myocardium. Similarly, GAG`s were distributed in the leaflets and wall, but could hardly be observed in the myocardium. In the leaflets, the layer containing the most GAG`s was the *spongiosa*. A high content of GAG`s was also present at the base of the leaflets, in the connection area.

In the decellularisation processes used in this study, hypotonic buffer was used to lyse the cells using osmosis. The mode of action of SDS is to solubilise the lipid bi-layer of the cells and form micelles which incorporate the biological membrane and its associated proteins. SDS has been shown to achieve better results in porcine heart valve tissue decellularisation whilst maintaining the histoarchitecture and biomechanical properties of the tissues when compared to a series of other detergents such as triton X-100. Trypsin treatment of the pulmonary wall tissue leads to loosening of the interfibrillar spaces (Bader *et al.*, 1998; Bader *et al.*, 2000), and could also be applied in tissue decellularisation (Kasimir *et al.*, 2003; Leyh *et al.*, 2003). Trypsin treatment was included as an additional step in order to achieve complete decellularisation of the aortic wall (Wilcox *et al.*, 2005). The utilisation of trypsin treatment was also considered in this project to decellularise porcine pulmonary roots. DNAse and RNAse treatment was applied to digest nucleic acids. Hypertonic buffer was used to further remove cellular proteins and α-gal epitopes. The activation of proteases in natural tissues during decellularisation can lead to extensive autolysis of ECM proteins and can cause major damage to the structure and function of the scaffold (Bodnar *et al.*, 1986; Courtman *et al.*, 1994; Pachence, 1996, Walles *et al.*, 2003). Protease inhibitors were thus necessary

in all stages of decellularisation to maintain the ECM components. EDTA was selected to inhibit the matrix metalloproteases, and aprotinin was used as a broad-spectrum inhibitor of serine proteases such as the members of the plasminogen activation cascade (Booth *et al.,* 2002). The protease inhibitors were not applied prior to and during nuclease treatment in order not to compromise the action of nucleases.

Decellularisation Method 1 was based on the method reported by Wilcox *et al.* (2005). This method was developed for the decellularisation of whole porcine aortic roots, and it was based on the decellularisation method reported by Booth *et al.* (2002) for aortic valve leaflet. For leaflets *in situ* in the aortic root, 0.1% (w/v) SDS was sufficient to lyse the cells and 0.03 % (w/v) SDS was sufficient to lyse the cells in excised leaflets which had a second free edge. However, since the aortic wall is much thicker than the leaflet itself, 0.1% (w/v) SDS was not sufficient to lyse all the cells in the whole aortic root (Wilcox *et al.*, 2005). Thus, both 0.1% (w/v) SDS and 2.25×10^4 Unit.ml^{-1} trypsin were used for decellularisation. During trypsin treatment, the leaflets were protected by cotton wool soaked with 50% (v/v) FBS in PBS so that the thin, fragile leaflets were not damaged by trypsin digestion. On the other hand, the cotton wool made it difficult for the enzyme to enter the leaflet root connection area, making it difficult to achieve complete digestion of the connection area. Wilcox *et al.* (2005) made another attempt to decellularise the whole aortic root by thinning the aortic root wall to allow maximal diffusion of SDS and trypsin. The connective tissue layer as well as a thin layer of the valve wall was peeled from the outside using fine tip forceps. This method produced completely decellularised whole aortic roots with excellent leaflet kinematics, hydrodynamic performance, and biomechanical characteristics (Korossis *et al.,* 2005).

Following decellularisation of the porcine pulmonary roots in the present study, four areas of the valve roots were closely observed, namely the leaflet, the wall, the myocardium, and the connection of the leaflet to the root. The first three sites were examined because they represented a particular structure of the root. The latter was selected because it was the thickest site within the whole root, and the most difficult to decellularise, since it was difficult for the detergent or enzymes to enter the central area of the tissue in this region.

Following decellularisation with Method 1, no cells were observed in the leaflets, wall, or myocardium. However, cells or cell residues were observed in the leaflet root

connection area, by the edge of the myocardium. When magnified to 400 ×, the blue stained residues in this area appeared very similar to the cells of the fresh pulmonary root in the same area. To further investigate the extent of decellularisation using this method on pulmonary roots, Hoechst staining was performed. Bright blue fluorescence, representing DNA or its residues, was observed in the same area where the cell nuclei were observed in H&E stained sections.

According to Method 2, which was a modification of Method 1, two cycles of 0.1% (w/v) SDS buffer treatment were applied to improve cell removal in the connection area. Neither peeling of an external layer of the pulmonary artery or trypsin treatment was performed in Method 2, with the consideration that since the pulmonary artery is thinner than the aorta, extra steps in decellularisation might not be necessary for the porcine pulmonary artery. Using Method 2, no cells were observed in the leaflet, pulmonary wall, myocardium, or the leaflet-root connection area. In addition the gross histoarchitecture of the ECM was successfully retained. However, cells or cell residues were observed in regions of the outside surface of the pulmonary wall featuring a 'fluffy' layer of connective tissue. Millers staining showed that connective tissue including elastin was present in this layer. Further Hoechst staining revealed diffuse blue fluorescence in this area, indicating that cells were lysed during decellularisation but that DNA was not totally cleared from this layer. The reason for this was probably because the outside of the pulmonary artery was covered with fat and connective tissue, and trimming during dissection alone did not eliminate it. Owing to this, cellular content was trapped in that region by the connective tissue during decellularisation.

Decellularisation Method 3 was based on Method 2, with the peeling procedure included again in order to remove the connective tissue which trapped the cellular contents. In total six porcine pulmonary roots were decellularised according to Method 3. Histological staining showed no evidence of cells using this method. No cells were observed in H&E stained sections, and no fluorescence was observed after Hoechst staining. Miller's staining results showed no obvious changes in the distribution of elastin, whereas the histoarchitecture of the tissue was well retained. Compared to the histological results reported by Wilcox *et al.* (2005) for decellularised aortic roots, the pulmonary roots decellularised by Method 3 achieved similar results.

Uniaxial tensile testing has been used in the majority of studies on the biomechanical properties of heart valve tissues (Lee *et al.*, 1984a, b; Vesely & Noseworthy, 1992; Stradins *et al*., 2004). Uniaxial tensile testing was carried out on fresh and decellularised (Method 3) porcine pulmonary leaflets and on fresh, peeled fresh and decellularised (Method 3) pulmonary arteries. The reason for adding the additional control group of peeled fresh pulmonary arteries was that the peeling procedure was very likely to affect the mechanical properties of the tissue.

The stress-strain behaviour of porcine pulmonary leaflets and pulmonary arteries demonstrated similar trends to the results described in previous studies (Jennings, 2001; Korossis *et al*., 2002; Stradins *et al*., 2004; Korossis *et al*., 2005; Seebacher *et al*., 2007), with the typical quasi-linear behaviour characterised by a low modulus region during the elastin phase and high modulus region during the collagen phase. The stress-strain properties of the pulmonary leaflets indicated the reduced extensibility and increased strength of the circumferential specimens compared to the radial specimens. This was due to the anisotropy of the valvular tissue inherited by the directionality of the ECM.

The decrease ($p<0.05$) in the failure stress of the decellularised radial leaflet group compared to the fresh control indicated a loss of strength of the leaflets in their radial direction after decellularisation according to Method 3. However, in the results for porcine aortic leaflets reported by Korossis *et al*. (2002), significant differences were only observed for the elastin phase slope in circumferential and radial directions, and the collagen phase slope of the circumferential specimens, but not for the failure stress or strain. The decrease in the failure stress of the radial leaflet group was most likely to have been caused by the additional 0.1 % (w/v) SDS treatment that was used in Method 3.

Method 4 was very similar to Method 3. The only difference was the scraping of the outer surface of the adventitia of the pulmonary artery instead of peeling an external layer prior to decellularisation. The purpose of Method 4 was to test the effect of scraping in the decellularisation of the porcine pulmonary root. The peeling procedure removed connective tissue as well as a layer of the adventitia of the pulmonary artery. Although it has been shown by Korossis *et al.* (2005) that the peeling of aorta did not compromise the strength of the tissue since no significant difference was observed in the failure stress, in the present study a significant difference in the failure stress for the

circumferential direction between the fresh and decellularised (Method 3) pulmonary arteries was found. One reason for the different result between the porcine aorta and the porcine pulmonary artery was because the pulmonary artery is naturally thinner than the aorta, so peeling a layer could have removed a larger portion of the pulmonary artery wall. Hence, the mechanical properties of the acellular pulmonary artery were affected more by the removal of a larger portion of the wall. Another reason could have been that the peeling was not consistent. It was really difficult to control the tissue thickness to be peeled. Peeling techniques would also vary from person to person. Following decellularisation using Method 4, no cells or cell residues were identified from both H&E staining and Hoechst stained sections. Special attention was paid to the adventitial surface of the pulmonary artery, where cell nuclei were likely to be trapped if no peeling was carried out (Method 2). No fluorescence was observed upon Hoechst staining. Decellularisation according to Method 4 confirmed the success in removing cell components by scraping the adventitia of the porcine pulmonary arteries. However, no further evaluation of the acellular scaffold was carried out since it was realised that the two cycles of 0.1 % (w/v) SDS would still damage the pulmonary valve leaflets.

Decellularisation Method 5 was developed with purpose view to retaining the leaflet biomechanical properties as much as possible after decellularisation. In Method 5, the scraping technique that was included in Method 4 was applied because of its success in removing the cellular components trapped on the outer surface of the adventitia of the pulmonary artery. Method 5 also incorporated only one cycle of 0.1 % (w/v) SDS buffer wash in order to minimise the effect on the leaflet biomechanics. Scraping and trypsin treatment were utilised to aid decellularisation of the pulmonary artery and the leaflet connection. In the six roots that were subject to decellularisation according to Method 5, histology showed complete decellularisation of the leaflets, pulmonary arteries and myocardium bars for all roots. However, Hoechst staining indicated that two out of the six roots treated featured cell nucleic residues in their leaflet connection regions. The reason that two roots out of the six were not completely decellularised was probably due to the increased size of these roots or due to the pulmonary arteries being thicker compared to the other four roots.

Since no whole cells were identified after decellularisation with Method 5, but only nucleic residues were recognised in two out of six pulmonary roots, an additional nuclease wash was included in decellularisation Method 6 to completely remove the cell

nuclei. Complete decellularisation was achieved using decellularisation Method 6 according the histology results. All of the six roots were decellularised with their histoarchitectures well retained as shown in the Figure 3.40 and Figure 3.41. Further characterisation of the decellularised porcine pulmonary roots according to Method 6 will be discussed in subsequent chapters.

3.6 Conclusion

A decellularisation method for porcine pulmonary valve root was developed based on the original method described by Wilcox *et al.* (2005). The method with two cycles of 0.1 % (w/v) SDS buffer washes and peeling of the pulmonary artery (Method 3) achieved complete decellularisation. Although the histoarchitecture of the tissue was retained after decellularisation, uniaxial tensile testing to failure indicated a significant decrease ($p<0.05$; t-test) in the failure stress of the decellularised radial leaflet and circumferential wall groups compared to the fresh control. No significant differences were observed in the other biomechanical parameters between treated and native leaflet and pulmonary wall tissues ($p \geqslant 0.05$). Another method which achieved complete decellularisation of the whole porcine pulmonary root was developed using trypsin treatment on the scraped adventitia of the pulmonary artery, one cycle of 0.1 % (w/v) SDS buffer wash and two cycles of nuclease buffer washes (Method 6). H&E and Hoechst staining results showed complete decellularisation. Further evaluation of decellularisation Method 6 will be discussed in Chapter 4 and Chapter 5.

Chapter 4

Biological Characterisation of Fresh and Acellular Porcine Pulmonary Valve conduits

4.1 Introduction

The acellular porcine pulmonary root scaffold produced by decellularisation should ideally be biocompatible with complete cell removal and retention of the ECM. The porcine pulmonary root scaffold should also not be immunogenic when used in human transplantation. Thus it was important to assess the extent of decellularisation and removal of major antigens. The decellularisation procedure designed for cell removal however has the potential to alter the native histoarchitecture and composition of the ECM. The detergents and enzymes remaining in the scaffold after decellularisation could also be toxic to cells. Should this happen, the function of the scaffold (such as the support of cell repopulation) could be compromised and hence could negate the advantages gained by the use of natural scaffolds. Therefore, following the production of the decellularised porcine pulmonary roots, the biological characteristics of the scaffolds required investigation for: (i) the extent of cell and cellular component removal, (ii) the retention of ECM components, and (iii) the biocompatibility of the scaffold.

The determination of the extent of DNA removal following decellularisation has been considered very important in the assessing of the success of a decellularisation method. The removal of DNA can be qualitatively assessed by histological staining (i.e. Hoechst staining) and/or determination of the residual DNA content in tissue (Gilbert *et al*., 2009; Boer *et al*., 2011). DNA represents an easy quantifiable integral part of the cell. Thus, the determination of residual DNA content in decellularised tissue can provide understanding of cell removal. Moreover, porcine DNA remnants have been suggested to be immunogenic following the implantation of porcine derived scaffolds (Zheng *et al*., 2005; Lotze *et al*., 2007, Nagata et al., 2010). It was unlikely that the decellularisation process would, however, remove 100 % of the total DNA. Previous studies have shown that trace amounts of DNA are present in experimental and commercially available naturally derived scaffolds (Gilbert *et al*., 2009; Boer *et al*.,

2011; Wilshaw *et al*., 2011). Short lengths of remnant DNA (less than 300 bp) however, are unlikely to be of concern, since they would be subject to degradation via enzymatic breakdown to nucleotides for use by the cells after implantation (Bennett *et al*., 1985; McCoy *et al*., 2004; Gilbert *et al*., 2007; Gilbert *et al*., 2009). On the other hand, the remnant DNA fragments in the decellularised scaffold should not be able to be functional to encode xenogenic cellular protein components.

In addition to DNA, other components from dead cells have been reported to initiate host immune responses (Nagata *et al*., 2010). For the successful production of a tissue-engineered heart valve from porcine material, elimination of any residual inflammatory stimulus in the matrix is crucial. In particular, the α-gal epitope is known to be involved in rejection of xenogeneic organ transplants and causes hyperacute immune reactions since high titres of preformed anti-α-gal antibodies are present in normal humans (Sandrin & McKenzie, 1994; Kobayashi *et al*., 1999). The first decellularised porcine heart valve substitute, SynerGraft, which was commercially introduced in Europe by CryoLife (Kennesaw, GA), failed early in children with disasterous consequences because of a severe inflammatory reaction (Simon *et al*., 2003) which was subsequently shown to be most likely due to incomplete removal of the α-gal epitope by the decellularisation procedure (Kasimir *et al*., 2005).

The detection of particular cytoskeletal components indicative of particular cell types is able to provide supportive evidence for the extent of cell removal following decellularisation. The presence of these components can be determined by immunohistochemical labelling with antibodies. Alpha-SMA, vWF, desmin and vimentin represent the cytoskeleton components of the different cell types in the porcine heart root tissue. Alpha-SMA is present in high amounts in vascular smooth muscle cells. The protein is localised in microfilament bundles of smooth muscle (Skalli *et al*., 1989). vWF is a glycoprotein involved in haemostasis. The basic vWF monomer is a 2050-amino acid protein. It is produced constitutively in endothelium, megakaryocytes, and subendothelial connective tissue, and expressed in membrane and cellular vesicles. Thus, vWF is commonly used as a marker for the detection of endothelial cells (Sadler, 1998). Desmin is a protein of 52 kD which has been identified as the constitutive subunit of the intermediate filaments in skeletal, cardiac, and smooth muscle (Lazarides & Hubbard, 1976; Small & Sobieszek, 1977; Geisler & Weber, 1982; Li *et al*., 1997). In skeletal and cardiac muscles, the staining of desmin is confined to the Z-bands giving a

characteristic striated appearance. Vimentin is a cytoskeletal component in fibroblasts and smooth muscle cells.

The ECM is constantly undergoing remodelling (assembly and degradation). It has a dynamic interaction with the resident cells in response to changes in the microenvironment. The ECM regulates cell behavior by influencing cell proliferation, survival, shape, migration and differentiation (Bornstein & Sage, 2002; Daley *et al*., 2008; Vorotnikova *et al*., 2010; Barkan *et al*., 2010; Crapo *et al*., 2011). It is highly likely that the 3-dimensional structure and composition of the ECM both contribute to these effects. The ECM consists of a complex mixture of structural and functional proteins. The primary components are fibrous structural proteins (e.g. collagens, laminins, fibronectin, vitronectin and elastin), specialised proteins (e.g. growth factors, small matricellular protein) and proteoglycans. The precise composition varies from tissue to tissue (Badylak, 2002; Daley *et al*., 2008).

Collagen is the most abundant ECM protein in mammals. Collagens are synthesized by fibroblasts predominantly, but epithelial cells may also synthesize some collagens. There are at least 30 different collagen genes in the human genome which combine in a variety of ways to create over 20 different types of collagen fibrils (Bateman *et al*., 1996). Collagen types I, II and III which have a long-recognised characteristic fibre bundle structure are the most abundant collagen types. Collagen type IV forms a two-dimensional reticulum and is a major component of the basement membrane. The basic conformation of collagen is the triple-helix structure. This was first deduced from high angle x-ray diffraction studies on collagen type I in tendon (Rich & Crick, 1961; Fraser & MacRae, 1983). Each of the three polypeptide chains in the molecule forms an extended left-handed helix with 3.3 amino acids per turn, which is stablilised by the high imino acid content. The three chains are supercoiled around a common axis in a right-handed way to form the triple-helix. In this helical structure, a glycine residue occurs every third amino acid. Glycine is the smallest amino acid thus allows the close packing along the central axis and hydrogen bonding between the three chains. Therefore, collagens have the general structure of $(\text{Glycine-X-Y})_n$ with X and Y frequently being the amino acids (a.a.) proline and hydroxyproline. The hydroxyproline is important for stabilising the collagen triple helix structure by the formation of extra hydrogen bonds. The number of repeats (n) varies in different collagen types. In the case of the fibrillar collagens, this helix-forming glycine-X-Y repeat is continuous over

the approximately 1000 amino acid length of the three α-chain subunits of the molecule, while the non-fibrillar collagens commonly contain imperfections and non-collagenous interruptions in the helical sequence (Bateman *et al*., 1996).

The elastin molecule is a chemically inert and extremely hydrophobic protein. It is insoluble under most conditions including strong alkali in the fully cross-linked form. This is because at least 60 % of the a.a. side chains in elastin are non-polar. These properties of insoluble elastin make it one of the most stable proteins in the body. Elastic tissues are characterised by their rubber-like properties, including long range extensibility and the capacity to return to their original dimensions when the stress is removed (Gleary & Gibson, 1996). Elastin is secreted from the cells as a soluble protein of 60,000-70,000 molecular weight called tropoelastin. The tropoelastin associates with fibrillin rich microfibrillar components to allow assembly into elastic fibres. These are cross-linked within the ECM to form 3-dimentional networks by the action of copper dependent lysyl oxidase (Ayad *et al*., 1994). Other properties of elastin include promotion of cell adhesion and elastin peptides have been shown to be chemotactic (Ayad *et al*., 1994; Kielty *et al*., 2002).

The GAG`s are an important family of highly functionalised, linear, and negatively charged polysaccharides present in animal tissues which with the exception of hyaluronic acid are covalently bound to a protein core in macromolecular assemblies known as proteoglycans (Yeung *et al*., 2001; Mavrilas *et al*., 2005). GAG`s play important roles in the binding of growth factors and cytokines, water retention, and the gel properties of the ECM. The heparin binding properties of numerous cell surface receptors and of many growth factors (e.g. fibroblast growth factor family, vascular endothelial cell growth factor) make the heparin-rich GAG`s essential components of the ECM as substrates for cell growth (Badylak, 2002; Badylak, 2004). The GAG`s present in the ECM include chondroitin sulfates A and B, heparin, heparin sulphate and keratan sulphate (Entwistle *et al*., 1995; Hodde *et al*., 1996).

Proteoglycans are proteins substituted with at least one GAG chain (Ayad *et al*., 1994; Vogel, 1994). GAG`s in the ECM are linked covalently to a core protein except for the hyaluronan. The number and length of GAG chains attached to a core protein may vary. Proteoglycans of the ECM are generally divided into three categories based on the GAG type: those with chondroitin sulphate or dermatan sulphate chains, those with heparin

sulphate chains, and those substituted with keratan sulphate. The proteoglycans have been shown to be important in the physical behaviour of connective tissues. They confer lubrication either between tissues (joints) or between collagen and elastin fibres (Ayad *et al*., 2004).

The ECM plays an important role in heart valve function in maintaining the normal physical and mechanical properties. The principle ECM components of the native valve are collagen (type I (~74%), type III (~24%), type V (~2%)), elastin and proteoglycans (Taylor *et al*., 2006b). Each component is responsible for the unique physical and mechanical properties for valve function. The heart valve tissue composes of about 50 % collagen and 13 % elastin by dry weight (Bashey *et al*., 1967). Collagen fibrils confer mechanical and tensile strength, but are stiff with limited extensibility. Elastin is highly extensible but has very low stiffness, existing as a sponge-like matrix of fibres and sheets with tubular openings surrounding and interconnecting the collagen fibre bundles. The elastin in the heart valve leaflets maintains the specific wave-like configuration of collagen fibre orientation and returns to its original state after loading (Scot & Vesely *et al*., 1995; Vesely, 1998). The highly negatively charged GAG side chains of the proteoglycans produce a hydrated gel-like substance, which allows interaction with other matrix molecules. In addition, the GAGs are involved in the function and survival of endothelial and possibly other cells (Taylor *et al*., 2006b).

Fibronectin is a multifunctional adhesive protein which has a primary role in cell attachment. It is a large glycoprotein with a size of approximately 450 kDa, and consisting of two chains held together by disulfide bonds (Ramzi *et al*., 1999). Fibronectin exists in a soluble protomeric form in blood plasma and as an insoluble multimeric form in the ECM. It is produced by fibroblasts, chondrocytes, endothelial cells and macrophages as well as certain epithelial cells (Hynes, 1990). Fibronectin contains binding domains for collagen, heparin, some proteoglycans, DNA, hyaluronic acid, and fibrin (Haralson & Hassell, 1995). The cells bind to fibronectin via receptors that recognise the specific amino acid sequence of the tripeptide arginine-glycine-aspartic acid (RGD). The RGD recognition element plays a key role in cell-matrix adhesion (Ramzi *et al*., 1999). These structural domains also provide the chemical basis for the diverse biological functions of fibronectin including the regulation of growth, differentiation, cell shape, and migration, as well as its interactions with other matrix components (Haralson & Hassell, 1995; Magnus *et al*., 1998).

The reaction of the host to the implantation of natural or synthetic materials may be in the form of regeneration or rejection. Failure to remove the reagents used during the decellularisation of the tissue might cause adverse effects such as cytotoxicity and calcification. SDS detergent used in the decellularisation process in this study is cytotoxic as it disrupts cell membranes (Newby *et al*., 2000). EDTA and aprotinin have also been reported to be cytotoxic (Koulaouzidou *et al*., 1999; Rakhi *et al*., 2004). PAA which was used for sterilisation of the decellularised heart roots in this study has also been reported to be a potent cytotoxic disinfectant (Sagripanti & Bonifacino, 2000). To ensure that the reagents used in the decellularisation protocol were removed adequately from the tissues, it would be necessary to carry out *in vitro* biocompatibility tests.

The acellular porcine pulmonary valve plus roots used in all of the studies in this chapter were produced using decellularisation Method 6 (described in Section 3.4.8.1). The extent of decellularisation, the presence and location of ECM proteins and cytoskeletal proteins, the presence of antigenic α-gal epitopes and the *in vitro* biocompatibility of the decellularised porcine pulmonary root scaffold were assessed in this Chapter.

4.2 Aims and objectives

Aims:

The aims of this chapter were to investigate the effects of decellularisation of porcine pulmonary roots using the method developed in Chapter 3 on the biological characteristics of the tissue.

Objectives:

- To determine the effects of decellularisation on the histoarchitecture of the decellularised matrix by comparison with fresh porcine pulmonary roots.
- To determine the effects of decellularisation on the total amount of DNA and the presence of functional DNA by comparison with fresh porcine pulmonary roots.
- To determine the effects of decellularisation on the presence of specific matrix and cytoskeletal proteins by comparison with fresh porcine pulmonary roots.
- To determine the presence of α-gal epitope in the decellularised matrix by comparison with fresh pulmonary roots.
- To determine the biocompatibility of the acellular scaffold using *in vitro* techniques.

4.3 Methods

Decellularisation of porcine pulmonary roots was performed according to the methodology described in Section 3.4.8 (Method 6). Six roots were decellularised and used for histology, immunohistochemistry and investigation of the expression of α-gal. Six roots were decellularised and utilised for DNA extraction and PCR analysis. Another six roots were decellularised and used for contact cytotoxicity (for pulmonary leaflets) and extract cytotoxicity (for pulmonary arteries) analyses.

4.3.1 Histology

Histology was used to determine the histoarchitecture of the decellularised porcine pulmonary heart valve conduits. Tissue samples from six decellularised roots from different animals were fixed with 10 % (v/v) NBF for 24 to 48 h. Histological evaluation was performed as described in Section 2.2.7. Tissue sections of 10 µm were prepared longitudinally such that the leaflet, pulmonary artery and myocardium all appeared on the same tissue section. At least 10 sections were collected every 20 sections, and these sections were all examined by histology to study the effects of decellularisation. The H&E stain was used to study the tissue architecture and cell distribution. The Hoechst stain was performed to locate cell nuclei or DNA residues in the tissue. Miller's stain was used to identify the distribution of elastin in the tissue. The Alcian blue stain was used to identify the GAG`s in tissue. The slides were viewed using light microscopy or fluorescent microscopy with a DAPI filter.

4.3.2 DNA quantification

DNA quantification was used to determine the total remaining DNA in porcine pulmonary roots following decellularisation. By comparing the DNA levels in decellularised and the fresh tissue, the efficiency of DNA removal by the decellularisation process could be determined. The greater extent of DNA removal during decellularisation the better, however, it is very difficult to remove 100 % of DNA from the tissue. During decellularisation, the porcine DNA was cleaved into small fragments by nuclease treatment and fragments removed by the wash procedures. A small amount of remaining DNA was acceptable as long as it did not contain any coded functional genes which might be introduced into the patient following implantation. The effect of decellularisation on DNA removal was therefore further assessed by PCR

using selected functional genes as targets. This was to determine if the remaining DNA in the tissue after decellularisation contained any large fragments of DNA that may have been functional.

4.3.2.1 DNA extraction

DNA was extracted from fresh and decellularised porcine pulmonary roots using a commercially available DNeasy blood and tissue kit from QIAgen.

DNA was extracted from tissues from six fresh and six decellularised porcine pulmonary roots. DNA was extracted from 4 different regions (leaflet, pulmonary artery, myocardium, and leaflet connection) of the porcine pulmonary roots. For each region from each root, triplicate samples were taken for DNA extraction.

Each sample consisted of 25 mg tissue, which was macerated using a scalpel blade and placed in a sterile 1.5 ml microcentrifuge tube. Buffer ATL (180 µl) and proteinase K (20 µl), both from the QIAgen kit, were mixed with the macerated tissue by vortexing, and incubated at 56 °C for three hours or until the tissue was completely digested. Pulse vortexing (5 to 10 s) was performed every 30 min to disperse the sample. Each sample was vortexed for 15 s at the end of the incubation. Buffer AL (200 µl) from the QIAgen kit was added to the sample, and mixed thoroughly immediately by vortexing and 200 µl of ethanol (100 %, v/v) was added, and mixed thoroughly immediately by vortexing. Each sample was transferred to a separate DNeasy Mini spin column placed in a 2 ml collection tube, and centrifuged at 6,000 × g for 1 min. The flow-through was discarded together with the collection tube. The DNeasy Mini spin column was placed in a fresh 2 ml collection tube, and Buffer AW1 (500 µl) was added to the column. The DNeasy membrane at the bottom of the DNeasy Mini spin column was dried by centrifuging at 15,000 × g for 3 min. The flow-through was discarded together with the collection tube. The DNeasy Mini spin column was placed in a clean 1.5 ml microcentrifuge tube, and Buffer AE (200 µl) was added directly to the centre of the DNeasy membrane. After incubation for 1 min, the 1.5 ml microcentrifuge tube was centrifuged for 1 min at 6,000 × g to elute. The extracted DNA was in Buffer AE in the flow-through. The DNeasy Mini spin column was discarded. The extracted DNA was subjected to quantification immediately or stored at – 20 °C until needed.

4.3.2.2 DNA quantification by spectrophometry

The concentration of extracted DNA was determined spectrophometrically using a Nanodrop spectrophotometer. Buffer AE (2 µl) was used as a blank. Extracted DNA sample (2 µl) was loaded onto the Nanodrop, and the absorbance was determined at 260 nm. Three readings were taken for each sample, and the mean was considered as the absorbance of the sample. The DNA concentration ($ng.\mu l^{-1}$) in the sample was directly displayed in the Nanodrop software. This concentration was used to calculate the DNA weight/tissue weight (µg/mg) according to:

$$\text{DNA weight/tissue weight } (\mu g/mg) = \frac{C \times 200}{25 \times 1000}$$

where *C* represents the DNA concentration in the Buffer AE ($ng.\mu l^{-1}$). The volume of the Buffer AE containing extracted DNA was 200 µl. The total weight for each tissue sample was 25 mg.

The mean ± 95 % C.I. of the DNA weight/tissue weight ($\mu g.mg^{-1}$) for each region of fresh (n=6) or decellularised (n=6) tissue was calculated.

4.3.2.3 Polymerase chain reaction (PCR)

4.3.2.3.1 Target genes and primers

The presence of four functional genes in fresh and decellularised porcine pulmonary roots was studied: glyceraldehyde 3-phosphate dehydrogenase (GAPDH), swine leukocyte antigen 2 (SLA-2), β 2-microglobulin and β actin. The complete or partial coding sequences were obtained from the nucleotide database (http://www.ncbi.nlm.nih.gov/nuccore). The coding sequences used in this study are listed in Appendix 1. Primers were designed using Primer 3 programme (Version 0.4.0) to have a product length of 150 to 250 base pairs (bp). All primers were custom-made by Sigma, and made to a working concentration of 20 mM using 1 × Tris-EDTA (TE) buffer (pH 8.0, 10 mM Tris, 1 mM EDTA). The information for target genes and primers is shown in Table 4.1.

Table 4.1 Target genes and primers used for PCR analysis

Target gene	Primer sequences 5' – 3'	Predicted product length (bp)
GAPDH	Forward: GGGCATGAACCATGAGAAGT Reverse: AAGCAGGGATGATGTTCTGG	230
SLA-2	Forward: ACCTTCCAGAGCATGTACGG Reverse: CCTTCCCCATCTCCAGGTAT	250
β 2-microglobulin	Forward: GAAAAACGGGGAGAAGATG Reverse: GTGATGCCGGTTAGTGGTCT	189
β actin	Forward: ACATCTGCTGGAAGGTGGAC Reverse: ACATCTGCTGGAAGGTGGAC	210

4.3.2.3.2 PCR conditions

For each primer pair, gradient PCR with a range of different melting temperatures (Tm) was first applied to determine a suitable Tm. PCR was then performed with the suitable Tm and a suitable concentration of each component. Fresh porcine pulmonary wall (Valve 3) DNA extract was used for GAPDH gradient PCR, and the fresh porcine pulmonary leaflet (Valve 1) DNA extract was used for gradient PCR for SLA-2, β 2-microglobulin and β actin. For each PCR reaction, a blank reaction with all of the reaction components except the gene template was included to control for contamination.

Gradient PCR for GAPDH, SLA-2, β 2-microglobulin and β actin

The gradient PCR mixture used for GAPDH, SLA-2, β 2-microglobulin and β actin genes comprised PCR master mix, nuclease-free water, forward and reverse primers and the template DNA in the quantities indicated below.

	Sample (µl)
PCR master mix (2×) (Fermentas)	25
Nuclease-free water (Fermentas)	21
F primer	1
R primer	1
Template DNA	2
Total	50

The gradient PCR programme used for GAPDH, SLA-2, β 2-microglobulin and β actin genes is given below, with the different Tm ranges for each gene.

STEP	Temprature (°C)	Time	Cycles
Initial denaturation	95	3 min	1
Denaturation	95	30 s	
Annealing	*	30 s	35
Extension	72	30 s	
Final extension	72	10 min	1
End			

*: Tm used for GAPDH: 55.4 °C, 56.3 °C, 57.5 °C, 59.2 °C, 61.4 °C, 63.9 °C, 66.1 °C, 67.7 °C; Tm used for SLA-2, β 2-microglobulin and β actin: 53.6 °C, 54.9 °C, 57.0 °C, 59.6 °C, 62.6 °C, 65.2 °C, 67.2 °C, 68.2 °C.

PCR for GAPDH

The PCR mixture used for GAPDH gene PCR comprised PCR master mix, nuclease-free water, forward and reverse primers and the template DNA in the quantities shown below.

	Sample (µl)	Blank (µl)
PCR master mix (2×) (Fermentas)	25	25
Nuclease-free water (Fermentas)	21	23
F primer	1	1
R primer	1	1
Template DNA	2	0
Total	50	50

The programme used for GAPDH gene PCR is listed below, with 3 min denaturation, 35 cycles of the PCR (annealing temperature: 56 °C) and 10 min final extension.

STEP	Temprature (°C)	Time	Cycles
Initial denaturation	95	3 min	1
Denaturation	95	30 s	
Annealing	56	30 s	35
Extension	72	30 s	
Final extension	72	10 min	1
End			

PCR for SLA-2

The PCR mixture used for SLA-2 gene PCR comprised PCR master mix, nuclease-free water, forward and reverse primers and the template DNA in the quantities shown below.

	Sample (µl)	Blank (µl)
PCR master mix (2×) (Fermentas)	25	25
Nuclease-free water (Fermentas)	23.4	24.4
F primer	0.3	0.3
R primer	0.3	0.3
Template DNA	1	0
Total	50	50

The programme used for SLA-2 gene PCR is shown below, with 3 min denaturation, 35 cycles of the PCR (annealing temperature: 55 °C) and 10 min final extension.

STEP	Temprature (°C)	Time	Cycles
Initial denaturation	95	3 min	1
Denaturation	95	30 s	
Annealing	55	30 s	35
Extension	72	30 s	
Final extension	72	10 min	1
End			

PCR for β 2- microblobulin

The PCR mixture used for β 2- microblobulin gene PCR comprised PCR master mix, nuclease-free water, forward and reverse primers and the template DNA in the quantities shown below.

	Sample (µl)	Blank (µl)
PCR master mix (2×) (Fermentas)	25	25
Nuclease-free water (Fermentas)	22.4	24.4
F primer	0.3	0.3
R primer	0.3	0.3
Template DNA	2	0
Total	50	50

The programme used for β 2- microblobulin gene PCR is shown below, with 3 min denaturation, 35 cycles of the PCR (annealing temperature: 55 °C) and 10 min final extension.

STEP	Temprature (°C)	Time	Cycles
Initial denaturation	95	3 min	1
Denaturation	95	30 s	
Annealing	55	30 s	35
Extension	72	30 s	
Final extension	72	10 min	1
End			

PCR for β actin

The PCR mixture used for β actin gene PCR comprised PCR master mix, nuclease-free water, forward and reverse primers and the template DNA in the quantities shown below.

	Sample (µl)	Blank (µl)
PCR master mix (2×) (Fermentas)	25	25
Nuclease-free water (Fermentas)	21	23
F primer	1	1
R primer	1	1
Template DNA	2	0
Total	50	50

The programme used for β actin gene PCR is shown below, with 3 min denaturation, 35 cycles of the PCR (annealing temperature: 55 °C) and 10 min final extension.

STEP	Temprature (°C)	Time	Cycles
Initial denaturation	95	3 min	1
Denaturation	95	30 s	
Annealing	55	30 s	35
Extension	72	30 s	
Final extension	72	10 min	1
End			

4.3.2.3.3 DNA agarose gel electrophoresis

Agarose gel electrophoresis was used to identify and separate DNA fragments after PCR. Commercially available E-gels (Invitrogen) of 0.8 % (for gradient PCR products)

and 4% (for PCR products) were used. The E-gels contained 0.8 % (w/v) or 4 % (w/v) agarose and ethidium bromide. The gels were run for 15 min for the 0.8 % gels and 30 min for the 4 % gels at 12 V in an E-gel Powerbase™ (Invitrogen). The migration rate of DNA on the agarose gel after electrophoresis corresponded to the molecular size. The more bp`s the DNA, the slower it migrated on the gel. Quick-Load® PCR marker (Biolabs) and E-gel® low range quantitative DNA ladders (Invitrogen) were used to determine the sizes of DNA fragments (Table 4.2 & Table 4.3). By comparing to the bands of the markers, the sizes of DNA fragments in the samples were determined.

Table 4.2 Quick-Load® PCR marker (Biolabs)

Fragments	Quick-Load® PCR marker (Biolabs) (Conc. 30 ng.10 µl^{-1})	
	Base pairs	Mass (ng)
1	766	62
2	500	40
3	300	48
4	150	61
5	50	89

Table 4.3 E-gel® low range quantitative DNA ladder (Invitrogen)

Fragments	E-gel® low range quantitative DNA ladder (Invitrogen) (Conc. 175 ng. 10 µl^{-1})	
	Base pairs	Mass (ng)
1	2,000	100
2	800	40
3	400	20
4	200	10
5	100	5

For each sample that was loaded on the gel, 9 µl of PCR product was mixed with 1 µl of 10× Blue Juice™ gel loading buffer (Invitrogen). The DNA ladder was loaded at 10 µl per well.

4.3.3 Immunohistochemical evaluation of decellularised pulmonary roots

Specific matrix and cytoskeletal proteins were localised using immunohistochemical labelling. Fresh (n=6 from separate animals) and decellularised (n=6 from separate animals) pulmonary root tissue samples were fixed with either 10 % (v/v) NBF or Zinc

fixation solution and immunohistochemical evaluation was performed as described in Section 2.2.8. Each tissue sample was serially sectioned at 10 μm and a minimum of 3 sections per sample were evaluated using immunohistochemistry. For each tissue sample, immunohistochemistry was performed for a section incubated with specific antibody, a section incubated with an isotype control antibody of the same concentration, and a section incubated with antibody diluent alone (no primary antibody as a negative control) at the same time to verify antibody specificity and rule out non-specific antibody binding. The porcine pulmonary leaflets, pulmonary artery and myocardium were carefully examined for antibody specific binding. Slides were examined using light microscopy. The antibodies used in this study were specific to: α-SMA, vWF, desmin, vimentin, fibronectin, collagen-IV and α-gal.

4.3.4 *In vitro* biocompatibility assays

In order to determine the biocompatibility of the decellularised tissues *in vitro*, decellularised porcine pulmonary valve leaflets were assessed using a qualitative contact cytotoxicity assay and decellularised porcine pulmonary artery wall was assessed using a quantitative extract cytotoxicity assay. For each assay, two types of cells were used: 3T3 murine fibroblasts and L929 murine fibroblasts. The cells were obtained from the European Collection of Animal Cell Cultures and resurrected from frozen, cultured and passaged as described in Section 2.2.9. 3T3 murine fibroblasts at passage 11 and L929 murine fibroblasts at passage 24 were used for contact cytotoxicity assay. 3T3 murine fibroblasts at passage 13 and L929 murine fibroblasts at passage 26 were used for the extract cytotoxicity assay.

4.3.4.1 Contact cytotoxicity assay

Tissue samples (2 of approx 5 mm^2) were dissected aseptically from the central part of each of six leaflets (from different decellularised porcine pulmonary roots). The leaflet samples were stored in PBS temporarily to avoid dehydration. The samples were attached to the centre of each well of a six-well tissue culture plate using collagen gel prepared from rat tails (prepared by Andrew Aldridge) and sterile 0.1 M NaOH (2:1). The collagen gel took about 20 min to set. A drop of cyanoacrylate contact adhesive was placed in the centre of control wells (n=3). This was used as a positive control, as it

has been demonstrated to produce a reproducible cytotoxic response. Collagen gel (20 µl) was carefully added to the centre of negative control wells. The gel was neutralised with 10 µl of 0.1 M sterile NaOH. This served as a negative control as collagen gel from rat tail is biocompatible. All the wells containing samples, positive and negative controls were washed three times using sterile PBS, each for 10 min. Cells (3T3 and L929) were added to each well at a concentration which allowed the cells to become approximately 80 % confluent at a final volume of 2 ml (i.e. approximately 3×10^5 cells per well in DMEM cell culture medium). The plates were covered and incubated at 37 °C in 5 % (v/v) CO_2 in air for 48 h. Following incubation, the culture medium was carefully aspirated, and the wells were gently washed using PBS containing calcium and magnesium. The cell layers were fixed with 10 % (v/v) NBF for 10 min. Following fixation, the 10 % (v/v) NBF was carefully aspirated and the cell monolayers were stained using Giemsa solution (2 ml per well) for 5 min. The wells were then gently rinsed with running tap water until the water ran clear. The plates were air dried at room temperature before microscopy. A bright-field microscope was used to observe any changes in cell morphology and density.

4.3.4.2 Extract cytotoxicity assay

4.3.4.2.1 Extract cytotoxicity assay

Pulmonary arteries (n=6, from separate animals) from decellularised porcine pulmonary roots were finely macerated and placed into sterile 1.5 microcentrifuge tubes. The tubes containing tissue were re-weighed to determine the weight of tissue. DMEM (1ml per 100 mg tissue) was added before incubation at 37 °C for 72 h on a blood rotator at 30 rpm. Following incubation, the tissue-containing microcentrifuge tubes were centrifuged at 15,000 × g for 15 min. The supernatants (tissue extracts) were collected. The sterility of the tissue extracts was checked by plating onto agar plates. Three types of plate were used for each sample: nutrient agar (NA, plates incubated at 37 °C for 48 h), heated blood agar (HBA, plates incubated at 37 °C for 48 h), and Saboraud dextrose agar (SAB, plates incubated at 30 °C for 72 h). The tissue extracts were stored at –20 °C until needed. Cells (3T3 of P13 and L929 of P26) were seeded into a 96-well plate at a confluence of approximately 80 % (approximately 1×10^4 cells per well), and incubated overnight at 37 °C in 5% (v/v) CO_2 in air. The tissue extracts were thawed at

37 °C on the day of test. The cell culture medium was aspirated from the 96-well plate, and replaced with 100 µl of DMEM containing 20% (v/v) FBS, 200 $U.ml^{-1}$ penicillin, 200 $U.ml^{-1}$ streptomycin, and 200 µM L-glutamine. Test reagents of 100 µl (the tissue extracts, n=6 for each root) were added to appropriate wells. The positive controls (n=6) consisted of 200 µl 40 % (v/v) DMSO in DMEM. The negative controls (n=6) consisted of 200 µl cell culture medium alone. The 96-well plates with cells were incubated at 37 °C in 5 % (v/v) CO_2 in air for 48 h. The cell viability was then determined using the ATPLite-M® assay.

4.3.4.2.2 ATPLite-M® assay for cell viability

Solutions:

- Mammalian cell lysis solution: stored at 4 °C.
- Substrate solution: one vial of lyophilised substrate solution was reconstituted by adding 25ml of substrate buffer. The substrate solution was made into 5 ml aliquots and stored at -20 °C in the dark.

Methods:

The ATPLite-M® assay was used to determine cell viability following the manufacture's instruction. ATPLite-M® reagents were allowed to warm to room temperature. For each well containing cells in the 96-well plate, the original culture medium was aspirated from the well, and 50 µl of fresh cell culture medium added to each well. Mammalian cell lysis solution (50 µl) was added into each well and incubated at room temperature with agitation at 500 rpm for 5 min. Solution (100 µl) from each well was then transferred into a 96-well Optiplate™. Substrate solution (50 µl) was added to each well and the Optiplate™ was agitated at 500 rpm for five min. The luminescence was measured using TopCount™. Data was expressed as counts per minute (cpm).

4.4 Results

4.4.1 Histological evaluation of decellularised porcine pulmonary roots

Histology was used to determine if the decellularisation process affected the histoarchitecture of the porcine pulmonary roots and the extent of decellularisation. Tissue sections were stained with H&E (Figure 4.1), Hoechst (Figure 4.2), Miller's (Figure 4.3) and Alcian blue (Figure 4.4).

No blue stained cells were observed in any of the sections following H&E staining (Figure 4.1) of the decellularised porcine pulmonary roots. Pink/red stained connective tissue (collagen and elastin) was observed in the pulmonary leaflet, pulmonary artery and myocardium. In the porcine pulmonary leaflet (Figure 4.1 A), there was more collagen and elastin distributed in the *ventricularis* and *fibrosa* layers than the *spongiosa* layer, since the red staining was deeper in *ventricularis* and *fibrosa* but lighter in *spongiosa*. The structure of the *ventricularis* and the *fibrosa* appeared to be more organised and more compact than the *spongiosa*. The myocardium bundles were regularly arranged as shown in Figure 4.1 B. No damage to the pulmonary artery, either the luminal side or the adventitial layer, was observed as shown in Figure 4.1 C and Figure 4.1D. The connective tissue structure was aligned parallel to the long axis of the pulmonary artery. In the leaflet connection area, the histoarchitecture seemed to be intact (Figure 4.1 E). No damage was observed to the structure of connective tissue.

Images of the decellularised pulmonary root tissue stained with Hoechst are shown in Figure 4.2. No fluorescence indicating cell nuclei was observed throughout the whole pulmonary roots. This result provided further evidence of removal of cells from porcine pulmonary roots after decellularisation. The ECM was stained brighter with Hoechst in the myocardium (Figure 4.2 B) than in the pulmonary leaflet and artery (Figure 4.2 A, C, D). In Miller's stained images (Figure 4.3), it was observed that a large amount of elastin fibres was distributed in the pulmonary wall (Figure 4.3 C). The *ventricularis* seemed to have larger elastin content than the *fibrosa*. After Alcian blue staining, blue coloured GAG`s were not readily observed in the leaflet and pulmonary wall tissues (Figure 4.4 A, C), but were evident in the leaflet connection and in the myocardium (Figure 4.4 B, D).

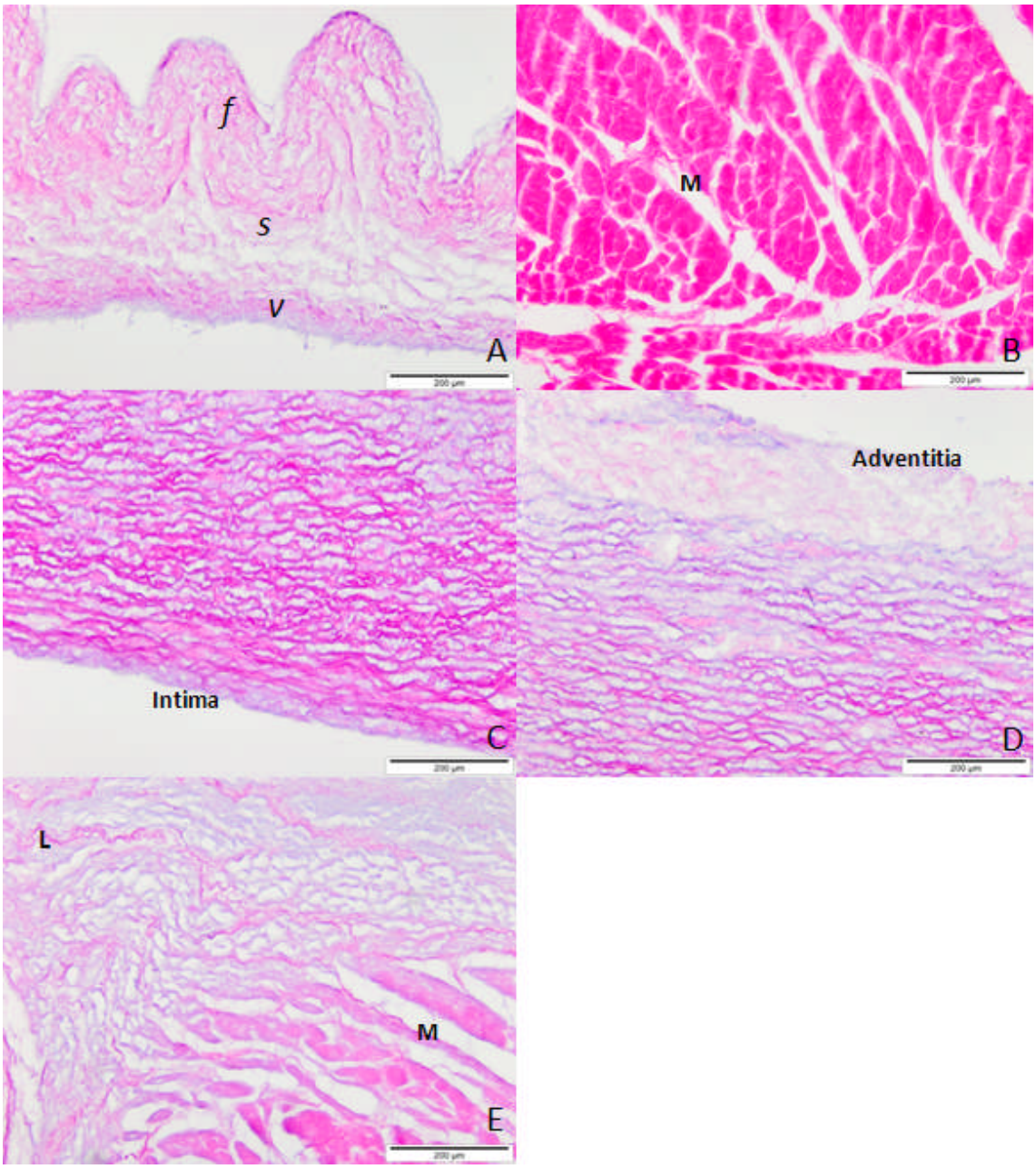

Figure 4.1 Sections of decellularised porcine pulmonary root tissue stained with H&E. (A) Pulmonary valve leaflet, 100 × (*v*: *ventricularis*; *s*: *spongiosa*; *f*: *fibrosa*); **(B)** Myocardium, 100 ×; **(C)** The lumen surface of the pulmonary wall, 100 ×; **(D)** The adventitial surface of the pulmonary wall, 100 ×; **(E)** Leaflet connection, 100 ×. M: myocardium; L: leaflet. Scale bars are: all 200 µm.

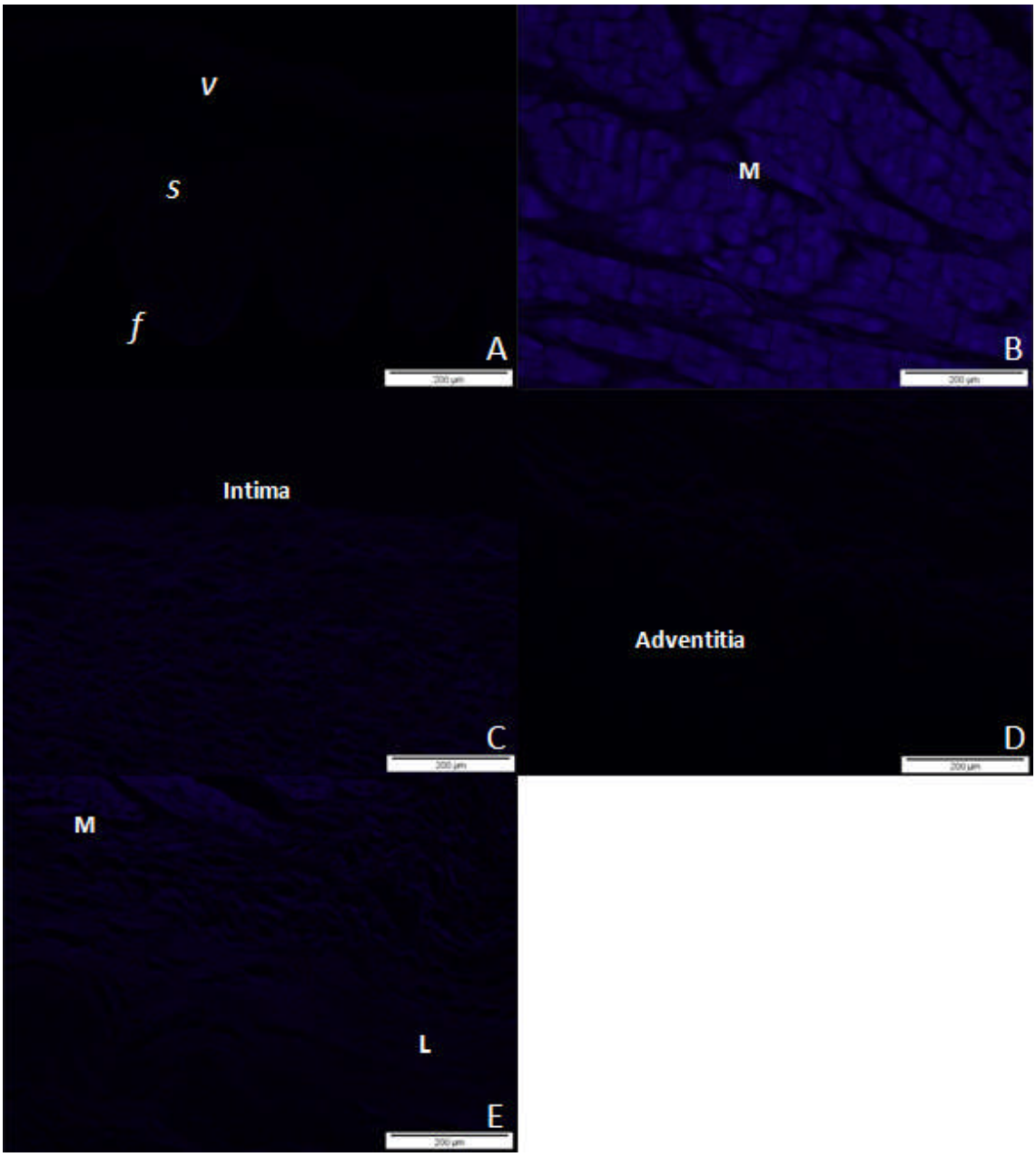

Figure 4.2 Sections of decellularised porcine pulmonary root tissue stained with Hoechst. (A) Pulmonary valve leaflet, 100 × (*v*: *ventricularis*; *s*: *spongiosa*; *f*: *fibrosa*); **(B)** Myocardium, 100 ×; **(C)** The lumen surface of the pulmonary wall, 100 ×; **(D)** The adventitial surface of the pulmonary wall, 100 ×; **(E)** Leaflet connection, 100 ×. M: myocardium; L: leaflet. Scale bars are: all 200 µm.

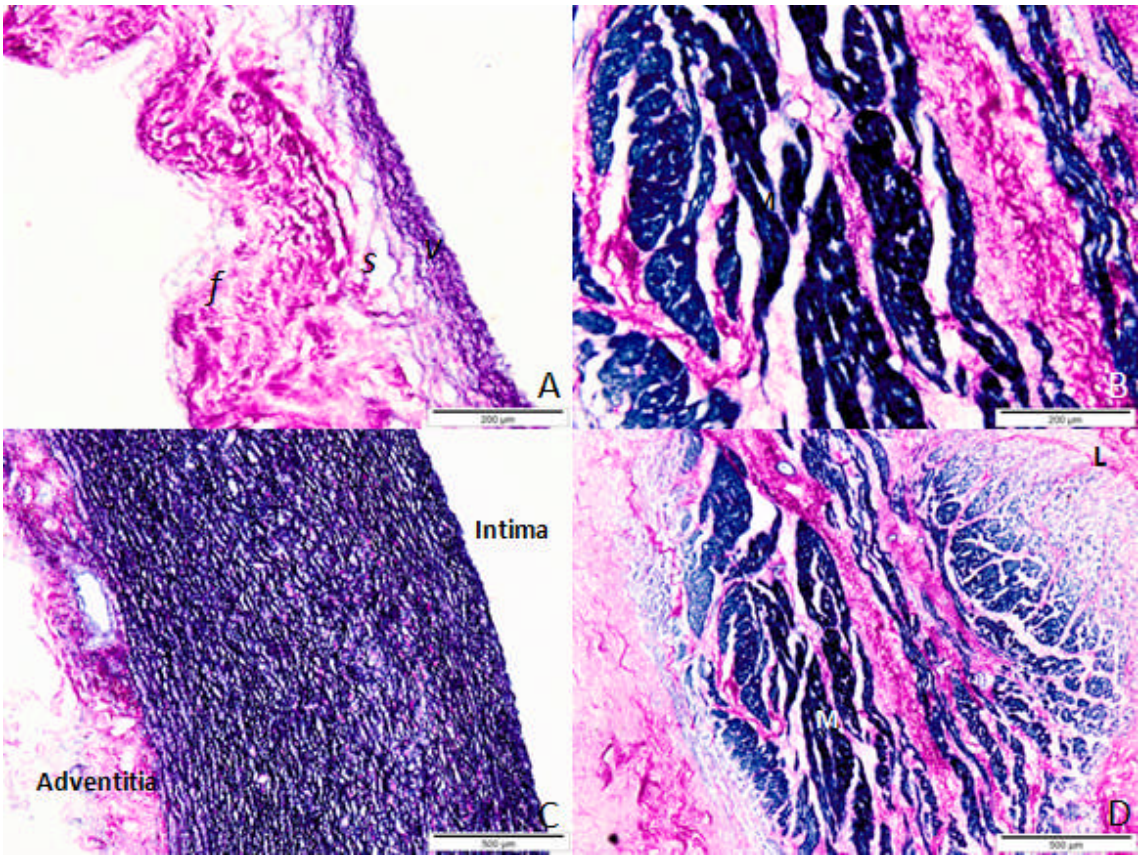

Figure 4.3 Sections of decellularised porcine pulmonary root tissue stained with Miller's. (A) Pulmonary valve leaflet, 100 × (*v*: *ventricularis*; *s*: *spongiosa*; *f*: *fibrosa*); **(B)** Myocardium, 100 ×; **(C)** The pulmonary wall, 40 ×; **(D)** Leaflet connection, 40 ×. M: myocardium; L: leaflet. Scale bars are: (A), (B) 200µm; (C), (D) 500 µm.

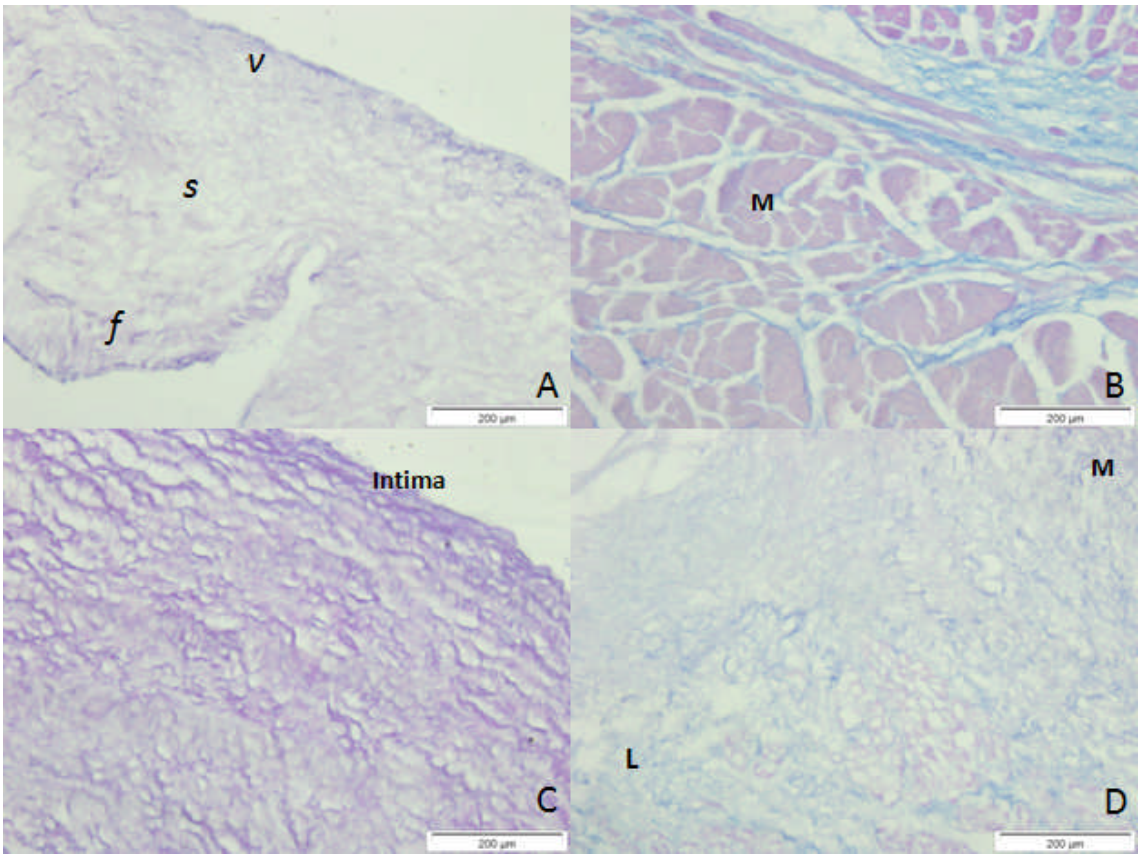

Figure 4.4 Sections of decellularised porcine pulmonary root tissue stained with Alcian blue. (A) Pulmonary valve leaflet, 100 × (*v*: *ventricularis*; *s*: *spongiosa*; *f*: *fibrosa*); **(B)** Myocardium, 100 ×; **(C)** The pulmonary wall, 100 ×; **(D)** Leaflet connection, 100 ×. M: myocardium; L: leaflet. Scale bars are: all 200 µm.

4.4.2 DNA content analysis of fresh and decellularised porcine pulmonary roots

4.4.2.1 DNA spectrophometry

The DNA extracted from fresh and decellularised porcine pulmonary roots was quantified using nanodrop spectrophotometry. The results are shown in Figure 4.5 and Table 4.4. For all of the four regions (leaflet, pulmonary artery, myocardium, and leaflet connection) of decellularised porcine pulmonary roots (n=6 from different animals) there was a significant reduction in DNA content compared to fresh samples ($p<0.05$, students t-test). Greater than 90 % of the DNA was removed from the porcine pulmonary roots after decellularisation.

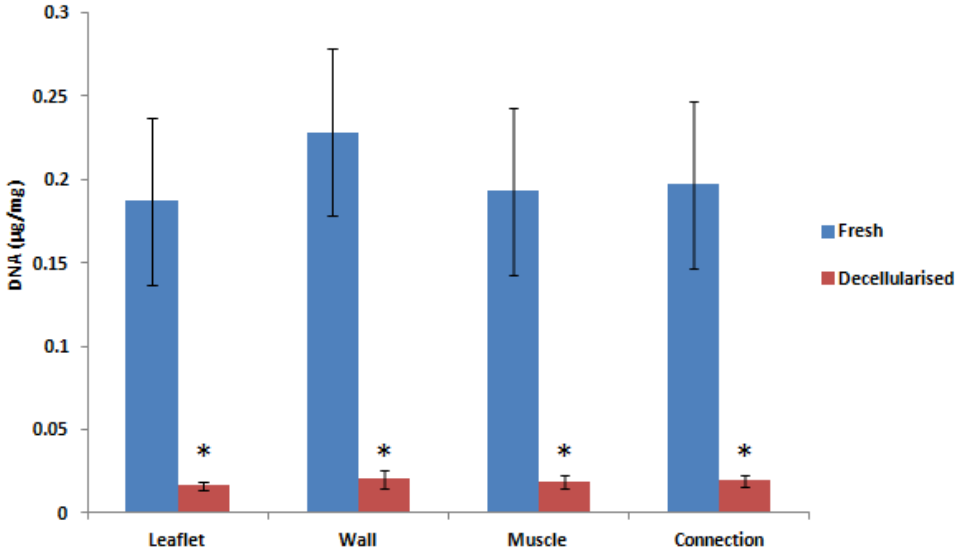

Figure 4.5 DNA content of fresh and decellularised porcine pulmonary root tissue determined by Nanodrop spectrophotometry at 260 nm. Data is presented as the mean (n=6) ± 95 % C.I.. Data was analysed using the students t-test, which showed a significant reduction of DNA content in decellularised tissue compared to the fresh tissue of the same region ($p<0.05$ *).

Table 4.4 DNA content of fresh (n=6) and decellularised (n=6) porcine pulmonary root tissue determined by Nanodrop spectrophotometry at 260 nm (mean ± 95 % C.I.) and percentage of DNA removal after decellularisation.

	DNA content of fresh tissue (µg.mg^{-1})	DNA content of decellularised tissue (µg.mg^{-1})	Percentage of DNA removal (%)
Leaflet	0.187±0.021	0.016±0.003	91.27
Wall	0.228±0.029	0.020±0.006	91.04
Myocardium	0.193±0.019	0.019±0.004	90.10
Connection	0.197±0.020	0.020±0.004	90.01

4.4.2.2 PCR

4.4.2.2.1 Gradient PCR results for GAPDH, SLA-2, β 2-microglobulin and β actin

Gradient PCR with a range of different Tm was used to determine the suitable PCR conditions for each gene. The agarose gel image for GAPDH gradient PCR is shown in Figure 4.6. Different Tm`s of 55.4 °C to 67.7 °C were used. The PCR product was

detected in Lane 2-7. The product band was most obvious in Lanes 2-4 (which had a Tm range of 55.4°C to 57.5°C). It was decided from this result that 56 °C was to be used as the melting temperature for GAPDH PCR.

The agarose gel image for SLA-2 is shown in Figure 4.7. Tm`s of 53.6 °C to 68.2 °C were used. The PCR product was detected in Lanes 2-7. The product band appeared to be most bright in lane 3 (which had a Tm of 54.9 °C). It was decided from this result that 55 °C was to be used as the melting temperature for SLA-2 PCR.

The agarose gel image for β 2-microglobulin is shown in Figure 4.8. Tm`s of 53.6 °C to 68.2 °C were used. The PCR product band was observed on Lane 2-7. The clearest bands were observed in Lane 2-5 (which had a Tm range of 53.6 °C to 59.6 °C). It was decided from this result that 55 °C was to be used as the melting temperature for β 2-microglobulin PCR.

The agarose gel image for β actin is shown in Figure 4.9. Tm's for gradient PCR ranged from 53.6 °C to 68.2 °C. The PCR product band was observed in all of the lanes that loaded with samples (Lane 2-9). In Lane 2-7, a second band was observed on the gel at around 150 bp. The PCR product seemed to have the highest concentration in Lane 3 (Tm=57.0 °C). However, since the concentration of the second band was also the highest, the Tm for Lane 2 (54.9 °C) was considered as a better option because at this melting temperature, the PCR product had a clear band whilst the unwanted band was less clear. It was decided 55 °C was to be used as the melting temperature for β actin PCR.

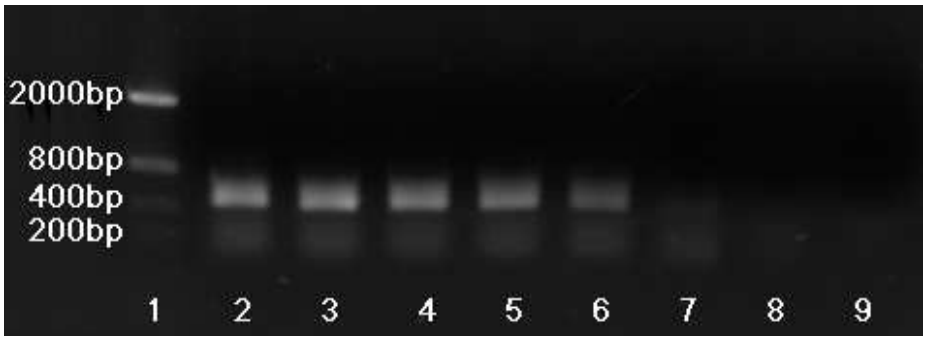

Figure 4.6 Gradient PCR products for GAPDH on a 0.8 % E gel. Lane 1: E-gel® low range quantitative DNA ladder (Invitrogen); Lane 2-9: DNA from fresh porcine pulmonary wall with Tm of 55.4 °C, 56.3 °C, 57.5 °C, 59.2 °C, 61.4 °C, 63.9 °C, 66.1 °C, and 67.7 °C. Lane 2-7 showed a band at around 600bp on the gel.

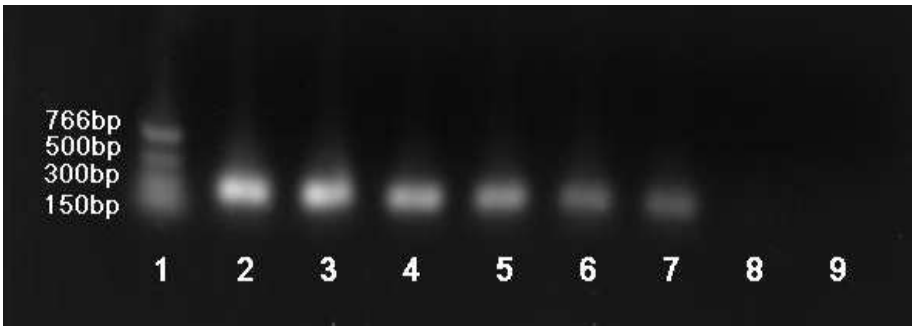

Figure 4.7 Gradient PCR products for SLA-2 on a 0.8 % E gel. Lane 1: Quick-Load® PCR marker (Biolabs); Lane 2-9: DNA from fresh porcine pulmonary leaflet with Tm of 53.6 °C, 54.9 °C, 57.0 °C, 59.6 °C, 62.6 °C, 65.2 °C, 67.2 °C, and 68.2 °C. Lane 2-7 showed a band at around 250 bp on the gel.

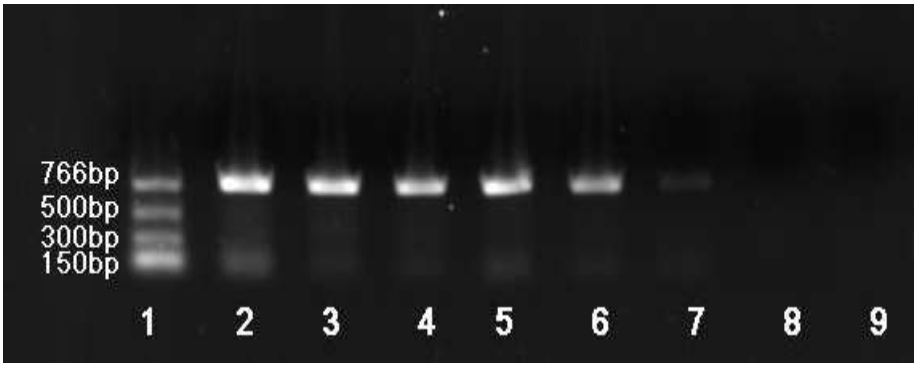

Figure 4.8 Gradient PCR products for β 2-microglobulin on a 0.8 % E gel. Lane 1: Quick-Load® PCR marker (Biolabs); Lane 2-9: DNA from fresh porcine pulmonary leaflet with Tm of 53.6 °C, 54.9 °C, 57.0 °C, 59.6 °C, 62.6 °C, 65.2 °C, 67.2 °C, and 68.2 °C. Lane 2-7 showed a band at around 760 bp on the gel.

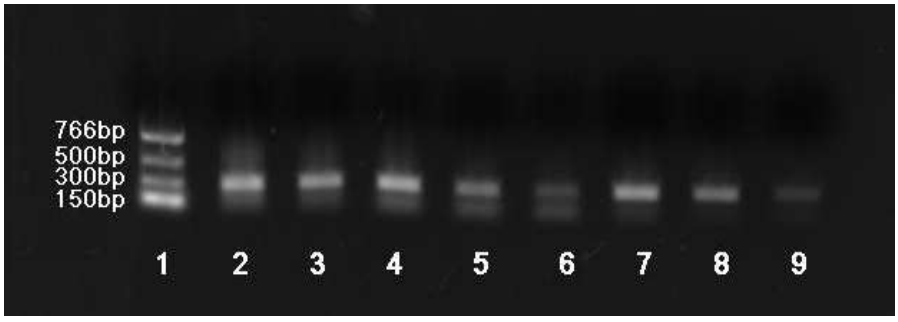

Figure 4.9 Gradient PCR products for β actin on a 0.8 % E gel. Lane 1: Quick-Load® PCR marker (Biolabs); Lane 2-9: DNA from fresh porcine pulmonary leaflet with Tm of 53.6 °C, 54.9 °C, 57.0 °C, 59.6 °C, 62.6 °C, 65.2 °C, 67.2 °C, and 68.2 °C. Lane 2-9 showed a band at around 300 bp on the gel.

4.4.2.2.2 PCR results for GAPDH, SLA-2, β 2-microglobulin and β actin

PCR was used to detect the presence of functional genes in DNA extracted from fresh and decellularised porcine pulmonary roots. The gel image of GAPDH PCR is shown in Figure 4.10. A clear band localised at around 600 bp was observed in DNA extracted from fresh porcine pulmonary leaflet, artery, myocardium and leaflet connection tissue. No band was observed in the decellularised samples or the blank reaction.

The gel image of SLA-2 PCR is shown in Figure 4.11. A clear band of a size around 250 bp was observed in fresh porcine pulmonary leaflet, artery, myocardium and leaflet connection. No band was observed in DNA extracted from the decellularised samples or the blank reaction.

The gel image of β 2-microglobulin PCR is shown in Figure 4.12. A clear band of around 760 bp was observed in DNA extracted from fresh porcine pulmonary leaflet, artery, myocardium and leaflet connection tissue. No band was observed in the PCR product with template DNA from decellularised tissue or the blank reaction.

The gel image of β actin PCR is shown in Figure 4.13. A clear band of around 300 bp was observed in DNA extracted from fresh porcine pulmonary leaflet, artery, myocardium and leaflet connection tissue. No band was observed in the PCR product with template DNA from decellularised tissue or the blank reaction.

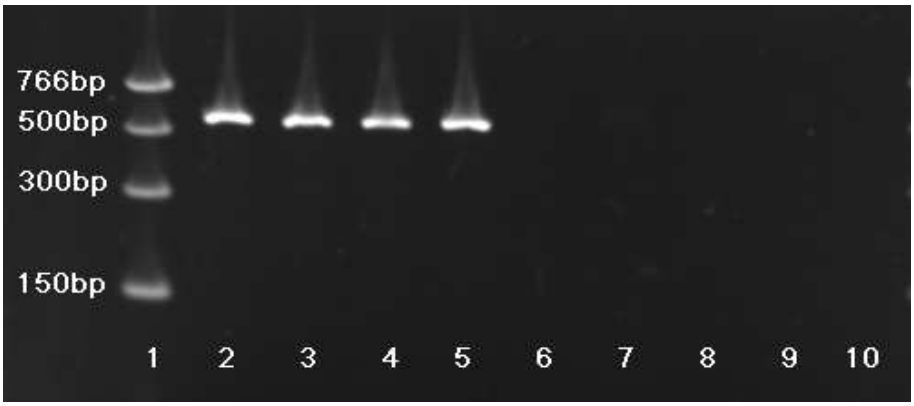

Figure 4.10 PCR products for GAPDH on a 4 % E gel. Lane 1: Quick-Load® PCR marker (Biolabs); Lane 2-5: fresh porcine pulmonary leaflet, fresh porcine pulmonary wall, fresh porcine myocardium, fresh porcine pulmonary leaflet connection; a band at around 600 bp is present on the gel. Lane 6-9: decellularised porcine pulmonary leaflet, decellularised porcine pulmonary wall, decellularised porcine myocardium, decellularised porcine pulmonary leaflet connection; no band is present on the gel. Lane 10: blank; no band is present on the gel.

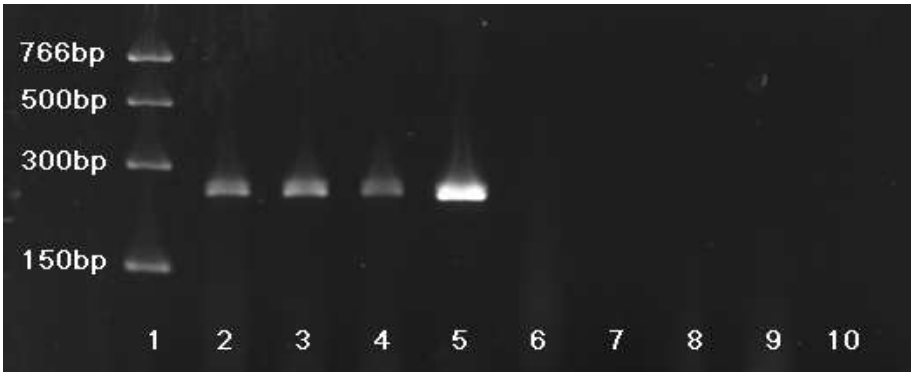

Figure 4.11 PCR products for SLA-2 on a 4 % E gel. Lane 1: Quick-Load® PCR marker (Biolabs); Lane 2-5: fresh porcine pulmonary leaflet, fresh porcine pulmonary wall, fresh porcine myocardium, fresh porcine pulmonary leaflet connection; a band at around 250 bp is present on the gel. Lane 6-9: decellularised porcine pulmonary leaflet, decellularised porcine pulmonary wall, decellularised porcine myocardium, decellularised porcine pulmonary leaflet connection; no band is present on the gel. Lane 10: blank; no band is present on the gel.

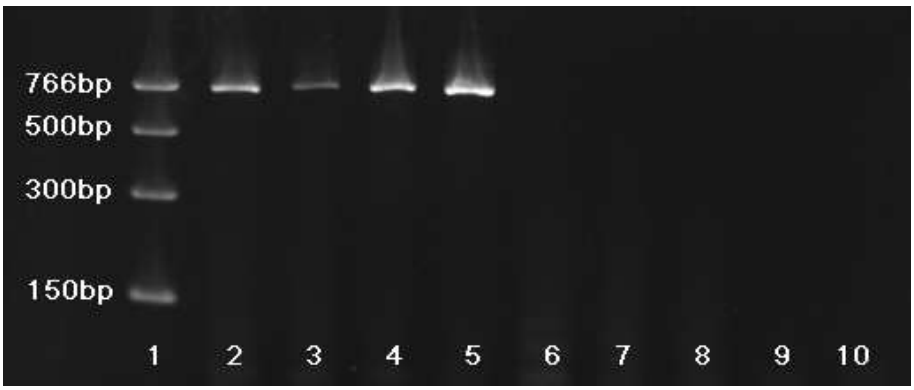

Figure 4.12 PCR products for β 2-microglobulin on a 4 % E gel. Lane 1: Quick-Load® PCR marker (Biolabs); Lane 2-5: fresh porcine pulmonary leaflet, fresh porcine pulmonary wall, fresh porcine myocardium, fresh porcine pulmonary leaflet connection; a band at around 760 bp is present on the gel. Lane 6-9: decellularised porcine pulmonary leaflet, decellularised porcine pulmonary wall, decellularised porcine myocardium, decellularised porcine pulmonary leaflet connection; no band is present on the gel. Lane 10: blank; no band is present on the gel.

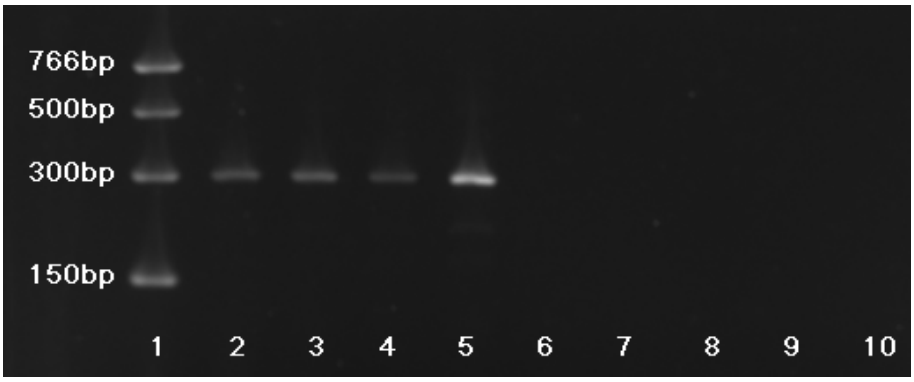

Figure 4.13 PCR products for β actin on a 4 % E gel. Lane 1: Quick-Load® PCR marker (Biolabs); Lane 2-5: fresh porcine pulmonary leaflet, fresh porcine pulmonary wall, fresh porcine myocardium, fresh porcine pulmonary leaflet connection; a band at around 300 bp is present on the gel. Lane 6-9: decellularised porcine pulmonary leaflet, decellularised porcine pulmonary wall, decellularised porcine myocardium, decellularised porcine pulmonary leaflet connection; no band is present on the gel. Lane 10: blank; no band is present on the gel.

4.4.3 Immunohistochemical evaluation of fresh and decellularised porcine pulmonary roots

Antibody labelling was used to localise specific proteins in porcine pulmonary roots. By comparing the images of the fresh and decellularised samples, it was possible to determine if there was any change in specific matrix and cytoskletetal components and the extent removal of the α-gal epitope during the decellularisation process.

4.4.3.1 Alpha smooth muscle actin (α-SMA)

The images of porcine pulmonary root tissue sections labelled with antibody to α-SMA are shown in Figure 4.14. The surfaces of fresh porcine pulmonary leaflet were stained brown (positive with α-SMA antibody) especially the ventricular surface (Figure 4.14 A). The cells within the pulmonary artery were also stained with a deep brown colour, with the ECM of the pulmonary artery stained a light brown colour. The blood vessels within the myocardium and the pulmonary artery were also stained positive (Figure 4.14 D, Figure 4.14 G). No brown coloured staining was observed in the decellularised leaflet, myocardium or wall (Figure 4.14 B, E, and H). The ECM of the decellularised

porcine pulmonary root had background staining of brown colour, which appeared more positive than the isotype control for the leaflet and wall tissue (Figure 4.14).

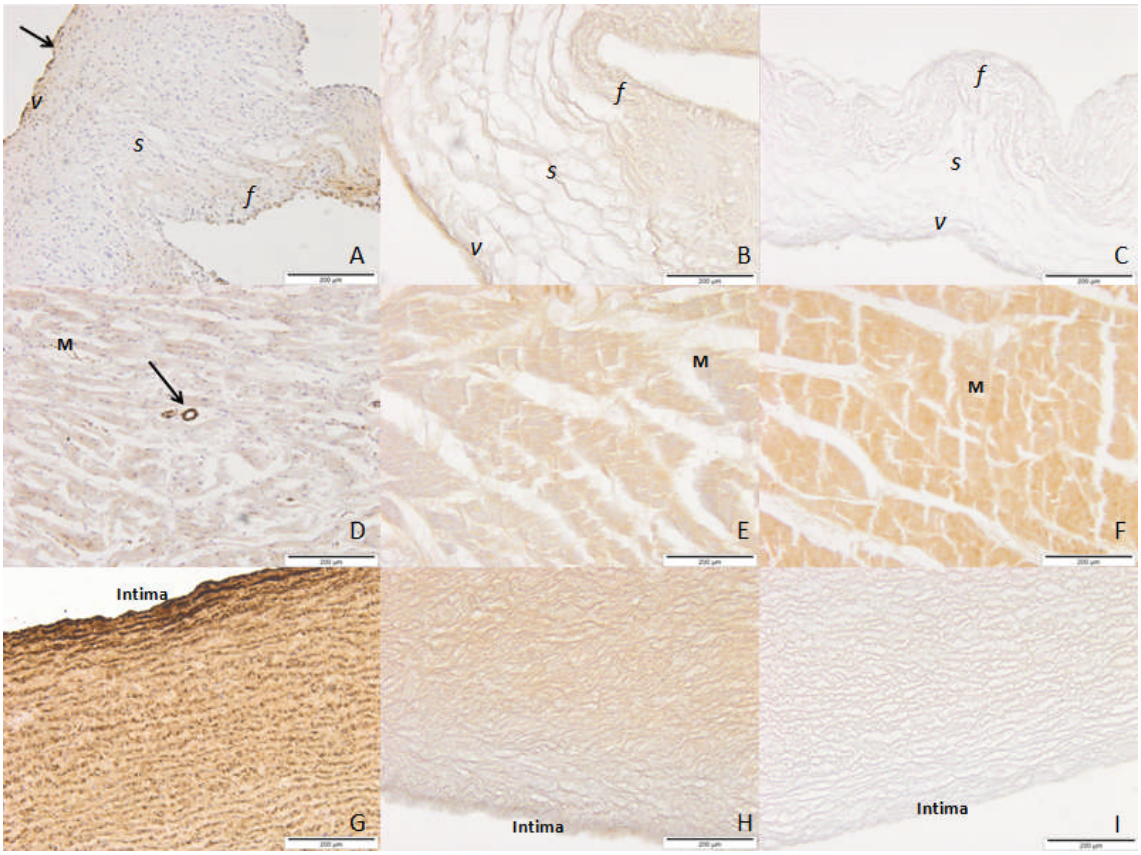

Figure 4.14 Localisation of α-SMA in fresh and decellularised porcine pulmonary root tissue. (A) Fresh pulmonary valve leaflet, 100 ×, the arrow indicates the ventricular side of the pulmonary leaflet that has been positively stained; **(B)** Decellularised pulmonary valve leaflet, 100 ×; **(C)** Decellularised pulmonary valve leaflet isotype control, 100 ×; **(D)** Fresh myocardium, 100 ×, the arrow indicates a blood vessel in the myocardium that has been positively stained; **(E)** Decellularised myocardium, 100 ×; **(F)** Decellularised myocardium isotype control, 100 ×; **(G)** The lumen surface of the fresh pulmonary wall, 100 ×; **(H)** The lumen surface of the decellularised pulmonary wall, 100 ×; **(I)** The lumen surface of the decellularised pulmonary wall isotype control, 100 ×. *v*: *ventricularis*; *s*: *spongiosa*; *f*: *fibrosa*; M: myocardium; L: leaflet. Scale bars are: all 200 µm.

4.4.3.2 Von Willebrand factor (vWF)

The images of porcine pulmonary root tissue sections stained with antibodies to vWF are shown in Figure 4.15. Positive staining (brown colour) were observed in the endothelial layers of the fresh pulmonary leaflets (Figure 4.15 A), as well as the

endothelial layer of the lumen of the fresh pulmonary artery (Figure 4.15 G). The small blood vessels within the fresh myocardium and the connective tissue layer of the adventitia of the fresh pulmonary artery were also positively stained (Figure 4.15 D, J). No positive staining was observed in the decellularised porcine pulmonary roots (Figure 4.15 B, E, H, K) or the isotype control sections (Figure 4.15 C, F, I, L).

4.4.3.3 Desmin

Images of porcine pulmonary root tissue sections labelled with antibodies to desmin are shown in Figure 4.16. The myocardium tissue was stained brown for both fresh and decellularised sections (Figure 4.16 D, E). Some small brown coloured areas were observed within the connective tissue layer on the adventitia of fresh pulmonary artery (Figure 4.16 J). No brown colour was observed in the sections stained with the isotype control.

4.4.3.4 Vimentin

The results of porcine pulmonary root tissue labelled with antibodies to vimentin are shown in Figure 4.17. Cells throughout the fresh porcine pulmonary leaflet, myocardium and artery were stained brown (Figure 4.17 A, D, G, J). No positive staining was observed throughout the decellularised tissue (Figure 4.17 B, E, H, K). No brown colour was observed in the sections stained with the isotype control.

4.4.3.5 Fibronectin

Following labelling using a monoclonal antibody against fibronectin, the results indicated that the fresh and decellularised porcine pulmonary root tissues were stained positive throughout (Figure 4.18). The fresh pulmonary leaflets and wall were more intensely stained compared to the decellularised leaflets and wall, however the staining in the fresh and decellularised myocardium was similar. The darkest colour was observed in the surfaces of the pulmonary leaflets and arteries in both fresh and decellularised tissue sections. The regions close to the surfaces of decellularised pulmonary artery had a lighter brown colour than the centre of the pulmonary artery (Figure 4.18 H, K). Minimal brown colour was observed in the sections stained with the isotype control.

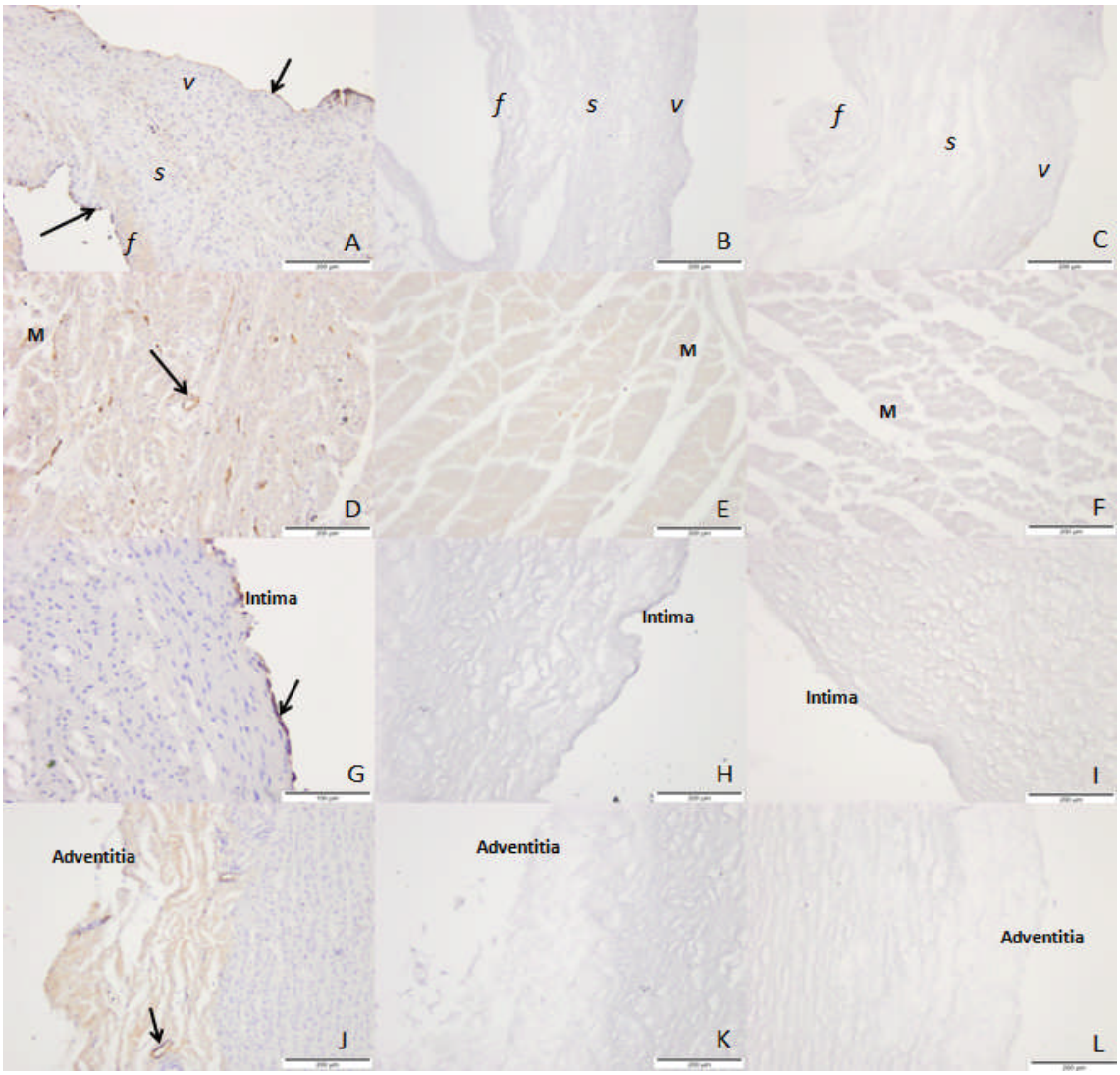

Figure 4.15 Localisation of vWF in fresh and decellularised porcine pulmonary root tissue. (A) Fresh pulmonary valve leaflet, 100 ×, the arrows indicate the surfaces of pulmonary leaflet that has been positively stained; **(B)** Decellularised pulmonary valve leaflet, 100 ×; **(C)** Decellularised pulmonary valve leaflet isotype control, 100 ×; **(D)** Fresh myocardium, 100 ×, the arrow indicates a blood vessel in the myocardium that has been positively stained; **(E)** Decellularised myocardium, 100 ×; **(F)** Decellularised myocardium isotype control, 100 ×; **(G)** The lumen surface of the fresh pulmonary wall, 200 ×, the arrow indicates the surface cell layer of pulmonary wall that has been positively stained; **(H)** The lumen surface of the decellularised pulmonary wall, 100 ×; **(I)** The lumen surface of the decellularised pulmonary wall isotype control, 100 ×; **(J)** The adventitial surface of the fresh pulmonary wall, 100 ×, the arrow indicates a blood vessel that has been positively stained; **(K)** The adventitial surface of the decellularised pulmonary wall, 100 ×; **(L)** The adventitial surface of the decellularised pulmonary wall isotype control, 100 ×. *v*: *ventricularis*; *s*: *spongiosa*; *f*: *fibrosa*; M: myocardium; L: leaflet. Scale bars are all 200 µm except for (G), 100 µm.

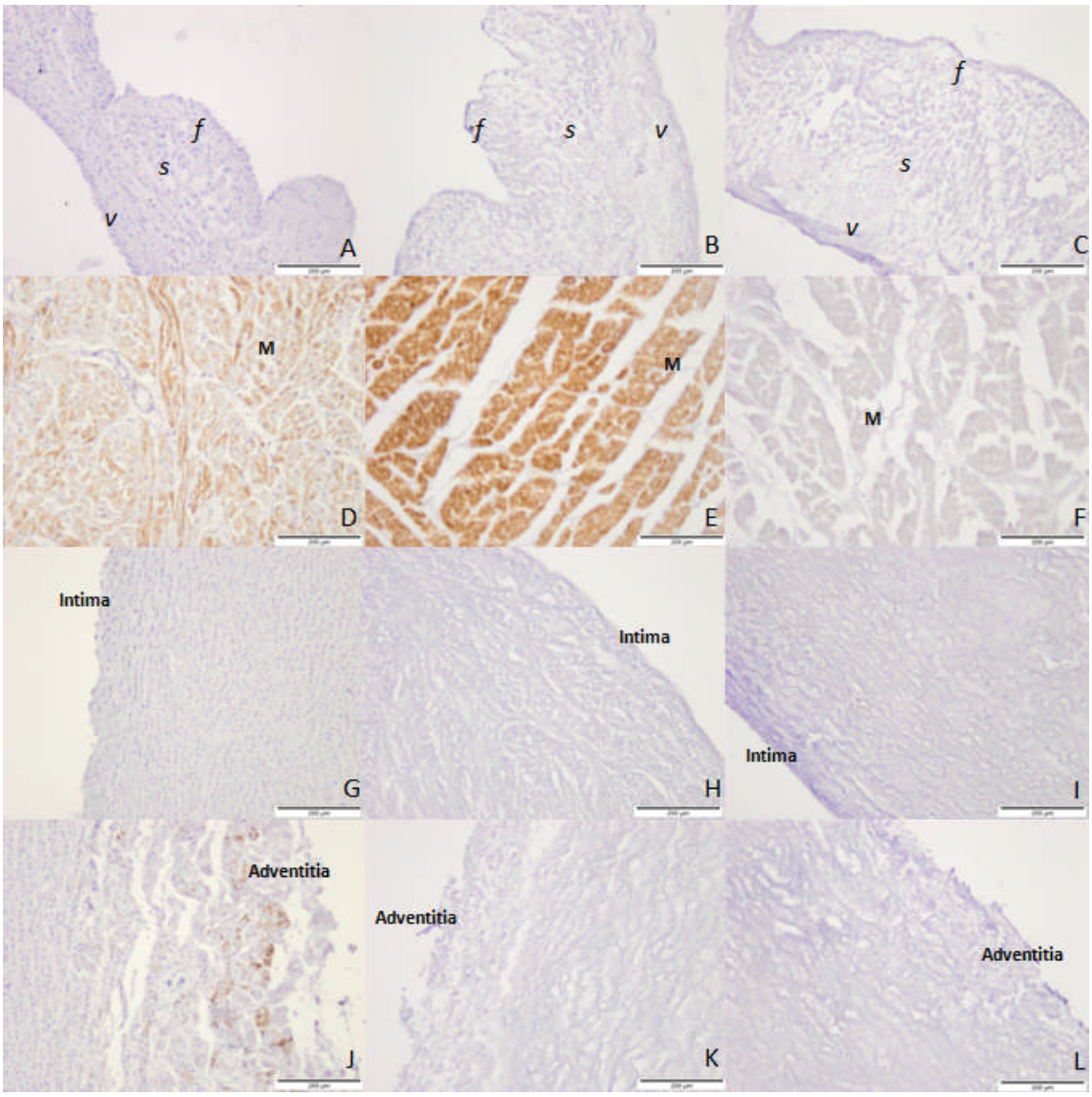

Figure 4.16 Localisation of desmin in fresh and decellularised porcine pulmonary root tissue. (A) Fresh pulmonary valve leaflet, 100 ×; **(B)** Decellularised pulmonary valve leaflet, 100 ×; **(C)** Decellularised pulmonary valve leaflet isotype control, 100 ×; **(D)** Fresh myocardium, 100 ×; **(E)** Decellularised myocardium, 100 ×; **(F)** Decellularised myocardium isotype control, 100 ×; **(G)** The lumen surface of the fresh pulmonary wall, 100 ×; **(H)** The lumen surface of the decellularised pulmonary wall, 100 ×; **(I)** The lumen surface of the decellularised pulmonary wall isotype control, 100 ×; **(J)** The adventitial surface of the fresh pulmonary wall, 100 ×; **(K)** The adventitial surface of the decellularised pulmonary wall, 100 ×; **(L)** The adventitial surface of the decellularised pulmonary wall isotype control, 100 ×. *v*: *ventricularis*; *s*: *spongiosa*; *f*: *fibrosa*; M: myocardium; L: leaflet. Scale bars are: all 200 µm.

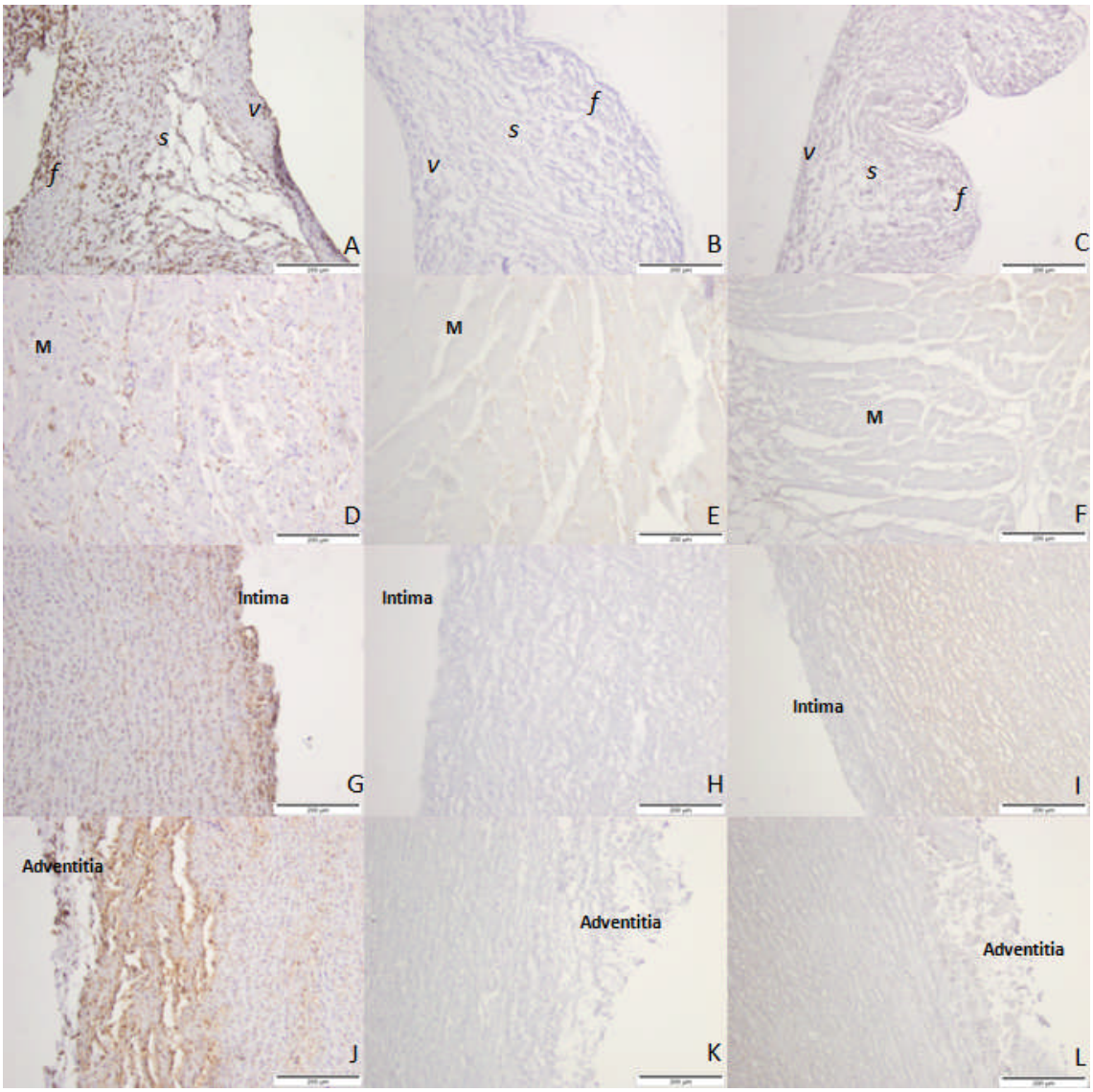

Figure 4.17 Localisation of vimentin in fresh and decellularised porcine pulmonary root tissue. (A) Fresh pulmonary valve leaflet, 100 ×; **(B)** Decellularised pulmonary valve leaflet, 100 ×; **(C)** Decellularised pulmonary valve leaflet isotype control, 100 ×; **(D)** Fresh myocardium, 100 ×; **(E)** Decellularised myocardium, 100 ×; **(F)** Decellularised myocardium isotype control, 100 ×; **(G)** The lumen surface of the fresh pulmonary wall, 100 ×; **(H)** The lumen surface of the decellularised pulmonary wall, 100 ×; **(I)** The lumen surface of the decellularised pulmonary wall isotype control, 100 ×; **(G)** The adventitial surface of the fresh pulmonary wall, 100 ×; **(H)** The adventitial surface of the decellularised pulmonary wall, 100 ×; **(L)** The adventitial surface of the decellularised pulmonary wall isotype control, 100 ×. *v*: *ventricularis*; *s*: *spongiosa*; *f*: *fibrosa*; M: myocardium; L: leaflet. Scale bars are: 200 µm.

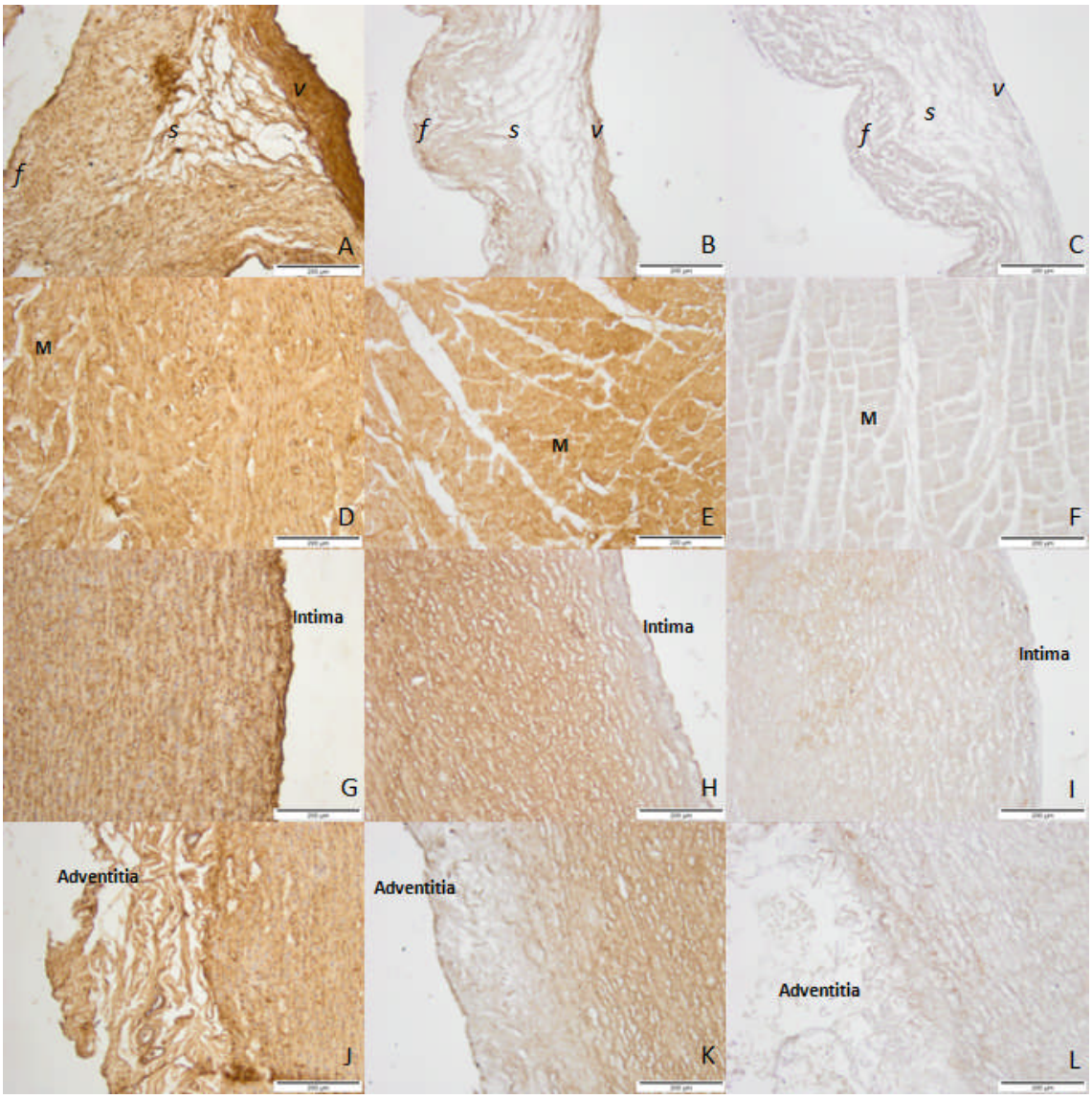

Figure 4.18 Localisation of fibronectin in fresh and decellularised porcine pulmonary root tissue. (A) Fresh pulmonary valve leaflet, 100 ×; **(B)** Decellularised pulmonary valve leaflet, 100 ×; **(C)** Decellularised pulmonary valve leaflet isotype control, 100 ×; **(D)** Fresh myocardium, 100 ×; **(E)** Decellularised myocardium, 100 ×; **(F)** Decellularised myocardium isotype control, 100 ×; **(G)** The lumen surface of the fresh pulmonary wall, 100 ×; **(H)** The lumen surface of the decellularised pulmonary wall, 100 ×; **(I)** The lumen surface of the decellularised pulmonary wall isotype control, 100 ×; **(J)** The adventitial surface of the fresh pulmonary wall, 100 ×; **(K)** The adventitial surface of the decellularised pulmonary wall, 100 ×; **(L)** The adventitial surface of the decellularised pulmonary wall isotype control, 100 ×. *v*: *ventricularis*; *s*: *spongiosa*; *f*: *fibrosa*; M: myocardium; L: leaflet. Scale bars are: all 200 µm.

4.4.3.6 Collagen IV

The results of porcine pulmonary root tissue labelled with antibody to collagen IV are shown in Figure 4.19. A brown line was observed on the surfaces of the fresh porcine pulmonary leaflets (Figure 4.19 A) as well as the lumen surface of the fresh pulmonary artery (Figure 4.19 G). Positive staining was also observed in the blood vessels within the connective tissue layer outside the adventitia of fresh porcine pulmonary artery (Figure 4.19 J). Following decellularisation, no evidence of the presence of collagen IV was found in any location within the porcine pulmonary root (Figure 4.19 B, E, H, K). No brown colour was observed in the sections stained with the isotype control.

4.4.3.7 α-gal

Images of porcine pulmonary root tissue labelled with antibody to α-gal are shown in Figure 4.20. The endothelial layer of the pulmonary leaflet and VIC`s (Figure 4.20 A) and the small blood vessels in the myocardium (Figure 4.20 D) were stained brown. No brown colour was observed in the pulmonary artery (Figure 4.20 G). No evidence of positive staining was observed throughout the decellularised porcine pulmonary roots (Figure 4.20 B, E, H). No brown colour was observed in the sections stained with the isotype control.

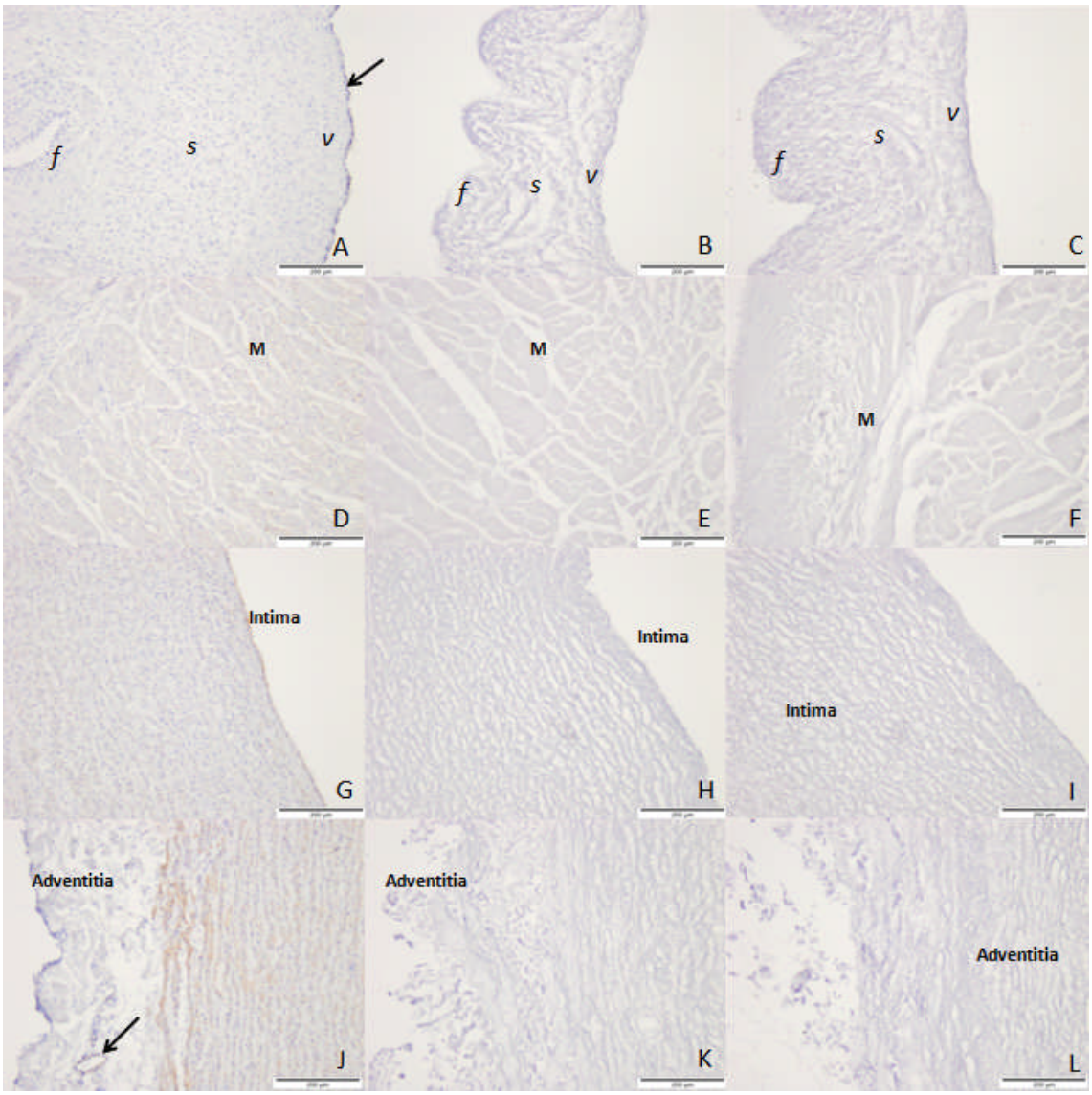

Figure 4.19 Localisation of collagen IV in fresh and decellularised porcine pulmonary root tissue. (A) Fresh pulmonary valve leaflet, 100 ×, the arrow indicated the surface of pulmonary leaflet that has been positively stained; **(B)** Decellularised pulmonary valve leaflet, 100 ×; **(C)** Decellularised pulmonary valve leaflet isotype control, 100 ×; **(D)** Fresh myocardium, 100 ×; **(E)** Decellularised myocardium, 100 ×; **(F)** Decellularised myocardium isotype control, 100 ×; **(G)** The lumen surface of the fresh pulmonary wall, 100 ×, the arrow indicated the surface layer of pulmonary wall that has been positively stained; **(H)** The lumen surface of the decellularised pulmonary wall, 100 ×; **(I)** The lumen surface of the decellularised pulmonary wall isotype control, 100 ×; **(J)** The adventitial surface of the fresh pulmonary wall, 100 ×, the arrow indicates a blood vessel that has been positively stained; **(K)** The adventitial surface of the decellularised pulmonary wall, 100 ×; **(L)** The adventitial surface of the decellularised pulmonary wall isotype control, 100 ×. *V*: *ventricularis*; *s*: *spongiosa*; *f*: *fibrosa*; M: myocardium; L: leaflet. Scale bars are: all 200 µm.

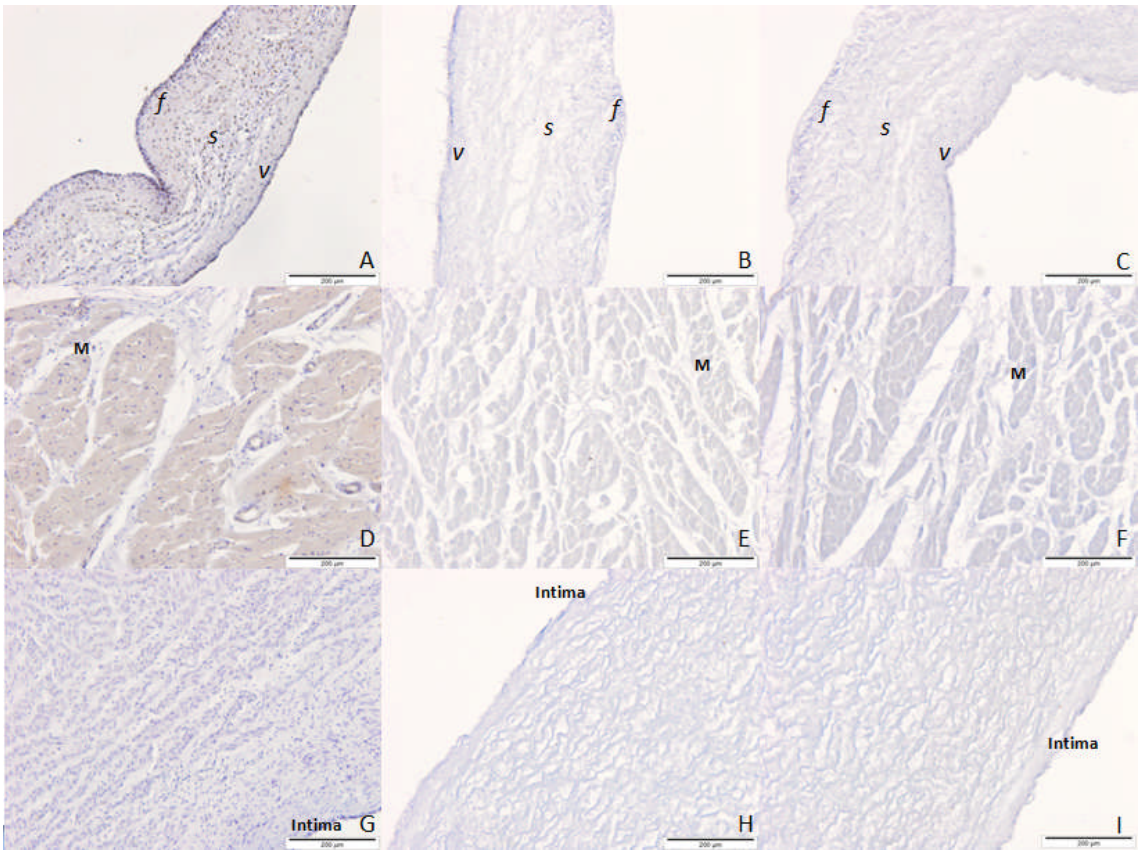

Figure 4.20 Localisation of α-gal in fresh and decellularised porcine pulmonary root tissue. (A) Fresh pulmonary valve leaflet, 100 ×; **(B)** Decellularised pulmonary valve leaflet, 100 ×; **(C)** Decellularised pulmonary valve leaflet isotype control, 100 ×; **(D)** Fresh myocardium, 100 ×; **(E)** Decellularised myocardium, 100 ×; **(F)** Decellularised myocardium isotype control, 100 ×; **(G)** The lumen surface of the fresh pulmonary wall, 100 ×; **(H)** The lumen surface of the decellularised pulmonary wall, 100 ×; **(I)** The lumen surface of the decellularised pulmonary wall isotype control, 100 ×. *v*: *ventricularis*; *s*: *spongiosa*; *f*: *fibrosa*; M: myocardium; L: leaflet. Scale bars are: all 200 µm.

4.4.4 *In vitro* biocompatibility assays

Contact cytotoxicity assay and extract cytotoxicity assay were used in this study to evaluate the *in vitro* biocompatibility of the decellularised porcine pulmonary root tissue. The effect of the decellularised tissue on the cell growth (murine 3T3 fibroblasts and murine L929 fibroblasts) was evaluated.

4.4.4.1 Contact cytotoxicity assay

The contact cytotoxicity assay was used to study the *in vitro* biocompatibility of the decellularised porcine pulmonary valve leaflets by culturing cells directly in contact with the tissue. The images (Figure 4.21; Figure 4.22) taken by microscopy recorded the cell growth and morphology after culture. When 3T3 cells and L929 cells were cultured with cyanoacrylate contact adhesive (positive control), no evidence of cells was found in a circular area around the adhesive. Cells started to appear at about 1,500 µm far from the edge of the cyanoacrylate contact adhesive (Figure 4.21 A; Figure 4.22 A). Collagen gel (negative control) had no effect on either of the cell types that were used in this study (Figure 4.21 B; Figure 4.22 B). Cells were able to grow to the edge and into the collagen gel. The contact cytotoxicity results of the 6 porcine pulmonary roots indicated the decellularised leaflets had no effect in changing the cell growth or cell morphology for both cell types (Figure 4.21 C, D, E, F, G, H; Figure 4.22 C, D, E, F, G, H). Cells grew in contact with the decellularised tissue. No difference was observed between the morphology of cells cultured with decellularised porcine pulmonary leaflets and cell cultured with the collagen gel.

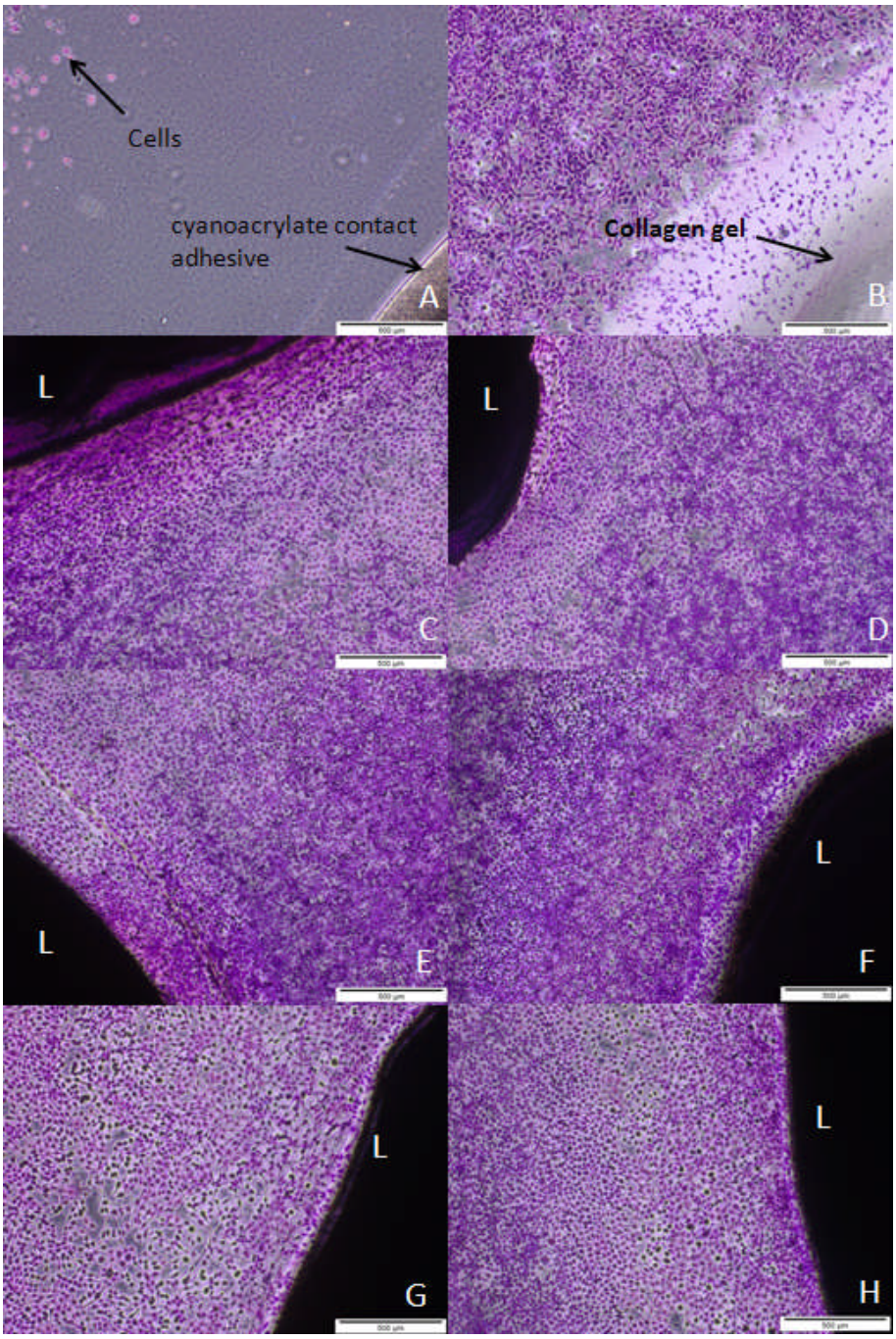

Figure 4.21 Contact cytotoxicity assays of decellularised porcine pulmonary valve leaflets following 48 h culture with murine 3T3 fibroblasts. (A) Cyanoacrylate contact adhesive (positive control), 40 ×, the arrow indicates cells; **(B)** Collagen gel (negative control), 40 ×; **(C)** Porcine pulmonary valve leaflet 1, 40 ×; **(D)** Porcine pulmonary valve leaflet 2, 40 ×; **(E)** Porcine pulmonary valve leaflet 3, 40 ×; **(F)** Porcine pulmonary valve leaflet 4, 40 ×; **(G)** Porcine pulmonary valve leaflet 5, 40 ×; **(H)** Porcine pulmonary valve 6, 40 ×. L: leaflet. Scale bars are: all 500 µm.

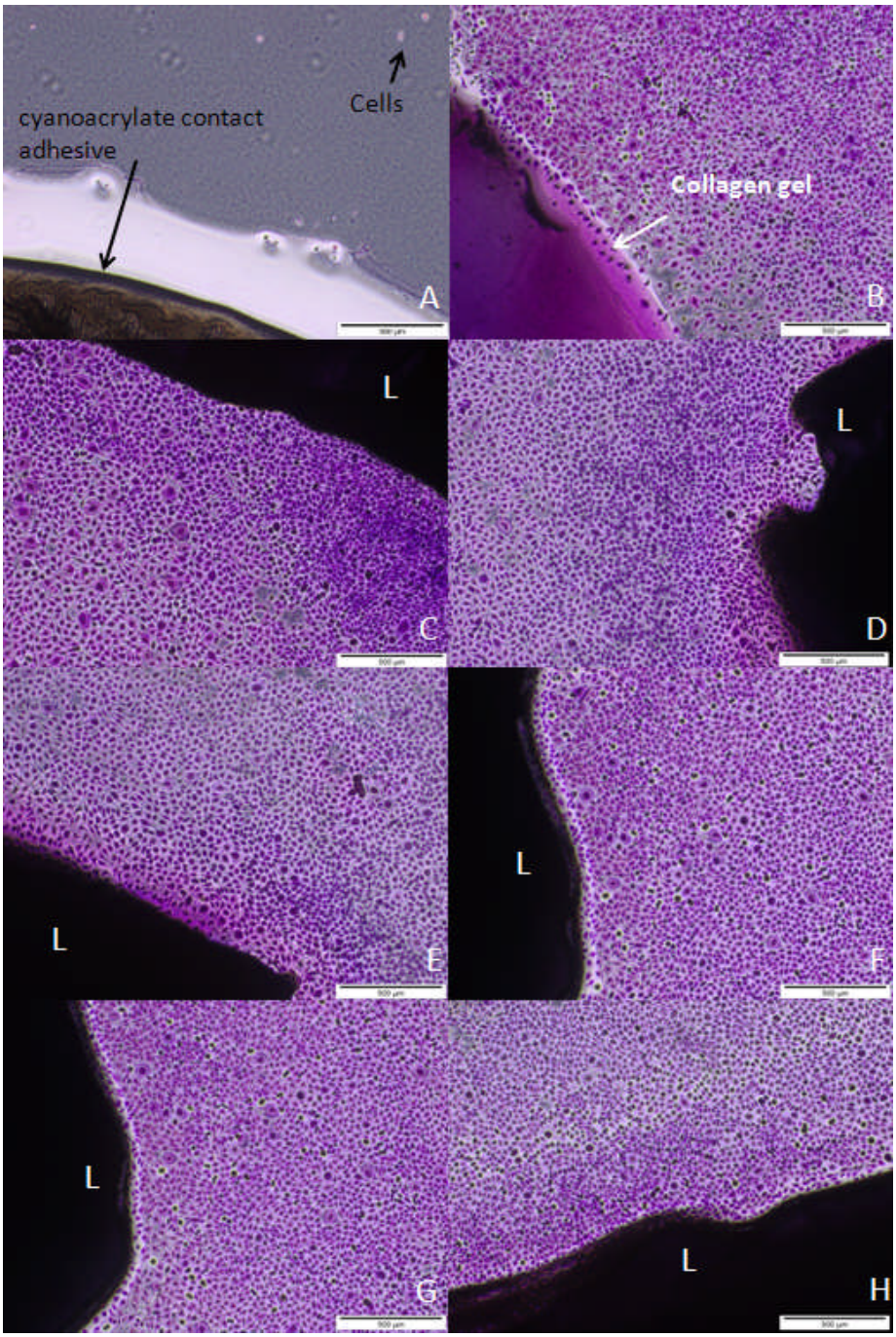

Figure 4.22 Contact cytotoxicity assays of decellularised porcine pulmonary valve leaflets following 48 h culture with murine L929 fibroblasts. (A) Cyanoacrylate contact adhesive (positive control), 40 ×, the arrow indicates cells; **(B)** Collagen gel (negative control), 40 ×; **(C)** Porcine pulmonary valve leaflet 1, 40 ×; **(D)** Porcine pulmonary valve leaflet 2, 40 ×; **(E)** Porcine pulmonary valve leaflet 3, 40 ×; **(F)** Porcine pulmonary valve leaflet 4, 40 ×; **(G)** Porcine pulmonary valve leaflet 5, 40 ×; **(H)** Porcine pulmonary valve 6, 40 ×. L: leaflet. Scale bars are: all 500 µm.

4.4.4.2 Extract cytotoxicity assay

The extract cytotoxicity assay was used to determine the effect of soluble components of decellularised porcine pulmonary artery on the viability of 3T3 cells and L929 cells. The relative ATP levels of cells following culture with tissue extracts are shown in Figure 4.23 (for murine 3T3 fibroblasts) and Figure 4.24 (for murine L929 fibroblasts). Data was analysed using one way ANOVA. The relative ATP levels were significantly lower in the positive control (cultured with DMSO; $p<0.05$) compared to the negative control (cells cultured in cell culture medium) for both cell types. The mean relative ATP content of the cells cultured with the 6 decellularised porcine pulmonary artery extracts showed no significance difference compared with the negative control for both cell types. When comparing the relative ATP level between individual decellularised pulmonary roots and the negative control, a significant reduction in ATP levels was observed in 3 out of 6 decellularised pulmonary artery extracts cultured with 3T3 cells. No significant difference was observed between individual decellularised pulmonary artery extracts and the negative control when cultured with L929 cells.

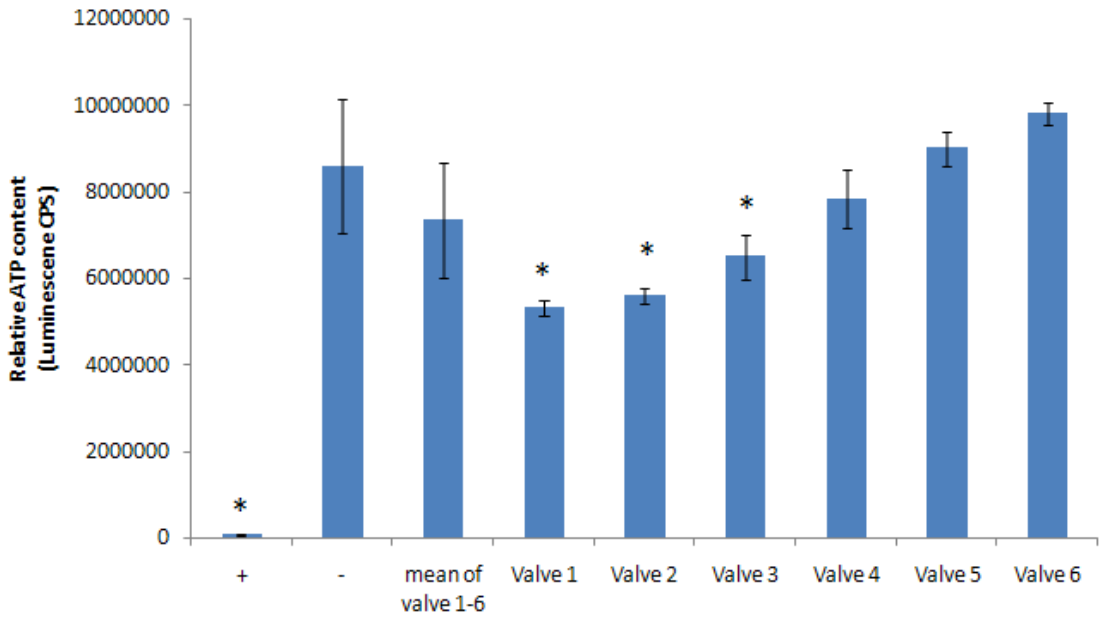

Figure 4.23 Cell viability of murine 3T3 fibroblasts following 72 h cultured *in vitro* with decellularised porcine pulmonary artery extracts. Data is presented as the mean (n=6) ± 95 % confidence limits. Data was analysed using one way ANOVA followed by calculation of the MSD by the T-method ($p<0.05$). +: DMSO positive control; -: cell culture medium negative control. "*" indicates a significant difference when compared with the negative control group.

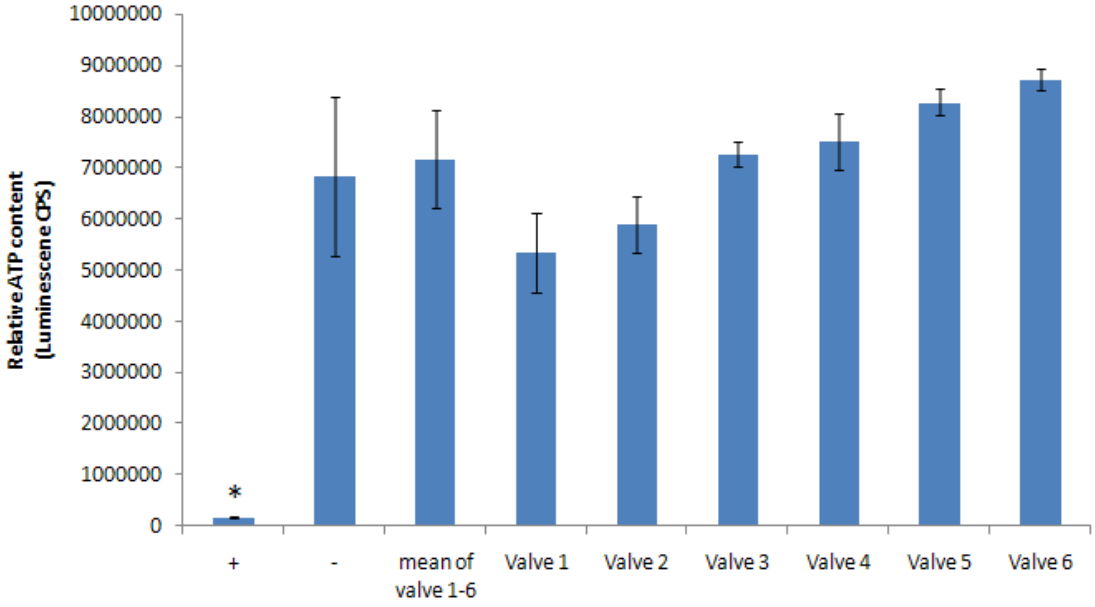

Figure 4.24 Cell viability of murine L929 fibroblasts cultured *in vitro* with decellularised porcine pulmonary arteries extracts following 72 h. Data is presented as the mean (n=6) ± 95 % confidence limits. Data was analysed using one way ANOVA followed by calculation of the MSD by the T-method ($p<0.05$). +: DMSO positive control; -: cell culture medium negative control. "*" indicates a significant difference when compared with the negative control group.

4.5 Discussion

In this chapter, the biological characteristics of the acellular porcine pulmonary roots were evaluated and compared to fresh tissues. The decellularisation method used to obtain the acellular tissue in this chapter was referred to as 'Method 6' in Chapter 3. This method involved trypsin treatment of the adventitial surface of the scraped pulmonary artery, together with 1 cycle of SDS-hypotonic buffer treatment and 2 cycles of nuclease treatment. This method was developed with care to remove the cells while causing minimal damage to the ECM.

Histology was used to evaluate the extent of decellularisation and the integrity of the ECM. H&E and Hoechst stained images showed no evidence of cell presence in the decellularised tissue, which indicated the removal of cells throughout the decellularised porcine pulmonary roots. H&E staining showed no evidence of damage to the decellularised tissue, and the histoarchitecture of the ECM was not altered following decellularisation. The connective tissue distribution in the acellular porcine pulmonary valve leaflet was comparable to the fresh tissue. The density of connective tissue (pink/red in H&E stain) in the leaflets was much higher in the *fibrosa* and *ventricularis* than that in *spongiosa*. The myocardium bundles and the pulmonary artery structure were not changed after decellularisation. The elastin fibre distribution was not altered after decellularisation as revealed by Miller's staining. However, an absence of GAG`s was observed in acellular pulmonary leaflet and artery tissues following Alcian blue staining. This revealed a difference from the fresh tissue, in which GAG`s were observed in the leaflets, pulmonary wall and the leaflet connection. This indicated a significant amount of GAG was lost during the decellularisation procedure. A similar finding was reported by Miradraee (2005) for human pericardium tissue decellularisation, Stapleton (2008) for porcine meniscus tissue decellularisation and Cheng *et al*. (2009) in porcine cartilage. In the above studies, SDS was also used as a detergent during decellularisation. SDS has been reported to remove GAG`s from tissue (Gilbert *et al*., 2006; Yang *et al.*, 2010). The lost of GAG`s may have aided the success in decellularisation because the removal of GAG`s would allow increased access of the decellularisation reagents to diffuse into the tissue. GAG`s are, however, very important components in the loosely arranged *spongiosa* layer of the porcine pulmonary leaflets, and are believed to perform an important role in the integrity and mechanical properties of the leaflets. Thus, although no evidence of change in the structure of the leaflet ECM

was observed by histology, it will be essential to evaluate the hydrodynamic properties of the acellular porcine pulmonary root, in order to assess the functional significance of GAG loss.

The amount of DNA removal is very important in evaluating the success of decellularisation. DNA was extracted and the total quantities of DNA in fresh (n=6) and decellularised (n=6) porcine pulmonary roots were quantified by spectrophotometry at 260 nm, which is the most straight-forward method for DNA quantification. The fresh samples demonstrated around 0.2 μg DNA per mg tissue. After decellularisation, the DNA content demonstrated a reduction of more than 90 % throughout the porcine pulmonary root tissue. The majority of DNA was therefore successfully removed after decellularisation. A limitation of this method was: the DNA concentration detected by Nanodrop spectrophotometry is only accurate when it reaches a certain level. The lowest end of sensitivity of the nanodrop spectrophotometer is 2 $ng.\mu l^{-1}$, which was very close to the readings for decellularised samples. Thus, it is highly likely that the actual amount of DNA removed following decellularisation was even greater than the percentage presented in this study. In future studies, the amount of DNA in tissue could be assessed by extracting DNA from a greater mass of decellularised tissue, in order to obtain more accurate result of the DNA removal effect of decellularisation.

PCR was used to determine target gene expression in porcine pulmonary root tissue. Housekeeping genes of GAPDH (involved in carbohydrate metabolism), SLA-2 (porcine histocompatibility antigen), β 2-microglobulin (involved in the expression of MHC class I molecules) and β actin (a cytoskeleton actin that is important in cell motility, structure and integrity) were selected as target genes (Eisenberg & Levanon, 2003; Barber *et al*., 2005). Housekeeping genes were selected because they are universal in cell DNA and the expression of the genes remains constant in the tissues, thus providing a reliable standard to investigate the presence of any remaining functional DNA in the tissue.

The same DNA extracts for Nanodrop spectrophotometry were used for PCR. Gradient PCR was conducted initially to determine the appropriate Tm for each gene. Fresh tissue DNA extracts provided sufficient template DNA to study appropriate PCR conditions. Fresh porcine pulmonary artery DNA extracted from valve No 3 was used as the template for GAPDH gradient PCR, and fresh porcine pulmonary valve leaflet

DNA extracted from Valve No 1 was randomly selected to be used as the template for gradient PCR for SLA-2, β 2-microglobulin and β actin. The concentrations of primer and template for PCR were also optimised to obtain maximum product yields (data not shown). Once the PCR conditions for each gene had been determined, all of the samples from fresh and decellularised porcine pulmonary roots were subjected to PCR. For each PCR, a blank reaction containing all reaction components except the DNA template was included to ensure no contamination (DNA from other sources) was introduced during the experiment. No contamination was observed in any of the reactions. The results of fresh DNA extract PCR analyses showed single clear product bands on the gels. The GAPDH PCR had a predicted product size of 230 bp, but the PCR products had a size of around 600 bp. The β 2-microglobulin PCR had a predicted product size of 189 bp, but the PCR products had a size of around 760 bp. The β actin PCR was predicted to have a product size of 210 bp while the actual amplified fragments were around 300 bp. The reason that the PCR product sizes were larger than predicted was because: mRNAs which only included the exons were used for primer design and product size prediction, but fresh porcine pulmonary root tissue DNA extract contained the complete genomic DNA which included both exons and introns. When the PCR primers targeted a gene fragment which included the complete or part of two or more exons, the actual PCR product would contain the introns between those exons that were amplified from the genomic DNA. The SLA-2 PCR product had a size of around 250 bp, which is the same as predicted. The fact that no PCR product band was seen in any of the decellularised samples indicated that no template of the target genes was present in the decellularised tissue extracts. This result provided further evidence of the successful removal of DNA after decellularisation.

Immunohistochemical labelling was used to localise specific proteins in the porcine pulmonary roots. Tissue sections stained with α-SMA were observed to be positively stained in fresh pulmonary artery and small blood vessels within the porcine pulmonary root tissue. This was as expected since smooth muscle cell is the major cell type in fresh arteries and vessels. Positive staining was also observed on the surface layer of the fresh pulmonary leaflets especially in the *ventricularis*. It has been reported that the smooth-muscle-like cells are distributed in the *ventricularis* and *spongiosa* due to the pressure level on the leaflets (DellaRocca *et al*., 2000). The result from this study was in agreement with the study conducted by Bertiplaglia *et al*. (2003) in which smooth

muscle cells distributed more prevalent in the *ventricularis* than in the *fibrosa*. Residual α-SMA was detected in the matrix of the decellularised porcine pulmonary roots indicating that upon cell lysis, some of the intracellular protein may have remained in the matrix. A blast search for similarity of the porcine and human α-SMA was carried out using the NCBI online tool BlastP. The porcine and human α-SMA sequences had 100 % (377/377 a.a.) identity. Thus, the residual α-SMA would not be antigenic if the xenogenic acellular scaffold was transplanted into humans. Tissue sections stained with vWF, which is a marker for the endothelial cells, were shown to be positive in the endothelial cell layers on the surface of the fresh pulmonary leaflets and the pulmonary artery, as well as the small blood vessels in the porcine pulmonary root tissue. The staining was negative throughout the decellularised porcine pulmonary root tissue, indicating the successful removal of the endothelial cells following decellularisation. The level and localisation of desmin remained the same after decellularisation. Desmin is a cytoskeletal protein expressed by muscle cells. A blast search for similarity of the porcine and human desmin was done using the NCBI online tool BlastP. The porcine desmin sequence had 98 % (463/470 a.a.) identity to the human desmin. Query coverage (the length coverage of high scoring pairs) of 100 % had also been identified. Because of the very high similarity of the porcine and human desmin proteins, it is unlikely the remaining desmin would be antigenic if the xenogenic decellularised scaffold was transplanted into humans. Positive staining for vimentin was observed in all cells in the fresh porcine pulmonary root tissue because it is a very important cytoskeletal component. No evidence of vimentin expression was found in the acellular porcine pulmonary roots, which was a result of the successful cell removal during the decellularisation procedure.

The levels of fibronectin appeared to be lower in decellularised leaflet and artery tissues compared to fresh, and most fibronectin was lost in the surface exposed regions indicating that the protein may have been partially removed during the wash processes. Collagen IV was used in immunohistochemistry as a marker to detect the presence of the basement membrane. The basement membrane is a specialised form of the ECM that supports and facilitates the growth of epithelial cell populations, thus is considered very important in the endothelialisation of tissue engineered scaffolds after implantation (Brown *et al*., 2006b). In this study, sections of fresh samples showed specific staining in the basement membrane of pulmonary leaflets and arteries. The decellularised

samples on the other hand, showed the complete removal of collagen IV. The removal of basement membrane is not in agreement with studies reported by others which also used SDS as a decellularisation detergent for porcine pulmonary heart valve tissue (Tudorache *et al*., 2007). Recent experimental results in the laboratory conducted by Dr Stacy-Paul Wilshaw have demonstrated that the PAA sterilisation treatment is responsible for the basement membrane removal during decellularisation of arteries. Therefore, PAA treatment may not be the ideal method of sterilisation and it may be necessary to develop an alternative method to replace the PAA treatment in order to retain the basement membrane to support the endothelial cell attachment after transplantation.

The α-gal epitope is the major xenoantigen causing hyperacute rejection. If α-gal epitope remained in the decellularised tissue scaffold, it may have the potential to incite a strong inflammatory response if implanted due to the presence of anti-α-gal antibodies in humans (Simon *et al*., 2003). The presence of the α-gal epitope was detected and localised using immunohistochemistry in this study. The results revealed the absence of α-gal in the decellularised porcine pulmonary roots. Further quantitative analysis of the α-gal levels should be carried out in the future to validate this study.

Contact cytotoxicity assays were performed to determine the effect of any remaining chemicals within the porcine pulmonary valve leaflets on the growth of murine 3T3 fibroblasts and murine L929 fibroblasts *in vitro*. The results indicated that the cells proliferated normally around and in direct contact with the decellularised porcine pulmonary leaflets. The cell morphology remained normal when cultured with the decellularised tissue. The decellularised porcine pulmonary leaflets were not cytotoxic to cells. Extract cytotoxicity assays were applied to quantify cell viability (murine 3T3 fibroblasts and murine L929 fibroblasts) after culturing with the soluble extracts of the decellularised porcine pulmonary arteries by detecting their relative cell ATP content. The mean level of relative ATP for the six porcine pulmonary arteries showed no significant difference compared with the negative controls for both cell types. To look at each sample individually, 3 out of 6 samples showed significant reduction in the relative ATP levels compared with the negative control for 3T3 cells. All of the 6 samples showed no significant difference in the relative ATP levels compared to the negative control for L929 cells. In this study, three times 30 min washes with PBS at 37 °C were applied at the end of decellularisation to remove any remaining chemicals. These results

showed that it will be necessary to increase the final wash process duration to help remove remaining chemicals in individual pulmonary arteries, and thus provide biocompatible scaffolds. The contact and extract cytotoxicity results are in agreement of the results obtained by Wilcox *et al*. (2005), who also used 0.1 % (w/v) SDS and trypsin in porcine aortic heart valve decellularisation.

4.6 Conclusion

The decellularisation method for porcine pulmonary roots used in this chapter applied trypsin treatment on the adventitial surface of the scraped pulmonary artery, together with 1 cycle of hypotonic SDS buffer treatment and 2 cycles of nuclease treatment (referred to as 'Method 6' in Chapter 3). Histology results confirmed that complete decellularisation was achieved using this method, with histoarchitecture well retained. The levels of collagen and elastin remained qualitatively similar in porcine pulmonary roots after decellularisation, but a loss of GAG`s was observed by Alcian blue staining of tissue sections. Nanodrop spectrophotometry results showed that greater than 90 % of DNA was successfully removed throughout the porcine pulmonary roots following decellularisation. House keeping genes GAPDH, SLA-2, β 2-microglobulin and β actin were not detected by PCR in decellularised tissue. Immunohistochemistry results further confirmed the absence of cells in the decellularised scaffolds. However, the basement membrane protein collagen IV was removed following decellularisation. The major xenoantigen α-gal was not detected in decellularised tissue by immunohistochemistry. *In vitro* cytotoxicity assays demonstrated the decellularised pulmonary leaflets were not cytotoxic to murine 3T3 and L929 fibroblasts. *In vitro* extract cytotoxicity assays demonstrated the decellularised pulmonary arteries were not cytotoxic to L929 fibroblasts, while 3 out of 6 decellularised pulmonary artery samples under test significantly decreased the viability of murine 3T3 fibroblasts. In conclusion, the decellularised porcine pulmonary root scaffold demonstrated cell removal with good biocompatibility. The biomechanical properties of the acellular porcine pulmonary roots will be further evaluated in the next chapter.

Chapter 5

Biomechanical & Hydrodynamic Characterisation of Fresh and Acellular Porcine Pulmonary Valve Roots

5.1 Introduction

As discussed in the previous chapter, the acellular porcine pulmonary root scaffold demonstrated cell removal and good biocompatibility. This chapter describes, the biomechanical and hydrodynamic assessments of the acellular pulmonary roots in terms of low-strain-rate uniaxial tensile loading to failure testing and pulsatile flow testing, respectively. Uniaxial tensile testing was utilised to determine the stress-strain behaviour of the decellularised root tissues, whereas near physiological pulsatile flow testing was used to evaluate the mean pressure drop across the acellular valves during the cardiac cycle and their effective orifice area (EOA). Pulsatile flow testing was also used to assess the kinematics and the bending stress and strain of the free leaflet edge of the acellular valves during the cardiac cycle. During all three types of assessment, the performance of the decellularised roots was compared to the performance of the native pulmonary root.

5.2 Aims and objectives

Aims:

The aim of the work described in this chapter was to investigate the effects of the decellularisation method developed in Chapter 3 on the biomechanical and hydrodynamic characteristics of porcine pulmonary roots.

Objectives:

- To assess the effects of decellularisation on the uniaxial tensile properties of the decellularised tissues by comparison to fresh porcine pulmonary root tissues.
- To characterise the hydrodynamic behaviour of fresh and decellularised porcine pulmonary roots under simulated pulsatile flow conditions.
- To determine the leaflet kinematics of fresh and decellularised porcine pulmonary roots under simulated pulsatile flow conditions.

5.3 Methods

5.3.1 Uniaxial tensile testing

The biomechanical properties of native and decellularised (Method 6, Section 3.4.8.1) porcine pulmonary roots were assessed under uniaxial tensile loading to failure testing, according to the methodology described in Section 2.2.10. Circumferential (n=6) and axial (n=6) specimens were dissected from scraped fresh and decellularised porcine pulmonary arteries. The size of the pulmonary artery specimens was 5 mm in width by approximately 20 mm in length. Following mounting in the holder, the actual test length (initial gauge length) of the pulmonary wall specimens was 10 mm. Circumferential (n=6) and radial (n=6) specimens were also dissected from the left pulmonary leaflets of fresh and decellularised (Method 6, Section 3.4.8.1) pulmonary roots and tested under uniaxial tensile loading to failure. The pulmonary leaflet specimens were 3 mm in width by approximately 15 mm in length. Following mounting in the holder, the test length (initial gauge length) of the leaflet specimens was 6 mm, which similar to the case of the pulmonary wall, gave a testing aspect ratio of 2:1. In order to obtain a more representative set of data, the specimens of each of the control and test groups were procured from the pulmonary roots of different animals. The results for the control (fresh) and test (decellularised) groups were compared with respect to the anatomical direction (circumferential vs. axial wall and circumferential vs. radial leaflet) and with respect to treatment (fresh vs. decellularised). Moreover, the results for the pulmonary wall were also compared to the results obtained from the fresh intact pulmonary arteries described in Section 3.4.5. The wall and leaflet groups are listed in Tables 5.1 and 5.2, respectively.

Table 5.1 The test and control groups used in the uniaxial tensile testing of porcine pulmonary arteries.

	Fresh intact		Scraped fresh		Decellularised (Method 6)	
	C	A	C	A	C	A
No of samples	7	6	6	6	6	6

C: circumferential direction; A: axial direction. Fresh intact refers to the group the testing of which was described in Section 3.4.5.

Table 5.2 The test and control groups used in the uniaxial tensile testing of porcine pulmonary leaflets.

	Fresh		Decellularised (Method 6)	
	C	R	C	R
No of samples	6	6	6	6

C: circumferential direction; R: radial direction.

The recorded force and extension data was converted to stress and strain, respectively, as described in Chapter 2 (Section 2.2.10.4), and the elastin and collagen phase slopes, transition stress and strain, and failure stress and strain were obtained from the stress-strain responses of each specimen. Subsequently, each of the aforementioned biomechanical parameters were averaged over the number of specimens in each of the control and test groups. The stress-strain responses of the specimens in each group were further processed in Origin 8.0 software package, which was used to generate the mean stress-strain response for each group. In order to do this, a cubic spline was fitted to each data set (stress-strain response of each specimen) and the data set was extrapolated/interpolated up to the mean failure strain of the particular control or test group. The data set for each group then had the same normalised strain, thus the combined mean stress-strain curves could be generated for each test groups. Subsequently, 100 data points (out of approximately 3,000) were interpolated from each data set, at 100 equally-spaced intervals (the same for all samples in a particular group) of the engineering strain into 100 equal portions. The interpolated data sets of the specimens in each group were then averaged over the number of specimens in each group to produce the mean stress-strain behaviour of the group. The mean stress-strain curves do not present the true stress-strain behaviour of each specimen. However, the mean trend of each test group could be visualised by these mean stress-strain behaviour curves.

5.3.2 Hydrodynamic function testing

5.3.2.1 The pulsatile flow simulator

The pulsatile flow simulator used in this study was originally developed by Fisher *et al.* (1986) (Figure 5.1). It was designed to mimic the function of the left or right side of the

heart for testing prosthetic valves in the mitral/tricuspid or aortic/pulmonary position. The simulator allows valves to be repeatedly tested under standard controllable pulsatile flow conditions. The simulator comprised a pulsatile pump (positive displacement linear actuator, Model SP3891, Vivitro Systems Inc, Victoria BC, Canada), a viscoelastic impedance adapter, two test chambers for testing valves in the aortic/pulmonary or mitral/tricuspid valve positions, a ventricular and an atrial chamber, a compliance chamber or afterload, silicon tubing simulating the peripheral circulation, a peripheral resistance tap, and the pressure and flow measurement (Model PT43-604, Vivitro Systems Inc, Victoria BC, Canada) instruments. The simulator was controlled and monitored by the ViviTest software (Vivitro Systems Inc, Victoria BC, Canada) which was installed in the attached computer. The ViviTest software was also used to record and process the data during testing. The blood substitute used in the simulator was physiological saline (0.9 % w/v NaCl).

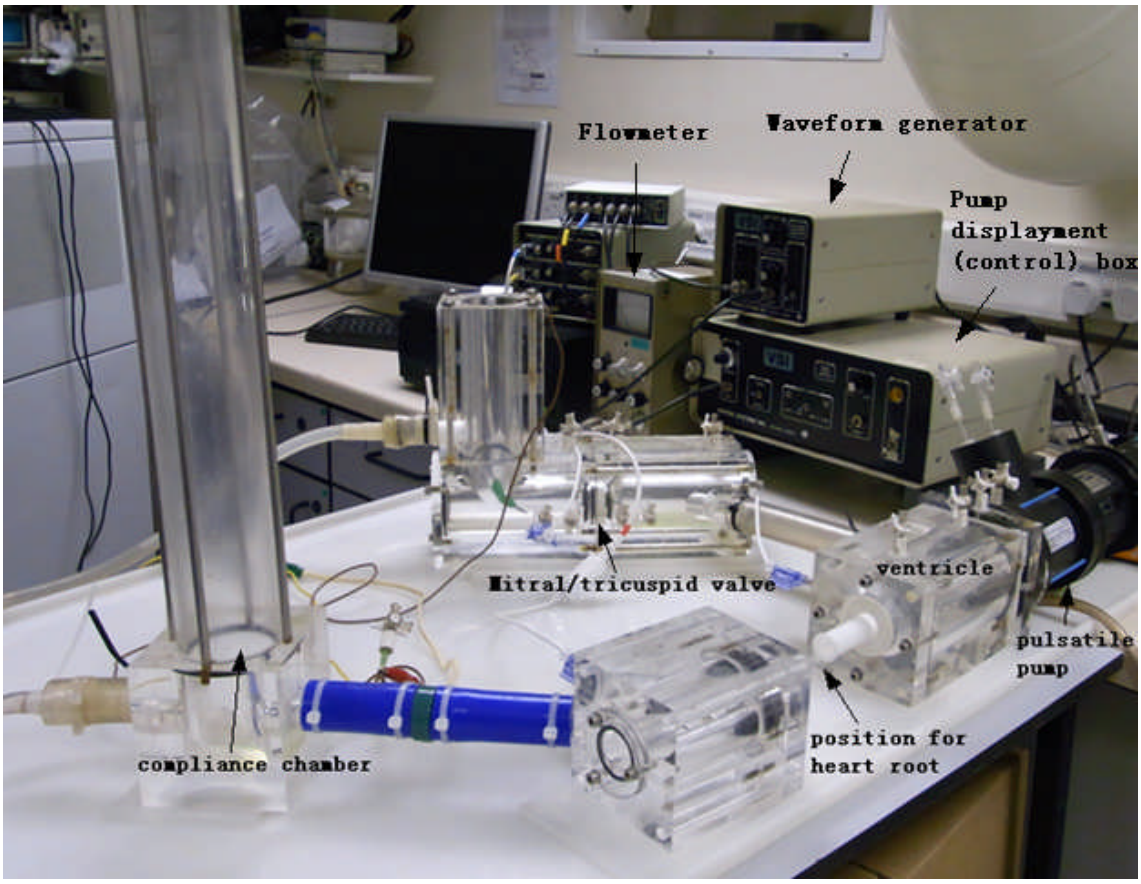

Figure 5.1 The pulsatile flow simulator. The simulator comprised a pulsatile pump (positive displacement linear actuator), a viscoelastic impedance adapter, two test chambers for testing valves in the aortic/pulmonary or mitral/tricuspid valve positions, a ventricular and an atrial chamber, a compliance chamber or afterload, silicon tubing simulating the peripheral circulation, a peripheral resistance tap, and the pressure and flow measuring instruments.

The schematics of the pulsatile flow simulator are shown in Figure 5.2. The waveform of the pulsatile flow was produced by a programmable waveform generator (Model WG5891, Vivitro Systems Inc, Victoria BC, Canada). The waveform generator was able to reproduce 5 different waveforms to match the blood flow characteristics of the cardiac cycle. However, only waveform C (sinusoidal) was used throughout this study since in previous studies (Jennings, 2001) it has been found to produce smoother mean pressure difference versus root mean square flow characteristics for tissue roots. During this study, the pulmonary roots were tested at the aortic/pulmonary test section (Figure 5.2 B), which comprised a ventricular chamber and pulmonary artery chamber. The ventricular chamber was attached to the linear actuator. The pulmonary artery was simplified as a straight tube with a diameter of 28 mm. The tissue root under investigation was mounted in-between the ventricular chamber and the pulmonary artery. The aortic chamber was connected to the afterload downstream, via stiff tubing of 25 mm in diameter. An electromagnetic flowmeter, which was used to measure the flow rate of the test medium, was incorporated in the tube. The afterload consisted of a vertical Perspex cylinder partially filled with saline and partially with air, which was sealed to the atmosphere. The afterload chamber acted as a damper in the pulsatile flow rig circulation, by minimising the abrupt peaks in the flow and pressure waveforms, which resulted from the flow of the incompressible test fluid in the rigid sections of the simulator. Physiological pressure ranges in the simulator were created by adjusting the variable peripheral resistance tap downstream of the afterload. The pressure in the simulated peripheral circulation was monitored by a pressure gauge attached to the top of the cylinder. The afterload was connected to the atrial reservoir via silicon rubber tubing, which featured the peripheral resistance tap. The atrial reservoir was opened to the atmosphere and produced a constant pressure head to the mitral/tricuspid valve section during systole. A 29 mm Bjork-Shiley tilting disc valve was used as the standard test valve in the mitral/tricuspid position throughout this study. The mitral/tricuspid valve section was connected to the ventricular chamber by a stiff tube, 25 mm in length.

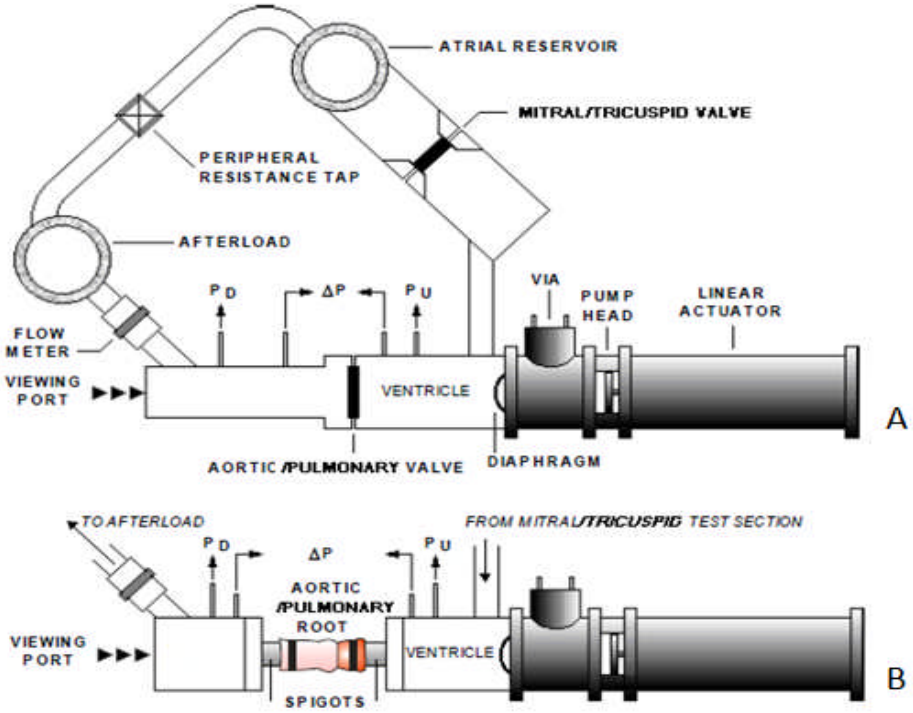

Figure 5.2 Schematic diagrams of the pulsatile flow simulator set up for mechanical valve testing in the aortic/pulmonary position (A), and for whole tissue root testing in the aortic/pulmonary position (B) (modified from Korossis, 2002).

Valve function in the pulsatile flow simulator was assessed by measuring the pressure difference across and flow through the test valve or valve root placed in the pulmonary position. An electromagnetic flowmeter (Spectramed Blood Flow Meter, Model SP2202) and electromagnetic probe were used to measure the flow through the valve under test. The probe was positioned approximately 200 mm downstream of the pulmonary valve position, and contained an electromagnet that produced a pulsed magnetic field at right angles to the direction of fluid flow. As the conducting fluid passed through this magnetic field, a pulsatile voltage was produced, which was directly proportional to the fluid velocity. The flow meter had a range of 10 $ml.min^{-1}$ to 30 $L.min^{-1}$, with a full scale output signal voltage of ±1.414 V pulsatile, and ±1.414 V DC mean. The pulsatile reading gave the undamped output. For direct recording purposes the mean flow signal was produced. The pressure difference across the valve under test was monitored using a Gaeltec differential pressure transducer (Model 3CT/Perspex), which had a measuring range of 0 to 200 mmHg and a sensitivity of 5 µV/V/mm Hg and an excitation voltage of ± 5 V. For the testing of tissue roots, the pressure transducers were connected at 25

mm upstream and 50 mm downstream of the root. The atrium pressure transducer was placed 50 mm upstream of the reference mechanical tricuspid valve.

5.3.2.2 Calibration of the pulsatile flow simulator

Prior to testing, the pressure transducers were calibrated with reference pressures of 0 and 200 mm Hg using a manometer. A standard test valve (Bjork-Shiley Monostrut 23 mm) was tested before each use of the simulator under the conditions listed in Table 5.3. The acquired data was compared to the historical data. Deviations from the previous recordings of ± 5 % were considered as acceptable, and indicated that the simulator was in its proper working condition.

Table 5.3 Test conditions used in the hydrodynamic function testing for Bjork-Shiley Monostrut 23 mm standard test valve.

Condition	Waveform	Heart rate (bpm)	Stroke volume (ml)	Cardiac output ($L.min^{-1}$)	Systematic pressure (mm Hg)
1	C	60	60	3.60	120/80
2	C	72	70	5.04	120/80
3	C	80	80	6.40	120/80
4	C	100	80	8.00	120/80
5	C	120	80	9.60	120/80

5.3.2.3 Tissue preparation

The porcine pulmonary roots were dissected according to the methodology described in Section 2.2.4. The size of the roots used for the pulsatile flow testing was approximately 18 mm, as sized by the obturators. The lengths of the myocardial skirt and the pulmonary artery of the tested roots were kept as long as possible during dissection in order to be able to mount the roots onto the spigots of the pulsatile flow simulator. The thickness of the myocardial skirt was trimmed to approximately 5 mm throughout. The fresh roots were tested within 10 h of slaughter. In total six fresh and six decellularised porcine pulmonary roots were tested. Both fresh and decellularised roots were kept in PBS prior to testing.

5.3.2.4 Testing procedure

All porcine pulmonary roots were tested under the three different pulsatile flow conditions listed in Table 5.4.

Table 5.4 Test conditions used in the hydrodynamic function testing for porcine pulmonary roots.

Condition	Waveform	Heart rate (bpm)	Stroke volume (ml)	Cardiac output ($l.min^{-1}$)	Pulmonary pressure (mm Hg)
1	C	60	60	3.60	35/5
2	C	72	70	5.04	45/10
3	C	80	70	5.60	50/10

The pressure and flow transducers were connected to the pulsatile flow simulator at the positions described in Section 5.3.2.1. The porcine pulmonary root under investigation was mounted with cable ties to appropriate sizes of acetal spigots which were prepositioned in the rig. PBS was pipetted onto the root surface at regular intervals during testing to prevent the tissue from drying out. The test rig was filled with saline and degassed with a syringe. The appropriate linear actuator waveform and heart rate (cycling rate) were set on the waveform generator. The actuator was set going by adjusting its stroke on the actuator control box, until the stroke volume monitored by the computer reached the required value (± 0.1 ml) at each test condition. The pulmonary pressures (systolic/diastolic) of each condition were obtained by completely releasing the pressure resistance tap. The pressures applied at each condition were the minimum pressures that could be obtained by this pulsatile flow simulator at the required cardiac output. These pressures were the closest pressures to the physiological pulmonary pressures that the rig could generate. When the test rig conditions were stabilised, the Vivitest software was run in data acquisition mode for ten cycles, and the pressure and flow data was stored in ACQ format files for subsequent analysis. Three test runs were performed at each condition for each root. The means of each hydrodynamic parameter were considered as the obtained value at each condition for each root. A high speed camera (Redlake® MotionScope, Model PCI 1000S) was used to record the motion of the heart valve leaflets during the cardiac cycle at flow condition 2 (72 bpm / 70 ml) and using a recording rate of 250 frames per second.

5.3.2.5 Data processing

The ACQ files recorded during each test run with each root, including the signal histories from the pressure transducers, the electromagnetic flow meter and the stroke of the linear actuator. Following testing, the ACQ files were analysed using the Vivitest analysis software. The differential pressure and flow waveforms were displayed on the computer screen, and the reference points were marked manually. An illustration of the differential pressure and flow waveform, together with the seven reference points is shown in Figure 5.3.

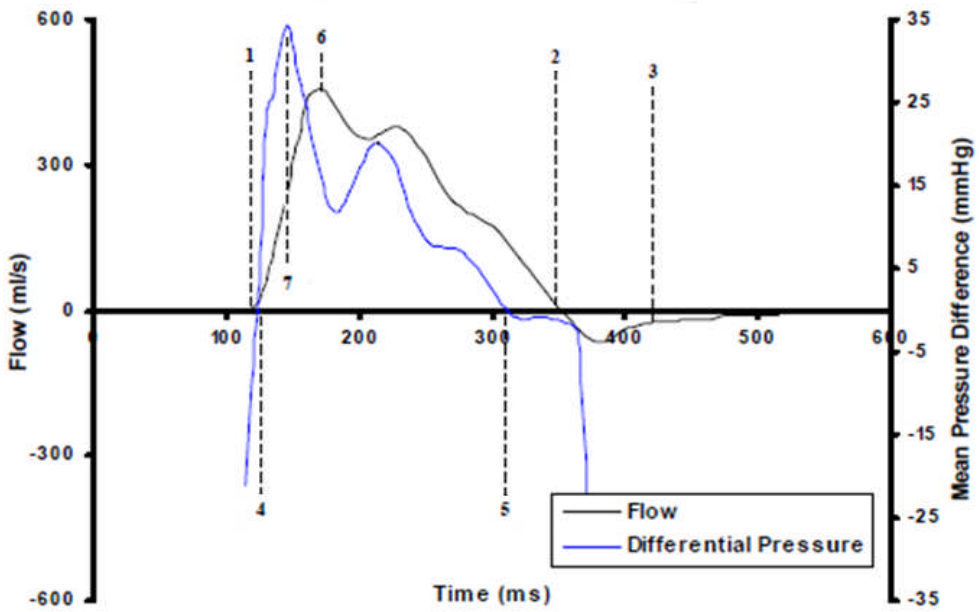

Figure 5.3 Differential pressure signals and flow waveform showing the reference time points used in data analysis. 1: Start of forward flow; 2: End of forward flow; 3: End of closing regurgitation; 4: Start of positive pressure difference; 5: End of positive pressure difference; 6: Maximum flow; 7: Maximum pressure (adapted from Korossis 2002).

The reference time points allowed the analysis to be performed during the forward flow interval (1-2), valve closing interval (2-3), valve closed interval (3-1), valve opening interval (1-6), valve closing interval (6-2), total systole (1-3), pressure-flow interval (4-2), and pressure-pressure interval (4-5). The function of the tested roots was assessed by means of the mean pressure difference across the valve (Δp), the root mean square forward flow through the valve (Q_{RMS}), and the valve EOA. The Δp across each valve was measured in the pressure-flow interval (4-2) as a function of the Q_{RMS}. The EOA is a measure of the resistance to the flow through the valve under test, and it was also

analysed in the pressure-flow interval. The calculation of the EOA was based on the formula that was derived by Gabbay *et al.* (1978) experimentally:

$$\mathrm{EOA} = \frac{\mathrm{Q_{RMS}}}{51.6 \times \sqrt{\Delta \mathrm{p}}}$$

The calculation of the three parameters was carried out by the Vivitest analysis programme based on the flow and differential pressure signals and the manually marked reference points. The calculated results were exported as .TXT files and transferred to a Microsoft Excel® (Version 2007) spreadsheet for statistical analysis. The results for each root were averaged over the number of test runs at each flow condition (n=3). All results were presented as means ± 95 % C.I.. The results for the fresh and decellularised roots were analysed by the Student's t-test, and the statistical significance was determined at the 95 % confidence level.

5.3.2.6 Image and leaflet bending deformation analysis

The leaflet kinematics of fresh (n=6) and decellularised (n=6) porcine left pulmonary leaflets was analysed during a complete cardiac cycle at pulsatile flow condition 2 (72 bpm/70 ml). During testing, the images were recorded using a high speed camera (Redlake® MotionScope, Model PCI 1000S) at a recording rate of 250 frames per second. Due to the anatomical obstructions, the motion of only one leaflet could usually be recorded in full for the whole duration of the cardiac cycle and thus, only the left pulmonary leaflets were used in the assessment of the bending deformation of the leaflet free edge. The acquired video sequences allowed the opening, open, closing and closed phase characteristics of the valves to be described. The opening, open, closing and closed phase durations, the shapes and bending deformations of the free edge of the left leaflets at four different time points (start opening, fully open, start closing, fully closed) were assessed.

The leaflet reference state (t=0) was defined at the instance where the leaflets were fully closed immediately prior to the start of the opening phase. This was denoted as start opening (SO). The fully open (FO) point referred to the beginning of the fully open leaflet phase. The start closing (SC) point was identified as the first point of the closing phase of the leaflets. The fully closed (FC) point was identified as the time point when the valve leaflets closed fully for the first time after opening. The opening, open, closing and closed phases referred to the time intervals between SO and FO, FO and SC, SC

and FC, and FC and SO of the next cardiac cycle, respectively. The phase durations were determined by counting the number of video frames between the reference points (SO, FO, SC, FC, SO) and multiplying it by the frame acquisition interval (4 ms).

The leaflet bending deformation was determined by the curvature of the leaflet free edge. The curvatures at each of the phase points (SO, FO, SC, FC) for each valve leaflet studied, were calculated along the circumferential direction according to the deformation of their free edge. The video frames corresponding to the phase points studied, were extracted from the video sequences using the Corel Photo Paint (Version X4) manufacture software package. Once extracted, the frames were further processed in Image Pro Plus (Version 4.51) manufacture software package by mapping the free edge of each leaflet at each of the phase points. In order to do this, each frame was calibrated using the measured internal diameter (19 mm) of the spigots used to mount the pulmonary artery of the roots in the pulsatile flow simulator, which was visible in the video frames captured. In order to improve the accuracy the edge of the spigot was placed as close to the leaflets as possible, without obstructing their motion during pulsatile flow testing.

Subsequently, a reference origin was defined at the same position for all frames analysed, which ensured that for any valve the co-ordinates of each leaflet had the same frame of reference at all time points. The shape of the leaflet free edge was then digitised by drawing along the leaflet free edge a polyline consisting of n points connected by n-1 straight lines (n was typically between 25 and 40), and the coordinates of the points (X_n, Y_n) were recorded. The calculation of the curvature required that there was one-to-one mapping of the free leaflet edge and that the domain of X_n values were monotonically increasing (i.e. $X_{n+1}>X_n$). Unless the condition of monotony was satisfied, the video frame was rotated until $X_{n+1}>X_n$ was satisfied. The X_n, Y_n co-ordinates of each point making up the polyline were exported to Microsoft Excel® for further analysis.

A cubic spline was fitted to the variably spaced (X_n, Y_n) data points of the leaflet free edge in the Origin (Version 8.0) software package. Equally spaced (X_i, Y_i) data points were interpolated from the cubic spline at 94 fixed intervals. From the interpolated, equally spaced (X_i, Y_i) data points the K_i at each fixed interval along the spline was calculated. A smoothing routine was then used to eliminate the possibility of

introducing false curvatures when the shape of the leaflet free edge was digitised. This resulted in the calculation of an average curvature ($K_{i,avg}$) profile. The rationale behind the averaging routine, together with the relevant formulae, is described in Appendix 2. The $K_{i,avg}$ profile of each left leaflet at each time point was calculated in Microsoft Excel®. The $K_{i,avg}$ was then used to calculate the average bending radius ($R_{i,avg}$) as:

$$R_{i,avg} = \frac{1}{K_{i,avg}}$$

Subsequently, the minimum bending radius (maximum deformation) for each leaflet at each phase point studied was calculated. The results for the fresh and decellularised valves were compared using the Student's t-test at the 95 % significance level.

5.4 Results

5.4.1 Biomechanics of fresh and decellularised porcine pulmonary roots

As discussed in Chapter 4, the decellularised porcine pulmonary roots demonstrated removal of cells and cell nuclei with the biological properties and histoarchitecture well retained. The biomechanical properties of the tissues were assessed under uniaxial tensile loading to failure in order to assess the effect of the decellularisation treatment on the mechanical behaviour of the porcine pulmonary leaflet and arterial wall.

5.4.1.1 Biomechanical characterisation of the pulmonary leaflets

The mean stress-strain behaviour and the individual stress-strain behaviours for each test sample of the fresh and decellularised pulmonary left leaflet groups is illustrated in Figure 5.4 (circumferential) and Figure 5.5 (radial). The curves demonstrated the typical quasi-linear characteristics of biological tissue with a low modulus region during the elastin phase and a high modulus region during the collagen phase, followed by specimen failure. The statistical analysis demonstrated no significant difference between the fresh and decellularised groups for the elastin phase slope (Figure 5.6), the collagen phase slope (Figure 5.7), the transition stress (Figure 5.8), the transition strain (Figure 5.9), the failure stress (Figure 5.10), and the failure strain (Figure 5.11) in the circumferential or radial directions. In addition, there was no significant difference in the leaflet thickness between the two groups along the radial direction (Figure 5.12). The results indicated a significant decrease ($p=0.009$) in the leaflet thickness of the decellularised circumferential group (Figure 5.12). The elastin slope of the leaflet pulmonary leaflet in the circumferential direction ($7.55\times10^{-4} \pm 2.86\times10^{-4}$ GPa) was about two fold compared to that in the radial direction ($3.42\times10^{-4} \pm 1.19\times10^{-4}$ GPa) (Figure 5.6). The collagen slope, transition stress and failure stress of the left pulmonary leaflet in the circumferential direction were about 10 fold compared to those in the radial direction (Figure 5.7; Figure 5.8; Figure 5.10). The transition and failure strains of the left pulmonary leaflet in the circumferential direction were at similar level of those in the radial direction.

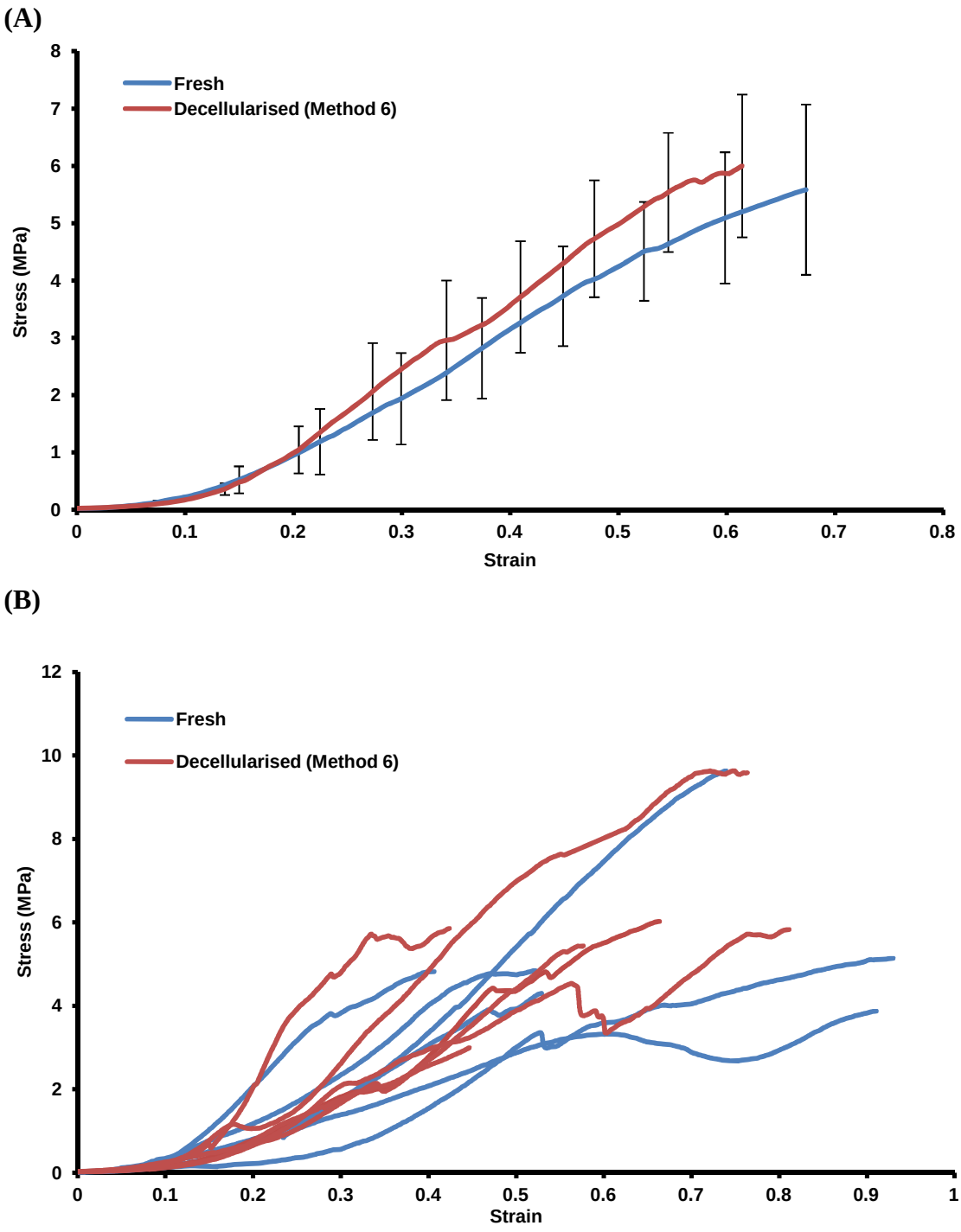

Figure 5.4 Stress-strain behaviour of the fresh and decellularised circumferential left pulmonary leaflet groups. (A) Mean stress-strain behaviour of the fresh and decellularised circumferential left pulmonary leaflet groups (n=6). Error bars indicate the 95% C.I.s. **(B)** Individual stress-strain behaviour of the fresh and decellularised circumferential left pulmonary leaflet groups (n=6).

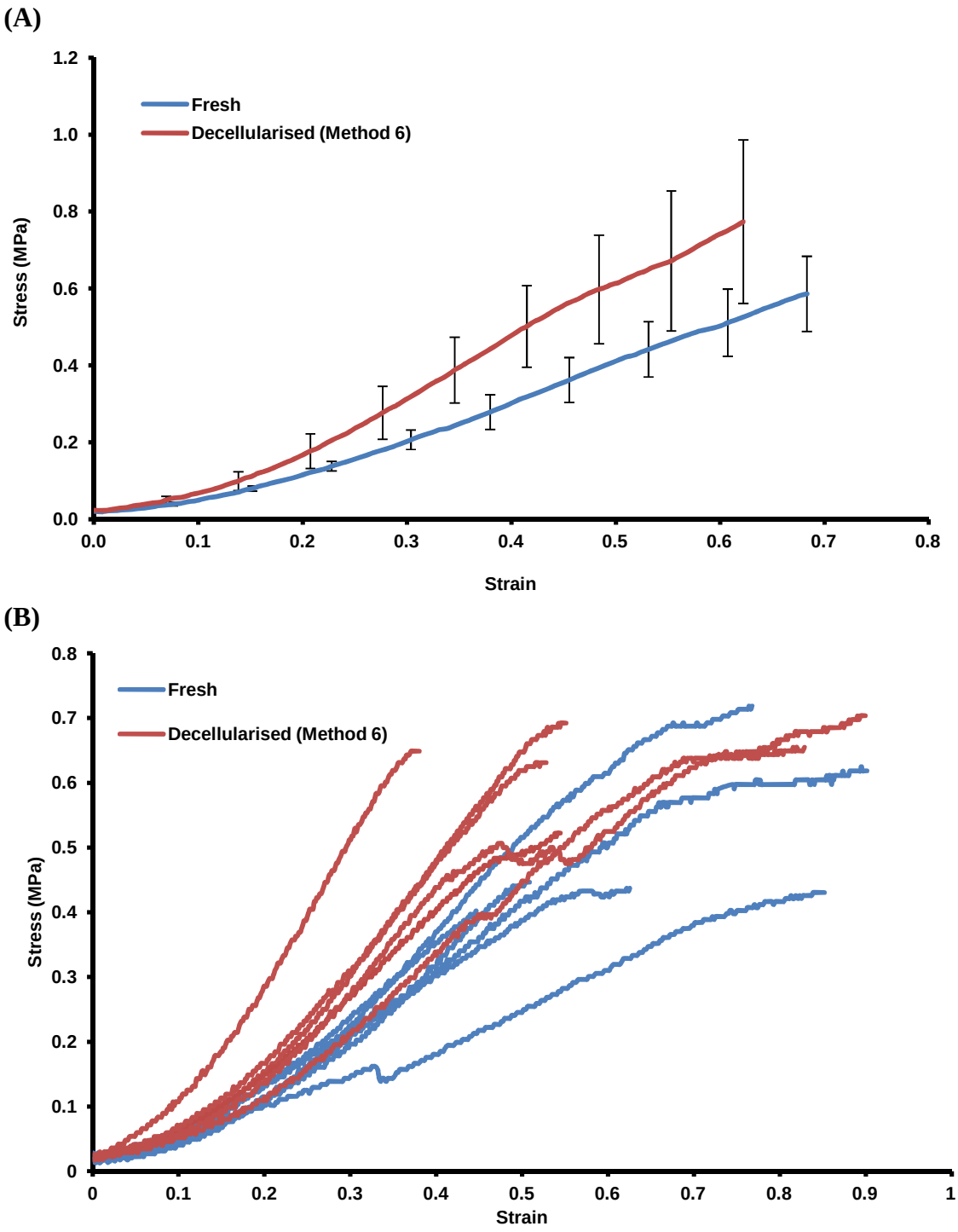

Figure 5.5 Stress-strain behaviour of the fresh and decellularised radial left pulmonary leaflet groups. (A) Mean stress-strain behaviour of the fresh and decellularised radial left pulmonary leaflet groups (n=6). Error bars indicate the 95% C.I.s. **(B)** Individual stress-strain behaviour of the fresh and decellularised radial left pulmonary leaflet groups (n=6).

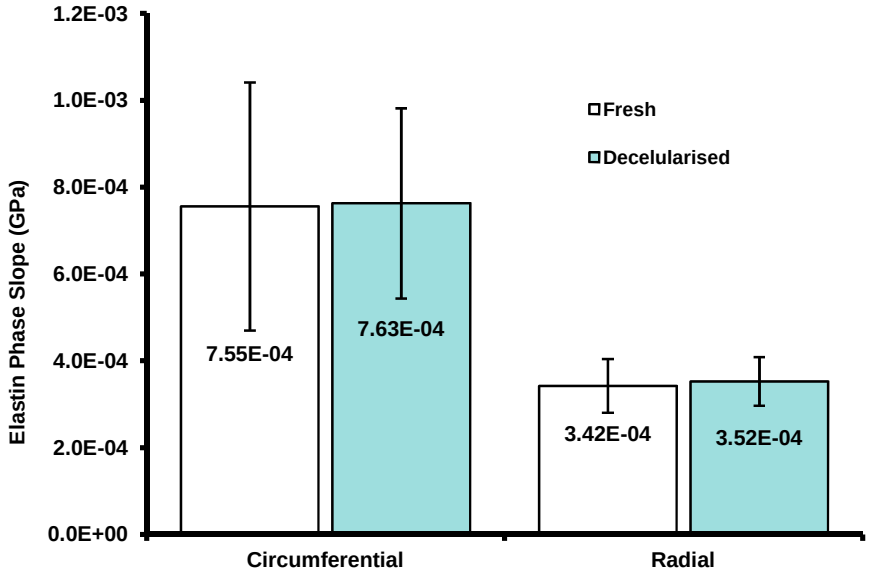

Figure 5.6 Average elastin phase slope for the fresh and decellularised left pulmonary leaflet groups (n=6). The error bars indicate the 95% C.I.s. There was no significant difference between fresh and decellularised tissue.

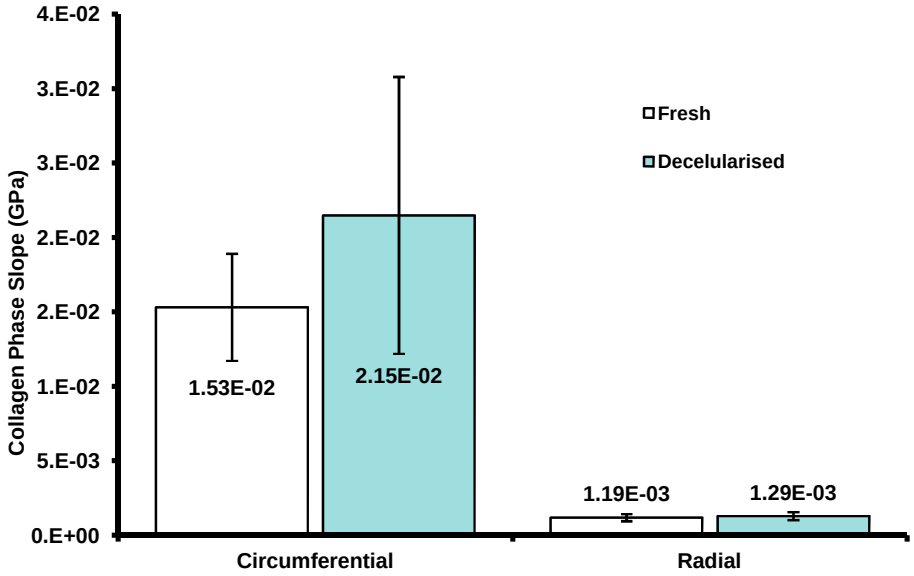

Figure 5.7 Average collagen phase slope for the fresh and decellularised left pulmonary leaflet groups (n=6). The error bars indicate the 95% C.I.s. There was no significant difference between fresh and decellularised tissue.

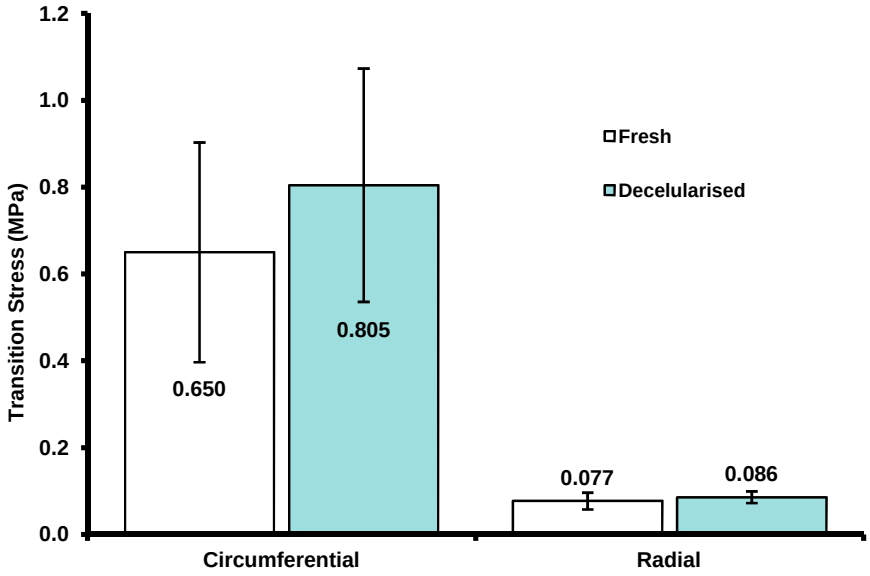

Figure 5.8 Average transition stress for the fresh and decellularised left pulmonary leaflet groups (n=6). The error bars indicate the 95% C.I.s. There was no significant difference between fresh and decellularised tissue.

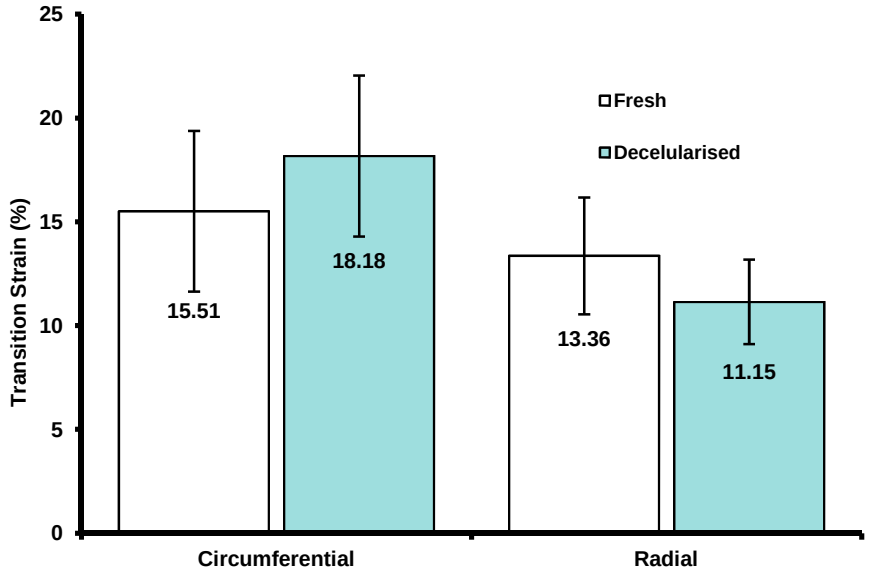

Figure 5.9 Average transition strain for the fresh and decellularised left pulmonary leaflet groups (n=6). The error bars indicate the 95% C.I.s. There was no significant difference between fresh and decellularised tissue.

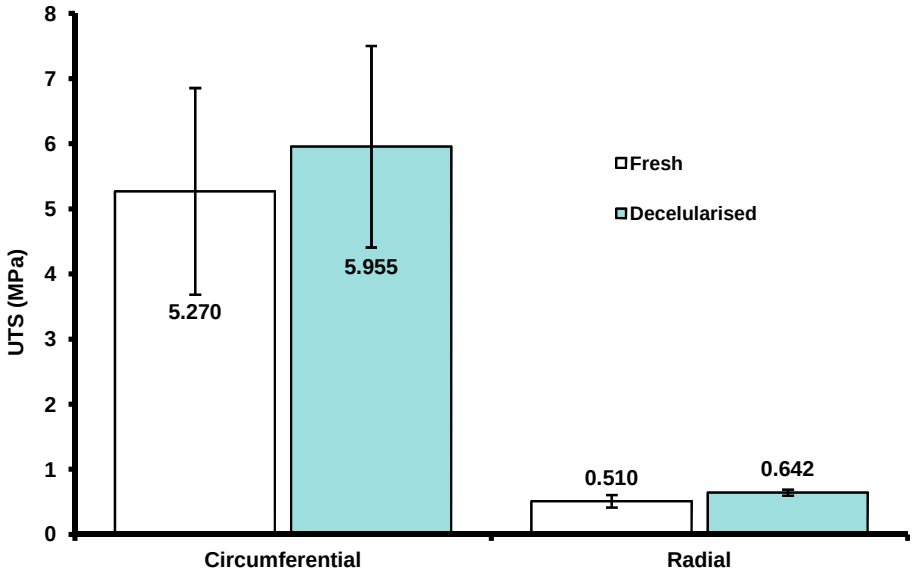

Figure 5.10 Average ultimate tensile stress for the fresh and decellularised left pulmonary leaflet groups (n=6). The error bars indicate the 95% C.I.s. There was no significant difference between fresh and decellularised tissue.

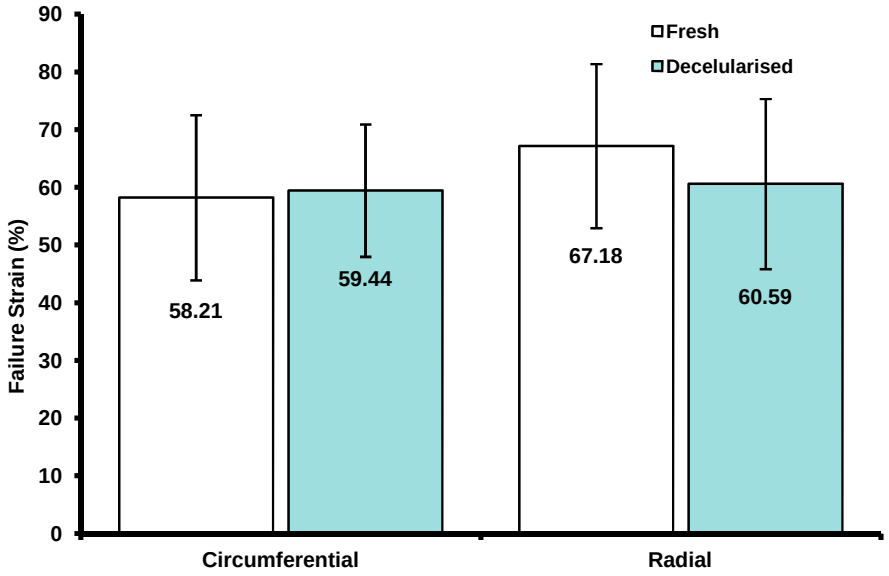

Figure 5.11 Average failure tensile strain for the fresh and decellularised left pulmonary leaflet groups (n=6). The error bars indicate the 95% C.I.s. There was no significant difference between fresh and decellularised tissue.

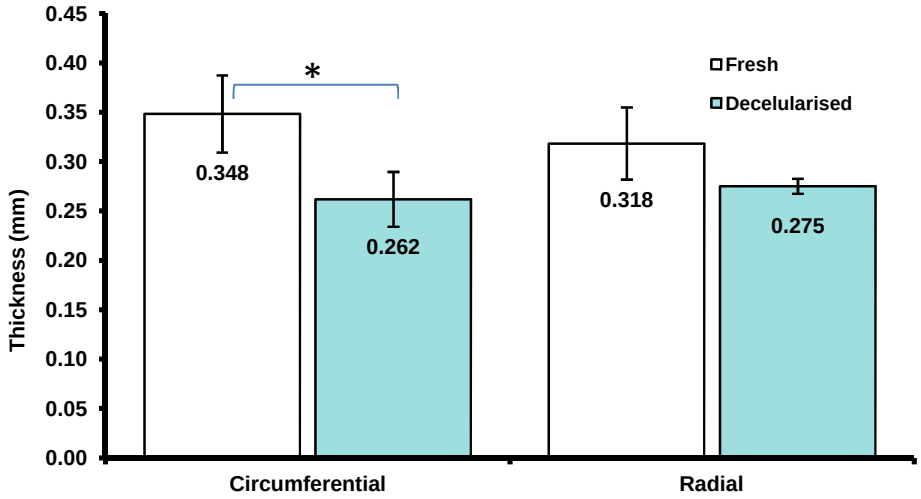

Figure 5.12 Average thickness for the fresh and decellularised left pulmonary leaflet groups (n=6). The error bars indicate the 95% C.I.s. There was no significant difference between fresh and decellularised tissue in the radial direction. A significant difference was observed in the circumferential direction (p=0.009). The asterisk indicates significant difference between the marked groups.

5.4.1.2 Biomechanical characterisation of the pulmonary artery

The effect of decellularisation on the biomechanics of the pulmonary artery was also studied under uniaxial tensile loading. A fresh pulmonary artery group (data presented in Section 3.4.5.2) was used as control. Since scraping of the outer surface of the pulmonary artery was applied during the decellularisation method, a second control group of fresh pulmonary arteries treated with the same scraping method was used. In total, 6 pulmonary artery groups were tested, including circumferential and axial decellularised (n=6), circumferential (n=7) and axial (n=6) fresh and the circumferential and axial scraped fresh (n=6). Statistical significance was determined using one way ANOVA followed by calculation of the MSD using the T-method ($p<0.05$).

The mean stress-strain behaviour of the pulmonary artery groups and the individual stress-strain behaviours for each test sample are illustrated in Figure 5.13 (circumferential) and Figure 5.14 (axial). As with the case of the pulmonary leaflets, all pulmonary artery groups demonstrated the typical quasi-linear behaviour of biological tissues. However, in this case, the extent of the elastin phase was markedly increased compared to the pulmonary leaflets, which was evidence of the increased elastin content of the pulmonary artery wall. The results for the elastin and collagen phase slopes,

transition stress and strain, and failure stress and strain, for the control and test groups are illustrated in Figure 5.15 through to Figure 5.21.

The results indicated no significant difference between the three groups for the following parameters: the collagen phase slope in the circumferential and axial directions (Figure 5.16), the transition stress in the circumferential and axial directions (Figure 5.17), the transition strain in the circumferential direction (Figure 5.18), the failure stress in the circumferential and axial direction (Figure 5.19), and the failure strain in the circumferential and axial direction (Figure 5.20). Significant differences were found in the elastin phase slope between the fresh group and the decellularised group in the circumferential and the axial directions (Figure 5.15), the transition strain between the fresh group and the decellularised group in the axial direction (Figure 5.18), the thickness between the scraped fresh and the decellularised groups in the circumferential and axial directions, and the thickness between the fresh and the decellularised groups in the axial direction (Figure 5.21). The mechanical testing data of elastin and collagen slopes, and the transition and failure stresses of the pulmonary artery of the circumferential and axial directions had a ratio of approximately 3:2. Similar to the pulmonary leaflets, the transition and failure strains of the pulmonary artery had a similar level for both directions.

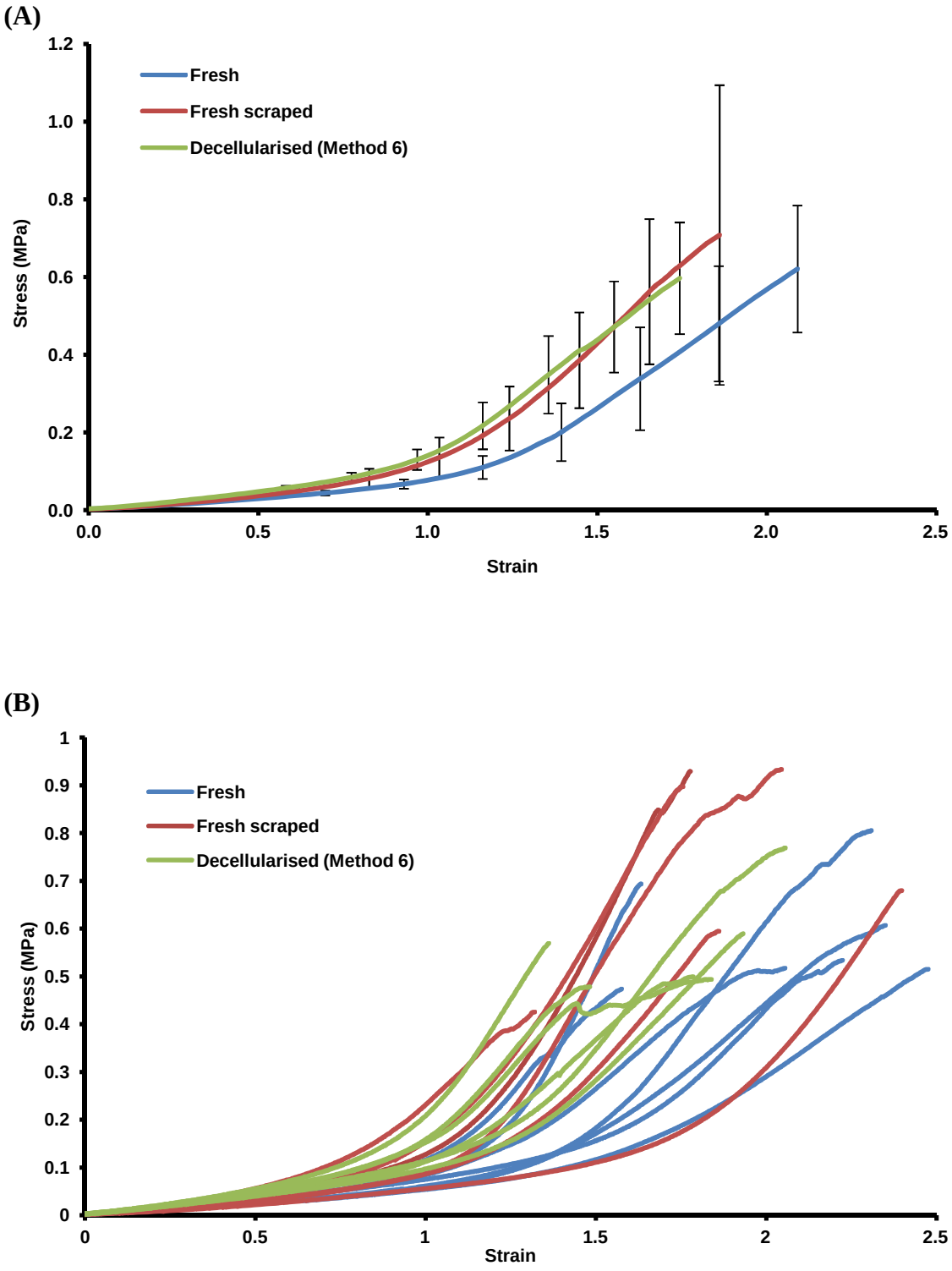

Figure 5.13 Stress-strain behaviour for the fresh (n=7), scraped fresh (n=6) and decellularised (n=6) circumferential pulmonary artery groups. (A) Mean stress-strain behaviour for the fresh (n=7), scraped fresh (n=6) and decellularised (n=6) circumferential pulmonary artery groups. The error bars indicate the 95 % C.I.s. **(B)** Individual stress-strain behaviour for the fresh (n=7), scraped fresh (n=6) and decellularised (n=6) circumferential pulmonary artery groups.

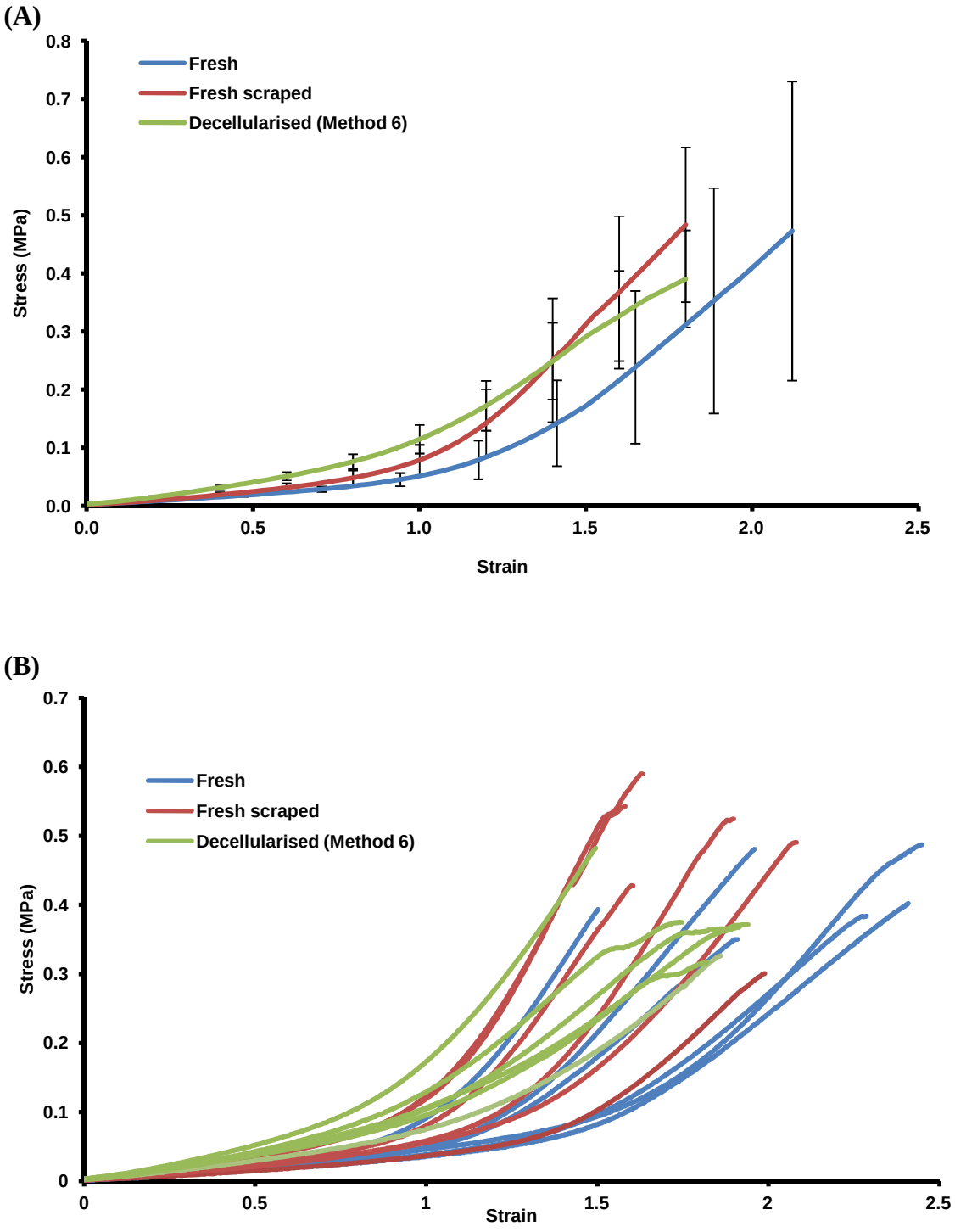

Figure 5.14 Stress-strain behaviour for the fresh (n=7), scraped fresh (n=6) and decellularised (n=6) axial pulmonary artery groups. (A) Mean stress-strain behaviour for the fresh (n=7), scraped fresh (n=6) and decellularised (n=6) axial pulmonary artery groups. The error bars indicate the 95 % C.I.s. **(B)** Individual stress-strain behaviour for the fresh (n=7), scraped fresh (n=6) and decellularised (n=6) axial pulmonary artery groups.

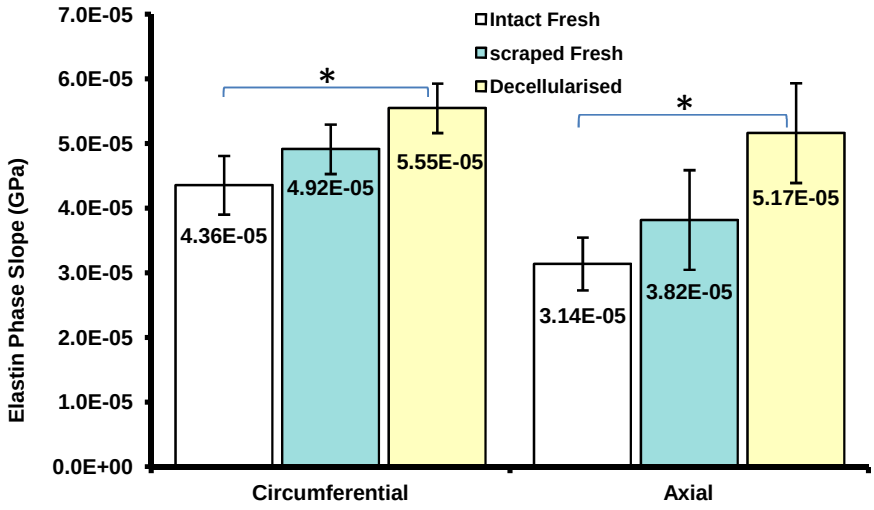

Figure 5.15 Average elastin phase slope for the fresh (circumferential: n=7; axial: n=6), scraped fresh (n=6) and decellularised (n=6) pulmonary artery groups along the circumferential and axial directions. The error bars indicate the 95 % C.I.s. No significant difference was found between the groups in the circumferential or axial directions except for between the fresh and decellularised groups in both directions. The asterisk indicates significant difference between the marked groups.

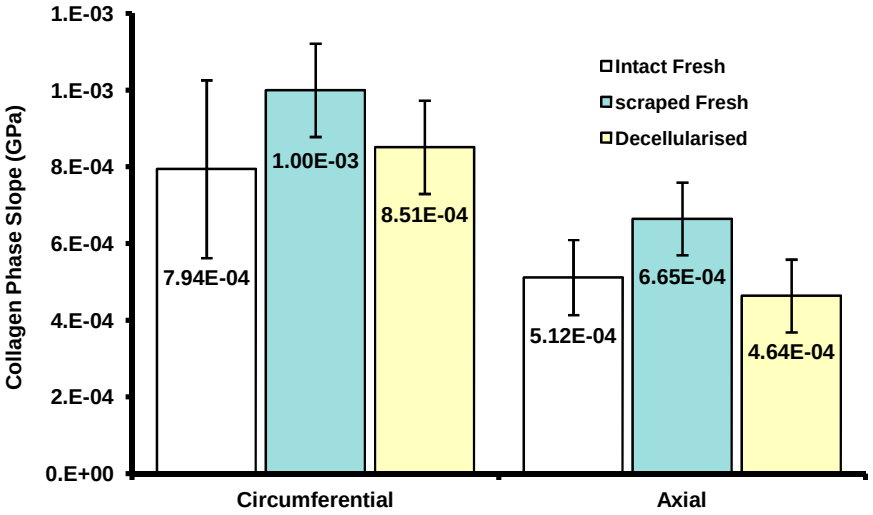

Figure 5.16 Average collagen phase slope for the fresh (circumferential: n=7; axial: n=6), scraped fresh (n=6) and decellularised (n=6) pulmonary artery groups along the circumferential and axial directions. The error bars indicate the 95 % C.I.s. There was no significant difference between the groups in the circumferential or axial direction.

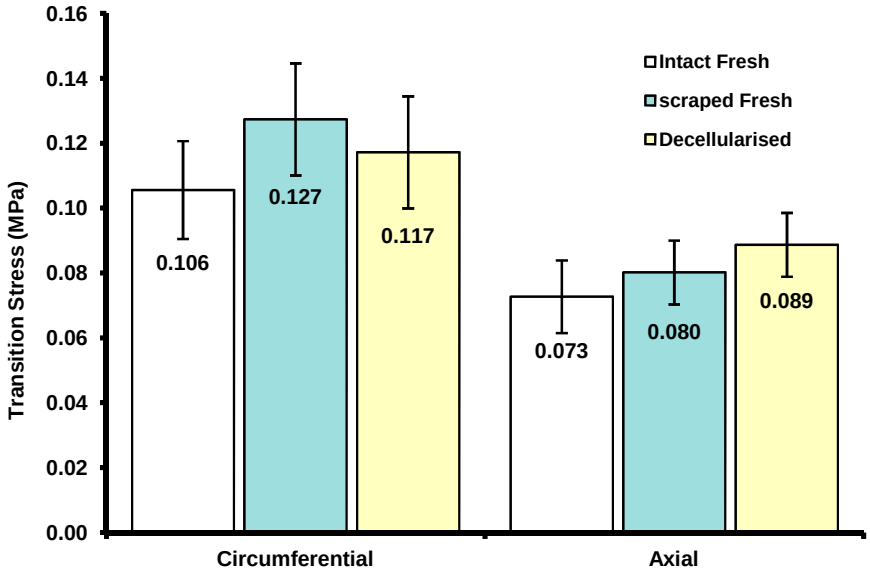

Figure 5.17 Average transition stress for the fresh (circumferential: n=7; axial: n=6), scraped fresh (n=6) and decellularised (n=6) pulmonary artery groups along the circumferential and axial directions. The error bars indicate the 95 % C.I.s. There was no significant difference between the groups in the circumferential or axial direction.

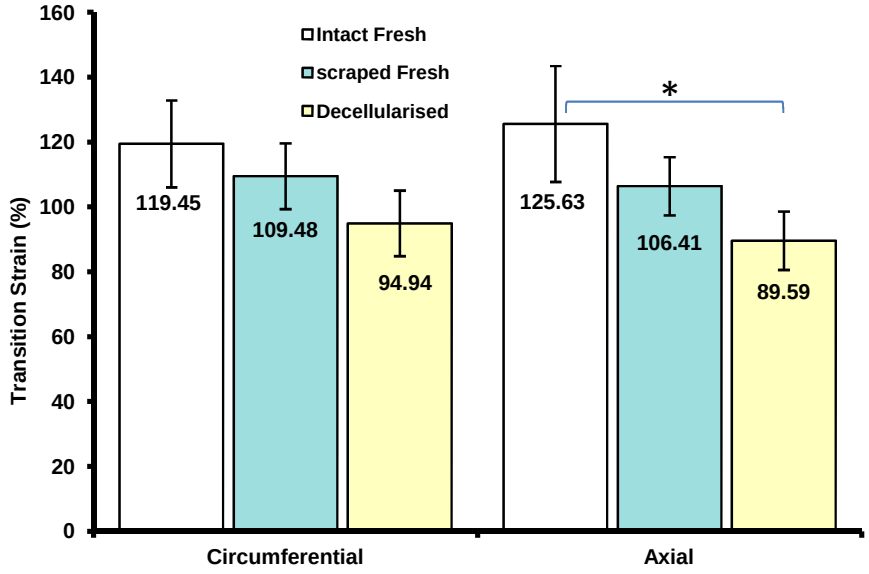

Figure 5.18 Average transition strain for the fresh (circumferential: n=7; axial: n=6), scraped fresh (n=6) and decellularised (n=6) pulmonary artery groups along the circumferential and axial directions. The error bars indicate the 95 % C.I.s. No significant difference was found between the groups in the circumferential or axial directions except for between the fresh and decellularised groups in the axial direction. The asterisk indicates significant difference between the marked groups.

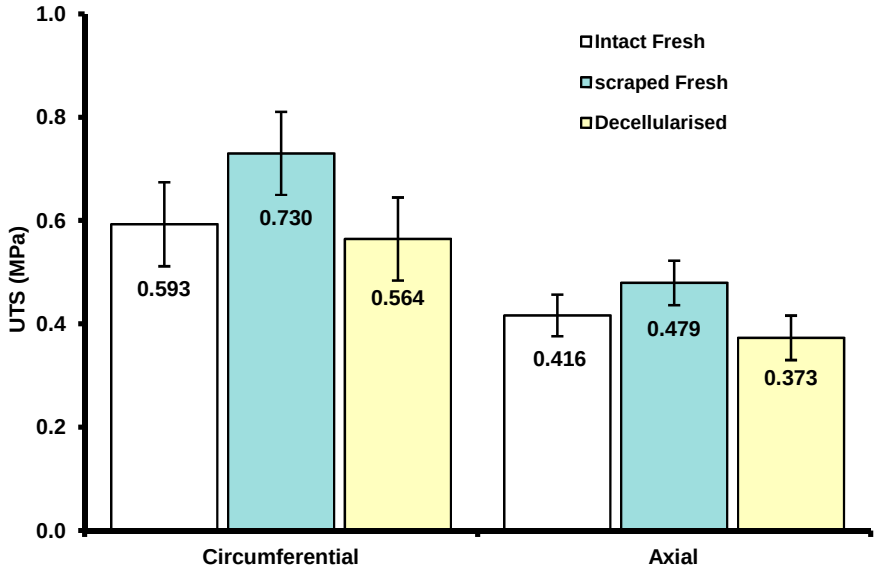

Figure 5.19 Average ultimate tensile stress for the fresh (circumferential: n=7; axial: n=6), scraped fresh (n=6) and decellularised (n=6) pulmonary artery groups along the circumferential and axial directions. The error bars indicate the 95% C.I.s. There was no significant difference between the groups in the circumferential or axial direction.

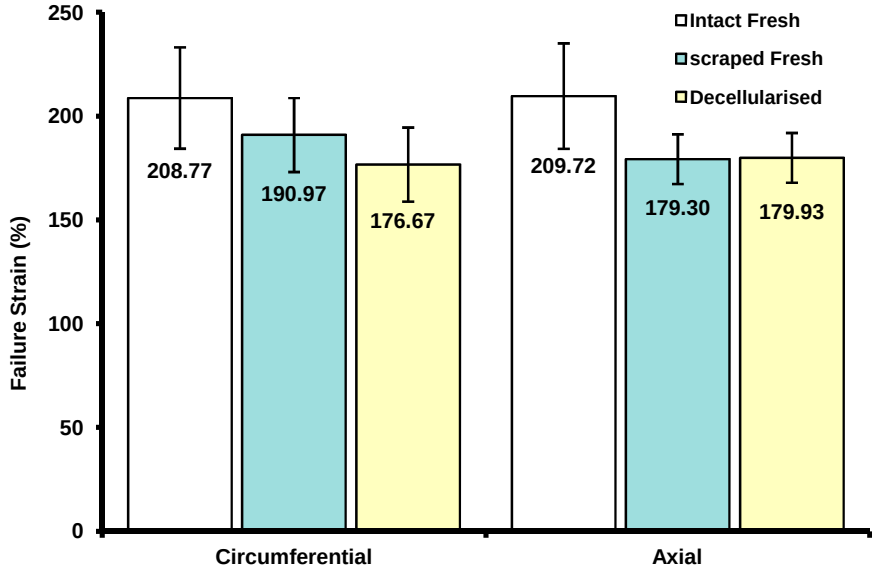

Figure 5.20 Average failure tensile strain for the fresh (circumferential: n=7; axial: n=6), scraped fresh (n=6) and decellularised (n=6) pulmonary artery groups along the circumferential and axial directions. The error bars indicate the 95 % C.I.s. There was no significant difference between the groups in the circumferential or axial direction.

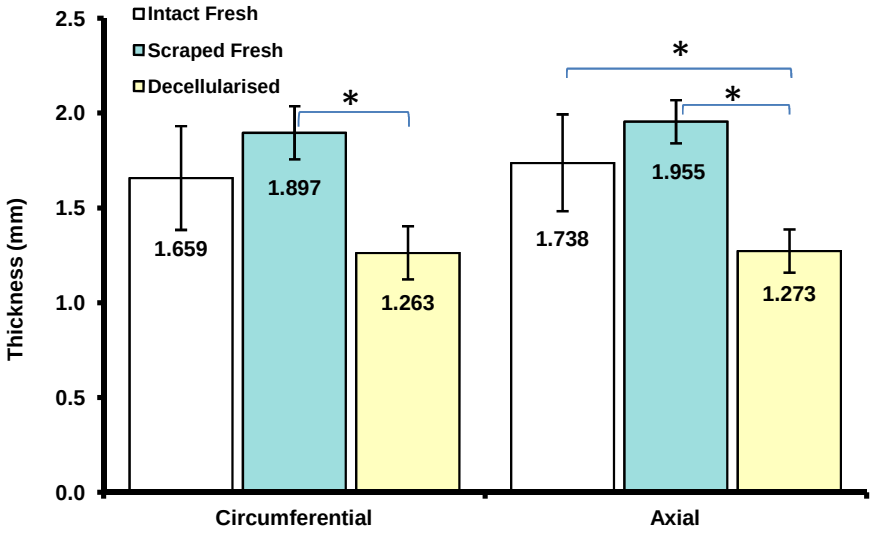

Figure 5.21 Average thickness for for the fresh (circumferential: n=7; axial: n=6), scraped fresh (n=6) and decellularised (n=6) pulmonary artery groups along the circumferential and axial directions. The error bars indicate the 95% C.I.s. No significant difference was found between the groups in the circumferential or axial directions except for between the scraped fresh and the decellularised groups in the circumferential and axial directions, and the fresh and the decellularise groups in the axial direction.

5.4.2 Hydrodynamic assessment of fresh and decellularised pulmonary roots

The hydrodynamic function of the fresh (n=6) and decellularised (n=6) porcine pulmonary roots was assessed in terms of the mean pressure difference across the valve (Δp), the root mean square forward flow (Q_{RMS}) through the valve, and the valve effective orifice area (EOA). The mean pressure difference across a heart valve is indicative of the degree of obstruction to blood flow, with lower pressure differences corresponding to lower resistance to flow. The EOA was calculated from the pressure and flow measurements and it was normalised with respect to flow. Larger EOAs corresponded to smaller pressure differences.

The mean pressure difference averaged over the number of valves in the fresh and decellularised groups at each test condition was plotted as a function of the corresponding averaged Q_{RMS} (Figure 5.22). Overall the repeatability of the tests was quite adequate as indicated by the considerably small error bars. No significant difference was observed for test condition 1 or 3 (Table 5.2) in the Q_{RMS} or Δp between the fresh and decellularised groups. However, significant differences were found at test condition 2 (72 bpm/70 ml), with a Δp of 5.57 ± 0.37 mm Hg (mean ± 95% C.I.) and a

Q_{RMS} of 181.67 ± 1.87 ml.s^{-1} recorded for the fresh group, and a Δp of 4.50 ± 0.79 mm Hg and a Q_{RMS} of 169.39 ± 18.54 ml.s^{-1} recorded for the decellularised group (p=0.012 and 0.035, respectively).

The average EOA of the fresh (n=6) and decellularised (n=6) groups at each test condition is shown in Figure 5.23. No significant difference was observed in any of the test conditions between the two groups (p>0.05).

5.4.3 Leaflet kinematics of fresh and decellularised pulmonary roots

The leaflet kinematics of the fresh and decellularised pulmonary roots was assessed by recording their leaflet motion during a test run at condition 2 (72 bpm/70 ml). The leaflet kinematics was assessed during the opening, open, closing and closed phases. The durations of the opening, open, closing and closed phases averaged over the number of leaflets studied in the fresh (n=6) and decellularised (n=6) groups are shown in Figure 5.24. The opening phase duration of the decellularised group (188.7 ms) was considerably longer than that of the fresh roots (108.7 ms), and the mean of the closed phase duration of the decellularised roots (284.0 ms) was much shorter than that of the fresh ones (372.0 ms). However, no statistically significant difference was observed between the fresh and decellularised groups in any of the phases studied.

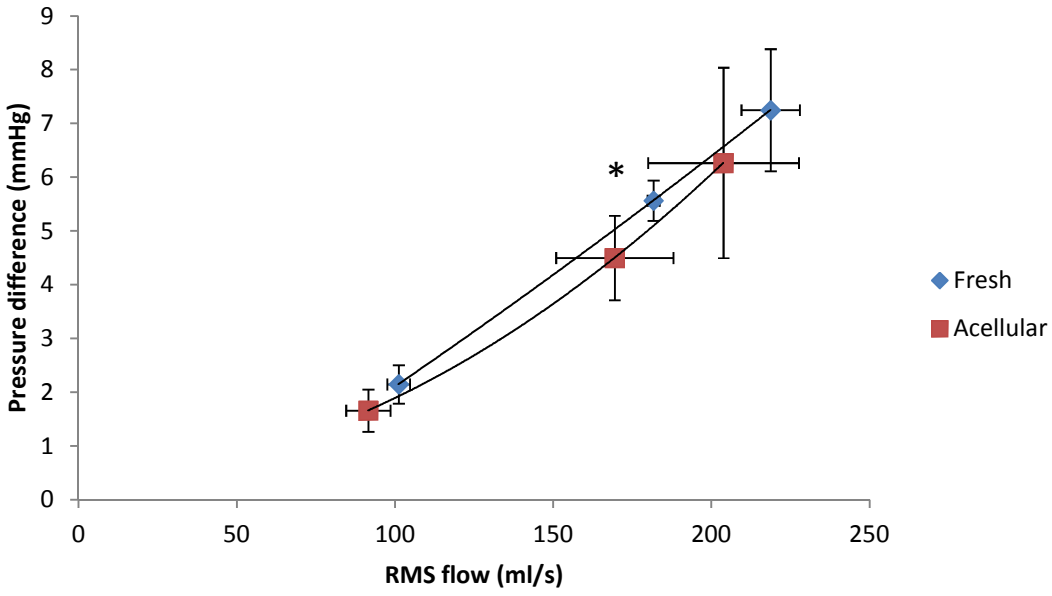

Figure 5.22 Average Δp versus average Q_{RMS} for the fresh (n=6) and decellularised (n=6) groups at the 3 test conditions. Error bars indicate 95% C.I.s. The asterisk indicates significant difference at flow condition 2 (72 bpm/70 ml).

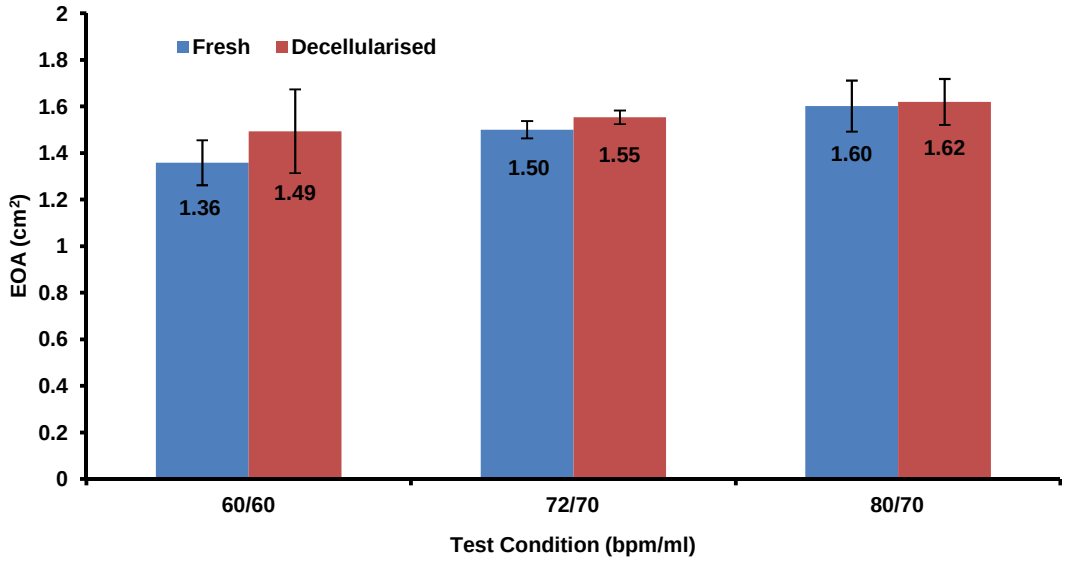

Figure 5.23 Average EOA for the fresh (n=6) and decellularised (n=6) porcine pulmonary roots at each test conditions. The error bars indicate the 95% C.I.s. No significant differences were found between the two groups.

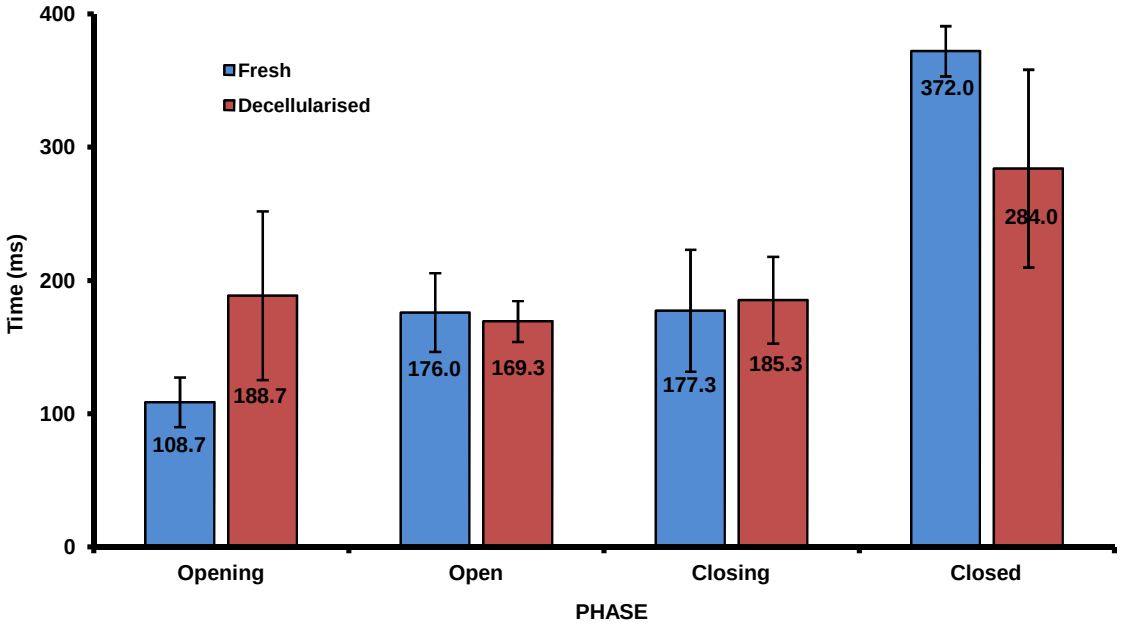

Figure 5.24 Phase times for the fresh (n=6) and decellularised (n=6) pulmonary roots at test condition 2. The error bars indicate the 95% C.I.s. No significant differences were found between the two groups.

Both fresh and decellularised valves demonstrated a synchronous opening and closing leaflet motion, as illustrated in the frames in Figure 5.25 and Figure 5.26 for a representative fresh and decellularised valve, respectively. All valves demonstrated fully closed leaflet configurations with no visible leakage orifices or coaptation flaws

during diastole. At peak systole, the fully opened valve configuration was circular for all fresh and decellularised valves. The free leaflet edge shapes generated by the interpolated X_i, Y_i data points, as described above, and the corresponding averaged leaflet curvatures ($K_{i,avg}$) for the representative fresh and decellularised valves are also illustrated in Figure 5.25 and Figure 5.26, respectively.

The variation of the averaged minimum bending radius (maximum deformation) during the cardiac cycle, calculated for the start opening, fully open, start closing and fully closed leaflet configurations, and averaged for the fresh (n=6) and decellularised (n=6) left pulmonary leaflet groups is illustrated in Figure 5.27. In all four configurations, both leaflet groups demonstrated similar variation in their minimum bending radius during the cardiac cycle. No significant difference was observed between the fresh and the decellularised groups.

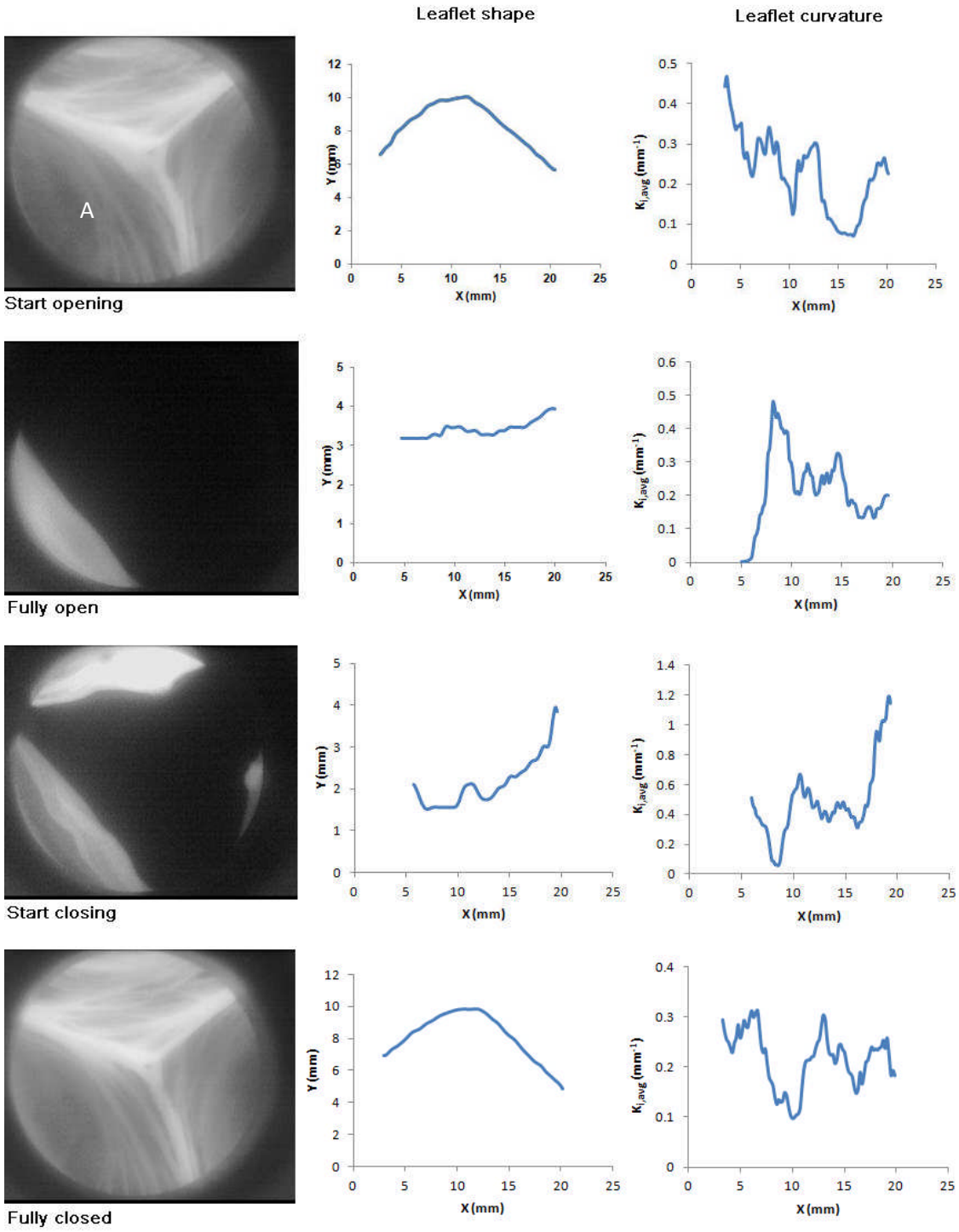

Figure 5.25 Sequence of video images and curves showing the deformation and corresponding curvatures of the left pulmonary leaflet (leaflet A) of a representative fresh valve at start opening, fully open, start closing, and fully closed positions.

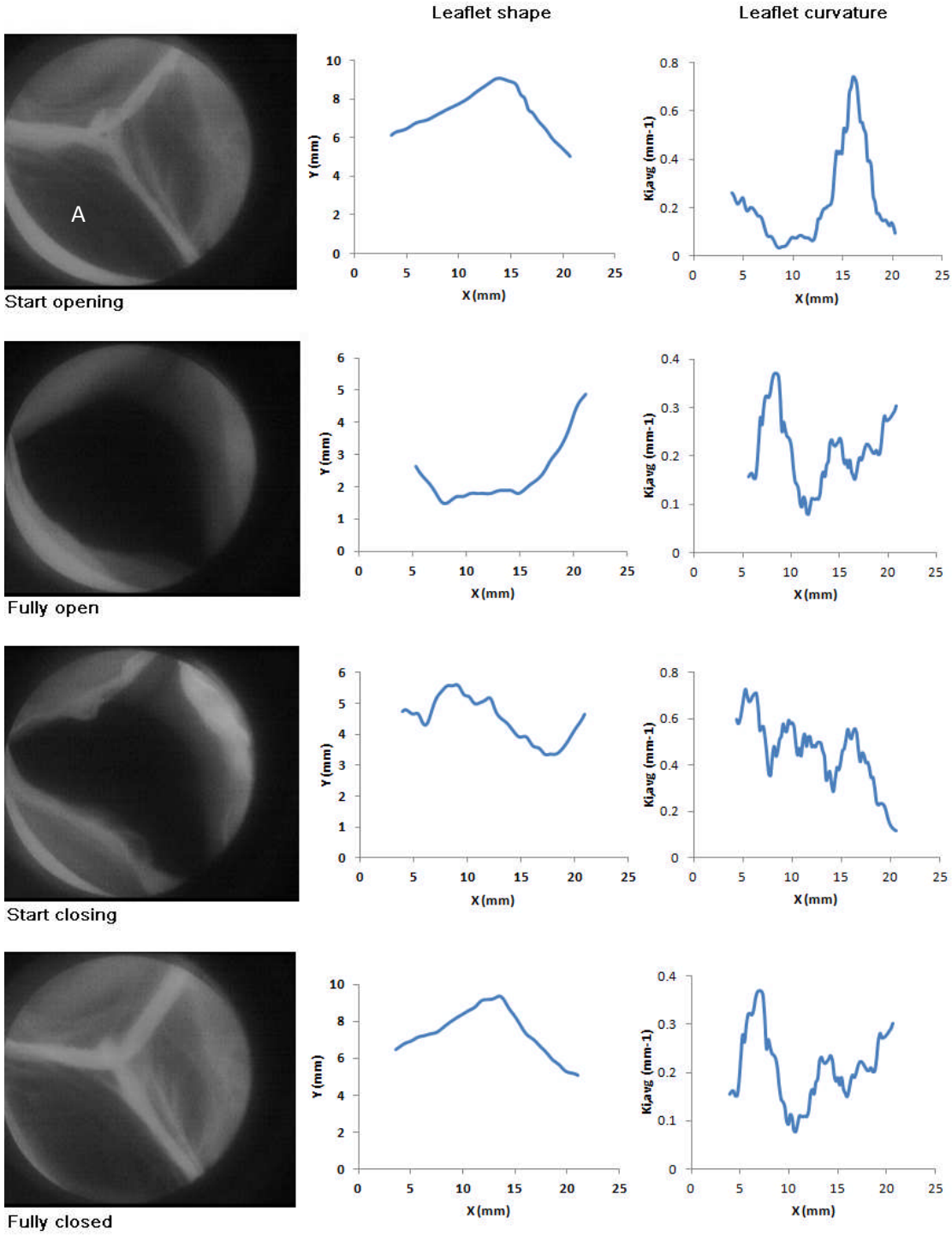

Figure 5.26 Sequence of video images and curves showing the deformation and corresponding curvatures of the left pulmonary leaflet (leaflet A) of a representative decellularised valve at start opening, fully open, start closing, and fully closed positions.

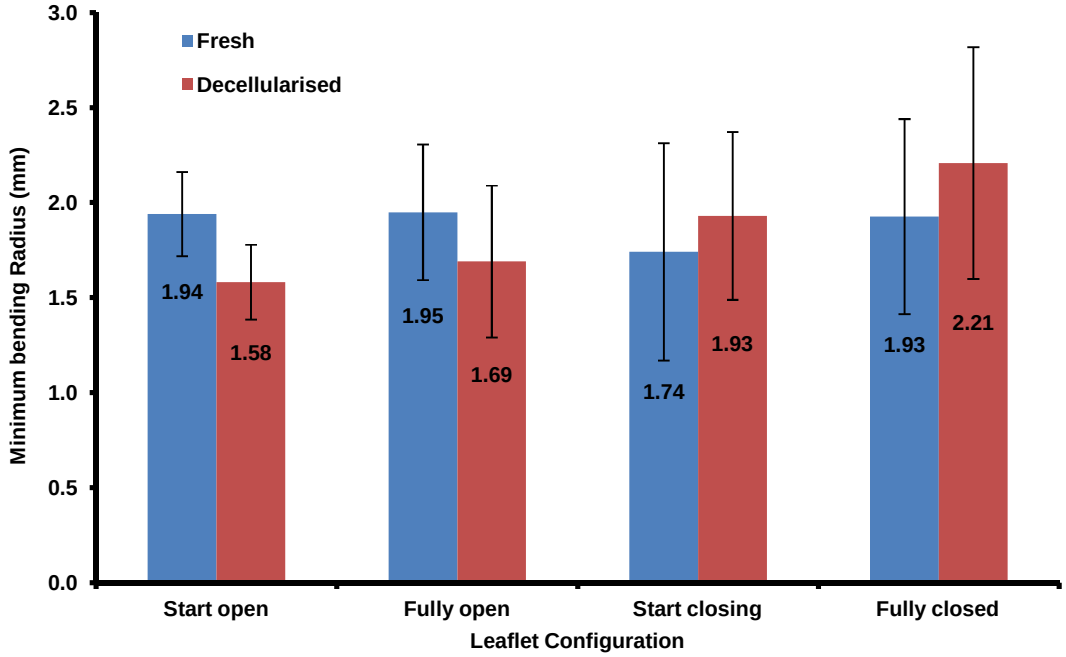

Figure 5.27 Average minimum bending radius at start opening, fully open, start closing and fully closed positions for the fresh (n=6) and decellularised (n=6) left pulmonary leaflets. The error bars indicate the 95% C.I.s. No significant differences were found between the two groups at any of the time points studied.

5.5 Discussion

Following the characterisation of the biological properties in Chapter 4, the biomechanical characteristics of the acellular porcine pulmonary roots were assessed and compared to fresh tissue in this chapter. The decellularisation method used to produce the acellular tissue used in the studies presented in this chapter was referred to as 'Method 6' in Chapter 3. Uniaxial tensile testing was carried out to determine the biomechanical properties of the acellular pulmonary leaflets and arteries by comparison to the fresh tissues. The hydrodynamic function and leaflet motion of the acellular pulmonary roots were assessed by pulsatile flow testing and compared to the fresh control.

The stress-strain behaviour of both fresh and decellularised groups demonstrated the typical quasi-linear behaviour of biological tissue, with a low modulus region during the elastin phase and a high modulus region during the collagen phase. This trend was similar to the results obtained for the fresh and decellularised tissues (Method 3 in Chapter 3) and described in Chapter 3, as well as to the results described in previous studies (Jennings, 2001; Korossis *et al*., 2002; Stradins *et al*., 2004; Korossis *et al*., 2005; Seebacher *et al*., 2007).

In the uniaxial tensile tests of the fresh and decellularised (Method 3 in Chapter 3) pulmonary leaflets described in Chapter 3, the samples were randomly selected from the three leaflets in the pulmonary valve for both the circumferential and radial directions. However, in the uniaxial tensile testing described in the present chapter, only the left pulmonary leaflets were used in order to minimise tissue inhomogeneity effects. Moreover, in the tensile testing results described in Chapter 3 for the pulmonary leaflets decellularised according to Method 3, a significant decrease ($p<0.05$) was observed in the failure stress along the radial direction, which led to the conclusion that the pulmonary valve tissue decellularised according to this method may not be competent to be used in heart valve replacement surgery.

The tensile testing results presented in the present chapter for the decellularised left pulmonary leaflets (Method 6 as described in Chapter 3) showed no significant difference in any of the tensile testing parameters when compared to the fresh tissue. These results were in general agreement with the results reported by Korossis *et al*. (2002), who applied 1 cycle of 0.1 % (w/v) SDS to decellularised porcine aortic leaflets.

This result confirmed the hypothesis raised in Chapter 3 that the additional cycle of SDS treatment (Method 3 in Chapter 3) would compromise the mechanical behaviour of the pulmonary leaflets. The fact that the elastin slope of the left pulmonary leaflet (both fresh and decellularised) in the circumferential direction was about two fold compared to that in the radial direction, the collagen slope and transition failure stresses in the circumferential direction were about 10 fold compared to those in the radial direction confirmed the anisotropy property of the leaflets. Gerosa *et al*. (1994) reported a fourfold difference in the mechanical properties of the circumferential and radial directions within a human valve, and Christie & Barratt-Boyes (1995) showed the circumferential/radial ratio of mechanical parameters to be 6.0 for porcine aortic leaflets. In the study carried out by Korossis (2002), which applied a very similar testing method to the present study on porcine fresh and decellularised aortic leaflets, the elastin slope of the leaflet (both fresh and decellularised) in the circumferential direction was about two fold greater than that in the radial direction, the circumferential/radial ratio of collagen slope was about 15, and the circumferential/radial ratio of the transition and failure strain was approximately 6. The data presented in this study were in agreement with the trends in the previous studies.

Nevertheless, the present study indicated a significant decrease in the thickness of the decellularised left pulmonary leaflets compared to the fresh leaflets in the circumferential direction. This was probably due to the different sizes of valve roots used for the fresh and decellularised groups, which was in turn due to the limitation of the tissue supply from the local abattoir. The difference in the leaflet thickness, however, did not affect the comparison of the relevant biomechanical parameters (elastin and collagen phase slopes, transition and the failure stress) between the different groups since these parameters were normalised with respect to the specimen thickness.

The biomechanical properties of the decellularised pulmonary artery were determined in both circumferential and axial directions, and compared to two control groups: the fresh group and the scraped fresh group. Scraping of the outer surface of the adventitia of pulmonary artery was applied in the decellularisation protocol. Thus, in order to identify the mechanical effect of scraping, a control group of scraped fresh porcine pulmonary arteries was included in the study. The same tensile testing results for the fresh group used in Chapter 3 were also used for comparison in the present chapter. The pulmonary artery group used in this chapter, which was decellularised according to Method 6

(Section 3.4.8.1), demonstrated a significantly decreased elastin phase slope in both the circumferential and axial directions, and decreased transition strain in the axial direction compared to the fresh control. No significant difference was observed in the tensile parameters between the acellular and the scraped fresh control groups. In the study conducted by Korossis *et al*. (2005), in which a similar decellularisation method with trypsin and 0.1 % (w/v) SDS was used on porcine aortic arteries, similar changes to the acellular tissue were also described. The reduction in elastin phase slope indicated that the decellularisation treatment produced a more compliant tissue in the initial elastin phase (physiological range). Similar to the pulmonary leaflets, the pulmonary artery also showed anisotropic properties. In the present study, the circumferential/axial ratio of mechanical parameters was approximately 3:2 for the pulmonary artery. In the study conducted by Korossis (2002), the ratio was determined to be approximately 4:1 for porcine aorta. The anisotropic properties of the porcine pulmonary artery were therefore less apparent than for the pulmonary leaflet and the porcine aorta.

Despite the differences between the acellular and the fresh pulmonary artery groups, the treatment did not compromise the strength of the tissue since no significant difference was observed in the failure stress. As discussed in Chapter 3, the peeling of the relatively thin pulmonary artery, which was applied in decellularisation Method 3, could have caused the significant reduction in the tissue strength. It has been confirmed by the results shown in this chapter that the scraping of the adventitial surface of the pulmonary artery did not compromise the strength of the tissue whilst decellularisation was achieved. Thus, scraping instead of peeling an outer layer of the adventitia of the porcine pulmonary artery was considered as an optimal method for removing the connective tissue from the outer surface of the pulmonary artery during decellularisation. A significant decrease in the thickness of the decellularised pulmonary artery was observed in both the circumferential and the axial directions compared to the fresh control. This result was in agreement with that of the pulmonary leaflets. As discussed previously, the decrease in pulmonary artery thickness was probably due to variability of the tissue supply from the local abattoir.

The hydrodynamic function of the acellular porcine pulmonary roots was assessed in comparison to the fresh tissue using simulated pulsatile flow testing. The purpose was to assess the effect of the decellularisation treatment on the hydrodynamic parameters of the porcine pulmonary roots. Three conditions were used for the hydrodynamic function

assessment as described in Section 5.3.2.4. The pressure ranges used in this study were the minimum pressure ranges that could be achieved by the pulsatile flow simulator at each flow condition. These pressures were close to physiological pulmonary pressures, and since the intention for the decellularised pulmonary valve scaffolds is to be used for the replacement of the native pulmonary valve following the Ross procedure, the particular pressures were deemed appropriate for assessing the function of the pulmonary scaffolds.

No significant difference was observed in the mean pressure difference and the Q_{RMS} between the acellular and the fresh pulmonary roots at flow condition 1 and 3 (Figure 5.22). However, a significant decrease in the mean pressure difference and Q_{RMS} of the decellularised groups compared to the fresh control was observed at flow condition 2. In general, the performance of the acellular roots was superior to that of the fresh roots since lower mean pressure differences across the acellular roots were observed. The fresh pulmonary roots had a mean pressure difference of 4.5 ± 0.79 mm Hg (95 % C.I.) at flow condition 2, which corresponded very well with the previous study carried out by Nagy *et al*. (2000), who demonstrated a mean pressure difference for fresh porcine pulmonary roots of 4.6 ± 2.6 mm Hg at very similar testing conditions. The results of the mean pressure difference and Q_{RMS} in this study also corresponded well to the results reported by Weerasena *et al*. (1992) for the fresh pulmonary roots tested at pulmonary pressures.

The EOA showed no significant difference between the decellularised and fresh pulmonary roots at each of the three flow conditions used. The average EOA for all flow conditions and all fresh roots was 1.49 ± 0.08 cm^2 (95 % C.I.), and the corresponding average EOA for the decellularised roots was 1.55 ± 0.10 cm^2. The EOA of fresh porcine pulmonary valve reported by Jennings (2001) ranged from 1.82 to 4.04 cm^2 with a root size of approximately 23 mm. The flow conditions used by Jennings (2001) were similar to this ones used in this study, except that the pressure was 120/80 mm Hg, which was much higher than the pressure used in this study (45/10 mmHg). Higher pulmonary pressures lead to larger dilation of the root, thus resulting in larger EOA`s. Nagy *et al*. (2000) tested fresh porcine pulmonary roots with sizes ranging from 20 mm to 25 mm, and demonstrated an average EOA of 2.69 ± 0.53 cm^2 at flow condition (72 bpm/70 ml) and pulmonary pressure of 25/10 mmHg. In this study, the

average EOA was smaller compared to the previous studies, but this was due to the smaller pulmonary root size (approximately 18 mm) used.

Korossis (2002) conducted hydrodynamic function testing of decellularised porcine aortic roots treated with 0.1 % (w/v) SDS. In that study, the decellularised aortic roots demonstrated a significant decrease in the Δp and significant increase in the EOA compared to fresh aortic valves. In the present study, in which 0.1 % (w/v) SDS was also used for the decellularisation of the porcine pulmonary roots, similar finding was observed for the mean pressure difference, and no significant difference was observed for the EOA between the fresh and decellularised roots. This demonstrated the consistency of the changes in the hydrodynamic function of porcine heart valves treated with 0.1 % (w/v) SDS.

The leaflet kinematics of the decellularised pulmonary roots were assessed at test condition 2 (72 bpm/ 70 ml) and compared to the leaflet kinematics of fresh pulmonary roots. During opening, all fresh and decellularised roots demonstrated the same stellate, triangular and circular configurations as described for the semilunar valves by Thubrikar *et al*. (1979). All decellularised roots demonstrated a circular configuration at peak systole (FO) and no visible leakage orifices or coaptation flaws during diastole (FC). The average durations of opening, open, closing and closed phases for the fresh group (n=6) were 108.7 ± 18.6 ms (mean ± 95 % C.I.), 176.0 ± 29.6 ms, 177.3 ± 45.7 ms and 372.0 ± 18.8 ms, respectively. These phase durations in this study were in good agreement with the times estimated by Jennings (2001), who reported corresponding durations of 100, 183, 90, and 457 ms for fresh porcine pulmonary roots. The differences between the durations in this study and those reported by Jennings (2001) were most likely due to the small sample size (only one sample) used in the study by Jennings (2001). The phase durations in this study are in a very good agreement with the results reported by Korossis (2002) for the fresh aortic roots, in which the mean durations were 89.5, 160.8, 188.7 and 396.0 for opening, open, closing, and closed phases based on 10 samples. The phase durations of the decellularised porcine pulmonary roots (n=6) in the present study showed no statistically significant difference compared to the fresh control. It was noticed however, that the duration of 188.7 ± 63.2 ms obtained for the opening phase of the decellularised group was increased compared to the opening phase duration of 108.7 ± 18.6 ms for the fresh control. This result was in agreement with that reported by Korossis (2002) who used a very similar method for the

decellularisation of porcine aortic roots. In the study by Korossis (2002), the increased duration of the opening phase of the decellularised aortic roots was attributed to the increased compliance of the leaflets, which caused them to take longer time to respond to the dilation of the aorta generated by the increase in pressure during systole. In the present study, however, no significantly increased compliance of the pulmonary leaflets was observed, as demonstrated by the similar elastin phase slopes (no significant difference) of the fresh and decellularised leaflet groups.

Finally, no significant difference was observed in the minimum bending radius of the fresh and decellularised left pulmonary leaflets at the start opening, fully open, start closing, and fully closed configurations. This result further proved that the decellularised pulmonary leaflets demonstrated similar characteristics to the fresh control.

5.6 Conclusion

The decellularisation method for porcine pulmonary roots used in this chapter incorporated trypsin treatment on the adventitial surface of the scraped pulmonary artery, together with 1 cycle of SDS-hypotonic treatment and 2 cycles of nuclease treatments (referred to as 'Method 6' in Chapter 3). Uniaxial tensile testing indicated no significant difference ($p > 0.05$; t-test) between the fresh and acellular left pulmonary leaflets in all biomechanical parameters studied. Although the elastin phase slope showed a significant decrease ($p < 0.05$; ANOVA) for the acellular pulmonary artery compared to the fresh tissue, the strength of the pulmonary arteries following decellularisation was not compromised significantly. The hydrodynamic performance of the pulmonary roots was grossly preserved following decellularisation. The decellularised pulmonary leaflets demonstrated similar leaflet kinematics and deformation compared to the fresh leaflets. Overall the decellularised porcine pulmonary roots demonstrated very good biomechanical and hydrodynamic function compared to the fresh control. These results indicate that the decellularised porcine pulmonary valve scaffold has the potential to be used for at least short term implantation in the pulmonary position.

Chapter 6

Investigation of fresh porcine pulmonary valve conduits in a novel heart valve bioreactor

6.1 Introduction

A major challenge in tissue engineering is to create viable and functional replacement heart valves that have the ability to remodel and regenerate *in vivo* after transplantation. Although some of the currently available acellular heart valves have been assessed for their biological and biomechanical properties, and have been used clinically either cell seeded or non-seeded (Dohmen *et al*., 2007; Mulinari *et al*., 2008; da Costa *et al*., 2009; da Costa *et al*., 2010; Dohmen *et al*., 2011), there are currently no *in vitro* models for investigating the regeneration of acellular cardiac valves. The *in vivo* remodelling of tissue engineered heart valves will probably display considerable variation between patients, due to inherent biological heterogeneity between individuals in physiological tissue remodelling potential (Schoen, 2011). The current scientific data are insufficient to understand the complex mechanobiological stimuli and signalling mechanisms *in vivo* (Gandaglia *et al*., 2011). In order to determine the mechanisms by which VIC and VEC regenerate acellular heart valves, it would be valuable to be able to study this process *in vitro*. Evidence has shown that biomechanical simulation has a significant impact on cell behaviour including *in vitro* differentiation. Moreover, physiological hemodynamic conditioning has been shown to promote new tissue development (Gandaglia *et al*., 2011). *In vitro* mechanical conditioning which reproduces the developmental process of native heart valves is considered important for the study of functional heart valve tissue engineering (Hjortnaes *et al*., 2009). The matrix remodelling and cellular regeneration of an acellular heart valve scaffold may be possible to study *in vitro* with a bioreactor device which can mimic the physiological conditions *in vivo*. Using a bioreactor, the mechanisms by which the biochemical or biomechanical environment influences the interaction between the valvular cell types or between cells and scaffold could be studied (Berry *et al*., 2010).

A heart valve bioreactor is a device that is able to recapitulate the biological and physiological environment of the heart and the circulatory system (Carrier *et al*., 1999).

Both mechanical and biochemical conditions are crucial for maintaining heart valve tissue viability in a bioreactor, namely the concentration of O_2 and CO_2, pH, temperature, nutrients, flow conditions and physiological pressure. The maintenance of a sterile culture environment is essential. There are generally two types of heart valve bioreactors: the static bioreactor and the dynamic bioreactor. The static bioreactors do not provide culture medium circulation. Both static and dynamic bioreactors can provide consistent O_2 and CO_2 concentration, suitable pH, temperature and nutrients. Flow conditions and physiological pressure, which are important elements for the function of a heart valve, are however provided only by dynamic bioreactor systems (Gandaglia *et al*., 2011). In order to mimic physiological flow and pressure conditions, dynamic bioreactors have been designed to deliver culture medium under pulsatile flow that simulates *in vivo* pressure (80-120 mmHg for the systemic circulation in the left heart, and 15-35 mmHg for the pulmonary circulation in the right heart), heart rate (60-100 bpm), and stroke volume (50-70 ml). To achieve such conditions, peristaltic, centrifugal, or pneumatic pumps have been used, coupled with programmable waveform generators that recreate cardiac physiological flow. Moreover, a compliance chamber to simulate the elastic loading sustained *in vivo* by the arteries is usually included. This chamber is responsible for the delay and shape of the pressure waveform (Ruel & Lachance, 2009). In addition, a flow resistor is usually positioned downstream of the heart valve to simulate the vasculature narrowing in precapillary arterioles, capillaries and veins (Gandaglia *et al*., 2011).

A dynamic heart valve bioreactor generally consists of the following components: a ventricle chamber driven by a motor (mechanical, pneumatic, or electric) which is able to provide physiological pressure and flow conditions; a system to control and adjust compliance and resistance; a chamber to house the heart valve; probes and sensors for measuring and adjusting flow and pressure, temperature, pH, O_2 and CO_2 concentrations plus hardware, and software to control the whole system (Dvir *et al*., 2006). Moreover, a dynamic heart valve bioreactor should also have the potential to allow the setting and adjusting of parameters such as stroke volume and number of cycles, as well as the possibility to remove or add fresh medium under sterile conditions. Ideally, the heart valve under culture should be visible and monitored during the whole culture period (Gandaglia *et al*., 2011).

Although the ultimate goal of these studies was to use a heart valve bioreactor to study the regeneration of acellular pulmonary heart valve scaffolds by appropriate cell types, suitable conditions to apply during culture in order to maintain valve function and cell viability in the bioreactor had to be determined using fresh tissue. In this chapter, fresh porcine pulmonary roots were cultured in dynamic conditions in a novel heart valve bioreactor and compared to valves cultured in static culture for one week, and the histology, cell viability, expression of cellular and matrix proteins were compared to fresh tissue which was not subject to organ culture.

6.2 Aims and objectives

Aims:

The aims of this chapter were to determine the conditions for the culture of fresh porcine pulmonary roots under sterile conditions in a dynamic heart valve bioreactor and a static culture system, and to compare the tissue properties with fresh porcine pulmonary roots.

Objectives:

- To determine the cell distribution and tissue histoarchitecture of fresh porcine pulmonary roots cultured statically and dynamically in a heart valve bioreactor and to compare with fresh, non-cultured tissue.
- To detect and localise specific matrix and cellular proteins in dynamically and statically cultured fresh porcine pulmonary roots and to compare with fresh, non-cultured tissue.
- To determine cell viability in the dynamic and static cultured porcine pulmonary roots compared to fresh non-cultured roots.

6.3 Methods

6.3.1 Pulmonary root tissue culture medium

The medium used in this study for pulmonary root tissue culture in both dynamic and static culture systems was DMEM with 10 % (v/v) FBS, 100 $U.ml^{-1}$ penicillin, 100 $U.ml^{-1}$ streptomycin, 250 $ng.ml^{-1}$ amphotericin B, 25 $\mu g.ml^{-1}$ gentamicin, 100 µM L-glutamine, and 0.1 % (v/v) anti foaming reagent polypropylene glycol. The medium was prepared fresh and used immediately.

6.3.2 Porcine pulmonary root tissue preparation

The fresh porcine pulmonary roots used in this chapter were dissected as described in Section 2.2.4. The dissection procedure was carried out aseptically in a Class II safety cabinet. All the roots were used immediately after dissection. The length of the myocardium skirt of the dissected porcine pulmonary root was kept at around 2.5 cm, and the myocardium skirt was thinned to have a thickness of around 3 mm. The length of the myocardium skirt in the roots dissected for culture was longer than those subject to decellularisation. The reason for this was that when sewing the porcine pulmonary root to the tissue holder of the dynamic bioreactor, the three pulmonary leaflets needed to reside in the middle of the holder in order to free the annulus for expansion during dynamic culture. Only when the annulus was free, could the porcine pulmonary heart valve leaflets open and close properly during dynamic culturing (data not shown). The roots used for static culture were kept the same as those used for dynamic culture. The integrity of the whole roots was carefully examined before they were placed in the culture system. An image of a dissected fresh porcine pulmonary root for dynamic and static culture is shown in Figure 6.1.

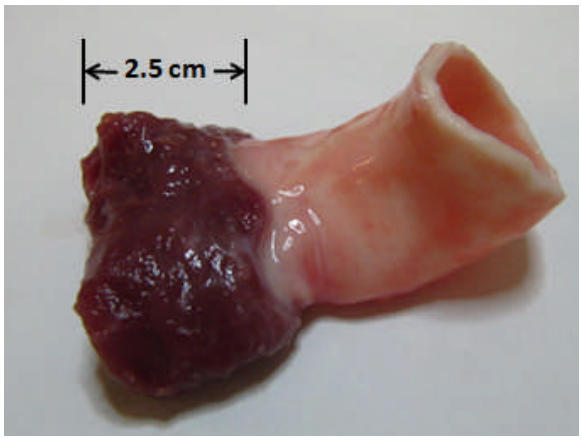

Figure 6.1 A fresh porcine pulmonary root dissected for dynamic or static culturing.

6.3.3 The dynamic and static heart root culture systems

6.3.3.1 The dynamic culture system

A dynamic heart valve bioreactor designed by Dr Sotirios Korossis was used in this study for the dynamic culture of fresh porcine pulmonary roots. A schematic image of the bioreactor in its vertical section is shown in Figure 6.2, and images of the bioreactor are shown in Figure 6.3. This bioreactor worked by mimicking either the left or the right side of the heart. There were three main parts of the bioreactor: the pump, the left/right heart simulator and the biostat.

The bioreactor was driven by an electric pump (Vivitro systems Inc, Canada; Industrial Devices Corporation, CA, USA), which was attached to a control panel to obtain the desired pumping rate, stroke volume and waveform. The pump directly provided pressure to the water inside the membrane housing chamber during pumping, so the silicone membrane which was attached on top of the membrane housing chamber expanded in response to the pressure. The expansion of the silicone membrane produced pressure in the ventricular chamber, which was connected to the membrane housing chamber, thus forcing medium circulation inside the culture system. The silicone membrane also provided separation of the sterile ventricular chamber and the non-sterile electric pump so that the internal environment of the circulation system which contained the tissue was kept sterile. The pulmonary valve roots were placed in stations which were positioned downstream of the ventricular chamber. There were six stations

in total, and when attached encompassed the main body of the bioreactor. Thus, this bioreactor was designed to be able to accommodate six valve roots at the same time. Viewing windows with glass were incorporated at both ends of each station, to allow monitoring of valve root behaviour during the culture process. The pulmonary root was fitted onto a holder which was then positioned into a heart root station (Figure 6.3 B). Images of a fresh porcine pulmonary valve root during culture which were taken from the viewing window of the root station are shown in Figure 6.4. During operation, the ventricular chamber was pressurised, and the culture medium was forced to circulate through the pulmonary valves in the stations, the compliance chamber, the atrial reservoir, the mechanical valve (which represented either the mitral valve in the left heart or the tricuspid valve in the right heart), and back to the ventricular chamber (Figure 6.2). A peripheral resistance was positioned between the compliance chamber and the atrial reservoir in order to mimic the vasculature narrowing in precapillary arterioles, capillaries, and veins. The peripheral resistance could be adjusted manually to control the internal pressure of the circulating system. The internal pressure was monitored with a pressure meter residing on top of the compliance chamber (Figure 6.3 A). The medium temperature, pH and O_2 concentration were monitored and controlled by the biostat (Model ADI 1025, Applikon® Biotechnology) which was connected to the left/right heart simulator (Figure 6.3 C). The medium in the medium resevoir of the biostat was continuously stirred. A heating wrap was placed around the resevoir to maintain the temperature of the medium at 37 °C. The culture medium circulated between the bioreactor and medium resevoir of the biostat, and the circulation rate was monitored so the level of the medium was dynamically balanced. The constant medium circulation made the composition and the parameters of the medium inside the left/right heart simulator and the biostat the same.

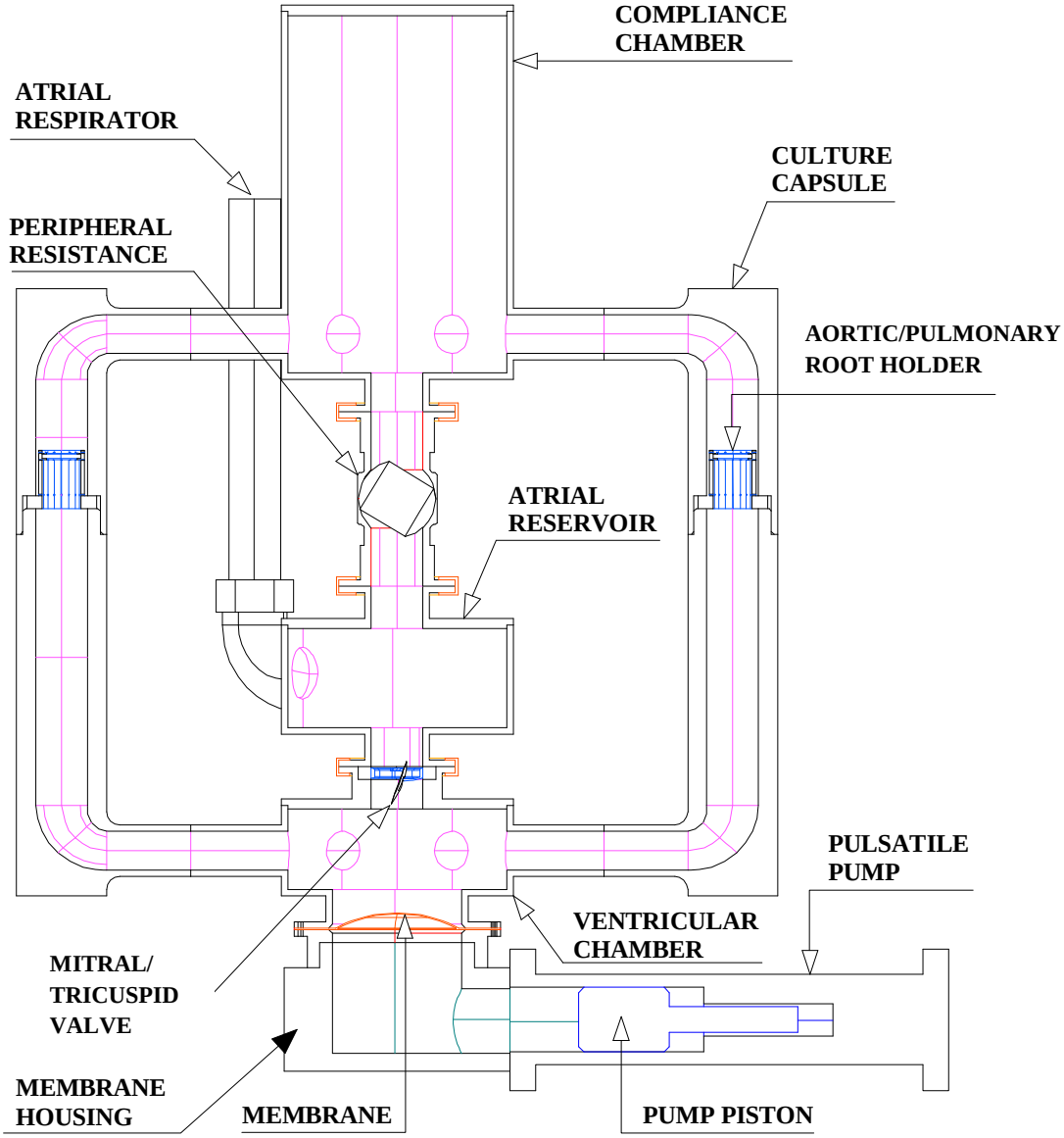

Figure 6.2 A schematic picture of the 6-station dynamic heart valve bioreactor. The bioreactor was driven by an electric pump which directly provided pressure to the water inside the membrane housing chamber during pumping, so the silicone membrane which was attached on top of the membrane housing chamber was expanded in response to the pressure. The expansion of the silicone membrane produced pressure on the ventricular chamber, which was connected to the membrane housing chamber, thus forcing medium circulation inside the culture system. The tissue roots were placed in the stations which were positioned downstream of the ventricular chamber. During operation, the ventricular chamber was pressurised, and the culture medium was forced to circulate through the pulmonary heart valves in the stations, the compliance chamber, the atrial reservoir, the mechanical valve (which represented either the mitral valve in the left heart or the tricuspid valve in the right heart), and back to the ventricular chamber. A peripheral resistance was positioned between the compliance chamber and the atrial reservoir in order to mimic the vasculature narrowing in precapillary arterioles, capillaries, and veins.

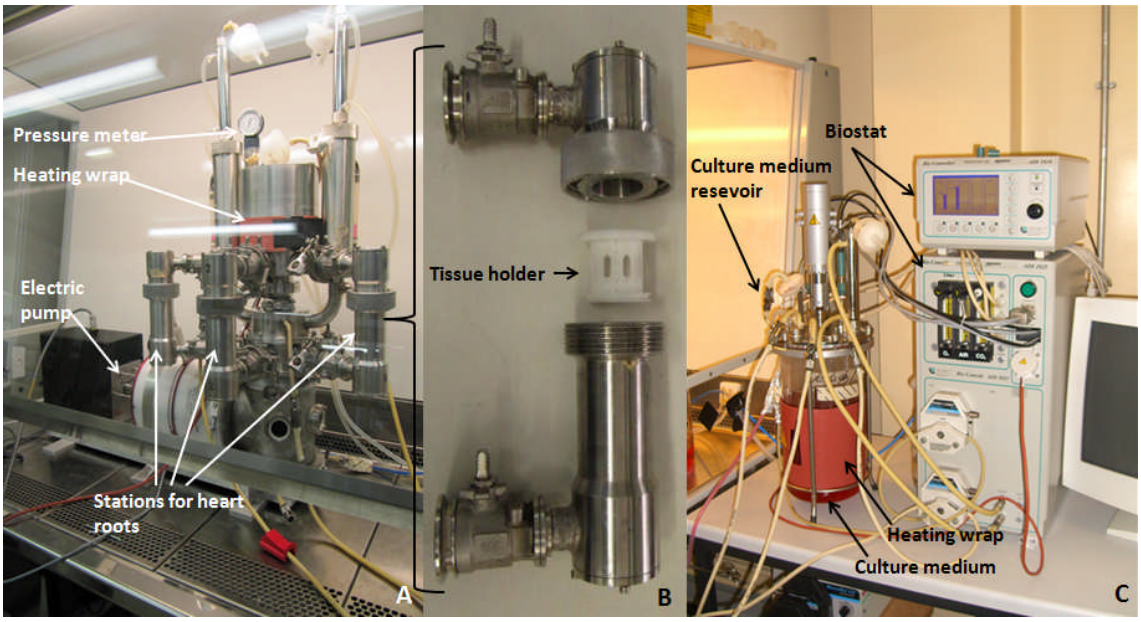

Figure 6.3 The 6-station dynamic heart valve bioreactor. (A) The left/right heart simulator and the pump inside a Class II safety cabinet; **(B)** An opened heart root station with illustration of the heart root holder position; **(C)** The biostat and culture medium resevoir connected to the bioreactor.

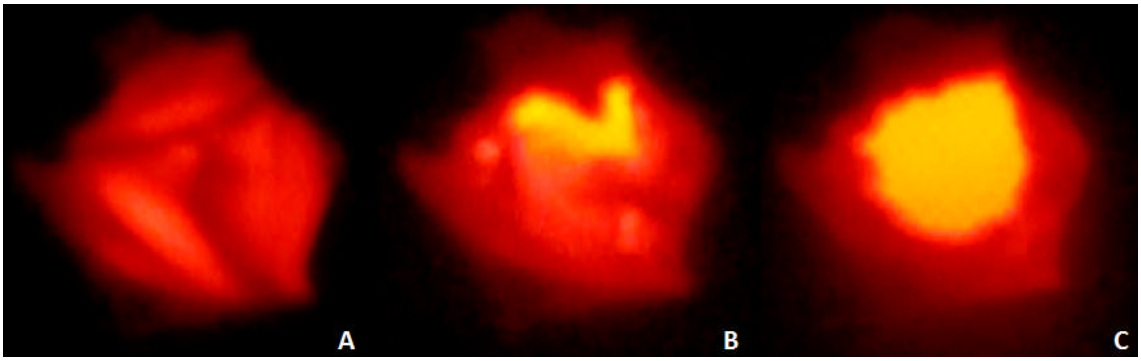

Figure 6.4 Images of a fresh porcine pulmonary valve root during dynamic culture. The images were taken from the viewing window of the heart valve station. **(A)** Fully closed fresh pulmonary valve; **(B)** Fresh pulmonary valve during opening; **(C)** Fully opened fresh pulmonary valve.

6.3.3.2 The static culture system

The static culture system for valve roots is shown in Figure 6.5. The system consisted of three 250 ml tissue culture pots. Each pot was able to accommodate one pulmonary root. There were four valves on the lid of each pot for air-in and out, and medium-in and out.

A sterile filter was positioned upstream of the air-in valve in order to block any microorganisms from the air entering the culture. When the system was working, 5 % (v/v) CO_2 in air was continuously bubbled into the bottom of each pot. The pressure of the 5 % (v/v) CO_2 in air was monitored by a pressure meter (Figure 6.5 B) that was connected upstream of the air-in valve sterile filter. The pressure used in the culture system was 0.5 $L.min^{-1}$ (this value was for the 3 pots together, so each of them was 1/3 of this value). Tests had shown that a flow rate of 0.5 $L.min^{-1}$ in this system would keep the oxygen level in the medium of the static culture pots at 21%. The whole system except for the pressure meter was placed in a 37 ° C incubator.

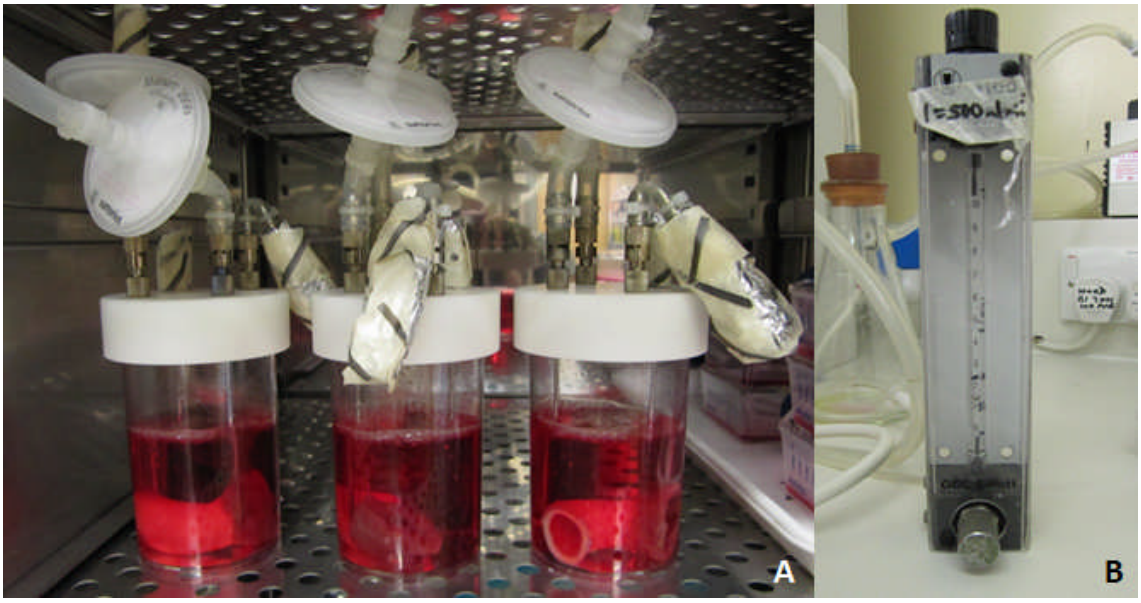

Figure 6.5 The static heart valve culture system. (A) The static heart valve culture pots inside the incubator; **(B)** The pressure meter.

6.3.4 Sterilisation of the heart valve culture systems

The sterility of the heart valve culture systems was crucial to the success of culture experiments with porcine pulmonary roots. Autoclaving was carried out as described in Section 2.2.3.2, and dry heat sterilisation was carried out as described in Section 2.2.3.1.

Prior to experiments, the dynamic bioreactor, the static bioreactor and the biostat culture medium resevoir and tubing were soaked in 1% (v/v) Trygene for 1 hour, with all the valves open, and all the parts separated. All of the air filters were taken off the system.

The parts of the bioreactor and the medium resevoir were then rinsed in running tap water until clear. Following that, all the parts of the bioreactor and the biostat culture medium resevoir were rinsed in distilled water three times. The parts were air-dried on the bench, and the air filters were assembled in their correct positions. Autoclaving was used to sterilise the heart valve bioreactor. Prior to autoclaving, all of the valves were opened, and covered with double layers of foil and fixed with autoclave tape, including the air filters. The mechanical valve was kept in place during autoclaving. To autoclave the biostat culture medium resevoir, the lid of the medium tank was loosely fixed, and around 50 ml of distilled water was in the resevoir to protect the pH probe during autoclaving. All of the connecting tubes were also cleaned and autoclaved prior to use. Trygene (1 %, v/v) was pumped into the tubes and they were soaked for 1 hour, and then Trygene was completely rinsed by pumping tap water through the tubes until the water ran clear. The final step was to pump distilled water through the tubes. The tubes were left on the bench to dry before autoclaving. Both ends of the tubes were opened and covered with double layers of foil, and sealed loosely with autoclave tape prior to autoclaving. Valve root holders and sealing rings for valve root holders were autoclaved separately in autoclave bags. All the parts that were autoclaved were left to completely dry in 37 °C drying room for one week prior to use. Dissection tools, along with bioreactor fixing clips were sterilised by dry heat sterilisation.

6.3.5 The dynamic culture of fresh porcine pulmonary roots

6.3.5.1 Suturing the fresh porcine pulmonary root onto the tissue holder

In order to position the pulmonary valves in the stations of the bioreactor, a root holder was specially designed (Figure 6.6 A). Small holes for suturing were made on both sides of the holder. Dissected fresh porcine pulmonary valve roots were sutured onto the holder aseptically in a Class II safety cabinet with 3/0 non-absorbable polypropylene monofilament suture with a 3/8c, 24mm needle (Premilene®). The myocardium was sutured onto the holder first. The pulmonary artery was then sutured onto the holder with the pulmonary root positioned in its natural state (not to disturb to its natural bending). The extra length of the pulmonary artery was trimmed off after suturing. The tissue was rinsed in PBS every few minutes during the suturing procedure to prevent the tissue from drying and to maintain the maximum viability of the cells in the porcine

pulmonary root. Sealing rings were used on both sides of the holder when it was placed in the bioreactor station to ensure the medium circulated only through the porcine pulmonary roots. Images of a pulmonary valve root holder with a fresh porcine root sutured in place are shown in Figure 6.6 B, C, and D.

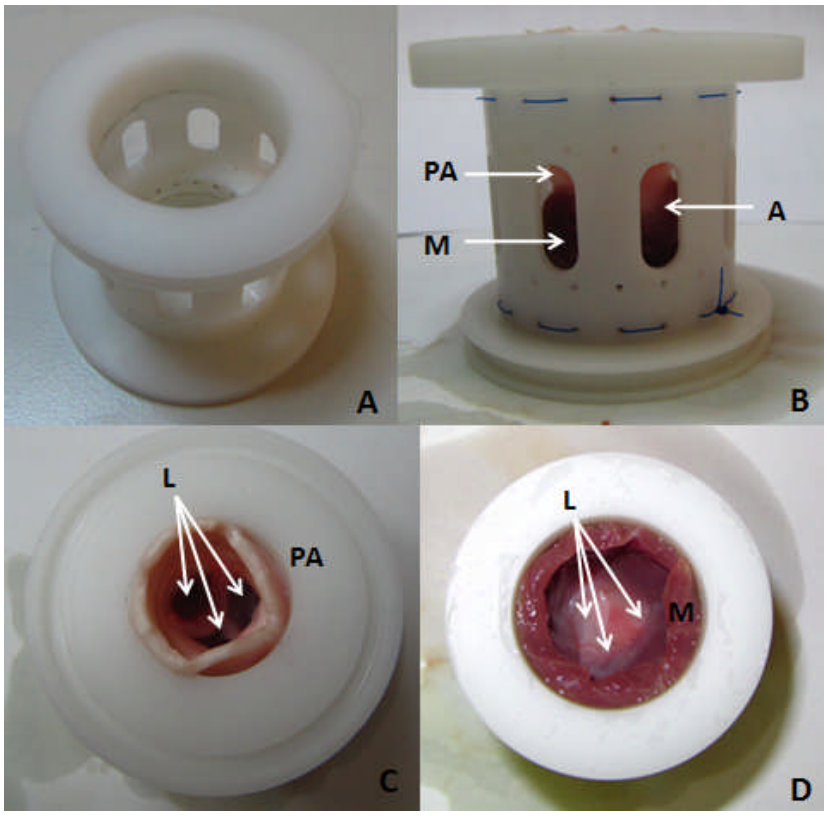

Figure 6.6 Suturing of a fresh porcine pulmonary root onto a holder for the dynamic bioreactor. (A) An image of a pulmonary valve root holder for the heart valve dynamic bioreactor; **(B)** An image of a pulmonary valve root holder for the heart valve dynamic bioreactor with a fresh porcine pulmonary valve root sutured in place; **(C)** An image of a pulmonary valve root holder for the heart valve dynamic bioreactor with a fresh porcine pulmonary heart root sutured in place (a view from the pulmonary artery side); **(D)** An image of a pulmonary valve root holder for the heart valve dynamic bioreactor with a fresh porcine pulmonary heart root sutured in place (a view from the myocardium skirt side). A: leaflet annulus; M: myocardium skirt; PA: pulmonary artery; L: pulmonary leaflet.

6.3.5.2 Tissue disinfection

Each of the sutured fresh porcine pulmonary roots with the holder were incubated in 100 ml Cambridge antibiotics solution in a 250 ml container for 16-17 h at 4 °C for surface disinfection before culturing in the dynamic bioreactor. The Cambridge

antibiotics solution (Sigma) consisted of 14.7 $g.L^{-1}$ Medium 199, 0.2 $g.L^{-1}$ vancomycin HCl USP, 0.2 $g.L^{-1}$ polymyxin B sulphate, 2.5 million $unit.L^{-1}$ nystatin, 0.25 $g.L^{-1}$ imipenem/cilastatin sodium and 4 $g.L^{-1}$ gentamicin sulphate.

6.3.5.3 The dynamic culture procedure

The dynamic heart valve bioreactor was assembled aseptically in the class II safety cabinet, and connected to the biostat. Tissue culture medium was aseptically pumped into the bioreactor (~ 5 L) and the biostat medium resevoir (~ 5 L). A valve root station with a mechanical valve was fitted to the bioreactor. The bioreactor was operated with the culture medium and mechanical valve for a period of one week prior to inserting any fresh pulmonary roots in order to check for sterility and equilibrate the system. During this period, the culture medium was equilibrated to the required O_2 concentration, pH, and temperature. After everything was balanced, the pump was set at 60 bpm, and produced a stroke volume of 4.2 $L.min^{-1}$. A sinusoidal waveform was used. The pressure inside the bioreactor during operation was 15-33 mmHg. The culture medium within the bioreactor and the chemostat had an O_2 concentration of 21 %, and the pH was pH 7.4. The temperature of the medium was 37 °C. The same conditions were applied to the dynamic culture of fresh porcine pulmonary roots. After the bioreactor had operated with a mechanical valve for one week, three fresh porcine pulmonary roots were dissected and sutured onto valve root holders aseptically. The holders were placed in the stations for valve roots prior to fitting the stations to the bioreactor. The station with the mechanical valve was removed at this stage. The three fresh porcine pulmonary roots were cultured in the dynamic bioreactor for one week. Following culture, the roots were removed from the stations, and the cultured roots were assessed for cell viability and examined by histology and immunohistochemistry.

6.3.6 The static culture procedure of fresh porcine pulmonary roots

The static culture system was assembled in a Class II safety cabinet. Three fresh pulmonary roots were dissected and disinfected in Cambridge antibiotics solution for 16-17 h at 4 °C, prior to being placed in the three pots of the static culture system individually. Culture medium (150 ml) was used for the culture of each fresh porcine

pulmonary root in each pot. The culture system was then placed in a 37 °C incubator with 5 % (v/v) CO_2 in air continuously bubbled into the culture medium. The three fresh porcine pulmonary roots were cultured in the static system for one week, and the cultured roots were assessed for cell viability and examined by histology and immunohistochemistry.

6.3.7 Histology

Following culture of fresh porcine pulmonary roots in the dynamic (n=3) and static (n=3) systems, histology was carried out to determine the cell distribution and tissue histoarchitecture. Tissue samples for histology were fixed with 10 % (v/v) NBF for 24 to 48h, and histology was carried out as described in Section 2.2.7. Tissue sections for histology were collected when the leaflet, pulmonary artery and myocardium all appeared on the same sections. The H&E stain was used to study the cell distribution and tissue histoarchitecture. The Hoechst stain was used to study the localisation of cell nuclei. Each tissue sample was serially sectioned at 10 μm, and at least 3 sections were stained. Slides were viewed with a bright-field microscope or a fluorescent microscope with a DAPI filter after staining.

6.3.8 Immunohistochemistry

Immunohistochemistry was utilised to localise specific matrix and cellular proteins in tissue sections. Porcine pulmonary root samples (n=3 for dynamic cultured tissue; n=3 for static cultured tissue) were fixed with 10 % (v/v) NBF or zinc fixation solution, and immunohistochemical analyses were performed as described in Section 2.2.8. A minimum of 3 sections per sample from serial sections of 10 μm were evaluated. Sections from each tissue sample were incubated with specific antibody, isotype control of the same concentration as the antibody, and antibody diluent (omitting the primary antibody as a negative control). Antibody specific binding was carefully examined using light microscopy. Monoclonal antibodies used in this study were specific to: α-SMA, vWF, desmin, vimentin, fibronectin, and collagen-IV.

6.3.9 Live/dead staining of porcine pulmonary leaflets

6.3.9.1 Live/dead staining

Solutions:

Live/dead stain solution was prepared using PBS at pH 7.6, and comprised 1mM calcein AM and 1mM ethidium homodimer-1 (1.2 µl calcein and 5 µl of ethidium homodimer-1 in 5ml of PBS pH 7.6).

Method:

Live/dead staining was used to visualise the viability of cells in the pulmonary leaflets. Pulmonary leaflet tissue was dissected and placed into individual wells of a 12-well tissue culture plate. Live/dead stain solution was added into each well to completely cover the tissue. The plate was fitted with its lid, and incubated at room temperature in the dark for 45 min. The tissue was washed three times in TBS pH 7.6 for 10 min on a plate rocker. The tissue was then wet mounted with glycerol: DABCO (1:9) onto a microscope slide and covered with a glass coverslip. The tissue was viewed using a confocal microscope (Zeiss LSM510 META) and a conventional fluorescent long pass filter. Live cells were stained green while dead cells were stained red.

6.3.9.2 Confocal Microscopy

A Zeiss LSM510 META confocal microscope was used to examine the cell viability in the leaflet tissue. The pre-stained porcine pulmonary leaflets were wet mounted with glycerol/DABCO (1:9) onto a microscope slide and covered with a glass coverslip. The two laser injectors of the confocal microscope, Argon/2 and HeNel1 were turned on, and the live/dead assay setting was selected using the LSM510 control programme. The signals of the two dyes from the live/dead stain assay were captured at 448 nm (for calcein), and 514 nm (for ethidium homodimer-1) at different depths of the tissue. Images were captured using the 40 times magnification observation lens.

6.3.10 Cell viability assay (MTT assay) for porcine pulmonary leaflets

Solutions:

- MTT (3-(4,5-Dimethylthiazol-2-yl)-2,5-diphenyltetrazolium bromide) solution: 5mg.ml^{-1} MTT was made in PBS pH 7.6. This solution was stored in a foil wrapped container in -20 °C, and thawed to room temperature when used.
- DMSO

Method:

The MTT assay was used to study the cell viability within the heart valve leaflet tissue. Tissue samples of 20 mg were macerated with a scalpel blade, weighted, and then placed in 1.5 ml microtubes. MTT solution (200 µl) and 400 µl PBS were added to each microtube. The tubes were incubated on a blood rotator at 30 rpm for 2.5 h at 37 °C. Following incubation, the tubes were centrifuged in a micro centrifuge at 6,000 g for 5 min, the supernatant was removed and 1ml of DMSO was added into each tube. The tubes were further incubated on the blood rotator at 30 rpm for 17 h at 37 °C, centrifuged at 6,000 g for 5 min in a micro centrifuge. Aliquots of 200 µl supernatant were transferred from the micro tubes to a clear flat-bottomed 96-well plate. The absorbance was read at 570 nm with a reference filter at 630 nm. DMSO was used as a blank. The readings for acellular pulmonary leaflet samples were compared to those of the fresh tissue, in order to compare the cell viability. Data was analysed by one way ANOVA followed by calculation of the MSD using the T-method.

6.4 Results

6.4.1 The fresh porcine pulmonary roots cultured in dynamic and static culture systems for one week

After culture for one week in the dynamic and static culture systems, the porcine pulmonary roots were removed. Images of the cut-open porcine pulmonary roots are shown in Figure 6.7. No damage was seen to the pulmonary leaflets or any other parts of the roots for both dynamic and static cultured tissue. No apparent change in gross tissue morphology was observed. The porcine pulmonary leaflets and pulmonary arteries were found to have taken up the pink colour of the phenol red in the tissue culture medium.

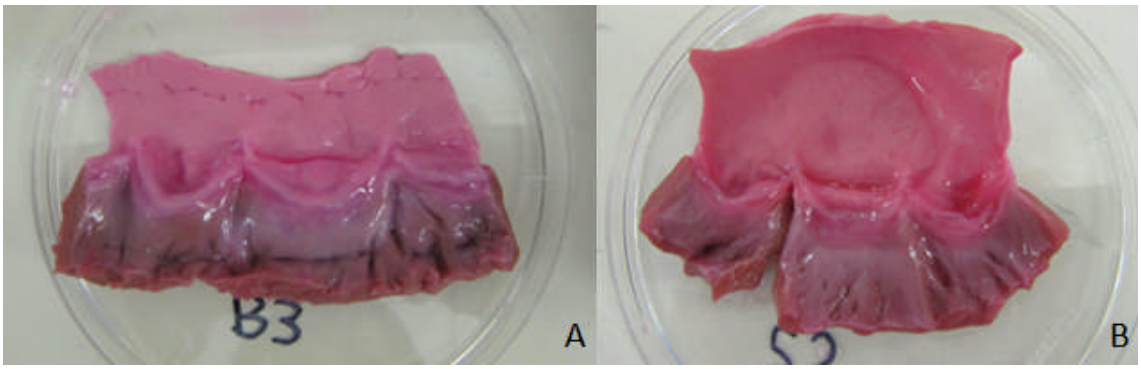

Figure 6.7 Images of cut-open fresh porcine pulmonary roots after one week of culture in the dynamic and static culture systems. (A) An image of a cut-open fresh porcine pulmonary root cultured in the dynamic culture system for one week; **(B)** An image of a cut-open fresh porcine pulmonary root cultured in the static culture system for one week.

6.4.2 Histological evaluation of fresh porcine pulmonary valve conduits cultured in the dynamic and static heart root culture systems for one week

Tissue sections of the porcine pulmonary roots cultured in the dynamic and static culture systems for one week were stained with H&E and Hoechst. Histology images of the pulmonary roots cultured in the dynamic system are shown in Figure 6.8 (H&E) and Figure 6.9 (Hoechst). Histology images of the pulmonary roots cultured in the static system are shown in Figure 6.10 (H&E) and Figure 6.11 (Hoechst). Cells that were

stained blue after H&E staining were observed throughout the dynamic and static cultured porcine pulmonary roots (Figure 6.8 & Figure 6.10). The connective tissues that were stained red could be seen in the pulmonary leaflets, pulmonary artery and myocardium. The loosely arranged *spongiosa* and the more organised *ventricularis* and *fibrosa* in the pulmonary leaflets were recognised (Figure 6.8 A & figure 6.10 A). The tips of the pulmonary leaflets remained intact after culturing in the dynamic and static systems (Figure 6.8 B & Figure 6.10 B). In the H&E images for myocardium (Figure 6.8 C & Figure 6.10 C), the cross-sectioned myocardium bundles were observed. The connective tissue and smooth muscle cells were aligned parallel to the long axis of the pulmonary arteries after culture (Figure 6.8 D, E; Figure 6.10 D, E). Hoechst staining results further confirmed the cell distribution was throughout the whole porcine pulmonary roots cultured in the dynamic and static systems (Figure 6.9 & Figure 6.11). Cells were recognised in both the endothelial region and the internal region of the pulmonary leaflets and pulmonary arteries.

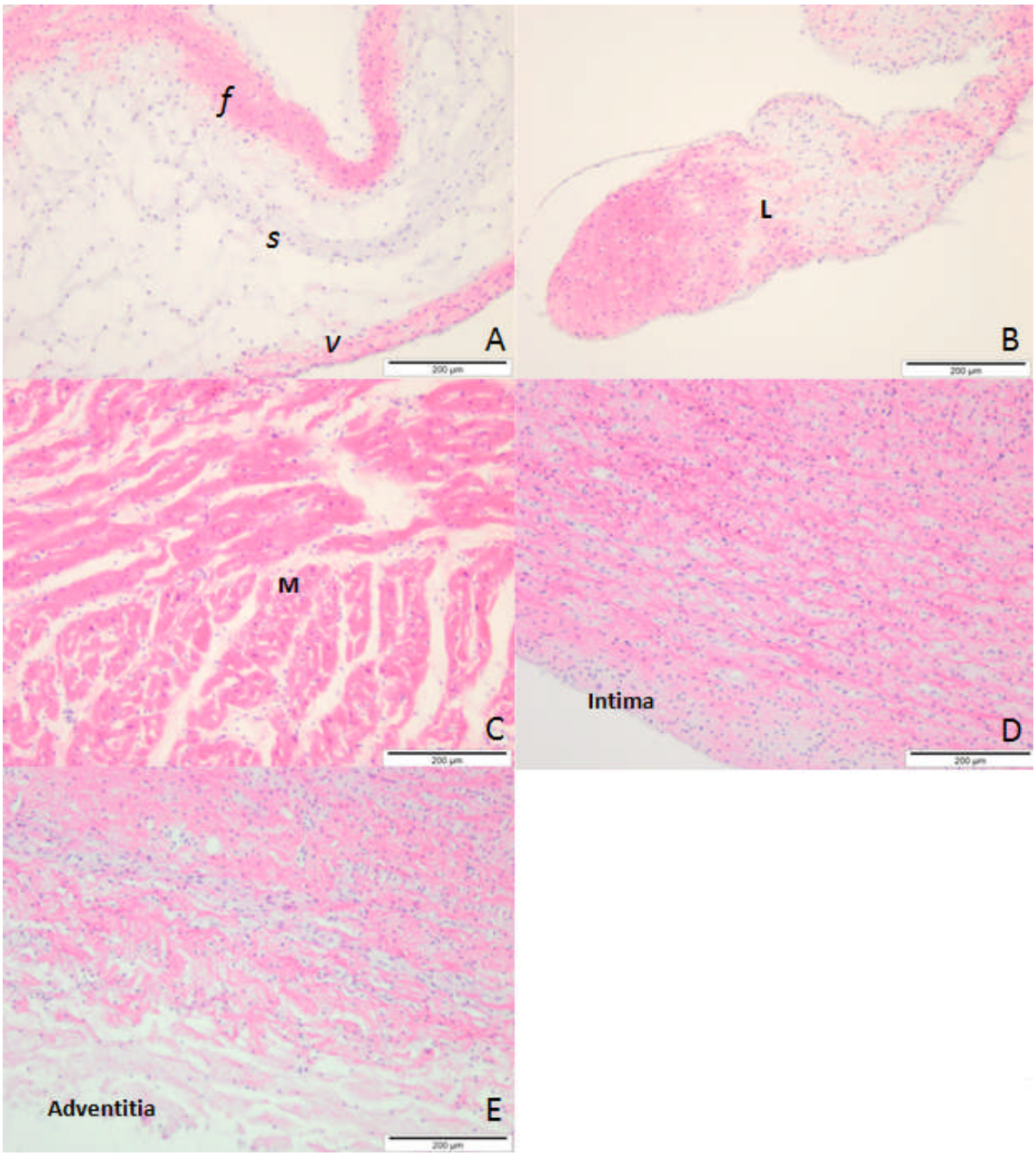

Figure 6.8 Sections of fresh porcine pulmonary root tissue cultured in the dynamic system for one week stained with H&E. (A) Pulmonary valve leaflet, 100 × (*v*: *ventricularis*; *s*: *spongiosa*; *f*: *fibrosa*); **(B)** The tip of the pulmonary valve leaflet, 100 ×; **(C)** Myocardium, 100 ×; **(D)** The lumen surface of the pulmonary artery, 100 ×; **(E)** The adventitial surface of the pulmonary artery, 100 ×. M: myocardium; L: leaflet. Scale bars are: all 200 µm.

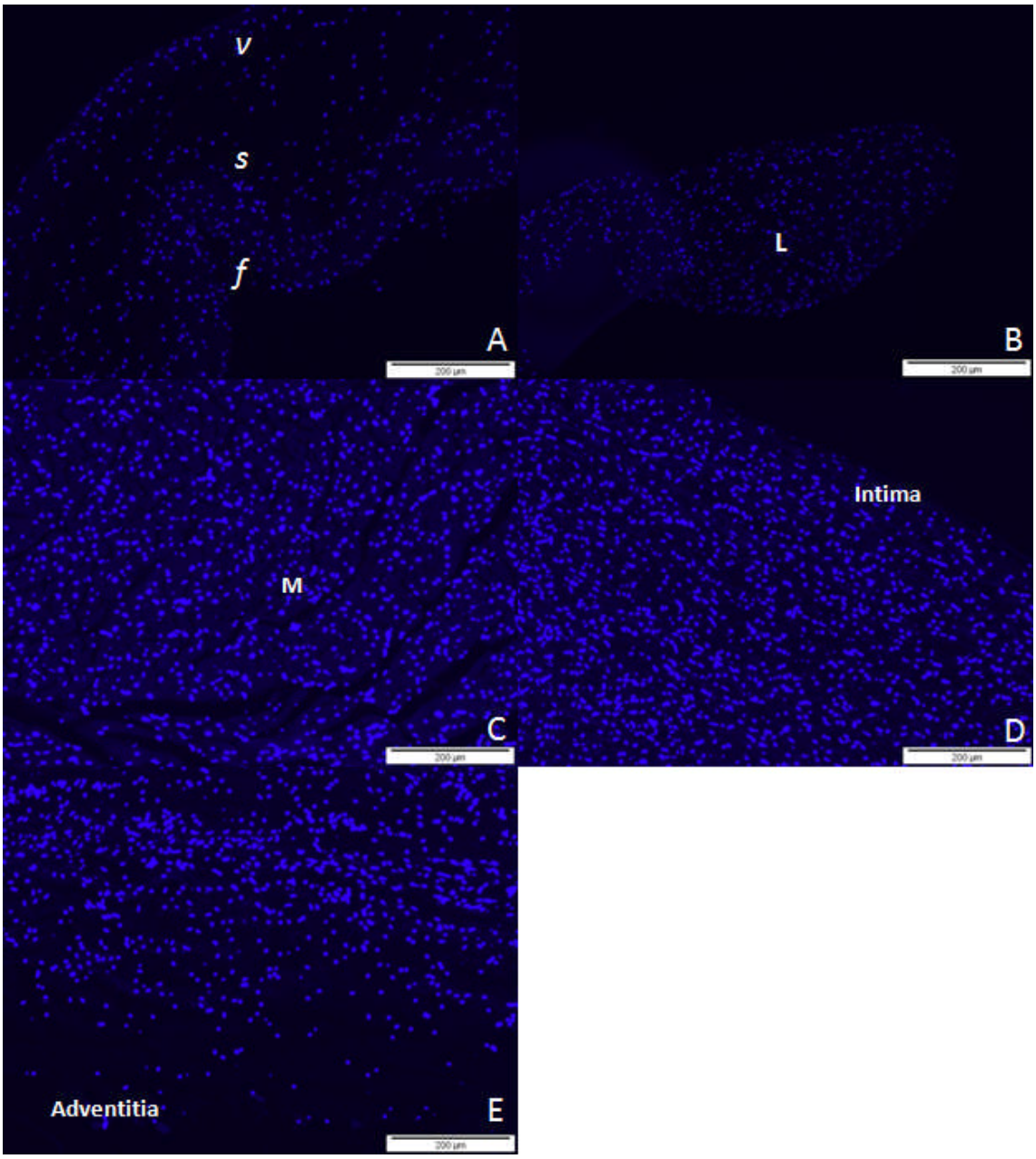

Figure 6.9 Sections of fresh porcine pulmonary root tissue cultured in the dynamic system for one week stained with Hoechst. (A) Pulmonary valve leaflet, 100 × (*v*: *ventricularis*; *s*: *spongiosa*; *f*: *fibrosa*); **(B)** The tip of the pulmonary valve leaflet, 100 ×; **(C)** Myocardium, 100 ×; **(D)** The lumen surface of the pulmonary artery, 100 ×; **(E)** The adventitial surface of the pulmonary artery, 100 ×. M: myocardium; L: leaflet. Scale bars are: all 200 µm.

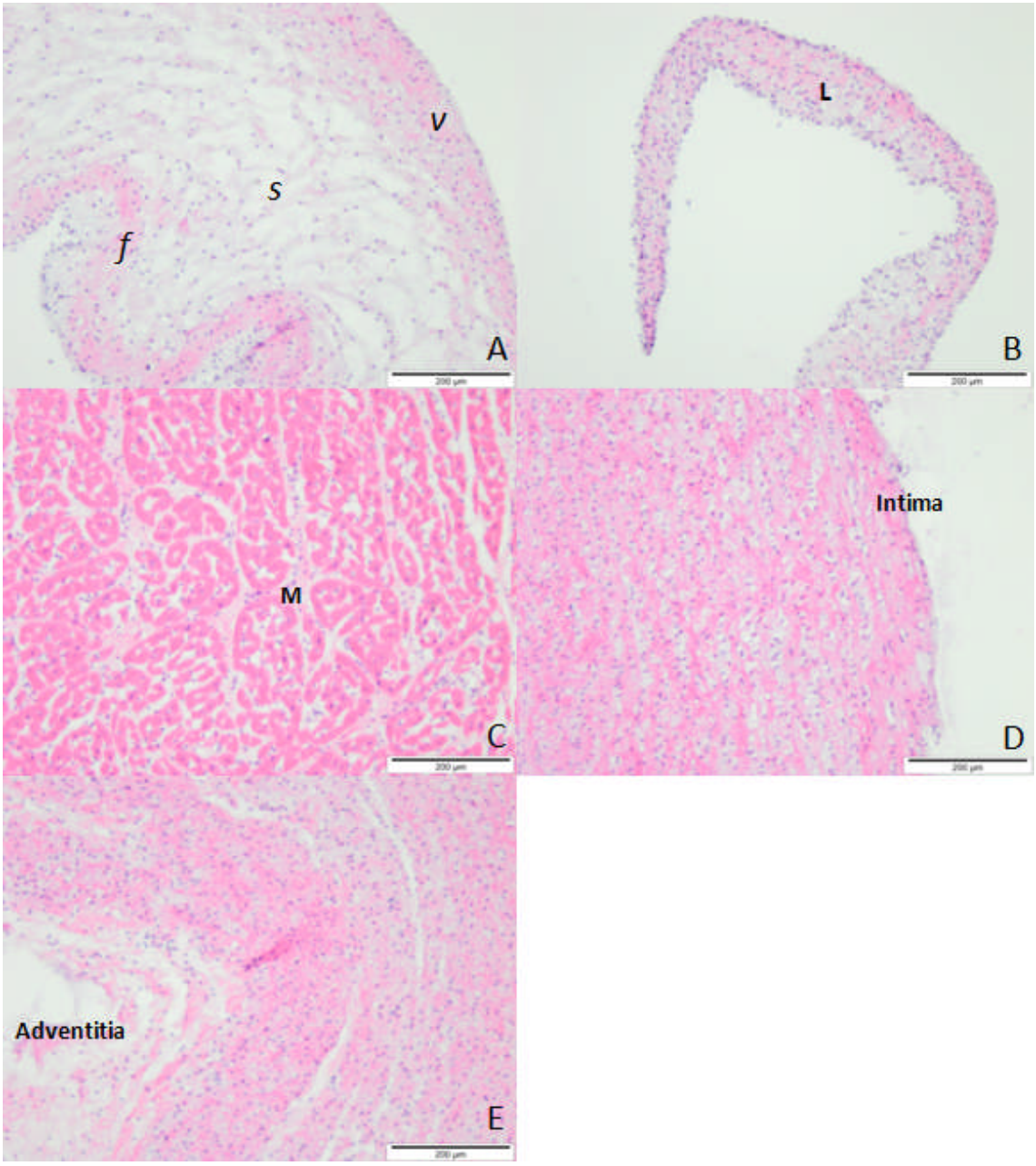

Figure 6.10 Sections of fresh porcine pulmonary root tissue cultured in the static system for one week stained with H&E. (A) Pulmonary valve leaflet, 100 × (*v*: *ventricularis*; *s*: *spongiosa*; *f*: *fibrosa*); **(B)** The tip of the pulmonary valve leaflet, 100 ×; **(C)** Myocardium, 100 ×; **(D)** The lumen surface of the pulmonary artery, 100 ×; **(E)** The adventitial surface of the pulmonary artery, 100 ×. M: myocardium; L: leaflet. Scale bars are: all 200 µm.

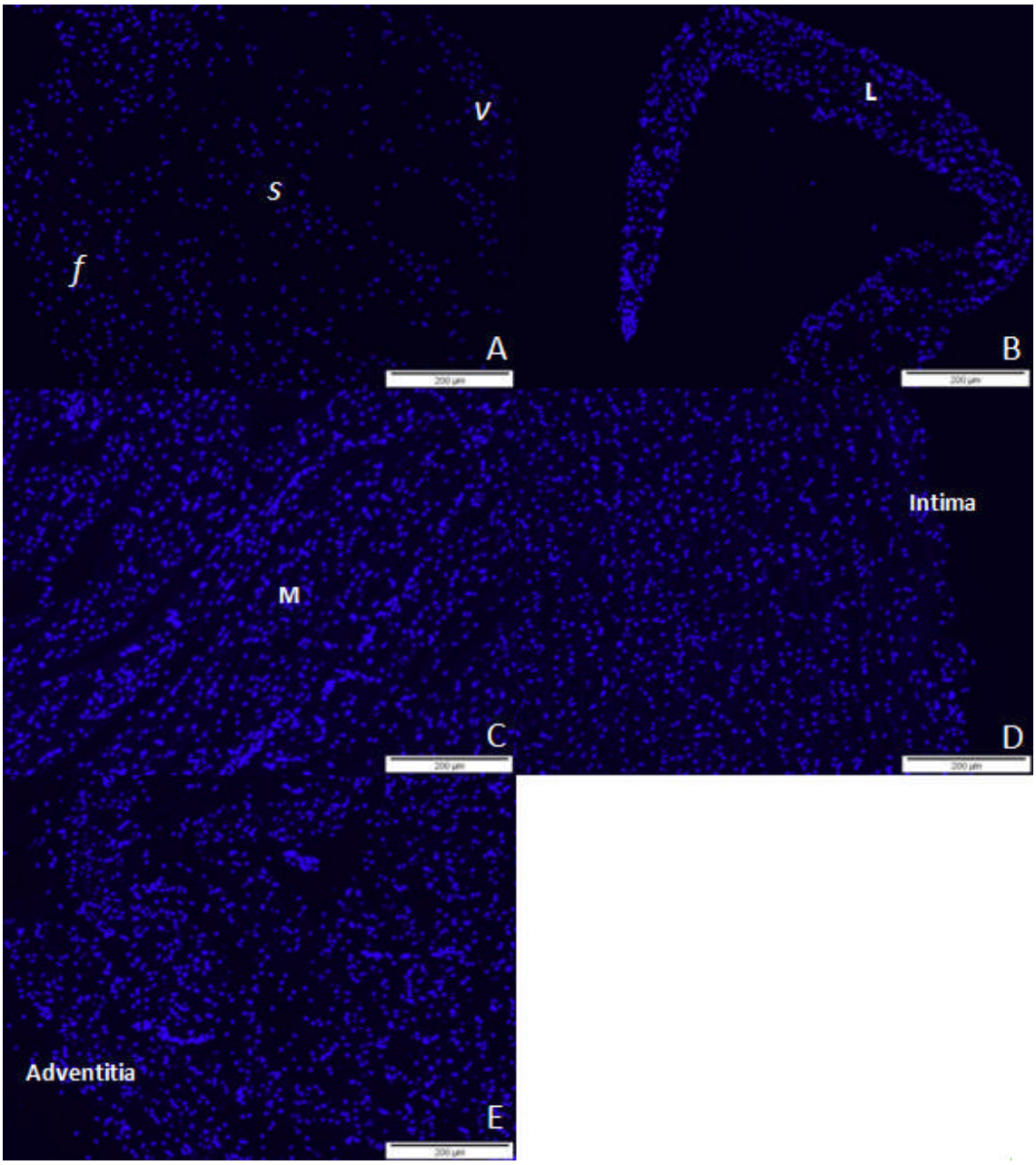

Figure 6.11 Sections of fresh porcine pulmonary root tissue cultured in the static system for one week stained with Hoechst. (A) Pulmonary valve leaflet, 100 × (*v*: *ventricularis*; *s*: *spongiosa*; *f*: *fibrosa*); **(B)** The tip of the pulmonary valve leaflet, 100 ×; **(C)** Myocardium, 100 ×; **(D)** The lumen surface of the pulmonary artery, 100 ×; **(E)** The adventitial surface of the pulmonary artery, 100 ×. M: myocardium; L: leaflet. Scale bars are: all 200 µm.

6.4.3 Immunohistochemical evaluation of fresh porcine pulmonary valve conduits cultured in the dynamic and static heart root culture systems for one week

Specific cytoskeletal and ECM proteins of the porcine pulmonary roots cultured in dynamic and static systems for one week were localised using immunohistochemical stainings. All negative control sections (including isotype controls and omission of primary antibody controls) showed an absence of staining.

6.4.3.1 Alpha-SMA

The images of porcine pulmonary root tissue sections labelled with α-SMA are shown in Figure 6.12 (cultured in the dynamic system) and Figure 6.13 (cultured in the static system). The ventricular surface of the pulmonary leaflet that was cultured in the dynamic system was positively stained with α-SMA antibody (Figure 6.12 A). However, no staining was observed in the leaflets cultured in the static system (Figure 6.13 A). Positive staining was also observed in the blood vessels within the myocardium of dynamic and static culture porcine pulmonary roots (Figure 6.12 B; Figure 6.13 B). The cells within the pulmonary arteries from both dynamic and static cultured porcine pulmonary roots were stained positive, while the ECM of the pulmonary arteries stained a light brown colour (Figure 6.12 C; Figure 6.13 C). No positive staining was observed in the tissue sections stained with isotype control (Figure 6.12 D, E, F; Figure 6.13 D, E, F).

6.4.3.2 vWF

The images of porcine pulmonary root tissue sections stained for vWF are shown in Figure 6.14 (cultured in the dynamic system) and Figure 6.15 (cultured in the static system). No brown coloured positive staining was observed in the pulmonary leaflets or the luminal surface of the pulmonary arteries of either the dynamic cultured or the static cultured porcine pulmonary roots (Figure 6.14 A, C; Figure 6.15 A, C). This result indicated a loss of endothelial cells in the porcine pulmonary roots after dynamic and static culturing. However, the small blood vessels within the myocardium and the adventitial connective tissue layer of the pulmonary arteries were stained positive (Figure 6.14 B, D; Figure 6.15 B, D). No positive staining was observed in the tissue sections stained with isotype control (Figure 6.14 E, F; Figure 6.15 E, F).

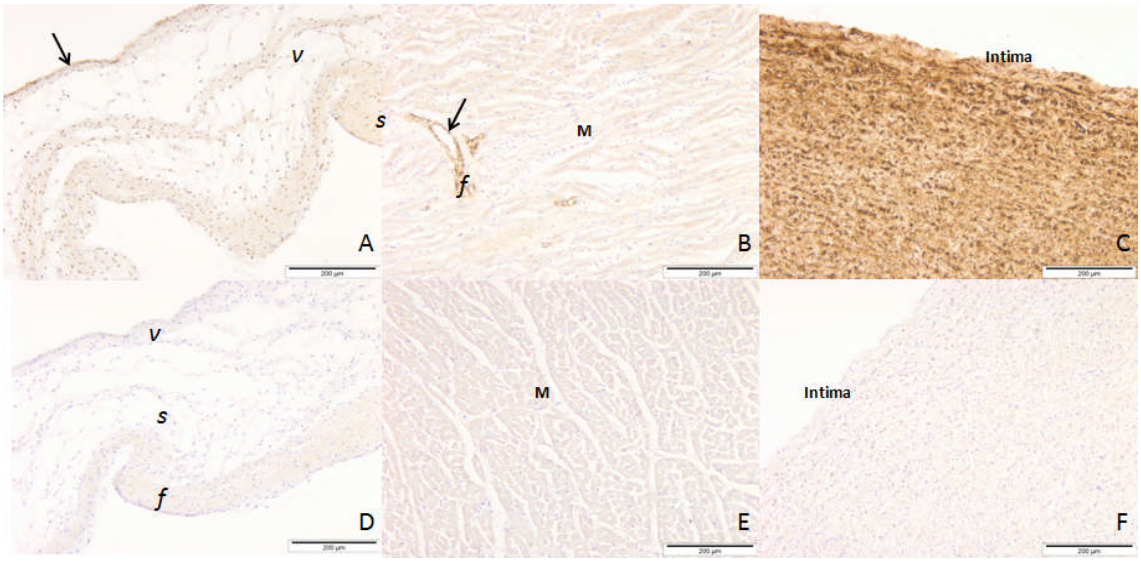

Figure 6.12 Localisation of α-SMA in fresh porcine pulmonary root tissue cultured in the dynamic system for one week. (A) Pulmonary valve leaflet, 100 ×, the arrow indicates the ventricular side of the pulmonary leaflet that has been positively stained; **(B)** Myocardium, 100 ×, the arrow indicates a blood vessel in the myocardium that has been positively stained; **(C)** Pulmonary wall, 100 ×; **(D)** Pulmonary valve leaflet isotype control, 100 ×; **(E)** Myocardium isotype control, 100 ×; **(F)** Pulmonary wall isotype control, 100 ×. *v*: *ventricularis*; *s*: *spongiosa*; *f*: *fibrosa*; M: myocardium. Scale bars are: all 200 µm.

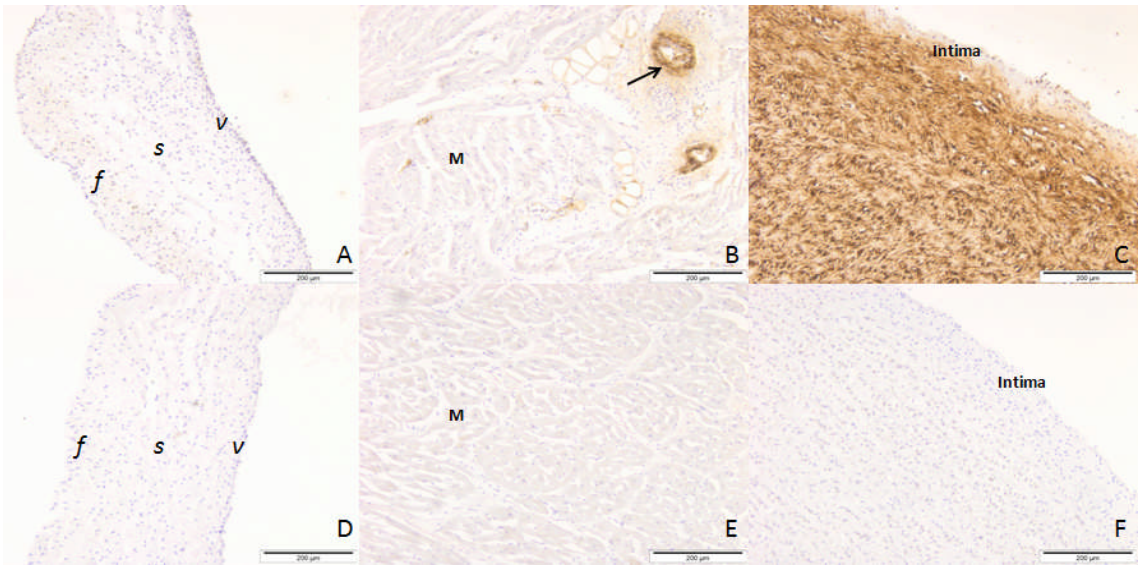

Figure 6.13 Localisation of α-SMA in fresh porcine pulmonary root tissue cultured in the static system for one week. (A) Pulmonary valve leaflet, 100 ×; **(B)** Myocardium, 100 ×, the arrow indicates a blood vessel in the myocardium that has been positively stained; **(C)** Pulmonary wall, 100 ×; **(D)** Pulmonary valve leaflet isotype control, 100 ×; **(E)** Myocardium isotype control, 100 ×; **(F)** Pulmonary wall isotype control, 100 ×. *v*: *ventricularis*; *s*: *spongiosa*; *f*: *fibrosa*; M: myocardium. Scale bars are: all 200 µm.

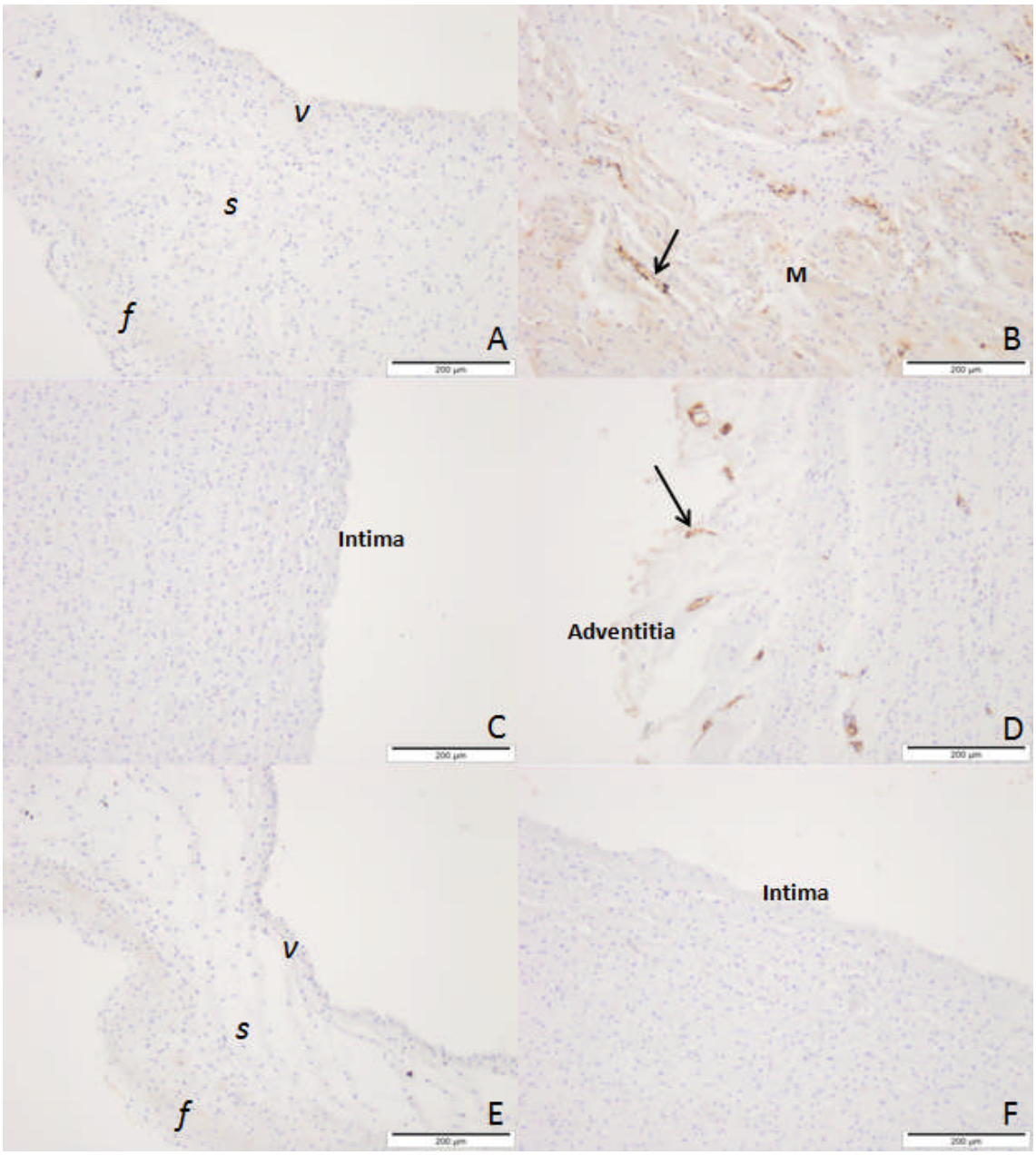

Figure 6.14 Localisation of vWF in fresh porcine pulmonary root tissue cultured in the dynamic system for one week. (A) Pulmonary valve leaflet, 100 ×; **(B)** Myocardium, 100 ×, the arrow indicates a blood vessel in the myocardium that has been positively stained; **(C)** The lumen surface of the pulmonary wall, 100 ×; **(D)** The adventitial surface of the pulmonary wall, 100 ×, the arrow indicates a blood vessel that has been positively stained; **(E)** Pulmonary valve leaflet stained with isotype control, 100 ×; **(F)** Pulmonary wall stained with isotype control. *v*: *ventricularis*; *s*: *spongiosa*; *f*: *fibrosa*; M: myocardium. Scale bars are: all 200 µm.

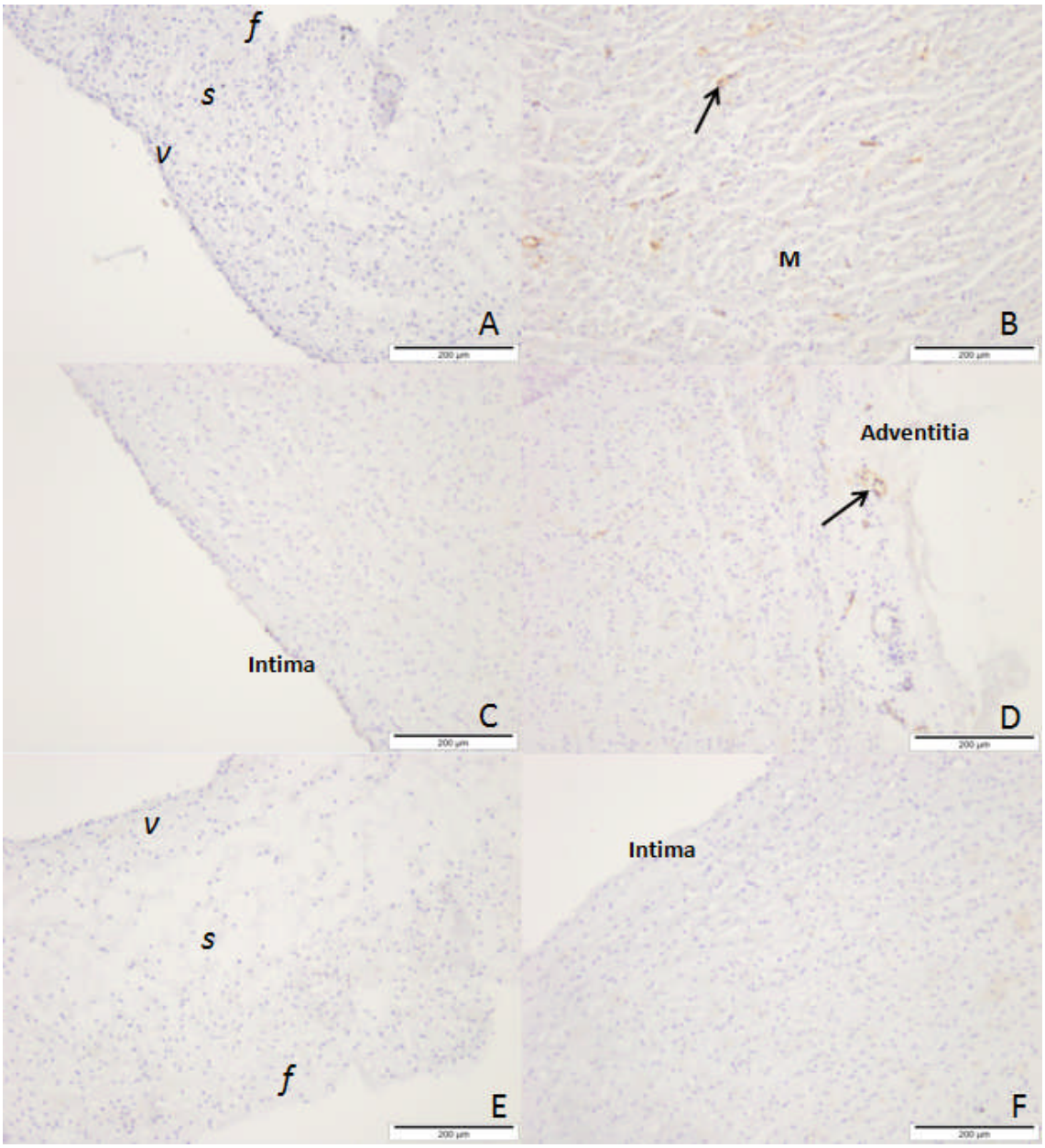

Figure 6.15 Localisation of vWF in fresh porcine pulmonary root tissue cultured in the static system for one week. (A) Pulmonary valve leaflet, 100 ×; **(B)** Myocardium, 100 ×, the arrow indicates a blood vessel in the myocardium that has been positively stained; **(C)** The lumen surface of the pulmonary wall, 100 ×; **(D)** The adventitial surface of the pulmonary wall, 100 ×, the arrow indicates a blood vessel that has been positively stained; **(E)** Pulmonary valve leaflet stained with isotype control, 100 ×; **(F)** Pulmonary wall stained with isotype control. *v*: *ventricularis*; *s*: *spongiosa*; *f*: *fibrosa*; M: myocardium. Scale bars are: all 200 µm.

6.4.3.3 Desmin

Images of porcine pulmonary root tissue sections labelled with a monoclonal antibody against desmin are shown in Figure 6.16 (cultured in the dynamic system) and Figure 6.17 (cultured in the static system). The myocardium of the dynamic cultured pulmonary roots was stained positive (Figure 6.16 B). No positive staining was observed in the static cultured pulmonary root sections. No positive staining was observed in the tissue sections stained with isotype control (Figure 6.16 E, F; Figure 6.17 E, F).

6.4.3.4 Vimentin

Following labelling using a monoclonal antibody against vimentin, the results indicated that the cells within the porcine pulmonary roots cultured in the dynamic and static systems for one week were stained positive (Figure 6.18; Figure 6.19). The cells within the myocardium of the static cultured porcine pulmonary roots (Figure 6.19 B) were stained less intensely than those of the dynamic cultured porcine pulmonary roots (Figure 6.18 B). No positive staining was observed in the tissue sections stained with isotype control (Figure 6.18 E, F; Figure 6.19 E, F).

6.4.3.5 Fibronectin

The porcine pulmonary roots cultured in the dynamic and static system for one week were stained brown throughout following labelling with fibronectin (Figure 6.20; Figure 6.21). The darkest colour was observed in the surfaces of the pulmonary leaflets and the lumen surface of the pulmonary arteries. No positive staining was observed in the tissue sections stained with isotype control (Figure 6.20 E, F; Figure 6.21 E, F).

6.4.3.6 Collagen IV

The images of porcine pulmonary root sections stained for collagen IV are shown in Figure 6.22 (cultured in the dynamic system) and Figure 6.23 (cultured in the static system). The darkest brown colour indicating positive staining was observed on the surfaces of the porcine pulmonary leaflets (Figure 6.22 A; Figure 6.23 A) as well as the lumen surface of the fresh pulmonary artery (Figure 6.22 C; Figure 6.23 C). The ECM of porcine pulmonary arteries and myocardium were also stained a light brown colour.

No positive staining was observed in the tissue sections stained with the isotype control (Figure 6.22 E, F; Figure 6.23 E, F).

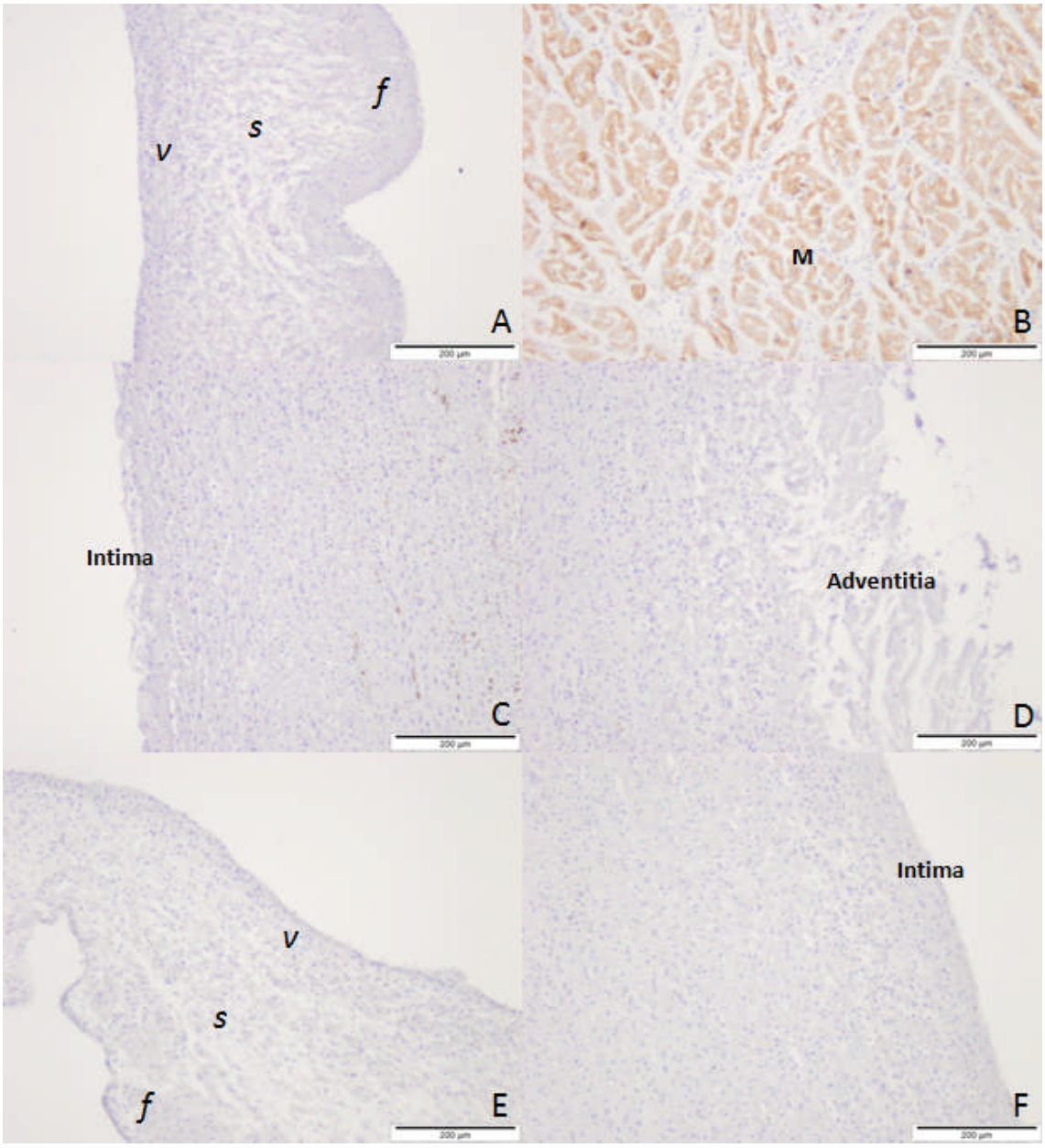

Figure 6.16 Localisation of desmin in fresh porcine pulmonary root tissue cultured in the dynamic system for one week. (A) Pulmonary valve leaflet, 100 ×; **(B)** Myocardium, 100 ×; **(C)** The lumen surface of the pulmonary wall, 100 ×; **(D)** The adventitial surface of the pulmonary wall, 100 ×. M: myocardium; **(E)** Pulmonary valve leaflet stained with isotype control, 100 ×; **(F)** Pulmonary wall stained with isotype control. *v*: *ventricularis*; *s*: *spongiosa*; *f*: *fibrosa*; M: myocardium. Scale bars are: all 200 µm.

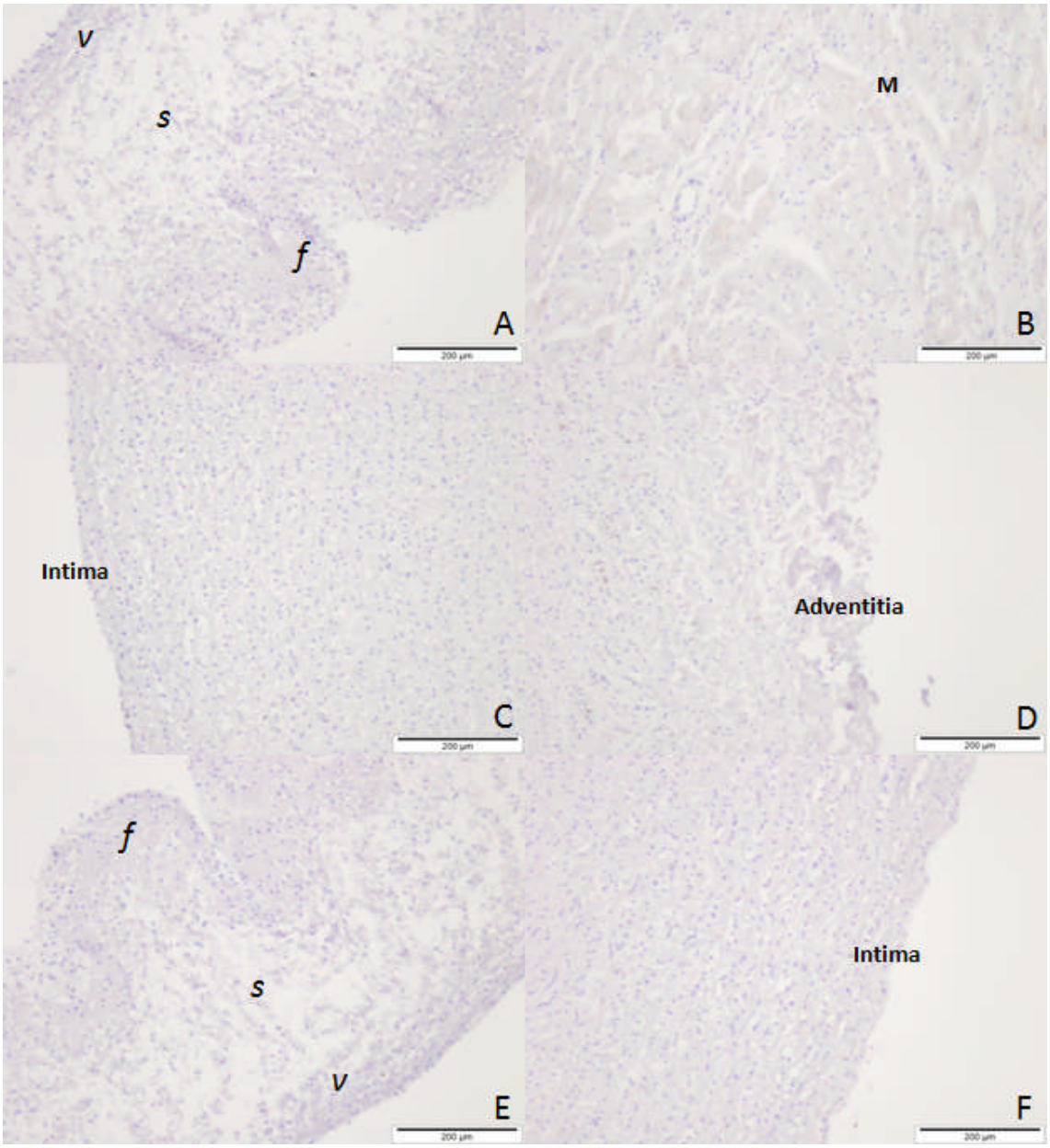

Figure 6.17 Localisation of desmin in fresh porcine pulmonary root tissue cultured in the static system for one week. (A) Pulmonary valve leaflet, 100 ×; **(B)** myocardium, 100 ×; **(C)** the lumen surface of the pulmonary wall, 100 ×; **(D)** the adventitial surface of the pulmonary wall, 100 ×; **(E)** pulmonary valve leaflet stained with isotype control, 100 ×; **(F)** Pulmonary wall stained with isotype control. *v*: *ventricularis*; *s*: *spongiosa*; *f*: *fibrosa*; M: myocardium. Scale bars are: all 200 µm.

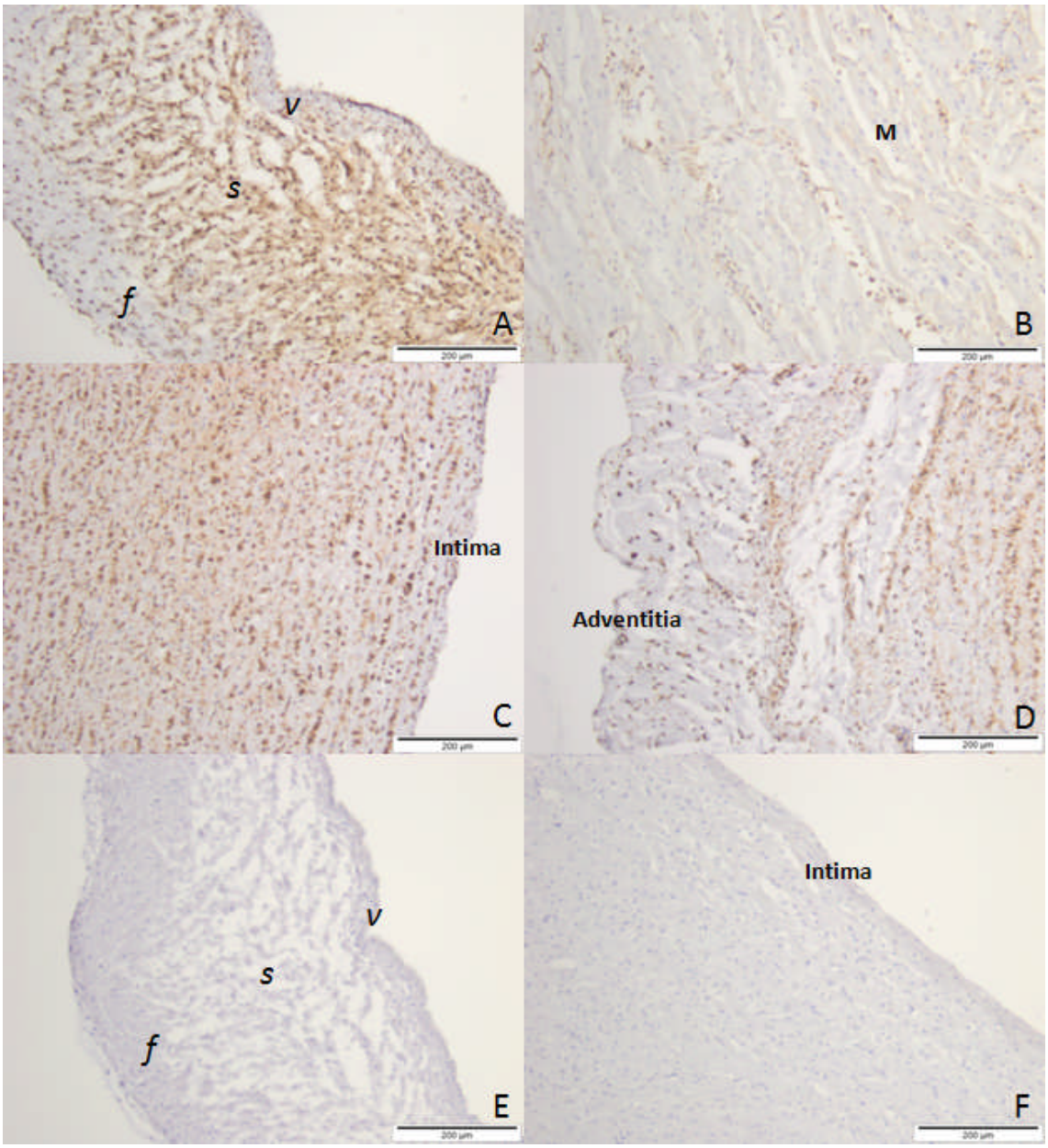

Figure 6.18 Localisation of vimentin in fresh porcine pulmonary root tissue cultured in the dynamic system for one week. (A) Pulmonary valve leaflet, 100 ×; **(B)** Myocardium, 100 ×; **(C)** The lumen surface of the pulmonary wall, 100 ×; **(D)** The adventitial surface of the pulmonary wall, 100 ×; **(E)** Pulmonary valve leaflet stained with isotype control, 100 ×; **(F)** Pulmonary wall stained with isotype control. *v*: *ventricularis*; *s*: *spongiosa*; *f*: *fibrosa*; M: myocardium. Scale bars are: all 200 µm.

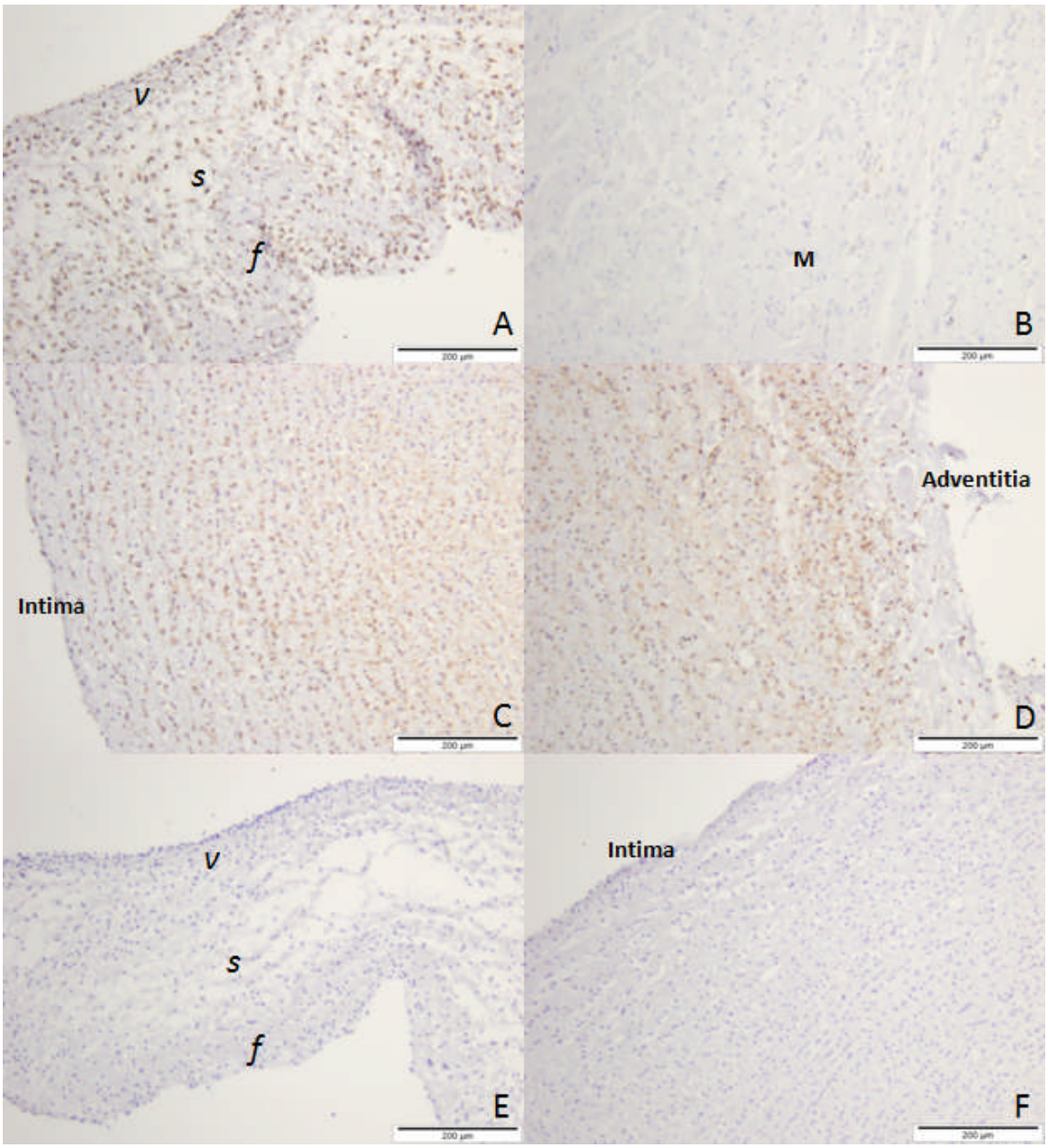

Figure 6.19 Localisation of vimentin in fresh porcine pulmonary root tissue cultured in the static system for one week. (A) Pulmonary valve leaflet, 100 ×; **(B)** myocardium, 100 ×; **(C)** the lumen surface of the pulmonary wall, 100 ×; **(D)** the adventitial surface of the pulmonary wall, 100 ×; **(E)** pulmonary valve leaflet stained with isotype control, 100 ×; **(F)** pulmonary wall stained with isotype control. *v*: *ventricularis*; *s*: *spongiosa*; *f*: *fibrosa*; M: myocardium. Scale bars are: all 200 µm.

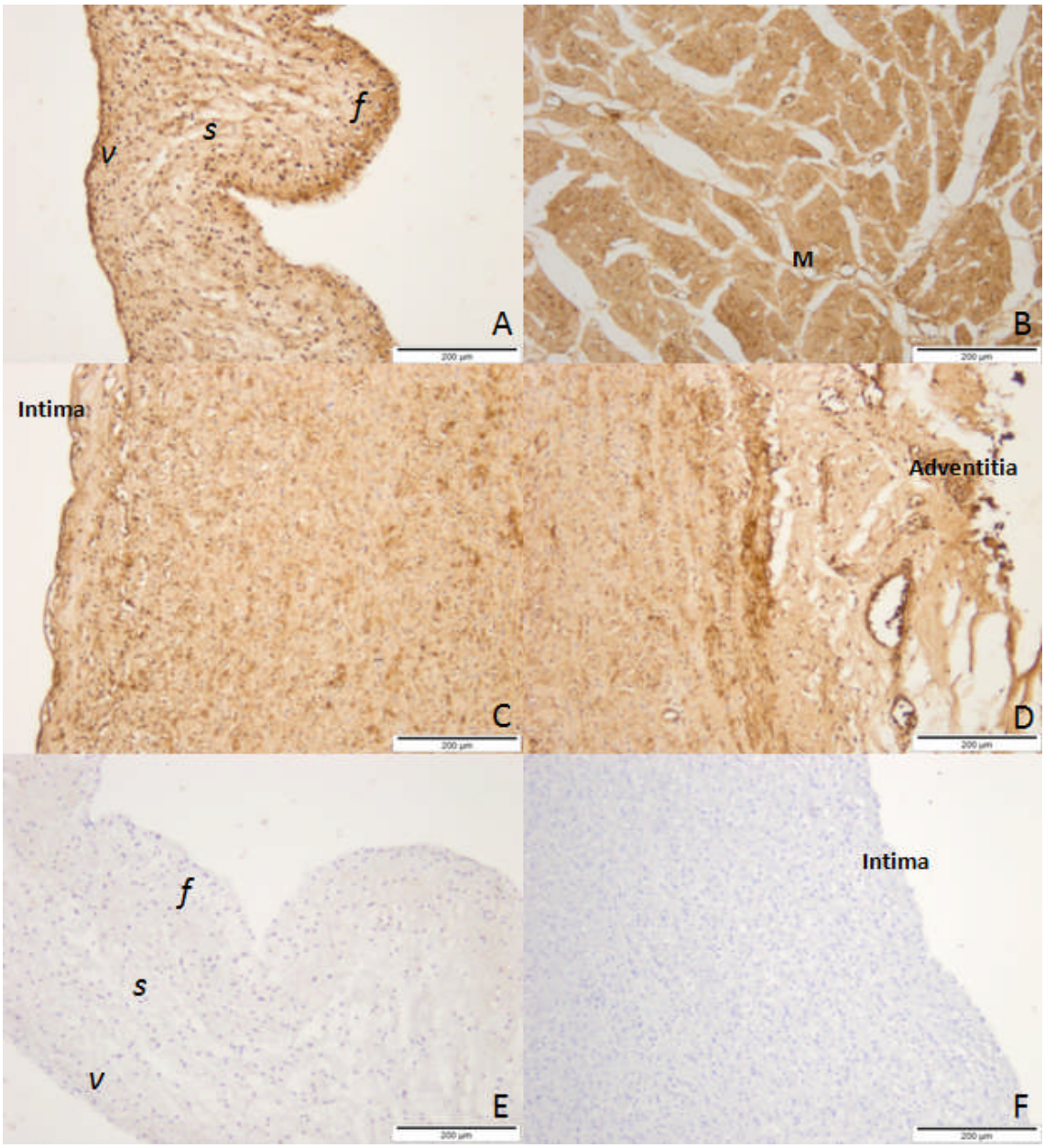

Figure 6.20 Localisation of fibronectin in fresh porcine pulmonary root tissue cultured in the dynamic system for one week. (A) Pulmonary valve leaflet, 100 ×; **(B)** Myocardium, 100 ×; **(C)** The lumen surface of the pulmonary wall, 100 ×; **(D)** The adventitial surface of the pulmonary wall, 100 ×; **(E)** Pulmonary valve leaflet stained with isotype control, 100 ×; **(F)** Pulmonary wall stained with isotype control. *v*: *ventricularis*; *s*: *spongiosa*; *f*: *fibrosa*; M: myocardium. Scale bars are: all 200 µm.

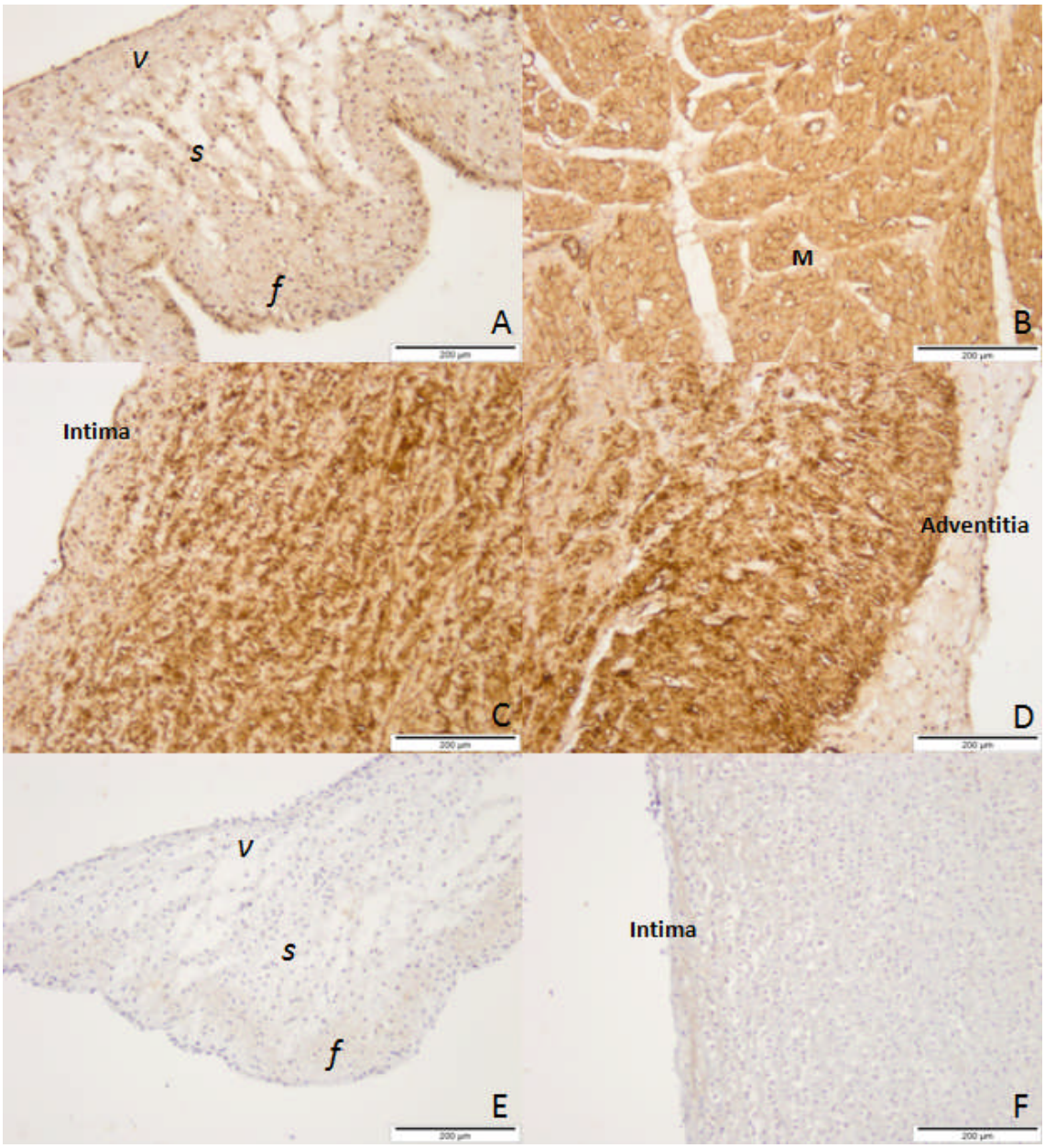

Figure 6.21 Localisation of fibronectin in fresh porcine pulmonary root tissue cultured in the static system for one week. (A) Pulmonary valve leaflet, 100 ×; **(B)** Myocardium, 100 ×; **(C)** The lumen surface of the pulmonary wall, 100 ×; **(D)** The adventitial surface of the pulmonary wall, 100 ×; **(E)** Pulmonary valve leaflet stained with isotype control, 100 ×; **(F)** Pulmonary wall stained with isotype control. *v*: *ventricularis*; *s*: *spongiosa*; *f*: *fibrosa*; M: myocardium. Scale bars are: all 200 µm.

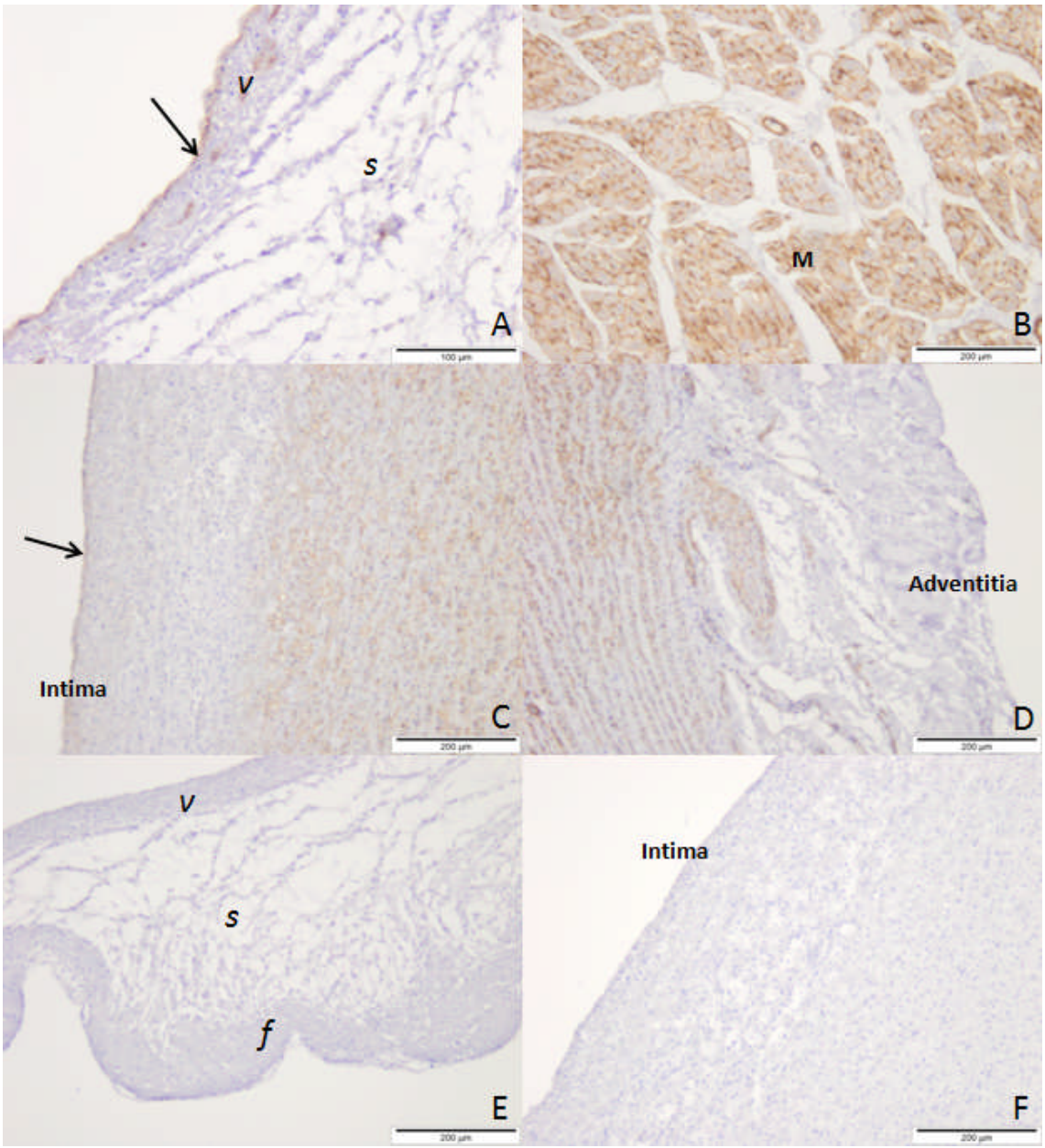

Figure 6.22 Localisation of collagen IV in fresh porcine pulmonary root tissue cultured in the dynamic system for one week. (A) Pulmonary valve leaflet, 200 ×, the arrow indicates the surface of pulmonary leaflet that has been positively stained; **(B)** Myocardium, 100 ×; **(C)** The lumen surface of the pulmonary wall, 100 ×, the arrow indicates the surface layer of pulmonary wall that has been positively stained; **(D)** The adventitial surface of the pulmonary wall, 100 ×; **(E)** Pulmonary valve leaflet stained with isotype control, 100 ×; **(F)** Pulmonary wall stained with isotype control. *v*: *ventricularis*; *s*: *spongiosa*; *f*: *fibrosa*; M: myocardium. Scale bars are: Scale bars are all 200 µm except (A), 100 µm.

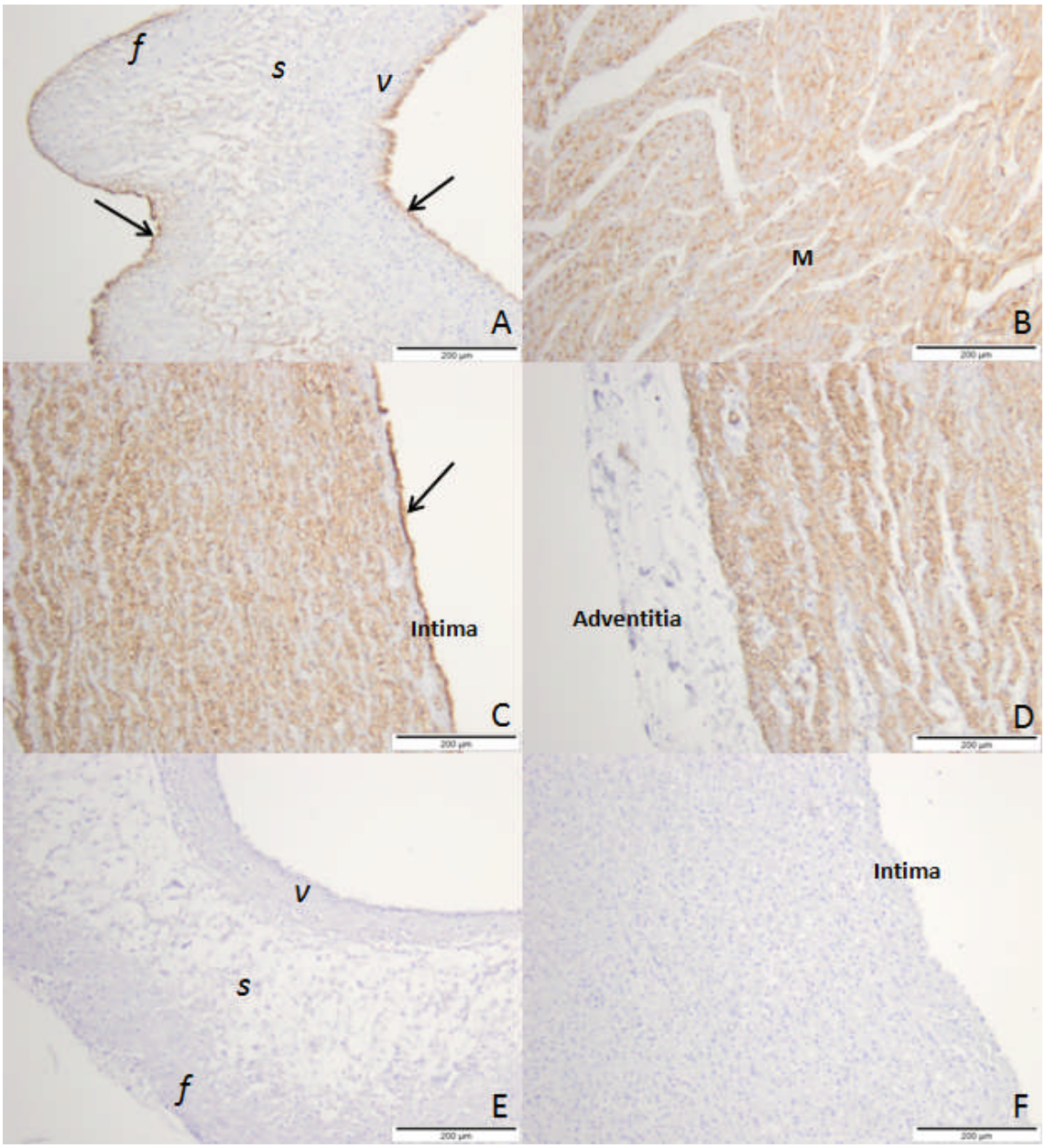

Figure 6.23 Localisation of collagen IV in fresh porcine pulmonary root tissue cultured in the static system for one week. (A) Pulmonary valve leaflet, 100 ×, the arrows indicates the surfaces of pulmonary leaflet that has been positively stained; **(B)** Myocardium, 100 ×; **(C)** The lumen surface of the pulmonary wall, 100 ×, the arrow indicates the surface layer of pulmonary wall that has been positively stained; **(D)** The adventitial surface of the pulmonary wall, 100 ×; **(E)** Pulmonary valve leaflet stained with isotype control, 100 ×; **(F)** Pulmonary wall stained with isotype control. *v*: *ventricularis*; *s*: *spongiosa*; *f*: *fibrosa*; M: myocardium. Scale bars are: all 200 µm.

6.4.4 Live/dead staining for porcine pulmonary leaflets

The viability of cells in the porcine pulmonary leaflets was assessed using live/dead stain, in which viable cells were stained green and dead cells were stained red. The cells on the surface of the pulmonary leaflets following staining were observed using confocal microscopy. The pulmonary leaflets of fresh, 10 % (v/v) NBF treated (for 1 h), dynamic cultured, and static cultured porcine pulmonary roots were stained and examined. Fresh leaflets that had not been cultured were used as negative control, and the 10 % (v/v) NBF treated leaflets were used as positive control. The results are shown in Figure 6.24. Most cells appeared to be green in the image of fresh leaflet (Figure 6.24 A) with approximately 10 % cells stained red. The cells appeared to reside close to each other in the image for the fresh sample. All of the cells were stained red in the 10 % (v/v) NBF treated leaflet (Figure 6.24 B). Most cells were stained both green and red in the sections of dynamic and static cultured porcine pulmonary leaflets (Figure 6.24 C, D). The size of the cells appeared to be a lot smaller than the ones in the fresh leaflets.

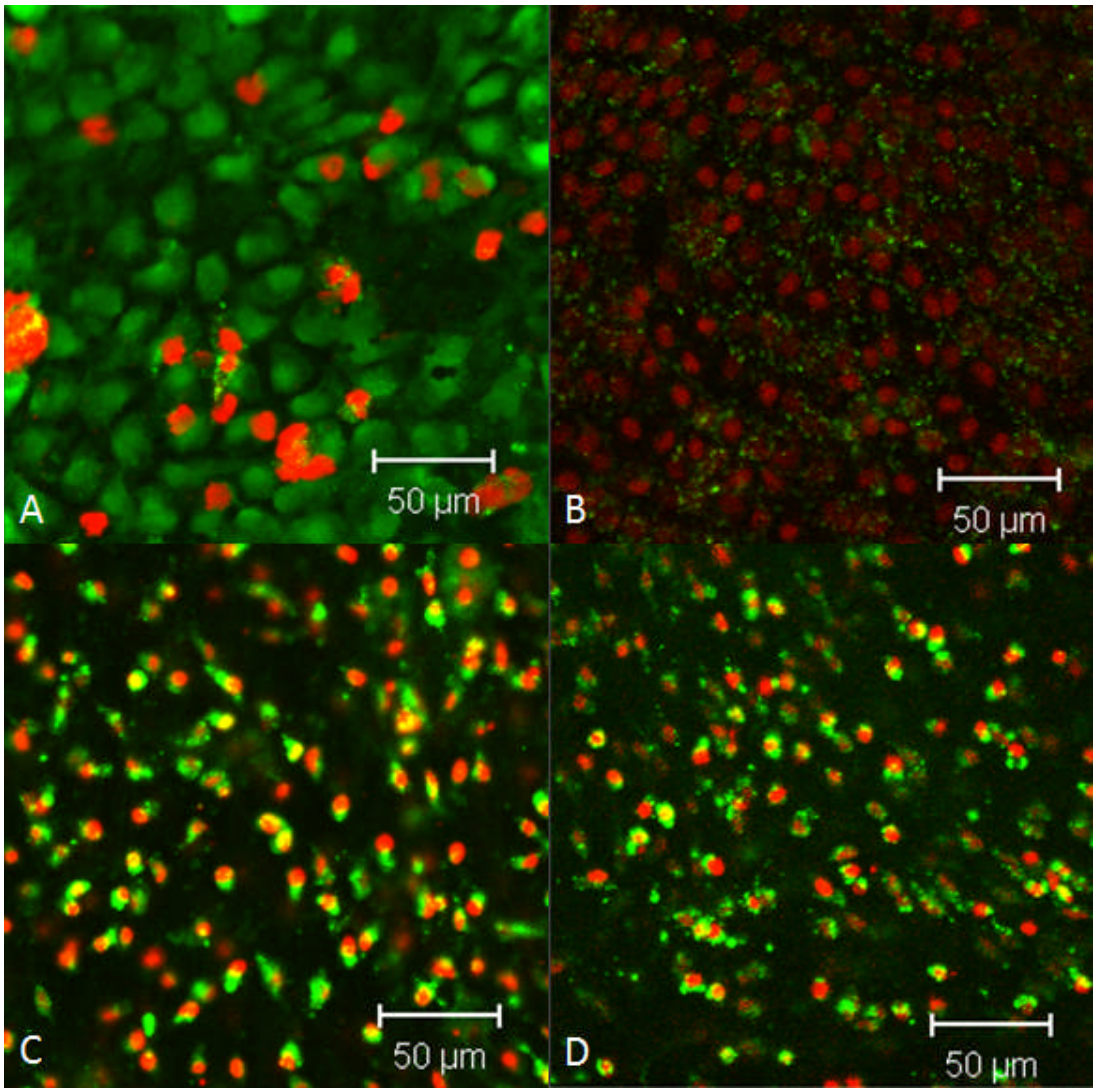

Figure 6.24 Sections of the porcine pulmonary leaflets stained with live/dead stain. **(A)** Fresh porcine pulmonary leaflet, 400 ×; **(B)** Fresh porcine pulmonary leaflet fixed with 10 % (v/v) for 1 h, 400 ×; **(C)** Porcine pulmonary leaflet cultured in the dynamic system for one week, 400 ×; **(D)** Porcine pulmonary leaflet cultured in the static system for one week, 400 ×.

6.4.5 Cell viability assay (MTT assay) for porcine pulmonary leaflets

The viability of cells in the porcine pulmonary leaflets was further assessed quantitatively using MTT assay. The assay was performed on porcine pulmonary leaflets from fresh, 10 % (v/v) NBF treated (for 1 h), dynamic cultured, and static cultured porcine pulmonary roots. The fresh leaflets were used as positive control, and the 10 % (v/v) NBF treated leaflets (tissue with dead cells) were used as negative control for cell viability. The absorbance was read at 570 nm with a reference filter at

630 nm. Data was analysed by one way ANOVA. The results are shown in Figure 6.25, which indicated a significant decrease of the cell viability in the 10 % (v/v) NBF treated leaflets, dynamic cultured and static cultured samples compared to the fresh sample. The cell viability of the dynamic cultured and static cultured leaflet samples was significantly higher in comparison with that of the 10 % (v/v) NBF treated leaflet sample.

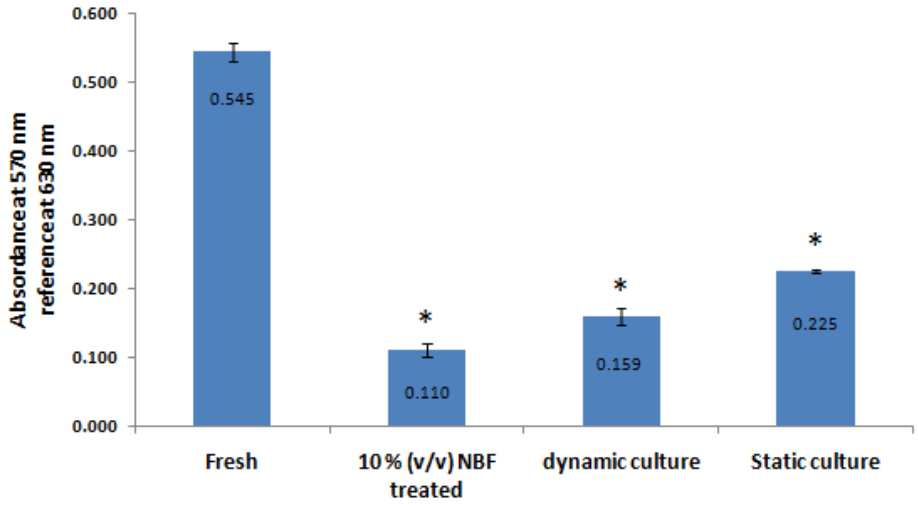

Figure 6.25 Cell viability of porcine pulmonary leaflets determined by MTT assay. Data is presented as the mean (n=3) ± 95 % C.I.. Data was analysed using one way ANOVA followed by calculation of the MSD using the T-method ($p<0.05$) "*" indicated significant difference when compared with the fresh leaflet group.

6.4.6 Study the effect of Cambridge antibiotics on cell viability and the endothelial cells in fresh porcine pulmonary heart roots

The immunohistochemistry results indicated a loss of endothelial cell layers in the dynamic and static cultured porcine pulmonary leaflets and the lumen surface of the pulmonary arteries. From the live/dead staining results and the MTT assay results, it was observed that the cell viability in the porcine pulmonary leaflets was significantly reduced after dynamic and static culture compared with that of the fresh tissue. Since Cambridge antibiotics solution was used for the disinfection of porcine pulmonary roots before culturing in the dynamic and static system, it was deemed necessary to study the

effect of Cambridge antibiotics on the leaflet cell viability and the presence of endothelial cells on the porcine pulmonary roots.

6.4.6.1 Method

Five conditions were applied to the fresh porcine pulmonary roots in order the study the effect of Cambridge antibiotics prior to evaluation:

(1) Fresh porcine pulmonary roots dissected within 4 hours of slaughter;

(2) Fresh porcine pulmonary roots stored in PBS for 16-17 h at 4 °C;

(3) Fresh porcine pulmonary roots stored in DMEM cell culture medium for 16-17 h at 4 °C;

(4) Fresh porcine pulmonary roots cultured in Cambridge antibiotics solution in the static culture system with continuous pumping of 5 % (v/v) CO_2 in air at 37 °C for 16-17 h.

(5) Fresh porcine pulmonary roots stored in Cambridge antibiotics solution for 16-17 h at 4 °C.

Conditions (1), (2), (3) and (4) were used as controls; condition (5) was the same procedure that was taken prior to the porcine pulmonary roots being cultured in the dynamic and static systems.

The leaflet cell viabilities of the treated and non treated porcine pulmonary roots were studied using MTT. Sections of the pulmonary roots were labelled with monoclonal antibody to von Willebrand factor to study the presence of the endothelial cells.

6.4.6.2 Results

6.4.6.2.1 Cell viability assay (MTT assay) for porcine pulmonary leaflets

Following the MTT assay, the absorbance was read at 570 nm with a reference filter at 630 nm. The data was analysed using one way ANOVA. The results are shown in Figure 6.26. A significant difference increase in cell viability for the leaflets cultured

with DMEM cell culture medium for 16-17 h at 4 °C compared to fresh leaflets. No other significant differences were found.

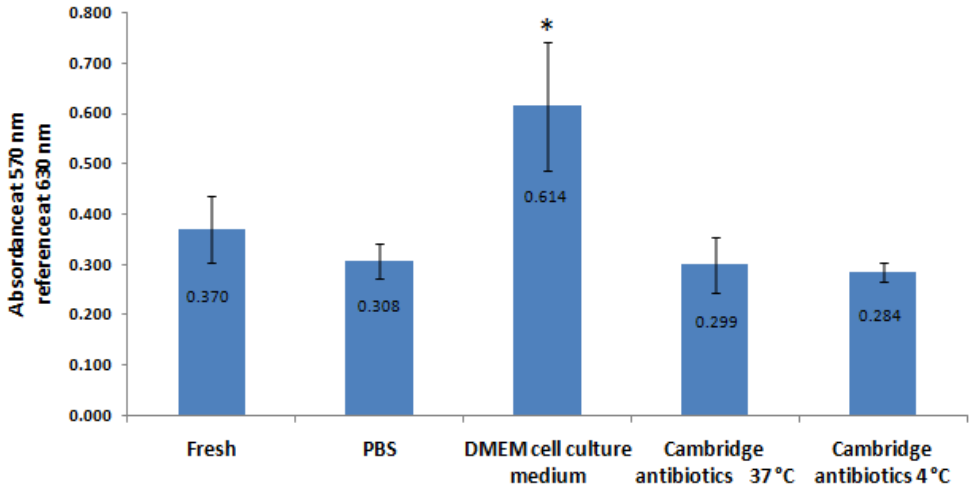

Figure 6.26 Cell viability of porcine pulmonary leaflets determined by MTT assay. Data is presented as the mean (n=3) ± 95 % C.I.. Data was analysed using by one way ANOVA followed by calculation of the MSD using the T-method ($p<0.05$). "*" indicated significant difference when compared with the fresh leaflet group.

6.4.6.2.2 Immunohistochemistry evaluation of porcine pulmonary roots labelled with vWF

The non treated and treated porcine pulmonary root sections were labelled with monoclonal antibody against vWF to study the presence of endothelial cells. The results are shown in Figure 6.27 for fresh tissue, Figure 6.28 for tissue stored in PBS for 16-17 h at 4 °C, Figure 6.29 for tissue stored in DMEM culture medium for 16-17 h at 4 °C, Figure 6.30 for tissue cultured in Cambridge antibiotics solution in the static culture system for 16-17 h at 37 °C, and Figure 6.31 for tissue stored in Cambridge antibiotics solution for 16-17 h at 4 °C. Positive staining was observed on both surfaces of pulmonary leaflets and the lumen surface of the pulmonary artery of the fresh, PBS stored, and DMEM cell culture medium stored porcine pulmonary roots (Figure 6.27 A &C; Figure 6.28 A&C, Figure 6.29 A&C). The small blood vessels in the myocardium of Cambridge antibiotics stored tissue (at 4 °C and 37 °C) were stained positive, but no

brown colour was recognised on the surfaces of the pulmonary leaflets and pulmonary arteries of the above two groups (Figure 6.30 B, Figure 6.31 B).

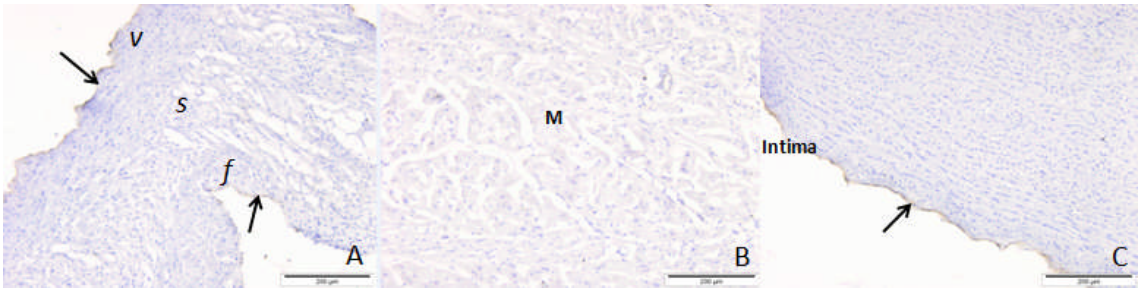

Figure 6.27 Localisation of vWF in fresh porcine pulmonary root tissue. (A) Pulmonary valve leaflet, 100 × (*v*: *ventricularis*; *s*: *spongiosa*; *f*: *fibrosa*), the arrows indicate the surfaces of the pulmonary leaflet that has been positively stained; **(B)** Myocardium, 100 ×; **(C)** The lumen surface of the pulmonary wall, 100 ×, the arrow indicates the surface cell layer of the pulmonary wall that has been positively stained; M: myocardium. Scale bars are: all 200 µm.

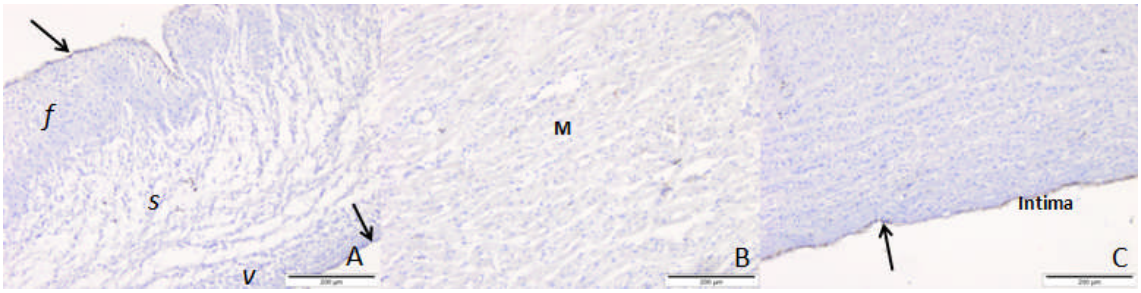

Figure 6.28 Localisation of vWF in fresh porcine pulmonary root tissue stored in PBS for 16-17 h at 4 °C. (A) Pulmonary valve leaflet, 100 × (*v*: *ventricularis*; *s*: *spongiosa*; *f*: *fibrosa*), the arrows indicates the surfaces of the pulmonary leaflet that has been positively stained; **(B)** Myocardium, 100 ×; **(C)** The lumen surface of the pulmonary wall, 100 ×, the arrow indicates the surface cell layer of the pulmonary wall that has been positively stained; M: myocardium. Scale bars are: all 200 µm.

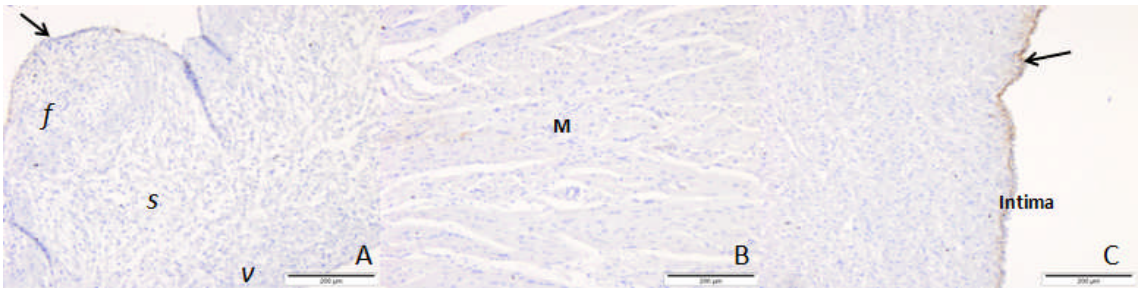

Figure 6.29 Localisation of vWF in fresh porcine pulmonary root tissue stored in DMEM culture medium for 16-17 h at 4 °C. (A) Pulmonary valve leaflet, 100 × (*v*: *ventricularis*; *s*: *spongiosa*; *f*: *fibrosa*), the arrow indicates the surface of the pulmonary leaflet that has been positively stained; **(B)** Myocardium, 100 ×; **(C)** The lumen surface of the pulmonary wall, 100 ×, the arrow indicates the surface cell layer of the pulmonary wall that has been positively stained; M: myocardium. Scale bars are: all 200 µm.

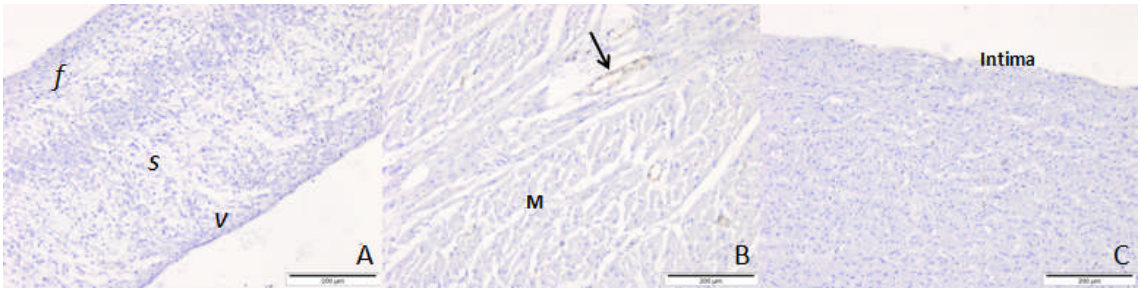

Figure 6.30 Localisation of vWF in fresh porcine pulmonary root tissue cultured in Cambridge antibiotics solution in the static culturing system for 16-17 h at 37 °C. (A) Pulmonary valve leaflet, 100 × (*v*: *ventricularis*; *s*: *spongiosa*; *f*: *fibrosa*); **(B)** Myocardium, 100 ×, the arrow indicates a blood vessel that has been positively stained; **(C)** The lumen surface of the pulmonary wall, 100 ×; M: myocardium. Scale bars are: all 200 µm.

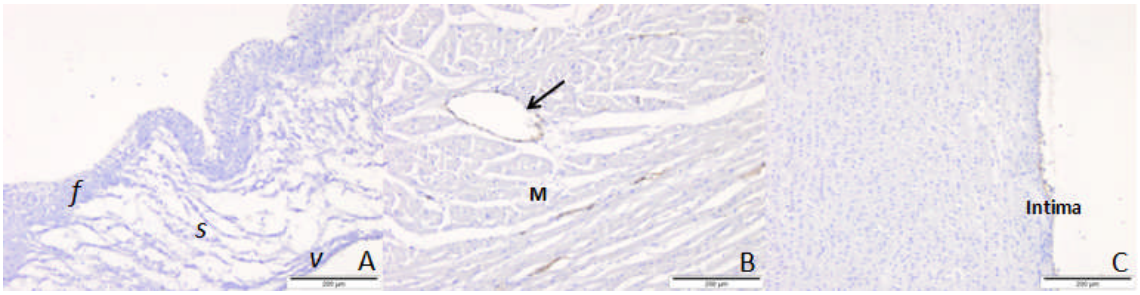

Figure 6.31 Localisation of vWF in fresh porcine pulmonary root tissue stored in Cambridge antibiotics solution for 16-17 h at 4 °C. (A) Pulmonary valve leaflet, 100 × (*v*: *ventricularis*; *s*: *spongiosa*; *f*: *fibrosa*); **(B)** Myocardium, 100 ×, the arrow indicates a blood vessel that has been positively stained; **(C)** The lumen surface of the pulmonary wall, 100 ×; M: myocardium. Scale bars are: all 200 µm.

6.5 Discussion

This chapter has described the culture of fresh porcine pulmonary roots in the dynamic and static heart root culture systems. Fresh porcine pulmonary roots were dissected and cultured in the systems for one week. The cultured roots were characterised and compared with the fresh tissue. The development of a fully functional heart valve bioreactor which is able to provide physiological biological and mechanical environment of the heart and circulatory system is still under research (Chen & Hu, 2006; Mertsching & Hansmann, 2009; Shaikh *et al*., 2009; Ruel *et al*., 2009; Vismara *et al*, 2010; Berry *et al*., 2010). In order to validate the performance of heart valve bioreactor systems it is necessary to investigate their capacity to support the viability and function of fresh cardiac valves.

During the one week-culture in the dynamic and the static systems, the pulmonary roots were observed daily. No changes were observed in the pulmonary root morphology during this time. The pulmonary leaflets opened and closed properly during the culture period in the dynamic bioreactor. The porcine pulmonary roots were taken out of the culture systems, the roots were cut open, and the leaflets were examined for damage. No damage was observed on the pulmonary leaflets of the roots that were cultured either dynamically or statically. These results demonstrated the dynamic conditions applied during culture did not have any effect on the pulmonary leaflet morphology, and did not alter the pulmonary leaflets' behaviour. The pulmonary leaflets and the pulmonary arteries were stained pink following the culture. However, this was due to the penetration of the DMEM medium, and did not affect the biological and mechanical behaviour of the tissue.

H&E and Hoechst staining was utilised to evaluate the distribution of cells and the integrity of the pulmonary root tissue. The results were compared with the histological images of the fresh porcine pulmonary roots (Section 3.4.1). The cell distribution and density of the dynamic and static cultured porcine pulmonary roots appeared to be no different compared to that of the fresh tissue. No damage to the tissue was observed, and the integrity, shape and distribution of the connective tissue fibres were well preserved after culture in the dynamic and static systems in comparison with the fresh tissues. No difference was observed in cell distribution and tissue ECM between the dynamic and static cultured porcine pulmonary roots. The culture conditions of the

dynamic and the static systems did not result in any overt cell loss or changes to the porcine pulmonary roots.

The immunohistochemistry results of the dynamic and static cultured porcine pulmonary roots were compared with the results of the fresh roots which were described in Section 4.4.3. The results of the dynamic cultured porcine pulmonary roots were in agreement with the fresh tissue when labelled with α-SMA. The static cultured porcine pulmonary leaflets were however markedly negative for α-SMA. Since positive staining was observed in the *ventricularis* of the fresh pulmonary leaflets, the results indicated the loss of α-SMA in the static cultured pulmonary leaflets. Previous studies have shown that the smooth-muscle-like cells are distributed in the *ventricularis* in the semilunar valves because this layer faces the blood flow and bears the most pressure during leaflet function (DellaRocca *et al*., 2000; Bertiplaglia *et al*., 2003). In the mitral valves, α-SMA has also been reported to positively label the arterial side of the leaflet, which is also the side that is most stressed (Dal-Bianco *et al*., 2009). Since the *ventricularis* in the static cultured pulmonary leaflet was in a condition that did not bear any pressure during culture, it is hypothesised that the flow pressure during leaflet function is important for the cells in the *ventricularis* of pulmonary leaflets to have smooth-muscle cell properties. The dynamic culture system, which mimicked the physiological hydrodynamic conditions, contributed to retaining the smooth-muscle-like cell properties in the *ventricularis* of the pulmonary leaflets during the culture process.

The tissue sections of dynamic and static cultured porcine pulmonary roots labelled with vWF showed positive staining in the small blood vessels in the myocardium and the connective tissue on the adventitial surface of the pulmonary artery, which was in agreement with the results of the fresh tissue. However, the fact that no positive staining was observed on the surfaces of pulmonary leaflets and the lumen surfaces of the pulmonary arteries indicated a loss of endothelial cells following culture in the dynamic and static systems. The VEC`s are believed to regulate vascular tone, inflammation, thrombosis and remodelling (Leask *et al*., 2003; Sacks & Yoganathan, 2007). Thus, it was considered important that the valve root culture system had the potential to accommodate and maintain the viability and function of the endothelial cells on the pulmonary valve leaflets. The dynamic and static culture techniques in this study however failed to support the retention of endothelial cells. The reasons could be: (1) the process during the preparation of porcine pulmonary roots prior to culture had

accidentally removed or damaged the endothelial cells; (2) the culture medium used during dynamic and static culture was not appropriate for endothelial cell viability (i.e. lack of growth factor); (3) or/and the hydrodynamic conditions in the dynamic bioreactor was not appropriate to retain the cells. The fact that the loss of endothelial cells was mainly in areas that were exposed directly to the external environment (the surfaces of pulmonary leaflets and pulmonary arteries, but not the internal tissue e.g. myocardium and pulmonary arteries), lead to the hypothesis that the loss of endothelial cells was due to the solutions/medium that had contacted directly with the tissue. Thus, in this study, Cambridge antibiotics solution, which was used for tissue disinfection prior to culture, was evaluated for its effect on endothelial cell retention.

The immunohistochemical results of the fibronectin labelled porcine pulmonary roots following both dynamic and static culture were very similar to that of the fresh tissue, indicated the retention of this root ECM protein after culture. In the images of desmin and vimentin labelled porcine pulmonary roots following the dynamic culture, it was observed that the distribution and the strength of positive staining were in agreement with that of the fresh tissue. However, in the static cultured myocardium, the brown colour was lighter than that of the fresh tissue. These results indicated that the level of desmin and vimentin were reduced in the cardiac muscle cells that were cultured statically. Thus, although the myocardium was not contracting in the dynamic culture system, the medium flow and the stress provided during leaflet opening and closing could still be important to the function of the cardiac muscle cells. Nevertheless, since the acellular pulmonary heart roots would not consist of any cardiac muscle cells, and the myocardium in the pulmonary root grafts that were subject to replacement surgery would only be necessary as a suturing material during surgery and not be intended to have functional cells, the viability of the myocardium cells was not of a major interest in the study of the performance of the culture systems. The positive staining for collagen IV, which served as a marker for the basement membrane, was found at the same locations as that of the fresh tissue. The basement membrane remained intact after the fresh porcine pulmonary roots had been cultured in the dynamic and static systems for one week.

Live/dead cell staining was used to visualise the viability of pulmonary leaflet cells using confocal microscopy. The confocal microscope captured cells from the layer that was closest to the surface of the tissue. The captured cells of fresh porcine pulmonary

leaflet sample were mostly alive and arranged close to each other. Judging from the shape, size (~20 µm) and arrangement of the cells, they were considered to be endothelial cells. The cells observed in the dead tissue control (10 % v/v NBF treated porcine pulmonary leaflets) were all dead and smaller in size compared to the cells from the fresh tissue. However, since dead cells shrink in size, and to judge from their arrangement, the cells were considered to be endothelial cells as well. The cells observed in the dynamic and static cultured porcine pulmonary leaflets were mostly dead, although a small number of the cells were alive (green colour only). Cells that took up both green-coloured calcein dye and red-coloured ethidium homodimer-1 dye indicated that they were dying, and they were considered as 'dead cells'. From the size and arrangement of the cells, it was concluded that these cells from cultured porcine pulmonary leaflets that were captured by confocal microscopy were VIC`s. This result further indicated the loss of the endothelial layer in the dynamic and static cultured porcine pulmonary leaflets.

The viability of cells from the porcine pulmonary leaflets was further assessed by MTT assay, with the fresh tissue as the positive control, and the 10 % (v/v) NBF treated dead tissue as the negative control. Although the cell viability of the dynamic and static cultured leaflet tissue were significantly higher than the dead tissues control, neither was comparable to the fresh tissue control. The reason for the reduction in cell viability following tissue culture could be: (1) the tissue processing method prior to culturing had affected the cell viability; (2) the culture medium used in the culture system was not suitable for the cell viability; (3) the hydrodynamic conditions were not suitable to maintain the viability of the porcine pulmonary leaflet cells. Regardless, the cell viability data indicated the hydrodynamic conditions used during culture did not promote cell viability in comparison to the static culture.

The Cambridge antibiotics solution that was used for tissue surface disinfection prior to dynamic and static culture of porcine pulmonary roots could have contributed to the loss of endothelial cell layers and the reduction in leaflet cell viability of the cultured tissues. The MTT cell viability assay and immunohistochemical labelling with vWF were used to assess the tissue properties after treatment with Cambridge antibiotics. The leaflet cell viability was not significantly different between the Cambridge antibiotics cultured tissue (either at 4 °C or 37 °C) and the fresh leaflet or the PBS treated leaflets. This result indicated the pre-disinfection with antibiotics solution procedure did not affect the

cell viability of the pulmonary leaflet tissue. The cell viability of tissue stored in DMEM cell culture medium was significantly higher than that of the fresh tissue, indicating that DMEM cell culture medium was suitable for the growth and repopulation of cells in the porcine pulmonary leaflets. The differences between the standard DMEM cell culture medium and the culture medium used in the valve root culture systems were: the latter contained 250 $ng.ml^{-1}$ amphotericin B, 25 $\mu g.ml^{-1}$ gentamicin and 0.1 % (v/v) anti foaming reagent polypropylene glycol. The 250 $ng.ml^{-1}$ amphotericin B and 25 $\mu g.ml^{-1}$ gentamicin were standard dose used in tissue culture, thus should not have any effect on the reduction of leaflet cell viability. The 0.1 % (v/v) of polypropylene glycol was also a standard dose used as an anti foaming purpose. A study by Routledge *et al*. (2011) has also shown that a concentration of up to 1 % (v/v) of polypropylene glycol does not affect the growth rate of cells. Thus, of the three possible reasons that could affected the cell viability during dynamic and static culture of porcine pulmonary roots, the Cambridge antibiotics and the tissue culture medium were excluded. Since the static culture system did not mimic the physiological conditions for heart valve leaflet functioning, after culturing for one week, the reduction of cell viability in porcine pulmonary leaflets was not unexpected. However, the cell viability assay results for the dynamic cultured tissue have highlighted the need to further study the conditions to apply in the system for valve root culture, or even to modify the system itself in order to improve the leaflet cell viability during the dynamic culture.

The results of porcine pulmonary root sections labelled with anti-vWF clearly indicated the effect of Cambridge antibiotics solution in removing the endothelial cells. The Cambridge antibiotics solution was initially used by the National Blood & Transplant Tissue Services for the disinfection of cryopreserved allografts. The maintenance of cell viability was less of a consideration than the disinfection of the tissue prior to transplantation. Thus, for the purpose of this study, which was to maintain the cell and tissue properties of the fresh porcine pulmonary root tissue during culture, and eventually to repopulate the cells in the acellular tissue in the dynamic valve root culture system, Cambridge antibiotics solution was not an ideal choice for surface disinfection prior to tissue culture. However, because the dynamic valve root culture system had failed to provide cultured porcine pulmonary root tissue with satisfying leaflet cell viability and the limitation of time in this project, no further steps were taken to choose

a suitable disinfection solution. Further attempts could be to exclude certain components in the Cambridge antibiotics cocktail that could possibly affect the viability of endothelial cells, and/or to reduce the doses of certain components. Sterility tests could be applied to optimise the disinfection solution.

6.6 Conclusion

Fresh porcine pulmonary roots were dissected, disinfected and cultured in dynamic and static heart root culture systems for one week prior to characteriseation and comparison with fresh tissue. Histology results showed no changes in cell distribution or alterations in the ECM structure of the dynamic and static cultured porcine pulmonary roots. Immunohistochemical results indicated a loss of endothelial cells in both dynamic and static cultured porcine pulmonary valve leaflets. Further studies confirmed this result was due to the use of Cambridge antibiotics solution for tissue disinfection prior to culturing. The porcine pulmonary leaflet cell viabilities were significantly reduced following culture in the dynamic and static systems. These experiments indicated the need to further study the conditions to apply in the system for valve root culture, or even to modify the system itself in order to improve leaflet cell viability during dynamic culture. The culture of fresh porcine pulmonary roots in the dynamic and static systems for one week had partially retained the natural properties of the tissue.

Chapter 7

General Discussion

Heart valve dysfunction is a leading cause of death in the modern world. Among the four human heart valves, the aortic valve is most often replaced. Replacement valves may be mechanical, bioprosthetic, cryopreserved homografts or autografts. The Ross procedure (Ross, 1967) is a surgical technique used to treat severe aortic valve disease in young patients in which the patient's own pulmonary valve is used to replace the diseased aortic valve. The pulmonary autograft is considered to be the best substitute for the diseased aortic valve since it is a living tissue with very similar structure to the aortic valve. The pulmonary valve used to reconstruct the right ventricular outflow tract is usually a cryopreserved homograft. Cardiac valve replacements each have their own advantages and disadvantages. However, none of the replacement options is ideal. Tissue engineering offers an opportunity to create an "ideal replacement valve" which would overcome almost all of the limitations of currently available replacement valves, including the risk of thromboembolism, requirement for life-time anticoagulation therapy, poor durability and abnormal hydrodyanics. In addition, for the paediatric population, tissue-engineered heart valves may be considered to be the optimal potential solution for valve replacement since they should have the potential to grow, repair and remodel (Sapirsten & Smith, 2001; Booth, *et al*., 2002; Veseley, 2005).

The overall aim of this study was to produce and characterise an acellular porcine pulmonary root conduit. The long term goal is to translate the acellular valved conduit for use in the clinic as a replacement valve, in particular in the Ross procedure to reconstruct the right ventricular outflow tract. During the course of this study, a decellularisation process was developed which was shown to remove the xenogeneic cells from the porcine pulmonary root with minimum effect on the histoarchitecture and composition of the ECM. The biomechanical and hydrodynamic function of the decellularised porcine pulmonary root was characterised and compared to fresh untreated tissue. In addition, attempts were made to investigate the culture conditions required to maintain valve function and cell viability in a novel dynamic heart valve bioreactor using fresh porcine pulmonary roots.

The decellularisation process is the key step in determining the success of production of an acellular xenogeneic heart valve conduit. Residual cellular material can be antigenic and can reduce the capacity of the acellular scaffold to remodel *in vivo* which would negate the advantages of using a biological scaffold (Brown *et al*., 2009; Burch *et al*., 2010; Crapo *et al*., 2011). A fully decellularised porcine heart valve scaffold should have similar biological, histological and mechanical characteristics to the native tissue with close to 100 % of cells and cell remnants removed.

Various attempts have been made to produce a decellularised heart valve scaffold. In early attempts, freeze-drying was used for heart valve decellularisation (Curtil *et al*., 1997). However, not surprisingly decellularisation of the scaffold was not achieved since the approach made no attempt to physically remove dead cell components. Subsequent attempts to decellularise heart valves focused on the use of hypo-and hypertonic solutions to lyse the cells and detergents such as Triton X-100 (Bader *et al*., 1998; Wang *et al*., 2005) or 1 % (w/v) SDS (Courtman *et al*., 1994) to solublise cell membranes and enzymes such as trypsin (Schenke-Layland *et al*., 2003; Yang *et al*., 2010). However, the results were not ideal since, for example, the use of trypsin was reported to disrupt the elastin and collagen network of the ECM leading to changes in the mechanical properties of the tissue (Yang *et al*., 2009); Triton X-100 did not achieve adequate decellularisation of the whole valve root (Grause *et al*., 2005) and 1% (w/v) SDS changed the mechanical properties of valve leaflet tissue (Courtman *et al.*, 1994). A more effective way to achieve decellularisation of heart valve tissues without affecting the integrity of the ECM is to utilise a combination of gentle treatments. A successful method for the decellularisation of porcine aortic valve leaflets was developed by Booth *et al*. (2002) using a combination of hypotonic buffer and low concentration (0.03-0.1% w/v SDS) in the presence of proteinase inhibitors. The approach taken was based on the hypothesis that the previous report of damage to ECM, was not due to SDS treatment but caused by the release of numerous proteinases from the cells following lysis. The acellular scaffold was shown to retain biomechanical properties (Korossis *et al*., 2002). This process was further developed for whole porcine aortic roots by Wilcox *et al*. (2005) with the addition of 1.25% (w/v) trypsin treatment to the thinned aortic wall. The method also incorporated a freeze-thaw cycle at the beginning, and a nuclease treatment cycle following the SDS-hypotonic wash. Following treatment, the major structural components of the valve ECM were observed

to be successfully maintained through histological analysis, and functional analysis showed the valve leaflets to be fully competent under physiological pressures (120 mm Hg) along with physiological leaflet kinematics (Korossis *et al*., 2005).

In this study, the development of the decellularisation process for porcine pulmonary roots was based on that developed by Wilcox *et al*. (2005) for porcine aortic roots. Porcine aortic and pulmonary roots share very similar structures, but still have anatomical differences. In total six decellularisation methods were tested on porcine pulmonary roots. Basic histological assessment with H&E and Hoechst staining was used to assess the extent of cell removal from the tissue. Method 3, which incorporated two cycles of SDS-hypotonic buffer washes with no trypsin treatment on the thinned pulmonary artery and one cycle of nuclease treatment, showed cell removal throughout the pulmonary root. The tissue histoarchitecture was well retained as determined by histology. However, in subsequent biomechanical assessment using uniaxial tensile testing, it was found that the tensile properties, namely the failure stress of the pulmonary leaflet in the radial direction and the failure stress of the pulmonary artery in the circumferential direction were significantly reduced compared to the fresh tissue. These results indicated a loss of strength in the decellularised pulmonary roots which was not the case for the aortic roots decellularised following the original protocol (Korossis *et al*., 2005) developed by Wilcox *et al*. (2005). Biomechanical properties play a very important role in the function of heart valve tissue. By comparison of the modified and the original decellularisation methods, it was concluded that the loss of leaflet strength was probably due to the application of the additional cycle of 0.1 % (w/v) SDS-hypotonic buffer, since SDS has been reported to affect the mechanical properties of the tissue, probably due to its effects on protein/protein interactions of importance to the integrity of a collagenous matrix (Courtman *et al*., 1994). Although Booth *et al*. (2002) and Wilcox *et al*. (2005) had successfully minimised the effects of SDS on the ECM proteins by using a low concentration (0.1 % w/v) of SDS for aortic root decellularisation, it was highly likely that the additional 0.1 % (w/v) SDS-hypotonic buffer wash caused the loss of leaflet strength in the thin and delicate pulmonary leaflets. In addition, although the same process of peeling the outer layer of the pulmonary wall was taken in this study to the process reported by Wilcox *et al*. (2005) and Korossis *et al*. (2005) for the aortic wall, the peeling of the pulmonary artery wall was most likely

to have caused a reduction in its strength due to the fact that the pulmonary artery is naturally thinner than the aorta.

Further development of the decellularisation process for porcine pulmonary roots therefore used only one cycle of 0.1 % (w/v) SDS-hypotonic buffer as in the original protocol developed by Wilcox *et al.* (2005) and omitted peeling the pulmonary artery wall. This led to the development of Method 6, which used 1.25% (w/v) trypsin digestion on the adventitial surface of the scraped pulmonary artery, one cycle of 0.1 % (w/v) SDS-hypotonic buffer wash and two cycles of nuclease treatment. This process was shown to achieve removal of cells as demonstrated by an absence of cells and an absence of DNA throughout the tissue following staining with DNA specific fluorescent Hoechst dye.

The DNA in the decellularised porcine pulmonary roots was extracted from individual parts of the conduits including the leaflets, pulmonary artery, myocardium and leaflet connection with the purpose to determine the levels of residual DNA and the presence of functional genes in comparison to fresh tissues. The levels of residual DNA in the pulmonary roots were determined by Nanodrop spectrophotometry. The results indicated that greater than 90% of the DNA had been removed from all parts of the conduits by the decellularisation process. A limitation of the experimental procedure used to assess the DNA levels was that the absorbance values for the DNA extracted from the decellularised tissue were at the lowest sensitivity of the Nanodrop spectrophotometer. Thus, the actual reduction in total DNA levels in the decellularised tissues was likely to have been inaccurate with the actual levels of residual DNA being lower than the estimated values. A solution to this problem would be to start the DNA extraction with greater masses of decellularised tissue (e.g. 10 times more mass of tissue than used in this study). The quantity of residual DNA recovered would then be proportionally higher and more accurate readings obtained using Nanodrop spectrophotometry. Although it is unlikely that any decellularisation procedure would remove 100 % of the DNA, it is generally accepted that short lengths of remnant DNA (less than 300 bp) would not to be of concern in the decellularised scaffold (McCoy *et al*., 2004; Gilbert *et al*., 2009). PCR was performed to detect the presence of functional genes which would encode xenogenic cellular protein components in the decellularised scaffold with target product lengths shorter than 250 bp. GAPDH, SLA-2, β 2-microglobulin and β actin genes were not detected in the decellularised porcine

pulmonary leaflet, pulmonary artery, leaflet connection or myocardium. These results provided evidence for an absence of functional DNA in the decellularised pulmonary roots. This approach to assessing the extent of DNA removal from acellular xenogeneic cardiac valves has not been previously reported by others in the field.

Particular cytoskeletal components of the different cell types within the pulmonary roots were assessed by immunohistochemical labelling to further determine the extent of decellularisation. There was no evidence for the presence of vWF or vimentin. This provided evidence for the successful removal of endothelial and fibroblast cells. However, there was evidence of residual levels of the intracellular proteins α-SMA and desmin in the decellularised scaffold. Similarity searches of porcine and human α-SMA revealed 100 % identity. Porcine desmin had 98 % identity to human desmin. Hence it was considered unlikely that these residual proteins would be of immunological concern following implantation in Man.

The connective tissue distribution in the ECM of the decellularised porcine pulmonary root was comparable to the fresh tissue as determined by H&E and Miller's elastin staining. However, a significant reduction in the level of GAG`s was observed in the pulmonary leaflet and pulmonary arteries following decellularisation as determined by Alcian blue staining. Similar findings of GAG loss have been reported for different types of tissues that were also decellularised using SDS (Mirsadraee, 2005; Stapelton, 2008; Cheng *et al*., 2009). The use of SDS in the decellularisation method was most likely to have caused this result (Gilbert *et al*., 2006; Yang *et al*., 2010). Since GAG is the major component in the *spongiosa* of the pulmonary leaflets and believed to perform an important role in the integrity and mechanical properties of the leaflets, it was important to examine the effect of GAG loss on the function of acellular pulmonary valves through hydrodynamic testing. Although not performed in this study, the level of GAG`s can be determined quantitatively using the dimethylene blue assay and it will be important to quantify the GAG loss in future studies. The other major components of the ECM such as collagen and elastin can also be quantitatively assessed using biochemical assays. Future studies should also investigate total collagen and elastin levels in acellular valve tissues compared to fresh tissues to provide better understanding of the effects of the SDS based decellularisation treatment on the ECM of the valvular tissue.

The integrity of the ECM was also assessed by immunohistochemical labelling of specific ECM proteins, fibronectin (a multifunctional adhesive EMC protein for cell attachment) and collagen IV (a basement membrane marker). The results indicated a reduction in the level of fibronectin and a total loss of collagen IV in the decellularised porcine pulmonary roots. The removal of fibronectin was most likely due to the continuous washing procedure during decellularisation based on the fact that the regions close to the surface of tissue had lost more fibronectin than the internal parts of the tissue. The loss of collagen IV in the decellularised scaffold indicated the loss of basement membrane. The basement membrane is considered very important in tissue endothelialisation (Brown *et al*., 2006). Thus, the pulmonary root scaffold produced in this study may not be able to be repopulated with endothelial cells either *in vitro* or *in vivo*. It will be important to determine whether loss of basement membrane collagen IV does have an effect on the endothelialisation of the acellular pulmonary heart valve conduits *in vitro* and *in vivo* in future studies. As discussed in Chapter 4, recent findings in the laboratory by Dr Stacy-Paul Wilshaw have shown that the PAA sterilisation treatment is responsible for loss of collagen IV during decellularisation of arteries. It is therefore highly likely PAA was also responsible for the removal of basement membrane in the pulmonary roots in this study. This could easily be tested in future studies of porcine pulmonary valve conduits decellularised with and without PAA sterilisation. Sterilisation of the decellularised scaffold is a prerequisite for any future *in vivo* studies and clinical translation and hence, if loss of basement membrane collagen IV does affect endothelialisation it will be necessary to investigate alternative sterilisation methods in future studies. Alternative methods that could be investigated include alternative chemical sterilising agents such as hydrogen peroxide and ethanol, γ-irradiation, ethylene oxide or electron-beam sterilisation. Gorschewsky *et al*. (2005) reported that acid or solvent sterilisation caused ECM damage. γ-irradiation is known to induce free radical formation and this may alter the mechanical properties of the ECM through cross-linking of collagens (Rosatio *et al*., 2008; Freytes *et al*., 2008; Sun & Liung, 2008; Grouk *et al*., 2008). There is also a possibility that scaffolds could become cytotoxic after sterilisation treatment (Moreau *et al*., 2000). Ethylene oxide sterilisation is only effective in the absence of water and would require the tissue to be freeze dried prior to treatment, which may affect the integrity of the scaffold. A future direction could be to investigate the use of low dose γ-irradiation or electron-beam sterilisation on

the integrity and biomechanical properties of the acellular pulmonary heart valve conduit.

Immunohistochemistry was also used to detect the presence of the xenoantigen, the α-gal epitope in the decellularised scaffolds. The presence of α-gal in the xenogeneic scaffold could cause inflammation following implantation in Man. The failure of the first acellular porcine heart valve implanted in patients, the Synergraft^{TM} , with disasterous consequences was reportedly due to the presence of residual cells expressing α-gal (Simon *et al*., 2003). For the acellular porcine pulmonary heart valve conduit produced in this study, there was no evidence of residual α-gal throughout the tissue. A limitation of this part of the study was that the determination of the presence of α-gal by immunohistochemistry was only qualitative. It is possible to quantify the levels of α-gal in tissues using an anti-α-gal antibody absorption assay followed by an ELISA to detect unbound antibodies (Stapleton *et al*., 2008). Although this was not carried out during the present study, this analysis will be important to perform in future studies.

In addition, the potential presence of porcine endogenous retrovirus (PERV) is another important concern in the use of tissues derived from pigs. There is a possibility that PERV introduced into patients through implantation of tissues of porcine origin could recombine with a latent human virus with serious consequences (Hammer, 2003; Boneva & Folks, 2004). Given the lack of detectable functional DNA in the acellular porcine pulmonary valve conduits it is unlikely that any functional retroviral DNA would be present in the tissues, however, it will be important to confirm this through use of PCR using PERV specific primers

In vitro biocompatibility studies were carried out to determine whether the decellularised porcine pulmonary heart valve conduit contained any residual reagents that were cytotoxic to cells. The acellular leaflet tissue was shown to be biocompatible using contact cytotoxicity tests with 3T3 and L929 fibroblasts. An extract cytotoxicity assay was used to assess the *in vitro* biocompatibility of the decellularised pulmonary arteries. The experiments showed that extracts from 3 out of 6 replicate acellular arterial tissues had a significant effect on the growth of 3T3 cells but not L929 cells. This revealed that the wash procedure used in the final stages of the decellularisation process was not consistently removing all of the residual chemicals from the thicker pulmonary

artery tissue and that increased washes would be required to ensure a reproducibly biocompatible acellular pulmonary heart valve conduit.

Biomechanical testing provided information on any changes in the stress-strain behaviour of the pulmonary valve leaflet and artery tissues following decellularisation. Biomechanical testing also provided an indirect assessment of the integrity of the major structural components of the ECM (elastin and collagen). The stress-strain behaviour of both fresh and decellularised leaflet and pulmonary artery tissues demonstrated typical quasi-linear trends, which were in agreement with the previous studies of the biomechanical properties of cardiac valve tissues (Jennings, 2001; Stradins *et al*., 2004; Seebacher *et al*., 2007). The pulmonary leaflet and artery tissues showed reduced extensibility and increased strength when tested in uniaxial tensile tests in the circumferential direction compared to the radial direction. This finding supported the anisotropy of the valvular tissue indicated by the directionality of the ECM. The anisotropy in the pulmonary leaflets was more apparent than that in the pulmonary artery. No significant difference was observed for any of the mechanical parameters between the fresh and decellularised leaflets, or the fresh and decellularised pulmonary arteries, with the exception of the elastin phase slope of the pulmonary artery in both directions which showed a significant decrease in the decellularised tissue. This finding indicated that decellularisation resulted in a more compliant tissue in the elastin phase within the physiological range. The results indicated that the strength of the pulmonary leaflets and arteries were not compromised following decellularisation. The results obtained in the present study were in general agreement with the results reported by Korossis (2002), who tested the mechanical properties of porcine aortic root tissues which had been decellularised using a very similar method based on 0.1 % (w/v) SDS.

Pulsatile flow testing at physiological pulmonary pressures was carried out to investigate the hydrodynamic function of the decellularised porcine pulmonary roots in comparison to the fresh tissue. No significant difference was observed in the EOA for any of the test conditions between decellularised and fresh pulmonary roots. The Q_{RMS} of the decellularised pulmonary roots showed no significant difference compared to the fresh group except for flow condition 2 (72 bpm/70 ml), during which a significant decrease was observed in the pulmonary roots following decellularisation. Interestingly, the lower Q_{RMS} indicated better performance of the roots following decellularisation treatment. The data obtained was in very good agreement with the previously reported

studies for porcine pulmonary roots (Nagy *et al*., 2000). The leaflet kinematics was assessed by recording the leaflet motion during a test run in the pulsatile flow testing. The results demonstrated a circular configuration when the valves were fully open, and no visible leakage orifices or coaptation flaws were observed in all decellularised valves. There was no significant difference in the phase durations of opening, fully open, closing and fully closed phases for the decellularised and the fresh valves, and the results were in very good agreement with the previous study reported by Korossis *et al*. (2005). No significant difference was observed in the minimum bending radius of the fresh and decellularised pulmonary leaflets. No damage to the hydrodynamic function and leaflet kinematics of the porcine pulmonary roots following decellularisation was observed.

Overall the biological, biomechanical and hydrodynamic characterisation of the acellular porcine pulmonary heart valve conduits indicated that the decellularisation process had produced minimum changes to the properties of the tissues. This indicated that the acellular porcine pulmonary cardiac valve conduits were suitable for further studies of their regenerative capacity *in vitro* and *in vivo*. In order to progress to studies of the *in vitro* regeneration of the acellular scaffolds, it was necessary to develop appropriate physiological physically interactive culture conditions. This led to preliminary studies using a novel “in house” heart valve bioreactor. Fresh porcine pulmonary roots were cultured in the heart valve bioreactor for one week in an attempt to determine whether the physically interactive culture conditions in the bioreactor could maintain tissue viability and function in comparison to fresh tissue and tissue cultured statically. The cell density and parenchymal cell distribution in the porcine pulmonary roots cultured in the bioreactor for 7 days were maintained as compared to the fresh tissue and the ECM histoarchitecture showed no overt changes as determined by H&E and Hoechst staining.

Qualitatively the levels and distribution of fibronectin and collagen IV remained the same in both dynamic and static cultured pulmonary roots when compared to the fresh tissue. Interestingly, however, there was a qualitative reduction in the levels of vimentin and desmin in the myocardium of the statically cultured tissue but no difference between the fresh and dynamically cultured tissues. This suggested that dynamic flow and stress conditions provided during leaflet opening and closing could be important to the function of the cardiac muscle cells. The levels and distribution of α-SMA in the

dynamically cultured porcine pulmonary roots was no different to the fresh tissue. There was however, a lack of α-SMA expression in the *ventricularis* of the leaflets in the statically cultured pulmonary roots. It has been reported that the *ventricularis* in the semilunar valve leaflets contains smooth muscle-like cells because this layer faces the blood flow and bears the most pressure during leaflet function (DellaRocca *et al*., 2000; Bertiplaglia *et al*., 2003). This interesting result therefore led to the hypothesis that pressure due to flow on the *ventricularis* during leaflet opening and closing might play an important role in the distribution of smooth-muscle-like cells in the *ventricularis* in the pulmonary leaflets. Unfortunately, a lack of von Willebrand factor expression on the surfaces of the pulmonary leaflets or pulmonary artery in either the dynamically or statically cultured roots indicated a loss of endothelial cells. This finding was also supported by the live/dead cell staining of the leaflets. Further investigation indicated that the Cambridge antibiotic solution which was used for surface disinfection of the pulmonary roots was responsible for the loss of endothelial cells. Therefore, in order to maintain the presence and viability of the endothelial cells in the pulmonary roots during tissue culture, it will be essential to develop an alternative disinfection solution.

Unfortunately, neither the dynamically or statically cultured tissue retained viability at the level of the fresh tissue control. Hence, the conclusion was that the conditions within the heart valve bioreactor did not promote tissue viability in comparison to static culture. The loss of tissue viability was not due to the treatment with Cambridge antibiotics. It is possible that the thickness of the tissue in the pulmonary artery wall was too great to allow adequate nutrient diffusion, even under dynamic culture conditions. Studies have shown that oxygen diffusion into heart valve leaflet tissue is limited to a depth of 300-500 microns (Wang *et al*., 2008; Wang *et al*., 2009). If cells were dying in the thickness of the arterial wall, this could have had an effect on the viability of the cells in the leaflets. In future studies of the behaviour of the fresh pulmonary valve conduits in the bioreactor it may be necessary to reduce the thickness of the artery wall in order to maintain tissue viability to study the effects of dynamic culture on leaflet viability and function.

Acellular biological scaffolds for cardiac valve replacement may be used either pre-seeded with the patient's own autologous cells prior to implantation or implanted directly with a view to the patient's own endogenous cells repopulating the scaffolds and regenerating the tissues *in vivo*. When this project commenced, both strategies were

considered as options for the future clinical translation of the scaffolds. Some researchers believe that pre-seeding of acellular xenografts with autologous endothelial cells is necessary for clinical success (Dohmen *et al*., 2002). However, harvesting of cells from patients and pre-seeding of scaffolds is a time consuming and risky procedure. In addition, this approach would not be possible for the majority of patients requiring a cardiac valve replacement.

It would be desirable if acellular cardiac valve scaffolds remodelled and regenerated *in vivo* following implantation. This approach has the advantage of an "off the shelf" solution for the majority of patients. Interestingly, the clinical use of acellular allogeneic and xenogeneic heart valves in cardiac valve replacement surgery heart has advanced considerably since the start of this project. Currently, commercially available acellular pulmonary valve grafts include the SynerGraft™ pulmonary homograft (Cyrolife Inc, USA) and the Matrix P™ porcine pulmonary valve (AutoTissue, Germany).

The early results for the SynerGraft™ pulmonary homograft appear to be good, demonstrating that this approach is safe. The implanted acellular allogeneic scaffolds have been shown to have comparable hemodynamic performance, and have been shown to be as competent as cryopreserved homografts according to current experience (Brown *et al*., 2010; Brown *et al*., 2011), although further long term follow up will be needed to evaluate the long term success of the SynerGraft™ pulmonary homografts. To date, however, there are no apparent clinical advantages to the use of the SynerGraft™ pulmonary homograft over traditional cryopreserved homografts. The real test will be the comparative performance at 8-12 years, when the cryopreserved homografts begin to fail due to calcification and degeneration. It is important to recognise that, if, as anticipated, the SynerGraft™ pulmonary homograft cardiac valve shows advantages over cryopreserved homografts in the longer term, there will still be limitations of availability since the tissue is derived from human donors.

The use of xenogeneic tissue, as with the Matrix P™ porcine pulmonary grafts has the advantage of unlimited availability in a range of different sizes. However, a number of studies have reported inflammatory responses to the Matrix P™ porcine pulmonary grafts associated with predominantly peripheral conduit narrowing (Bayrak *et al*., 2010; Ruffer *et al*., 2010; Mahler & Butcher, 2011). It is interesting to speculate whether the decellularisation process used in the production of the Matrix P™ porcine pulmonary

graft is adequately quality controlled, especially in light of the Cryolife experience with the SynerGraft™ technology applied to porcine pulmonary cardiac valves (Simon *et al*., 2003).

There have been other reports that have demonstrated the successful repopulation of decellularised heart valve scaffolds either in animal studies or clinical use (Kim *et al*., 2004; da Costa *et al*., 2007). In particular, da Costa *et al.* (2009; 2010) reported on the successful clinical use of non-pre-seeded decellularised allogeneic pulmonary and aortic roots produced using the process based on 0.1 % (w/v) SDS developed by Booth *et al*. (2002) and Wilcox *et al*. (2005). The acellular pulmonary homografts were used in the Ross procedure for right ventricular outflow tract reconstruction and demonstrated stable structural integrity, low rate of calcification, and adequate hemodynamics in early and midterm clinical results (da Costa *et al.,* 2009). Although the acellular allogeneic grafts used by da Costa *et al*. (2009; 2010) would suffer from limited availability, the clinical studies have shown promising results for the use of 0.1 % (w/v) SDS decellularisation in the production of acellular homografts. The application of a similar decellularisation process to porcine tissue in this study may offer a solution to achieve similar promising clinical results while solving the problem associated with the limited availability of homografts.

In this study, a decellularisation method for porcine pulmonary roots was developed based on the use of 0.1 % (w/v) SDS. Cell removal was achieved with the majority of ECM biological characteristics well retained. The scaffold demonstrated excellent biomechanical and hydrodynamic performance. The decellularised pulmonary leaflets showed similar leaflet kinematics and deformation compared to the fresh tissue. Minor modifications to the decellularisation process are still needed in order to produce a reproducibly biocompatible scaffold with the basement membrane retained. Further assessment of the decellularised porcine pulmonary root scaffold is required, in particular quantitative determination of α-gal. Overall the decellularised porcine pulmonary roots have excellent potential for development of a tissue engineered solution for right ventricular outflow tract reconstruction during the Ross procedure.

Appendix 1

Coding sequences for Sus scrofa Glyceraldehyde 3-phosphate dehydrogenase (GAPDH), Swine leukocyte antigen (SLA), beta 2-microglobulin (β 2-microglobulin) and beta actin (β actin)

1. Sus scrofa glyceraldehyde 3-phosphate dehydrogenase (GAPDH) mRNA, complete cds

CTCTCTGCTCCCTCCCCGTTCCACAGACAGCCGTGTGTTCCGTGCATTGCCAGGTAAAGCCTGGCGGAGT
GGAGCCACAAGGTTCGAGGACTGGTCCAAAGGGACCGGGGGCCGTGCGCGGTCTGGGAGTGTGGGTGCGG
GCCCGGCTGGGGGCCGGAGTTGTGCTGCGCCGGCCGGGCCCCTGCATTGCGGGTTGAGGGGGAGGAAGGA
CGTGCAGAAGAGCAGAGCGAGGATGGAGGCCACTGGGGGAGGGGCGGGGAGGGCACCGTCGGGCTCCAGC
CGCTTTGCCCCGCGATCTAATGTTCTCTTTCCTCTGCCGGCAGCCGCGTCCCTGAGACACGATGGTGAAG
GTCGGAGTGAACGGATTTGGCCGCATCGGGCGCCTGGTCACCAGGGCTGCTTTTAACTCTGGCAAAGTGG
ACATTGTCGCCATCAATGACCCCTTCATTGACCTCCACTACATGGTCTACATGTTCCAGTATGATTCTAC
CCATGGCAAATTCCACGGCACAGTCAAGGCTGAGAATGGGAAGCTTGTCATCAATGGAAATCCCATCACC
ATCTTCCAGGAGCGAGATCCCGCCAAAATCAAATGGGGCGATGCTGGTGCTGAGTATGTCGTGGAGTCCA
CTGGTGTCTTCACGACCATGGAGAAGGCTGGGGCTCACTTGAAGGGGGGAGCCAAAAGGGTCATCATCTC
TGCCCCTTCTGCTGATGCCCCCATGTTTGTGATGGGCATGAACCATGAGAAGTATGACAACAGCCTCAAG
ATCATCAGCAATGCCTCCTGTACCACCAACTGCTTGGCACCCCTGGCCAAGGTCATCCATGACAACTTCG
GCATCGTGGAAGGACTCATGACCACAGTCCATGCCATCACTGCCACCCAGAAGACTGTGGATGGCCCCTC
TGGGAAACTGTGGCGTGATGGCCGAGGGGCTCTCCAGAACATCATCCCTGCTTCTACTGGTGCTGCCAAG
GCTGTGGGCAAGGTCATCCCTGAGCTCAACGGGAAGCTCACTGGCATGGCCTTCCGTGTCCCTACTGCCA
ACGTGTCGGTTGTGGACCTGACCTGCCGTCTGGAGAAACCTGCCAAATATGATGACATCAAGAAGGTGGT
GAAGCAGGCGTCCGAGGGCCCCCTCAAGGGCATCCTGGGCTACACTGAGCACCAGGTTGTGTCCTCTGAC
TTTAACAGTGACACTCACTCTTCTACCTTTGATGCTGGGGCTGGCATTGCCCTCAACGACCACTTTGTCA
AGCTCATTTCCTCGTACGACAATGAATTTGGCTACAGCAACAGGGTGGTGGACCTCATGGTCCACATGGC
CTCCAAGGAGTAAGAGCCCCTGGACCACCAACCCCAGCAAGAGCACGCGAGGAGGAGAGAGGCCCTCAGT
CGTCGGGGATGCACAGCCC

2. Sus scrofa SLA-2 mRNA for MHC class I antigen, complete cds, allele: SLA-2-TPK (1119bp)

AGATGCGGGTCAGGGGCCCTCAAGCCATCCTCATTCCGCTGTCGGGGGCCCTGGCCCTGACCGGGACCCA
GGCGGGTTCCCACTCCCTGAGCTATTTCTACACCGCCGTGTCCCGGCCCGACCGCGGGGACTCCCGCTTC
CTCACCGTCGGGTACGTGGACGACACGCAGTTCGTGCGGTTCGACAGCGACGCCCCGAATCCGAGGGAGG
AGCCGCGGGTGCCGTGGATACAGCAGGAGGGGCAGGACTATTGGGATAGGAACACGCAGATTTACAAGGA
AACCGCACAGATTTACAGAGTGGGCCTGAACAACCTGCGCGGCTACTACAACCAGAGCGAGGCCGGGTCT
CACACCTTCCAGAGCATGTACGGCTGCGACGTGGGACCAGACGGGCTCTTCCTCCGCGGGTACAGTCAGG
ACGCCTACGACGGCGCCGATTACGTCGCCCTGAACGAGGACCTGCGCTCCTGGACCGCGGCGGACACGGC
GGCTCAGATCACCAAGCGCAAGAGGGAGGCGGCCGATGCGGCGGAGCAGTGGAGGAGCTACCTGCGGGGC
ACGTGTATGGAGGGGCTCCGCAGATACCTGGAGATGGGGAAGGACACGCTGCAGCGCGCAGAGCCTCCAA
AGACACATGTGACCCGCCACCCCAGCTCTGACCTGGGGGTCACCTTGAGGTGCTGGGCCCTGGGCTTCTA
CCCTAAGGAGATCTCCCTGACCTGGCAGCGCGAGGGCCAGGACCAGAGCCAGGACATGGAGCTGGTGGAG
ACCAGGCCCTCAGGGGATGGGACCTTCCAGAAGTGGGCGGCCCTGGTGGTGCCTCCTGGAGAGGAGCAGA
GCTACACCTGCCATGTGCAGCACGAGGGCCTGCAGGAGCCCCTCACCCTGAGATGGGACCCTCCTCAGCC
CCCCGTCCCCATCGTGGGCATCATTGTTGGCCTGGTTCTGGTCCTGGTCACTGGAGCCGTGGTGACTGGA
GTTGTGATCTGGAGAAAGAAGCGCTCAGGTGAAAAAGGAGGGAGCTACACTCAGGCTGCAGGCAGTGACA
GTGCCCAGGGCTCCGATGTGTCCCTTACCAAGGATCCTAGAGTGTGAGACAGCTGCCTTGTGGGGACTG

3. Sus scrofa beta 2-microglobulin mRNA, complete cds (543bp)

AAGGGTCTTAAAACTTTTTAAATCAAGTCAACCACTTTTCACACCGCTCCAGTAGCGATGGCTCCCCTCG
TGGCCTTGGTCCTGCTCGGGCTGCTCTCACTGTCTGGCCTGGATGCGGTCGCGCGTCCCCCGAAGGTTCA
GGTTTACTCACGCCACCCAGCGGAAAACGGAAAGCCAAATTACCTGAACTGCTATGTATCTGGGTTCCAT
CCGCCCCAGATTGAAATTGATTTGCTGAAAAACGGGGAGAAGATGAACGCGGAGCAGTCAGACCTGTCTT
TCAGCAAGGACTGGTCTTTCTACCTTCTGGTCCACACTGAGTTCACTCCTAACGCTGTGGATCAGTATAG
CTGCCGCGTGAAGCACGTGACTCTCGATAAGCCCAAGATAGTTAAGTGGGATCGAGACCACTAACCGGCA
TCACAGAGATTATGAAGATGCTGCATCTGGGTTGGATGAATCCAAATTCTGATTTGTTGCTTTTTAATAC
TGATAAGCTTTTATACTTTATGCACATAAATCAGAAATCGTATTGATGTTACC

4. Sus scrofa beta actin mRNA, partial cds (706bp)

ATGTTTGAGACCTTCAACACGCCGGCCATGTACGTGGCCATCCAGGCTGTGCTGTCCCTGTACGCCTCTG
GCCGCACCACTGGCATTGTCATGGACTCTGGGGATGGGGTCACCCACACGGTGCCCATCTACGAGGGGTA
CGCCCTGCCCCACGCCATCCTGCGTCTGGACCTGGCTGGCCGGGACCTGACCGACTACCTCATGAAGATC
CTCACGGAGCGGGGCTACAGCTTCACCACCACGGCCGAGCGGGAGATCGTGCGGGACATCAAGGAGAAGC
TCTGCTACGTCGCCCTGGACTTCGAGCAGGAGATGGCCACGGCCGCCTCCTCCTCCTCCCTGGAGAAGAG

CTACGAGCTGCCCGACGGGCAGGTCATCACCATCGGCAACGAGCGCTTCCGGTGTCCAGAGGCGCTCTTC
CAGCCCTCCTTCCTGGGCATGGAGTCCTGCGGCATCCACGAGACCACCTTCAACTCGATCATGAAGTGCG
ACGTGGACATCAGGAAGGACCTCTACGCCAACACGGTGCTGTCTGGCGGGACCACCATGTACCCCGGCAT
CGCCGACAGGATGCAGAAGGAGATCACGGCCCTGGCGCCCAGCACCATGAAGATCAAGATCATCGCCCCT
CCCGAGCGCAAGTACTCCGTGTGGATCGGGGGCTCCATCCTGGCCTCGCTGTCCACCTTCCAGCAGATGT
GGATCA

Appendix 2

Determination of leaflet average curvature

The mathematical rationale for the determination of the leaflet average curvature has been described by Courden *et al.* (1995a, 1995b). The cubic spline, s(x), was fitted to the transformed data (X_{α},trans, Y_{α},trans), using a standard numerical routine integrated into the Origin programme (Version 8.0). The spline was represented in its B-spline form as: C_kN_k

$$s(x) = \sum_{k=1}^{J} c_k N_k(x)$$

Where $N_k(x)$ is the normalised 3rd degree B-spline, and c_k are the spline coefficients estimated by the routine. A further numerical routine was used to evaluate the spline at 90 equally spaced points (X_i, Y_i) along the curve.

The curvature Ki at each point along the spline was calculated according to [Gere & Timoshenko (1984)]:

$$K_i = \left| \frac{\left(\frac{d^2y}{dx^2}\right)_i}{\left(1+\left(\frac{dy}{dx}\right)_i^2\right)^{3/2}} \right|$$

Where the derivatives were evaluated at each point using the central difference expressions, given by:

$$\left(\frac{dy}{dx}\right)_i = \frac{y_{i+1} - y_{i-1}}{2\delta x}$$

and

$$\left(\frac{d_2y}{dx^2}\right)_i = \frac{y_{i+1} - y_{i-1}}{2\delta x}$$

Since any leaflet has a finite thickness when viewed using the image analysis system it was possible to introduce false local curvatures when defining the leaflet using a polyline. This concept is illustrated in Figure B.1. In order to eliminate the effect of these false curvatures that may have contaminated the data, an average value of curvature was calculated according to the formula:

$$K_{i,avg} = \frac{K_{i-(n-1)/2} + \cdots + K_{i-1} + K_i + K_{i+1} + \cdots + K_{i+(n-1)/2}}{n}$$

The value of n was chosen to satisfy the following condition:

$$l_n \geq 10 \times t$$

Where t is the thickness of the leaflet, n is an odd integer and l_n is parameter defining a length of leaflet over which the average curvature is calculated. The ensured a sufficient aspect ratio between l_n and t to allow the use of thin shell bending theory to calculate the bending stresses in the leaflet ($t/ l_n < 0.1$). The fresh left pulmonary leaflets had an average thickness of 0.348 mm, and the decellularised left pulmonary leaflets had an average thickness of 0.262 mm. The value n of 13 was used.

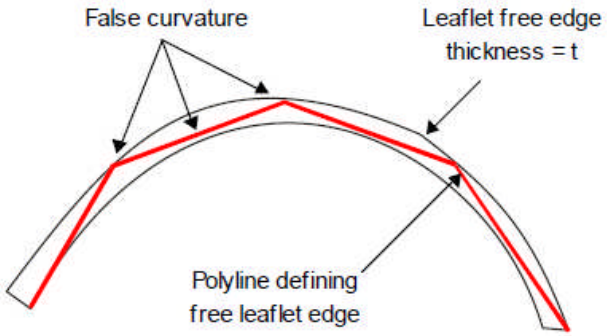

Figure B.1 Schematic of possible false curvature.

Appendix 3

List of presentations

Ji Luo, John Fisher, Zhongmin Jin, Eileen Ingham, and Sotirios Korossis (2009) **Biomechanical and Histological Characterisation of Low Concentration SDS Decellularised Porcine Pulmonary Valvular Scaffold.** 11th Annual White Rose Work in Progress Meeting, York. Poster presentation.

Ji Luo, Sotirios Korossis, Zhongmin Jin, John Fisher, Eileen Ingham (2009) **Biomechanical testing of low concentration SDS decellularised porcine pulmonary valves.** The Society of Heart Valve Diseases 5th Biennial meeting, Berlin. Poster presentation.

Ji Luo, John Fisher, Zhongmin Jin, Eileen Ingham, and Sotirios Korossis (2009) **Biomechanical and Histological Characterisation of Low Concentration SDS Decellularised Porcine Pulmonary Valvular Scaffold**. Tissue Engineering and Regenetive Medicine International Society (TERMIS) World Congress, Seoul. Poster presentation.

J Luo, John Fisher, Zhongmin Jin, Eileen Ingham, Sotirios Korossis (2010) **Biomechanical Testing of Low-Concentration SDS Decellularised Porcine Pulmonary Valves.** Tissue and Cell Engineering Society meeting, Manchester. Poster presentation.

Ji Luo, John Fisher, Zhongmin Jin, Daniel Thomas, Sotirios Korossis and Eileen Ingham (2010) **Biomechanical and Histological Characterisation of Trypsin and Low Concentration SDS Decellularised Porcine Pulmonary Valvular Scaffold.** 12th Annual White Rose Work in Progress Meeting, Leeds. Oral presentation.

References

Allen, R.A., Seltz, L.M., Jiang, H., Kasick, R.T., Sellaro T.L., Badylak, S.F., *et al.* (2010) Adrenal extracellular matrix scaffolds support adrenocortical cell proliferation and function *in vitro*. *Tissue. Eng. Part A*, 16(11), 3363–3374.

Arts, T., Meerbaum, S., Reneman, R., Corday, E. (1983) Stresses in the closed mitral valve: a model study. *J. Biomech*., 16(7), 539-547.

Asahara, T. Murohara, T., Sullivan, A., *et al*. (1997) Isolation of putative progenitor endothelial cells for angiogenesis. *Science*, 275, 964-967.

Ayad, S., Boot-Handford, R., Humphries, M.J. Kadler, K.E., Shuttleworth, A. (1994) *the extracellular matrix. Facts book*, 2nd edn. London, Academic Press Limited.

Bader, A., Schilling, T., Teebken, O.E., *et al.* (1998) Tissue engineering of heart valves – human endothelial cell seeding of detergent acellularized porcine valves. *Eur. J. Cardiothorac. Surg.*, 14, 279-284.

Bader, A., Steinhoff, G., Strobl, K., *et al*. (2000) Engineering of human vascular aortic tissue based on a xenogenec starter matrix. *Transplantation*, 70, 7-14.

Badylak, S.F., Tullius, R., Kokini, K., Shelbourne, K.D., Klootwyk, T., Voytik, S.L., *et al.* (1995) The use of xenogeneic small intestinal submucosa as a biomaterial for Achilles tendon repair in a dog model. *J. Biomed. Mater. Res.*, 29, 977–985.

Badylak, S.F. (2002) The extracellular matrix as a scaffold for tissue reconstruction. *Semin Cell Dev. Biol.*, 13(5), 377-383.

Badylak, S.F. (2004) Xenogeneic extracellular matrix as a scaffold for tissue reconstruction. *Transplant immunology*, 12, 367-377.

Badylak, S.G., Gilbert, T.W. (2008) Immune response to biologic scaffold materials.

Seminars in Immunology, 20, 109-116.

Bairati, A. Debiasi., S. (1981) Presence of a smooth muscle system in aortic valve leaflets. *Anat. Embryol*., 161, 327-340.

Barber, R.D., Harmer, D.W., Coleman, R.A., Clark, B.J. (2005) GAPDH as a housekeeping gene: analysis of GAPDH mRNA expression in a panel of 72 human tissues. *Physiological Genomics*, 21, 389-395.

Barkan, D., Green, J.E., Chambers, A.F. (2010) Extracellular matrix: a gatekeeper in the transition from dormancy to metastatic growth. *Eur. J. Cancer*, 467, 1181–1188.

Barnett, S.D., Ad, N. (2009) Surgery for aortic and mitral valve disease in the United States: a trend of change in surgical practice between 1998 and 2005. *J. Thorac. Cardiovasc. Surg.*, 137(6), 1422-1429.

Barratt-Boyes, B.G., Roche, A.H.G., Whitlock, R.M.L. (1977) Six year review of the results of freehand aortic valve replacement using an antibiotic sterilized homograft valve. *Circulation*, 55, 353-361.

Bashey, R.I., Torii, S., Angrist, A. (1967) Age-related collagen and elastin content of human heart valves. *J. Gerontol.*, 22 (2), 203-208.

Bateman, J.F., Lamande, S.R., Ramshaw, A.M. (1996) *Collagen Superfamily* in *Extracellular Matrix* (Comper, W.D. ed.), 22-67, Amsterdam, Harwood Academic Publishers.

Bechtel, J. F., Muller-Steinhardt, M., Schmidtke, C., Brunswik, A., Stierle, U., & Sievers. H. H. (2003) Evaluation of the decellularized pulmonary valve homograft (SynerGraft), *J. Heart Valve Dis.*, 12**,** 734-739.

Bechtel, J.F., Stierle, U., Sievers, H. (2008) Fifty-two Months' mean follow yp of decellularied SynerGraft™-treated pulmonary valve allografts. *J. Heart Valve Dis.*, 17(1), 98-104.

Bennett, R.M., Gabor, G.T., Merritt, M.M. (1985) DNA binding to human leukocytes. Evidence for a receptor-mediated association, internalization, and degradation of DNA. *J. Clin. Invest*., 76(6), 2182-2190.

Bernal, J.M., Rabaso, J.M, Lopez, R., *et al*., (1995) Durability of the Carpentier-Edwards porcine bioprosthesis: role of age and valve position. *Ann. Thorac. Surg.*, 60, 248-252.

Bernard, A., Mahmoodi, M., *et al*. (1989) A semi supported xenografts. *Journal of Thoracic &Cardiovascular Surgery*, 37, 313-315.

Berrebi, A.J., Carpentier, S.M., Phan, K.P., *et al*. (2001) Results of up to 9 years of high-temperature-fixed valvular bioprostheses in a young population. *Ann. Thorac. Surg*., 71(5 Suppl.), S353-S355.

Berry, J.L., Steen, J.A., Williams, K., Jourdan, J.E., Atala, A., Yoo, J.J. (2010) Bioreactors for development of tissue engineered heart valves. *Ann. of Biomedical Engineering*, 38(11), 3272-3279.

Bertiplaglia, B., Ortolani, F., Petrelli, L., Gerosa, G., Spina, M., Pauletto, P., Casarotto, D., Machini, M., and Sartore, S. (2003) Cell characterization of porcine aortic valve and decellularized leaflets repopulated with aortic valve interstitial cells: the vesalio project (vitalitate exornatum succadaneum aorticum labore ingenioso obtenibitur). *Annals of Thoracic Surgery*, 75, 1274–1282.

Bhairi, S.M. (1997) A guide to the properties and uses of detergents in biology and biochemistry: Calbiochem-Novabiochem Corporation.

Bhairi, S.M., Mohan, C. (2007) Detergents: a guide to the properties and uses of detergents in biological systems. Calbiochem®.

BiologyDaily (2005) [Internet] Available from http://biosphere.biologydaily.com/help/node/5409 [accessed 2nd Oct, 2011]

Bjork, B.O. (1969) A new tilting disk prosthesis. *Scand. J. Thorac. Cardiovasc. Surg.*, 3, 1-10.

Bodnar, E., Olsen, E.G., Florio, R., Dobrin, J. (1986) Damage of porcine aortic valve tissue caused by the surfactant sodium dodecylsulphate. *Thorac. Cardiovasc. Surg.*, 34, 82-85.

Boer, U., Lohrenz, A., Klingenberg, M., Pich A., Haverich, A., Wilhelmi, M. (2011) The effect of detergent-based decellularisation procedures on cellular proteins and immunogenicity in equine carotid artery grafts. *Biomaterials*, 32, 9730-9737.

Bokros, J.C. (1989) Carbon in prosthetic heart valve. *Ann. Thorac. Surg*., 48, S49-50.

Boneva, R., Folks, T. (2004). Xenotransplantation and risks of zoonotic infections. *Annuals of Medicine*, 36, 504-517.

Booth, C., Korossis, S.A., Wilcox, H.E., Watterson, K.G., Kearney, J.N., Fisher, J., Ingham, E. (2002) Tissue engineering of Cardiac valve prostheses I: Development and histological characterization of an acellular porcine scaffold. *The Journal of Heart Valve Disease*, 11, 457-462.

Bornstein, P., Sage, E.H., (2002) Matricellular proteins: extracellular modulators of cell function. *Curr. Opin. Cell Biol.*, 145, 608–616.

Boudoulas, H., Vavuranakis, M., Wooley, C.F. (1994) Valvular heart diseases: the influence of changing etiology on nosology. *J. Heart Valve Dis*., 3(5), 516-526.

Brockbank, K.G., Lightfoort, F.G., Song, Y.C., Taylor, M.J. (2000) Interstitial ice formation in cryopreserved homografts: a possible cause of tissue deterioration and calcification *in vivo*. *J Heart Valve Dis*, 9, 200-206.

Brody, S., Pandit, A., (2007) Approaches to heart valve tissue engineering scaffold design. *Journal of Biomedical Materials Research Part B: Applied Biomaterials*, 83B

(1), 16–43.

Bronzino, J.D. (2000) *Biomedical Engineering*. 2nd edn, Springer.

Broom, N.D. (1978) Simultaneous morphological and stress-strain studies of the fibrous components in the wet heart valve leaflet tissue. *Connect Tiss. Res*., 6, 37-50.

Brown, J.W., Ruzmetov, M. *et al*. (2006a) The Ross-Konno procedure in children: outcomes, autograft and allograft function, and reoperations. *Ann. Thorac, Surg.*, 82, 1301-1307.

Brown, B., Lindberg, K., Reing, J., Stolz, D.B., Badylak, S.F. (2006b) The basement membrane component of biologic scaffolds derived from extracellular matrix. *Tissue engineering*, 12(3), 519-26.

Brown, B.N., Valentin, J.E., Stewart-Akers, A.M., McCabe G.P., Badylak, S.F. (2009) Macrophage phenotype and remodeling outcomes in response to biologic scaffolds with and without a cellular component. *Biomaterials*, 30(8), 1482–1491.

Brown, B.N., Fruend, J.M., Li, H., Rubin, P.J., Reing, J.E., Jeffries, E.M., *et al.* (2011) Comparison of three methods for the derivation of a biologic scaffold composed of adipose tissue extracellular matrix. *Tissue Eng. Part C Methods*., 17(4), 411-421.

Brown, J.W., Ruzmetov, M., Vijay, P., *et al*. (2001) clinical outcomes and indicators of normalization of left ventricular dimensions after Ross procedure in children. *Semin. Thorac. Cardiovasc. Surg.*, 13, 28-34.

Brown, J.W., Elkins, R.C., Clarke, D.R., *et al*. (2010) Performance of the CryoValve SG human decellularized pulmonary valve in 342 patients compared to the conventional CryoValve at a mean follow-up of 4 years. *J. Thorac. Cardiovasc. Surg.*, 139, 339-348.

Brown, J.W., Ruzmetov, M., Eltayeb, O., Rodefeld, M.D., Turrentine, M.W. (2011) Performance of SynerGraft decellularized pulmonary homograft in patients undergoing a Ross procedure. *Ann. Thorac. Surg.*, 91, 416-423.

Burch, P.T., Kaza, A.K., Lambert, L.M., Holubkov, R., Shaddy, R.E., Hawkins, J.A. (2010) Clinical performance of decellularized cryopreserved valved allografts compared with standard allografts in the right ventricular outflow tract. *Ann. Thorac. Surg.*, 90(4), 1301–1305.

Burcin, E., Cooper, D.K.C. (2008) Update: cardiac xenotransplantation. *Curr. Opin. Organ Transplant*, 13(5), 531-535.

Butany, J., Ahluwalia, M.S. Munroe, C., Fayet, C., Ahn, C., Blit, P., Kepron, C, Cusimano, R., Leask, R.L. (2003a) Mechanical heart valve prostheses: identification and evaluation (erratum). *Cardiovascular Pathology Pathology*, 12, 322-344.

Butany, J., Fayet, C., Ahluwalia, M.S., Blit, P., Ahn, C., Munroe, C., Israel, N., Cusimano, R.J., Leask, R.L. (2003b) Biological replacement heart valves: identification and evaluation. *Cardiovascular Pathology*, 12, 119-139.

Butany, J., Luk, A., Leong, S.W., Leong, M.M., Singh, G., Thangaroopan, M., Williams. W. (2007a) A Carpentier-Edwards porcine-valved dacron conduit: at twenty-five years. *Int. J. Cardiol.*117(1) e13-e16.

Butany, J., Leong, S.W., Cunningham, K.S., D'Cruz, G., Carmichael, K., Yau, T.M. (2007b) A 10-year comparison of explanted Hancock-II and Carpentier-Edwards supraannular bioprostheses. *Cardiovasc. Pathol*., 16(1), 4-13.

Butcher, J.T., Nerem, R.M. (2004) Porcine aortic valve interstitial cells in three dimensional culture: comparison of phenotype with aortic smooth muscle cells. *J. Heart valve Dis*., 13, 485-486.

Butcher, J.T., Penrod, A.M., Garcia, A.J., Nerem, R.M. (2004) Unique morphology and focal adhesion development of valvular endothelial cells in static and fluid flow enviroments. Arterioscler. *Thromb. Basc. Biol*., 24, 1429-1434.

Butterfield, M., Fisher, J., *et al*. (1990) Fresh and glutaraldehyde preserved frame

mounted homograft and porcine bioprosthetic heart vales: leaflet geometry dynamics and function. In: *Clinical implant materials* (Eds. Heimke, E. *et al*.), Elsevier Science Publishers. 9, 523-528.

Carew, E.O., Garg, A., Barber, J.E., Vesely, I. (2004) Stress relaxation preconditioning of porcine aortic valves. *Annals. Of Biomedical Engineering*, 32(4), 563-572.

Carrier, R.L., Papadaki, M., Rupnick, M., Schoen, F.J., Bursac, N., Langer, R., Freed, L.E., Vunjak-Novakovic, G. (1999) Cardiac tissue engineering: cell seeding, cultivation parameters, and tissue construct characterization. *Biotechnol Bioeng*, 64, 580-589.

Cebotari, S., Lichtenberg, A., Tudorache, I., Hilfiker, A., Mertsching, H., Leyh, R., Breymann, T., Kallenbach, K., Maniuc, L., Batrinac, A., Repin, O., Maliga, O., Ciubotaru, A., Haverick, A. (2006) Clinical application of tissue engineered human heart valves using autologous progenitor cells. *Circulation*, 114, 1132-1137.

Chamberlain, G., Fox, J., Ashton, B., Middleton, J. (2007) Concise review: mesenchymal stem cells: their phenotype, differentiation capacity, immunological features, and potential for homing. *Stem Cells*, 25, 1739-1749.

Chen, H., Hu, Y. (2006) Bioreactors for tissue engineering. *Biotechnol. Lett*., 28, 1415-1423.

Chen, R.N., Ho, H.O., Tsai Y.T., Sheu, M.T. (2004) Process development of an acellular dermal matrix (ADM) for biomedical applications. *Biomaterials*, 25(13), 2679–2686.

Cheng, H., Tsui, Y., Cheung, K., Dan, D., Chan, B. (2009) Decellularization of chondrocyte-encapsulated collagen microspheres: a three-dimensional model to study the effects of acellular matrix on stem cell fate. *Tissue Engineering: Part C*, 15 (4), 697-706.

Chevallay, B., Herbage, D. (2000) Collagen-based biomaterials as 3D scaffold for cell cultures: Applications for tissue engineering and gene therapy. *Med. Biol. Eng. Comput*., 38, 211–218.

Christie, G.W., Barratt-Boyes, B.G. (1995) Mechanical properties of porcine pulmonary valve leaflets: How do they differ from aortic leaflets? *Ann Thorac Surg*, 60, 195-199.

Christoforou, N., Gearhart, J.D. (2007) Stem cells and their potential in cell-based cardiac therapies. *Progress in Cardiovascular Diseases*, 49(6), 396-413.

Cicha, I., Ruffer, A., Cesnjevar, R., *et al*. (2011) Early obstruction of decellularized xenogeneic valves in pediatric patients: involvement of inflammatory and fibroproliferative processes. *Cardiovascular Pathology*, 20(4), 222-231.

Clark, R.E. (1973) Stress-strain characteristics of fresh and frozen human aortic and mitral leaflets and chordate tendineae. *J. Thorac. Cardiovasc. Surg*., 66(2), 202-208.

Clarke, D.R., Campbell, D.N., Hayward, A.R., Bishop, D.A. (1993) Degeneration of aortic valve allografts in young recipients. *J. Thoracic. Cardiovasc. Surg.*, 105, 934-941.

Cleary, E.G., Gibson, M.A. (1996) *Elastic tissue, elastin and elastin associated microfibrils* in *Extracellular Matrix* (Comper, W.D. ed.), 22-67, Amsterdam, Harwood Academic Publishers.

Collins, J.J. (1991) The evolution of artificial heart valves. *New England Journal of Medicine*, 324, 624.

Concha, M., Aranda, P.J., Casares, J., Merino, C., *et al.* (2004) The Ross procedure. *J. Card. Surg*., 19, 401-409.

Connolly, J.M., Alferiev, I., Kronsteiner, A., Lu, Z., Levy, R.J. (2004)Ethanol inhibition of porcine bioprosthetic heart valve cusp calcification is enhanced by reduction with sodium borohydride. *The Journal of Heart valve disease*, 13, 487-493.

Cooper, D.K., Good, A.H., Koren, E., Oriol, R., Malcolm, A.J., Ippolito, R.M., Neethling, F.A., Ye, Y., Romano, E., Zuhdi, N. (1993) Identification of alpha-galactosyl and other carbohydrate epitopes that are bound by human anti-pig anti-bodies: relavance

to discordant xenografting in man. *Transpl. Immunol*., 1, 198-205.

Corden, J.M., David, T., Fisher, J. (1995a) Determination of the curvatures and bending strains in open trileaflet heart valves. *Proceedings of the Institution of Mechanical Engineers*, Part H, 209 (H2), 121-128.

Corden, J.M., David, T., Fisher, J. (1995b) *In vitro* determination of the curvatures and bending strains acting on the leaflets of polyurethane trileaflet heart valves during leaflet motion, *Proceedings of the institution of Mechanical Engineers*, Part H, 209，243-253.

Courtman, D.W., Pereira, C.A., Kashef, V., McComb, D., Lee, J.M., Wilson, G.J. (1994) Development of pericardial acellular matrix biomaterial: biochemical and mechanical effects of cell extraction. *Journal of Biomedical Materials Research*, 28, 655-666.

Cox, B., Emili, A. (2006) Tissue subcellular fractionation and protein extraction for use in mass-spectrometry-based proteomics. *Nat. Protoc.*, 1(4), 1872–1878.

Crapo, P.M., Gilbert, T.W., Badylak, S.F. (2011) An overview of tissue and whole organ decellularisation processes. *Biomaterials*, 32, 3233-3243.

Curtil, A., Pegg, D.E., Wilson, A. (1997) Freeze drying of cardiac valves in preparation for cellular repopulation. *Cryobiology*, 34, 13-22.

Cuy, J.L., Beckstead, B.L., Brown, C.D., Hoffman, A.S., Giachelli, C.M. (2003) Adhesive protein interactions with chitosan: Consequences for valve endothelial cell growth on tissue-engineering materials. *J. Biomed. Mater Res*., 67, 538–547.

Da Costa F. D., Dohmen P. M., Lopes S. V., Lacerda G., Pohl F., Vilani R., Da Costa A.M.B., Vieira E. D., Yoschi S., Konertz W., da Costa, A.I. (2004) Comparison of cryopreserved homografts and decellularized porcine heterografts implanted in sheep. *Artif. Organs*, 28, 366-370.

Costa, F. Pereira, E., Barboza, L., *et al*. (2005a) Ten-Year experience with the Ross

operation. *Arq. Bras. Cardiol*., 87, 531-538.

Da Costa, F.D., Dohmen, P.M., Duarte, D., von Glenn, C., Lopes, S.V., Filho, H.H., *et al*. (2005b) Immunological and echocardiographic evaluation of decellularised versus cryopreserved allografts during the Ross operation. *Eur. J. Cardiothorac. Surg.*, 27(4), 572-578.

Da Costa, F., Dohmen, P., Vieira, E., Lopes, S.V., Colatusso, C., Pereira, E.W.L., Matsuda, C.N., Cauduro., S. (2007) Ross operation with decelularized pulmonary allografts: medium-term results. *Rev. Bras. Cir. Cardiovas.*, 22(4), 454-462.

Costa, F.D.A, Santos, L.R., Collatusso, C., Matsuda, C.N., Lopes, S.A.V., Caudoro, S., Roderjan, J, Ingham, E. (2009) Thirteen years' experience with the Ross operation. J. *Heart valve Dis*., 18 (1), 84-94.

Da Costa, F.D., da Costa, A.C., Prestes, R., Domanski, A.C., Balbi, E.M., Ferreira, A.D., Lopes, S.V. (2010) The early and midterm function of decellularized aortic valve *allografts. Ann. Thorac. Surg*., 90(6), 1854-1860.

Dagum, P., Green, G.R., Nistal., F.J., Daughters, G.T., Timek, T.a., Foppiano, L.E., Bolger, A.F., Ingels Jr., N.B., Miller, D.C. (1999) Deformational dynamics of the aortic root: models and physiologic determinants. *Circulation*, 100(19 Suppl.), 1154-1162.

Dal-Bianco, J.P., Aikawa, E., Bischoff, J., Guerrero, J.L., Handschumacher, M.D., Sullivan, S., Johnson, B., Titus, J.S., Iwamoto, Y., Robert, J.W., Levine, A., Carpentier, A. (2009) Active Adaptation of the Tethered Mitral Valve: Insights Into a Compensatory Mechanism for Functional Mitral Regurgitation, *Circulation*, 120, 334-342.

Daley, W.P., Peters, S.B., Larsen, M. (2008) Extracellular matrix dynamics in development and regenerative medicine. *J. Cell Sci*., 121, 255-264.

David, H., Boughner, D.R., Vesely, I., Gerosa, G. (1994a) The pulmonary valve: is it mechanically suitable for use as anaortic valve replacement? *ASAIO Journal*, 40, 206-

212.

David, T.E., Feindel, C.M. *et al*. (1994b) Aortic valve replacement with a stentless porcine aortic valve. *Journal of Thoracic & Cardiovascular Surgery*, 108, 1030-1036.

David, T.E. Armstrong, S., Sun, Z. (1995) The Hancock II bioprosthesis at ten years. *Ann. Thorac. Surg*., 60, S229-234.

Davies, P.F. (1997) Mechanisms involved in endothelial responses to hemodynamic forces, *Atherosclerosis*, 131, S15-S17.

DeBakey, M.E., Discussion of Braunwald, N.S., Tatooles, C., Turina, M. *et al*. (1971) New development in the design of fabric covered prosthetic heart valves, *J. Thorac. Cardiovasc. Surg.*, 62, 673-682.

DellaRocca, F., Sartore, S., Guidolin, D., Bertiplaglia, B., Gerosa, G., Casarotto, D., and Pauletto, P. (2000) Cell composition of the human pulmonary valve: A comparative study with the aortic valve - the vesalio project. *Annals of thoracic surgery*, 70, 1594–1600.

Diaz-Jauanen, E., Strichland, r.G.,Williams, R.C. (1975) Studies of human lymphocytes in the newborn and the aged. *Am. J. Med*., 58, 620-628.

Dignan, R., O'Brien, M., Hogan, P, Passage, J., Stephens, f., Thornton, A., Harrocks, S. (2000) Influence of HLA matching and associated factor on aortic valve homograft function. *The Journal of Heart Valve Disease*, 9, 504-511.

Dimmerler, S., Aiche, A., Vasa, M., *et al*. (2001) HMG-CoA reductase inhibitor (statins) increase endothelial progenitor cells via the PI 3-kinase/Akt pathway. *J. Clin. Invest*., 108, 391-397.

Dimmerler, S., Zeiher, A.M., Schneide, M.D. (2005) Unchian my heart: the scientific foundations of cardiac repair. *J. Clin. Invest*., 115, 572-583.

Dohmen, P.M., Lembcke, A., Hotz, H., Kivelitz, D., Konertz, W.F. (2002) Ross operation with a tissue engineered heart valve. *Ann. Thorac. Surg*., 74, 1438-1442.

Dohmen, P. M., Ozaki, S., Nitsch, R., Yperman, J., Flameng, W., & Konertz. W. (2003) A tissue engineered heart valve implanted in a juvenile sheep model. *Med. Sci. Monit*. 9, BR97-BR104.

Dohmen, P. M., Costa, F., Lopes, S. V., Yoshi, S., Souza, F. P., Vilani, R., da Costa M. B., & W. Konertz. (2005) Results of a decellularized porcine heart valve implanted into the juvenile sheep model. *Heart Surg. Forum,* 8, E100-E104.

Dohmen, P.M., Lembcke, A., Holinski, S., Kivelitz, D., Braun, J.P., Pruss, A., Konertz, W. (2007) Mid-term clinical results using a tissue-engineered pulmonary valve to reconstruct the right ventricular outflow tract during the Ross procedure. *Ann. Thorac. Surg*., 84(3), 729-736.

Dohmen, P.M., Lembcke, A., Holinski, S., Pruss, A., Konertz, W. (2011) Ten years of clinical results with a tissue-engineered pulmonary valve. *Ann. Thorac. Surg*., 92(4), 1308-1314.

Dreger, S.A., Thomas, P., Sachlos, E., Chester, A.H., Czernuszka, J.T., Taylor, P.M., yacoub, M.H. (2006) Potential for synthesis and degradation of extracellular matrix proteins by vave interstitial cells seeded onto collgen scaffolds. *Tissue engineering*, 12(9), 2533-2540.

Du, L., Wu, X., Pang, K., Yang, Y. (2011) Histological evaluation and biomechanical characterisation of an acellular porcine cornea scaffold. *Br. J. Ophthalmol*., 95(3), 410-414.

Dvir, T., Benishti, N., Shachar, M., Cohen, S.A. (2006) A novel perfusion bioreactor providing a homogenous milieu for tissue regeneration. *Tissue Eng*., 12, 2843-2852.

Edmunds, J.H. Jr. (1987) Thrombotic and bleeding complications of prosthetic heart vales. *Annals of Thoracic Surgery*, 44, 430-445.

Eisenberg, E., Levanon, E.Y. (2003). Human housekeeping genes are compact. *TRENDS in Genetics*, 19 (7), 362–365.

Emery, R.W., Mettler, E., Nicoloff, D.M. (1979) A new cardiac prosthesis. The St Jude Medical cardiac valve: *In vivo* results. *Circulation*, 60, 48-54.

Entwistle, J., Zhang, S., Yang, B., *et al*. (1995) Characterization of the murine gene encoding the hyaluronan receptor RHAMM. *Gene*, 163(2), 233-238.

Fang, N., Xie, S., Wang, S., Gao, H., Wu, C., Pan, L. (2007) Constriction of tissue-engineered heart valves by using decellularized scaffolds and endothelial progenitor cells. *Chin. Med. J.*, 120(8), 696-702.

Farivar, R.S., Chen, R.H., adams, D.H. (2001) Xenotransplantation and the endothelium. *Graft*, 4, 355-364.

Farivar, R.S., Filsoufi, F., Adams, D.H. (2003) Mechanisms of Galα1-3Galβ1-4GlcNAc-R (αGal) expression on porcine valve endothelial cells. *Surgery for acquired cardiovascular disease*, 125, 306-341.

Ferraresi, C., Manuello, B.A., Mazza, L., Maffiodo, D., Franco, W. (1999) One-dimensional experimental mechanical characterisatin of porcine aortic root wall. *Med Biol. Eng. Comput*., 37, 202-207.

Filip, D.A., Radu, A., Simionescu, M. (1986) Interstitial cells of the heart valve possess characteristics similar to smooth muscle cells. *Circ. Res*., 59, 310-320.

Fisher, J., Jack, R., Wheatley, D.J. (1986) Design of a function test apparatus for prosthetic heart valves. Initial results in the mitral position. *Clinical Physics & Physiological Measurements*, 7, 63-73.

Fisher, J., Wheatley, D.J. (1988) Hydrodynamic function of ten prosthetic heart valves in the aortic position. *Clin. Phys. Physiol. Meas.*, 9(4), 307-317.

Fisher, J., Watterson, K. (1997) Comparative mechanics of pulmonary an aortic porcine bioprosthetic valve leaflets. In *Advances in Anticalcifica and Antidegenerative Treatment of Heart Valve Bioprostheses*, Chapter 5, Edited by Shlomo Gabbay and David J Wheatley, Silent Partners Inc., Austin.

Fitzpatrick, J.C., Clark, P.M., Capaldi, F.M. (2010) Effect of decellularisation protocol on the mechanical behaviour of porcine descending aorta. International journal of biomatirials, doi: 10.1155/2010/620503.

Fraser, R.B.D., MacRae, T.P., Miller, A., Suzuki, E. (1983) Molecular conformation and packing in collagen fibrils. *J. Mol. Biol*., 167, 497-521.

Freytes, D.O., Badylak, S.F., Webster, T.J., Geddes, L.A., Rundell, A.E. (2004) Biaxial strength of multilaminated extracellular matrix scaffolds. *Biomaterials*, 25, 2353–2361.

Freytes, D.O., Stoner, R.M., Badylak, S.F. (2008) Uniaxial and biaxial properties of terminally sterilized porcine urinary bladder matrix scaffolds. *J. Biomed. Mater Res. B. Appl. Biomater*, 84(2), 408–414.

Fukuhara, S., Tomita, S., yamashiro, S., *et al*. (2003) Direct cell-cell interaction of cardiomyocytes is key for bone marrow stromal cells to go into cardiac lineage *in vitro*. *J. Thorac. Cardiovasc. Surg.*, 125, 1470-1480.

Funamoto, S., Nam, K., Kimura, T., Murakoshi, A., Hashimoto, Y., Niwaya, K., *et al.* (2010) The use of high-hydrostatic pressure treatment to decellularize blood vessels. *Biomaterials*, 31(13), 3590–3595.

Gabbay, S., McQueen, D.M. *et al*. (1978) *In vitro* hydrodynamic comparison of mitral valve prostheses at high flow rates. *Journal of Thoracic & Cardiovascular Surgery*, 76, 771-788.

Galili, U., Rachmilewitz, E.A., Peleg, A., Flechner, I. (1984) A unique natural human IgG antibody with anti-alpha-galactosyl specificity. *J. Exp. Med.*, 160, 1519-1531.

Galili, U., Macher, B.A., Buehler, J., Shohet, S.B. (1985) Human natural anti-alpha-galactosyl IgG. II. The specific recognition of alpha (1-3) –linked galactose residues. *J. Exp. Med*., 162, 573-582.

Galili, U., Swanson, K. (1991) Gene sequences suggest inactivation of alpha-1,3-galactosyltransferase in catarrhines after the divergence of apes from monkeys. *Proc. Natl. Acad. Sci. USA*, 88, 7401-7404.

Gandaglia, A., Bangno, A., Naso, F., Spina, M., Gerosa, G. (2011) Cells, scaffolds and bioreactors for tissue-engineered heart valves: a journey from basic concepts to contemporary developmental innovations. *European Journal of Cardio-thoracic Surgery*, 39, 523-531.

Geisler, N., Weber, K. (1982) The amino acid sequence of chicken muscle desmin provides a common structural model for intermediate filament proteins. *Eur. Mol. Biol. Organ*, 1, 1649–1656.

Gere, J.M., Timoshenko, S. (1984) Mechanics of materials, 2nd SI edition, Wadsworth International, 352.

Gerosa, G., Ross, D.N., Bruche, P.E., Dziatkowiak, A., Mohammad, S., Norman, D., Davies, J., Sbarbati, A., Casarotto, D (1994) Aortic valve replacement with pulmonary homografts: early experience. *J. Thorac. Cardiovasc. Surg*., 107, 424-437.

Gilbert, T.W., Freund, J.M., Badylak, S.F. (2009) Quantification of DNA in Biologic scaffold Materials. *Journal of Surgical Research*, 152, 135-139.

Gilbert, T.W., Sellaro, T.L., Badylak, S.F. (2006) Decellularization of tissues and organs. *Biomaterials*, 27, 3675-3683.

Gilbert, T.W., Stewart-Akers, A.M., Simmons-Byrd, A., Badylak, S.F. (2007) Degradation and remodeling of small intestinal submucosa in canine Achilles tendon repair. *J. Bone Joint Surg. Am.*, 89(3), 621-630.

Giusti, S., Bogetti, M.E., Bonafina, A., Fiszer de Plazas, S. (2009) An improved method to obtain a soluble nuclear fraction from embryonic brain tissue. *Neurochem. Res.*, 34(11), 2022–2029.

Goldstein, S., Clarke, D.R., Walsh, S.P., Black, K.S., O'Brien, M.F. (2000) Transpecies heart valve transplant: advanced studies of a bioengineered xeno-autograft. *Ann. Thorac. Surg.*, 70(6), 1962-1969.

Gong, G., Seifter, E., Lyman, W.D., Factor S.M., Blau, S., Frater, R.W. (1993) Bioprosthetic cardiac valve degeneration: role of inflammatory and immune reactions. *J. Heart valve Dis*., 2, 684-693.

Gorschewsky, O., Puetz, A., Riechert, K., Klakow, A., Becker, R. (2005) Quantitative analysis of biochemical characteristics of bone-patellar tendon-bone allografts. *Biomed. Mater Eng.*, 15(6), 403-411.

Gouk, S.S., Lim, T.M., Teoh, S.H., Sun, W.Q. (2008) Alterations of human acellular tissue matrix by gamma irradiation: histology, biomechanical property, stability, in vitro cell repopulation, and remodeling. *J. Biomed. Mater Res. B. Appl. Biomater.*, 84(1), 205–217.

Grabenwoger, M., Sider, J. *et al*. (1996) Impact of glutaraldehyde on calcification of pericardial bioprosthetic heart valve material. *Annals of Thoracic Surgery*, 62, 772-774.

Grayson, A.C., Voskerician, G., Lynn, A., Anderson, J.M., Cima, M.J., Langer, R. (2004) Differential degradation rates in vivo and in vitro of biocompativle poly (lactic acid) and poly (glycolic acid) homo- and co-polymers for a polymeric drug-delivery microchip. *J. Biomater. Sci. Poym. Ed.*, 15, 1281-1304.

Grauss, R.W., Hazekamp, M.G., Oppenhuizen, F., van Munsteren, C.J., Gittenberger-de Groot, A.C., DeRuiter, M.C. (2005) Histological evaluation of decellularised porcine aortic valves: matrix changes due to different decellularisation methods. *Eur. J. Cardiothorac. Surg.*, 27(4), 566–571.

Gross, L, Kugel, M.A. (1931) Topographic anatomy and histology of the valves in the human heart. *Am. J. Pathol.*, 7, 445-473.

Gulati, A.K. (1988) Evaluation of acellular and cellular nerve grafts in repair of rat peripheral nerve. *J. Neurosurg.*, 68, 117–123.

Grunkemeier, G.L, Rahimtoola, S.H. (1990) Artificial heart valves. *Annal. Review of Medicine*, 41, 251-263.

Grunkemeier, G.L., Li, H.H., Naftel, D.C., Starr, A., Rahimtoola, S.H. (2000) Long term performance of heart valve prostheses. *Curr. Probl. Cardiol.*, 25, 73-154.

Gunatillake, P.A., Adhikari, R. (2003) Biodegradable dynthetic polymers for tissue engineering. *European Cells and Materials*, 5, 1-16.

Hammer, C. (2003). Xenotrasplantation: the good, the bad, and the ugly or how far are we to clinical application? *Transplantion Proceedings*, 35, 1256-1257.

Haralson, M. A. & Hassell, J. R. (1995). Extracellular Matrix, A Practical Approach. Oxford University Press. New york.

Hawkins, J. A., Hillman, N. D., Lambert, L. M., Jones, J., Di Russo, G. B., Profaizer, T., Fuller, T. C., Minich, L. L., Williams, R. V., & Shaddy, R. E. (2003) Immunogenicity of decellularized cryopreserved allografts in pediatric cardiac surgery: comparison with standard cryopreserved allografts. *J. Thorac. Cardiovasc. Surg.*, 126**,** 247-252.

Hilbert, S.L., Yanagida, R., Souza, J., Wolfinbarger, L., Jones, A.L., Krueger, P., *et al.* (2004) Prototype anionic detergent technique used to decellularize allograft valve conduits evaluated in the right ventricular outflow tract in sheep. *J. Heart Valve Dis.*, 13, 831–840.

Hilfiker, A., Kasper, C., Hass, R., Haverich, A. (2011) Mesenchymal stem cells and progenitor cells in connective tissue engineering and regenerative medicine: is there a

future for transplantation? *Langenbecks Arch Surg*., 396(4), 489-497.

Hjortnaes, J., Bouten, C.V.C, Van Herwerden, L.A., Grundeman, P.F., Kluin, J. (2009) Translating autologous heart valve tissue engineering from bench to bed. *Tissue Eng*., 15, 307-317.

Hodde, J.P., Badylak, S.F., Brightman, A.O., Voytik-Harbin, S.L. (1996) Glycosaminoglycan content of small intestinal submucosa: a bioscaffold for tissue replacement. *Tissue engineering*, 2, 209-217.

Hodde, J.P., Hiles, M. (2002) Virus safety of a porcine-derived medical device: evaluation of a viral inactivation method. *Biotechnol. Bioeng.*, 79(2), 211–216.

Hoerstrup, S.P., Sodian, R., Daebritz, S., Wang, J., Bacha, E.A., Martin, D.P., Moran, A.M., Guleserian, K.J., Sperling, J.S., Kaushal, S., Vacanti, J.P., Schoen F.J., Mayer, J.E. (2000) Functional living trileaflet heart valves grown *in vitro*. *Circulation*, 102, 44–49.

Hogan, P.G., O'Brien, M.F. (2003) Improving the allograft valves: Does the immune response matter? *The Journal of Thoracic and Cardiovascular Surgery*, 126(5), 1251-1253.

Hokken, R.B., Bartelings, M.M., Bogers, J.J.C., Gittenberger-de Groot, A.C. (1997) Morphology of the pulmonary and aortic roots with regard to the pulmonary autograft procedure. *J. Thorac. Cardiovasc. Surg*., 113, 453-461.

http://en.wikipedia.org/wiki/File:Diagram_of_the_human_heart_(cropped).svg (Diagram of the human heart)

Hudson, T.W., Liu, S.Y., Schmidt, C.E., (2004) Engineering an improved acellular nerve graft via optimized chemical processing. *Tissue Eng.*, 10(9–10), 1346–1358.

Hynes, R.O. (1990). Fibronectins. Springer-Verlag Inc, New York.

Jackson, D.W., Grood, E.S., Wilcox, P., Butler, D.L., Simon, T.M., Holden, J.P. (1988)

The effects of processing techniques on the mechanical properties of bone–anterior cruciate ligament–bone allografts. An experimental study in goats. *Am. J. Sports Med*, 16, 101–105.

Jackson, D.W., Grood, E.S., Cohn, B.T., Arnoczky, S.P., Simon, T.M., Cummings, J.F. (1991) The effects of in situ freezing on the anterior cruciate ligament. An experimental study in goats. *J. Bone Joint Surg. Am.*, 73, 201–213.

Jamieson, W.R., Burr, L.H., Tyers, G.F., *et al.* (1995) Carpentier-Edwards supra-annular porcine bioprosthesis: clinical performance to twelve years. *Ann. Thorac. Surg*., 60, S235-240.

Jashari, R., Goffin, Y., Van Hoeck, B., Vanderkelen, A., Du Verger ,A., Fan, Y., Holovska, V., Fagu, A., Brahy, O. (2010) Belgian and European experience with the European Homograft Bank (EHB) cryopreserved allograft valves.--assessment of a 20 year activity. *Acta. Chir. Belg*., 110(3), 280-290.

Jennings, L.M. (2001) The pulmonary bioprosthetic valve, PhD Thesis, Mechanical engineering Department, University of Leeds.

Jiang, W.H., Ma, A.Q., Zhang, Y.M. *et al*. (2005) Migration of intravenously grafted mesenchymal stem cells to injured heart in rats. *Sheng Li Xue Bao*, 57, 566-572.

Jockenhoevel, S., Zund, G., Hoerstrup, S.P., Chalabi, K., Sachweh, J.S., Demircan, L., Messmer, B.J., Turina, M. (2001) Fibrin gel—Advantages of a new scaffold in cardiovascular tissue engineering. *Eur. J. Cardiothorac. Surg.*, 19, 424–430.

Joziasse, D.H., Shaper, J.H., Jabs, E.W., Sahper, N.L. (1991) Characterization of an alpha 1,3-galactosyltransferase homologue on human chromosome 12 that is organized as a processed pseudogene. *J. Biol. Chem.*, 266, 6991-6998.

Kano, M., Masuda, Y., Tominaga, T., *et al*. (2001) Collagen synthesis and collagenase activity of cryopreserved heart valves. *J. Thorac. Cardiobasc. Surg*., 122, 706-711.

Kasimir, M.T., Rieder, E., Seebacher, G., *et al.* (2003) Comparison of different decellulariszation procedures of porcine heart valves. *Int. J. Artif. Organs*, 26, 421-427.

Kasimir, M.T., Rieder, E., Seebacher, G., Nigisch, A., Dekan, B., Wolner, E., Weigel, G., Simon, P. (2006) Decellularization does not eliminate thrombogenicity and inflammatory stimulation in tissue-engineered porcine heart valves. *J. Heart Valve Dis.*, 15, 278-286

Kitagawa, T., Masuda, Y., Tominaga, T., Kano, M. (2001) Cellular biology of cryopreserved allograft valves. *J. Med. Invest*., 48, 123-132.

Kitamura, S., Yagihara, T., Kobayashi, J., Nakajima, H., Toda, K., Fujita, T., Ichikawa, H., Ogino, H., Nakatani, T., Taniguchi, S. (2011) Mid- to long-term outcomes of cardiovascular tissue replacements utilizing homografts harvested and stored at Japanese institutional tissue banks. *Surg. Today*, 41(4), 500-509.

Kazuo, N., Knott-Craig, C.J., Lane, M.M., Chandrasekaren, K., Overholt, E.D., Elkins, R.C. (1999) Cryopreserved homograft valves in the pulmonary position: risk analysis for intermediate-term failure. *J. Thorac. Cardiovasc. Surg.*, 117, 141-147.

Khan, S. (1998) Prosthetic heart valve information Page. [Internet] available from: http://www.csmc.edu/cvs/md/valve/vlvtypes.html [Accessed 19th Dec 2007]

Kilian, E., Fries, F., Kowert, A., Vogt, F., Kreuzer, E., Reichart, B. (2010) Homograft implantation for aortic valve replacement since 15 years: results and follow-up. *Heart Surg. Forum*, 13(4), E238-E242.

Kim, W.G., Park, J.K., Lee, W.Y. (2002) Tissue-engineered heart valve leaflets: an effective method of obtaining acellularized valve xenografts. *Int. J. Artif. Organs*, 25 (8), 791-797.

Kim, W.G., Lee, W.Y., Mi Kim, J., Moon, H.J. (2004) tissue-engineered acellularized valve xenografts: a comparative animal study between plain acellularized xenografts and autologous endothelial cell seeded acellularised xenografts. *Int. J. Artif. Organs*,

27(6), 501-508.

Knight, R.L., Booth, C., Wilcox, H.E., Fisher, J., Ingham, E. (2005) Tissue engineering of cardiac valves: re-seeding of acellular porcine aortic valves matrices with human mesenchymal progenitor cells. *The journal of heart valve disease*, 14, 806-813.

Knight, R.L., Wilcox, H.E., Korossis, S.A., Fisher, J., Ingham, E. (2008) Acellular matrices for the tissue engineering of cardiac valves. *J. Engineering in Medicine Proc. IMechE.*, 222 Part H, 129-143.

Kobayashi, J. (2011) Stentless aortic valve replacement: an update. *Vasc. Health Risk Manag.*, 7, 345-351.

Kohn, J., Abramson, S., Langer, R. (2004) *Bioresorbable and bioerodible materials. In: Biomaterials Science:* An Introduction to Materials in Medicine, 2nd edn, (edited by Ratner, B. D., Hoffman, A. S., Schoen, F. J., Lemons, J. E.) Orlando, Academic Press.

Kolf, C.M., Cho, E., Rocky, S.T. (2007) Biology of adult mesenchymal stem cells: regulation of niche, self-renewal and differentiation. *Arthritis research & Therapy*, 9(1), 204.

Kon, N.D., Cordell, A.R., Adair, S.M., *et al*. (1999) Aortic root replacement with the freestyle stentless porcine aortic root bioprosthesis. *Ann. Thorad. Surg*., 67, 1609-1615.

Konakci, K.Z., Bohle, B., Blumer, R., *et al*. (2005) Alpha-Gal on bioprostheses; xenograft immune response in cardiac surgery. *European Journal of Clinical Investigation*, 35, 17-23.

Konertz, W., Dohmen, P.M., Liu, J., Beholz, S., Dushe, S., Posner, S., Lembcke, A., Erdbrugger, W. (2005) Hemodynamic characteristics of the Matrix P decellularized xemograft for pulmonary valve replacement during the Ross oeration. *J. Heart Valve Dis*., 14, 78-81.

Konertz, W., Angeli, E., Tarusinov, G., Christ, T., Kroll, J., Dohmen, P.M., Krogmann,

O., Franzbach, B., Napoleone, C., Gargiulo, G. (2011) Right ventricular outflow tract reconstruction with decellularised porcine xenografts in patients with congenital heart disease. *J. Heart. Valve Dis.*, 20(3), 341-347.

Korossis, S.A., Booth, C., Wilcox, H.E., Watterson, K.G., Kearney, J.N., Fisher, J., Ingham, E. (2002) Tissue engineering of cardiac valve prostheses II: biomechanical characterization of decellularized porcine aortic heart vales. *The Journal of Heart Valve Disease*, 11, 463-371.

Korossis, S.A., Wilcox, H.E., Watterson, K.G., Kearney, J.N., Ingham, E., Fisher, J. (2005) In-vitro assessment of the functional performance of the decellularized intact porcine aortic root. *The Journal of Heart Valve Disease,* 14 (3), 408-422.

Koulaouzidou, E.A., Margelos, J., Beltes, P., Kortsaris, A.H. (1999). Cytotoxic effects of different concentrations of neutral and alkaline EDTA solutions used as root canal irrigants. *Journal of endodontics*. 25(1), 21-23.

Ku, C., Johnson, P.H., Batten, P. *et al*. (2006) Collagen synthesis by mesenchymal stem cells and aortic valve interstitial cells in response to mechanical stretch. *Cardiovascular Research*, 71, 548-556.

Kuwaki, K., Tseng, Y.L., Dor, F.J., Shimizu, A., Houser, S.L., Sanderson, T.M., Lancos, C.J., Prabharasuth, D.D., Cheng, J., Moran, K., Hisashi, Y., Mueller, N., Yamada, K., Greenstein, J.L., Hawley, R.J., Patience, C., Awwad, M., Fisman, J.A., Robson, S.C., Schuurman, H.J., Sachs, D.H., Cooper, D.K. (2005) Heart transplantation in baboons using alpha 1,3-galactosyltransferase gene-knockout pigs as donors: initial experience. *Nat. Med.*, 11, 29-31.

Lai, L., Kolber-Simonds, D., Park, K.W., Cheong, H.T., Greenstein, J.L., Im, G.S., Samuel, M., Bonk, A., Rieke, A., Day, B.N., Murphy, C.N., Carter, D.B., Hawley, R.J., Prather, R.S. (2002) Production of alpha-1,3-galactosyltransferase knockout pigs by nuclear transfer coning. *Science*, 295,1089-1092.

Langer, R., Vacanti, J.P. (1993) Tissue engineering. *Science*, 260, 920-926.

Lanza, R., Langer, R., Vancanti, J. Edt. (2007) *Principles of tissue engineering*, 3rd edn. San Diego, Elsevier Academic Press.

Latif, N., Sarathchandra, P., Thomas, P., Antoniw, J., Baten, P., Chester, A.H., Taylor, P.M., Yacoub, M.H. (2007) Characterization of structural and signaling molecules by human valve interstitial cells and comparison to human mesenchymal stem cells. *The Journal of Heart Valve Disease*, 16, 56-66.

Lazarides, E., Hubbard, B.D. (1976) Immunological characterization of the subunit of the 100A filaments from muscle cells. *Proc. Natl. Acad. Sci. USA*, 73, 4344–4348.

Leask, R.L., Jain, N., Butany, J. (2003) Endotheliam and valvular diseases of the heart. *Microsc. Res. Tech*., 60, 129-137.

Lee, J.M., Courtman, D.W., Boughner, D.R. (1984a) The glutaraldehyde-stablized porcine aortic valve xenograft I. Tensile viscoelastic properties of the fresh leaflet material. *J. Biomed. Mater. Res.*, 18, 61-77.

Lee, J.M., Boughner, D.R., Courtman, D.W. (1984b) The glutaraldehyde-stabilized porcine aortic valve xenograft II. Effect of fixation with or without pressure on the tensile viscoelastic properties of the leaflet material. *J. Biomed. Mater. Res.*, 18, 79-98.

Lee, J.A. (2006) Medline Plus [Internet] available from http://www.nlm.nih.gov/medlineplus/ency/ imagepages/18092.htm [accessed 8th Dec, 2007]

Lee, D.J., Steen, J., Jordan, J.E., Kincaid, E.H., Kon, N.D., Atala, A., Berry, J., Yoo, J.J. (2009) Endothelialization of heart valve matrix using a computer-assisted pulsatile bioreactor. *Tissue Eng. Part A*, 15, 807–814.

Lee, C., Park, C.S., Lee, C.H., Kwak, J.G., Kim, S.J., Shim, W.S., Song, J.Y., Choi, E.Y., Lee, S.Y. (2011) Durability of bioprosthetic valves in the pulmonary position: long-term follow-up of 181 implants in patients with congenital heart disease. *J. Thorac.*

Cardiovasc. Surg., 142(2), 351-358.

Lefrak, E.A., Starr, A. (1979) *Cardiac valve prostheses*. Appleton-Century-Crofts, New York.

Lehr, E.J., Rayat, G.R., Chiu, B., Churchill, T., McGann L.E., Coe, J.Y., *et al.* (2011) Decellularization reduces immunogenicity of sheep pulmonary artery vascular patches. *J. Thorac. Cardiovasc. Surg*., 141, 1056-1062

Levick, J.R. (2003) *An introduction to cardiovascular physiology*. 4th edn, London, Arnold.

Levy, M.N., Pappano, A.J. (2007) *Cardiovascular physiology*. 9th edn, Philadephia, Mosby, Inc.

Lewis, K.B., Teller, D.C., Fry, J., Lasser, G.W., Bishop, P.D. (1993) Crosslinking kinetics of the human transglutaminase, factor XIII[A2], acting on fibrin gels and g-chain peptides. *Biochemistry*, 36, 995–1002.

Leyh, R.G., Whilhelmi, M., Reba, P., *et al.* (2003) *In vivo* repopulation of xenogeneic and allogeneic acellular valve matrix conduits in the pulmonary circulation. *Ann. Thorac. Surg.*, 75, 1457-1463.

Li, Z., Mericskay, M., Agbulut, O., Butler-Browne, G., Carlsson, L., Thornell, L.E., Babinet, C., Paulin, D. (1997) Desmin Is Essential for the Tensile Strength and Integrity of Myofibrils but Not for Myogenic Commitment, Differentiation, and Fusion of Skeletal Muscle. *J. Cell Biol*., 139 (1), 129–144.

Lila, N., Mcgregor, C., Carpentier, S., Rancic, J., Byrne, G.W., Carpentier, A. (2010) Gal knockout pig pericardium: new source of material for heart valve bioprostheses. *J. Heart Lung Transplant*, 29, 538-543.

Livi, U., Abdulla, A., Parker, R., Olsen, E.J., Path, F.R.C., Ross, D.N. (1987) Viability and morphology of aortic and pulmonary homografts. *J. Thorac. Cardiovasc. Surg.*, 93,

755-760.

Llevadot, J., Murasawa, S., Kureishi, Y., *et al*. (2001) HMG-CoA reductase inhibitors (statins) increase endothelial progenitor cells via the PI 3-kinase/Akt pathway. *J. Clin. Invest*., 108, 391-397.

Lockie, K.J., Butterfield, M., Fisher, J., Juster, N.P., Watterson, K., Davies, G.A. (1993) Geometry of homograft valve leaflets: Effect of dilation of the aorta and the aortic root. *Ann Thorac Surg*., 60, 374-378.

Lockie, K.J., Fisher, J., Juster, N.P., Davies, G.A., Watterson, K. (1994) Biomechanics of glutaraldehyde-treated porcine aortic roots and valves. An investigation of the effect of predilation of the elastic aortic root. *J. Thorac. Cardiovasc. Surg.*, 108(6), 1037-1042.

Lotze, M.T., Deisseroth, A., Rubartelli, A. (2007) Damage associated molecular patternmolecules. *Clin. Immunol.*, 124, 1-4.

Lower, R., Stofer, R.C., Shumway, E.N. (1960) Autotransplantation of the pulmonic valve into the aorta. *J. Thorac. Cardiovasc. Surg.*, 17, 176-177.

Magnus, K. Magnusson & Deane F. (1998). Fibronectin: structure, assembly, and cardiovascular implications. *Arteriosclerosis Thrombosis and Vascular Biology.* 18(9), 1363-1370.

Mahler, G.J., Butcher, J.T. (2011) Inflammatory regulation of valvular remodeling: The Good (?), the bad, and the ugly. International Journal of Inflammation. Doi: 10.4061/2011/721419.

Majumdar, M.K, Thiede, M.A., Mosca, J.D. *et al*. (1998) Phenotypic and functional comparison of cultures of marrow-derived mesenchymal stem cells (MSC) and stromal cells. *J. Cell Physiol*., 176, 57-66.

Makino, S., Fukuda, K., Miyoshi, S., *et al*. (1999) Cardiomycytes can be generated from marrow stromal cells in vitro. *J. Clin. Invest.*, 103, 697-705.

Manji, R.A., Zhu, L.F., Nijjar, N.K., Rayner, D.C., Korbutt, G.S., Churchill, T.A., Rajotte, R.V., Koshal, A., Ross, D.B. (2006) Glutaraldehyde-fixed bioprosthetic heart valve conduits calcify and fail from xenograft rejection. *Circulation*, 114, 318-327.

Marks, C., Marks, P. H. (1993) *Fundamentals of Cardiac surgery.* London, Chapman& Hall.

Marron, K., Yacoub, M.H., Polak, J.M., Sheppard, M.N., Fagan, D., Whitehead, B.F., de Leval, M.R., Anderson, R.H., Wharton, J. (1996) Innervation of human atrioventricular and arterial valves. *Circulation*, 94, 368-375.

Martini, F.H. (1995) *Fundamentals of anatomy and physiology*. 3rd Edn, Prentice-Hall.

Martini, F.H. (2006) *Fundamentals of anatomy and physiology*. 7rd Edn, Prentice-Hall.

Mavrilas, D., Sinouris, E.A., Vynios, D.H., Papageorgakopoulou, N. (2005) Dynamic mechanical characteristics of intact and structurally modified bovine pericardial tissues. *J. Biomech*, 38, 1483-1490.

Mayne, A.S.D., Christie, G.W., Smaill, B.H., Hunter, P.J., Barratt-Boyes B.G. (1989) An assessment of the mechanical properties of leaflets from four second-generation porcine bioprosthese with biaxial testing techniques. *J. Thorac. Cardiovasc. Surg*., 98, 170-180.

McCoy, S.L., Kurtz, S.E., Hausman, F.A., *et al*. (2004) Activation of RAW264.7 macrophages by bacterial DNA and lipopolysaccharide increases cell surface DNA binding and internalization. *J. Biol. Chem.*, 279(17), 17217-17223.

McGregor, C.G.A., Carpentier, A., Lila, N., Logan, J.S., Byrne, G.W. (2011) Cardiac xenotransplantation technology provides materials for improved bioprosthetic heart valves. *J. Thorac. Cardiovasc. Surg*., 141, 269-275.

Medical image reference center/cardiovascular (2000) [Internet] available from http://medirec.ncvc.go.jp/g7/owa/refsearch.ref_detail?regist=200408115737 [accessed

3rd Dec, 2007]

Mendelson, K. & Schoen, F.J. (2006) Heart valve tissue engineering: concepts, approaches, progress, and challenges. *Annals of Biomedical Engineering*, 34(2) 1799-1819.

Mercuri, J.J., Lovekamp, J.J., Simionescu, D.T., Vyavahare, N.R. (2007) Glycosaminoglycan-targeted fixation for improved bioprosthetic heart valve stabilization. Biomaterials, 28, 496–503.

Merryman, W.D., Youn, I., Lukoff, H.D., Krueger, P.M., Guilak, F., Hopkins, R.A., Sacks, M.S. (2006) Correlation between heart valve interstitial cell stiffness and transvalvular pressure: implications for collagen biosynthesis, *Am. J. Physil. Heart Circ. Physiol., 290*, H224-H231.

Mertsching, H., Hansmann, J. (2009) Bioreactor technology in cardiovascular tissue engineering. *Adv Biochem Engin/Biotechnol*., 112, 29-37.

Messier, R.H., Bass, B.L., Domkowski, P.W., Hopkins, R.A. (1999) Institial cellular and matrix restoration of cardiac valves after cryopreservation. J. *Thorac. Cardiovasc. Surg*., 118, 36-49.

Meyer, S.R., Chiu, B., Churchill, T.A., Zhu, L., Lakey, J.R., Ross, D.B. (2006) Comparison of aortic valve allograft decellularization techniques in the rat. *J. Biomed. Mater Res. A,* 79(2), 254–262.

Mikos, A.G., Temenoff, J.S. (2000) Formation of highly porous biodegradable scaffolds for tissue engineering. *Electron J. Biotechnol,* 3, 114-119.

Mirsadraee, S (2005) Tissue engineering of pericardium. PhD Thesis, School of Medicin, University of Leeds.

Mirsadraee, S., Wilcox, H. E., Korossis, S. A., Kearney, J. N., Watterson, K.G., Fisher, J., Ingham, E. (2006) Development and characterization of an acellular human

pericardial matrix for tissue engineering. *Tissue Engineering*, 12, 763-773.

Mol, A., Driessen, N.J., Rutten, M.C., Hoerstrup, S.P., Bouten, C.V., Baaijens, F.P. (2005) Tissue engineering of human heart valve leaflets: a novel bioreactor for a strain-based conditioning approach. *Ann. Biomed. Eng*., 33, 1778-1788.

Moreau, M.F., Gallois, Y., Basle, M.F., Chappard, D. (2000) Gamma irradiation of human bone allografts alters medullary lipids and releases toxic compounds for osteoblast-like cells. *Biomaterials*, 21(4), 369-376.

Mulholland, D.L., Gotlieb, A.I. (1996) Cell biology of valvular interstitial cells. *Can. J. Cardiol*., 12, 231-236.

Mulinari, L.A., Navarro, F.B., Pimentel, G.K., Miyazaki, S.M., Binotto, C.N., Pelissari, E.C., Miyague, N.I., da Costa, F.D. (2008) The use and midium-term evaluation of decellularized allograft cusp in the surgical treatment of the tetralogy of fallot. *Rev. Bras. Cir. Cardiovasc*., 23(2), 197-203.

Nagata, S., Hanayama, R. (2010) Autoimmunity and the clearance of dead cells. *Cell*, 140(5), 619-630.

Nagy, Z.L., Fisher, J., Walker, P.G., Watterson, K.G. (2000) The *in vitro* hydrodynamic characteristics of the porcine pulmonary valve and root with regard to the Ross procedure. *The Journal of Thoracic and Cardiovascular Surgery*, 120(2), 284-290.

Navarro, F.B., Costa, F.D.A., Mulinari, L.A., Pimentel, G.K., Roderjan, J,G., Vieira, E.D., Noronha, L., Miyague, N.I. (2010) Evaluation of the biological behaviour of decellularized pulmonary homografts: an experimental sheep model. *Rev. Bras. Cir. Cardiovasc*, 25(3), 377-387.

Newby, C.S., Barr, R.M., Greaves, M.W., Mallet, A.I. (2000). Cytokine release and cytotoxicity in human keratinocytes and fibroblasts induced by phenols and sodium dodecyl sulfate. *The Journal of investigative dermatology.* 115(2), 292-298.

Niwaya, K., Knott-Craig, C.J., Lane, M.M., Chandrasekaren, K., Overholt, E.D., Elkins, R.C. (1999) Cryopreserved homograft valves in the pulmonary position: risk analysis for intermediate-term failure. *J. Thorac. Cardiovasc. Surg*., 117(1), 141-146.

O'Brien, M.F. Stafford, E.G. *et al*. (1987) A comparison of aortic valve replacement with viable cryopresserved and fresh allografts valves with a note on chromosomal studies. *Journal of Thoracic & Cardiovascular Surgery*, 94, 812-823.

O'Brien, M.F., Goldstein, S., Walsh, S., Black, K.S., Elkins, R., Clarke, D. (1999) The SynerGraft valve: a new acellular (nonglutaraldehyde-fixed) tissue heart valve for autologous recellularization first experimental studies before clinical implantation. *Semin Thorac Cardiovasc Surg*, 11(4 Suppl 1), 194-200.

Oei, F.B.S., Welters, M.J.P., Vaessen, L.M.B., Stegmann, P.A., ogers, A.J.J.C., Weimar, W. (2000) Induction of cytotoxic T lymphocytes with destructive potential after cardiac valve homograft implantation. *The Journal of Heart valve Disease*, 9, 761-468.

Oei, F.B., Stegmann, A.P., van der Ham, F., *et al*., (2002) The presence of immune stimulatory cells in fresh and cryopreserved donor aortic and pulmonary valve allografts. *J. Heart valve Dis*., 11, 315-324.

Ohnishi, S., Nagaya, N. (2007) Prepare cells to repair the heart: mesenchymal stem cells for the treatment of heart failure. *Am. J. Nephro.*, 27, 301-307.

Ohshima, N., Yanagi, K., Miyoshi, H. (1997) Packed-bed type reactor to attain high density culture of hepatocytes for use as a bioartificial liver. Artif. Organs, 21, 1169-1176.

Okamura, K., Chiba, C., Iriyama, T., Itoh, T., Maeta, H., Ijima, H., Mitsui, T., Hori, M. (1980) Antigen depressant effect of glutaraldehyde for aortic heterografts with a valve, with special reference to a concentration right fit for the preservation of grafts. *Surgery*, 87,170-176.

Oriol, R., Ye, Y., Koren, E., Cooper, D.K. (1993) Carbohydrate antigens of pig tissues

reacting with human natural antibodies as potential targets for hyperacute vascular rejection in pig-to-man organ xenotransplantation. *Transplantation*, 56, 1433-1442.

Orlic, D., Kajstura, J., Chimenti, S., Limana, F., Jakoniuk, I., Quaini, F., Nadal-Ginard, B., Bodine, M., Leri, A., Anversa, P. (2001) Mobilized bone marrow cells repair the infarcted heart, improving function and survival. *Proc. Natl. Acad. Sci*., 98, 10344-10349.

Oswald, J., Boxberger, S., Jorgensen, B., Feldmann, S., Ehninger, G., Bornhauser, M., Werner, C. (2004) Mensenchymal stem cells can be differentiated into endothelial cells *in vitro*. *Stem Cells*, 22, 377-384.

Owen, S.C., Shoichet, M.S. (2010) Design of three-dimentional biomimetic scaffolds. *J. Biomed. Mater Res. Part A*, 94A, 1321-1331.

Oxenham, H., Bllomfield, P., Wheatley, D.J., Lee, R.J., Cunningham, J., Prescott, R.J., Miller, H.C. (2003) Twenty years comparison of a Bjork-Sjiley mechanical heart valve with porcine bioprotheses. *Heart*, 89, 715-721.

Pachence, J.M. (1996) Collagen-based devices for soft tissue repair. *Journal of Biomedical Materials Research*, 33, 35-40.

Patel, N., Solanki, E., Picciani, R., Cavett, V., Caldwell-Busby, J.A., Bhattacharya, S.K. (2008) Strategies to recover proteins from ocular tissues for proteomics. *Proteomics*, 8(5), 1055–1070.

Petersen, T.H., Calle, E.A., Zhao, L., Lee, E.J., Gui L., Raredon, M.B. *et al.* (2010) Tissue-engineered lungs for in vivo implantation. *Science*, 329 (5991), 538–541.

Phelps, C.J., Koike, C., Vaught, T.D., Boone, J., Wells, K.D., Chen, S.H., Ball, S., Specht, S.M., Polejaeva, I.A., Monahan, J.A., Jobst, P.M., Sharma, S.B., Lamborn, A.E., Garst, A.S., Moore, M., Demetris, A.J., Demetris, A.J., Rudert, W.A., Bottino, R., Bertera, S., Trucco, M., Starzl, T.E., Dai, Y., Ayares, D.L. (2003) Production of alpha 1,3-galactosyltransferase-deficient pigs. *Science*, 299, 411-414.

Pruss, A., Kao, M., Kiesewetter, H., von Versen, R., Pauli, G. (1999) Virus safety of avital bone tissue transplants: evaluation of sterilization steps of spongiosa cuboids using a peracetic acid–methanol mixture. *Biologicals.*, 27, 195–201.

Rahimtoola, S.H. (2010) Choice of prosthetic heart valve in adults an update. *J. Am. Coll. Cardio*l., 5, 2413-2426.

Ramzi, S., Vinay Kumar, C, Collins, T., eds. (1999). Robbins pathological basis of disease. Philadelphia, PA: WB Saunders Co.

Rapoport, H. S., Connolly, J. M., Fulmer, J., *et al*. (2007) Mechanisms of the in vivo inhibition of calcification of bioprosthetic porcine aortic valve cusps and aortic wall with triglycidylamine/mercapto bisphosphonate. *Biomaterials*, 28, 690-699.

Ravazzola, M., Orci, L. (1989) Alpha-smooth muscle actin, a differentiation marker of smooth muscle cells, is present in microfilamentous bundles of pericytes. *J. Histochem. Cytochem.*, 37(3), 315-321.

Rector and Visitors (University of Virginia) (2007) [Internet] Cardiovascular diseases. available from http://www.healthsystem.virginia.edu/uvahealth/adult_cardiac/valves.cfm [accessed 7th Dec, 2007]

Reing, J.E., Brown, B.N., Daly, K.A., Freund, J.M., Gilbert T.W., Hsiong, S.X., *et al.* (2010) The effects of processing methods upon mechanical and biologic properties of porcine dermal extracellular matrix scaffolds. *Biomaterials*, 31(33), 8626–8633.

Rich, A., Crick, F.H.C (1961) the molecular structure of collagen. *J. Mol. Biol*., 3, 483-506.

Rieder, E., Kasimir, M.T., Silberhumer, G., Seebacher, G., Wolner, E., Simon, P. (2004) Decellularization protocols of porcine heart valves differ importantly in efficiency of cell removal and susceptibility of the matrix to recellularization with human vascular

cells. *J. Thorac. Cardiovasc. Surg*, 127(2), 399–405.

Robarts *et al*. (1997) [Internet] Background of heart valves and their function. available from http://heartlab.robarts.ca/what.is.2.html [accessed 8th Dec, 2007]

Roberts, T.S., Drez, D., McCarthy, W., Paine, R. (1991) Anterior cruciate ligament reconstruction using freeze-dried, ethylene oxide-sterilized, bone–patellar tendon–bone allografts. Two year results in thirty-six patients. *Am. J. Sports Med.*, 19, 35–41.

Routledge, S.J., Hewitt, C.J., Bora, N., Bill, R.M. (2011) Antifoam addition to shake flask cultures of recombinant Pichia pastoris increases yield. *Microb. Cell Fact*., 22,10-17.

Rosario, D.J., Reilly, G.C., Ali, Salah, E., Glover, M., Bullock, A.J., Macneil, S. (2008) Decellularization and sterilization of porcine urinary bladder matrix for tissue engineering in the lower urinary tract. *Regen. Med.*, 3(2), 145-156.

Ross, D.N. (1962) Homograft replacement of the aortic valve. *Lancet*, 2, 487.

Ross, D.N. (1967) Replacement of aortic and mitral valves with a pulmonary autograft. *Lancet*, 2, 956-969.

Ross, D.N. (1989) The versatile homograft and autograft valve. *Annals of Thoracic Surgery*, 48, 569-570.

Ruel, J., Lachance, G. (2009) A new bioreactor for the development of tissue – engineered heart valves. *Annals of Biomedical Engineering*, 37(4), 674-681.

Ruffer, A., Purbojo, A., Cicha, I., Glockler, S.P., Dittrich, S., Cesnjevar, R.A. (2010) Early failure of xenogenous de-cellularised pulmonary valve conduits – a word of caution! *European Journal of Cardio-thoracic Surgery*, 38, 78-85.

Sacks, M.S., Yoganathan, A. (2007) Heart valve function: a biomechanical perspective. *Phil. Trans. R. Soc. B*., 362, 1369-1391.

Sacks, M.S., Merryman, W.D., Schmidt, D.E. (2009) On the biomechanics of heart valve function. *Journal of Biomechnics*, 42, 1804-1824.

Sadler, J.E., (1998) Biochemistry and genetics of von Willebrand factor. *Annu. Rev. Biochem.*, 67, 395–424.

Sagripanti, J.L., Bonifacino, A. (2000) Cytotoxicity of liquid disinfectants. *Surgical Infection* (Larchmt), 1(1), 3-14.

Sacks, M.S., Yoganathan, A.P. (2007) Heart valve function: a biomechanical perspective. *Phil. Trans. R. Soc*., 362, 1369-1391.

Sales, V.L., Mettler, B.A., Engelmayr, G.C. Jr., Aikawa, E., Bischoff, J., Martin, D.P., Exarhopoulos, A., Moses, M.A., Schoen, F.J., Sacks, M.S., Mayer, J.E. Jr. (2010) Endothelial progenitor cells as a sole source for ex vivo seeding of tissue-engineered heart valves. *Tissue Eng. Part A*, 16(1), 257-267.

Sapirstein, J.S., Smith, P.K. (2001) The “ideal” replacement heart valve. *American Heart Journal*, 141(5), 856-860.

Sauren, A.A.H.J., Kuijpers, W., Van Steenhoven, A.A., Veldpause, F.E. (1980) Aortic valve histology and its relation with mechanics: Preliminary report. *J. Biomech.*, 13, 97-104.

Schenke-Layland, K., Vasilevski, O., Konig, F., Riemann, I., Halbhuber, K.J., Wahlers, T., Stock, U.A. (2003) Impact of decellularisation of xenogeneic tissue on extracellular matrix intergrity for tissue engineering of heart valves. *Struct. Biol*., 143, 201-208.

Schmidt, D., Breymann, C., Weber. A., *et al*. (2004) Umbilical cord blood derived endothelial progenitor cells for tissue engineering of vascular grafts. *Ann. Thorac. Surg.*, 78, 2094-2098.

Schmidt, D., Stock, U.A., Hoerstrup, S.P. (2007) Tissue engineering of heart valves

using decellularized xenogeneic or polymeric starter matrices. *Phil. Trans. R. Soc. B*, 362, 1505-1512.

Schmidt, C.E., Baier, J.M. (2000) Acellular vascular tissues: natural biomaterials for tissue repair and tissue engineering. *Biomaterials*, 21, 2215-2231.

Schoen, F.J., Titus, T., Lawrie, G.M. (1982) Bioengineering aspects of heart valve replacement. *Annals. of Biomedical Engineering*, 10, 97-128.

Schoen, F.J., Levy, R.J., (1986) Pathophysiology of bioprosthetic heart valve calcification. In *Biologic & bioprosthetic valves.* Eds. Bodnar, E. & Yacoub, M.H. Yorke Medical Books, New York. 418-429.

Schoen, F.J., Mitchell, R.N., Jonas, R.A. (1995) Pathological considerations in cryopreserved allograft heart valves. *J. Heart valve Dis*., 4, 72-75.

Schoen, F.J. (1998) Pathological findings in explanted clinical bioprosthetic valves fabricated from photooxidised bovine pericardium. *Journal of heart valve diseases*, 7, 174-179.

Schoen, F.J. (1999a) Future directions in tissue heart valves: impact of recent insights from biology and pathology. *Journal of Heart Valve Disease*, 8, 350-358.

Schoen, F. J. (1999b). Future Directions in Tissue Heart Valves: Impact of Recent Insights from Biology and Pathology. *Journal of Heart Valve Disease*. 8, 350-358.

Schoen, F.J. (2001) Are immune mechanisms important in tissue heart valve failure? A debate. *J. Heart Valve Dis*., 10, 458-459.

Schoen, F.J., Levy, R.J. (2005) Calcification of tissue heart valve substitutes: progress toward understanding and prevention. *Ann. Thorac. Surg.*, 9, 1072-1080.

Schoen, F.J. (2011a) Mechanisms of Function and Disease of Natural and Replacement Heart Valves. *Annu. Rev. Pathol.*, [Epub ahead of print].

Schoen, F.J. (2011b) Heart valve tissue engineering: *quo vadis*? *Current Opinion in Biotechnology*, 22, 698-705.

Schenke-Layland, K., Opitz, F., Gross, M., Doring, C., Halbhuber, K.J., Schirrmeister, F., Wahlers, T., Stock, U.A. (2003) Complete dynamic repopulation of decellularized heart valves by application of defined physical signals – an *in vitro* study. *Cardiovasc. Res.*, 60, 497-509.

Schurch, W., Seemayer, R.A., Gabbiani, G. (1998) The myofibroblast: a quarter century after its discovery. *Am. J. Surg. Pathol.*, 22, 141-147.

Scott, M., Vesely, I (1995) Aortic valve cusp microstructure: the role of elastin, *Ann. Thorac. Surg.* 60 (2 Suppl), S391–S394.

Seddon, A.M., Curnow, P., Booth, P.J (2004) Membrane proteins, lipids and detergents: not just a soap opera. *Biochimi. Biophys. Acta.*, 1666 (1-2), 105-117.

Seebacher, G., Grasl, C., Grasl, C., Stoiber, M., Rieder, E., Kasimir, M., Dunkler, D., Simon, P., Weigel, G., Schima, H. (2007) Biomechanical properties of decelularized porcine pulmonary valve conduits. *Artificial Organs*, 32(1), 28-35.

Seliktar, D., Black, R.A, Vito, R.P., Nerem, R.M. (2000) Dynamic mechanical conditioning of collagen-gel blood vessel constructs induces remodeling *in vitro*. *Ann. Biomed Eng.*, 28, 351-362.

Senthilnathan, V., Treasure, T., Grunkemeier, G., *et al*. (1999) Heart valves: which is the best choice? *Cardiovasc. Surg*., 7, 393-397.

Shaikh, F.M., O'Brien, T.P., Callanan, A., Kavanagh, E.G., Burke, P.E., Grace, P.A., McGloughlin, T.M. (2009) New pulsatile hydrostatic pressure bioreactor for vascular tissue-engineered constructs. *Artificial organs*, 34(2), 1525-1594

Shi, G. Wang, C., Lu, N., Wang, S., Bei, J. (2002) Fabrication of cell scaffolds of poly-

L-lactic acid) and poly (L-lactic-*co*-glycolic acid). *Polym. Adv. Technol*., 13, 227.

Shinoka, T., Breuer, C.K., Tanel, R.E., Zund, G., Miura, T., Ma, P.X., Langer, R., Vacanti, J.P., Mayer, J.E. Jr. (1995) Tissue engineering heart valves: Valve leaflet replacement study in a lamb model. *Ann. Thorac. Surg*., 60, S513–S516.

Shinoka, T., Ma, P.X., Shum-Tim, D., Breuer, C.K., Cusick, R.A., Zund, G., Langer, R., Vacanti, J.P., Mayer, J.E. Jr. (1996) Tissue-engineered heart valves. Autologous valve leaflet replacement study in a lamb model. *Circulation*, 94, II164–II168.

Shinoka, T., Shum-Tim, D., Ma, P.X., Tanel, R.E., Langer, R., Vacanti, J.P., Mayer, J.E. Jr. (1997) Tissue-engineered heart valve leaflets: Does cell origin affect outcome? *Circulation*, 96, II102–II107.

Sierra, D.H. (1993) Fibrin sealant adhesive systems: A review of their chemistry, material properties and clinical applications. *J. Biomater. Appl.*, 7, 309–352.

Simionescu, D.T. (2004) Prevention of calcification in bioprosthetic heart valves: challenges and perspectives. *Expert Opin. Biol. Ther.*, 4, 1971-1985.

Simon, P., Kasimir, M.T., Seebacher, G., Wigel, G., Ullrich, R., Salzer-Muhar, U., Rieder, E., Wolner, E. (2003) Early failure of the tissue engineered porcine heart valve SYNERGRAFT in pediatric patients. *Eur. J. Cardiothorad. Surg*., 23, 1002-1006.

Sloth, E., Houlind, K.C., Oyre, S., Kim, W.Y., Pedersen, E.M., Jorgensen, H.S., Hasenkam, J.M (1994) Three-dimensional visualization of velocity profiles in the human main pulmonary artery with magnetic resonance phasevelocity mapping. *Am. Heart J*. 128, 1130-1138.

Small, J.V., Sobieszek, A. (1977) Studies on the function and composition of the 10-nm (100-Å) filaments of vertebrate smooth muscle. *J. Cell Sci*., 23, 243–268.

Sodian, R., Hoerstrup, S.P., Sperling, J.S., Daebritz, S.H., Martin, D.P., Schoen, F.J., Vacanti, J.P., Mayer, J.E. (2000) Tissue engineering of heart valves: *in vitro* experience.

Ann. Thorac. Surg., 70, 140–144.

Sodian, R., Hoerstrup, S.P., Sperling, J.S. *et al*. (2000) Evaluation of biodegradable, three-dimensional matrices for tissue engineering of heart valves. *ASAIO J*., 46, 107-110.

Sodian, R., Loebe, M., Hein, A., *et al*. (2002) Application of stereolithography for scaffold fabrication for tissue engineered heart valves. *ASAIO*, 48, 12-16.

Sokal, R.R., Rohlf, F.J. (1981) Biometry, 2nd edn. New York: W. H. Freeman & Company.

St Jude Medical, Inc. (2007) [Internet] available from: http://www.ctsnet.org/stjude/product/25 [accessed 18th Dec 2007]

Standring, S. (2008) *Gray's Anatomy—The anatomical basis of clinical practice*. 14th Edn, UK, Elsevier Limited.

Stapleton, T (2008) Development and characterisation of an acellular porcine medial meniscus for use in tissue engineering. PhD Thesis, Faculty of Biological Scienses, University of Leeds.

Stapleton, T.W., Ingram, J., Katta, J., Knight, R., Korossis, S., Fisher, J., Ingham, E. (2008) Development and characterization of an acellular porcine medial meniscus for use in tissue engineering. *Tissue Eng. Part A*, 14 (4), 505-518.

Starr, A., Edwards, M.L. (1961a) The shielded ball valve prosthesis. *J. Thorac. Cardiovasc. Surg.*, 42, 673.

Starr, A., Edwards, M.L. (1961b) Mitral replacement: The shielded ball valve prothesis. *Ann. Surg*., 154, 726-740.

Starr, A. Herr, R.H., Wood, J.A. (1967) Mitral replacement: Review of six years' experience, *J. Thorac. Cardiovasc. Surg*., 54, 333-358.

Starr, A., Fessler, C.L., Grunkemeier, G., He, G. (2002) Heart valve replacement surgery: past, present and future. *Clinical and Experimental Pharmacology and Physiology*, 29, 735-738.

Stock, U.A., Vacanti, J.P. (2001) Cardiovascular physiology during fetal development and implications for tissue engineering. *Tissue Eng.*, 7, 1–7.

Stock, U.A., Schenke-Layland, K. (2006) Performance of decellularized xenogeneic tissue in heart valve replacement. *Biomaterials*, 27, 1-2.

Stradins, P., Lacis, R, Ozolanta, I., Purina, B., Ose, B., Feldmane, L., Kasyano, V. (2004) Comparison of biomechanical and structural properties between human aortic and pulmonary valve. *European Journal of Cardio-thoracic Surgery*, 26, 634-639.

Suh, J.K., Matthew, H.W. (2000) Application of chitosan-based polysaccharide biomaterials in cartilage tissue engineering: A review. *Biomaterials*, 21, 2589–2598.

Sun, W.Q., Leung, P. (2008) Calorimetric study of extracellular tissue matrix degradation and instability after gamma irradiation. *Acta. Biomater.*, 4(4), 817–826.

Sung, H.W., Yoganathan, A.P. (1990) Secondary flow velocity patterns in a pulmonary artery model with varying degrees of valvular pulmonic stenosis: pulsatile *in vitro* studies. *J. Biomech. Eng.*, 112, 88-92.

Sung, H.W., Philpot, E.F., Nanda, N.C., Yoganathan, A.P. (1990) Axial flow velocity patterns in a pulmonary artery model with varying degrees of valvular pulmonic stenosis: pulsatile *in vitro* studies. *J. Biomech.*, 23, 563-578.

Sutherland, F.W.H., Perry, T.E., Yu, Y., *et al*. (2005) From stem cells to viable autologous semilunar heart valve. *Circulation*, 111, 2783-2791.

Sutton, J.P., Ho, S.Y., Anderson, R.H. (1995) The forgotten interleaflet triangles: a review of the surgical anatomy of the aortic valve. *Annals of Thoracic Surgery*, 59, 419-427.

Tavakkol, Z., Gelehrter, S., Goldberg, C. S., Bove , E. L., Devaney, E. J., Ohye, R. G. (2005) Superior durability of SynerGraft pulmonary allografts compared with standard cryopreserved allografts. *Ann. Thorac. Surg.* 80, 1610-1614.

Taylor, P.M., Batten, P., Brand, N.J., Thomas, P.S., Yacoub, M.H. (2003) The cardiac valve interstitial cell. *Int. J. Niochem. Cell. Biol*., 35, 113-118.

Taylor, P.M., Sachlos, E., Dreger, S.A., Chester, A.H., Czernuszka, J.T., Yacoub, M.H. (2006a) Interaction of human valve interstitial cells with collagen matrices manufactured using rapid prototyping. *Biomatirials*, 27, 2733-3737.

Taylor, P. M., Cass, A. E.G., Yacoub, M.H. (2006b) Extracellular matrix scaffolds for tissue engineering heart valves. *Progress in Pediatric Cardiology*, 21(2), 215-225.

Terrovitis, J.V, Bulte, J.W.M., Sarvananthan, S., Crowe, L.A., Sarathchandra, P., Batten, P., Sachlos, E., Chester, A.H., Czernuszka, J.T., Firmin, D., Taylor, P., Yacoub, M.H. (2006) Magnetic resonance imaging of ferumoxide-labeled mesenchymal stem cells seeded on collagen scaffolds-relevance to tissue engineering. *Tissue engineering*, 12(10), 2765-2774.

Texas Heart Institute (2007) [Internet] available from http://www.texashemtinstitute.org/HIC/ Anatomy/anatomy2.cfm [accessed 2nd Dec, 2007]

Thom, T., Haase, N., Rosamond, W. *et al.* (2006) Heart disease and stroke statistics-2006 update. A report from the American Heart Association Statistics Committee and Stroke Statistics Subcommittee. *Circulation*, 113, e85-e151.

Thubrikar, M., Bosher, P.L., Nolan, S.P. (1979) The mechanism of opening of the aortic valve. *Journal of Thoracic & Cardiovascular Surgery*, 77, 863-870.

Thubrikar, M.J., Heckman, J.L., Nolan, S.P. (1993) High speed cine-radiographic study of aortic valve leaflet motion. *J. Heart valve Dis*., 2(6), 653-661.

Trantina-Yates, A., Weissenstein, C., Human, P., Zilla, P. (2001) Stentless bioprosthetic heart valve research: sheep versus primate model. *Ann. Thorac. Surg*., 71(Suppl.), S422-S427.

Treasure, T. (1990) Which heart valve should you use? *Lancet*, 336, 1115-1117.

Tudorache, I., Cebotari, S., Sturz, G., Kirsch, L., Hurschler, C., Hilfiker, A., Haverich, A., Lichtenberg, A. (2007) Tissue engineering of heart valves: biomechanical and morphological properties of decellularized heart valves. *J Heart Valve Dis*., 16(5), 567-573.

Tuzlakoglu, K., Reis, R.L. (2009) Biodegradable polymeric fiber structures in tissue engineering. *Tissue Engineering Part B*, 15, 17-27

Uccelli, A., Moretta, L., Pistoia, V. (2006) Immunoregulatory function of mesenchymal stem cells. *Eur. J. Immunol*., 81, 1390-1397.

University of Utah Cardiovascular Pathology Index (2007a) [Internet] available from http://library.med.utah.edu/WebPath/CVHTML/CV003.html [accessed 8th Dec, 2007]

University of Utah Cardiovascular Pathology Index (2007b) [Internet] available from http://library.med.utah.edu/WebPath/CVHTML/CV002.html [accessed 8th Dec, 2007]

Valentin, J.E., Turner, N.J., Gilbert, T.W., Badylak, S.F. (2010) Functional skeletal muscle formation with a biologic scaffold. *Biomaterials*, 31(29), 7475–7484.

van Gorp, M.J., Steyerberg, E.W., van der Graaf, Y. (2004) Decision Guidelines for Prophylactic Replacement of Björk-Shiley Convexo-Concave Heart Valves Impact on Clinical Practice. *Circulation*, 109, 2092-2096.

Versily, I. (1998) The role of elastin in aortic valve mechanics, *J. Biomech.*, 31 (2), 115–123.

Vesely, I., Boughner, D., Song, T. (1988) Tissue buckling as a mechanism of bioprosthetic vale failure. *Annals. of Thoracic Surgery*, 46, 302-305.

Vesely, I., Noseworthy, R. (1992) Micromechanics of the fibrosa and the ventricularis in aortic valve leaflets. *J. Biomech.*, 25, 101-113.

Vesely, I., Casarotto, D.C., Gerosa, G. (2000) Mechanics of cryopreserved aortic and pulmonary homografts. *J. Heart Valve Dis.*, 9, 27-37.

Vesely, I. (2005) Heart valve tissue engineering. *Circ. Res*., 97, 743-755.

Villa, M.L., DeBiasi, S., Pilotto, F., (1980) Residual heteroantigenicity of glutaraldehydetreated porcine cardiac valves. *Tissue Antigens.*, 16, 62-69.

Vincentelli, A., Wautot, F., Juthier, F. *et al*. (2007) *In vivo* autologous recellularization of a tissue-engineered heart valve: are bone marrow mesenchymal stem cells the best candidates? *Evolving Technology*, 424-432.

Vismara, R., Soncini, M., Talo, G., Dainese, L., Guarino, A., Redaelli, A., Fiore, G.B. (2010) A bioreactor with compliance monitoring for heart valve grafts. *Annals. of Biomedical Engineering*, 38(1), 100-108.

Vogel, K.G. (1994) *Glycosaminoglycans and proteoglycans* in *Extracellular matrix assembly and structure* (Yurchenco, P.D., Birk, D.E., Mecham, R.P. ed.), pp 243-279, San Diego, Academic Press Inc.

Vorotnikova, E., McIntosh, D., Dewilde, A., Zhang, J., Reing, J.E., Zhang, L. *et al*. (2010) Extracellular matrix-derived products modulate endothelial and progenitor cell migration and proliferation in vitro and stimulate regenerative healing *in vivo*. *Matrix Biol.*, 298, 690–700.

Vyavahare N.R., Hirsch, D., Lerner, E., *et al*. (1998) prevention of calcification of glutaraldehyde-crosslinked orcine aortic cusps by ethanol preincubation: mechanistic studies of protein structure and water-biomaterial relationships. *J. Biomed. Mater. Res.*,

40, 577-585.

Walker, G.A., Masters, K.S., Shal, D.N, Anseth, K.S., Leinwand, L.A. (2004) Valvular myofibroblast activation by transforming growth factor-beta: implications for pathological extracellular matrix remodeling in heart valve disease. *Circ. Res.*, 95, 253-260.

Walles, T., Puschmann, C., Haverich, A., Mertsching, H. (2003) Acellular scaffold implantation – no alternative to tissue engineering. *International Journal of Artificial Organs*, 26, 225-234.

Wang, L., Korossis, S., Ingham, E., Fisher, J., Jin, Z. (2008) Computational simulation of oxygen diffusion in aortic valve leaflet tissue for tissue engineering applications. *Journal of Heart Valve Disease*, 17, 700-709.

Wang, L., Wilshaw, SP., Korossis, S., Fisher, J., Jin, Z., Ingham, E. (2009) Factors influencing the oxygen consumption rate of aortic valve interstitial cells: application to tissue engineering. *Tissue Engineering Part C*, 15, 355-363.

Wang, K.X., Zhang, J.F., Zhan, Q.P., Jian, X.H. (2005) Effect of trypsin and Triton-X 100 for decellularisation of porcine aortic heart valves. *Di Yi Jun Yi Da Xue Xue Bao*, 25 (1), 22-25.

Ward, K.E., Elkins, R.C., Overholt, E.D., *et al.* (1997) Evaluation of cryopreserved homografts in right ventricular outflow tract after the Ross procedure: intermediate-term follow up. *J. Heart Valve Dis.*, 6, 130–133.

Weatley, D., Will, M. (2004) Mitral valve replacement with mechanical or bioprosthetic valve. *MMCTS*, doi: 10.1510/mmcts.2004.001024

Weerasena, N., Lockie, K.J., Butterfield, M., Fisher, J., Kearney, J.N., Davies, G.A. (1992) The hydrodynamic function and leaflet dynamics of aortic and pulmonary roots and valves: an in vitro study. *European Journal of Cardiothoracic Surgery*, 6, 350-356.

Wernly, J.A., Crawford, M.H. (1998) Choosing a prosthetic heart valve. *Cardiol. Clin*., 16, 491-504.

Wilcox, H.E., Korossis, S.A., Booth, C., Watterson, K.G., Kearney, J.N., Fisher. J., Ingham, E. (2005) Biocompatibility and recellularization potential of an acelluar porcine heart valve matrix. *The journal of heart valve disease.* 14, 228-237.

Wilshaw, S., Kearney, J.N., Fisher, J., Ingham, E. (2006) Production of an acellular amniotic membrane matrix for use in tissue engineering. *Tissue Engineering*, 12, 2117-2129.

Wilshaw, S., Rooney, P., Berry, H., Kearney, J., Homer-Vanniasinkam, S., Fisher, J., Ingham, E. (2011) Development and characterisation of acellular allogeneic arterial matrices. *Tissue Engineering*, doi: 10.1089/ten.TEA.2011.0287.

Wilson, G.J., Courtman, D.W., Klement, P., Lee, J.M., Yeger, H. (1995) Acellular matrix: a biomatirials approach for coronary-artery bypass and heart valve replacement. *Ann. Thorac. Surg*., 60 (Suppl.), S353-S358.

Winters, R.N., Obriot, P. (2007) Mitral valve repair. *AORN Journal*, 85(1), 152-166.

Women's Heart Foundation (2007) [Internet] available from http://www.womensheart.org/content/ HeartSurgery/heart_valve_replacement.asp [accessed 15th Dec]

World Invisible (2007) [Internet] available from http:///www.worldinvisible.com/apologet/ humbody/heart.htm [accessed 2nd Dec, 2007]

Wu, X.E., Rabkin-Aikawa, E., Guleserian, K.J., Perry, T.E., Masuda, Y., Sutherland, F.W., Schoen, F.J., Mayer, J.E., Bischoff, J. (2004) Tissue-engineered microvessels on three-dimensional biodegradable scaffoldsusing human endothelial progenitor cells. *Am. J. Physiol. Heart Circ. Physiol.*, 287, H480-487.

Xu, C.C., Chan, R.W., Tirunagari, N. (2007) A biodegradable, acellular xenogeneic scaffold for regeneration of the vocal fold lamina propria. *Tissue Eng.*, 13(3), 551–566.

Xu, H., Wan, H., Sandor, M., Qi, S., Ervin. F., Harper, J.R., *et al.* (2008) Host response to human acellular dermal matrix transplantation in a primate model of abdominal wall repair. *Tissue Eng. Part A*, 14(12), 2009–2019.

Yang, B., Zhang, Y., Zhou, L., Sun, Z., Zheng, J., Chen, Y., Dai, Y. (2010) Development of a Porcine Bladder Acellular Matrixwith Well-Preserved Extracellular Bioactive Factors for Tissue Engineering. *Tissue Engineering: Part C*, 16 (5), 1201-1211.

Yang, M., Chen, C.Z., Wang, X.N., Zhu, Y.B., Gu, Y.J. (2009) Favorable effects of the detergent and enzyme extraction method for preparing decellularized bovine pericardium scaffold for tissue engineered heart valves. *J. Biomed. Mater Res. B Appl. Biomater.*, 91(1), 354–361.

Yeung, B.K.S., Chong, P.Y.C., Petillo, P.A. (2001) Synthesis of glycosaminoglycans. New York, Marcel Dekker, 425-429.

Yokose, S., Fukunaga, S., Tayama, E., Kato, S., Aoyagi, S. (2002) Histological and immunohitological study of cryopreserved aortic vave grafts: the possibility of a clinical application for cryopreserved aortic valve xenograft. *Artif. Organs*, 26, 407-415.

Zeltinger, J., Landeen, L.K., Alexander, H.G., Kidd, I.D., Sibanda, B. (2001) Development and characterization of tissue-engineered aortic valves. *Tissue Eng*, 7, 9–22.

Zhang, Q., Raoof, M., Chen, Y., Sumi, Y., Sursal T., Junger, W., *et al*. (2010) Circulating mitochondrial DAMPs cause inflammatory responses to injury. *Nature*, 464(7285), 104–107.

Zheng, M.H., Chen, J., Kirilak, Y., *et al*. (2005) Porcine small intestine submucosa (SIS) is not an acellular collagenous matrix and contains porcine DNA: Possible implications in human implantation. *J. Biomed. Mater. Res. B. Appl. Biomater.*, 73(1), 61-67.

Zhou, J., Quintero, L.J., Helmus, M.N., Lee, C., Kafesjian, R. (1997) Porcine aortic wall flexibility: fresh vs denacol fixed vs glutaraldehyde fixed. *ASAIO Journal*, 43, 470-475.
Zilla, P., Weissenstein, C., Bracher, M., *et al*. (1997) high glutaraldehyde concentrations reduce rather than increase the calcification of aortic wall tissue. *J. Heart valve Dis.*, 6, 490-491.

Zilla, P., Weissenstein, C., Human, P., Dower, T., von Oppell, U.O. (2000) High glutaraldehyde concentrations mitigate bioprosthetic root calcification in the sheep model. *Ann. Thorac. Surg.*, 70, 2091-2095.